
The effects of the 15q11.2 BP1-BP2
copy number variant on white matter microstructure

Ana Isabel Silva

School of Medicine, Cardiff University



Thesis submitted for the degree of

Doctor of Philosophy

2019

Declaration

STATEMENT 1 This thesis is being submitted in partial fulfilment of the requirements for the degree of *PhD*

Signed _____

Date _____

STATEMENT 2

This work has not been submitted in substance for any other degree or award at this or any other university or place of learning, nor is it being submitted concurrently for any other degree or award (outside of any formal collaboration agreement between the University and a partner organisation)

Signed _____

Date _____

STATEMENT 3

I hereby give consent for my thesis, if accepted, to be available in the University's Open Access repository (or, where approved, to be available in the University's library and for inter-library loan), and for the title and summary to be made available to outside organisations, subject to the expiry of a University-approved bar on access if applicable.

Signed _____

Date _____

DECLARATION

This thesis is the result of my own independent work, except where otherwise stated, and the views expressed are my own. Other sources are acknowledged by explicit references. The thesis has not been edited by a third party beyond what is permitted by Cardiff University's Use of Third Party Editors by Research Degree Students Procedure.

Signed _____

Date _____

WORD COUNT 53600 words

Thesis Summary

The effects of the 15q11.2 BP1-BP2 copy number variant on white matter microstructure

Altered white matter structure has been consistently reported in neurodevelopmental disorders. A key question is whether genetic risk variants that are associated with neurodevelopmental disorders, are also associated with changes in white matter. The 15q11.2 BP1-BP2 copy number variant (CNV) is emerging as a recognised syndrome and has been associated with several neurodevelopmental disorders, including autism spectrum disorders (ASD) and schizophrenia. The cytoplasmic *FMR1* interacting protein 1 (*CYFIP1*), a gene in this region, is involved in two distinct complexes, known to regulate actin cytoskeleton dynamics and protein translation - mechanisms that are crucial in white matter dynamics. This thesis describes a translational project combining a diverse set of multidisciplinary experiments to investigate the effects of the 15q11.2 BP1-BP2 CNV on white matter microstructure.

In Chapters 3 and 4, using diffusion tensor imaging (DTI) methods, I demonstrate a link between 15q11.2 BP1-BP2 CNV dosage and altered white matter microstructure in human carriers, where bidirectional CNV dosage leads to opposite changes in white matter measures.

In Chapters 5, 6 and 7, using a novel *Cyfp1* haploinsufficiency rat model to model the low dosage of *CYFIP1* in 15q11.2 BP1-BP2 deletion carriers, I investigate how this gene could contribute to the phenotype seen in Chapters 3 and 4. Combining DTI, histology and *in vitro* methods, I report that *Cyfp1* haploinsufficiency leads to thinning of the myelin sheath in the corpus callosum, and suggest that these changes are caused by abnormal mechanisms involving myelin basic protein distribution in mature oligodendrocytes.

In conclusion, these results show that variations at the 15q11.2 BP1-BP2 chromosomal region lead to white matter abnormalities, and suggest that *Cyfp1* influences myelination in the central nervous system in a rat model, providing an insight into a possible contribution made by low dosage of *CYFIP1* to 15q11.2 BP1-BP2 deletion associated phenotypes.

Acknowledgments

Foremost, I would like to express my sincere gratitude to my supervisors, Prof Jeremy Hall, Prof. Lawrence Wilkinson and Prof. David Linden, for their guidance and continuous support throughout the course of this PhD. Their encouragement, motivation and optimism were fundamental during these years, and I consider myself very lucky to have had the opportunity to be their student.

I extend my gratitude to everyone in NMHRI and CUBRIC, whom I had the pleasure to work alongside. In particular, I would like to thank Dr. Yasir Syed, who was invaluable during my laboratory work, for teaching me new techniques, as well as providing technical support and helpful discussions. Special thanks goes to Jenny Carter and Dr. Josephine Haddon for all their incredible support and friendship, and for helping me with all the animal work. I would like to thank the team at deCODE genetics institute in Iceland, in special Dr. Magnús Úlfarsson and Dr. Hreinn Stefansson, for giving me the opportunity to work in their team for 3 months.

Living in Cardiff has been a wonderful experience, and I owe it to many wonderful people I met during these years, especially my ‘Portuguese crew’ of friends who always made me feel at home, and provided me countless hours of laughter and (very importantly) delicious food! I am also grateful to all my friends outside of Cardiff, whom I miss deeply, and were very supportive during my academic life. A heartfelt thanks goes to Eduardo Terças, my forever friend, for always believing in me, and for always being there to bring me joy during difficult times.

I would also like to express my gratitude to my parents for their endless support, and for always believing in me (even when I didn’t!). My parents have been my role models in the past years, showing me that it is never too late to pursue my dreams and aspirations. Thank you for *everything*. A special thanks to my brother Bruno, for fruitful conversations and re-affirming my interest in psychiatry.

Finally, I would like to thank my partner, Jonathan Willow, who has made this whole experience very special. Thank you for all our adventures in nature, for loving all the living creatures as much as I do, and for showing me many of the magical things this world has to offer.

Data collection and funding

I was supported by funding from the Neuroscience and Mental Health Research Institute (NMHRI) at Cardiff University. This work is part of the DEFINE project, funded by the Wellcome Trust Strategic Award DEFINE grant (grant no. 100202/Z/12/Z). All the work was carried out according to the guidance of my supervisors, Prof. Jeremy Hall, Prof. Lawrence Wilkinson, and Prof. David Linden.

The imaging data from Iceland were collected, as part of the ongoing gene discovery work, at deCODE genetics institute in Reykjavik, Iceland. This work was supported by the Innovative Medicines Initiative Joint Undertaking grant (grant no. 115008 and 115300), of which resources were composed of European Federation of Pharmaceutical Industries and Associations in-kind contribution and financial contribution from European Union Seventh Framework Programme (EU-FP7/2007-2013) (grant no. 602450 (IMAGEMEND)) and FP7-People-2011-IAPP (grant no. 286213 (PsychDPC)). As part of a collaboration between Cardiff University and deCODE genetics institute, I spent 3 months in Iceland, where I pre-processed and analysed the imaging data under the supervision of Dr. Magnús Úlfarsson, Dr. Omar Gustafsson, Bragi Walters, and Dr. Hreinn Stefansson. The pre-processing of the imaging data was done with the support from Dr. Mark Drakesmith from Cardiff University.

The processed imaging data from UK Biobank were released to Cardiff University after application to the UK Biobank (project ref. 17044). These data were kindly provided by Dr. Xavier Caseras, and I performed the analyses of the data.

The creation of the *Cyfp1* haploinsufficiency rat model was done by a collaboration between Cardiff University and Horizon Discovery (St Louis, USA), under the DEFINE project grant, and core support from the NMHRI. Animal husbandry and care was done by the Joint Biological Services Unit personal at Cathays Animal Facility, at Cardiff University. The specification of the model was done by Dr. Simon Trent at Cardiff University.

The imaging data on the rat model was collected by Andrew Stewart and Dr. Yaniv Assaf. I performed the pre-processing and analyses of the imaging data with the guidance from Dr. Yaniv Assaf. For histology, the perfusions of the brains were done by Jenny Carter, Yateen Patel, Dr. Josephine Haddon, and Dr. Niels Haan. The preparation of the brain tissue for the transmission electron microscopy experiment and image acquisition were done by Dr. Christopher Von Ruhland, at the Central Biotechnology Services, at Cardiff University. The data were analysed by me. For immunofluorescence, I extracted and cut the brain in a cryostat. I also performed all the stainings and analysed the data. For the cell culture experiment, Dr. Yasir Syed and I generated the oligodendrocyte cultures, and I performed the staining and analyses of the data. All the laboratory work was done under the supervision of Dr. Yasir Syed.

Publications arising from the thesis

Chapter 3 has been published as a journal article in Biological Psychiatry:

Silva, Ana I., et al. "Reciprocal white matter changes associated with copy number variation at 15q11. 2 BP1-BP2: A diffusion tensor imaging study." *Biological psychiatry* 85.7 (2019): 563-572.

Chapters 5, 6 and 7 were published as a journal article in Nature Communications:

Silva, Ana I., et al. "Cyfip1 haploinsufficient rats show white matter changes, myelin thinning, abnormal oligodendrocytes and behavioural inflexibility." *Nature communications* 10.1 (2019): 3455.

Abbreviations

A

ABI interactor 1/2	ABI1/2
Actin-related protein 2/3	Arp2/3
Adult mathematical history questionnaire	AMHQ
Adult reading history questionnaire	ARHQ
Advanced chromosomal microarray	CMA
Attention deficit and hyperactivity disorder	ADHD
Autism spectrum disorder	ASD
Axial diffusivity	AD

B

Body Corpus Callosum	BCC
Bone morphogenic protein	BMP
Brain-derived neurotrophic factor	BDNF
Breakpoint	BP

C

Common variant common disease	CVCD
Copy number variant	CNV
Corpus Callosum	CC
<i>Cyfi1</i> haploinsufficiency	<i>Cyfi1</i> ^{+/-}
Cytoplasmic <i>FMRI</i> interacting protein 1	CYFIP1
2'-3'-cyclic nucleotide 3'-phosphodiesterase	CNP

D

Diffusion tensor imaging	DTI
Diffusion-weighted MRI	DWI

Intelligence quotient	IQ
Intracranial volume	ICV

J

John Hopkins University	JHU
-------------------------	-----

L

L-thyroxine	T4
Linear mixed effects	LME
Long-term depression	LTD
Long-term potentiation	LTP

M

Mammalian Target of Rapamycin	mTOR
Mean diffusivity	MD
Messenger RNA	mRNA
Miniature excitatory postsynaptic current	mEPSC
Miniature inhibitory postsynaptic current	mIPSC
Minimum essential medium Eagle	MEM
Myelin basic protein	MBP
Myelin-associated glycoprotein	MAG

N

N-methyl-D-aspartate	NMDA
Nck-associated protein 1	NCKAP1
Non-imprinted in Prader-Willi/Angelman syndrome 1 gene	NIPA1
Non-imprinted in Prader-Willi/Angelman syndrome 2 gene	NIPA2

O

Oligodendrocyte precursor cell	OPC
--------------------------------	-----

P

Paraformaldehyde	PFA
Phosphate buffered saline	PBS
Phosphatidylinositol 4,5-bisphosphate	PI(4,5)P2
Poly-L-Lysine	PLL
Prader-Willi Syndrome	PWS
Proteolipid protein	PLP

R

Radial diffusivity	RD
Radio frequency	RF
Rare variant common disease	RVCD
Region-of-interest	ROI
Repetition time	TR
Right and left Anterior Corona Radiata	ACR_R; ACR_L
Right and left Anterior Limb of the Internal Capsule	ALIC_R; ALIC_L
Right and left Cingulum (cingulate gyrus portion)	C_CG_R; C_CG_L
Right and left Cingulum (hippocampal portion)	C_HIP_R; C_HIP_L
Right and left Corticospinal tract	CST_R; CST_L
Right and left External Capsule	EC_R; EC_L
Right and left Inferior Longitudinal Fasciculus	ILF_R; ILF_L
Right and left Posterior Corona Radiata	PCR_R; PCR_L
Right and left Posterior Limb of the Internal Capsule	PLIC_R; PLIC_L

Right and left Posterior Thalamic Radiation	PTR_R; PTR_L
Right and left Superior Corona Radiata	SCR_R; SCR_L
Right and left Superior Longitudinal Fasciculus	SLF_R; SLF_L
Right and left Uncinate Fasciculus	UF_R; UF_L
S	
Single-nucleotide polymorphism	SNP
Splenium Corpus Callosum	SCC
T	
Threshold-free cluster-enhancement	TFCE
Total intracranial volume	TIV
Tract-Based Spatial Statistics	TBSS
Transfer RNA	tRNA
Transmission electron microscopy	TEM
Tri-iodothyroxine	T3
Tubulin gamma complex associated protein 5 gene	<i>TUBGCP5</i>
V	
Voxel-based morphometry	VBM
W	
WAVE regulatory complex	WRC
Wechsler Adult Intelligence Scale	WASI-I
Wild-type	WT
Wiskott-Aldrich syndrome protein family verprolin homologous protein	WAVE
Wiskott–Aldrich syndrome protein	WASP
α -amino-3-hydroxy-5-methyl-4-isoxazolepropionic acid	AMPA

List of Tables

Table 3.1- Subject characteristics.	65
Table 3.2 – Summary of between group TBSS analyses results.	69
Table 3.3- White matter tracts and abbreviations used.	70
Table 3.4 - Group differences between deletion and controls with NoCNV, duplications and NoCNV, and deletions and duplications carriers.	74
Table 4.1 - Subject characteristics of the UK Biobank sample.	104
Table 4.2 - White matter tracts and abbreviations used.	107
Table 4.3 - Group differences between deletion and controls with NoCNV, duplications and NoCNV, and deletions and duplications carriers.	110
Table 5.1 – Group differences between <i>Cyfp1^{+/-}</i> and WT rats.	142
Table 5.2 – Group differences between <i>Cyfp1^{+/-}</i> and WT rats in the 3 segments of the corpus callosum.	145

List of Figures

Figure 1.1 - Development of biomarkers in order to achieve a personalised diagnosis and treatment of neurodevelopmental disorders (NDD).	5
Figure 1.2 - Translational framework combining multi-modal imaging in animal models and humans.....	10
Figure 1.3 - Ideogram representing the chromosome 15.	12
Figure 1.4 - Penetrance and frequency of different CNVs in controls and different neurodevelopmental disorders.....	13
Figure 1.5 - Schematic representation of a neuron, and detailed view of the growth cone and main cytoskeletal components (filopodia, lamellipodia, microtubules and actin filaments).....	18
Figure 1.6 - Schematic illustration of CYFIP1 protein dynamics as an inhibitor of WAVE regulatory complex (WRC) and actin polymerisation.....	20
Figure 1.7 - Schematic illustration of CYFIP1-FMRP complex dynamics as an inhibitor of mRNA translation.....	22
Figure 1.8 - Diagram showing the different types of glial cells in relation to a neuron.	30
Figure 1.9 - Actin dynamics during oligodendrocyte differentiation and process extension.	34
Figure 1.10 - Model of myelin wrapping in the central nervous system.	36
Figure 1.11 – Schematic representation of MBP synthesis in oligodendrocytes.	41
Figure 1.12 – Schematic representation of the major myelin-key proteins PLP and MBP.	42
Figure 2.1- Conceptual diagram of image acquisition in MRI.....	49
Figure 2.2 – Diffusion-weighted spin echo sequence.....	51
Figure 2.3 – Diffusion tensor and DTI measures.	52
Figure 2.4 – Different approaches to analyse DTI data.	55
Figure 3.1 - TBSS whole-group voxel-based analysis.....	72
Figure 3.2 - Boxplots showing group differences for atlas-based segmentation analyses.	76

Figure 3.3 - Diverging bars for Cohen d' effect sizes for group differences when comparing deletion and duplication carriers versus controls.	78
Figure 3.4 - Cohen d' effect sizes for group differences when comparing deletion versus duplication carriers.....	80
Figure 3.5 - Linear age trajectories for deletion (red), NoCNV (yellow), and duplication (blue) groups.....	82
Figure 3.6 - Quadratic age trajectories for deletion (red), NoCNV (yellow), and duplication (blue) groups.	83
Figure 3.7 – Gender differences in Cohen d' effect sizes, when comparing deletion and duplication carriers versus controls.	85
Figure 3.8 - Gender differences in Cohen d' effect sizes, when comparing deletion versus duplication carriers.....	86
Figure 4.1 - Boxplots showing group differences for the UK Biobank TBSS-derived measures.	112
Figure 4.2 - Diverging bars for Cohen d' effect sizes for group differences when comparing deletion and duplication carriers versus controls.	114
Figure 4.3 – Cohen d' effect sizes for group differences when comparing deletion versus duplication carriers.....	116
Figure 4.4 – Cohen d' effect sizes in the samples from deCODE and UKBiobank.....	117
Figure 4.5 – Comparison between age trajectories in the deCODE Icelandic sample and UK Biobank sample.....	119
Figure 4.6 - Gender differences in Cohen d' effect sizes, when comparing deletion and duplication carriers versus controls.	121
Figure 5.1 – White matter skeleton used for the Tract-Based Spatial Statistics analysis.	135
Figure 5.2 – White matter binary masks used for segmentation of specific white matter tracts.	136
Figure 5.3 – Tractography of the corpus callosum.	137
Figure 5.4 – Colour-coded heat maps for fractional anisotropy.....	139
Figure 5.5 - TBSS whole-group voxel-based analysis, after FWE correction.	141
Figure 5.6 - Tractography of the splenium, body and genu of the corpus callosum. ...	144
Figure 5.7 - TBSS whole-group voxel-based analysis, after FDR correction.....	147

Figure 5.8 - Corpus callosum sub-regions in human (top) and rat (bottom) brain.....	151
Figure 6.1 – Illustration of sampling for transmission electron microscopy, and representative figures.....	161
Figure 6.2 - Schematic illustration of the axon and myelin sheath and calculation of the g-ratio and myelin thickness.....	163
Figure 6.3 - Number of axons in WT (n=5) and <i>Cyfp1</i> ^{+/-} (n=4) rats.	166
Figure 6.4 - Axon diameter in WT (n=5 animals, n=7148 axons) and <i>Cyfp1</i> ^{+/-} (n=4 animals, n=5979 axons) rats.....	167
Figure 6.5 - G-ratio in WT (n=5 animals, n=7148 axons) and <i>Cyfp1</i> ^{+/-} (n=4 animals, n=5979 axons) rats.....	168
Figure 6.6 - Myelin thickness in WT (n=5 animals, n=7148 axons) and <i>Cyfp1</i> ^{+/-} (n=4 animals, n=5979 axons) rats.....	170
Figure 6.7 – Number of oligodendrocyte lineage and mature cells in the corpus callosum of WT and <i>Cyfp1</i> ^{+/-} rats (n=7 each).	172
Figure 6.8 - MBP intensity levels in the corpus callosum of WT and <i>Cyfp1</i> ^{+/-} rats (n=7 each).....	173
Figure 7.1 - Schematic flow chart of the experimental protocol for cultivation of OPCs.	190
Figure 7.2 – Differentiation of oligodendrocyte lineage cells.....	192
Figure 7.3 - <i>In vitro</i> assessment of the percentage of oligodendrocyte (O4+) and mature oligodendrocyte (MBP+) cells.	194
Figure 7.4 - <i>In vitro</i> assessment of the percentage of mature oligodendrocytes in different stages of maturation, as indicated by the distribution of MBP staining in the cells.....	196
Figure 7.5 - <i>In vitro</i> assessment of the area of MBP distribution in oligodendrocytes at late stages of maturation.	198
Figure 8.1 - Proposed mechanisms through which <i>Cyfp1</i> haploinsufficiency could impact MBP mRNA transport and/or MBP translation inhibition in oligodendrocyte cells. ..	214
Figure 8.2 - Experiment design to test alterations in white matter microstructure after biconditional discrimination learning.	218

Table of Contents

THESIS SUMMARY	III
ACKNOWLEDGMENTS	V
DATA COLLECTION AND FUNDING	VI
PUBLICATIONS ARISING FROM THE THESIS	VIII
ABBREVIATIONS.....	IX
LIST OF TABLES.....	XIV
LIST OF FIGURES.....	XV
TABLE OF CONTENTS.....	XVIII
CHAPTER 1	1
GENERAL INTRODUCTION	1
1.1. THE COMPLEXITY OF NEURODEVELOPMENTAL DISORDERS	3
1.2. COPY NUMBER VARIANTS AND NEURODEVELOPMENTAL DISORDERS.....	5
1.2.1. <i>Neuroimaging studies in CNVs</i>	8
1.2.2. <i>Understanding the role of CNVs</i>	9
1.3. THE 15Q11.2 BP1-BP2 COPY NUMBER VARIANT	11
1.4. MOLECULAR FUNCTIONS OF THE <i>CYFIP1</i> GENE.....	16
1.4.1. <i>CYFIP1 role in actin cytoskeleton remodelling</i>	16
1.4.2. <i>CYFIP1 role in mRNA translation</i>	21
1.4.3. <i>Impact of Cyfip1 on dendritic and spine morphology and physiology</i>	23
1.5. AN EFFECT BEYOND SYNAPSES – NEURODEVELOPMENTAL DISORDERS AND WHITE MATTER	26
1.6. NEURODEVELOPMENTAL DISORDERS AND GLIAL CELLS.....	29
1.6.1. <i>The role of actin polymerisation on oligodendrocyte differentiation</i>	32
1.6.2. <i>The role of actin depolymerisation in myelin wrapping</i>	35
1.6.3. <i>The role of protein synthesis during myelination – MBP mRNA transport to localised translation</i>	39
1.7. THESIS AIMS	43
CHAPTER 2	45
GENERAL METHODS.....	45
2.1. ABSTRACT	47
2.2. ANIMALS	47
2.2.1. <i>Creation of the Cyfip1 haploinsufficiency rat model</i>	47

2.3.	DIFFUSION TENSOR IMAGING OF THE BRAIN	48
2.3.1.	<i>DTI data analyses</i>	53
CHAPTER 3.....		57
WHITE MATTER CHANGES ASSOCIATED WITH COPY NUMBER VARIATION AT 15Q11.2 BP1-BP2		57
3.1.	ABSTRACT.....	59
3.2.	INTRODUCTION	61
3.3.	MATERIAL AND METHODS	63
3.3.1.	<i>Participants</i>	63
3.3.2.	<i>Diffusion MRI acquisition and pre-processing</i>	65
3.3.3.	<i>Tract-Based Spatial Statistics Analysis (TBSS) of DTI</i>	66
3.3.4.	<i>Regional DTI Parameters analyses</i>	67
3.3.5.	<i>Age trajectories</i>	68
3.3.6.	<i>Sex differences</i>	68
3.4.	RESULTS.....	69
3.4.1.	<i>Between-group TBSS analysis</i>	69
3.4.2.	<i>Between-group regional analyses</i>	72
3.4.3.	<i>Age trajectories</i>	81
3.4.4.	<i>Sex Differences</i>	84
3.5.	DISCUSSION	87
3.5.1.	<i>Increased FA in 15q11.2 BP1-BP2 deletion carriers - how it relates to DTI findings in neurodevelopmental disorders and other CNVs</i>	87
3.5.2.	<i>Increased FA in 15q11.2 BP1-BP2 deletion carriers – Possible cellular causes</i>	89
3.5.3.	<i>White matter changes and relation with functional outcomes</i>	91
3.5.4.	<i>Age trajectories and gender differences</i>	93
3.5.5.	<i>Limitations of this study</i>	95
3.5.6.	<i>Conclusion</i>	96
CHAPTER 4.....		97
WHITE MATTER CHANGES ASSOCIATED WITH COPY NUMBER VARIATION AT 15Q11.2 BP1-BP2 – A REPLICATION STUDY FROM UK BIOBANK DATA.....		97
4.1.	ABSTRACT.....	99
4.2.	INTRODUCTION	101
4.3.	MATERIAL AND METHODS	102
4.3.1.	<i>Participants</i>	102
4.3.2.	<i>UK Biobank diffusion MRI acquisition and pre-processing</i>	104
4.3.3.	<i>Statistical analyses</i>	105
4.3.4.	<i>Age trajectories</i>	108
4.3.5.	<i>Sex differences</i>	108

4.4.	RESULTS	108
4.4.1.	<i>Between-group regional analyses.....</i>	108
4.4.2.	<i>Age trajectories.....</i>	118
4.4.3.	<i>Sex Differences.....</i>	120
4.5.	DISCUSSION.....	122
4.5.1.	<i>Similarities and differences between the UK Biobank sample and deCODE Icelandic sample 122</i>	
4.5.2.	<i>Age trajectories and gender differences.....</i>	124
4.5.3.	<i>Limitations of the study and future directions.....</i>	125
4.5.4.	<i>Conclusion</i>	126
CHAPTER 5	127
WHITE MATTER CHANGES ASSOCIATED WITH HAPLOINSUFFICIENCY OF CYFIP1 IN A NOVEL		
CRISPR/CAS9 ENGINEERED RAT MODEL.....		
5.1.	ABSTRACT	129
5.2.	INTRODUCTION.....	131
5.3.	MATERIALS AND METHODS	132
5.3.1.	<i>Rats.....</i>	132
5.3.2.	<i>Diffusion tensor imaging acquisition.....</i>	133
5.3.3.	<i>DTI data correction and DTI maps extraction.....</i>	133
5.3.4.	<i>Heat maps for differences in FA between WT and Cyfip1^{+/-} rats.....</i>	134
5.3.5.	<i>Tract-Based Spatial Statistics Analysis (TBSS) of DTI.....</i>	134
5.3.6.	<i>Quantification of TBSS differences.....</i>	135
5.3.7.	<i>Tractography.....</i>	137
5.3.8.	<i>Statistical analysis.....</i>	137
5.4.	RESULTS	138
5.4.1.	<i>Heat maps for differences in FA between WT and Cyfip1^{+/-} rats.....</i>	138
5.4.2.	<i>Between-group TBSS analysis – FWE correction.....</i>	140
5.4.3.	<i>Quantification of TBSS differences.....</i>	140
5.4.4.	<i>Tractography of the corpus callosum.....</i>	143
5.4.5.	<i>Between-group TBSS analysis – FDR correction.....</i>	146
5.5.	DISCUSSION.....	148
5.5.1.	<i>Contrast between 15q11.2 BP1-BP2 deletion in human carriers and Cyfip1 haploinsufficiency in the rat model.....</i>	148
5.5.2.	<i>Decreased FA in the corpus callosum of the Cyfip1^{+/-} rats – functional outcomes.....</i>	150
5.5.3.	<i>Decreased FA in Cyfip1^{+/-} rat model – Possible cellular causes.....</i>	152
5.1.1.	<i>Conclusion</i>	153
CHAPTER 6	155

INVESTIGATING THE EFFECT OF <i>CYFIP1</i> HAPLOINSUFFICIENCY ON WHITE MATTER IN RAT BRAIN - AN <i>IN VIVO</i> HISTOLOGICAL STUDY.....	155
6.1. ABSTRACT.....	157
6.2. INTRODUCTION	159
6.3. MATERIAL AND METHODS	159
6.3.1. <i>Rats</i>	159
6.3.2. <i>Transmission electron microscope</i>	160
6.3.3. <i>Immunofluorescence</i>	161
6.3.4. <i>Quantification and statistical analyses</i>	162
6.4. RESULTS.....	164
6.4.1. <i>Ultra-structural analysis of axons in the corpus callosum using transmission electron microscopy</i>	164
6.4.2. <i>Oligodendrocyte and MBP quantification in the corpus callosum and external capsule</i> .	171
6.5. DISCUSSION	174
6.5.1. <i>Myelin thinning in the <i>Cyfp1^{+/-}</i> rats – possible cellular mechanisms</i>	174
6.5.2. <i>Myelin thinning in the corpus callosum of <i>Cyfp1^{+/-}</i> rats – functional outcomes</i>	177
6.5.3. <i>Myelin thinning in the <i>Cyfp1^{+/-}</i> rat model and relationship with human data</i>	178
6.5.4. <i>Limitation of this study</i>	179
6.5.5. <i>Conclusion</i>	179
CHAPTER 7.....	181
INVESTIGATING THE EFFECT OF <i>CYFIP1</i> HAPLOINSUFFICIENCY ON RAT BRAIN OLIGODENDROCYTES - AN <i>IN VITRO</i> CELL CULTURE STUDY.....	181
7.1. ABSTRACT.....	183
7.2. INTRODUCTION	185
7.3. MATERIAL AND METHODS	186
7.3.1. <i>Generation of primary oligodendrocyte cultures</i>	186
7.3.2. <i>Preparation of tissue culture coating</i>	187
7.3.3. <i>Dissection of neonatal rat cortex for OPC isolation</i>	187
7.3.4. <i>Mechanical and chemical dissociation and preparation of cells for culture</i>	187
7.3.5. <i>Removal of microglia and isolation of OPCs from astrocyte monolayer</i>	188
7.3.6. <i>Immunofluorescence staining of cultures</i>	191
7.3.7. <i>Quantification and statistical analyses</i>	191
7.4. RESULTS.....	193
7.5. DISCUSSION	199
7.5.1. <i>Constrained MBP distribution in <i>Cyfp1^{+/-}</i> cultured oligodendrocytes – possible cellular mechanisms</i>	199
7.5.2. <i>Limitations of the study</i>	202

7.5.3. Conclusions.....	203
CHAPTER 8.....	205
GENERAL DISCUSSION.....	205
8.1. THESIS OVERVIEW	207
8.2. SUMMARY OF RESULTS	208
8.3. LINK BETWEEN HUMAN AND RAT MODEL FINDINGS	210
8.4. <i>CYFIP1</i> HAPLOINSUFFICIENCY AND OLIGODENDROCYTE FUNCTION – A PROPOSED MECHANISM	212
8.5. FUNCTIONAL OUTCOMES OF IMPAIRED MYELINATION IN <i>CYFIP1</i> ^{+/-} RATS	215
8.6. CONCLUSIONS AND FUTURE DIRECTIONS.....	219
REFERENCES.....	221
APPENDIX 1.....	263

Chapter 1

General Introduction

1.1. The complexity of neurodevelopmental disorders

Neurodevelopmental disorders encompass a wide spectrum of neuropsychiatric symptoms linked to abnormal development of the central nervous system, where general symptoms of these disorders emerge in early infancy/childhood and often persist through adulthood (*Palframan, 1997; Bishop and Rutter, 2009*). Autism spectrum disorders (ASD), intellectual disability, and attention deficit and hyperactivity disorder (ADHD) have been widely characterised as neurodevelopmental disorders (*Association, 2013*). Likewise, schizophrenia has also been proposed to result from neurodevelopment disturbances, but with symptoms usually emerging in early adulthood (*Owen and O'Donovan, 2017*). Clinically, these disorders are highly heterogeneous manifesting various degrees of social, cognitive, motor, language and affective deficits (*Association, 2013*), making diagnosis a lengthy and complex process. Given the importance of early detection and intervention in these disorders, a common goal in neurodevelopmental research is to discover 'indicators' of disruptions that confer a risk status and occur before any behaviour/clinical symptoms. These indicators are commonly termed as biomarkers and have been defined as "characteristics that are objectively measured and evaluated as indicators of normal biological processes, pathogenic processes, or pharmacologic responses to a therapeutic intervention" (*Biomarkers Definitions Working Group, 2001; Linden, 2012*).

Neuroimaging allows non-invasive access to the living brain and can be particularly useful for identifying core neurobiological mechanisms of neurodevelopmental disorders, and thus potential biomarkers in the brain (*Linden and Fallgatter, 2009; Linden, 2012*). With the development of new cutting-edge neuroimaging techniques, different aspects of brain structure (anatomical structure) and function (intrinsic physical properties of tissues) can be assessed, such as the morphology of grey and white matter, integrity and orientation of white matter tracts, brain activation patterns, connectivity between regions and networks, and neurochemistry (*Linden and Fallgatter, 2009; Linden, 2012; Silbersweig and Rauch, 2017*). Multimodal studies in patients with neurodevelopmental disorders, such as schizophrenia and ASD, have repeatedly shown abnormal effects on a structural and functional level (*Anagnostou and Taylor, 2011; Wheeler and Voineskos, 2014; Kambeitz et al., 2015; Ecker et al., 2015*). However, the high heterogeneity of these disorders is also reflected in neuroimaging studies, where inconsistent results are often found, making it difficult to identify specific

clinically robust biomarkers of disease (*Ecker and Murphy, 2014*). Furthermore, studies on patient cohorts do not answer the question of whether these differences were present before the onset of the disease (conferring risk to fall ill) or manifested over the course of illness (as a consequence of the illness).

Several clinical and preclinical studies have pointed to a complex interaction between genetic and environmental factors underlying pathogenesis in neurodevelopmental disorders (*Homberg et al., 2016*). Environment is known to play a key role in triggering abnormal brain development, given that the developing brain is highly plastic and sensitive to environmental changes (*Sale et al., 2014*). However, the high heritability estimates for these disorders suggest that much of the risk is inherited (*Gottesman, 1991; Abrahams and Geschwind, 2008; Rees et al., 2015*). For example, in schizophrenia, the heritability of the disorder is estimated to be between 60 to 80% (*Sullivan et al., 2012*). Advances in genetic technology and sequencing tools in the past few years have vastly expanded our knowledge of the genetics of neurodevelopmental disorders (*Hu et al., 2014*). It is known that the majority of neurodevelopmental disorders do not follow a strict Mendelian disease model where one gene is solely responsible for a given trait. Instead, current genetic models have established a polygenic nature for these disorders (*Hu et al., 2014*), identifying rare, common, and *de novo* risk alleles dispersed across a large number of genes. Interestingly, it has also become apparent that disorders like ASD, intellectual disability, schizophrenia and ADHD share risk alleles suggesting a common genetic aetiology across disorders (*Niemi et al., 2018*). Recent studies have further discovered that inheritance of one neurodevelopmental disorder also confers an increased risk for other disorders within the same family (*Kendler, 2010; Cheng et al., 2018*). For example, monozygotic twins were found to have a higher chance to develop ADHD or intellectual disability, if their co-twin had ASD (*Kendler, 2010*). Similarly, relatives of schizophrenia patients were found to be more likely to develop bipolar disorder, depression, and ASD, compared to the general population (*Cheng et al., 2018*).

The polygenic nature of these disorders, together with different interactions with environmental factors, likely underlie the phenotypic heterogeneity observed in behaviour and imaging studies (*Bruining et al., 2010*). Therefore, studies of genetically defined cohorts are needed in order to more precisely capture the biological aspects of subgroups within these neurodevelopmental disorders, which could allow more objective diagnoses, as well as more targeted interventions (**Figure 1.1**).

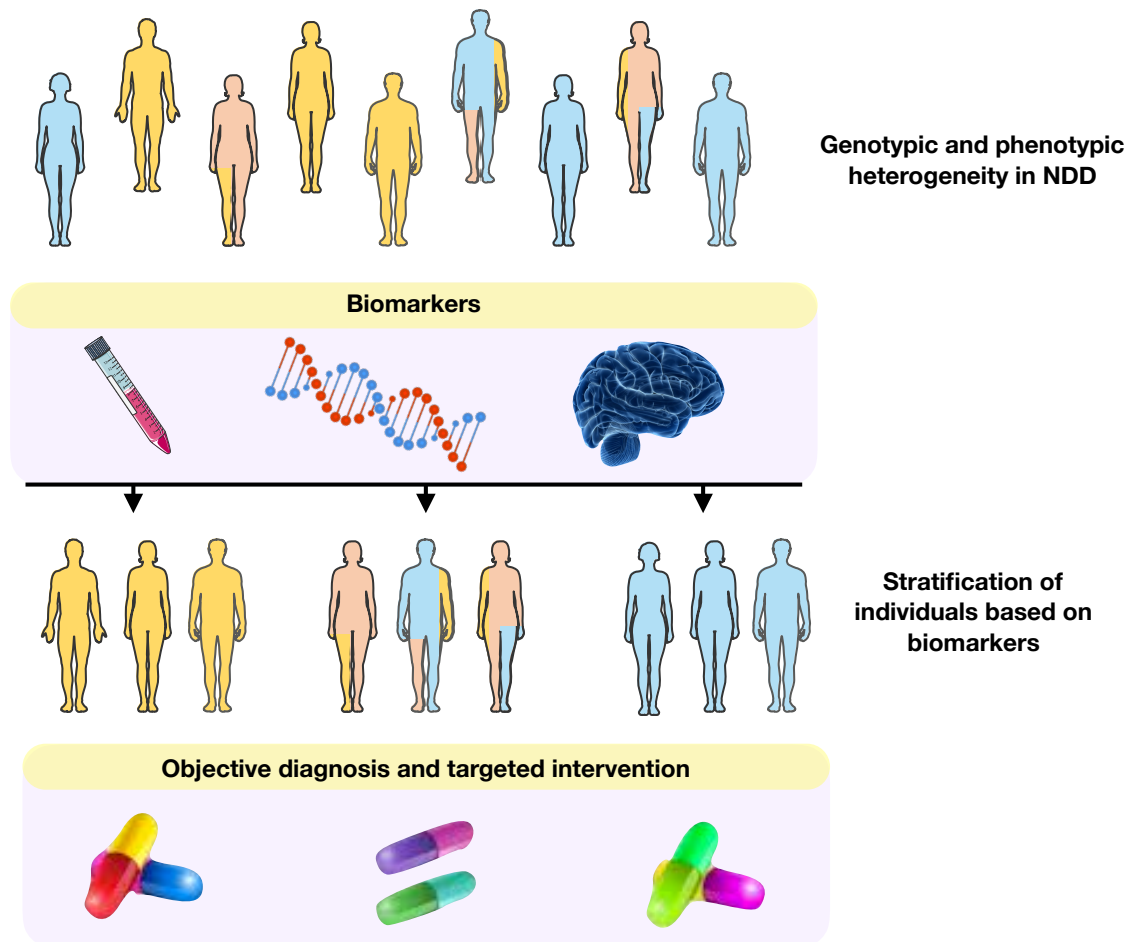


Figure 1.1 - Development of biomarkers in order to achieve a personalised diagnosis and treatment of neurodevelopmental disorders (NDD).

Clinical diagnoses based on general behaviour do not account for biological heterogeneity. The development of reliable biomarkers is crucial for early detection and phenotypic stratification of individuals leading to treatments and interventions designed to the patient's specific phenotype. Figure adapted from *Ecker and Murphy, 2014*.

1.2. Copy number variants and neurodevelopmental disorders

Identifying which genes and variants increase the risk for neurodevelopmental disorders and which mechanisms underlie their effect on brain function, is crucial for understanding the pathophysiology of these conditions. In this sense, large scale genotyping of the human and other mammalian genomes has provided powerful tools for understanding the functional/pathogenic implications of human genetic variation. Here, genetic variation is present in many forms. Single-nucleotide polymorphisms (SNPs) are individual base

changes and are the most common variants in the genome (*Ismail and Essawi, 2012*). Additionally, rare variations were also found in many locations throughout the genome (*Iafrate et al., 2004; Sebat et al., 2004*) and contribute to a substantial proportion of the genetic variability in humans. One type of rare variation is known as copy number variance. Copy number variants (CNVs) refer to microscopic deletions and duplications within the genome, involving more than 1000 base pairs in length but typically less than 5 megabases (*Feuk et al., 2006; Redon et al., 2006; Zhang et al., 2009; Alkan et al., 2011*), and may span many different genes.

Two genetic models have been proposed to explain the high complexity behind neurodevelopmental disorder phenotypes: the common variant common disease (CVCD) and the rare variant common disease (RVCD) models (*Malhotra and Sebat, 2012*). The CVCD model states that the genetic risk results from a combination of high frequency variants, which individually have a modest effect on risk (*Niemi et al., 2018*). For example, it is estimated that over 8000 SNPs contribute to schizophrenia, and together they are estimated to contribute to between 30% to 50% of the genetic predisposition (*Ripke et al., 2013*). However, individual SNPs typically have an odds ratio of around 1.10 each for schizophrenia risk (*Ripke et al., 2013*). In contrast, the RVCD model suggests that genetic risk is attributable to rare variants in the form of CNVs, single nucleotide variants (SNV, defined as point mutations with a frequency less than 1%), and small insertion/deletion (indel) mutations, which individually confer a considerably greater risk (*Malhotra and Sebat, 2012*). Although both models have important contributions, large rare CNVs show the strongest and most consistent associations with disease (*Kirov et al., 2014*). It is important to note that, although these variants have a higher penetrance than the combined effect of common variants, they only contribute to a minority (<10%) of cases of the common neurodevelopmental disorders (*Need et al., 2009; Purcell et al., 2014; Rees et al., 2014*). A question that has been raised is whether CNVs lead to the same phenotypes as common variants, or manifest in distinct forms, where they could be designated as specific syndromes (*Owen et al., 2010*). This has been argued for schizophrenia, however, against this idea studies have shown that CNV carriers who developed schizophrenia displayed symptoms that closely resemble those with no pathogenic CNVs (*Bassett et al., 2003*). Schizophrenia is found in carriers in the absence of any other disorder, suggesting that psychoses does not occur as a manifestation of another primary disorder (e.g. intellectual disability or epilepsy) (*Owen et al., 2010*). These findings suggest that both common and rare risk variants contribute towards

disease susceptibility for neurodevelopmental disorders. For the purposes of this thesis, which dealt with brain changes related to the 15q11.2 BP1-BP2 CNV, in this section I will focus on findings related to rare CNVs and associated risk of neurodevelopmental disorders.

The association of CNVs with neurodevelopmental disorders was only possible with advanced chromosomal microarray (CMA) technology, allowing extensive CNV analyses in very large case-control cohorts (*Morrow, 2010*). Several CNVs have been associated to neurodevelopmental disorders in genome-wide association studies (GWAS), including intellectual disability, ASD, epilepsy and schizophrenia (*Kirov, 2015*). To date, 11 CNVs have been consistently associated with risk of schizophrenia: these are deletions at 1q21.1, NRXN1, 3q29, 15q11.2, 15q13.3 and 22q11.2, and duplications at 1q21.1, 7q11.23, 15q11.2-q13.1, 16p13.1 and proximal 16p11.2 (*Rees et al., 2014, 2016*). Many of these CNVs were also shown to increase risk for intellectual disability, schizophrenia, ASD, ADHD, mood and anxiety disorders (*Guilmatre et al., 2009; Shinawi et al., 2010; Zufferey et al., 2012; Doherty and Owen, 2014; Rees et al., 2014; Hanson et al., 2015*). For example, ASD has been associated with both deletions and duplications at 16q11.2 and 1q21.1, as well as 22q11.2 deletion (*Doherty and Owen, 2014*). Several studies have estimated the risk of developing any one of these disorders when carrying each CNV by calculating its penetrance score (probability of developing the disease for individuals carrying the CNV). Although a number of CNVs have been associated with schizophrenia, these studies revealed overall modest penetrance values (from 2 to 7.4% in most CNVs) for the disorder, suggesting that these CNVs are neither sufficient nor necessary for the development of schizophrenia (*Kirov et al., 2014; Vassos et al., 2010*). However, the pathogenicity of these CNVs becomes apparent when considering the penetrance to other developmental disorders, like developmental delay and ASD, ranging from 10.6% for the 16p13.11 duplication to almost 100% for the 22q11.2 deletion in *Kirov et al., 2014*. Furthermore, given the incomplete penetrance of these CNVs, many carriers do not develop any clinical condition during their lifespan and are apparently healthy. However, these healthy carriers might still have an increased burden of cognitive or physical impairments (*Kendall et al., 2016*) and are extremely useful in studying the impact of these variants on brain- and cognitive phenotypes, without confounds such as secondary disease effects or medication.

1.2.1. Neuroimaging studies in CNVs

As stated in the beginning of this Introduction, neuroimaging studies on patient cohorts have shown that neurodevelopmental disorders lead to structural and functional changes in the brain, but fail to show if these changes are inherited and present before the onset of the disease, or manifested over the course of illness. Neuroimaging studies in relatives of these patients, who had not fallen ill, revealed extensive structural and functional brain changes, suggesting a degree of heritability of these phenotypes (*Scamvougeras et al., 2003; White et al., 2002; Belmonte et al., 2010; Thermenos et al., 2013*). Therefore, a key question for neurobiological research is whether genetic risk factors lead to disruptive neurobiological mechanisms that underlie the imaging phenotypes seen in neurodevelopmental disorders. Understanding these mechanisms is important for establishing biomarkers and may allow targeted design of new therapies. Here, as noted above, genetic neuroimaging studies in ‘clinically healthy’ CNV carriers can start answering this question by studying brain phenotypes on genetically defined populations that are not confounded by secondary disease effects.

The mechanisms through which CNVs affect brain and behaviour are poorly understood, where the rare occurrence of these CNVs and consequent difficulties in identifying sufficient subjects for study can pose practical problems in investigating their biological effects in humans. Neuroimaging studies in CNV cohorts have followed different approaches; some studies have looked at the impact of individual CNVs in the brain, whereas other studies have looked at a converging effect, combining data on different CNVs. Studies of individual CNVs are important for investigating the effect of targeted genes. These studies, mostly on small cohorts, have indeed shown that CNVs lead to brain abnormalities. For some CNVs, these changes were dependent on CNV dosage, and reciprocal effects were found in deletion and duplication carriers of the same CNV (*Chang et al., 2016*). However, as pointed out by *Drakesmith et al., 2019*, brain changes are highly heterogeneous across different CNVs where studies have shown increases (*Hoefl et al., 2007; Chang et al., 2016; Olszewski et al., 2017; Nuninga et al., 2018*) and decreases (*Eliez et al., 2000; Kates et al., 2001; Bearden et al., 2007*) in brain metrics, which is consistent with the notorious phenotypic heterogeneity seen in neurodevelopmental disorders. In an effort to detect convergent pathways common to different genetic variants, *Drakesmith et al., 2019* investigated morphological and microstructural alterations in the brain across CNVs and correlated these measures with

their penetrance to schizophrenia and developmental delay. Here, the authors found effects of penetrance for both disorders on medial white matter structures, more specifically a positive correlation with the curvature of the cingulum bundle and in the volumetric interrelationships between different segments of the corpus callosum. Furthermore, a recent study by *Warland et al., 2019* investigated combined data on subcortical brain volumes across schizophrenia-related CNVs, and compared these data to those of individuals who did not carry any pathogenic variant. The authors found a volume reduction in some subcortical structures in CNV carriers, these reductions were previously shown to be associated with schizophrenia.

The work developed in this thesis aims to understand the consequences of CNVs at the 15q11.2 BP1-BP2 region on brain structure and further elucidate possible cellular and molecular mechanisms underlying the pathogenicity of this CNV. For this work, two previous neuroimaging studies by *Stefansson et al., 2013* and *Ulfarsson et al., 2017* are of high relevance. The authors in both studies reported brain structural and functional abnormalities, using magnetic resonance imaging (MRI) data, in both deletion and duplication carriers whom did not have a clinical and/or self-reported diagnosis. In *Stefansson et al., 2013*, deletion carriers showed reduced grey matter volume in the perigenual anterior cingulate cortex (pACC) and in the left insula, as well as bilateral reductions in white matter volume in the temporal lobe and increases in the corpus callosum volume. Changes in the pACC and temporal lobe have also been reported in schizophrenia (*Baiano et al., 2007; Bora et al., 2011*). Interestingly, duplication resulted in reciprocal changes in the same regions showing alterations in the deletion carriers, presenting the first demonstration of dosage-dependent effects of CNVs on human brain structure. *Ulfarsson et al., 2017* replicated these results and further showed functional changes in the fusiform and angular gyri accompanied by a smaller fusiform gyrus in deletion carriers.

1.2.2. Understanding the role of CNVs

The ability to identify risk genes was a significant step in improving our understanding of human diseases. Following this, it was crucial to reveal the mechanisms by which these genetic variants influence risk for disorder. Although neuroimaging studies in CNV carriers have greatly contributed to finding convergent, as well as distinct,

impacts of these genetic variants on brain structure and function, these techniques do not provide enough resolution to further elucidate the cellular and molecular consequences underlying these effects. Currently, this may only be achieved using histological procedures that allow a careful examination of brain tissue. Histological studies in humans can only be performed using post-mortem tissue, thus relying on the availability of the tissue, making it difficult to control several variables like age, gender and conditions prior to death (*Monoranu et al., 2009*). In this regard, the fast progress in genome editing techniques, such as CRISPR, have led to the creation of invaluable animal and cellular models of human diseases that allow the study of molecular and cellular underpinnings of pathology (*McCarthy et al., 2014; Powell et al., 2017*). These models also allow the targeting of specific genes within a chromosomal region of interest, allowing the study of the role and effects of individual genes, which could explain the phenotypes associated with a particular CNV. Furthermore, advances in animal imaging protocols have allowed translational validity of these models by comparing human and animal imaging studies, increasing our confidence on the cellular findings in animals, as well as on translation of therapeutics to humans (**Figure 1.2**).

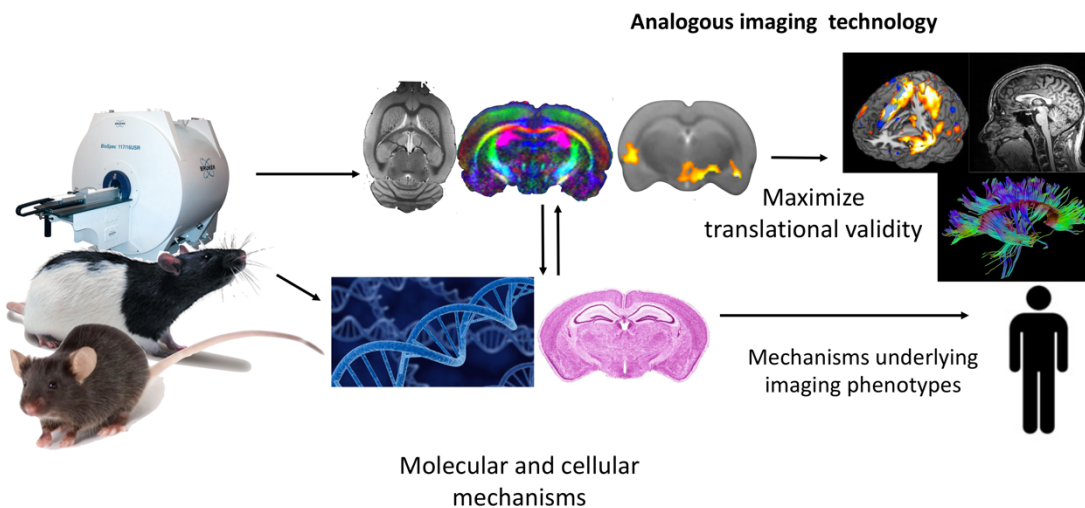


Figure 1.2 - Translational framework combining multi-modal imaging in animal models and humans. Similar imaging phenotypes increase our confidence on molecular and cellular findings in the rodent model, and may elucidate the mechanisms underlying the imaging phenotype in humans.

Given the high penetrance of CNVs for neuropsychiatric disorders, several animal models of these CNVs, as well as single genes within them, have been created. Some of these models were created for the following CNVs: 22q11.2 (*Mukai et al., 2008; S. R. Nilsson et al., 2016; Sigurdsson et al., 2010; Tamura et al., 2016; Van et al., 2017*), 7q11.23 (*Li et al., 2009*), 15q11-13 (*Nakatani et al., 2009*), 16p11.2 (*Horev et al., 2011*), 15q13.3 (*Fejgin et al., 2014; Forsingdal et al., 2016; S. R. O. Nilsson et al., 2016; Thelin et al., 2017*), 1q21.1 (*Nielsen et al., 2017*), and 15q11.2 BP1-BP2 (*Bozdagi et al., 2012; De Rubeis et al., 2013; Pathania et al., 2014; Hsiao et al., 2016*).

The work developed in this thesis is focused on the impact of 15q11.2 BP1-BP2 CNV on white matter microstructure. These findings are described in Chapter 3 and 4, and focus on the question of which gene, or genes, in this region could contribute to white matter abnormalities. To answer this question, it is important to understand the role of the different genes in this region and how they may individually, or collectively influence white matter microstructure. Here, different model organisms have been used to identify the roles of the genes within the 15q11.2 BP1-BP2 region. In the following section, I will elaborate on the clinical and cognitive findings related to this region, and further elaborate on findings related to individual genes within this region.

1.3. The 15q11.2 BP1-BP2 copy number variant

The chromosome 15q11-13 region contains 5 breakpoints (BP) that have been classified as CNVs (*Pujana et al., 2002; Locke et al., 2004*). The 15q11.2 BP1-BP2 (Burnside-Butler susceptibility locus) deletion has been gaining particular interest in Prader-Willi Syndrome (PWS) and Angelman syndrome studies, where deletions occur between the BP3 and BP1 or BP2. These have been classified as Type I when the deletion involves genes between the BP1 and BP3, or Type II when genes between BP2 and BP3 are deleted (**Figure 1.3**). Cognitive studies in PWS have suggested that Type I deletions often report more severe phenotypes, in particular learning and behavioural deficits, than Type II deletions (*Butler et al., 2004; Hartley et al., 2005; Varela et al., 2005; Sahoo et al., 2007*). This suggests a contributing role of the BP1-BP2 region to the severity of PWS-associated cognitive phenotypes.

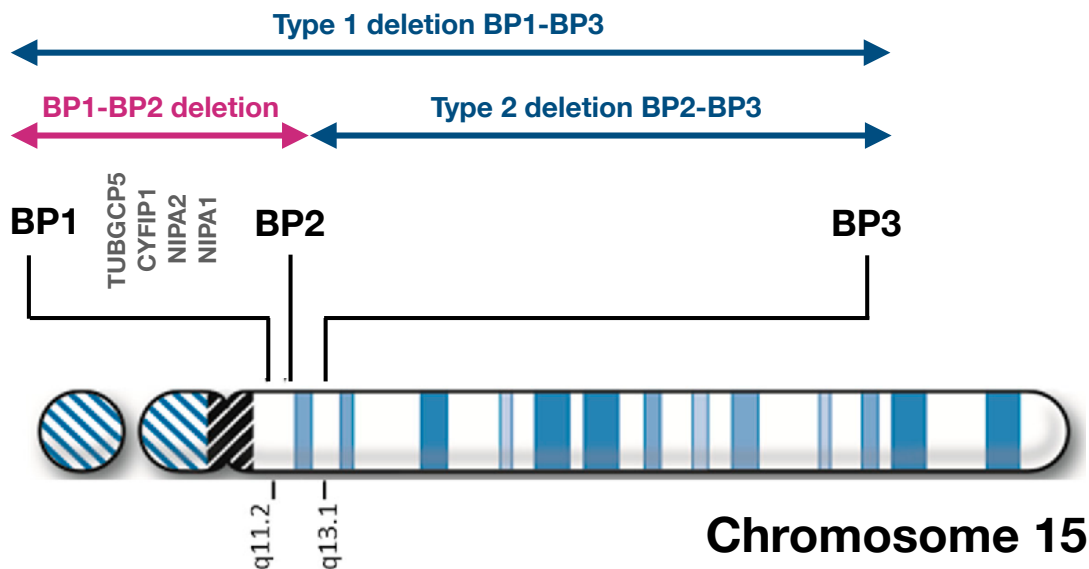


Figure 1.3 - Ideogram representing the chromosome 15.

The location of BP1 and BP2 (at the 15q11.2 band) and BP3 (at 15q13.1 band) are illustrated in the figure. Prader Willi Syndrome Type I deletion involving genes in the BP1-BP3 interval, and Type II deletions involving genes in the BP2-BP3 interval, are represented in this figure, as well as the BP1-BP2 region. Figure adapted from *Cox and Butler, 2015*.

The isolated BP1-BP2 region was first studied in *Murthy et al., 2007* in two individuals and further reported in nine individuals in *Doornbos et al., 2009*, where most of these individuals manifested behavioural and neurological abnormalities. A later study by *Burnside et al., 2011*, using a large cohort of patients, found that 0.86% of approximately 17 000 individuals had a deletion or duplication of the 15q11.2 BP1-BP2 region. Other reports have found 0.23% deletion carriers in 6 329 individuals, and 0.37% duplication carriers in 4 363 individuals (*Pinto et al., 2007; Jakobsson et al., 2008; Itsara et al., 2009*). In *Burnside et al., 2011*, having identified 69 deletion and 77 duplication carriers showing a range of symptoms consisting of language and motor delays, behavioural problems, ASD, seizures and occasionally mild dysmorphic features, the authors proposed that this was a susceptibility locus for neurological dysfunction. Similarly, a study by *Cafferkey et al., 2014* on a cohort of 14 605 patients (primarily paediatric) found 83 15q11.2 BP1-BP2 deletion carriers (0.57%), the majority presenting some form of behavioural disturbance or developmental/motor delays. Finally, a literature review of clinical features by *Cox and Butler, 2015*, from 200 individuals with the 15q11.2 BP1-BP2 deletion, has grouped these phenotypes into five categories: (1)

developmental (73% of cases) and speech (67%) delays; (2) dysmorphic ears (46%) and palatal anomalies (46%); (3) writing (60%) and reading (57%) difficulties, memory problems (60%) and verbal intelligence quotient (IQ) scores ≤ 75 (50%); (4) general behavioural problems (55%); and (5) abnormal brain imaging (43%). The deletion was also found to increase susceptibility to schizophrenia (*Stefansson et al., 2008; Kirov et al., 2009; Rees et al., 2014*) and epilepsy (*Valente et al., 2013*). Although all these findings point to an increased risk for neurodevelopmental disorders, the estimated penetrance is approximately 2% for schizophrenia and 10.4% for developmental delay/ASD (*Kirov et al., 2014*), which is considerably lower than other CNV deletions (**Figure 1.4A**). However, the frequency of this CNV is higher than other pathogenic CNVs (**Figure 1.4B**), and a recent study using ultra-high resolution CMA reported the 15q11.2 BP1-BP2 deletions as the most frequent finding in those with only ASD or those with ASD combined with intellectual disability and congenital anomalies (*Ho et al., 2016*).

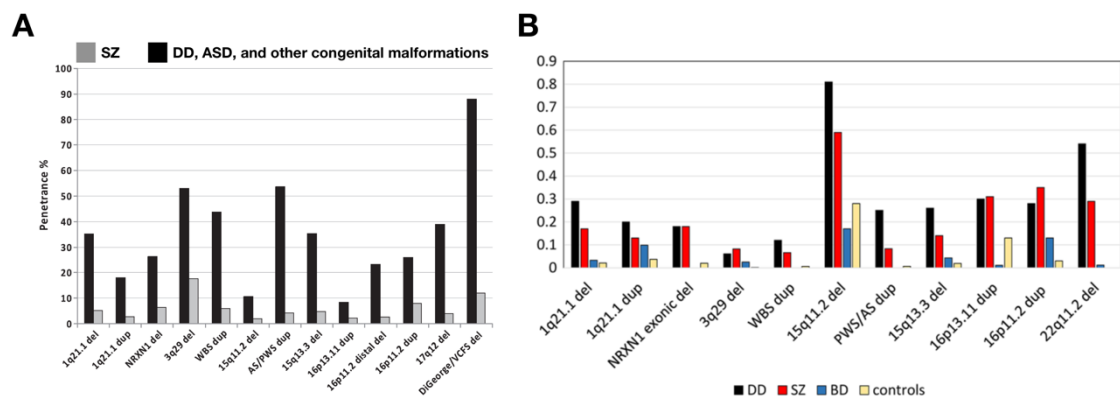


Figure 1.4 - Penetrance and frequency of different CNVs in controls and different neurodevelopmental disorders.

A Penetrance of schizophrenia-related CNVs for schizophrenia (represented in grey) and the combined group of development delay (DD), ASD, and various congenital malformations (CM) (represented in black). **B** Frequencies of CNVs in control groups (represented in yellow), individuals with DD/ASD/CM (represented in black), schizophrenia (represented in red) and bipolar disorder (represented in blue). The frequencies of the CNVs are represented in the y-axis. Figure 1.4A was taken from *Kirov et al., 2014*, and Figure 1.4B was taken from *Kirov, 2015*. PWS/AS, Prader-Willi /Angelman syndrome; del, deletion; dup, duplication; VCFS, velo-cardio-facial syndrome; WBS, Williams-Beuren syndrome.

The 15q11.2 BP1-BP2 duplication has been linked to a similar list of neurodevelopmental disorders, including intellectual disability, motor and speech delay, ASD, ADHD, ataxia, seizures and dysmorphic features, as summarised by a review of 52 subjects in *Burnside et al., 2011*. However, in a recent large-scale genetic study the duplication did not show a significant risk for developmental delay (*Coe et al., 2014*), and it is not considered a risk locus for schizophrenia (*Kirov et al., 2014*). Therefore, the pathogenicity of the duplication is still unclear, and more studies are needed in this matter.

As stated previously, carriers of CNVs who do not develop a clinical condition may still show cognitive and physical impairments. Both *Stefansson et al., 2013* and *Ulfarsson et al., 2017* showed dosage-dependent brain abnormalities in healthy carriers of the 15q11.2 CNV. When it comes to cognitive measures, in *Stefansson et al., 2013* the 15q11.2 BP1-BP2 deletion showed modest effects on neuropsychological tests but was strongly associated with difficulties in reading and mathematics, assessed by questionnaires designed to detect difficulties indicative of dyslexia and dyscalculia [adult reading history questionnaire (ARHQ) and adult mathematical history questionnaire (AMHQ)]. The structural and functional findings described in the previous section, also overlap with previous studies showing brain changes in dyslexia and dyscalculia, and may contribute to the cognitive phenotype in deletion carriers. Interestingly, although reciprocal effects in brain structure were found in association with both deletion and duplication, these opposite effects were not found for ARHQ and AMHQ scores, where the duplication carriers performed similar to controls with no pathogenic CNVs (*Stefansson et al., 2013*). Overall these results, together with the fact that the duplication seems to be less pathogenic on a clinical level than the deletion, suggest that the duplication may have a less damaging effect than the deletion.

Given the risk associated with the 15q11.2 BP1-BP2 deletion for neurodevelopmental disorders and cognitive impairment, it is important to identify which genes contribute to the observable phenotypes. The 15q11.2 BP1-BP2 region contains four genes (**Figure 1.3**): non-imprinted in Prader-Willi/Angelman syndrome 1 gene (*NIPAI*), non-imprinted in Prader-Willi/Angelman syndrome 2 gene (*NIPA2*), cytoplasmic *FMRI* interacting protein 1 (*CYFIP1*), and tubulin gamma complex associated protein 5 gene (*TUBGCP5*) (*Chai et al., 2003*). Supportive of the hypothetical role of BP1-BP2 region in the severity of PWS associated symptoms is a study by *Bittel et al., 2006*, where the authors found the amount of messenger RNA (mRNA) within the

BP1-BP2 region to explain between 24% to 99% of the phenotypic variability in behavioural and academic measures.

The four genes mentioned above are expressed in the central nervous system, and some work has been done to understand their individual roles. For example, *NIPAI* is known to mediate Mg^{2+} transport (*Rainier et al., 2003*), and has been associated with autosomal dominant hereditary spastic paraplegia and postural disturbances, which could result from impaired magnesium transfer (*Goytain et al., 2007*). Furthermore, *NIPAI* was also found to inhibit bone morphogenic protein (BMP) signalling via interaction with BMP receptor type II (*Tsang et al., 2009*). In a *Drosophila* model, *Wang et al., 2007* showed a role for BMP signalling in axonal microtubule maintenance and axonal transport, and further showed that this function is inhibited when the *Drosophila melanogaster NIPAI* ortholog *spichthyin* is mutated. The *NIPA2* gene encodes for proteins used in renal Mg^{2+} transport and metabolism, and mutations in this gene have been associated with childhood absence epilepsy (*Xie et al., 2014*). The *TUBGCP5* gene encodes a member of the gamma-tubulin small complex involved in microtubule nucleation and dynamics (*Murphy et al., 2001; Raynaud-Messina and Merdes, 2007*). This gene is highly expressed in the subthalamic nuclei, a region linked to obsessive-compulsive disorder and ADHD (*Grabli et al., 2004*). More is known about the *CYFIP1* gene. This gene is involved in two independent roles associated with actin remodelling and regulating mRNA translation through interactions with fragile X mental retardation protein (FMRP) (*De Rubeis et al., 2013*). Both functions are crucial for synapse development, axon targeting, and cytoskeleton organisation, processes that ultimately shape our brain and were found to be dysregulated in neurodevelopmental disorders (*Lee and Dominguez, 2010; Yan et al., 2016; Amorim et al., 2018*).

Each of these four genes have the potential to influence brain development and function. However, it is unknown to what extent they are associated with the increased risk for psychiatric disorders in 15q11.2 BP1-BP2 CNV carriers (*Cox and Butler, 2015*). Substantial rodent and human models have considered *CYFIP1* as a prominent candidate gene contributing to the 15q11.2 BP1-BP2 brain and psychological phenotypes (*Bozdagi et al., 2012; De Rubeis et al., 2013; Yoon et al., 2014; Pathania et al., 2014; Oguro-Ando et al., 2015; Nebel et al., 2016*). Moreover, a study looking at the relationship between SNPs across the 15q11.2 BP1-BP2 region and brain structures found an association between rs4778298, a common variant at *CYFIP1*, and variations in the surface area across the left supramarginal gyrus (*Woo et al., 2016*). This cortical structure is implicated

in speech and language, and could contribute to the language impairment seen in 15q11.2 BP1-BP2 deletion carriers. Most of the work was done in animal models and showed that dysregulations in *Cyfp1* gene have an effect on structure and function of synapses. In the following sections, I will elaborate on these findings elucidating the role of *CYFIP1* in the brain, and how dysregulations in this gene may affect synaptic morphology and physiology.

1.4. Molecular functions of the *CYFIP1* gene

As stated earlier in this Introduction, the creation of animal and cellular models allows the targeting of single genes in order to understand their individual roles. The first study modelling a reduction of *CYFIP1* was performed by *Schenck et al., 2003*, using a *Drosophila melanogaster* model with a *dCyfp* mutation. Using this model, *Schenck et al., 2003* were the first to identify the dual role of *CYFIP1*. Following this, *Bozdagi et al., 2012* created a *Cyfp1*-haploinsufficient mouse to model the low dosage of *CYFIP1* in 15q11.2 BP1-BP2 CNV deletion carriers. Here, complete knockout of *Cyfp1* was attempted but found to be embryonically lethal in the mouse (*Bozdagi et al., 2012; Pathania et al., 2014*) and fly (*Schenck et al., 2003; Zhao et al., 2013*).

1.4.1. *CYFIP1* role in actin cytoskeleton remodelling

CYFIP1 has a prominent role in cytoskeleton remodelling. The cytoskeleton of a cell is made of microtubules and actin filaments. Microtubules are the largest filament type, and are composed of a protein called tubulin. Actin filaments are essential for the formation and function of lamellipodia, also known as membrane ruffles at the cell periphery. These ruffles form processes that are called microspikes when the actin filaments do not project beyond the cell edge and filopodia when they do (*Small et al., 2002*). Lamellipodia are essential for cell motility, organisation of membrane domains, phagocytosis and the development of substrate adhesions (*Small et al., 2002*).

Actin is the most abundant intracellular protein in a eukaryotic cell, and can exist in two forms: as globular monomers (g-actin) or can form linear chains of these monomers in filamentous polymers (f-actin or actin filaments). In order to form actin

filaments, essential for lamellipodia formation, polymerisation of g-actin into f-actin must occur. Likewise, other processes require the rapid disassembly of f-actin into g-actin. This ability of g-actin to polymerise into f-actin and of f-actin to depolymerise into g-actin is an important property of actin, making the actin cytoskeleton extremely dynamic.

The actin cytoskeleton is involved in a variety of biological functions, and understanding the mechanisms underlying actin dynamics is critical in cell biology with important implications for health and disease. In earlier studies, three members of the Rho small guanosine triphosphatase (GTPase) family were found to be key regulators of actin dynamics, and play an important role in the organisation of the actin cytoskeleton (*Hall, 1998*). These were identified as Rho, Rac1, and Cdc42. Studies in 3T3 fibroblasts first showed that Rho activation lead to the assembly of contractile actin-myosin filaments (stress fibres) and associated focal adhesion complexes (*Ridley and Hall, 1992*). Rac1 was then analysed and found to drive actin polymerisation at the cell periphery to produce lamellipodia in mouse-derived Swiss 3T3- and human-derived KB cells (*Ridley et al., 1992; Nishiyama et al., 1994*). Later, activation of Cdc42 was found to also contribute to actin assembly and induce the formation of filopodia (*Kozma et al., 1995*). Although the effects of Rho GTPases on actin cytoskeletal dynamics were initially characterised in fibroblasts, later studies looked extensively at these effects in neuronal cells. Here, it was shown that axonal growth was driven by actin polymerisation within the growth cone – a highly dynamic structure at the end of the axon (**Figure 1.5**), consisting of lamellipodial and filopodial protrusions (*Hall, 1998; Dent and Gertler, 2003; Omotade et al., 2017*).

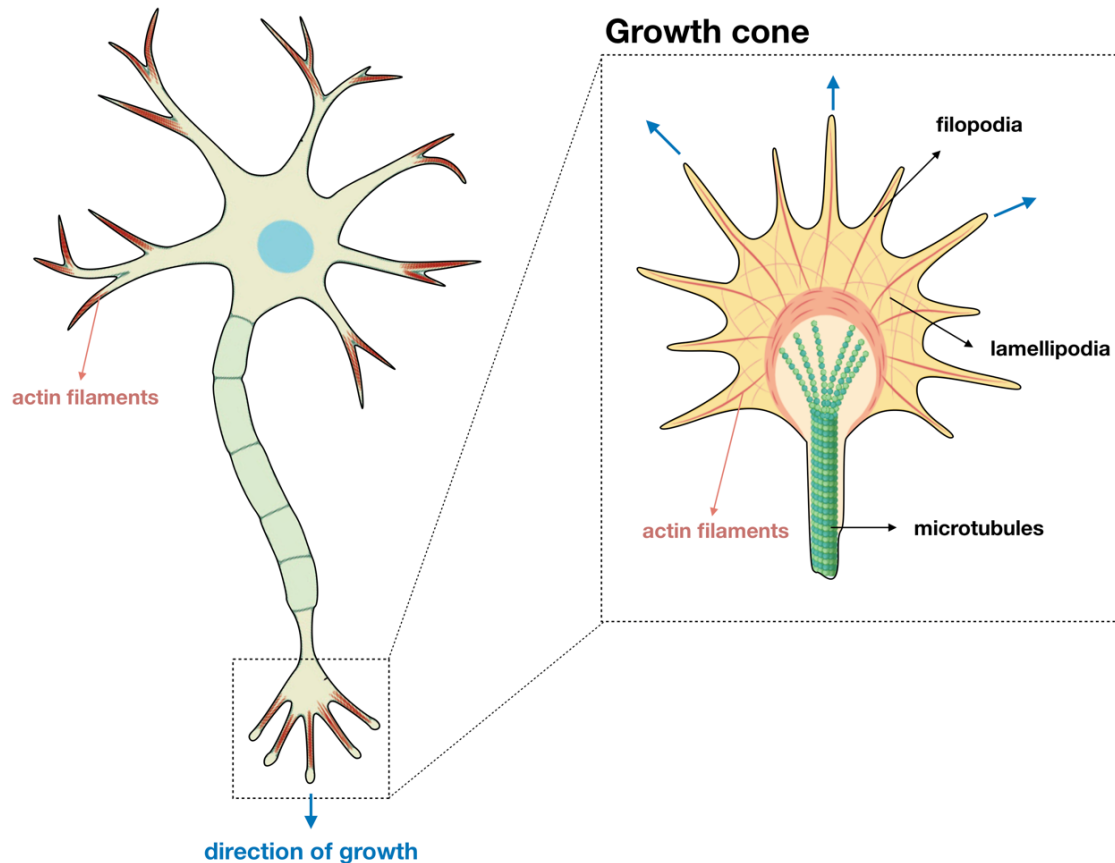


Figure 1.5 - Schematic representation of a neuron, and detailed view of the growth cone and main cytoskeletal components (filopodia, lamellipodia, microtubules and actin filaments).

It was suggested that the coordinated actions of Rho GTPases were possible through interactions with multiple target proteins (Hall, 1998). To better understand cellular cytoskeletal dynamics and lamellipodia formation, several studies were conducted to identify the protein targets of the small GTPase Rac1, leading to the discovery of a link between Rac1 and CYFIP1 protein. Using affinity purification methods in the bovine brain cytosol, CYFIP1 was found to be specifically co-purified with the active GTP-bound form of Rac1, but not with Rac1 in its inactive guanosine diphosphate (GDP)-bound state (Kobayashi et al., 1998). This interaction, established by the N-terminus of the CYFIP1 protein, was of particular interest since activation of Rac1 is essential for inducing actin polymerisation. CYFIP1 was first characterised as Rac1-associated protein 1 (Sra-1) in Kobayashi et al., 1998, since no interaction with the other Rho family members Cdc42 or Rho was found. This study provided the first functional

characterisation of CYFIP1, and showed that CYFIP1 co-sedimented with filamentous actin in KB cells, further suggesting a crucial role for a Rac1-CYFIP1 interaction in actin polymerisation and lamellipodia formation. The molecular pathway linking CYFIP1 to actin polymerisation through Rac1 activation was yet to be determined.

It was first shown that Cdc42 regulated actin assembly by activating the actin-related protein 2/3 (Arp2/3) through binding with N-WASP, a member of the Wiskott-Aldrich syndrome protein (WASP) family. After binding with Cdc42, N-WASP becomes active and binds to Arp2/3, generating filopodia (*Ma et al., 1998; Miki et al., 1998*). The Arp2/3 was also found to interact with the Wiskott-Aldrich syndrome protein family verprolin homologous protein (WAVE) regulatory complex (WRC) to initiate actin assembly. CYFIP1 is a member of this complex, which is an assembly of the proteins WAVE1/2/3, CYFIP1/2, Nck-associated protein 1 (NCKAP1), ABI interactor 1/2 (ABI1/2) and haematopoietic stem cell protein 300 (HSPC300) (*Dai and Pendergast, 1995; Shi et al., 1995; Eden et al., 2002; Kunda et al., 2003; Schenck et al., 2003; Chen et al., 2010*). Both the WASP and WAVE family proteins share a common domain architecture: a proline-rich stretch followed by a verprolin-homology central acidic (VCA) region located at the carboxyl terminus (*Kurisu and Takenawa, 2009*). The VCA simultaneously binds to an actin monomer (g-actin) and to Arp2/3 through the V and CA domain, respectively, to trigger actin polymerisation. In the WRC, the CYFIP1 protein binds to the VCA region, making it impossible to bind to Arp2/3, and therefore inhibiting WAVE activity (*Chen et al., 2010*). Rac1 was shown to activate WRC and trigger actin polymerisation, similar to how Cdc42 activates N-WASP protein. However, contrary to what was seen in Cdc42 and N-WASP interactions, Rac1 does not directly bind to the WAVE protein (*Pollard and Borisy, 2003; Chen et al., 2010*). Instead, Rac1 binds to CYFIP1, triggering a conformational change in the protein (*De Rubeis et al., 2013*) that releases the subcomplex of CYFIP1/2, NCKAP1 and ABI1/2 from the WRC (*Cory and Ridley, 2002; Eden et al., 2002; Derivery et al., 2009*). As a result, the VCA region of the WAVE protein becomes activated and able to bind to g-actin monomers and Arp2/3. This mechanism, summarised in **Figure 1.6**, supports the CYFIP1-Rac1 interactions in actin polymerisation, previously reported in *Kobayashi et al., 1998*.

Supportive of an inhibitory role of CYFIP1 in actin polymerisation is the fact that *Cyfp1* haploinsufficiency was shown to increase levels of f-actin in rodent and *Drosophila* models (*Schenck et al., 2003; Zhao et al., 2013; Pathania et al., 2014; Hsiao et al., 2016*). However, it is important to mention that some conflicting evidence has been

reported regarding the direction of change in f-actin levels. Although most studies have reported increased f-actin levels upon reduction of *Cyfp1* levels, *De Rubeis et al., 2013* found decreased f-actin levels in cortical neurons from 15-day-old *Cyfp1* heterozygous mice. Furthermore, other studies have proposed different versions of the WRC-actin assembly mechanism, suggesting that Rac1-binding triggers a conformational change in CYFIP1 that exposes the VCA domain without dissociation of CYFIP1 and other WRC members (*Ismail et al., 2009; Chen et al., 2010; Derivery and Gautreau, 2010*).

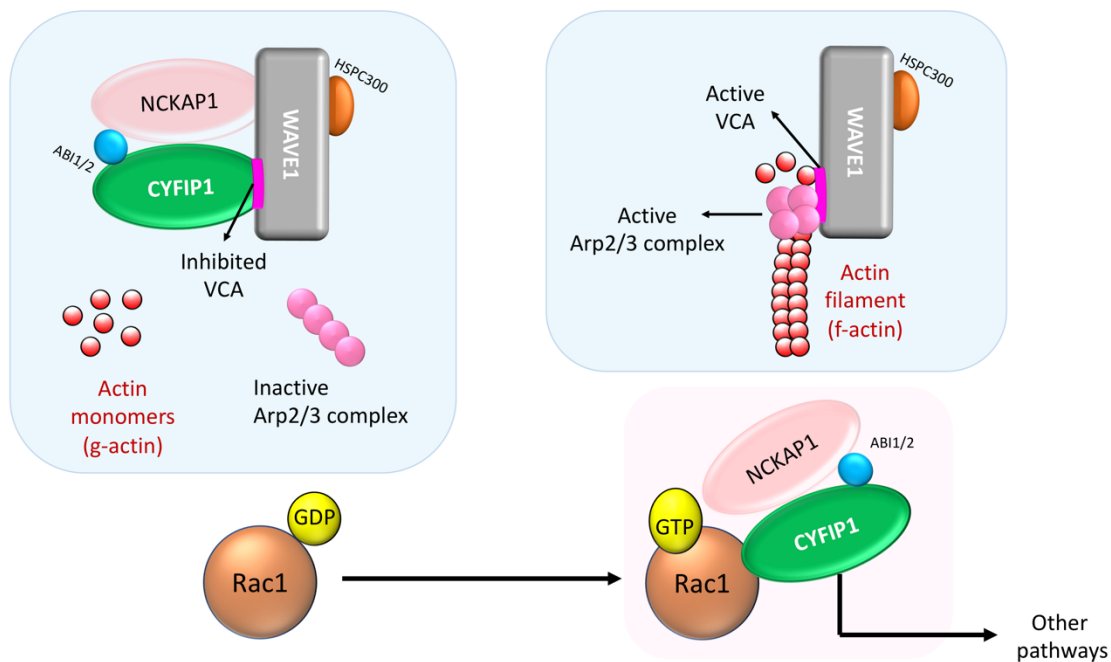


Figure 1.6 - Schematic illustration of CYFIP1 protein dynamics as an inhibitor of WAVE regulatory complex (WRC) and actin polymerisation.

When Rac1 is inactive (GDP-Rac1) CYFIP1 binds the VCA region of WAVE1 inhibiting this complex. Upon activation of Rac1, GTP-Rac1 binds to CYFIP1, inducing a conformational change that results in the release of the sub-complex CYFIP1/2, NCKAP1 and ABI1/2 sub-complex. Following this, the VCA region becomes free to interact with the Arp2/3 complex, which becomes active and starts polymerising actin (assembly of g-actin into f-actin). Scheme adapted from *Abekhoukh and Bardoni, 2014*.

1.4.2. CYFIP1 role in mRNA translation

CYFIP1 also plays an important role in regulating mRNA translation through interactions with FMRP. The control and fine regulation of protein translation is essential for both synaptic and axonal development in response to different developmental cues and other stimuli (*Martin et al., 2000; Steward and Schuman, 2003; Lin and Holt, 2008*). FMRP, encoded by the *FMR1* gene, is an RNA-binding protein that tightly regulates the localisation, stability, and translation of a large range of RNAs that are critical to neuronal development, synaptic plasticity and dendritic spine architecture (*Braat et al., 2015; Contractor et al., 2015; Richter et al., 2015; Banerjee et al., 2018*). Silencing of the *FMR1* gene results in fragile X syndrome (FXS), which is the most common form of inherited intellectual disability as well as the most frequent known cause of ASD (*Verkerk et al., 1991; Lozano et al., 2014*). In order to better understand the pathophysiology underlying FXS, a few studies have looked for interaction partners of FMRP. Here, *CYFIP1* was found to physically interact with the N-terminal part of FMRP (*Schenck et al., 2001*).

FMRP acts as a negative regulator of mRNA translation by binding to the L5 protein on the ribosomal 80S subunit, thus inhibiting the binding of transfer RNA (tRNA) and elongation factors to the ribosomal subunit (*Chen et al., 2014*). An additional mechanism of translation repression involves controlling the initiation of translation. In order for translation to begin the eukaryotic translation initiation factor (eIF4F) must bind to the modified guanosine molecule (termed cap) of the mRNA at the 5' end. This is established by the assembly of the eIF4A, eIF4G and eIF4E components of the eIF4F complex, a process often regulated by eIF4E-binding proteins (4E-BPs), which interfere with the eIF4E-eIF4G interaction (*Richter and Sonenberg, 2005*). Given that *CYFIP1* was identified as an FMRP interacting protein, different studies have looked at its involvement in translation control. Here, *CYFIP1* was found to also directly bind to eIF4E, acting as a 4E-BP protein and preventing eIF4E from binding to eIF4G (*Napoli et al., 2008; Di Marino et al., 2015*). The interactive domain of *CYFIP1* that binds to eIF4E forms a characteristic “reverse L shaped” structure that is also assumed by the canonical eIF4E-binding motif (*Marcotrigiano et al., 1999*). Therefore, this proposed mechanism suggests that FMRP can repress translation of target mRNAs through binding to *CYFIP1*. In a nutshell, FMRP recruits target mRNAs to *CYFIP1*, stabilising *CYFIP1* at the 5' end of the target mRNAs, which then binds eIF4E, preventing translation initiation (**Figure**

1.7) (Napoli *et al.*, 2008). Consistent with this mechanism, *Cyfp1* haploinsufficiency results in increased levels of newly synthesised FMRP-targeted mRNAs in a mouse model (Napoli *et al.*, 2008; Hsiao *et al.*, 2016).

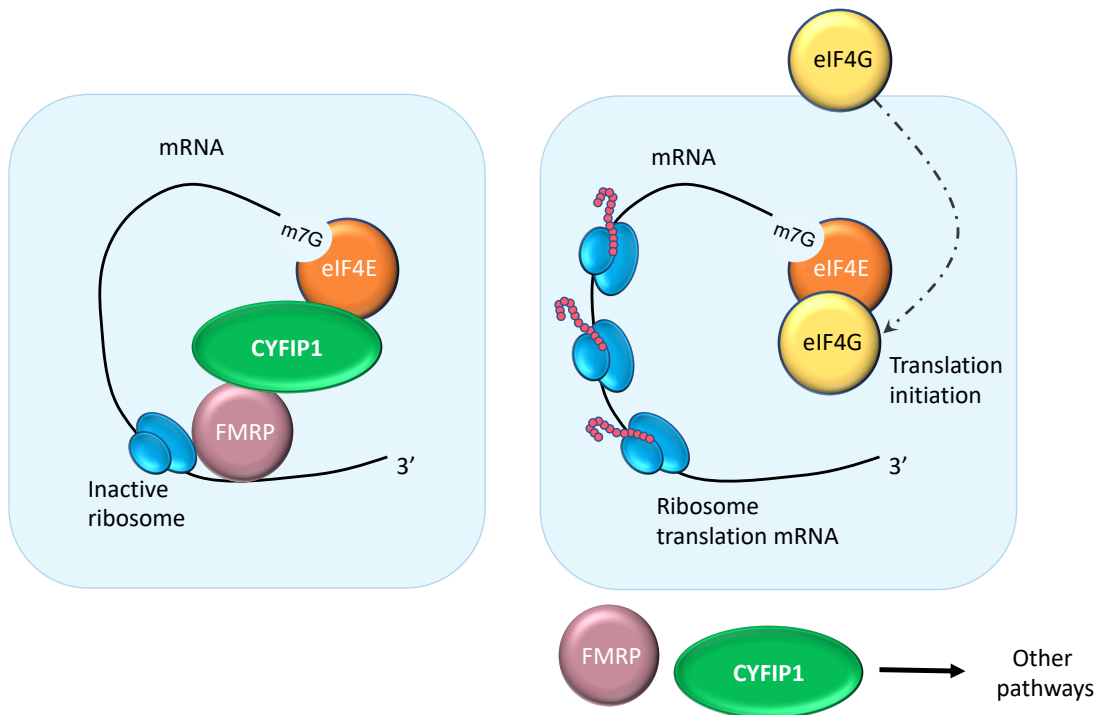


Figure 1.7 - Schematic illustration of CYFIP1-FMRP complex dynamics as an inhibitor of mRNA translation.

FMRP recruits target mRNAs to CYFIP1 stabilising CYFIP1 at the 5' end of the target mRNAs. CYFIP1 binds to eIF4E, preventing translation initiation. When CYFIP1 and FMRP are released from the complex, eIF4E is free to interact with eIF4G in order to assemble the eukaryotic translation initiation factor (eIF4F) and start translation. Scheme adapted from figure in *De Rubeis et al.*, 2013, and based on description from *Napoli et al.*, 2008.

It is widely accepted that CYFIP1 acts as a negative regulator in both actin polymerisation and mRNA translation. However, the structure of CYFIP1, when assembled in the WRC, does not allow CYFIP1 to simultaneously bind to eIF4E (Napoli *et al.*, 2008), and it was further shown that CYFIP1 can only interact with one of these pathways at a time (De Rubeis *et al.*, 2013). In *De Rubeis et al.*, 2013, the authors also found that CYFIP1 is exchanged between the FMRP-eIF4E complex and WRC, thereby linking protein translation to actin remodelling. Neuronal signalling can mediate the equilibrium of CYFIP1 between the two complexes. For example, translation is regulated by brain-derived neurotrophic factor (BDNF) or activation of group 1 metabotropic

glutamate receptors (mGluRs). Here, BDNF was found to activate Rac1, triggering the dissociation of CYFIP1 from eIF4E, thus releasing CYFIP1 and allowing mRNA translation (*Napoli et al., 2008; De Rubeis et al., 2013*). As mentioned above, activation of Rac1 was also suggested to trigger the dissociation of CYFIP1 from WRC, although some studies indicate that Rac1 activates the WRC complex without dissociation of its elements. This discrepancy in the literature reflects the complex nature of *CYFIP1*, and its implication in different cell pathways makes it a difficult subject to study. Nevertheless, several studies have looked at the impact of dysregulations in *CYFIP1* on neuronal function, especially on synaptic morphology and physiology using animal models. In the following section, I will summarise some of these studies.

1.4.3. Impact of *Cyfp1* on dendritic and spine morphology and physiology

Neurodevelopmental disorders have been linked to abnormalities in both dendritic architecture and synaptic formation (*see review Nakai et al., 2018*). These defects can produce network-wide effects in neuronal networks, ultimately resulting in aberrant cognitive processing. Several studies have indicated a key role of actin cytoskeletal dynamics in the establishment and maintenance of both dendritic arborisations and spines, as well as in driving rapid changes in spine morphology important for synaptic plasticity (*Basu and Lamprecht, 2018; Nakahata and Yasuda, 2018*). As stated in the beginning of the previous section, the actions of actin polymerisation during axonal growth can help elucidate how this mechanism influences the formation of dendrites and spines (**Figure 1.5**). Furthermore, also crucial for synaptic plasticity is the controlled and local synthesis of the right set of proteins at the synapses, modulating their activity (*Martin et al., 2000; Steward and Schuman, 2003*). Since *Cyfp1* was found to be highly enriched at inhibitory and excitatory synapses in mice (*Pathania et al., 2014; Davenport et al., 2019*), effects of *Cyfp1* dosage on density, size and shape of dendritic spines, as well as their role in synaptic plasticity have been investigated in several studies.

Several lines of evidence, from both *in vitro* and *in vivo* mouse models, propose a dosage-dependent effect of *Cyfp1* on spine maturation and morphology. Maturation of the spines is usually assigned to four morphological classes: mature (“stubby” and “mushroom”) and immature (long thin and filopodia). In *Pathania et al., 2014*, decreased levels of *Cyfp1* led to reduced dendritic complexity, as well as an increased number of

long and thin spines both *in vitro* and in the CA1 area of the hippocampus *in vivo*, whereas spine density remained unchanged. This phenotype was also seen in *De Rubeis et al., 2013*, where *Cyfp1*-silenced cortical neurons had a reduced number of mature spines, higher number of elongated immature-looking spines and increased spine length, compared to controls. Corresponding findings were obtained with overexpression models, where *Oguro-Ando et al., 2015* showed *in vitro*, using a human derived cell line SH-SY5Y, that overexpression of *CYFIP1* resulted in increased cell size and abnormal neurite outgrowth in neuron cells. These results were replicated in a mouse model both *in vitro* and *in vivo*. In the mouse, overexpression of *Cyfp1* also resulted in increases in dendritic complexity, spine density and proportion of pyramidal neurons showing a mature spine morphology (mature “stubby” spines), as well as an increase in abnormal-looking spines in the frontal cortex *in vivo*. These findings suggest a dosage-dependent effect of *Cyfp1*, where bidirectional dosage of *Cyfp1* leads to opposite changes on spine morphology. With the aim of showing further evidence of a *Cyfp1* dosage effect, *Abekhoukh et al., 2017* used RNA interference techniques to downregulate *Cyfp1* mRNA, and thus *Cyfp1* protein, levels in mouse neurons in order to achieve lower levels of the protein while bypassing the lethality of *Cyfp1* homozygous embryos. Using this technique, *Cyfp1* mRNA was successfully reduced by 70-80% and this led to a greater reduction in dendritic arborisation when compared to the other studies in *Cyfp1*-heterozygous mouse models.

An important characteristic of dendritic spines is the dynamic regulation of spine volume and density that underlie synaptic plasticity. This is mediated by stimuli that induce long-term potentiation (LTP) and long-term depression (LTD), leading to rapid changes in spine volume. LTP and LTD are both dependent on N-methyl-D-aspartate (NMDA)-type glutamate receptors activity. LTP occurs when the pre- and postsynaptic neurons are coincidentally active. In this condition, glutamate is released from the presynaptic bouton and binds the NMDA receptor, leading to the release of Mg^{2+} from the receptor, allowing the influx of large quantities of calcium. This maximal calcium influx through the receptor strengthens the synaptic connection. On the other hand, LTD is induced when presynaptic neurons are repeatedly activated without postsynaptic activity. However, the blockage of NMDA receptors by Mg^{2+} is incomplete, leading to some calcium influx. Presumably, this repeated occurrence of lower calcium influx triggers synaptic depression (*Lüscher and Malenka, 2012*). During LTP and LTD, a redistribution of α -amino-3-hydroxy-5-methyl-4-isoxazolepropionic acid (AMPA)-type

glutamate receptors occurs, where more receptors are added to potentiate the synapse, or receptors are removed to weaken synapses. In *Cyfp1*-heterozygous neurons, an increased mobility of AMPA receptor was found, indicating a lack of stability of these receptors (*Pathania et al., 2014*), which can have a marked impact on synaptic plasticity (*Huganir and Nicoll, 2013*). Furthermore, *Pathania et al., 2014* observed that spine shrinkage could be induced following NMDA administration in wild-type neurons, but no differences in spine volume were observed in *Cyfp1*-heterozygous cultured hippocampal neurons under the same conditions. *Bozdagi et al., 2012* also found enhanced mGluR-dependent LTD in hippocampal slices from 4- to 6-week-old *Cyfp1* heterozygous mice, while LTP remained unchanged. These findings were identical to those of *Fmr1*-knockout mice, suggesting a link to the mRNA translational pathway connecting FMRP and CYFIP1. Altogether, these results suggest a role of *Cyfp1* in activity-dependent changes in spine volume during synaptic plasticity.

One question arises from the findings of an impact of *CYFIP1* on dendritic spine morphology and maturation: which of the two *CYFIP1*-associated mechanisms (actin cytoskeleton dynamics or FMRP-target mRNAs translation) contribute to the observed phenotypes? Here, evidence showing dendritic spine effects in *Fmr1*-knockout mice might be of relevance. Both *Fmr1*-knockout and *Cyfp1*-heterozygous mice show an increase in dendritic spines with immature morphology, and fewer with mature morphology (*Grossman et al., 2006; He and Portera-Cailliau, 2013; De Rubeis et al., 2013; Pathania et al., 2014*). This phenotypic overlap suggests that regulation of protein synthesis, as a result of CYFIP1-FMRP complex action, may be essential for spine maturation. On the other hand, *Fmr1*-knockout mice exhibited increased spine density and dendritic complexity (*Nimchinsky et al., 2001; Abekhoukh et al., 2017*), which is similar to the findings in the *Cyfp1*-overexpression mouse model, but opposite to the *Cyfp1*-heterozygous model. Therefore, it is possible that reduced dendritic complexity may be linked to disruptions in actin cytoskeletal dynamics due to *Cyfp1*-Rac1 interactions, since Rho GTPases have been implicated in spine formation, maturation and stability (*Luo, 2002; Cingolani and Goda, 2008*). Actin dynamics in spines are also necessary for AMPA receptor trafficking (*Hanley, 2014*), and dysregulations in actin polymerisation could lead to the increased motility of these receptors seen in the *Cyfp1*-heterozygous mice (*Pathania et al., 2014*). In an attempt to answer the question of which mechanism is responsible for spine defects, *De Rubeis et al., 2013* looked at the individual impact of each complex. The authors created mouse mutants missing the

interaction with either eIF4E or NCKAP1 in order to separately study the impact of *Cyfp1* on mRNA synthesis and actin cytoskeleton dynamics, respectively. Here, both mutants failed to rescue the spine phenotype, suggesting that both *Cyfp1* complexes are equally important for spine formation.

Recently, *Cyfp1* was shown to be enriched both in excitatory and inhibitory synapses (Davenport *et al.*, 2019). Furthermore, in Davenport *et al.*, 2019 study, the effect of a complete conditional *Cyfp1* knockout, as well as its overexpression, on excitatory and inhibitory (E/I) balance was examined. Here, in cultured hippocampal neurons, *Cyfp1* overexpression led to a decrease in miniature inhibitory postsynaptic current (mIPSC) amplitude, increased miniature excitatory postsynaptic current (mEPSC) frequency and increase in the excitatory-to-inhibitory synaptic ratio, consistent with the findings on mIPSC and mEPSC. In contrast, forebrain-specific *Cyfp1*-knockout mice showed an increase in mIPSCs in CA1 pyramidal cells, increased inhibitory postsynaptic clustering and enhanced expression of neuroligin 3 and GABA_AR β -subunits *in vivo*. These results suggest a link between *CYFIP1* dosage and synaptic inhibition and excitation, leading to an altered E/I balance that can result in abnormal network connectivity (Osterweil, 2019). Conversely, a recently published study did not show any differences in phasic GABAergic inhibition, nor in properties of spontaneous IPSCs in DG granule cells from the hippocampus (Trent *et al.*, 2019). Differences between these findings may indicate a different effect of *Cyfp1* on different hippocampal subfields (DG vs CA1), or may be due to differences in gene dosage, since a full *Cyfp1*-knockout was used in Davenport *et al.*, 2019, whereas a *Cyfp1*-haploinsufficient mouse model was used in Trent *et al.*, 2019. Although full knockout models are relevant to investigate mechanisms and cell pathways of different proteins, in the context of human pathology the 15q11.2 BP1-BP2 deletion never results in *CYFIP1* homozygosity, as this is lethal.

1.5. An effect beyond synapses – neurodevelopmental disorders and white matter

Altogether, the above findings establish a link between dendrite formation and *Cyfp1* - associated mechanisms, suggesting a possible route by which *Cyfp1* haploinsufficiency could lead to neural dysfunction and result in psychiatric problems. Additionally, early evidence from a *Drosophila Cyfp1* null mutant model has showed a link between *dCyfp1*

haploinsufficiency and abnormal axonal growth, axonal pathfinding and axonal branching (*Schenck et al., 2003*). More recently, a study also found *Cyfp1* to be a mediator of axonal growth in zebrafish (*Cioni et al., 2018*). These observations suggest that *CYFIP1* might also influence different axonal characteristics, suggesting an impact beyond synapses. Although synaptic dysfunction is a major hallmark for neurodevelopmental disorders, multiple functional studies have emerged showing extensive brain connectivity changes associated with these disorders. While abnormal synapses can influence brain connectivity, this is mainly characterised by abnormal information transfer among neurons, which is established by axons in white matter.

The development of sophisticated techniques, such as diffusion tensor imaging (DTI) MRI, have allowed more detailed *in vivo* characterisation of axonal projections in the brain. DTI has the ability to quantify the diffusion of water molecules in the brain, as well as characterise the direction of their movement. This is particularly useful in white matter microstructure, where water molecules are constrained by the axon walls and forced to move preferentially along the main direction of the axons. Different tissue components contribute to this movement restriction, such as cell membranes, macromolecules, myelin sheaths and fibre tracts (*Beaulieu, 2002*). Therefore, any changes in these components affect the diffusion of water molecules, and this translates to alterations in DTI signal, making this a sensitive technique for detecting changes in white matter microstructure (*Beaulieu, 2002; Jones and Leemans, 2011; Soares et al., 2013*). Different measures can be extracted from DTI data. A more elaborate description of this technique, including the underlying physics and outcome measures, will be explained in the following chapter. In order to have a comparative measure between findings, most studies in literature use fractional anisotropy (FA), a measure that reflects how restricted the water molecules are, which is associated with axonal integrity. FA is decreased when water molecules are less restricted (random movement) and increased when these are more restricted (moving preferentially in one direction).

In the past few years, DTI has been widely used to explore white matter abnormalities in neurodevelopmental disorders. Generally, FA is globally decreased in patients, and lower FA values are usually associated with poorer cognitive performance in healthy populations, as well as in some clinical populations (*Taylor et al., 2004; Walther et al., 2011; Travers et al., 2012; Fitzsimmons et al., 2013*). There are exceptions, however. Increases in FA have been reported, in individuals with schizophrenia and ASD, in some white matter tracts that were associated with worse clinical or cognitive outcomes

(Hubl et al., 2004; Seok et al., 2007; Cheng et al., 2010). White matter abnormalities have also been detected in healthy individuals carrying neurodevelopmental CNVs, where white matter changes were reported in 16p11.2 (reciprocally for deletion and duplication) (Chang et al., 2016), in Williams syndrome (caused by deletions at the 7q11.23 region) (Hoefl et al., 2007), and in 22q11.2 deletion (Nuninga et al., 2018). Some of these findings will be explored in the discussion of Chapter 3.

As mentioned previously in this introduction, some evidence for regional changes in white matter volume were found in carriers of the 15q11.2 BP1-BP2 CNV (Stefansson et al., 2013; Ulfarsson et al., 2017). However, no studies to date have looked at white matter microstructural changes associated with the 15q11.2 BP1-BP2 region. The work developed in this thesis will begin with an investigation of white matter microstructural changes in deletion and duplication carriers of the 15q11.2 BP1-BP2 in two different populations using DTI methods. These findings are described in Chapters 3 and 4. This work raises the question of which gene, or genes, in this region could influence white matter. As mentioned, previous work has already suggested a link between *CYFIP1* and axonal growth and guidance, which may result in white matter abnormalities. Furthermore, DTI studies in FXS have shown extensive white matter abnormalities in patients (Barnea-Goraly et al., 2003; Haas et al., 2009; Green et al., 2015; Hall et al., 2016), which could be a consequence of dysregulations in the FMRP-CYFIP1 complex. Considering the role of actin dynamics and protein synthesis in cell differentiation and function, an impact of *CYFIP1* dysregulations on several other aspects of the central nervous system is likely. A striking example are the glial cells, which are dependent on actin dynamics to undergo morphological transitions during differentiation, as well as to move around and reshape their projections. Some evidence has suggested that *CYFIP1* may be expressed in glial cells, where a recent study has shown a highly expression of *Cyfp1* in microglia cells in mice (Haan et al., 2018, not peer-reviewed). Additionally, CYFIP1-interacting proteins were found to be expressed in glial cells; in particular, FMRP and WAVE1 were shown to be expressed in oligodendrocytes, the myelin producing cells of the central nervous system (Wang et al., 2004; Kim et al., 2006; Giampetruzzi et al., 2013). New lines of evidence have been proposing glial cells as essential modulators of neuronal function, where neuron-glia interaction has emerged as a potential contributor to pathogenesis of neurodevelopmental disorders (Bernstein et al., 2015; Jäkel and Dimou, 2017; C. Wang et al., 2015).

1.6. Neurodevelopmental disorders and glial cells

The growing evidence for neuronal dysfunction in neurodevelopmental disorders as a result of abnormalities in both synapses and axons has driven most of research to a “neuron-centric” hypothesis underlying mental illness. However, with recent advances in genetics and systematic biology, it has become increasingly clear that glial cells also play a crucial role in regulating neuronal function, and dysfunction in these cells may underlie several disrupted mechanisms in central nervous system diseases. The glial cell population can be subdivided into four major groups (*Jäkel and Dimou, 2017*): (1) microglia, (2) astrocytes, (3) oligodendrocytes, and (4) their progenitors NG2-glia (**Figure 1.8**).

Microglia are essential cells for maintaining homeostasis within the central nervous system, where they are also known to produce immune responses to inflammation (*Lenz and Nelson, 2018*). Besides surveying healthy tissue, microglia cells have also been shown to directly contact synapses, and play an important role in synaptic pruning and modulation during development (*Bar and Barak, 2019; Sellgren et al., 2019*). Abnormal microglia activity, morphology, and gene expression have been widely associated with neurodevelopmental disorders (*Vargas et al., 2005; Garey, 2010; Gupta et al., 2014*). In ASD and schizophrenia, increased numbers of microglia have been reported in post-mortem studies, along with evidence of increased microglia activation in patients from neuroimaging studies using positron-emission tomography (PET) and high-field MRI (*van Berckel et al., 2008*). Decreased synapse density in patients with schizophrenia has also been linked to excessive synaptic pruning as a result of dysregulations in microglia activity (*Sellgren et al., 2019*).

Astrocytes are the most abundant type of glial cells in the adult brain (*Jäkel and Dimou, 2017*). The roles of astrocytes encompass numerous aspects of brain physiology. Briefly, astrocytes provide structural and nutritional support for neurons and blood vessels, regulate water and ion homeostasis, modulate neurotransmitters, and secrete a number of cytokines that regulate inflammatory responses (*Sloan and Barres, 2014; C. Wang et al., 2015; Jäkel and Dimou, 2017*). Thus, astrocyte dysfunction may have a large effect on many processes in the brain. For example, astrocyte dysfunction can result in neurotransmitter dysfunction, which may contribute to pathology, and has been largely linked to schizophrenia (*Bernstein et al., 2015*).

Oligodendrocytes are the most investigated glial cells in neuropsychiatry. When mature, these cells are known to generate multiple layers of myelin membrane that insulate the axons, allowing a fast saltatory nerve conduction, as well as providing trophic support to axons (Nave, 2010).

NG2-glia were discovered more recently and, although characterised as precursors of mature oligodendrocytes within the oligodendrocyte lineage, they were considered an independent glial population due to their additional characteristics (Kettenmann and Verkhratsky, 2008). These cells are present in both grey and white matter through postnatal development and into adulthood. Furthermore, NG2-glia activate upon many types of injury or pathological conditions, by changing cell morphology and proliferation rate (Jin et al., 2018). Dysfunction of NG2-glia can result in abnormal development of oligodendrocytes.

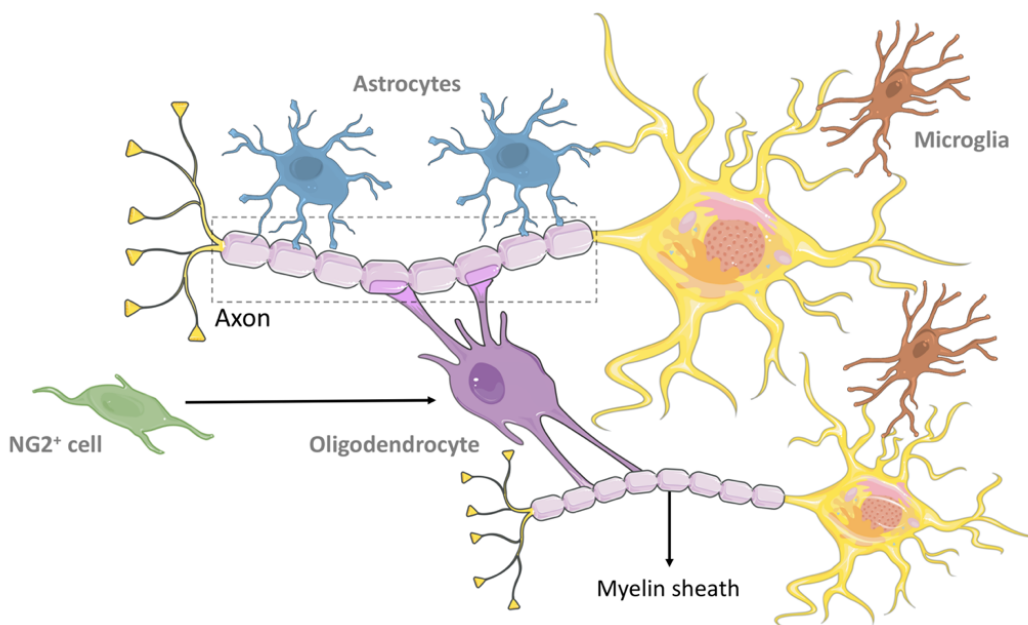


Figure 1.8 - Diagram showing the different types of glial cells in relation to a neuron.

Microglia are the immune cells in the brain removing toxic agents and dead cells from the brain. Astrocytes have a crucial role in providing structural and nutritional support for neurons. Oligodendrocytes produce myelin to insulate the axons. NG2-glia are the oligodendrocyte precursor cells. Image adapted from C. Wang et al., 2015.

A number of studies involving gene expression, animal models, and histological analysis of human post-mortem brain tissue have suggested that white matter abnormalities in neurodevelopmental disorders are related to neurobiological mechanisms affecting central nervous system myelination and myelin-producing cells (oligodendrocytes) (Flynn *et al.*, 2003; Vostrikov *et al.*, 2007; Fields, 2008; Roussos and Haroutunian, 2014). These studies have been highly predominant in schizophrenia, where altered expression of different genes associated with oligodendrocyte and myelin development was found (Hakak *et al.*, 2001), resulting in oligodendrocyte dysfunction (Uranova *et al.*, 2007; Mauney *et al.*, 2015) and myelin damage (Uranova *et al.*, 2001). It has been suggested that these changes could be caused by some types of medication, or drug abuse, affecting the expression of these genes, as well as white matter properties in patients with schizophrenia (Narayan *et al.*, 2007). However, a study by Hakak *et al.*, 2001 observed reduced expression of oligodendrocyte/myelin genes in a subset of patients who were off medication for a prolonged period of time. Furthermore, experimental manipulation of genes that regulate oligodendrocyte development and myelination caused behavioural changes characteristic of schizophrenia (Fields, 2008). Although not conclusive, these studies suggest a primary role for oligodendrocyte/myelin dynamics in schizophrenia. Fewer studies have looked at a relationship between ASD and oligodendrocyte dysfunction. Of relevance is a recent study, using an ASD mouse model, that showed reductions in both the number of oligodendrocytes and myelin thickness in important brain areas for social behaviour (Graciarena *et al.*, 2019).

The above findings suggest that changes in myelination might be a principal contributor to the abnormal network connectivity seen in neurodevelopmental disorders. Damage to myelin is a characteristic of multiple sclerosis, a known condition leading to motor problems and disability. Recently, myelination has also been proposed as having a dynamic role in learning (Fields, 2015). In fact, changes in myelination can alter the timing of arrival of action potentials in different regions of the brain, disturbing the temporal coherence of neuronal circuitry. Therefore, precise production of myelin in different regions of the brain is essential for normal brain function. Myelin is also required for long-term axonal integrity and survival (Griffiths *et al.*, 1998; Kassmann *et al.*, 2007). Generation of myelin occurs in the central nervous system by mature oligodendrocyte. Before maturation, oligodendrocytes undergo proliferation, migration, and changes in their cytoskeleton (Michalski and Kothary, 2015). When mature oligodendrocytes contact the axons, they extend a differentiated plasma membrane to produce myelin. Hence, actin

cytoskeletal dynamics is a major element driving oligodendrocyte differentiation and myelin wrapping. Moreover, an efficient and controlled transport and translation of proteins and lipids towards the axon-oligodendrocyte contact site is crucial for the production of large amounts of myelin (*Sherman and Brophy, 2005*). It is therefore plausible that dysregulations in these two processes could lead to abnormalities in the myelination process. By virtue of being involved in regulation of both actin dynamics and protein synthesis, dysregulations in *CYFIP1* could influence myelination and lead to white matter abnormalities and network dysfunction. For a better understanding of the potential role of *CYFIP1* on oligodendrocyte-myelin dynamics, in the following section I will elaborate on different aspects of oligodendrocyte differentiation and the myelination process.

1.6.1. The role of actin polymerisation on oligodendrocyte differentiation

Oligodendrocyte lineage cells represent all the oligodendrocyte cells in different stages of maturation, from early progenitors to mature myelinating-cells (**Figure 1.9A**). During development, oligodendrocyte precursor cells (OPCs) originate from neural stem and progenitor cells during late embryonic development (*Emery, 2010*). OPCs are also known as NG2-glia, and are highly proliferative and migrate through the central nervous system into different regions of the brain. A substantial number of NG2-glia persist in the adult brain (*Hughes et al., 2013*), and are thought to be responsible for myelin maintenance, where they are actively recruited for myelin remodelling and *de novo* myelination (*Young et al., 2013*). When these cells differentiate into oligodendrocytes, they extend multiple highly ramified processes. These processes will then contact unmyelinated axons, triggering myelination. This ability to extend long and complex processes is an important characteristic of oligodendrocytes, allowing the cell to myelinate multiple axons simultaneously (*Simons and Nave, 2016*). Oligodendrocyte differentiation represents one of the most significant changes in cell morphology, and is tightly regulated by several mechanisms involving actin, actomyosin- and tubulin-based cytoskeleton, and membrane adhesion complexes.

The rapid and sustained growth of oligodendrocyte is dependent on its two major cytoskeletal components: microtubules and microfilaments (f-actin), which act independently or together during oligodendrocyte differentiation (*Bauer et al., 2009*;

Michalski and Kothary, 2015). In immature oligodendrocytes, f-actin is highly concentrated at the leading edge of the processes. Lamellipodia, consisting of f-actin bundles, lead the growth of the processes by pushing against the membrane edge and generating extrusions of actin at the surface. These extrusions are also known as filopodia, as previously explained. It is noted that the growth of these processes is similar to that of a neuronal growth cone (see **Figure 1.5** for neuronal growth cone) (*Fox et al., 2006*). The oligodendrocyte growth cones have three different domains: a microtubule rich central domain, an f-actin rich peripheral domain, and a transient domain where microtubules and f-actin overlap (**Figure 1.9B**). A few exploratory microtubules penetrate the f-actin rich peripheral domain, and are thought to be important for directing growth. Mechanically, actin filaments and microtubules are different. Actin filaments have more flexibility and higher turnover rates than microtubules, enabling rapid re-organisation that is crucial for migration and growth (*Michalski and Kothary, 2015*). The microtubules in the oligodendrocytes have the central role of providing stability, increasing the levels of tubulin with maturation (*Lunn et al., 1997*). In the first days of differentiation, oligodendrocyte arborisation was shown to be highly dependent on actin and tubulin polymerisation. Highly branched oligodendrocytes start the process of maturation by establishing more distal interbranch connections with fewer invasions of microtubules (*Michalski and Kothary, 2015*). At the final stages of maturation, the oligodendrocytes undergo a shift from process outgrowth to membrane production, resulting in a progressively sparse cytoskeleton where the projections become thin and with an appearance similar to a spider's web (**Figure 1.9A**).

The role of actin polymerisation in early stages of oligodendrocyte differentiation and process extension is clear. Hence, several studies have investigated which polymerising proteins are present at the leading end of these processes. Although no study has looked at *CYFIP1* expression on oligodendrocytes, these cells were shown to express other actin-polymerising proteins, including the Arp2/3 complex, N-WASP, WAVE proteins, and the small Rho GTPases, Rac1, Cdc42 and RhoA (*Song et al., 2001; Fox et al., 2006; Kim et al., 2006; Bacon et al., 2007*). Therefore, it has been proposed that the WASP family members (N-WASP and WAVE1) are responsible for f-actin polymerisation at the leading end of the oligodendrocytes' processes, through interactions with Arp2/3 complex (**Figure 1.9B**). The fact that WAVE1 is expressed at the leading end of these processes may indicate that actin polymerisation occurs in the same way as explained previously for dendrite and spine formation in neurons. Therefore,

dysregulations in elements of the WRC, such as *CYFIP1*, could lead to abnormal oligodendrocyte differentiation. Furthermore, manipulation of different actin regulators led to abnormal oligodendrocyte-myelin dynamics, where oligodendrocyte differentiation and myelin wrapping were shown to be affected by knockouts of specific proteins: the WAVE1 and integrin-linked kinase (ILK) influences oligodendrocyte differentiation and axon ensheathment (*Kim et al., 2006; Michalski et al., 2016*), while the Arp2/3 complex influences process branching but not myelin wrapping (*Zuchero et al., 2015*), and Rho GTPases, Cdc42 and Rac1 regulate myelin sheath formation (*Thurnherr et al., 2006*). The influence of these proteins on myelination will be further elaborated in the discussion section of Chapter 6.

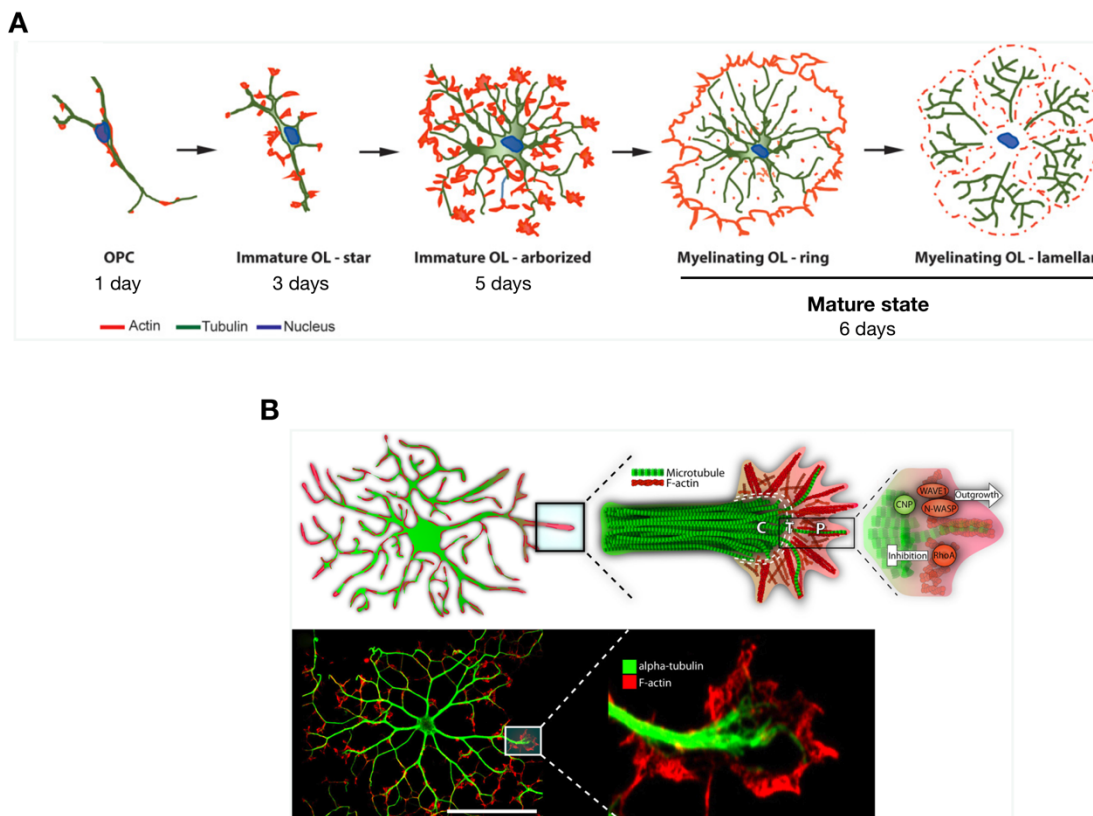


Figure 1.9 - Actin dynamics during oligodendrocyte differentiation and process extension.

A Dynamics of the oligodendrocyte cytoskeletal dynamics during differentiation process. Initially, OPCs extend long processes that create a star-shape oligodendrocyte. Here, actin filaments are present at the leading edge of the processes, and microtubules are present both in cell body and processes. After 3 days of differentiation *in vitro*, most oligodendrocytes form extensive and branched projections, a process highly dependent on actin and tubulin polymerisation. These highly complex oligodendrocytes start the process of maturation by establishing more distally interbranch connections of actin, which is preceded by actin

depolymerisation in the final step. After 6 days of differentiation *in vitro*, most oligodendrocytes show mature features. Figure taken from [Domingues et al., 2018](#). **B** Schematic representation of the cytoskeletal-mediated growth of the oligodendrocyte processes. Distribution of microtubules (in green) and f-actin (in red) in the oligodendrocyte cell. Oligodendrocyte growth cones have three different domains: a microtubule rich central domain (C), an f-actin rich peripheral domain (P), and a transient domain where microtubules and f-actin overlap (T). F-actin bundles (represented as long red stands) lead the growth of the processes by pushing against the membrane edge and generating filopodia. Key cytoskeleton assembly proteins that drive the spreading of oligodendrocyte processes are represented on the right. Below there is an immunofluorescent representation of an immature oligodendrocyte with f-actin in red and α -tubulin in green, with the growth-cone-like structure on the right. Scale bar: 50 μ m. Figure taken from [Michalski and Kothary, 2015](#).

1.6.2. The role of actin depolymerisation in myelin wrapping

As described by [Luse, 1959](#), myelination begins when the processes of an oligodendrocyte contacts an axon to form a specialised membrane junction. This is now known to be a specialised membrane domain for intercellular communication between the oligodendrocyte and the axon, which is carried out through cytoplasmic channels ([Pedraza et al., 2009](#); [Sobottka et al., 2011](#); [Wake et al., 2011](#); [Snaidero et al., 2014](#)). The mechanisms that drive the myelin wrapping around the axons have been a subject of debate. A recent study followed the axonal ensheathment by oligodendrocytes using high resolution imaging methods ([Snaidero et al., 2014](#)). Using a zebrafish model and electron microscopy, the authors employed a pressure-freezing technology to preserve high quality resolution of fine myelin structure, and looked at the shape of single myelin layers and their development over time. The authors showed that the oligodendrocytes form a triangular membrane upon connecting with the axon. Then, expansion of this membrane and consecutive wrapping of the axon occur due to an advancing inner tongue (leading edge) that deposits new layers underneath the previously formed membrane layers (see **Figure 1.10** for mechanism proposed by [Snaidero et al., 2014](#)). The individual layers of myelin expand laterally along the axon, wrapping the axon in concentric layers of membrane in a nonuniform manner ([Luse, 1959](#); [Sobottka et al., 2011](#); [Snaidero et al., 2014](#)). In order to form a stable myelin sheath, compaction of the membrane must occur, where cytoplasm is expelled from the layers between the outer tongue and the inner tongue, creating individual segments of mature myelin. The segments of mature myelin, still connected to the oligodendrocyte, are termed internodes, where the unmyelinated space between internodes forms the nodes of Ranvier, containing a high density of sodium

channels. Myelin sheaths enable the rapid saltatory conduction of action potential, by localising voltage-gated sodium channels in these Ranvier nodes (*Snaidero et al., 2014; Michalski and Kothary, 2015*). Altogether, these findings suggest that myelin grows via two distinct coordinated motions: the inner tongue leading the wrapping around the axon, and a lateral extension of myelin membrane towards the Ranvier node. Thus, both the inner tongue and the lateral edges stay in close contact with the axonal surface. The myelin membrane at the innermost, outermost and lateral edge regions remain uncompacted.

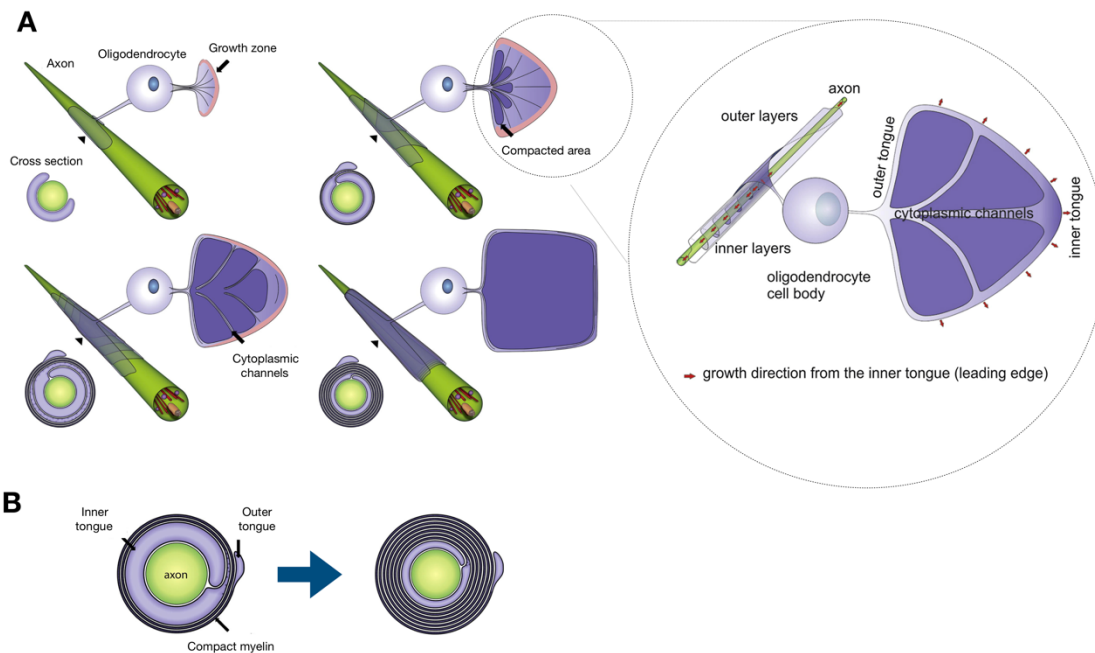


Figure 1.10 - Model of myelin wrapping in the central nervous system.

A Schematic representation of myelin ensheathment model in wrapped, unwrapped and cross section view. The unwrapped view shows the localisation of cytoplasmic channels, which connect the cell body of the oligodendrocyte to the growth zone of the inner tongue. The growth zone is represented by pink, while compact myelin is represented by dark purple. The wrapped view shows the position of the layers along the axon, whereas the cross section shows the stage of compaction during myelin growth. **B** Schematic representation of the myelin membrane layers in the early and later stages of myelin wrapping, indicating the inner and outer tongues, as well as compact myelin formation. Figures taken from *Snaidero et al., 2014*.

Although f-actin is abundant in oligodendrocyte projections, both *in vitro* and *in vivo* models showed that compact myelin does not contain f-actin (Nawaz *et al.*, 2015; Zuchero *et al.*, 2015), but contains high levels of g-actin. Two recent studies by Zuchero *et al.*, 2015 and Nawaz *et al.*, 2015 used complementary methods to demonstrate a highly dynamic mechanism involving actin remodelling during myelination, where actin assembly is essential for oligodendrocyte extension and wrapping initiation, and actin disassembly is crucial for myelin compaction and formation of mature myelin. Using Lifeact-RFP and an f-actin marker in developing zebrafish, Nawaz *et al.*, 2015 showed that f-actin is first widely expressed in oligodendrocytes in early stages, and then confined to the leading edges during maturation. Moreover, *in vitro* observations of the oligodendrocyte maturation process showed that the initially abundant f-actin, over time becomes concentrated at the leading edge of the cells, and it is lost when the processes are converted into myelin-like membrane sheets (**Figure 1.9A**) (Nawaz *et al.*, 2015; Zuchero *et al.*, 2015). It was further shown that the total actin levels remained unchanged, suggesting a transition from f-actin to g-actin (actin disassembly) during maturation. Consistent with this are the RNA sequencing data indicating that actin depolymerising proteins are significantly upregulated in myelinating oligodendrocytes (Zhang *et al.*, 2014). In order to investigate how actin depolymerisation drives myelin sheath formation, Nawaz *et al.*, 2015 used a laser trap and atomic force microscopy to show that loss of f-actin resulted in reduced membrane tension, facilitating membrane spreading and cell attachment. However, it is unknown whether this spreading mechanism would alone be sufficient to move the leading edge of the myelin membrane. The authors also proposed that f-actin is still present at the inner tongue during active growth, and could promote its extension. Zuchero *et al.*, 2015 on the other hand, addressed the role of actin assembly during myelin wrapping by inhibiting the Arp2/3 complex. Here, early inhibition of the Arp2/3 complex in oligodendrocyte differentiation led to impairments in oligodendrocyte branching and axon myelination. However, when Arp2/3 was conditionally deleted in oligodendrocytes after ensheathment, during active wrapping, no differences were found in the distribution or number of membrane wraps. This finding suggests that Arp2/3-dependent actin assembly is required for oligodendrocyte differentiation, but not for wrapping of myelin. Therefore, the two studies propose two mechanisms: Nawaz *et al.*, 2015 proposes that during myelination, actin polymerisation at the inner tongue is the driving force for myelin wrapping, while actin depolymerisation allows membrane spreading and myelin compaction; while Zuchero *et al.*, 2015 proposes that actin

depolymerisation alone provides the force to drive myelin wrapping. Although the exact mechanism is not yet fully understood, both studies show that a rapid switch from actin assembly to actin disassembly is required for myelin compaction and maturation.

Actin disassembly is controlled by cofilin and gelsolin family proteins, which are highly enriched in active myelinating oligodendrocytes. These proteins become active after their release from a phospholipid component of the plasma membrane, specifically phosphatidylinositol 4,5-bisphosphate (PI(4,5)P₂). Both *Nawaz et al., 2015* and *Zuchero et al., 2015* showed that, when cofilin1 is conditionally deleted, a significant reduction in myelin thickness is observed, providing additional evidence for a crucial role of actin disassembly in promoting myelin sheath formation. Myelin basic protein (MBP) is another major structural element of myelin in the central nervous system, interestingly also known to bind the PI(4,5)P₂ on the oligodendrocyte plasma membrane. Early studies using a *Shiverer* mouse model (in which the MBP protein is absent due to a mutation in the gene encoding MBP) showed that MBP is crucial for myelin membrane compaction and myelin wrapping (*Readhead et al., 1987*). Therefore, it is possible that somehow MBP could be linked to actin disassembly mechanisms. Noting this, *Zuchero et al., 2015* investigated the relationship between MBP and actin disassembly during myelination. Here, the authors found that MBP expression increases with actin disassembly, but MBP levels did not co-localise with actin filaments in oligodendrocytes. Furthermore, in the *Shiverer* mouse model, the authors found that, while f-actin levels dropped in wild-type mice during development, white matter in *Shiverer* mice maintained high levels of actin filaments, which was independent of the number of OPCs. These mice also showed an abnormal accumulation of f-actin in mature oligodendrocytes. The authors explored how MBP could influence actin disassembly. Since there was no evidence for co-localisation between MBP and actin filaments in oligodendrocytes, direct contact was unlikely. Since depolarising proteins were found to be enriched in myelinating oligodendrocytes, an interaction between MBP and these proteins was investigated. Here, the fact that MBP binds to the plasma membrane PI(4,5)P₂ component is highly relevant, since proteins like cofilin and gelsolin are kept inactive through their binding to this component. The authors tested the hypothesis that MBP could regulate actin disassembly by binding to membrane PI(4,5)P₂ and competing with cofilin and gelsolin, enabling their release and subsequent activation. This was supported by the fact that increases in MBP levels led to a complete block of cofilin1 binding and also blocked, to a lesser extent, the binding of gelsolin.

1.6.3. The role of protein synthesis during myelination – MBP mRNA transport to localised translation

In the central nervous system, the major myelin proteins include the proteolipid protein (PLP), 2'-3'-cyclic nucleotide 3'-phosphodiesterase (CNP), myelin-associated glycoprotein (MAG) and MBP (*Fulton et al., 2010*). PLP and MBP are the most abundant myelin proteins in the central nervous system, being widely distributed within the myelin sheath, and seem to play a key role in compaction of the multi-layered structure of mature myelin. MAG is localised at the lateral edges of the myelin membrane and may play a role in facilitating cell-to-cell interactions between myelin and axonal membranes during myelination. The role of CNP is less understood, and it has been proposed that CNP prevents the premature compaction of myelin by MBP at the inner tongue (*Snaidero et al., 2017*).

The synthesis of major myelin proteins, such as PLP and MBP, occurs in the oligodendrocyte, beginning when OPCs reach the maturation phase of differentiation and are considered pre-myelinating oligodendrocytes (*Baron and Hoekstra, 2010*). Generation of myelin is a complex process, where individual myelin proteins are expressed at different times, and transported to the myelin sheath by different mechanisms. Recent evidence has proposed a transcytotic transport mechanism for PLP, indicating transport of *de novo* synthesised PLP from the endoplasmic reticulum to the myelin membrane via the oligodendrocyte plasma membrane. This is followed by the subsequent internalisation and transport of PLP to the basolateral-surface-like myelin sheath. Newly arrived PLP appears to be internalised from the plasma membrane via clathrin-independent but cholesterol-dependent endocytosis. Data from mouse derived Oli-neu cell lines suggest that endosomal compartments may serve as sites of storage, prior to a neuronal signal-triggered delivery of the protein to the myelin membrane (*Baron et al., 2015*).

On the other hand, MBP was shown to be translated and inserted within the myelin membrane on site, at the oligodendrocyte-axonal contact region (*Colman et al., 1982*). It was found that large quantities of newly synthesised MBP protein can be detected in the myelin membrane as early as 2 minutes after translation (*Ainger et al., 1993*). Microinjection experiments with labelled MBP mRNA further revealed the formation of RNA transport granules, which are moved through the cytoplasm on microtubules to the distal ends of the oligodendrocyte processes, towards the myelin sheath (**Figure 1.11**)

(Ainger *et al.*, 1993; Carson *et al.*, 1997). It is therefore proposed that MBP mRNA is sorted into stress granules containing all necessary molecules for the translation of the mRNA, and is transported to the oligodendrocyte processes in a translationally inactive state (Müller *et al.*, 2013). In these granules, several proteins have been identified, that may play a role in the transport as well as inhibiting the premature mRNA translation. For example, it was proposed that the transport of these granules is mediated by the heterogeneous nuclear ribonucleoprotein hnRNP A2, which recruits hnRNP E1 to the granules to inhibit mRNA translation (White *et al.*, 2012). Furthermore, activation of Fyn kinase was shown to initiate mRNA translation through phosphorylation of hnRNP A2, which lead to the dissociation of hnRNP A2 and E1 from the stress granules, stimulating MBP synthesis (White *et al.*, 2008). The reason why MBP mRNA synthesis is repressed during transport is not fully understood. However, given its strong adhesive properties, this mechanism of local translation seems to be important for avoiding inappropriate adhesive interactions with other intracellular membranes (Müller *et al.*, 2013). This mechanism also allows a fast and selective production and insertion of MBP into myelin membranes, which may be important for the production of a defined amount of myelin in response to different determinants like axon diameter or activity (Müller *et al.*, 2013).

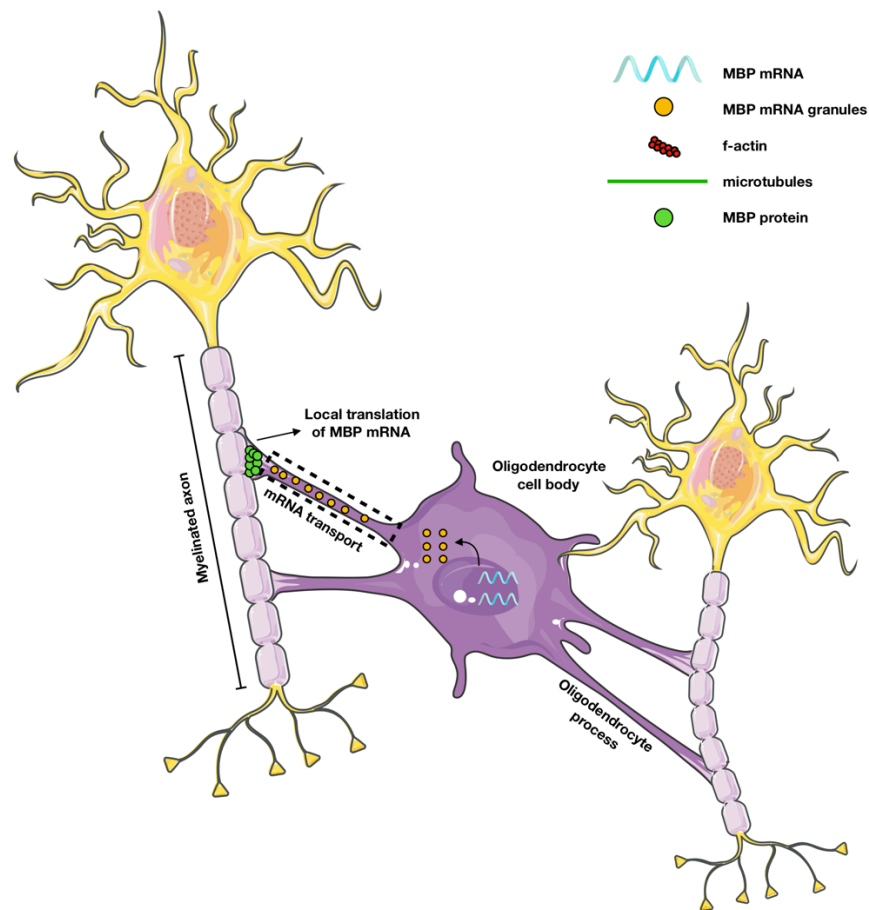


Figure 1.11 – Schematic representation of MBP synthesis in oligodendrocytes.

The synthesis of MBP occurs at the axon-oligodendrocyte contact site. This is possible through the transport of stress granules from the nucleus to the myelin membrane, that contain the mRNA, RNA binding proteins, motor proteins, and parts of the (possibly the entire) protein synthesis machinery, including ribosomes.

Both MBP and PLP have complementary roles during compaction of the myelin membrane. Myelin compaction starts with PLP mediating the correct apposition of the extracellular leaflets of the bilayer membrane, contributing to the stabilisation of the myelin membrane structure. This setup facilitates MBP to mediate the apposition of the internal surface, leading to the extrusion of cytoplasm and subsequent myelin compaction (**Figure 1.12**) (*Frank, 2000; Baron and Hoekstra, 2010*). MBP was shown to be the only myelin-specific vital and indispensable protein for myelin biogenesis. This was demonstrated in *Shiverer* mice, with findings of extensive hypomyelination in the central nervous system, shivering symptoms and premature death (*Readhead and Hood, 1990*). Different MBP isoforms are developmentally regulated and have different cellular distributions, which may reflect the multifunctionality of this protein family in myelin

maintenance. Furthermore, different roles have been assigned to this protein, which may explain the drastic phenotypes observed in its absence. As explained previously, MBP seems to play a role in actin disassembly during myelin wrapping, which is imperative for myelin formation (Zuchero *et al.*, 2015). The composition of the myelin membrane is unique compared to other membranes, with a high lipid to protein ratio (80:20). MBP is also thought to regulate this ratio by acting as a molecular filter, forming a cohesive protein meshwork blocking the diffusion of membrane proteins with a large cytosolic domain from entering myelin membrane sheaths (Aggarwal *et al.*, 2011). All these findings suggest that MBP is essential for many aspects of oligodendrocyte homeostasis and myelin formation.

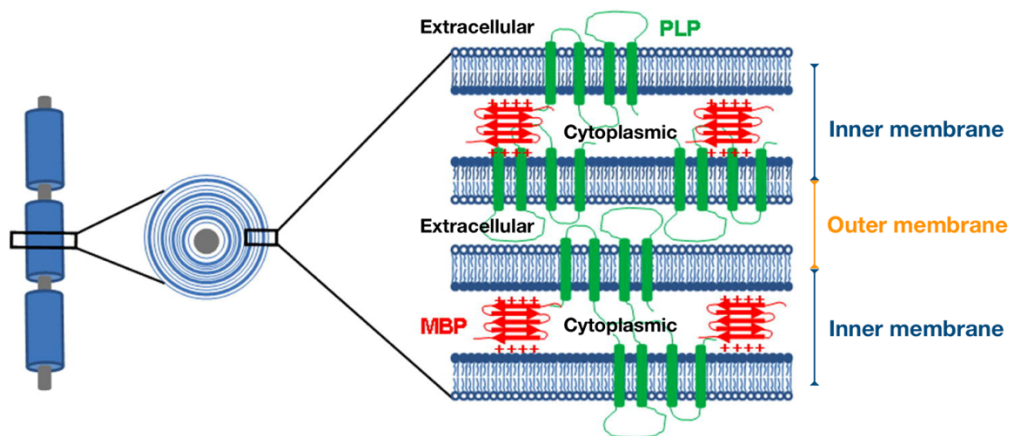


Figure 1.12 – Schematic representation of the major myelin-key proteins PLP and MBP.

Compact myelin is first formed by PLP, which is responsible for the apposition of the external surfaces of the myelin bilayer. This facilitates MBP in mediating the apposition of the internal surfaces and the extrusion of cytoplasm, forming a dense layer. Figure taken and adapted from Baron and Hoekstra, 2010.

The process of myelination involves the tightly-regulated coordination of several components, and many other aspects that are not mentioned in this introduction contribute to this process. Pre-myelinating oligodendrocytes extend and retract their processes into their environment with the aim of finding axons to myelinate (Hughes *et al.*, 2013). However, it is unclear whether this mechanism is dependent on axon-oligodendrocyte interactions or occurs randomly. It is known that oligodendrocytes continue to extend their processes, in the absence of any axons *in vitro* (Kachar *et al.*, 1986). However, it has also been noted that oligodendrocyte processes can recognise and ensheath only a

subset of axons in the central nervous system, leaving dendrites and neuronal cell bodies, as well as some axons, unmyelinated. Furthermore, individual oligodendrocytes respond to axons with different diameters by producing different amounts of myelin (*Almeida et al., 2011*). Therefore, the influence of axonal activity on oligodendrocyte differentiation and myelin production cannot be discounted. There is a clear synergistic relationship between neuronal activity and oligodendrocyte function that modifies myelin plasticity in the central nervous system. However, the signalling pathways contributing to this interaction are still poorly understood (*Bercury and Macklin, 2015*).

The above findings suggest that both transport and translation control of myelin-related proteins are essential for myelin formation. This plays together with highly dynamic changes in actin remodelling during oligodendrocyte differentiation and myelin formation. Given the known roles of *CYFIP1* in regulating both actin polymerisation and translation of some targeted mRNAs, it is of great interest to investigate the possible consequences of *CYFIP1* haploinsufficiency in oligodendrocyte differentiation and myelination process. Furthermore, it was found that FMRP is expressed in OPCs and immature oligodendrocytes (*Wang et al., 2004; Giampetruzzi et al., 2013*), whereas contradicting findings report both absence (*Wang et al., 2004*) and presence (*Giampetruzzi et al., 2013*) of FMRP in mature oligodendrocytes. It was proposed that FMRP could be a repressor of MBP synthesis leading to the inhibition of MBP expression in immature oligodendrocytes, which was validated in *in vitro* and *in vivo* experiments (*Wang et al., 2004; Giampetruzzi et al., 2013*). However, some results contradict this idea, where mature oligodendrocytes *in vitro* were shown to also express FMRP, and no differences in MBP expression were found between *Fmr1*-knockout and WT mice *in vivo* (*Giampetruzzi et al., 2013*). Nevertheless, the presence of both WAVE1 and FMRP in oligodendrocytes may indicate a role of CYFIP1-associated mechanisms in myelination. Disruptions in these mechanisms can ultimately lead to extensive white matter microstructural changes that can underlie the cognitive and clinical phenotypes associated with CNVs at the 15q11.2 BP1-BP2.

1.7. Thesis aims

The aim of this thesis is to investigate how variations in the 15q11.2 BP1-BP2 chromosomal region influence white matter microstructure. Using DTI methods, I first

established a link between variations at 15q11.2 BP1-BP2 CNV dosage and alterations of white matter microstructure in humans, some of these data were published in *Silva et al., 2019b*. Then, given the potential role of *CYFIP1* in 15q11.2 BP1-BP2 associated phenotypes, I then focused on looking at the impact of *Cyfp1* on white matter structure in a novel rat model. This *Cyfp1* haploinsufficiency rat model (hereafter designated *Cyfp1*^{+/-}), created in our laboratory using CRISPR/Cas9 technology, modelled the low dosage of *CYFIP1* in 15q11.2 BP1-BP2 deletion carriers. Using this model, white matter changes associated with *Cyfp1* haploinsufficiency were investigated. To this end, I combined DTI methods, allowing a whole-brain analysis, with *in vivo* and *in vitro* assessments of the cellular causes underlying these changes., some of these data were published in *Silva et al., 2019a*.

The experimental work in the thesis starts in Chapter 2 with a description of the *Cyfp1*^{+/-} animal model, together with a more detailed explanation of DTI. Following this, Chapter 3 will describe white matter microstructural changes associated with 15q11.2 BP1-BP2 CNV dosage. Here, DTI data from deletion and duplication carriers, drawn from a large genotyped population sample from Iceland and with no clinical diagnosis, will be analysed. In order to confidently establish a link between variations at 15q11.2 BP1-BP2 CNV and altered white matter microstructure, Chapter 4 will comprise a replication of these findings in a more heterogeneous sample drawn from the UK Biobank project. In the following chapters 5,6 and 7, I will focus on investigating the impact of *Cyfp1* haploinsufficiency on white matter microstructure in the *Cyfp1*^{+/-} rat model. First, Chapter 5 will comprise a DTI study, using analogous methods to the ones used for the human data in Chapter 3, where a whole-brain analysis will provide information on white matter regions affected by low dosage of *Cyfp1*. This information is used in Chapter 6, where a comprehensive ultrastructural analysis, using transmission electron microscopy (TEM), focused on the corpus callosum, allowing the investigation of changes in axon density and calibre, as well as myelin thickness in this structure. Finally, these analyses led to an *in vitro* assessment, where primary OPC cultures were used to investigate the effect of *Cyfp1* haploinsufficiency on oligodendrocyte differentiation. This study is described in Chapter 7 and is followed by a general discussion in Chapter 8, where wider implications of the experimental data, and suggestions and plans for future experiments will be discussed.

Chapter 2

General Methods

2.1. Abstract

This chapter will describe general methods used in more than one chapter in this thesis. First, I will briefly describe the procedures for the creation of the *Cyfp1*^{+/-} rat model, where additional technical details are provided in the Appendix 1. Then, I will elaborate on the DTI MRI technique, giving a brief overview of the underlying physics and DTI measures used in the thesis.

2.2. Animals

All procedures were carried out in accordance with the UK Animals Scientific Procedures Act (1986), the ARRIVE guidelines and the UK Home office License PPL 30/3135. All the rats used in this study were Long Evans and males. The rats were produced from breeding stocks held at Charles River (UK) using a wild-type (WT) x heterozygous design resulting in an average 1:1 WT to *Cyfp1*^{+/-} rat. The mutation was transmitted in Mendelian fashion with no sex bias and the rats were healthy and viable showing no general ill effects of the mutation. The rats were transported to Cardiff at 8 to 10 weeks of age. At Cardiff the rats were housed in mixed-genotype groups of 2 to 3 rats. The rats had daily free access to food and water and lived under the conditions of 12 hours light/day cycle (lights at 7:00 am), room temperature 21±2C°.

2.2.1. Creation of the *Cyfp1* haploinsufficiency rat model

The creation of the *Cyfp1*^{+/-} rat model was done by a collaboration between Cardiff University and Horizon Discovery (St Louis, USA) using CRISPR-Cas9 targeting (<https://www.horizondiscovery.com>). This was possible with the support from a Wellcome Trust Strategic Award, DEFINE. Briefly, CRISPR/Cas9 targeting of the exon 7 of the *Cyfp1* gene at the location 1: 36974-36977 led to the generation of a founder female Long Evans rat with a 4bp out of frame heterozygous deletion in exon 7, and a resulting bioinformatics prediction of an early stop codon in exon 8. A reduction in *Cyfp1* mRNA and protein were validated using qPCR and Western Blot to measure mRNA expression and protein level, respectively. Here, off target effects were assessed and excluded. The F1 founder female was mated with WTs at Horizon Discovery and

generated F2 progeny containing the mutation confirming germ-line transmission. Subsequent F2 generation positive males were exported to Charles River in Lyon, France for re-derivation by embryonic transfer. The resulting specific pathogen free (SPF) progeny were sent to Charles River, Margate, UK, for routine breeding, as explained above. Full information on the creation of the model, confirmation of the heterozygous deletion, assessment of off-target effects, re-derivation, breeding and genotyping can be found in Appendix 1. The data presented in Appendix 1 were kindly provided by Dr. Simon Trent at Cardiff University, who conducted the molecular specification of the novel heterozygous *Cyfp1* rat line.

2.3. Diffusion Tensor Imaging of the brain

The work developed in this thesis involved the use of DTI methods, allowing a non-invasive quantification of white matter microstructural changes in both human carriers of the 15q11.2 BP1-BP2 CNV (Chapters 3 and 4) and *Cyfp1*^{+/-} rats (Chapter 5). In order to understand the sensitivity of this technique to white matter changes, a description of the physical principles and measures taken will be described in this section.

More than 80% of the human body tissue is composed of water and fat that contain many hydrogen atoms. MRI is based on the principle of applying radio frequency (RF) pulses to excite these hydrogen nuclei (protons) in the tissues, and recording the energy released when they return to their relaxed state. Briefly, before entering the MRI scanner, the protons within the body are randomly oriented, and all present a uncoordinated wobbling motion, called precession (**Figure 2.1A**). The MRI scanner includes a powerful magnetic field. When entering the MRI scanner, the protons within the body will change their orientations to align with the direction of the scanner magnetic field (**Figure 2.1B**). Following this, the application of an RF pulse causes a 90° deflection in the orientation of the protons, that are now transversely oriented with the magnetic field (**Figure 2.1C**). The RF pulse also forces the protons to precess at the same time (in phase). When the RF is suspended, the deflected protons return to their previous orientation (aligned with the magnetic field), while emitting their stored energy (**Figure 2.1D**). The time they take to recover the initial orientation is called T₁. As they relax, they also start losing their coordinated motion, and their precessing becomes uncoordinated (out of phase). The time

it takes the protons to fall out of phase is called T_2 . When leaving the scanner, the protons return to their random orientations within the body (**Figure 2.1E**) (*Kagawa et al., 2017*).

During MRI acquisition, a series of short RF pulses are applied following a period of waiting, so the protons can recover and emit MR signal. The signal emitted from the protons is called magnetic echo, and the time between the RF pulse application and the resulting magnetic echo is called echo time (TE). In spin echo MRI imaging, double RF pulses are used, where the time between consecutive pulses is called repetition time (TR). Different tissues exhibit different T_1 and T_2 times, giving rise to different contrasts between tissues (**Figure 2.1F**). Here, manipulating the TE and TR will result in different contrasts of MR images.

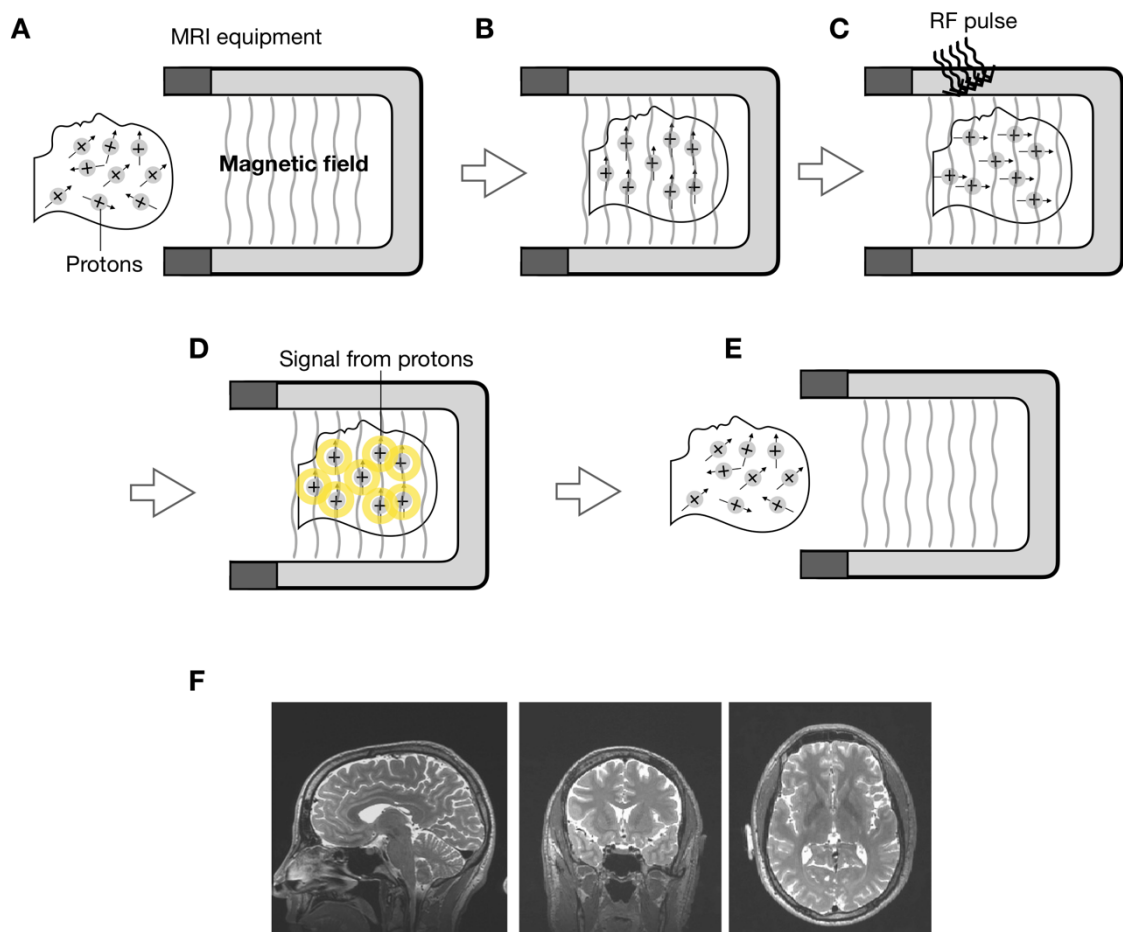


Figure 2.1- Conceptual diagram of image acquisition in MRI.

A Protons are usually oriented in random directions within the body. **B** When in contact with a powerful magnetic field, generated by the MRI magnet, the protons change their orientation to align with the magnetic field. **C** When an RF pulse is applied, the protons become deflected by 90° and start precessing

in synchrony (in phase) storing the energy from the RF pulse. **D** When the RF is suspended, the deflected protons return to their orientation, aligned with the magnetic field, and lose their coordinated precessing while emitting their stored energy. **E** After the scan, the protons become reoriented in random directions within the body. **F** Protons in different tissues will release energy in different speed, giving rise to the tissue contrast seen in MRI scans. Here, representative figures of MRI scans are shown. Figure adapted from *Kagawa et al., 2017*.

Diffusion-weighted MRI (DWI) is based on conventional MRI principles. DWI measures the dephasing of protons in the presence of a spatially-varying magnetic field. This is achieved by using several magnets, called gradients, in different directions that are rapidly switched ‘on’ and ‘off’. This setup is particularly useful to capture the diffusion of water molecules in the human brain (*Jones et al., 2013*). The diffusion of water molecules is characterised by a random motion, also known as Brownian motion. If not restricted, the water molecules will have an isotropic diffusion, moving freely in all directions. When restricted, the water molecules are forced to move in a certain direction, which is known as anisotropic diffusion. The mobility of water molecules in the brain is not always the same in different tissues. For example, in the cerebrospinal fluid (CSF), the water molecules usually display isotropic diffusion. On the other hand, water molecules movement is highly restricted in white matter by the axon walls and myelin sheaths, where diffusion is usually anisotropic (*Soares et al., 2013*).

When applying a gradient, the water molecules moving along the direction of the gradient will cause a signal attenuation. Hence, the degree of anisotropy (how restricted the water movement is) can be easily detected by observing variations in the MR signal when the direction of the gradient is changed. The degree of signal loss can be enhanced by increasing the strength and duration of the diffusion-encoding gradients which are characterised by the b value (s/mm^2). The first quantification of diffusion changes was pioneered by *Stejskal and Tanner, 1965*, who defined the Stejskal-Tanner equation for the b value:

$$b = \gamma^2 G^2 \delta^2 \left(\Delta - \frac{\delta}{3} \right)$$

where, γ is the gyromagnetic ratio, and G , δ , Δ are the amplitude, duration and interval of the diffusion gradient, respectively (**Figure 2.2**).

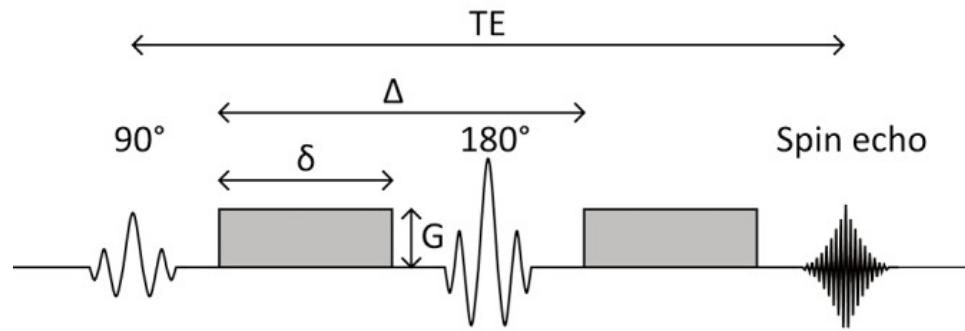


Figure 2.2 – Diffusion-weighted spin echo sequence.

The addition of the two gradients (represented by grey blocks) induces and then reverses a spatially-dependent phase shift. Figure taken from *Winston, 2012*.

DWI are acquired by applying many gradients in different directions, in order to calculate the dominant magnitude of water molecule diffusion within each image voxel. It is therefore understandable why this technique became increasingly popular to characterise white matter structure. As explained, water molecules that travel inside white matter fibres are forced to move within the axon walls. Therefore, by measuring the dominant magnitude of diffusion, we can infer the direction of movement of water molecules and therefore the orientations of the white matter fibres. Here, the introduction of the diffusion tensor (*P.J. Basser et al., 1994a; P.J. Basser et al., 1994b*) was essential for white matter characterisation and fibre reconstruction. The diffusion tensor is a symmetric 3x3 matrix, described by its eigenvalues ($\lambda_1, \lambda_2, \lambda_3$) and eigenvectors (e_1, e_2, e_3). This tensor, illustrated in **Figure 2.3B**, is calculated in each image voxel, where the eigenvalues represent the magnitude of diffusion and the corresponding eigenvectors reflect the direction of diffusion (*Soares et al., 2013*). The diffusion tensor shape reflects the degree of anisotropy; assuming an ellipsoidal shape when diffusion is anisotropic and a spherical shape when diffusion is isotropic. Colour-coded images indicating the direction of diffusion tensor can be used to represent fibre orientation. In **Figure 2.3A**, red, green and blue colours characterise the right-left, anterior-posterior, and superior-inferior directions of the fibre orientations, respectively (*Pierpaoli et al., 1996*).

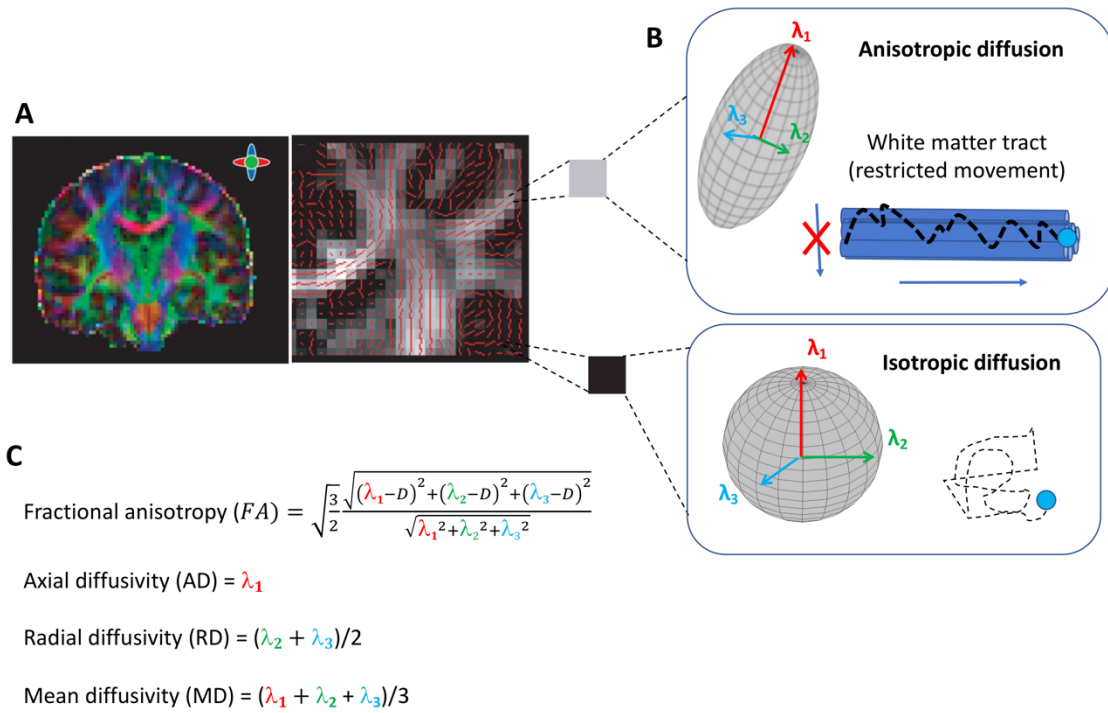


Figure 2.3 – Diffusion tensor and DTI measures.

Representation of **A** DTI images, **B** the diffusion tensor, and **C** quantitative measures extracted from DTI data. The diffusion tensor assumes an ellipsoidal shape when the diffusion of the water molecules is anisotropic. This is characteristic in white matter tracts, where the water molecules are forced to move along the axons. When diffusion is isotropic, the diffusion tensor assumes a spherical shape.

Various quantitative measures can be extracted from the diffusion tensor reflecting the degree of anisotropy of water molecules (*Soares et al., 2013*). In this thesis, the quantitative measures extracted from DTI data were FA, axial diffusivity (AD), radial diffusivity (RD) and mean diffusivity (MD), as shown in **Figure 2.3C**. FA derives from the standard deviation of the three eigenvalues and reflects the degree of anisotropy, ranging from 0 to 1, where values close to 0 reflect isotropic diffusion and values close to 1 reflect anisotropic (more restricted) diffusion. FA can be calculated with the following formula (*Pierpaoli and Basser, 1996*):

$$FA = \frac{\sqrt{\frac{3}{2} \frac{(\lambda_1 - D)^2 + (\lambda_2 - D)^2 + (\lambda_3 - D)^2}{\lambda_1^2 + \lambda_2^2 + \lambda_3^2}}}{1}$$

$$D = \frac{1}{3}(\lambda_1 + \lambda_2 + \lambda_3)$$

AD is the largest eigenvector (λ_1) and reflects the direction of water diffusivity. RD is the mean of the diffusivities perpendicular to the main axis of diffusion $[(\lambda_2+\lambda_3)/2]$. Finally, MD is the average diffusion across all directions $[(\lambda_1+\lambda_2+\lambda_3)/3]$. As explained previously, different tissue components contribute to the restriction of water movement in white matter microstructure, such as cell membranes, macromolecules, myelin sheaths and axon walls. Changes in any of these components can contribute to changes in anisotropy, making DTI a sensitive technique for detecting alterations in white matter microstructure that might not be detectable using conventional MRI (*Beaulieu, 2002*).

2.3.1. DTI data analyses

The DTI measures explained above can be extracted for each voxel, generating FA, AD, RD, and MD maps. The analysis of these maps can be performed using whole-brain approaches or confined to specific anatomical regions or white matter tracts (**Figure 2.4**). To this end, many studies have employed similar approaches to voxel-based morphometry (VBM), which was initially developed for analysis of structural MRI data (*Ashburner and Friston, 2000; Good et al., 2002*). VBM is an automated approach, where each DTI map is first registered into a standard space, and then voxel-wise statistics are carried out to find areas of the brain that correlate to the covariate of interest (e.g., carrier vs non-carrier). However, several concerns have been raised related to the exact alignment of very fine structures and to the standard practice of spatially smoothing data before computing voxel-wise statistics, which can greatly affect the final result (*Abe et al., 2010; Jones et al., 2005*). *Smith et al., 2006* developed a new approach to carry out voxel-by-voxel analysis, named Tract-Based Spatial Statistics (TBSS), which confines the analyses to a thinned white matter skeleton based on a “mean FA skeleton”. In this approach, DTI data is projected into a common space in a way that is not dependent on perfect nonlinear registration, and no spatial smoothing is necessary during image processing.

Single-voxel analyses is done by testing each voxel separately. This analysis is inherently limited given to the potential noise in each individual voxel. Furthermore, the

very large number of statistical tests involving tens of thousands of voxels requires adjusting the p-values for multiple comparisons, and this procedure may reveal only the voxels with higher noise, instead of real effects. Cluster-based threshold methods were shown to provide higher sensitivity to finding true signals than single-voxel analysis. In this method, clusters of multi-voxel data are compared to each other. However, a limitation of this method is the need to define, *a priori*, an initial cluster-forming threshold, which can largely impact results. Here, [Smith and Nichols, 2009](#) developed the Threshold-free cluster-enhancement (TFCE) method for enhancing cluster-like features in a statistical image, without having to previously define these clusters. This method was found to provide greater sensitivity in general, than commonly-used methods.

Region-of-interest (ROI) approaches, like atlas-based segmentation of DTI maps and tractography, allow the investigation of anatomically pre-defined brain regions. In both approaches, specific white matter tracts are defined and a mean DTI value is extracted from each tract. Atlas-based segmentation of DTI maps is done automatically by aligning all subjects to a template, where mean DTI values are extracted from regions delineated in the atlas. Tractography methods allow for an *in vivo* reconstruction of specific fibre pathways in the brain, providing a better tract-specific anatomical validity than segmentation of DTI maps. Using the information from the diffusion tensor, fibre tractography pieces together the orientation of diffusion in each voxel to infer fibre trajectories. Here, mathematical methods were developed to extract these trajectories within each voxel in discrete steps to form white matter tracts, allowing the visual representation of diffusion directions along white matter fibres ([Pierpaoli et al., 1996](#); [Mori et al., 1999](#); [Jones et al., 1999](#); [Catani et al., 2002](#)). This method relies on manually delineation of ROIs and visual inspection to exclude any tracts that do not belong to the tract-of-interest.

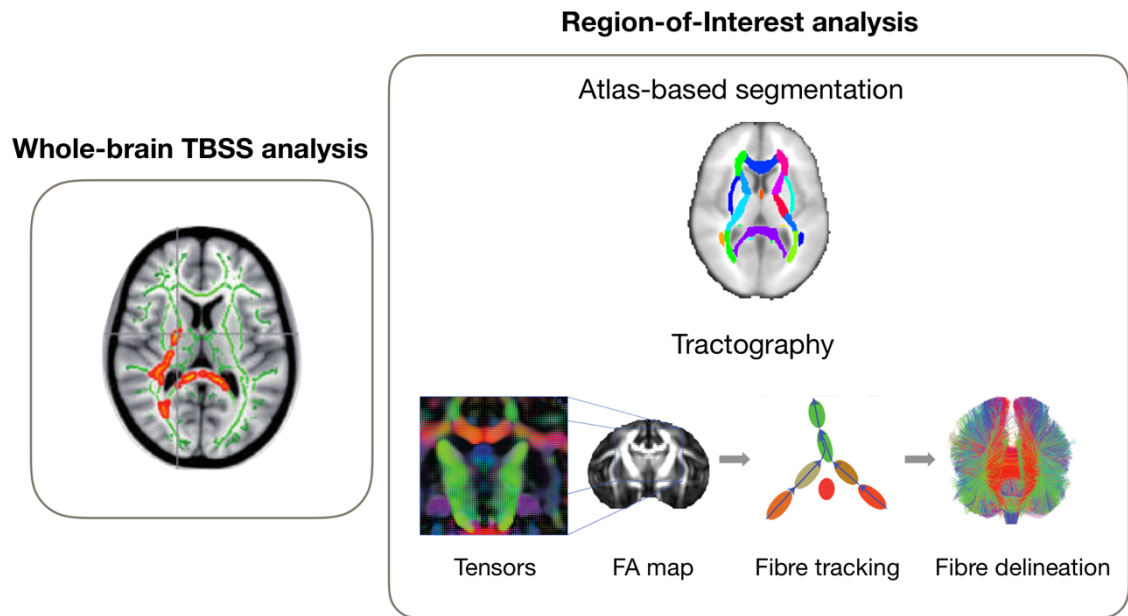


Figure 2.4 – Different approaches to analyse DTI data.

In whole-brain TBSS analysis, the analysis is confined to a thinned white matter skeleton (represented in green) based on a “mean FA skeleton”. Here, areas showing significant changes in DTI measures can be visualised by overlying a p-value map, where a threshold can be used (e.g., $p < 0.05$) to only visualise significant changes (represented in red). Regional-of-interest analyses can be done using an automated atlas-based segmentation, where mean values from defined regions are extracted from the DTI maps. Tractography allows the reconstruction of white matter tracts providing a better tract-specific anatomical validity.

A single white matter voxel contains hundreds of thousands of fibres, as well as other tissue components. In each voxel, distinctly different fibre configurations may be present. The presence of crossing fibres have a remarkable impact in DTI signal, where it has been reported that between 60% to 90% of white matter voxels contain crossing fibres (*Jeurissen et al., 2013*). Some methods have been developed to resolve this problem, but their application was not possible in this thesis (see discussion in Chapter 3). Furthermore, several cellular consequences can affect the DTI signal, making it difficult to interpret the physiological meaning of DTI outcomes. One way to validate and further explore cellular causes underlying DTI outcomes is by performing histology on the brain tissue. Nevertheless, DTI allows a non-invasive in vivo characterisation of white matter microstructure, where specific regions affected by a certain condition can be identified (*Jones et al., 2013*).

Chapter 3

White Matter Changes Associated With Copy
Number Variation at 15q11.2 BP1-BP2

3.1. Abstract

Background

The 15q11.2 BP1-BP2 CNV has been associated with a range of neurodevelopmental disorders including learning and motor delays, ASD, and schizophrenia. *CYFIP1* is a candidate gene in this region, and dysregulations in this gene are thought to be strongly associated with 15q11.2 BP1-BP2 associated phenotypes. *CYFIP1* gene product is known to play important roles in control of cytoskeletal dynamics and protein translation. The regulation of protein translation occurs due to interactions with FMRP, and absence of FMRP is known to cause FXS. Since abnormal white matter microstructure has been reported in both FXS and neurodevelopmental disorders, this study will investigate the impact of 15q11.2 BP1-BP2 dosage on white matter microstructure.

Methods

DTI data were collected from a sample of individuals divided in carriers of the 15q11.2 BP1-BP2 deletion (n=30), carriers of the reciprocal duplication (n=27), together with an IQ-matched control group of subjects with no large CNVs (n=19). All the subjects were recruited from a large genotyped population sample from Iceland and none had a clinical diagnosis. Here, brain-wide voxel differences were explored, using the TBSS method, and regional differences were further quantified using a regional atlas-based approach. Furthermore, age and gender interactions with 15q11.2 BP1-BP2 CNV dosage were also assessed.

Results

Global mirror effects (deletion > control > duplication) were found on FA, whereas effects in the opposite direction (duplication > control > deletion) were found in RD and MD. Significant white matter differences between groups were found between deletion and duplication carriers. The largest effect sizes for increased FA in the deletion carriers were found bilaterally in the posterior limb of the internal capsule, left inferior longitudinal fasciculus and in the left external capsule. Further preliminary and exploratory analyses suggest different trajectories of white matter integrity with age in each group, and different magnitude of effect in males and females.

Conclusions

These results show a reciprocal effect of the 15q11.2 BP1-BP2 CNV on white matter microstructure, providing evidence that reciprocal chromosomal imbalances may lead to opposite changes in brain structure. Findings in the deletion carriers overlap with previous white matter differences reported in FXS patients, suggesting common pathogenic mechanisms derived from disruptions of CYFIP1-FMRP complexes. These data begin to identify specific components of the neural phenotypes associated with copy number variation at 15q11.2 BP1-BP2 and thus neurobiological mechanisms of potential relevance to the increased risk for neurodevelopmental disorder associated with variation at this chromosomal locus.

3.2. Introduction

The 15q11.2 BP1-BP2 CNV microdeletion is emerging as a recognised syndrome and has been associated with developmental, speech, language, and motor delays (*Butler, 2017; Cox and Butler, 2015*), and also increased susceptibility for epilepsy (*de Kovel et al., 2010*), ADHD (*Cox and Butler, 2015*), ASD (*Chaste et al., 2014*), and schizophrenia (*Stefansson et al., 2008*). Not all the individuals with the microdeletion/microduplication are affected, and the genes in this region have variable expressivity. Previous research (*Stefansson et al., 2013*) has suggested that individuals with the deletion, and without a current clinical diagnosis, frequently report mild-to-moderate impairments in motor function and deficits across several cognitive domains, revealing more severe impairments in mathematics and reading skills; while individuals with the reciprocal duplication perform to a similar level as population control subjects with no large CNVs. In a recent study by *Ulfarsson et al., 2017*, these cognitive deficits in clinically healthy deletion carriers were shown to be accompanied by structural changes in the brain, as assessed by structural MRI, showing reciprocal structural effects between the deletion and the duplication, as well as different patterns of functional activation in the brain when combining functional MRI with tasks involving reading and mathematics. In both *Stefansson et al., 2013* and *Ulfarsson et al., 2017* studies, evidence of white matter macrostructural changes was found, where both studies reported increases in the corpus callosum (CC) volume in deletion carriers, and mirrored reductions in duplication carriers. However, the effects on white matter microstructure cannot be assessed using structural MRI, and DTI studies are needed.

Altered white matter microstructure has been consistently reported in developmental disorders. Several DTI studies in schizophrenia have suggested a degree of heritability of white matter phenotypes on the basis that disrupted white matter is also often observed in close relatives of these patients (*Baaré et al., 2001; White et al., 2002; Scamvougeras et al., 2003*). Therefore, a key question for neurobiological research is whether genetic risk factors contribute to neurobiological mechanisms that underlie white matter changes associated with developmental disorders, and more specifically whether individual CNVs that increase risk for neurodevelopmental disorders are also associated with changes in white matter and brain connectivity; and if so how disruptions in individual genes may contribute to these phenotypes. Previous studies have looked at white matter phenotypes in different CNVs, where white matter changes were reported

in 16p11.2 (reciprocally for the deletion and duplication) (Chang et al., 2016), in Williams syndrome (caused by deletions at the 7q11.23 region) (Hoeft et al., 2007), and in 22q11.2 deletion (Nuninga et al., 2018) CNVs. However, no study to date has looked at white matter microstructural changes associated with the 15q11.2 BP1-BP2 region.

The 15q11.2 BP1-BP2 region contains four genes: *NIPAI*, *NIPA2*, *CYFIP1*, and *TUBGCP5* (Chai et al., 2003). The four genes are highly conserved and expressed in the brain (Bittel et al., 2006) and may be of potential relevance to psychopathology. Moreover, mutations in each gene have been associated with different disorders: *NIPAI* with autosomal-dominant hereditary spastic paraplegia (Rainier et al., 2003), *NIPA2* with childhood absence epilepsy (Xie et al., 2014, p. 2), *TUBGCP5* with ADHD and obsessive-compulsive disorder (Grabli et al., 2004), and *CYFIP1* with increasing susceptibility to ASD (Toma et al., 2014) and schizophrenia (Tam et al., 2010). When it comes to mechanisms with potential impact on white matter integrity, *NIPAI* and *CYFIP1* were shown to be involved in mechanisms that, when dysregulated, have the potential to affect white matter microstructure. *NIPAI* was found to inhibit the BMP signalling via interaction with BMP receptor type II, which is crucial for typical axonal growth, guidance, and differentiation (Tsang et al., 2009). In a *Drosophila* model, enhanced BMP signalling resulted in abnormal distal axonal overgrowth at the presynaptic neuromuscular junction (X. Wang et al., 2007). *CYFIP1*, on the other hand, is known to be involved in a number of key brain plasticity-related functions, having a crucial role in actin remodelling during neural wiring (Eden et al., 2002; Steffen et al., 2004; Chen et al., 2010), in which dysregulations could result in changes in axonal density, organisation, and myelination (Dent and Gertler, 2003; Bauer et al., 2009; Kevenaar and Hoogenraad, 2015). Furthermore, *CYFIP1* protein is known to interact with FMRP, the gene product of *FMRI*, to regulate mRNA translation in neuronal dendrites, which underlies synaptic plasticity and brain development (De Rubeis et al., 2013; Napoli et al., 2008). Mutations in *FMRI* are causative for FXS, a condition associated with intellectual disability and a range of psychiatric symptoms (Lozano et al., 2014).

Abnormal white matter microstructure has been previously reported in FXS patients, where two recent studies (Green et al., 2015; Hall et al., 2016) used DTI to assess white matter microstructural changes in FXS patients, comparing this group with subjects without FXS but with similar IQ and levels of autistic symptoms (minimising confounding effects owing to intellectual ability). The authors found increased FA, as well as decreased RD and MD across several white matter tracts. Given the close

molecular links between CYFIP1 and FMRP, it is anticipated that some degree of phenotypic overlap may be present in FXS and 15q11.2 BP1-BP2 deletion.

In this chapter, DTI methods will be used to explore how variations in the 15q11.2 BP1-BP2 CNV region affect white matter microstructure in an adult sample. This sample was selected from the Icelandic population, and analysed through a collaboration with the deCODE genetics Institute in Iceland. None of the subjects included in the study had a clinical diagnosis of a neurodevelopmental disorder, thereby minimising the potential confound of illness-related effects such as psychotropic medication. Deletion and duplication carriers were compared to a sample of population controls with no large CNVs but matched IQ in order to evaluate the extent of any reciprocal effects on white matter microstructure. The analyses comprised a brain-wide voxel-based approach and a regional atlas-based analysis, allowing quantification of the magnitude of regional changes. This chapter further includes exploratory preliminary analyses looking at age trajectories in relation to DTI metrics and sex differences dependent on dosage. The aim of this study was to begin to identify specific components of the 15q11.2 BP1-BP2 phenotype and mechanisms of potential relevance to the increased risk for disorder.

3.3. Material and Methods

3.3.1. Participants

In total, 30 individuals with the 15q11.2 BP1-BP2 deletion, 27 with the reciprocal duplication, and 19 controls without large CNVs (NoCNV) were recruited from a large genotyped sample, as part of the ongoing gene discovery work in deCODE genetics institute, based in Reykjavik in Iceland. None of the subjects included in this study carried any other large CNVs. This study was possible through a collaboration involving Cardiff University and deCODE genetics institute. The gene discovery work in deCODE genetics institute involved the collection of genotypic and medical data from more than 160 000 volunteer participants, representing half of the Icelandic population, allowing large-scale studies of common diseases, and in particular neuroimaging studies on carriers of genetic risk variants for neurodevelopmental disorders (*Stefansson et al., 2013*). The sample was genotyped by Illumina HumanHap (300, 370, 610, 1M, 2.5M) and Illumina Omni (670, 1M, 2.5M, Express) SNP arrays. BeadStudio (Illumina, version 2.0) was used to call

genotypes, normalise signal intensity data and establish the log R ratio and B allele frequency at every SNP. Samples passing quality control were examined using PennCNV (*K. Wang et al., 2007*). All putative neuropsychiatric CNVs and other CNVs not known to be associated with schizophrenia or autism were visually inspected using DosageMiner software (developed at deCODE genetics). In 101 655 subjects, more than 1200 subjects carrying one or more neuropsychiatric CNVs were found (1.16% of the sample). More information can be found in the supplementary table 1 of *Stefansson et al., 2013* study.

The recruited subjects for this study were aged between 21 and 66 years old, and the number of females and males was the same (38 males and 38 females) and balanced in each condition group. Approval for this study was obtained from the National Bioethics Committee of Iceland and the Icelandic Data Protection Authority. Subjects were not included in the study if they had:

- 1) ICD-10 or DSM-IV diagnoses for schizophrenia, schizoaffective or bipolar disorder; if they were diagnosed with autism, intellectual disability, or developmental delay at the State Diagnostic and Counselling Centre of Iceland (serves children and adolescents with a disability);
- 2) Psychosis criteria on the MINI (*Sheehan et al., 1998*) interview;
- 3) Diagnosis for schizophrenia, schizoaffective, bipolar disorder, autism, intellectual disability, or developmental delay according to self-reports (or reports from parents) or if they were using antipsychotic medication.

The IQ scores were assessed using an Icelandic version of the Wechsler Adult Intelligence Scale (WASI-I) (*Woerner and Overstreet, 1999; Guðmundsson, 2016*) including four subtests: vocabulary and similarities, both tests of verbal IQ, and matrix reasoning and block design, both tests of performance IQ. The psychologists evaluating all subjects were blind to genotype. There were no significant differences in the IQs between groups (deletion vs NoCNV: $t = 1.37$, $p = 0.2$; duplication vs NoCNV: $t = 1.55$, $p = 0.1$), as assessed by an unpaired two-tailed t-test. It is important to notice that, although all the individuals with the deletion were tested, only 11 out of 19 NoCNV, and 26 out of 27 duplication groups were tested. Demographic information is described in **Table 3.1**, and family relationships between subjects are further described in Appendix 1. The recruitment, genotyping, cognitive testing, and collection of neuroimaging data was done at deCODE genetics institute before the beginning of this project.

Table 3.1- Subject characteristics.

Abbreviations used: F – Female, IQ - intelligence quotient, M – Male, NoCNV – with no large copy number variants, sd – standard deviation.

15q11.2 BP1-BP2	Mean age in years (sd, range)	Gender	IQ score^a (sd)	Number of subjects
Deletion	42.83 (12.5, 21 – 65)	14 M, 16 F	101.2 (13.8)	30
NoCNV	38.95 (10.56, 22 – 59)	12 M, 7 F	108.3 (16.9)	19
Duplication	43.48 (13.51, 22 – 66)	12 M, 15 F	100.8 (11.8)	27

^a Icelandic version of the WASI-I including four subtests (Vocabulary, Similarities, Block Design and Matrix Reasoning) (*Woerner and Overstreet, 1999*). The test was performed in all individuals with the deletion, in 11 out of 19 individuals with NoCNV and in 26 out of 27 individuals with the duplication.

3.3.2. Diffusion MRI acquisition and pre-processing

MRI data were acquired on a Philips Achieva 1.5T system (Phillips Healthcare, Eindhoven, The Netherlands). A diffusion-weighted spin-echo echo planar imaging (EPI) sequence with sensitivity encoding (SENSE) acceleration was used. 17 non-co-linear gradient diffusion-weighted images at $b=800$ s/mm² and one non-weighted ($b=0$ s/mm²) image were acquired with the following parameters: TE=72 ms, TR=9024 ms, 60 slices, slice thickness=2 mm, field-of-view (FoV)=240×240 mm, acquisition matrix=144×144, resulting in data acquired with a 1.67×1.67×2 mm voxel resolution.

DWI data were pre-processed using ExploreDTI v.4.8.3 (*Leemans et al., 2009*) in MATLAB R2015a (The MathWorks, Inc., Natick, Massachusetts, United States). First, the Brain Extraction Tool (BET, <http://www.fmrib.ox.ac.uk/fsl/>) was used to remove non-brain tissue. The EPI acquisition allows a rapid scanning, but is highly sensitive to inhomogeneities in the magnetic field, producing nonlinear geometric distortions, which can result in displacement of anatomical structures (*Wu et al., 2008*). The strong gradients used for diffusion encoding also create eddy currents, which contribute to increased geometric distortions. Within the ExploreDTI pipeline, eddy currents and head motion corrections were performed using an affine registration to the non-diffusion weighted B₀-images, with appropriate rotation of the encoding vectors (*Leemans and Jones, 2009*). EPI distortions were corrected by registering each image volume to high resolution T₁-

weighted images. Each DWI was nonlinearly warped to the T₁-weighted image using the FA maps from the DWIs as a reference. Warps were computed using Elastix (*Klein et al., 2010*), by using normalised mutual information as the cost function and constraining deformations to the phase-encoding direction (PA). The corrected DWIs were therefore transformed to the same (undistorted) space as the T₁-weighted structural images. ExploreDTI was used to generate whole-brain maps of FA, AD, RD, and MD.

3.3.3. Tract-Based Spatial Statistics Analysis (TBSS) of DTI

The corrected FA, AD, RD, and MD maps were analysed using the TBSS (*Smith et al., 2006*) tool available in FMRIB Software Library (FSL, <https://fsl.fmrib.ox.ac.uk/fsl/fslwiki>). TBSS is a whole-brain analysis that starts with a non-linear registration of the FA maps to a standard FA template, in this case the standard FMRIB58_FA (FSL FA adult template) was used. Following registration, a mean FA map was calculated, thinned and averaged to represent a study-specific mean FA skeleton. An optimal threshold of 0.2 was applied to the mean FA skeleton to exclude voxels that were primarily grey matter or cerebrospinal fluid (therefore with lower FA values), in order to create a binary white matter skeleton mask. Afterwards, all the AD, RD, and MD maps were also registered to the FMRIB58_FA template. Using the registered maps, the local FA-maxima, as well as the AD-, RD- and MD- maxima of each subject was projected onto the white matter skeleton.

General linear models were created to investigate copy number effects at 15q11.2 BP1-BP2. Statistically significant differences were first assessed with a multiple regression model (*duplication*>*NoCNV*>*deletion* and *deletion*>*NoCNV*>*duplication*). Total intracranial volume (TIV), age, and sex were included as covariates of no interest. Differences in DTI measures between groups were assessed using voxel-wise independent t-tests (deletion vs NoCNV, duplication vs NoCNV, and deletion vs duplication), where six different contrasts were used to assess group differences (**Table 3.2**). The randomize function from FSL was used with the TFCE approach (*Smith and Nichols, 2009*), generating cluster-size statistics based on 5000 random permutations. To correct for multiple comparisons, a family-wise error (FWE) approach was used with a threshold of $p < 0.05$. Anatomical white matter regions showing significant group

differences were identified with the John Hopkins University (JHU) white matter atlas (ICBM-DTI-81) (*Mori et al., 2005*).

3.3.4. Regional DTI Parameters analyses

Regional values of FA, AD, RD, and MD were obtained by averaging over the intersecting voxels between the white matter DTI maps with the JHU white matter atlas (ICBM-DTI-81), which comprises 48 tracts (*Mori et al., 2005*). From the atlas, the mean values from 30 segmented white matter tracts were considered for analyses (**Table 3.3**). Statistical analyses were carried out in RStudio statistical software *version 1.1.463* (R Foundation for Statistical Computing, Vienna, Austria). Before statistical analyses, all DTI variables within each white matter tract were checked for Gaussian distribution, using Shapiro-Wilk test, and for homogeneity of variance, using Levene's test ($p < 0.05$). Data that failed normality test were visual inspected using histograms and further Q-Q plots were examined to assure that residuals were normally distributed. Furthermore, data were inspected for outlier detection, where data points placed three standard deviations from the mean were considered outliers. Log-transformations were also applied for data that failed the normality check even after outlier removal. All the analyses were performed with all data points and with data after outlier removal and transformations. Both analyses lead to similar results, which showed that the results were not driven by outliers in the data. Therefore, results presented in this chapter include all the data points.

To investigate the effect of dosage within white matter regions, linear regression analyses were performed for each DTI measure and for each white matter tract, regression out age, sex and TIV as covariates of no interest. Following this, *post hoc* pairwise comparisons were performed to measure differences between groups (*deletion vs NoCNV*, *duplication vs NoCNV*, and *deletion vs duplication*). To account for multiple testing, the standard false discovery rate (FDR) method based on the Benjamini-Hochberg approach (*Benjamini and Hochberg, 1995*) was used, considering the relation between different white matter tracts and between DTI metrics. In Benjamini-Hochberg approach, a p-value is considered significant when the FDR corrected p-value ($p.adjust_i$) is smaller than 0.05, where $p.adjust_i$ is determined by the rank (R_i) of the p-value (p_i), after putting the individual p_i from each test in ascending order, and the number of tests (n): $p.adjust_i = p_i * (n/R_i)$.

After evaluating the statistical significance of these differences, the substantive significance was also determined by calculating Cohen's d effect sizes (*Cohen, 1977*). In order to investigate the magnitude of reciprocal effects in the deletion and duplication cohort, Cohen's d effect sizes were calculated comparing *deletion vs NoCNV* and *duplication vs NoCNV* and plotted using diverging bars. Cohen's d effect sizes were also calculated for differences between deletion and duplication cohorts. The Cohen's d effect sizes were calculated by measuring the standardised differences between two groups: $\text{adj_mean (group1)} - \text{adj_mean (group2)} / \text{standard deviation}$, where *adj_mean* is the adjusted mean of each group corrected for age, sex, and TIV. The adjusted mean of each group was computed using the residuals from the linear regression model: $\text{lm}(\text{genotype} \sim \text{age} + \text{sex} + \text{TIV})$. Cohen classified effect sizes as negligible ($d < 0.2$), small ($d > 0.2$), medium ($d > 0.5$), and large ($d > 0.8$), in accordance with *Cohen, 1977*.

3.3.5. Age trajectories

As a preliminary analysis, age-by-dosage and the quadratic age²-by-dosage interactions were also evaluated in the regional analysis for each white matter tract. For the white matter tracts showing a significant linear or quadratic interaction (without correction), linear or quadratic models were fit to global FA, MD, RD, and AD over age, separately for deletions, NoCNVs, and duplications.

3.3.6. Sex differences

In order to examine differences between male and female phenotypes in relation to CNV dosage, a sex-by-dosage interaction was also evaluated. As an exploratory investigation of sex differences, the effect sizes for the male and female cohorts were further analysed separately, in the same way described for the whole-group analysis.

3.4. Results

3.4.1. Between-group TBSS analysis

TBSS was used to assess group-wise microstructural differences in major white matter pathways throughout the brain. F statistics showed extensive significant differences in the direction *deletion*>*NoCNV*>*duplication* in FA, and *duplication*>*NoCNV*>*deletion* in AD, RD, and MD. Further pairwise comparisons showed extensive and global increased FA, and decreased AD, RD, and MD in deletion carriers compared to duplication carriers. These differences were seen in major white matter tracts, such as the corpus callosum (CC), superior longitudinal fasciculus (SLF), inferior longitudinal fasciculus (ILF), and internal capsule (IC). Moreover, the deletion also showed increased FA when compared with NoCNV in the posterior thalamic radiation (PTR). The duplication showed significantly increased AD when compared with NoCNV. The contrasts that gave rise to significant voxel-wise results ($p < 0.05$, FWE corrected) are summarised in **Table 3.2** and TBSS results are displayed in **Figure 3.1**.

Table 3.2 – Summary of between group TBSS analyses results.

Significant voxel-wise comparisons ($p < 0.05$) are presented with a + (less significant), ++ (more significant), and non-significant results ($p > 0.05$) by a –. All the p-values were corrected using the TFCE algorithm in TBSS.

Contrasts	Whole-group analysis			
	FA	AD	RD	MD
Del > NoCNV	+	–	–	–
NoCNV > Del	–	–	–	–
NoCNV > Dup	–	–	–	–
Dup > NoCNV	–	+	–	–
Del > Dup	++	–	–	–
Dup > Del	–	+	++	+

Table 3.3- White matter tracts and abbreviations used.

White matter tracts	Abbreviations
Genu Corpus Callosum	GCC
Body Corpus Callosum	BCC
Splenium Corpus Callosum	SCC
Right and left Corticospinal tract	CST_R; CST_L
Right and left Anterior Limb of the Internal Capsule	ALIC_R; ALIC_L
Right and left Posterior Limb of the Internal Capsule	PLIC_R; PLIC_L
Right and left Anterior Corona Radiata	ACR_R; ACR_L
Right and left Superior Corona Radiata	SCR_R; SCR_L
Right and left Posterior Corona Radiata	PCR_R; PCR_L
Right and left Posterior Thalamic Radiation	PTR_R; PTR_L
Right and left Inferior Longitudinal Fasciculus	ILF_R; ILF_L
Right and left External Capsule	EC_R; EC_L
Right and left Cingulum (cingulate gyrus portion)	C_CG_R; C_CG_L
Right and left Cingulum (hippocampal portion)	C_HIP_R; C_HIP_L
Right and left Superior Longitudinal Fasciculus	SLF_R; SLF_L
Right and left Uncinate Fasciculus	UF_R; UF_L

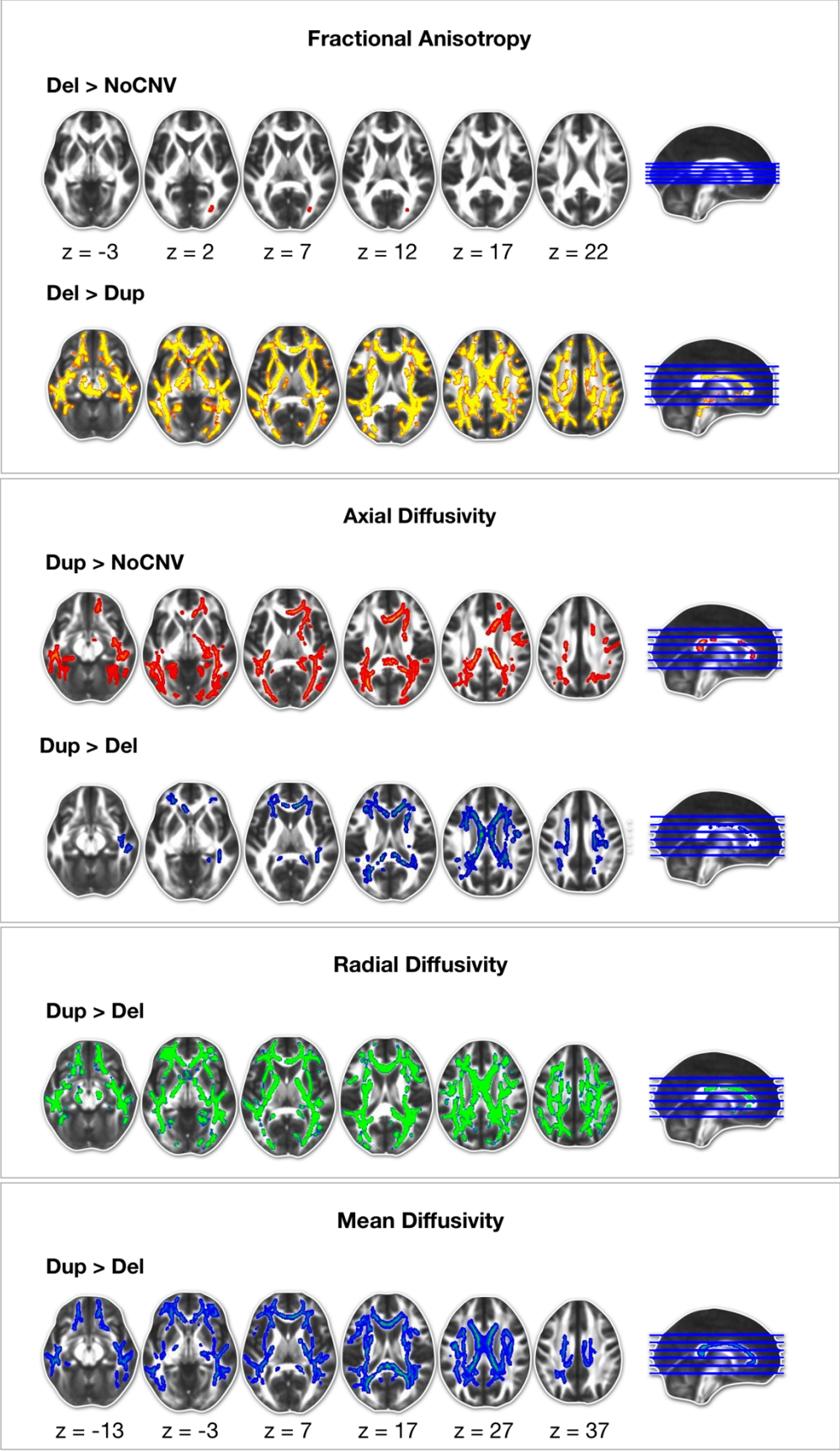


Figure 3.1 - TBSS whole-group voxel-based analysis.

Significant results for the two-sample t-test showing group differences between subjects with the deletion (Del, n=30), duplication (Dup, n=27), and no large copy number variants (NoCNV, n=19), for fractional anisotropy, axial diffusivity, radial diffusivity, and mean diffusivity maps. Here, only contrasts that gave rise to significant results after correction are displayed ($p < 0.05$, FWE corrected). Within the significant results, red and blue code for less significant results and yellow and green for more significant results. The deletion showed widespread increased FA compared with duplication and NoCNV groups, and decreased AD, RD, and MD compared with duplication group. The duplication showed increased AD compared with NoCNV group.

3.4.2. Between-group regional analyses

Results from the atlas-based segmentation analysis were consistent with the whole-brain TBSS analysis. Plots of the data confirmed the overall pattern of increased FA in the deletion compared to the duplication cohort, with the NoCNV group lying intermediate between these groups, and indicating a mirror effect of 15q11.2 BP1-BP2 dosage (**Figure 3.2**). The pairwise comparisons showed differences that, after FDR correction, were only significant between the deletion and duplication carriers (**Table 3.4**). **Figure 3.3** shows the Cohen's d effect sizes for deletion and duplication carriers when compared to the NoCNV group. Here, a clear reciprocal effect can be noticed, where deletion carriers predominantly show increased FA, and decreased RD and MD, whereas duplication carriers show decreased FA, and increased RD and MD. There were a few white matter tracts where a reciprocal effect was not observed: left anterior limb of the internal capsule (ALIC_L), right cingulum of the hippocampal portion (C_HIP_R), and left uncinate fasciculus (UF_L). Interestingly, deletion carriers showed an increased FA trend in all white matter tracts with exception of the fornix and right and left corticospinal (CST_R, CST_L), where reciprocal effects are seen in the opposite direction (decreased FA in deletion and increased FA in duplication carriers) – however, these effects were negligible. **Figure 3.3** also shows that, although the results are very consistent in FA, RD and MD metrics, changes in AD seem to be less consistent where increases and decreases in AD in different white matter changes are seen in deletion and duplication carriers.

The largest effect size for the significant differences seen between deletion and duplication carriers, was observed in the right and left posterior limb of the internal capsule (PLIC_R, PLIC_L) and in the left external capsule (EC_L) for increased FA and decreased RD in the deletion carriers **Figure 3.4**. Across the whole-brain (average FA

skeleton), the effect size was medium in FA (Cohen's $d = 0.74$), RD (Cohen's $d = -0.66$), and MD (Cohen's $d = -0.65$), and small for AD (Cohen's $d = -0.36$), according to Cohen's criteria (Cohen, 1977).

As some of the subjects were related, the data were reanalysed using only one member from each family. The results were consistent with initial findings/primary analyses. However, a few white matter tracts became non-significant, possibly due to the loss of power from reducing the sample to 65 subjects (Appendix 1).

Table 3.4 - Group differences between deletion and controls with NoCNV, duplications and NoCNV, and deletions and duplications carriers.

Effect of 15q11.2 BP1-BP2 CNV dosage are shown for FA, AD, RD, and MD. Groups were compared as defined in the dependent variable column, and the direction of effect is represented by a positive or negative value. Here only white matter tracts showing significant differences when comparing deletions to duplications carriers are shown. (* < 0.05, ** < 0.01, ***<0.001). White matter tracts abbreviations can be found on **Table 3.3**.

	Dependent variable	ROI	<i>t value</i>	<i>p-value</i>	<i>p-value (FDR)</i>	Effect size
FA	Del vs NoCNV	PLIC_R	2.54	0.013	0.28	0.77
		PLIC_L	1.97	0.05	0.42	0.57
		ILF_L	2.26	0.03	0.36	0.71
		EC_R	2.99	0.004	0.15	0.85
		EC_L	3.57	0.0006	0.08	1.03
		C_CG_L	1.48	0.14	0.47	0.42
	Dup vs NoCNV	PLIC_R	-0.64	0.52	0.78	-0.23
		PLIC_L	-1.66	0.1	0.78	-0.51
		ILF_L	-0.59	0.56	0.78	-0.21
		EC_R	0.19	0.85	0.93	0.003
		EC_L	-0.2	0.84	0.93	-0.15
		C_CG_L	-1.05	0.3	0.78	-0.36
	Del vs Dup	PLIC_R	3.68	0.0004	0.01*	1
		PLIC_L	4.20	0.00007	0.005**	1.19
		ILF_L	3.29	0.002	0.03*	0.85
		EC_R	3.26	0.002	0.03*	0.80
		EC_L	4.38	0.00004	0.005**	1.05
		C_CG_L	2.93	0.004	0.04*	0.77
AD	Del vs NoCNV	BCC	-2.52	0.01	0.28	-0.72
		PLIC_L	1.12	0.27	0.57	0.30
	Dup vs NoCNV	BCC	0.52	0.61	0.78	0.23
		PLIC_L	-1.37	0.18	0.78	-0.50
	Del vs Dup	BCC	-3.52	0.0008	0.02*	-0.88
		PLIC_L	0.88	0.005	0.04*	0.76

RD	Del vs NoCNV	PLIC_R	-1.81	0.07	0.43	-0.53
		PLIC_L	-1.81	0.08	0.43	-0.55
		ACR_R	-0.44	0.66	0.87	-0.15
		EC_R	-1.87	0.066	0.43	-0.58
		EC_L	-3.02	0.004	0.15	-0.95
		C_CG_L	-1.35	0.18	0.47	-0.39
	Dup vs NoCNV	PLIC_R	0.67	0.5	0.78	0.24
		PLIC_L	1.45	0.15	0.78	0.44
		ACR_R	2.11	0.04	0.62	0.64
		EC_R	0.55	0.58	0.78	0.21
		EC_L	0.34	0.73	0.89	0.15
		C_CG_L	1.38	0.17	0.78	0.46
	Del vs Dup	PLIC_R	-2.88	0.005	0.04*	-0.77
		PLIC_L	-3.77	0.0003	0.01*	-1.05
		ACR_R	-2.95	0.004	0.04*	-0.75
EC_R		-2.81	0.006	0.04*	-0.71	
EC_L		-3.89	0.0002	0.009**	-1.00	
C_CG_L		-3.16	0.002	0.03*	-0.84	
MD	Del vs NoCNV	BCC	-2.02	0.04	0.43	-0.62
		SCC	-0.61	0.54	0.76	-0.20
		ACR_R	-0.27	0.79	0.93	-0.10
		EC_L	-2.11	0.04	0.43	-0.68
	Dup vs NoCNV	BCC	0.68	0.5	0.78	0.24
		SCC	2.15	0.03	0.62	0.66
		ACR_R	2.3	0.02	0.62	0.69
		EC_L	0.51	0.61	0.78	0.18
	Del vs Dup	BCC	-3.13	0.003	0.03*	-0.80
		SCC	-3.19	0.002	0.03*	-0.83
		ACR_R	-2.96	0.004	0.04*	-0.76
		EC_L	-3.04	0.003	0.03*	-0.82

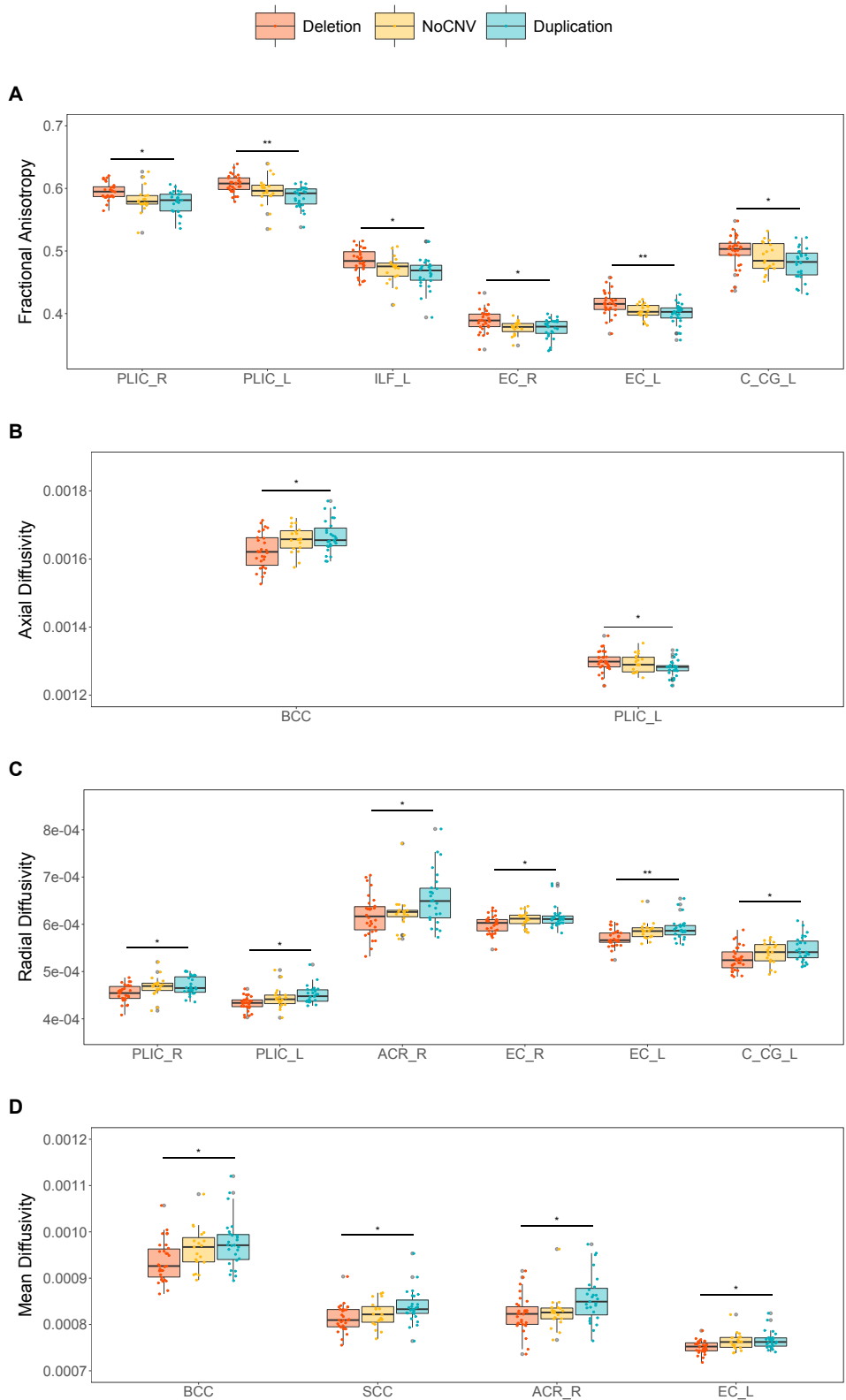
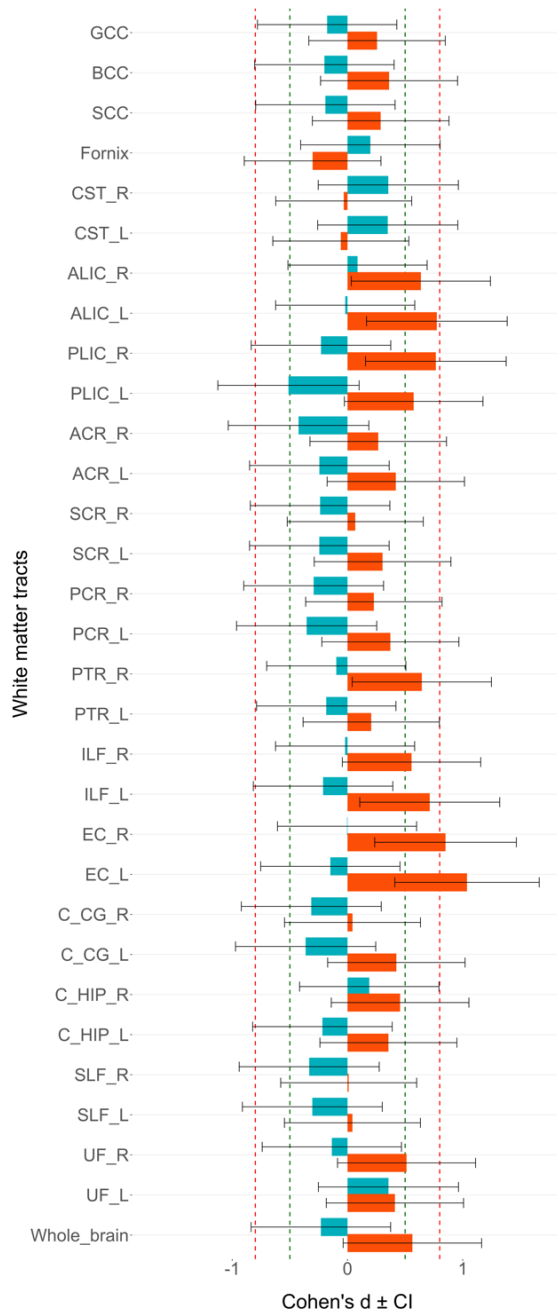


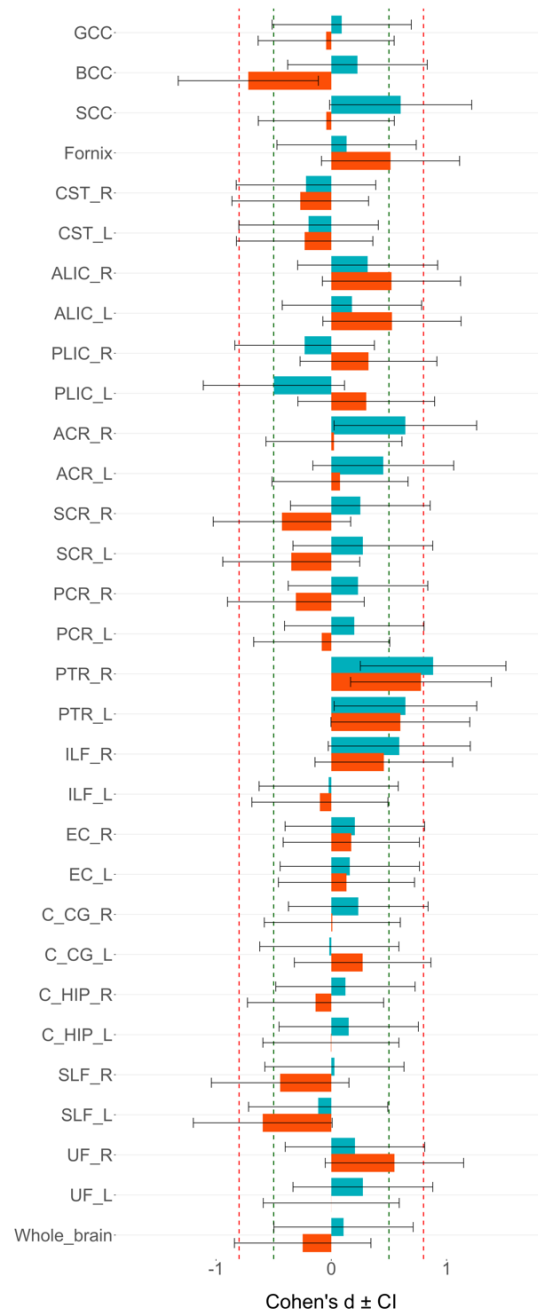
Figure 3.2 - Boxplots showing group differences for atlas-based segmentation analyses.

Significant pairwise group differences after FDR correction ($p < 0.05$) are shown for **A** fractional anisotropy, **B** axial diffusivity, **C** radial diffusivity and **D** mean diffusivity. * $p < 0.05$, ** $p < 0.01$, *** $p < 0.001$. White matter tracts (x axis) abbreviations can be found in **Table 3.3**.

A Fractional Anisotropy



B Axial Diffusivity



■ Deletion ■ Duplication

(Figure continues on next page)

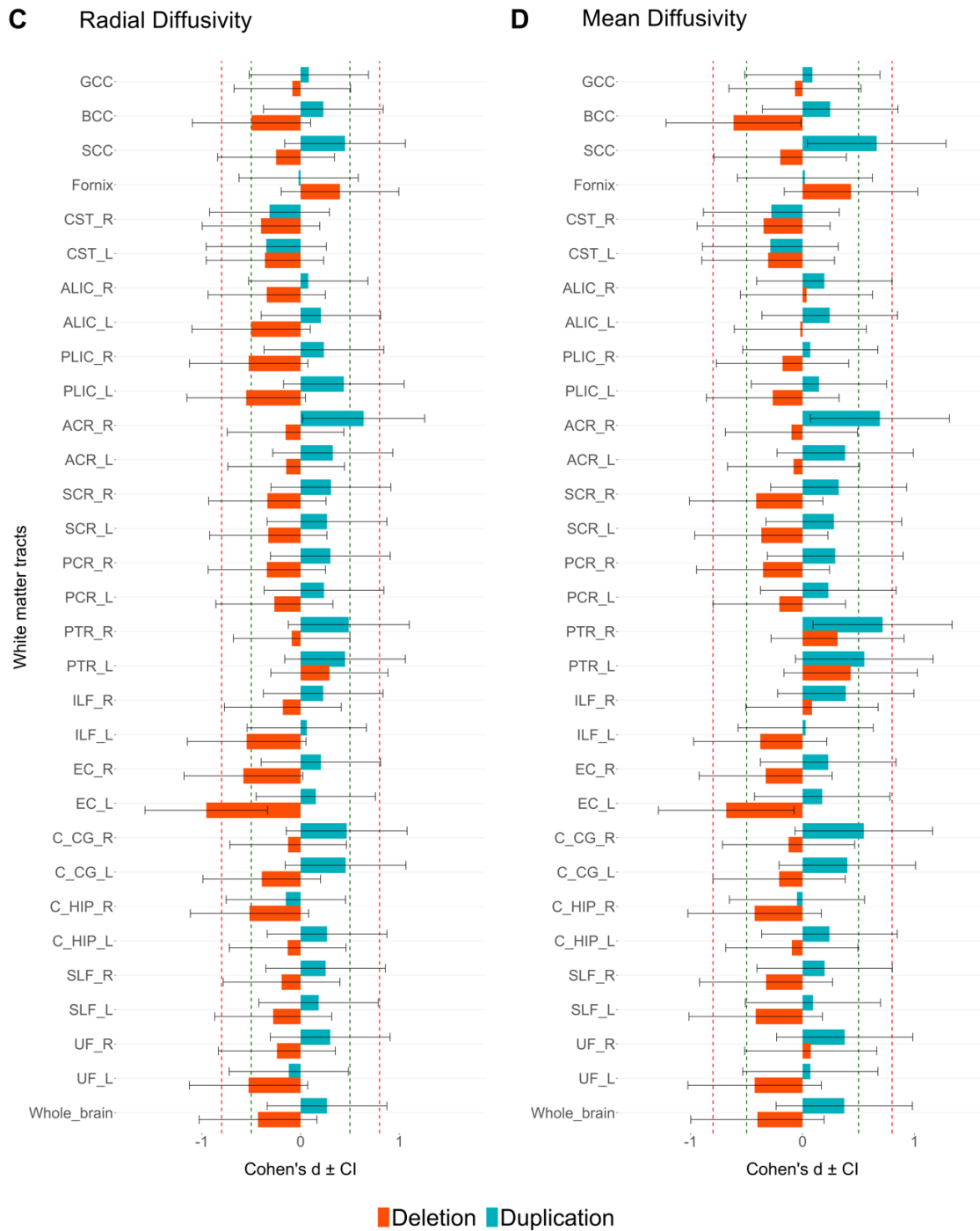
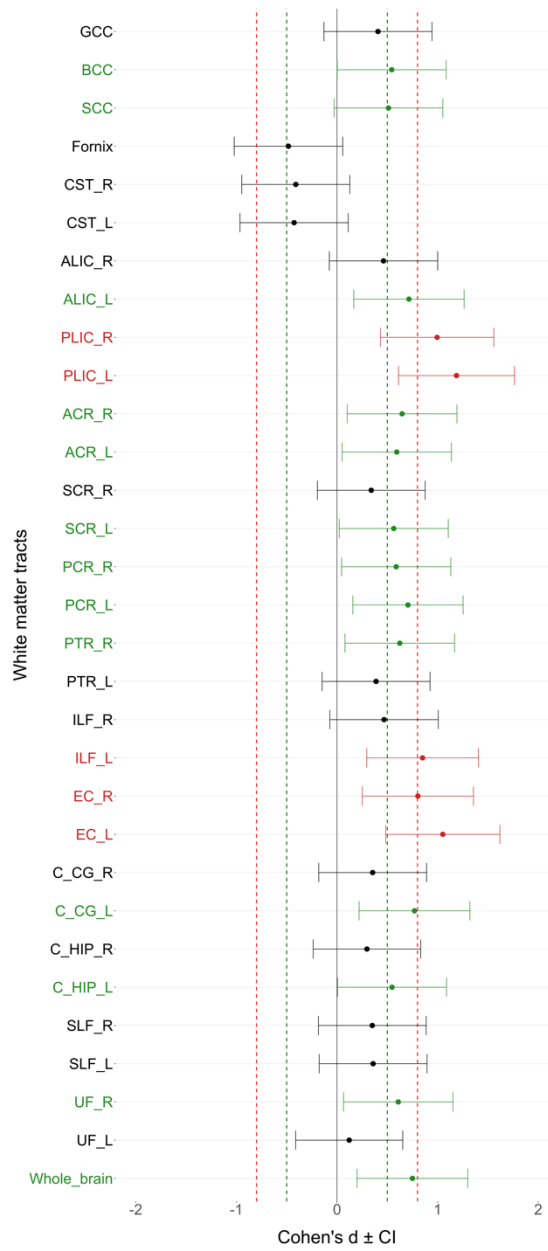


Figure 3.3 - Diverging bars for Cohen d' effect sizes for group differences when comparing deletion and duplication carriers versus controls.

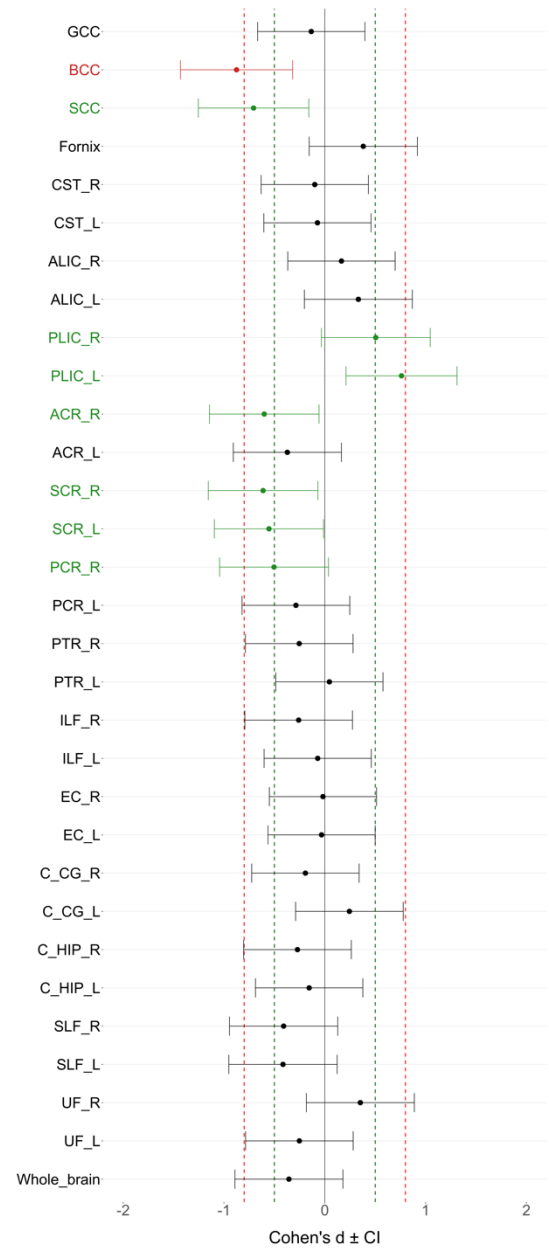
Diverging bars for Cohen d' effect sizes for group differences when comparing deletion and duplication carriers versus controls with no large copy number variants, for the different DTI metrics: **A** fractional anisotropy, **B** axial diffusivity, **C** radial diffusivity, and **D** mean diffusivity. The thresholds where an effect size is considered to be large (0.8) or medium (0.5), according to Cohen's criteria (Cohen, 1977), are represented by a vertical red or green dashed line, respectively. White matter tracts abbreviations can be found in **Table 3.3**.

Deletion vs Duplication

A Fractional Anisotropy



B Axial Diffusivity

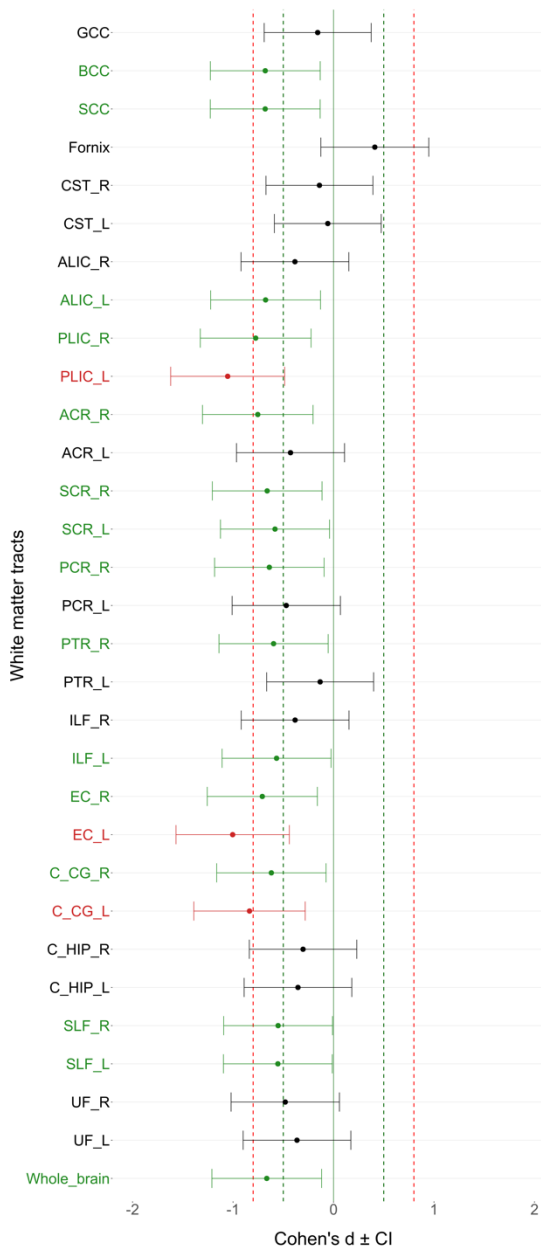


● small ● medium ● large

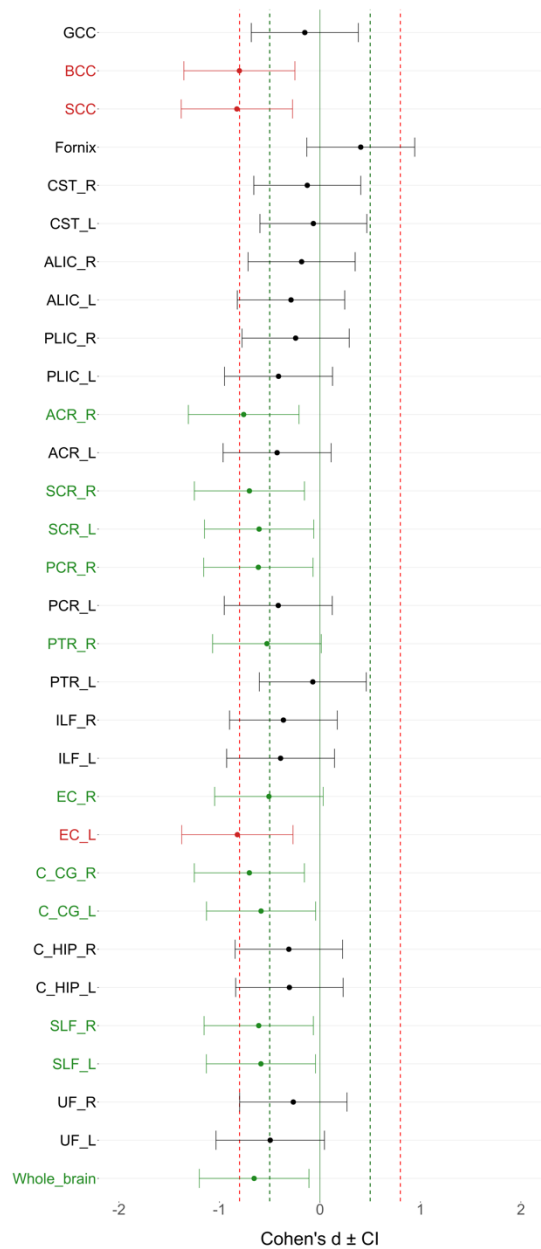
(Figure continues on next page)

Deletion vs Duplication

C Radial Diffusivity



D Mean Diffusivity



● small ● medium ● large

Figure 3.4 - Cohen d' effect sizes for group differences when comparing deletion versus duplication carriers.

Cohen d' effect sizes for group differences when comparing deletion versus duplication carriers for the different DTI metrics: **A** fractional anisotropy, **B** axial diffusivity, **C** radial diffusivity, and **D** mean diffusivity. The thresholds where an effect size is considered to be large (0.8) or medium (0.5), according to Cohen's criteria (*Cohen, 1977*), are represented by a vertical red or green dashed line, respectively. White matter tracts abbreviations can be found in **Table 3.3**.

3.4.3. Age trajectories

In order to examine differences in the effects of age on FA, AD, RD and MD between each group, age-by-dosage and age²-by-dosage interaction tests for each ROI were performed. A significant (p-value uncorrected) age-by-dosage interaction was observed in:

- 1) FA, bilaterally in the PLIC (PLIC_R; $F_{(2,65)}=4.29$, $p=0.02$ and PLIC_L; $F_{(2,65)}=3.25$, $p=0.04$), and in the right PCR (PCR_R; $F_{(2,65)}=4.5$, $p=0.02$);
- 2) AD, in the left PTR (PTR_L; $F_{(2,65)}=3.18$, $p=0.05$), and bilaterally in the C_HIP (C_HIP_R; $F_{(2,65)}=3.23$, $p=0.05$ and C_HIP_L; $F_{(2,65)}=3.8$, $p=0.03$);
- 3) RD, in the right PCR (PCR_R; ($F_{(2,65)}=3.36$, $p=0.04$), right C_HIP (C_HIP_R; $F_{(2,65)}=3.28$, $p=0.04$), and left SLF (SLF_L; ($F_{(2,65)}=3.32$, $p=0.04$);
- 4) MD, bilaterally in both the C_HIP (C_HIP_R; $F_{(2,65)}=3.94$, $p=0.02$ and C_HIP_L; $F_{(2,65)}=3.24$, $p=0.04$) and the SLF (SLF_R; $F_{(2,65)}=3.31$, $p=0.04$ and SLF_L; $F_{(2,65)}=3.33$, $p=0.04$).

Significant interactions with the quadratic term age²-by-dosage (p-value uncorrected) were observed in:

- 1) FA, in the splenium of the CC (SCC; $F_{(2,65)}=4.6$, $p=0.01$), right PTR (PTR_R; $F_{(2,65)}=4.72$, $p=0.01$), bilaterally in both the EC (EC_R; $F_{(2,65)}=5.88$, $p=0.004$ and EC_L; $F_{(2,65)}=7.09$, $p=0.002$) and uncinate fasciculus (UF_R; $F_{(2,65)}=3.4$, $p=0.04$ and UF_L; ($F_{(2,65)}=4.09$, $p=0.02$);
- 2) AD, in the right C_HIP (C_HIP_R; $F_{(2,65)}=3.55$, $p=0.03$);
- 3) RD, in the body of the CC (BCC, $F_{(2,65)}=3.77$, $p=0.03$), splenium of the CC (SCC; $F_{(2,65)}=4.29$, $p=0.02$), bilaterally in both the EC (EC_R; $F_{(2,65)}=3.46$, $p=0.04$ and EC_L; $F_{(2,65)}=5.12$, $p=0.009$) and UF (UF_R; $F_{(2,65)}=4.02$, $p=0.02$ and UF_L; $F_{(2,65)}=3.57$, $p=0.03$);
- 4) MD, in the body of the CC (BCC; $F_{(2,65)}=3.72$, $p=0.03$), right C_HIP (C_HIP_R; $F_{(2,65)}=4.93$, $p=0.01$), and right UF (UF_R; $F_{(2,65)}=3.28$, $p=0.04$).

In order to visualise these interactions, age trajectory plots are shown for the significant white matter tracts for deletion, NoCNV and duplication groups. For FA linear and quadratic interactions can be visualised in **Figures 3.5** and **3.6**, respectively.

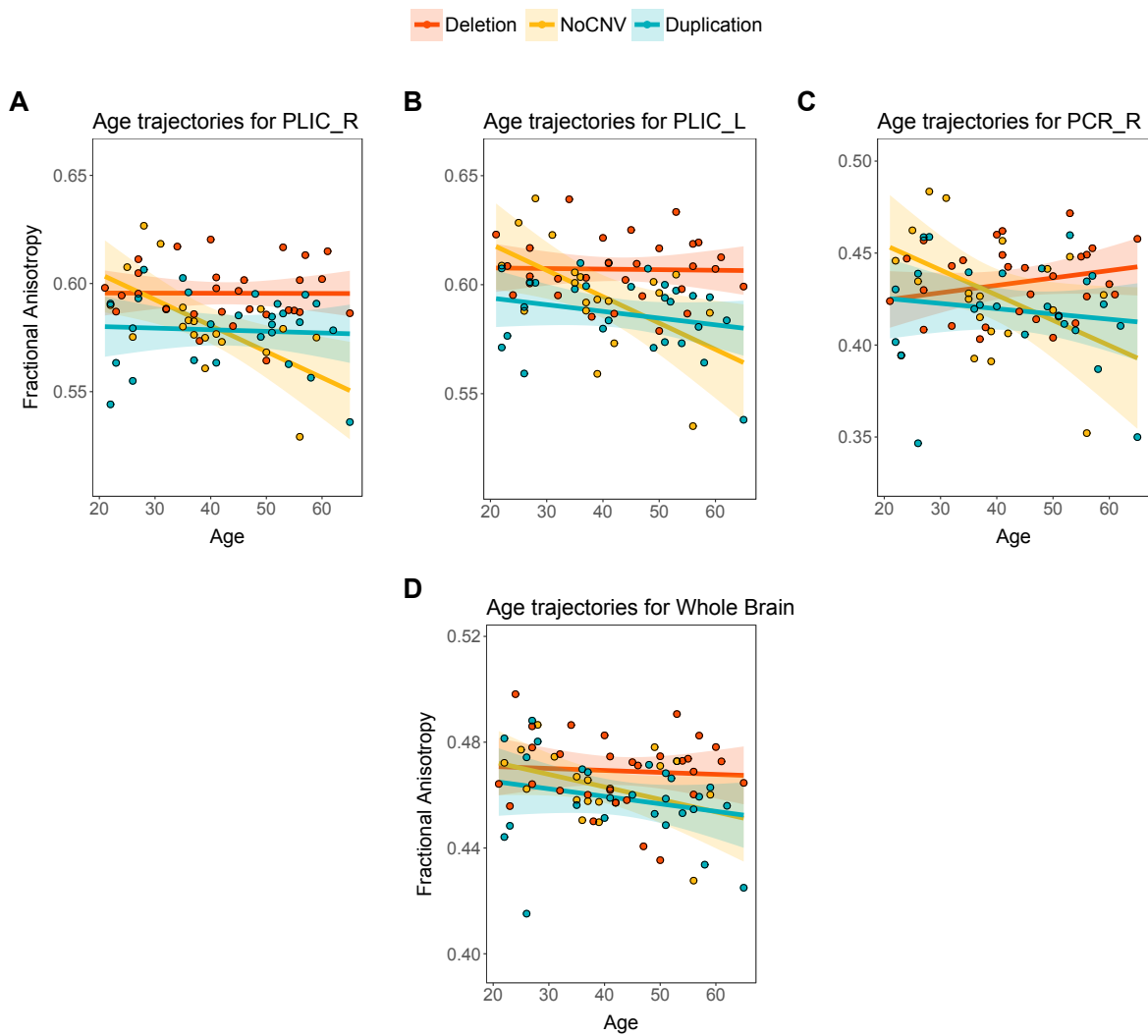


Figure 3.5 - Linear age trajectories for deletion (red), NoCNV (yellow), and duplication (blue) groups. Linear relationship between fractional anisotropy and age for the following white matter tracts: **A** PLIC_R, **B** PLIC_L, **C** PCR_R, and **D** averaged white matter skeleton (Whole Brain). Shaded regions represent 95% confidence intervals. White matter tracts abbreviations can be found in **Table 3.3**.

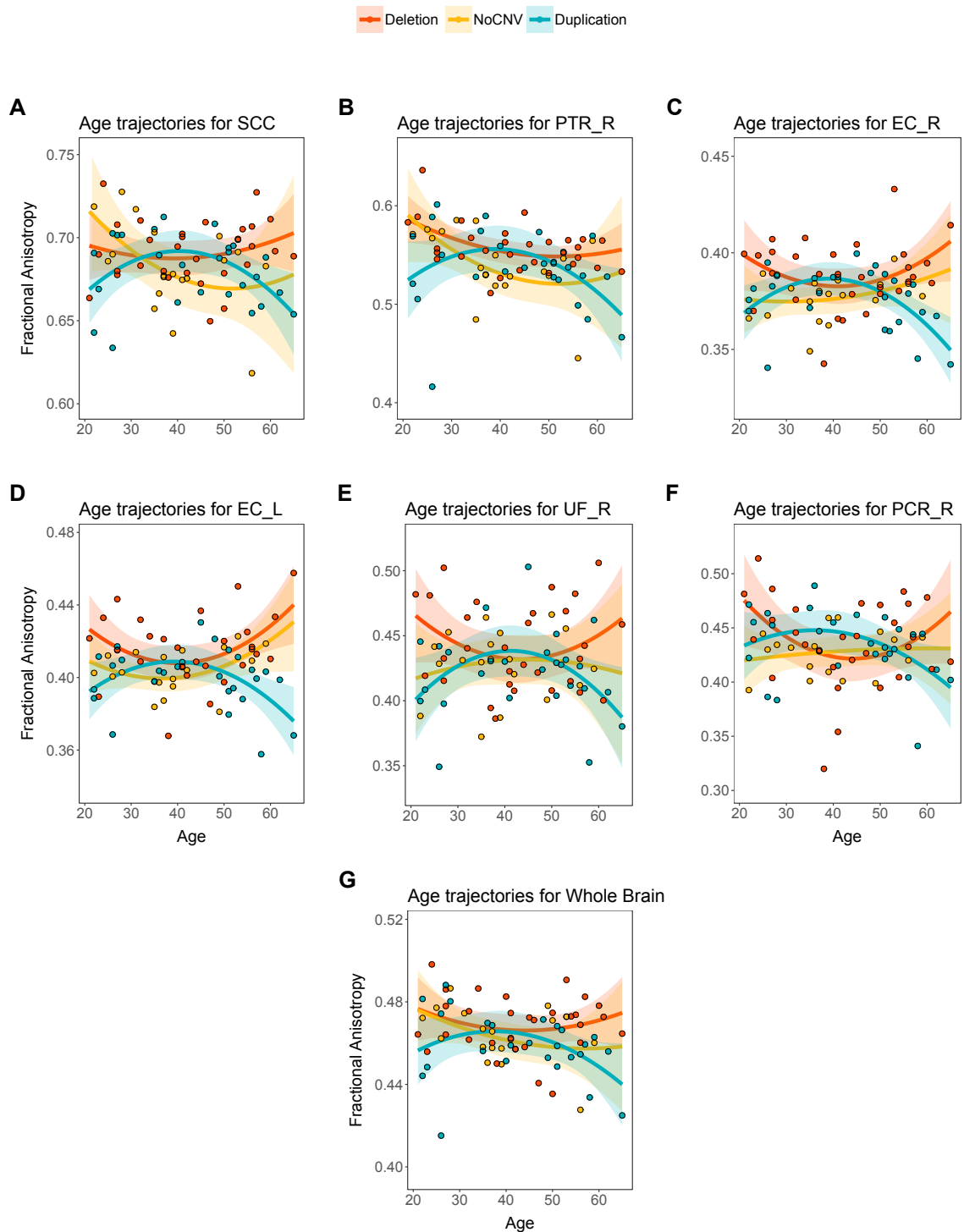


Figure 3.6 - Quadratic age trajectories for deletion (red), NoCNV (yellow), and duplication (blue) groups.

Quadratic relationship between fractional anisotropy and age for the following white matter tracts: **A** SCC, **B** PTR_R, **C** EC_R, **D** EC_L, **E** UF_R, **F** PCR_R, and **G** averaged white matter skeleton (Whole Brain). White matter tracts abbreviations can be found in **Table 3.3**.

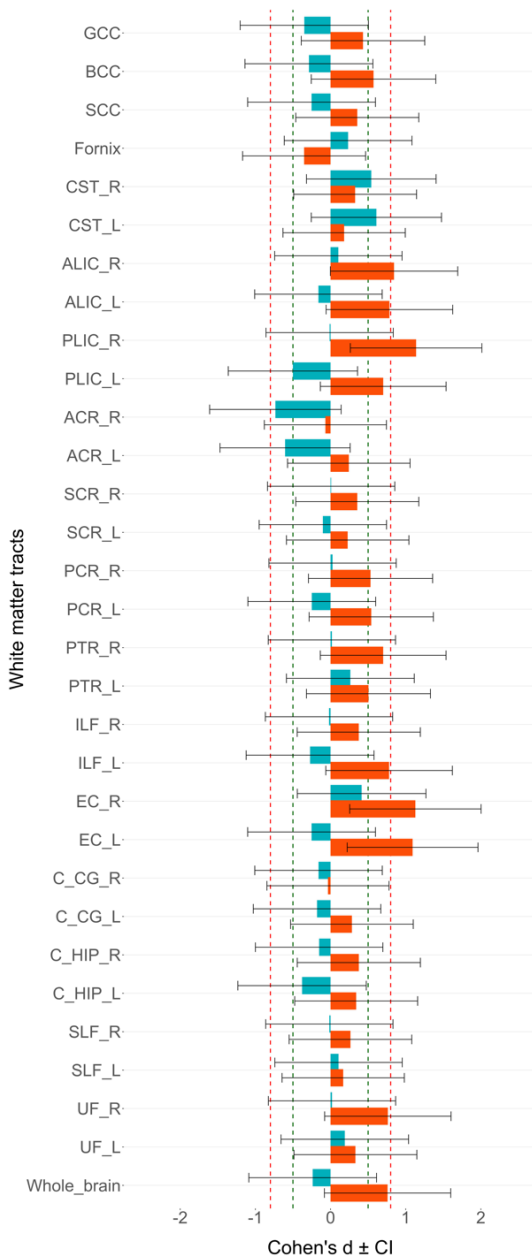
3.4.4. Sex Differences

A sex-by-dosage interaction model was used to investigate sex differences in relation to 15q11.2 BP1-BP2 dosage. No significant interaction effect was found across the whole-brain. However, when analysing the effect sizes for males and females separately, the male sub-group followed the same direction of effects seen in the whole-group analyses (increased FA in deletion carriers and decreased FA in duplication carriers), whereas in the female subgroup the reciprocal trend is not seen in the genu of the CC (GCC), BCC, CST_R, CST_L, right and left superior corona radiata (SCR_R, SCR_L), PCR_R, PTR_L, SLF_R, and SLF_L white matter tracts – instead, decreased FA in both deletion and duplication carriers is noted (**Figure 3.7**). It is also observable that, in female deletion carriers, there is a large effect size for decreased FA in the fornix, which is negligible in the male deletion carriers.

When analysing the effect sizes of the deletion vs duplication comparison, a significant difference in effect size was found between males and females, as assessed by a two-tailed paired t-test. Males showed larger effect sizes for increased FA ($t = 2.79$, p -value = 0.009) compared to females, and an overall large effect size in the whole-brain (Cohen's $d = 0.99$), whereas females showed a medium effect size (Cohen's $d = 0.52$), **Figure 3.8**. This result was expected since there were fewer reciprocal effects in the female subgroup. Of particular interest is the fact that, when analysing only the male carriers as opposed to the whole-group analyses, some additional white matter tracts showed a large effect size. In the male carriers the following white matter tracts showed differences with large effect sizes: GCC, BCC, ALIC_L, PLIC_R, PLIC_L, ACR_L, PCR_L, PTR_R, ILF_L, EC_R, and EC_L. Females, however, showed a large effect size for increased FA in the C_CG_L, that is not seen in the males.

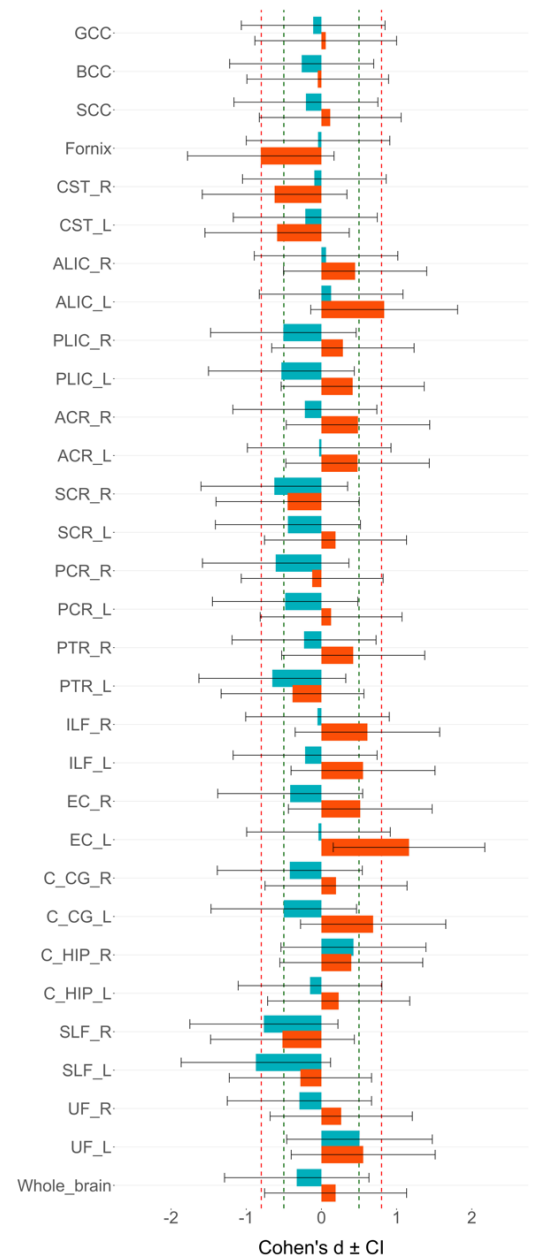
Males

A Fractional Anisotropy



Females

B Fractional Anisotropy



■ Deletion ■ Duplication

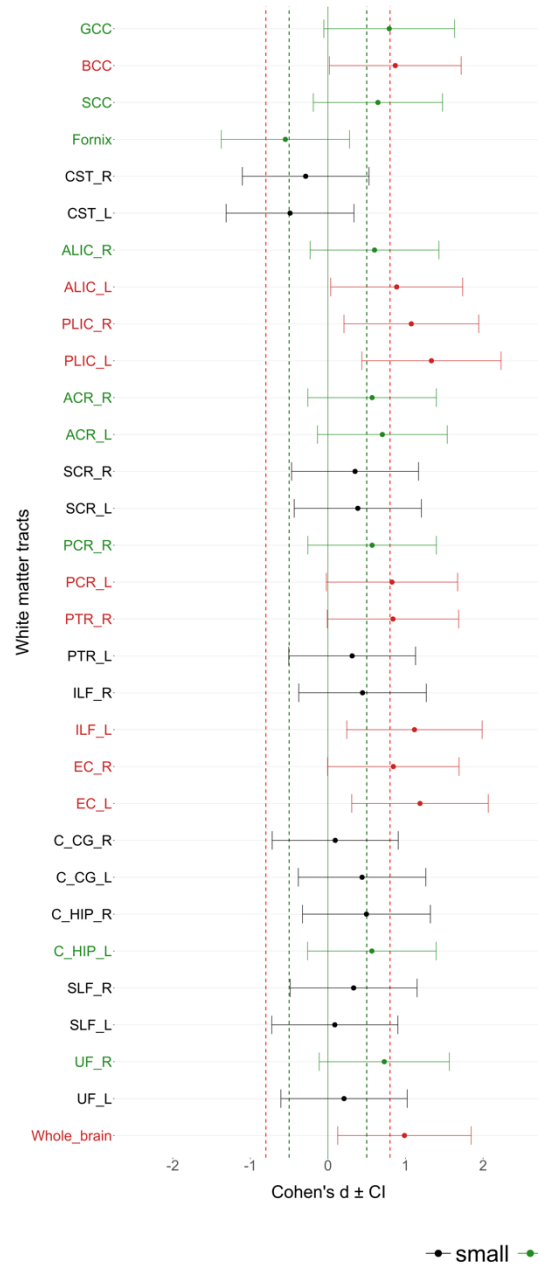
Figure 3.7 – Gender differences in Cohen d' effect sizes, when comparing deletion and duplication carriers versus controls.

Cohen d' effect sizes for group differences when comparing deletion and duplication carriers versus controls with no large CNV for fractional anisotropy in **A** males and **B** females. The thresholds where an effect size is considered to be large (0.8) or medium (0.5), according to Cohen's criteria (Cohen, 1977), are represented by a vertical red or green dashed line, respectively. White matter tracts abbreviations can be found in **Table 3.3**.

Deletion vs Duplication

Males

A Fractional Anisotropy



Females

B Fractional Anisotropy

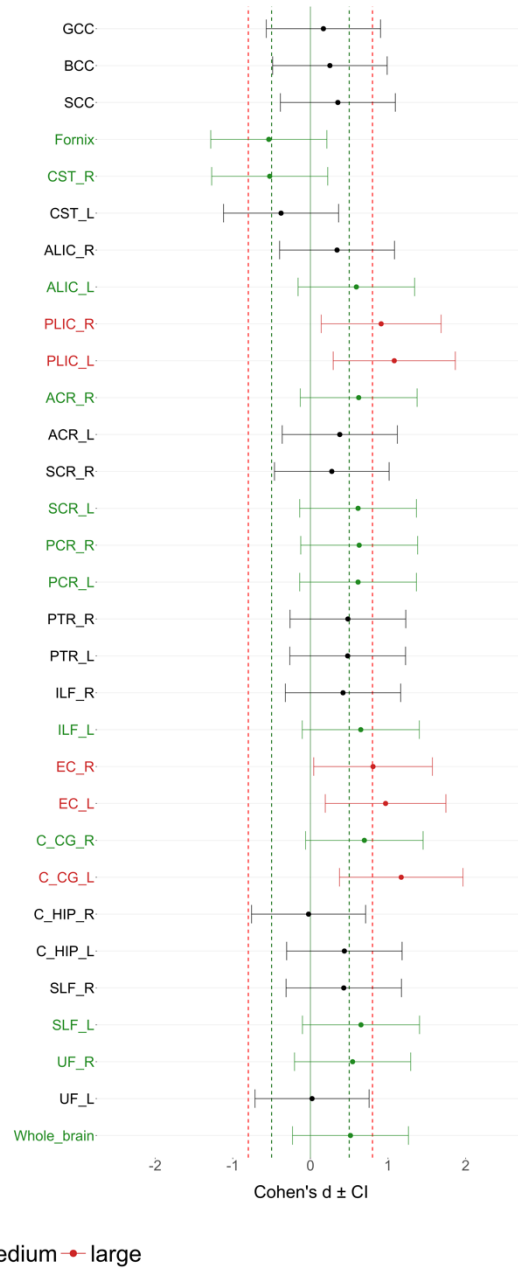


Figure 3.8 - Gender differences in Cohen d' effect sizes, when comparing deletion versus duplication carriers.

Cohen d' effect sizes for group differences when comparing deletion versus duplication carriers for fractional anisotropy in **A** males, and **B** females. The thresholds where an effect size is considered to be large (0.8) or medium (0.5), according to Cohen's criteria (*Cohen, 1977*), are represented by a vertical red or green dashed line, respectively. White matter tracts abbreviations can be found in **Table 3.3**.

3.5. Discussion

This was the first study to date looking at white matter microstructural changes associated with copy number variations in the 15q11.2 BP1-BP2 region. An initial whole-brain analysis showed significant widespread increased FA, and decreased AD, RD, and MD in 15q11.2 BP1-BP2 deletion carriers when compared to the duplication group. The whole-brain analyses also showed widespread increases in AD in the duplication group, compared to the NoCNV group. Quantification of these changes using a regional atlas-based approach indicated that, in most white matter tracts, the NoCNV group was intermediate between the deletion and duplication, evidencing a “mirrored phenotype” related to CNV dosage. The magnitude of the differences between the CNV carriers and NoCNV group revealed, however, that the deletion had a greater impact on white matter microstructure, by showing larger effect sizes than the duplication. In the regional analyses, only differences between the deletion and duplication carriers were significant after FDR correction, and the largest effects for these differences were seen bilaterally in the PLIC, ILF_L, and EC_L. Further preliminary analyses related to white matter changes progression with age suggests different direction of changes with age between groups. Finally, preliminary evidence of some sex differences was also found where females showed different direction of effects in some white matter tracts, compared to males and whole-group analyses, and males showed generally larger effect sizes than females.

3.5.1. Increased FA in 15q11.2 BP1-BP2 deletion carriers - how it relates to DTI findings in neurodevelopmental disorders and other CNVs

DTI has been widely used in identifying white matter phenotypes in neurodevelopmental disorders (*Taylor et al., 2004*), and changes in FA have been consistently reported in learning disabilities, schizophrenia (*Alba-Ferrara and de Erausquin, 2013*) and ASD (*Travers et al., 2012*). The general common finding in neurodevelopmental disorders points to reductions in FA in several white matter tracts (*Fitzsimmons et al., 2013*). DTI studies in advanced schizophrenia have consistently found reduced FA values in frontal regions, which correlated with cognitive and motor deficits (*Walther et al., 2011*). There are, however, some reports of increased FA in fibres connecting temporal regions (such as the superior longitudinal fasciculus), where increased FA values were found to be associated with increased severity of hallucinations

in schizophrenia patients (*Hubl et al., 2004; Rotarska-Jagiela et al., 2009; Seok et al., 2007; Shergill et al., 2007*); therefore contradicting the general idea that higher FA is always associated with better outcomes. Furthermore, only a few studies have investigated white matter microstructural phenotypes in the early preclinical stage, and current literature is inconsistent showing both increases and decreases in FA (*Francis et al., 2013; Gilmore et al., 2010; Satterthwaite et al., 2016*). In ASD research, adults with ASD often report general decreased FA in the brain, but most consistently in regions such as the corpus callosum, cingulum and regions of the temporal lobe (*Travers et al., 2012*). Recent longitudinal neuroimaging studies have supported a theory of atypical developmental trajectory of white matter microstructure in patients with ASD, where ASD children displayed abnormal age-related changes with higher FA and brain volume at younger ages, but lower FA and volume in older ASD children, when compared to typical developing children (*Cheng et al., 2010; Travers et al., 2015; McLaughlin et al., 2018*).

In this study, carriers of the 15q11.2 BP1-BP2 microdeletion showed consistent increases in FA. This result was surprising initially since the microdeletion has been strongly associated with dyslexia and dyscalculia, with a moderate increased risk for schizophrenia and ASD – all disorders that have been generally associated with global decreased FA in the brain. Given the highly genetic heterogeneity of these disorders, and the potential confounds associated with disease onset, DTI studies investigating the effect of individual neuropsychiatric genetic variations on the “healthy brain” have recently emerged. Surprisingly, several studies on carriers of other neurodevelopmental CNVs have also shown increases in FA. An example is the study by *Hoefl et al., 2007*, where individuals with Williams syndrome (caused by a hemizygous deletion of up to 28 genes on chromosome 7q11.23 (*Morris et al., 1988*)) reported increased FA in the superior longitudinal fasciculus, which was correlated with poor outcomes in a visuospatial construction task. Furthermore, increased FA was also reported in both children and adults carrying the 16p11.2 deletion, where reciprocal changes were found in the duplication (*Chang et al., 2016*). Finally, a recent study in patients with cognitive decline carrying the 22q11.2 deletion showed significant increased FA in the bilateral superior longitudinal fasciculus, the bilateral cingulum bundle, the left internal capsule and the left superior frontal-occipital fasciculus as compared with 22q11.2 deletion carriers without cognitive decline (*Nuninga et al., 2018*).

The biological nature of these changes reported in this, and in other CNV studies, is highly speculated, and increased FA could point to either a compensatory mechanism in response to primary deficits protecting against disease onset, or to a diffuse dysregulation of neuronal dynamics, increasing the risk for psychiatric disorder.

3.5.2. Increased FA in 15q11.2 BP1-BP2 deletion carriers – Possible cellular causes

DTI measures water diffusion, and water diffusion is highly sensitive to changes in the underlying tissue microstructure, making this a powerful method of assessing the orientation and integrity of white matter tracts. However, a major limitation of DTI is the difficulty of understanding the underlying cellular nature of these changes. DTI changes can either be attributed to microscopic factors, such as axonal properties (the diameter and number of axons) and myelin thickness, or to macroscopic factors, such as the coherence of axonal orientation within a voxel (parallel versus crossing fibres) (*Beaulieu, 2002*). Higher FA and reduced MD are usually associated with higher density, diameter, degree of organisation and myelination of axons. Changes in FA are modulated by changes in AD and RD: AD is thought to reflect fibre coherence, whereas RD is inversely correlated with myelin thickness and fibre density (*Wheeler-Kingshott and Cercignani, 2009; Aung et al., 2013*). Here, although all DTI changes seem to be consistent throughout the brain, regional analyses show increases and decreases in AD in different white matter tracts in deletion carriers (**Figure 3.3**). Since FA reflects the relative contribution of AD and RD and we find global increased FA, including in areas where AD is decreased, the RD contribution seems to be stronger. Hence, the increased FA and markedly decreased RD observed in the deletion carriers in the present study could potentially be driven by higher myelination or denser axonal packing, or both. It is also important to mention that reduction of white matter bundles in crossing fibre regions could also result in increased FA. Furthermore, areas with reduced AD could be a result of reduced axonal integrity.

A central question in addressing possible underlying mechanisms is how each gene within the 15q11.2 BP1-BP2 CNV region could contribute to the observed phenotype. It is known that all the four genes in this region are highly conserved and expressed in human central nervous system, therefore potentially playing a role in 15q11.2 BP1-BP2 associated phenotypes. Within these four genes, *NIPAI* and *CYFIP1*

were found to be involved in mechanisms that, when dysregulated, potentially impact white matter microstructure: (1) deletions of *NIPAI* gene could result in increased abnormal axonal density, through interactions with BMP signalling, leading to increased anisotropy in the white matter tracts; (2) whereas deletions in *CYFIP1* gene were already shown to impact dendritic branching (*De Rubeis et al., 2013; Pathania et al., 2014; Oguro-Ando et al., 2015*), and may as well result in changes in axonal density, organisation and myelination, due to its known effects on actin remodelling and interactions with FMRP (see General Introduction).

Recently, two articles (*Green et al., 2015; Hall et al., 2016*) by the same group reported increased FA and decreased RD and MD in FXS patients compared with IQ-matched control subjects. There is, therefore, a marked degree of overlap between changes in 15q11.2 BP1-BP2 deletion carriers and in FXS patients, consistent *a priori* with the suggested molecular link between CYFIP1 and FMRP. If these common neural mechanisms are the cause of the overlap in white matter phenotypes, the question arises on what cellular causes could explain these changes. Here, evidence that both FMRP and CYFIP1 influence diverse aspects of synaptic function, as well as effects on dendritic architecture, may be of relevance. In FXS patients and FXS animal models (mouse, *Drosophila*) a major phenotype consistently reported is the presence of dendritic spines that are longer, thinner and denser than normal (*Comery et al., 1997; Irwin et al., 2000; Abekhoukh et al., 2017*). Despite this increased dendritic complexity, mice harbouring deletions in the *Fmr1* gene were also shown to have increased ratio of immature-to-mature mushroom-shaped dendritic spines (*Comery et al., 1997; Abekhoukh et al., 2017*). In a mouse model, *Cyfp1* haploinsufficiency was shown to reduce dendritic complexity, as opposed to what was observed in the *Fmr1* mouse knockout model (*Pathania et al., 2014*). However, reduced levels of *Cyfp1* also lead to an increased number of immature spines in the hippocampus (*Pathania et al., 2014*). The common abnormal maturation of dendritic spines seen in both *Fmr1* knockout and *Cyfp1* heterozygous mice could be explained by altered processing, localisation, or translational regulation of mRNAs encoding pre- and post-synaptic proteins due to the absence of the CYFIP1-FMRP complex, whereas the opposite effects on dendritic complexity and length could be due to dysregulations of the WAVE regulatory complex caused by absence of CYFIP1 protein (*De Rubeis et al., 2013; Bardoni and Abekhoukh, 2014*). A study has also explored the impact of *Cyfp1* overexpression in a mouse model, showing a mirror phenotype characterised by increased dendritic length and complexity, with reduced number of

immature thin spines, and increased number of mature stubby and abnormal spines (Oguro-Ando et al., 2015). While the relationship between neuronal density and number of synapses per neuron is still not well understood, the observed increased FA in FXS (Green et al., 2015; Hall et al., 2016), and 15q11.2 BP1-BP2 (this study) could be caused by an increased neuronal density as an adaptive response to an increased number of immature spines and reduced functional synapses.

Further speculations as to cellular/molecular mechanisms underlying the observed white matter phenotype should, at this stage, be made with caution. DTI data are difficult to relate to underlying cellular changes, but ultrastructural magnetic resonance imaging methods could provide the necessary resolution to visualise and quantify myelin/axon density changes in the living human brain (Shi and Toga, 2017). However, a more comprehensive investigation would require histological studies of brains of human carriers *post mortem*, or animal studies. Translational models of human disease in animals are indeed a very attractive alternative to explore individual genotype-phenotype relationships, where direct access to brain tissue would allow an analysis of underlying cellular changes relevant to the DTI findings. Given the previous evidence highlighting *CYFIP1* as a strong candidate for the 15q11.2 BP1-BP2 phenotype, in this project I started to address these questions by exploring white matter changes in a novel *Cyfp1* haploinsufficiency rat model modelling the reduced dosage of *CYFIP1* in 15q11.2 BP1-BP2 deletion carriers (see Chapters 5-7).

3.5.3. White matter changes and relation with functional outcomes

This study showed that the 15q11.2 BP1-BP2 chromosomal region is associated with extensive global changes in white matter microstructure. However, some white matter tracts seemed to be more affected than others, showing larger effect sizes. The largest effects for increased FA were seen in the left ILF, left EC, and bilaterally in the PLIC, when comparing deletion to duplication carriers. These were accompanied with large effects for decreased RD in the left EC, and also bilaterally in the PLIC.

Motor delays are often reported in 15q11.2 BP1-BP2 deletion carriers (Cox and Butler, 2015). The PLIC is known to carry fibres from the corticospinal tract, carrying motor information from the primary motor cortex to the lower motor neurons in the spinal cord (Kretschmann, 1988). Therefore, the large effect sizes seen in the PLIC (**Figure 3.3**

and 3.4) are of high relevance, where increased FA could putatively be related to these motor deficits or may result from compensatory mechanisms – since decreased FA in the PLIC has previously been shown to correlate with poor motor outcomes in motor neuron disease (Puig *et al.*, 2011). Interestingly, and maybe indicative of a compensatory mechanism, AD was also increased in the PLIC bilaterally. The PLIC also carries sensory information from the thalamus to the cortex, a key sensorimotor relay area implicated in schizophrenia (Pergola *et al.*, 2015) and ASD (Schuetze *et al.*, 2016). In individuals with schizophrenia, decreased FA in the internal capsule has been reported (McIntosh *et al.*, 2005). However, functional studies in ASD patients have pointed to an increased functional connectivity between motor regions of the thalamus and cortex (Mizuno *et al.*, 2006). A longitudinal study by McLaughlin *et al.*, 2018 suggested that this was due to an atypical development trajectory of the thalamus and internal capsule in ASD patients, in which increasing connectivity through adolescence and adulthood was seen. In this present study, a significant (uncorrected) linear age-by-dosage interaction was found bilaterally in the PLIC for FA, where deletions and duplications seem to follow different developmental trajectories than NoCNV carriers (**Figure 3.5**) - FA values decrease with age in the NoCNV control group but maintain in the deletion carriers. Deletion carriers seem to have, in early adulthood, lower FA than NoCNV carriers and higher FA in later adulthood. Interestingly, a similar trajectory is seen in McLaughlin *et al.*, 2018 study, where reduced FA is seen in the PLIC of the youngest individuals with ASD (3-20 years old), compared with typical developing controls, and shift in young adulthood (~20 years), where the ASD group seems to have a more accentuated increased FA than the control group (Figure 2 in McLaughlin *et al.*, 2018 study). Understandably, a direct comparison between McLaughlin's study and this study cannot be made since the inclusion of a group of subjects under 20 years old would be needed, as well as a bigger sample with more individuals in each age interval. Although the present data does not allow any strong conclusion in this matter, this preliminary analysis may suggest possible differences in white matter development between early (~20 years) and late adulthood (~60 years). Furthermore, the increased FA in the PLIC of the 15q11.2 BP1-BP2 deletion carriers could be a result of an abnormal thalamus and IC development, which could arguably be associated with motor delays often reported in children with the deletion.

The 15q11.2 BP1-BP2 deletion was previously shown to confer a high risk of a combined phenotype of dyslexia and dyscalculia (Ulfarsson *et al.*, 2017). Reading involves a series of complex cognitive components that involve visual, phonological, and

semantic processes, where effective communication between specific brain areas is crucial. A number of DTI studies in dyslexic individuals have shown that white matter bundles connecting temporo-parietal and frontal areas have disrupted integrity, particularly in the superior longitudinal fasciculus (*Vandermosten et al., 2012*) - a key connection in phonological processing (*Yeatman et al., 2011*). In the 15q11.2 BP1-BP2 deletion, a large effect size for decreased AD was found in this white matter tract, compared to NoCNV (**Figure 3.3**), which could potentially be associated with worse reading outcomes, even though differences in FA were negligible. Significant increased FA in deletion carriers, when compared to duplication carriers, was also noted in the left ILF – a major white matter tract also involved in dyslexia and thought to be critical to semantic processing (*Menjot de Champfleury et al., 2013*). Furthermore, deletion carriers were previously shown to have a smaller fusiform gyrus (*Ulfarsson et al., 2017*), a structure that connects with ILF and shown to play a role in reading and mathematics (*Peters et al., 2018*). A large effect size was also found for differences in both FA and RD in the EC. The EC is a route for cholinergic fibres within the cholinergic circuitry, known to be highly associated with cognitive performance in schizophrenia (*Ross et al., 2010*). Finally, although of negligible effect, the only white matter tract reporting lower FA values in deletion carriers was the fornix – a compact bundle of white matter fibres projecting from the hippocampus (a brain structure frequently implicated in schizophrenia) to the septum, anterior nucleus of the thalamus and the mamillary bodies. The fornix has been shown to be implicated in cognitive disturbances and memory function in schizophrenia (*Fitzsimmons et al., 2009; Baumann et al., 2016*).

3.5.4. Age trajectories and gender differences

Atypical white matter development has been reported in longitudinal studies of ASD (*Cheng et al., 2010*) and schizophrenia (*Cropley et al., 2016*). As a preliminary exploratory investigation into developmental trajectories of white matter in 15q11.2 BP1-BP2 carriers, linear and quadratic models were fit to global FA, AD, RD, and MD over age, separately for deletion, NoCNV and duplication carriers (**Figure 3.5** and **3.6**). Studies of typical white matter development indicate a quadratic relationship between most DTI metrics and age, where FA typically increases from childhood to puberty, plateaus at early adulthood and decreases in later adulthood (*Krogsrud et al., 2016*). As seen in **Figures 3.5D** and **3.6G**, the NoCNV group follows a typical age trajectory with

gradual FA reduction in the whole-brain after early adulthood, whereas duplication carriers show increases in early adulthood and later reduction in adulthood, and deletion carriers seem to maintain or even slightly increase FA values with age. Although these results might be indicative of an atypical white matter development, it is important to note the preliminary nature and limitations of these data, and these analyses only aimed to explore possible interactions that need to be confirmed in larger samples. Furthermore, 19 controls are not enough for a reliable age trajectory analysis, and some variations can be seen in different white matter tracts, showing that the NoCNV controls not always follow the typical trajectory. In order to make a direct comparison with ASD and schizophrenia studies, a bigger sample with the inclusion of a younger group and homogeneous distribution of subject across different ages is required.

Gender bias has been repeatedly observed in neurodevelopmental disorders, evidencing an increased male prevalence and leading to the concept of a “female protective model”. As example are the epidemiologic studies showing a male-to-female ratio of 4:1 in ASD (*Fombonne, 2009*). In schizophrenia, males show an earlier age at onset, higher propensity to negative symptoms and substance abuse, and lower social functioning, whereas females often report more affective symptoms like mood disorders and depression (*Abel et al., 2010*). Although the molecular causality behind these sex differences is still unclear, it has been hypothesised that the female brain would require larger mutational burden to reach the ASD diagnostic threshold (*Jacquemont et al., 2014*). Moreover, variations in the 15q11.2 BP1-BP2 region were shown to have a greater impact on ASD-related phenotype in men than women (*Chaste et al., 2014*). In this current study, a sex-by-dosage interaction model was used to investigate sex differences in relation to CNV dosage. Since no interaction was found, an exploratory analyses was done looking at effect sizes separately for males and females, where males and females showed striking differences in the direction of effects in some white matter tracts and overall larger effect sizes in males than females (**Figure 3.7** and **3.8**). These preliminary results suggest that males might be more sensitive to mutations in this chromosomal region. Of interest, is also the large effect seen for decreased FA in the fornix of female deletion carriers compared to female NoCNV carriers (**Figure 3.7**). The fornix is part of the limbic system being involved in the regulation of emotional brain regions and, therefore, implicated in affective processing (*Whalley et al., 2015*). Since affective symptoms are more frequently reported in schizophrenia female patients, this could be associate with a higher sensitivity for changes in this region in female carriers.

3.5.5. Limitations of this study

A limitation of this study was the impossibility to correct for regions with crossing fibres, which are particularly challenging. Crossing fibres may have a remarkable impact in DTI analyses, as between 60% and 90% of white matter voxels contain crossing fibres (*Jeurissen et al., 2013*), which may override microscopic factors related to axonal or myelin structure. Several methods have been proposed to extract multiple fibre orientations from diffusion weighted images using tractography methods, but most of them rely on the high angular resolution diffusion imaging (HARDI) protocol. For instance, spherical deconvolution is a broadly used method in tractography, which is able to estimate fibre orientations present within each imaging voxel (*Tournier et al., 2008*). Unfortunately, this method did not work in the current data, probably due to lack of resolution. It is however important to note that differences were extensive to the whole-brain, and not specific to areas that are known to have more crossing fibres (e.g., between the corticospinal tract and the superior longitudinal fasciculus), making this less likely to be the main cause of group differences.

Another limitation was not including the IQ scores as a covariate in the analyses, and this was due to a lack of cognitive data on the NoCNV group. IQ is known to be associated with white matter integrity (*Watson et al., 2018*), and some of the group differences could be magnified by differences in IQ. However, the white matter changes did not follow the IQ trend, where both deletion and duplication showed a trend to decreased IQ compared to the NoCNV group, being more specific to the karyotype with reciprocal changes in FA.

The extensive mirrored effects on white matter reported here, and in previous structural MRI studies (*Stefansson et al., 2013; Ulfarsson et al., 2017*), suggest that 15q11.2 BP1-BP2 affects white matter microstructure in a dosage-dependent way. When it comes to neuropsychiatric and behavioural findings at this locus, the picture is less clear (*Butler, 2017*). The microdeletion has been associated with development delay, schizophrenia and ASD, whereas duplication is generally not considered as a risk locus for schizophrenia (*Kirov et al., 2014*) and has not come out as a significant risk variant for development delay in recent large-scale genetic studies (*Coe et al., 2014*). Moreover, the microdeletion has been shown to have a greater impact on cognitive function in individuals with no neurodevelopmental disorders, particularly in the acquisition of mathematical skills and reading, whereas duplication carriers performed similarly to the

NoCNV group (*Stefansson et al., 2013*). In line with these findings, the deletion showed greater impact on white matter microstructure, presenting larger effect sizes than the duplication (**Table 3.4** and **Figure 3.3**). As a limitation of this study, the lack of detailed cognitive data in this sample did not allow correlations between increased FA and cognition in deletion carriers.

3.5.6. Conclusion

Using whole-brain and regional-brain analyses, this study shows a consistent pattern of white matter microstructure alterations, which are consistent with recent DTI studies on FXS patients, beginning to reveal brain mechanisms underlying the complex routes to psychopathology mediated by mutations at the 15q11.2 BP1-BP2 CNV region. The reciprocal effects on white matter microstructure, described here, suggest that deviations from normal gene dosage in each direction can lead to abnormalities in brain development, underlining the importance of studying how reciprocal chromosomal imbalances impact neural processes, which might have important implications for therapeutic intervention.

Chapter 4

White Matter Changes Associated With Copy
Number Variation at 15q11.2 BP1-BP2 – a
replication study from UK Biobank data

4.1. Abstract

Background

Low replication rates are a concern across scientific disciplines, and replication studies have a growing importance in the scientific community. National and international biobanks and genotyped population cohorts are valuable resources in finding genetically defined cohorts, allowing the study of the effect of rare chromosomal mutations across different populations. In the previous chapter, evidence for a reciprocal effect of 15q11.2 BP1-BP2 CNV dosage on white matter microstructure was shown in an Icelandic sample. Here, a replication of these findings will be carried out in an independent sample, selected from the UK Biobank dataset.

Methods

DTI derived measures from different white matter tracts were obtained from the UK Biobank database, where measures from deletion (n=54) and duplication (n=55) carriers of the 15q11.2 BP1-BP2 CNV were compared to a large control group of individuals with no large CNVs (n=15663). Only participants with no clinical diagnosis were included in this study. Regional differences were quantified, where interactions with age and gender with CNV dosage were also explored.

Results

A pattern of reciprocal white matter changes was found, characterised by significant increases in FA in deletion carriers and opposite decreases in FA in duplication carriers, compared to the control group. Here, the largest effect sizes were found in the internal capsule and cingulum. Preliminary analyses of age and sex interactions with CNV dosage suggest different age trajectories in each group, whereas no sex differences were found in this sample.

Conclusions

This study replicated the findings from the previous chapter, showing again a reciprocal effect of 15q11.2 BP1-BP2 dosage on white matter microstructure. In both studies, the largest effect sizes were found in the internal capsule, revealing a higher sensitivity of this white matter tract to variations in this CNV region.

4.2. Introduction

Neuroscience in general, and neuroimaging in particular, have been overrun with a “reproducibility crisis” after several replication efforts have failed to reproduce many established effects (*Button et al., 2013; Ioannidis, 2005; Kappenman and Keil, 2017; Wager et al., 2009*). This frequent failure to replicate previous findings highlights the growing importance of independent replication studies before a result can be considered definitive (*Baker, 2016*). CNVs being rare genetic variations in the general population, and with consequent limited data based on relatively small sample sizes, complicate the detection of modest gene effect sizes, as well as the replication of findings in independent samples. Population cohorts such as Iceland’s deCODE project, used in the previous chapter, or the UK Biobank project, used in the present study, are remarkable initiatives providing large genotyped samples with sufficient numbers of CNV carriers to conduct quantitative imaging studies.

In collaboration with deCODE genetics Institute in Iceland, DTI data from an Icelandic sample were analysed, as described in the previous chapter, evidencing a dosage-dependent effect of 15q11.2 BP1-BP2 on white matter microstructure - specifically widespread increases in FA in deletion carriers. The largest effects were observed in the posterior limb of the internal capsule, left inferior longitudinal fasciculus, and left external capsule. Iceland is considered an homogeneous population, and the current gene pool descends from fewer ancestors (*Helgason et al., 2003*), reducing the background noise caused by genetic variation (*Heutink and Oostra, 2002*). Isolated populations, like Iceland, have been argued to confer a number of advantages in studying disease-causing genes, since the populations live in more uniform environments, have better genealogical and clinical records, have reduced genetic variability, and can have an enrichment of some phenotypes and diseases (*Peltonen et al., 2000*). Amongst all these advantages, there are also some concerns regarding the usability and replicability of findings in small isolated populations, that might not be as generalisable to more genetically diverse, heterogeneous populations (*Austin et al., 2003*).

Different large-scale national and international biobank initiatives have been created with the aim of gathering genetic information from more heterogeneous populations. An example is the UK Biobank, a large-scale prospective epidemiological study including approximately 500 000 people who are currently aged 40-69 years old,

from all around the United Kingdom. As part of this project, extensive data have been collected including different questionnaires, physical and cognitive measures, as well as biological samples, including genotyping. Furthermore, an imaging extension was included with the aim of collecting brain and body imaging data from 100 000 participants by 2020, with brain imaging including three modalities: structural MRI, resting and task-based functional MRI, and DTI MRI. All the imaging data undergoes an automated imaging processing pipeline, where artefacts are removed and images are rendered comparably across modalities and participants, generating thousands of image-derived phenotypes (IDPs). Example IDPs include volume of grey and white matter structures, and measures of functional and structural connectivity in distinct brain regions. The combination of large subject numbers with multimodal imaging data acquired using homogeneous hardware and software is a unique feature of UK Biobank.

In this chapter, the effect of 15q11.2 BP1-BP2 on white matter microstructure will be explored in a subsample of the UK Biobank dataset. To replicate the previous study, DTI-derived measures from different white matter tracts will be used, where deletion and duplication carriers of the 15q11.2 BP1-BP2 will be compared against a large cohort of controls with no large CNVs, comprising more than 15 000 subjects. All subjects with a clinical diagnosis of any neurodevelopmental disorder were excluded from this study. A similar statistical approach to the one used in Chapter 3 was employed, where regional differences in DTI-derived measures were quantified. Moreover, age trajectories and sex differences dependent on dosage were also explored in this chapter. The aim of this study was to test the replicability of the previous findings on white matter changes associated with the 15q11.2 BP1-BP2 CNV, in a larger and more genetically heterogeneous sample.

4.3. Material and Methods

4.3.1. Participants

The data used in this study is a subsample of participants from the UK Biobank project (www.ukbiobank.ac.uk). All subjects provided informed consent to participate in UK Biobank, and ethical approval was granted by the North West Multi-Centre Ethics committee. Data were released to Cardiff University after application to the UK Biobank (project ref. 17044). Genotyping in UK Biobank was done, initially in 50 000 participants,

using the Affymetrix UK BiLEVE Axiom array (807 411 probes), where the remaining participants were genotyped using the Affymetrix UK Biobank Axiom ® array (820 967 probes). The two arrays were tested and shown to be extremely similar (with over 95% common content). The sample processing at UK Biobank is further described in their documentation, available at: <https://biobank.ctsu.ox.ac.uk/crystal/refer.cgi?id=155581>. CNV calling was performed following the same procedure as described previously in *Kendall et al., 2016*. In brief, normalised signal intensity, genotype calls and confidence intervals were generated using ~750 000 biallelic markers that were further processed with PennCNV-Affy software (*K. Wang et al., 2007*). For quality control, individual samples were further excluded if they had >30 CNVs, a waviness factor >0.03 or <-0.03, or a call rate <96%. Following this, the final sample was reduced to n=17234 participants. Individual CNVs were also excluded if they were covered by <10 probes or had a density coverage of less than one probe per 20 000 base pairs (*Kendall et al., 2016*).

In order to replicate the findings of Chapter 3 only carriers of CNVs at the 15q11.2 BP1-BP2 locus and participants with no large CNVs (NoCNV) were selected. The breakpoints of this CNV were manually inspected, prior to this study, to confirm that they met the CNV calling criteria. Briefly, the CNV had to include the key genes in the region. None of the 15q11.2 BP1-BP2 deletion or duplication carriers included in this study carried any other large CNVs. For this study, only participants that self-referred to be White British or Irish descendent, and for whom genetic analysis confirmed European ancestry (*Legge et al., 2019*) were included. Additionally, in order to avoid disease causation effects, only participants with no personal history of severe neuropsychiatric disorders (i.e. schizophrenia, psychosis, ASD, dementia or intellectual disability) or medical/neurological conditions that could clearly impact white matter microstructure (i.e. alcohol or other substance dependency, Parkinson's, Alzheimer, multiple sclerosis or other neurodegenerative conditions) were selected. These exclusion groups were based on self-reported diagnosis from a doctor at any assessment visit or from hospital records (n=18 214). In total, data from 54 individuals with the 15q11.2 BP1-BP2 deletion, 55 with the reciprocal duplication, and 15663 controls with no large CNVs were included. The participants in this study were aged between 45 and 80 years old, and the number of females and males was balanced in each condition group. Demographic information is described in **Table 4.1**.

Table 4.1 - Subject characteristics of the UK Biobank sample.

Abbreviations used: F – Female, M – Male, NoCNV – with no large copy number variants, sd – standard deviation.

15q11.2 BP1-BP2	Mean age in years (sd, range)	Gender	Number of subjects
Deletion	63.57 (6.9, 49 – 77)	25 M, 29 F	54
NoCNV	62.76 (7.4, 45 – 80)	7388 M, 8275 F	15663
Duplication	63.24 (7.6, 46 – 77)	27 M, 28 F	55

4.3.2. UK Biobank diffusion MRI acquisition and pre-processing

The data used in this chapter were collected, pre-processed and made available by the UK Biobank, where the imaging-derived measures were generated by an image-processing pipeline developed and run on behalf of UK Biobank (*Alfaro-Almagro et al., 2018*). Complete details of the image acquisition and processing are freely-available on the UK Biobank website in the form of a protocol (<http://biobank.ctsu.ox.ac.uk/crystal/refer.cgi?id=2367>), Brain imaging Documentation (<http://biobank.ctsu.ox.ac.uk/crystal/refer.cgi?id=1977>) and in *Miller et al., 2016*. In this study, I only used the final DTI-derived measures, and a brief description of the pre-processing pipeline, used in the UK Biobank project, follows below.

The MRI data was collected in three dedicated imaging centres, equipped with identical scanners (3T Siemens Skyra, software VD13) using a standard SIEMENS 32-channel receive head coil. Briefly, the diffusion data was acquired using two b-values (b=1000 and 2000 s/mm²) with multiband acceleration factor of 3 (three slices are acquired simultaneously instead of just one). For each diffusion-weighted shell, 50 distinct diffusion-encoding directions were acquired. The diffusion preparation was a standard (monopolar) Stejskal-Tanner pulse sequence (**Figure 2.2** in General Methods) (*Sinnaeve, 2012*). The field of view was 104x104x72, imaging matrix 52x52, 72 slices with slice thickness 2mm, giving 2mm isotropic voxels. All the diffusion-weighted MRI data underwent quality-control procedures by UK Biobank before data release, which consisted in a combination of manual and automated checking and also included the

removal of data badly affected by movement artefacts (as described in the UK Biobank Brain Imaging Documentation). In this chapter only the derived measures from standard DTI data will be used, which are derived from the $b=1000$ s/mm² data. As described in *Alfaro-Almagro et al., 2018*, gradient distortion correction was applied using tools developed by the Freesurfer and Human Connectome Project groups, available at <https://github.com/Washington-University/Pipelines>. The Eddy tool from FSL, (<http://fsl.fmrib.ox.ac.uk/fsl/fslwiki/EDDY>) was then used to correct the data for head motion and eddy currents. The $b=1000$ shell (50 directions) was then fed into the DTI fitting tool DTIFIT, generating the whole-brain maps of FA, AD, RD, and MD.

The output was then used in two complementary analyses: one based on TBSS processing, and the other based on probabilistic tractography. Both analyses report a range of DTI-derived measures within different tract regions. However, for consistency with the previous chapter, only the TBSS-derived measures were used in this study. These were obtained by the alignment of the FA images onto a standard-space white matter skeleton, with alignment improved over the original TBSS skeleton-projection methodology through the high-dimensional FNIRT-based warping (*de Groot et al., 2013*). This was later validated through a comparison of 14 different alignment methods applied to UK Biobank data. The resulting standard-space warp was then applied to all DTI output maps. TBSS-derived measures were computed by averaging the skeletonised images of each DTI map within a set of 48 standard-space tract masks defined by the JHU white matter atlas (ICBM-DTI-81) (*Mori et al., 2005*).

4.3.3. Statistical analyses

The UK Biobank TBSS-derived measures (FA, AD, RD and MD) were used. From the available outputs, the mean values from 30 segmented white matter tracts were considered for analyses (**Table 4.2**). Statistical analyses were carried out in RStudio statistical software *version 1.1.463* (R Foundation for Statistical Computing, Vienna, Austria). Before statistical analyses, and to avoid the potential effect of extreme values, outlier values of FA, AD, RD and MD – defined as values ± 2.5 standard deviations from each group mean – in any white matter tract were removed from the analyses, the same cut-off used in a previous study using UK Biobank imaging derived measures *Warland et al., 2019*.

To investigate the effect of dosage, the same analysis used in the deCODE Icelandic sample (Chapter 3) was carried out, where linear regression analyses were performed for each DTI measure and for each white matter tract, regressing out age, sex and intracranial volume (ICV) as covariates of no interest. Following this, *post hoc* pairwise comparisons were performed to measure differences between groups (*deletion vs NoCNV*, *duplication vs NoCNV*, and *deletion vs duplication*). To account for multiple testing, the standard FDR method based on the Benjamini-Hochberg approach (*Benjamini and Hochberg, 1995*) was used (described in Chapter 3), considering the relation between different white matter tracts and between DTI metrics.

In order to investigate the magnitude of reciprocal effects in the deletion and duplication cohort, Cohen's d effect sizes were calculated comparing *deletion vs NoCNV* and *duplication vs NoCNV* and plotted using diverging bars. Cohen's d effect sizes were also calculated for differences between deletion and duplication cohorts. As described in Chapter 3, the adjusted means of each group and white matter tract were used in Cohen's d coefficient calculation, where the adjusted means were the residuals from the linear regression model: $\text{lm}(\text{genotype} \sim \text{age} + \text{sex} + \text{ICV})$. Cohen classified effect sizes as negligible ($d < 0.2$), small ($d > 0.2$), medium ($d > 0.5$), and large ($d > 0.8$) (*Cohen, 1977*).

Table 4.2 - White matter tracts and abbreviations used.

White matter tracts	Abbreviations
Genu Corpus Callosum	GCC
Body Corpus Callosum	BCC
Splenium Corpus Callosum	SCC
Right and left Corticospinal tract	CST_R; CST_L
Right and left Anterior Limb of the Internal Capsule	ALIC_R; ALIC_L
Right and left Posterior Limb of the Internal Capsule	PLIC_R; PLIC_L
Right and left Anterior Corona Radiata	ACR_R; ACR_L
Right and left Superior Corona Radiata	SCR_R; SCR_L
Right and left Posterior Corona Radiata	PCR_R; PCR_L
Right and left Posterior Thalamic Radiation	PTR_R; PTR_L
Right and left Inferior Longitudinal Fasciculus	ILF_R; ILF_L
Right and left External Capsule	EC_R; EC_L
Right and left Cingulum (cingulate gyrus portion)	C_CG_R; C_CG_L
Right and left Cingulum (hippocampal portion)	C_HIP_R; C_HIP_L
Right and left Superior Longitudinal Fasciculus	SLF_R; SLF_L
Right and left Uncinate Fasciculus	UF_R; UF_L

4.3.4. Age trajectories

In the previous chapter, a preliminary analysis was used to show the potential interaction between age and variations in 15q11.2 BP1-BP2 dosage on white matter microstructure. Here, the same analysis was performed in the UK Biobank sample, where age-by-dosage and the quadratic age²-by-dosage interactions were also evaluated in the regional analysis for each white matter tract.

4.3.5. Sex differences

In order to examine differences between male and female phenotypes in relation to CNV dosage, a sex-by-dosage interaction was also evaluated. Following this, the effect sizes for the male and female cohorts were analysed separately, in the same way described for the whole-group analysis.

4.4. Results

4.4.1. Between-group regional analyses

Group comparisons of DTI-derived measures revealed a pattern of white matter changes similar to the one reported in the deCODE Icelandic sample in Chapter 3. Again, increases in FA were seen in the deletion carriers, where duplication carriers showed overall decreases in FA, compared to the NoCNV group, confirming a reciprocal effect of 15q11.2 BP1-BP2 dosage on white matter microstructure (**Figure 4.1**). The pairwise comparisons, after FDR correction, revealed significant differences in FA between the deletion carriers and the NoCNV group in the ALIC_L, PLIC_R, PLIC_L, C_CG_R and C_HIPP_L white matter tracts, but the majority of significant differences were seen between deletion and duplication carriers, where significant effects on FA are found in ALIC_R, ALIC_L, PLIC_R, PLIC_L, PCR_L, EC_L, C_CG_R, C_HIPP_R, and C_HIPP_L (**Table 4.3**). No significant differences were found between the duplication carriers and the NoCNV group.

Figure 4.2 shows the Cohen's *d* effect sizes for deletion and duplication carriers when compared to NoCNV group. The effect sizes for these comparisons were overall small and the largest effect sizes were found in the anterior and posterior limb of the internal capsule, external capsule, and in both cingulate gyrus and hippocampal portion of the cingulum, where a reciprocal effect of 15q11.2 BP1-BP2 gene dosage can be seen in both FA and RD measures. In fact, when looking at comparisons between deletion and duplication carriers, the effect sizes were large in the posterior limb of the internal capsule, in both FA and RD, and medium in other white matter tracts, as shown in **Figure 4.3**, emphasising this reciprocal effect between deletion and duplication. **Figure 4.4** shows a comparison between the effect sizes found in both deCODE and UK Biobank samples for FA values comparisons. In both samples, the largest effect sizes were found for increased FA in deletion carriers in the anterior and posterior limbs of the internal capsule and also external capsule. Interestingly, the same trend of reduced FA in the fornix of the deletion carriers is seen, but again with negligible effect, according to Cohen's criteria (*Cohen, 1977*). However, in the UK Biobank sample a significant difference in MD was found in the fornix between deletion and duplication carriers, where deletion carriers show increased MD compared to the duplication (**Figure 4.1**). This increased MD was driven by increases in AD and RD in deletion carriers (**Figure 4.2**). There are however some differences between the samples. First, the effect sizes are overall smaller in the UK Biobank sample. Second, in the deCODE sample, increased FA is found consistently in all white matter tracts (with exception of the fornix and the corticospinal tract), whereas in the UK Biobank data some additional white matter tracts showed decreased FA trends in the deletion carriers (**Figure 4.3**). However, these decreases in FA were found to not be significant and are also considered negligible, according to Cohen's criteria (*Cohen, 1977*).

Table 4.3 - Group differences between deletion and controls with NoCNV, duplications and NoCNV, and deletions and duplications carriers.

Effects of 15q11.2 BP1-BP2 CNV dosage are shown for FA, AD, RD, and MD. Groups were compared as defined in the dependent variable column, and the direction of effect is represented by a positive or negative value. Here only white matter tracts showing significant differences when comparing deletions to duplications carriers are shown. (* < 0.05, ** < 0.01, ***<0.001). White matter tracts abbreviations can be found on **Table 4.2**.

	Dependent variable	ROI	<i>t value</i>	<i>p-value</i>	<i>p-value (FDR)</i>	Effect size (Cohen's d)
FA	Del vs NoCNV	ALIC_R	2.58	0.01	0.08	0.36
		ALIC_L	3.08	0.002	0.05*	0.43
		PLIC_R	3.2	0.001	0.04*	0.44
		PLIC_L	3.22	0.001	0.04*	0.44
		PCR_L	1.02	0.3	0.5	0.14
		EC_L	2.67	0.008	0.08	0.37
		C.CG_R	3.54	0.0004	0.04*	0.49
		C_HIP_R	1.81	0.07	0.2	0.25
		C_HIP_L	3.2	0.001	0.04*	0.44
	Dup vs NoCNV	ALIC_R	-2.05	0.04	0.2	-0.29
		ALIC_L	-1.69	0.09	0.3	-0.24
		PLIC_R	-2.67	0.008	0.2	-0.38
		PLIC_L	-2.75	0.006	0.2	-0.39
		PCR_L	-3.02	0.003	0.1	-0.43
		EC_L	-1.25	0.21	0.4	-0.18
		C.CG_R	-2.21	0.03	0.2	-0.31
		C_HIP_R	-2.5	0.01	0.2	-0.36
		C_HIP_L	-1.67	0.1	0.3	-0.24
	Del vs Dup	ALIC_R	3.27	0.001	0.02*	0.66
		ALIC_L	3.36	0.0008	0.01*	0.65
		PLIC_R	4.16	0.00003	0.002**	0.95
		PLIC_L	4.23	0.00002	0.002**	0.98
		PCR_L	2.88	0.004	0.04*	0.54
		EC_L	2.76	0.006	0.04*	0.57
		C.CG_R	4.06	0.00005	0.002**	0.78
		C_HIP_R	3.07	0.002	0.02*	0.59
		C_HIP_L	3.42	0.0006	0.01*	0.68

AD	Del vs NoCNV	PLIC_L	1.99	0.05	0.2	0.27
	Dup vs NoCNV	PLIC_L	-1.9	0.06	0.3	-0.27
	Del vs Dup	PLIC_L	2.75	0.006	0.05*	0.62
RD	Del vs NoCNV	PLIC_R	-2.13	0.03	0.2	-0.29
		PLIC_L	-2.67	0.008	0.08	-0.37
		C_CG_R	-2.82	0.005	0.06	-0.39
		UF_L	-2.6	0.009	0.08	-0.37
	Dup vs NoCNV	PLIC_R	2.46	0.01	0.2	0.35
		PLIC_L	2.44	0.01	0.2	0.35
		C_CG_R	1.96	0.05	0.3	0.28
		UF_L	1.93	0.05	0.3	0.27
	Del vs Dup	PLIC_R	-3.25	0.001	0.02*	-0.79
		PLIC_L	-3.62	0.0003	0.009*	-0.86
		C_CG_R	-3.38	0.0007	0.01*	-0.66
		UF_L	-3.2	0.001	0.02*	-0.68
MD	Del vs NoCNV	Fornix	0.67	0.01	0.08	0.36
	Dup vs NoCNV	Fornix	-1.55	0.12	0.3	-0.22
	Del vs Dup	Fornix	2.9	0.004	0.04*	0.51

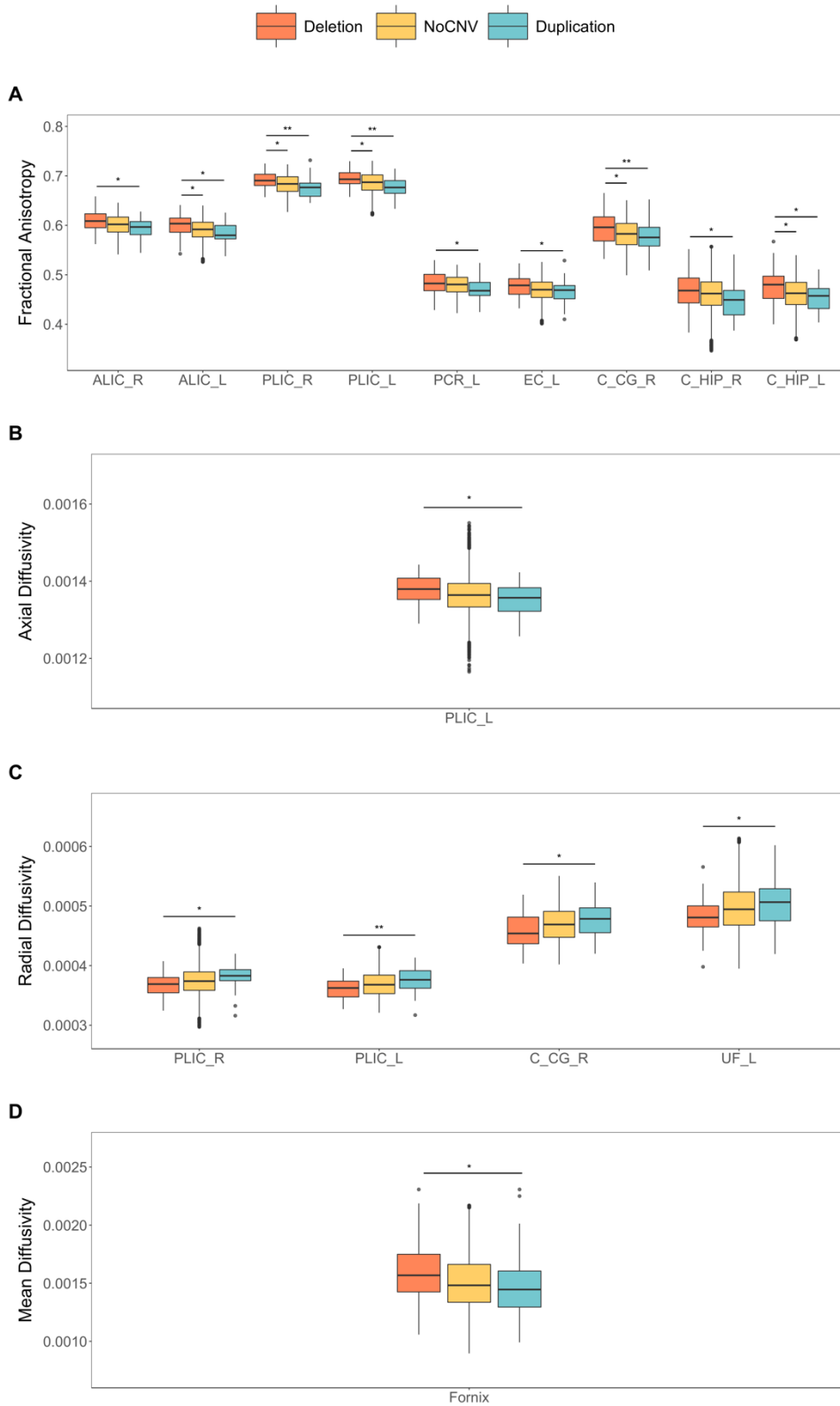
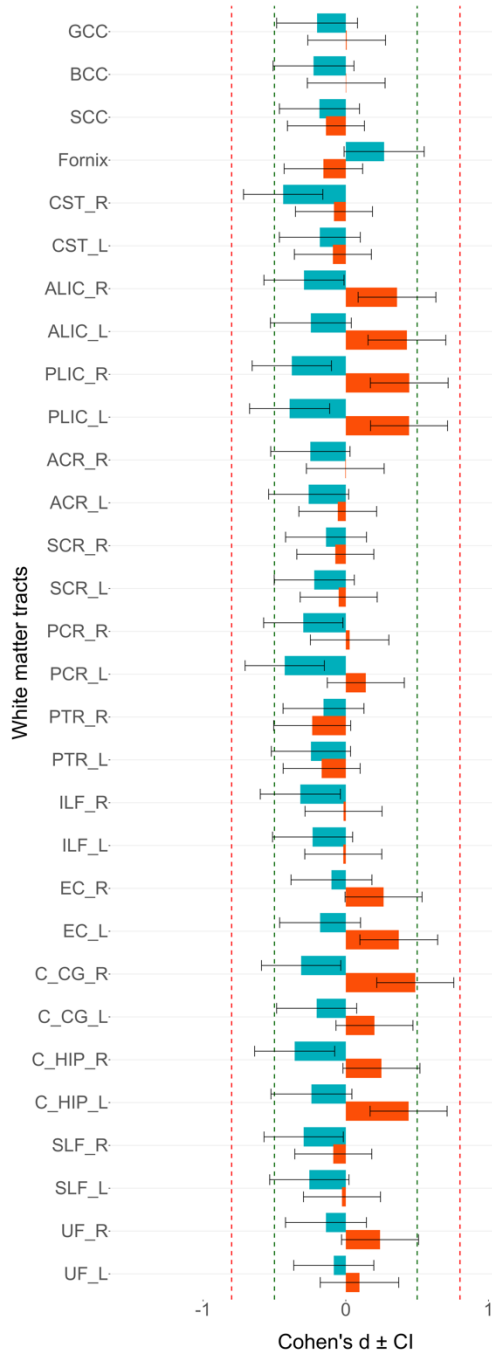


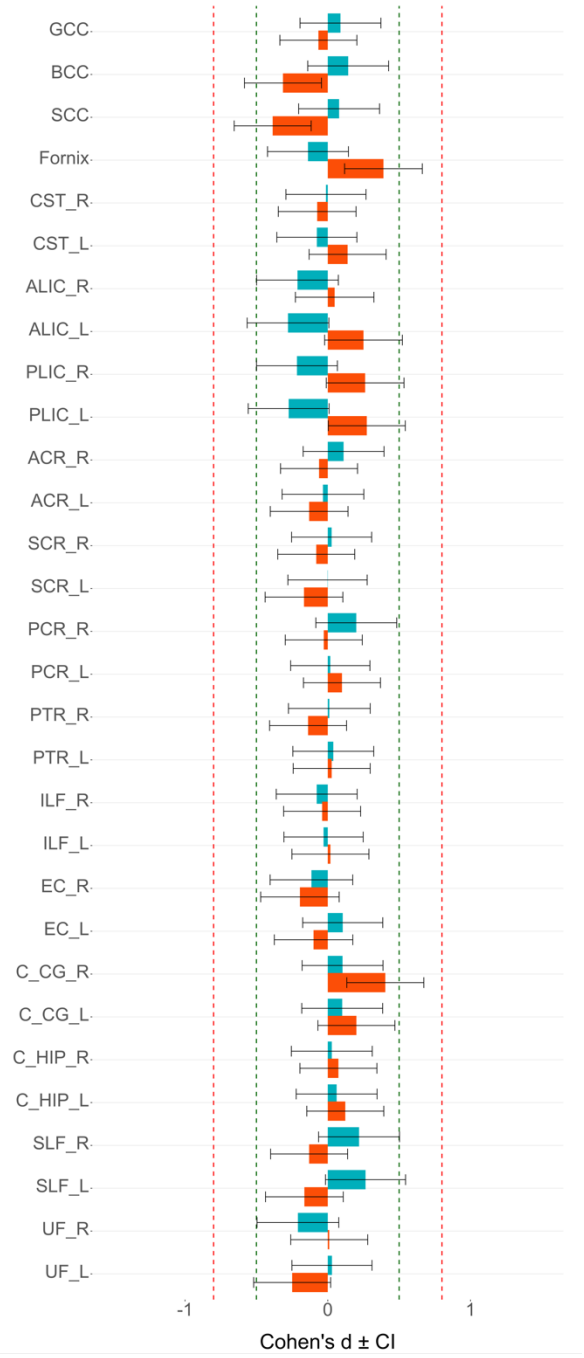
Figure 4.1 - Boxplots showing group differences for the UK Biobank TBSS-derived measures.

Only significant pairwise group differences after FDR correction ($p < 0.05$) are shown for **A** fractional anisotropy, **B** axial diffusivity, **C** radial diffusivity and **D** mean diffusivity. * $p < 0.05$, ** $p < 0.01$, *** $p < 0.001$. White matter tracts abbreviations can be found in **Table 4.2**.

A Fractional Anisotropy



B Axial Diffusivity



■ Deletion ■ Duplication

(Figure continues on next page)

C Radial Diffusivity

D Mean Diffusivity



Figure 4.2 - Diverging bars for Cohen d' effect sizes for group differences when comparing deletion and duplication carriers versus controls.

Diverging bars for Cohen d' effect sizes for group differences when comparing deletion and duplication versus controls with no large copy number variants for the different DTI metrics: **A** fractional anisotropy, **B** axial diffusivity, **C** radial diffusivity, and **D** mean diffusivity. The thresholds where an effect size is considered to be large (0.8) or medium (0.5), according to Cohen's criteria (Cohen, 1977), are represented by a vertical red or green dashed line, respectively. White matter tracts abbreviations can be found in **Table 4.2**.

Deletion vs Duplication

A Fractional Anisotropy

B Axial Diffusivity

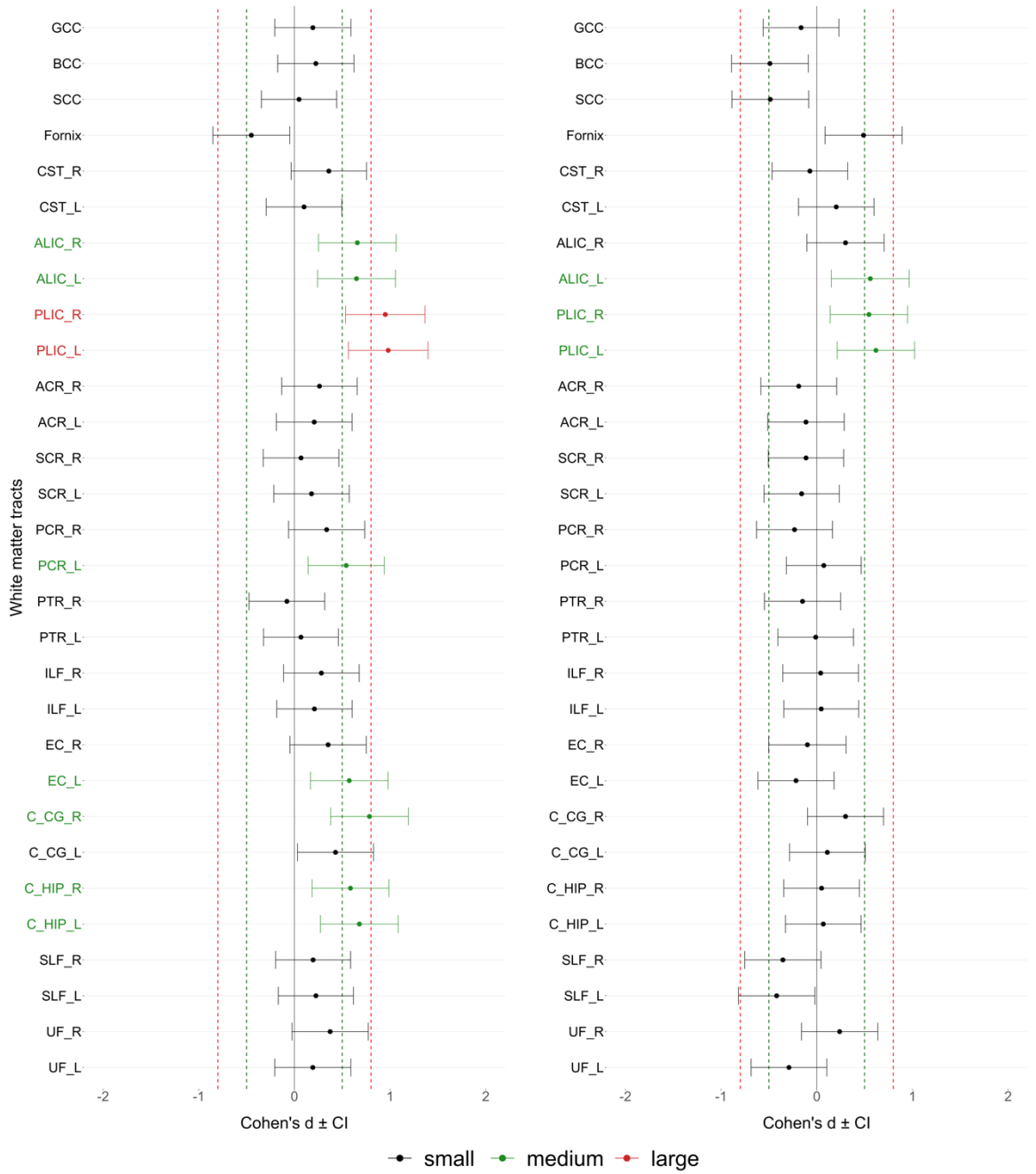
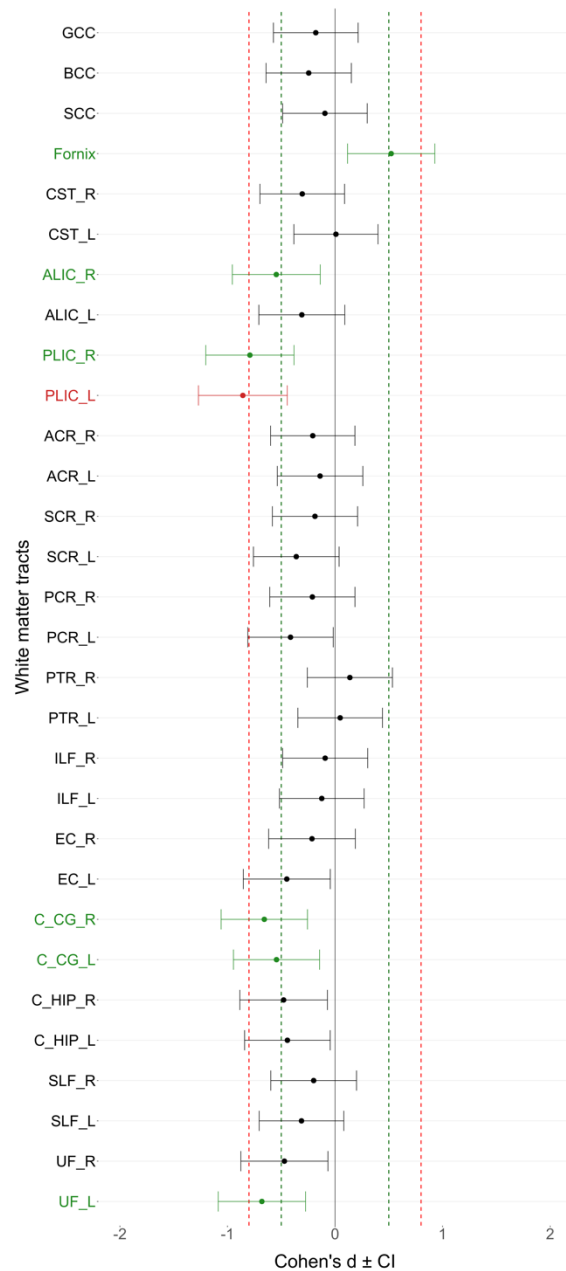


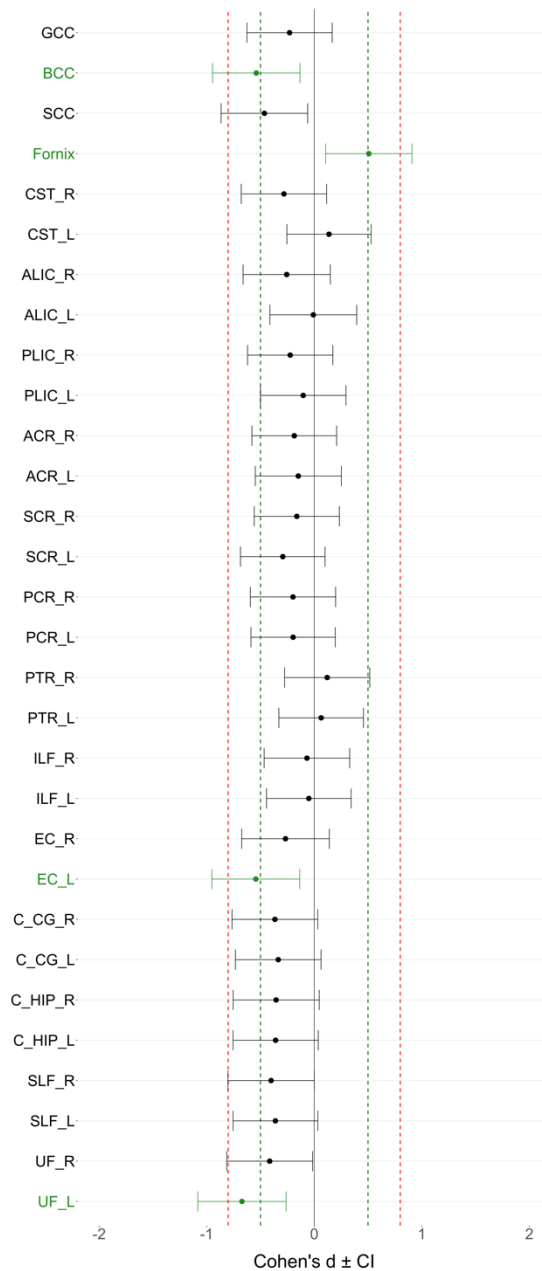
(Figure continues on next page)

Deletion vs Duplication

C Radial Diffusivity



D Mean Diffusivity



● small ● medium ● large

Figure 4.3 – Cohen d' effect sizes for group differences when comparing deletion versus duplication carriers.

Cohen d' effect sizes for group differences when comparing deletion versus duplication carriers for the different DTI metrics: **A** fractional anisotropy, **B** axial diffusivity, **C** radial diffusivity, and **D** mean diffusivity. The thresholds where an effect size is considered to be large (0.8) or medium (0.5), according to Cohen's criteria (Cohen, 1977), are represented by a vertical red or green dashed line, respectively. White matter tracts abbreviations can be found in **Table 4.2**.

deCODE sample

UKBiobank sample

A Fractional Anisotropy

B Fractional Anisotropy

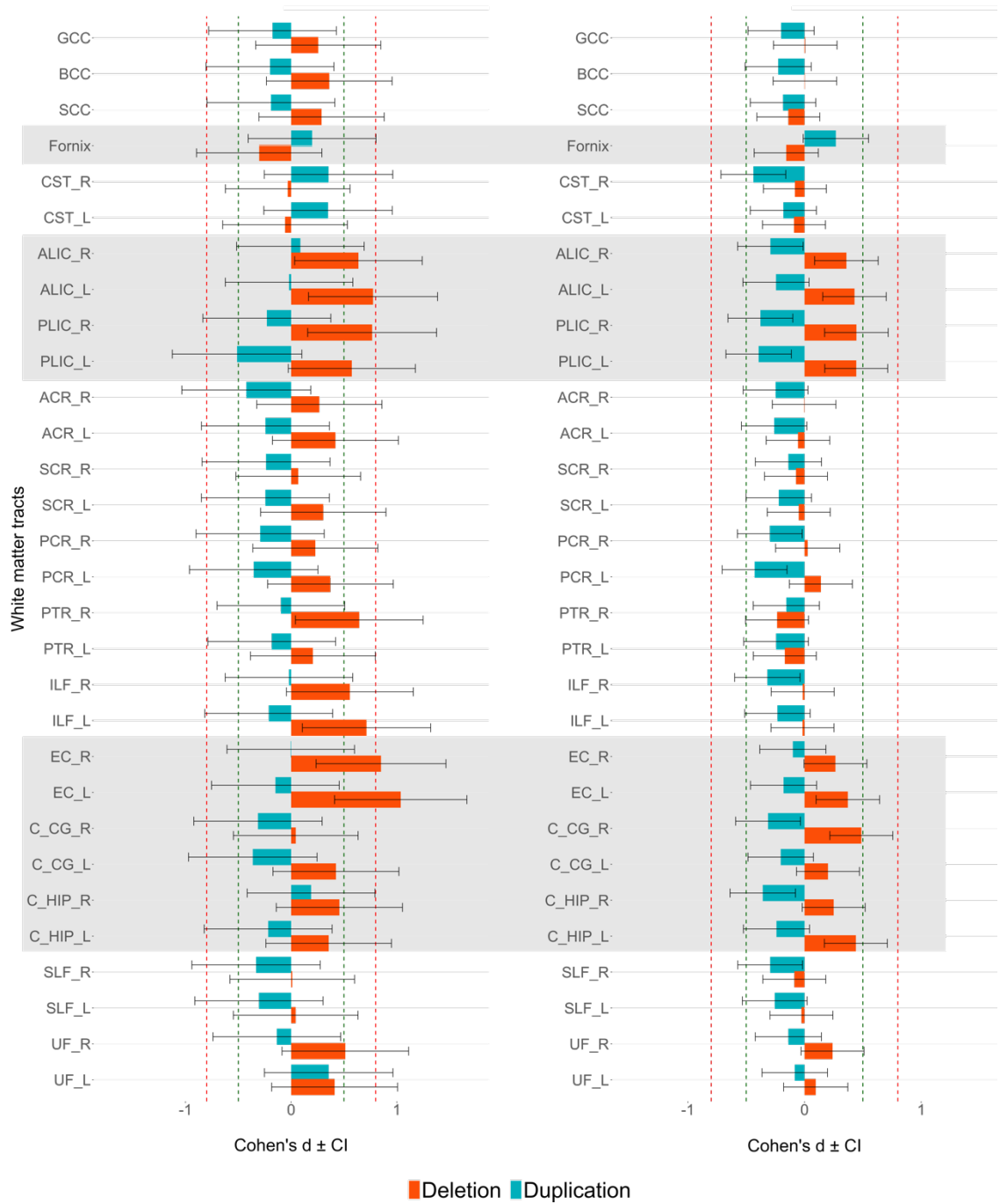


Figure 4.4 – Cohen d' effect sizes in the samples from deCODE and UKBiobank.

Cohen d' effect sizes for group differences when comparing deletion and duplication carriers versus controls with no large copy number variants for fractional anisotropy in the **A** deCODE sample, explored in Chapter 3, and **B** in the UK Biobank sample, explored in this chapter. The thresholds where an effect size is considered to be large (0.8) or medium (0.5), according to Cohen's criteria (Cohen, 1977), are represented by a vertical red or green dashed line, respectively. White matter tracts abbreviations can be found in **Table 4.2**.

4.4.2. Age trajectories

In the previous chapter, preliminary evidence of an interaction effect between age and CNV dosage was reported in the deCODE Icelandic sample. In the UK Biobank sample, only significant interactions were seen in AD in some white matter tracts. The weaker evidence for significant interactions between age and CNV dosage in the UK Biobank data might be attributable to the older age of the participants and the narrower age range of the sample. For comparison, the quadratic age trajectories for FA from the deCODE Icelandic and UK Biobank samples are plotted in **Figure 4.5** for the anterior and posterior limbs of the internal capsule, given the sensitivity of this region to variations in 15q11.2 BP1-BP2 in both samples. **Figure 4.5** illustrates a similar relationship between age progression and dosage in both samples, with FA decreasing in the NoCNV group with age, and maintaining or increasing in the 15q11.2 BP1-BP2 deletion carriers.

deCODE sample

UKBiobank sample

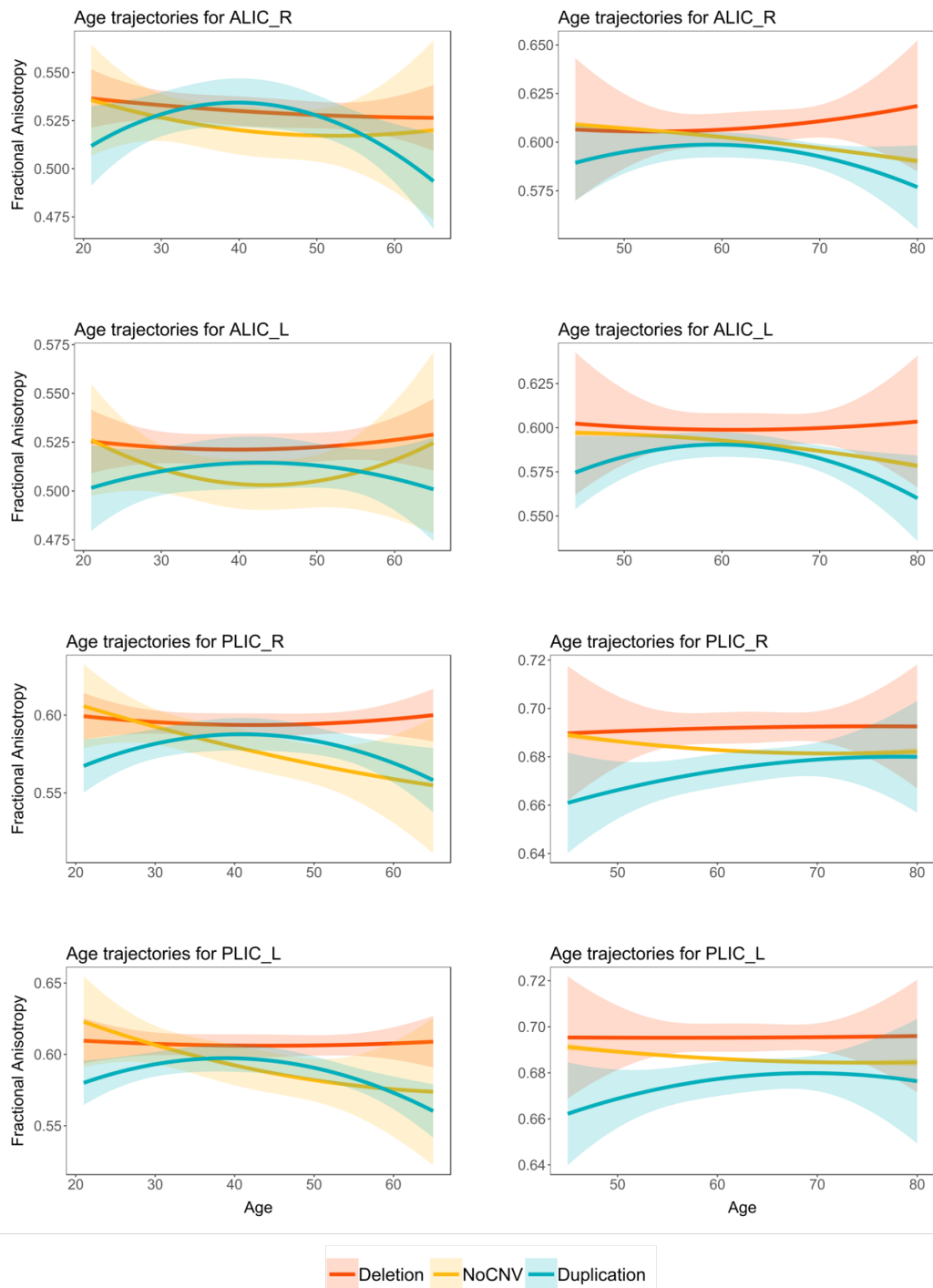


Figure 4.5 – Comparison between age trajectories in the deCODE Icelandic sample and UK Biobank sample.

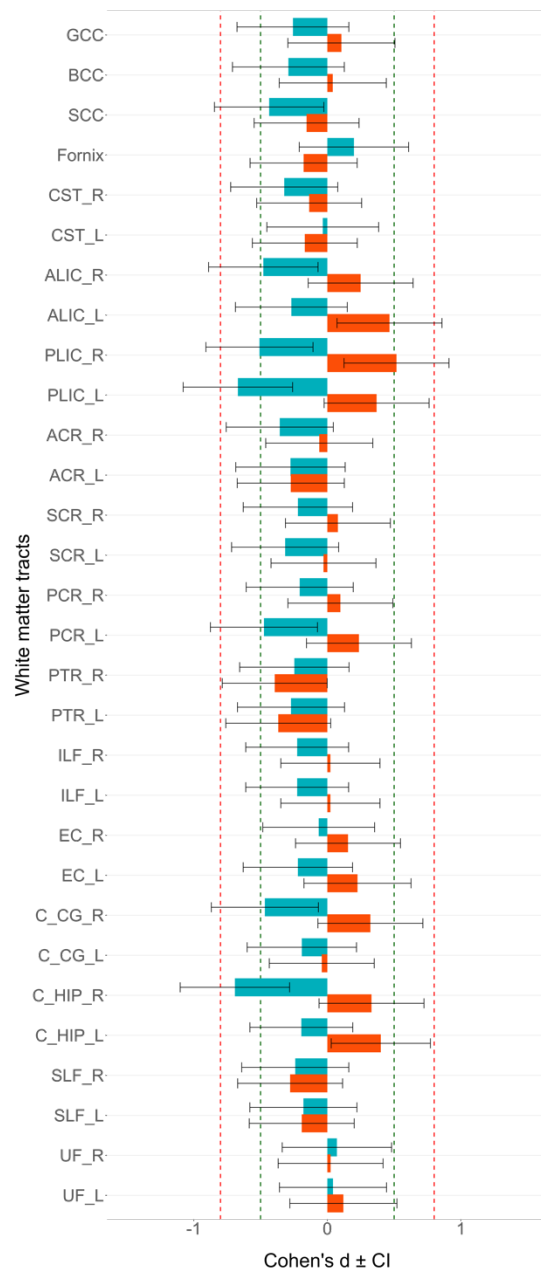
Quadratic age trajectories in deCODE Icelandic sample (left) and UK Biobank sample (right) for deletion (red), NoCNV (yellow), and duplication (blue) groups, showing the quadratic relationship between fractional anisotropy and age for the following white matter tracts: A ALIC_R, B ALIC_L, C PLIC_R, and D PLIC_L. Shaded regions represent 95% confidence intervals. White matter tracts abbreviations can be found in **Table 4.2**.

4.4.3. Sex Differences

A sex-by-dosage interaction model was also used to investigate sex differences in relation to 15q11.2 BP1-BP2 dosage. Similar to the findings in deCODE Icelandic sample, no significant interaction effect was found across the brain in the UK Biobank sample. However, contrary to the findings in the previous chapter, no differences in effect sizes were found when analysing males and females separately in the UK Biobank sample, where **Figure 4.6** shows similar direction and magnitude of effects in most white matter tracts. Moreover, no significant differences were found in the effect sizes of the deletion vs duplication comparison between males and females ($t=0.38$, $p=0.71$), as assessed using a two-tailed paired t-test.

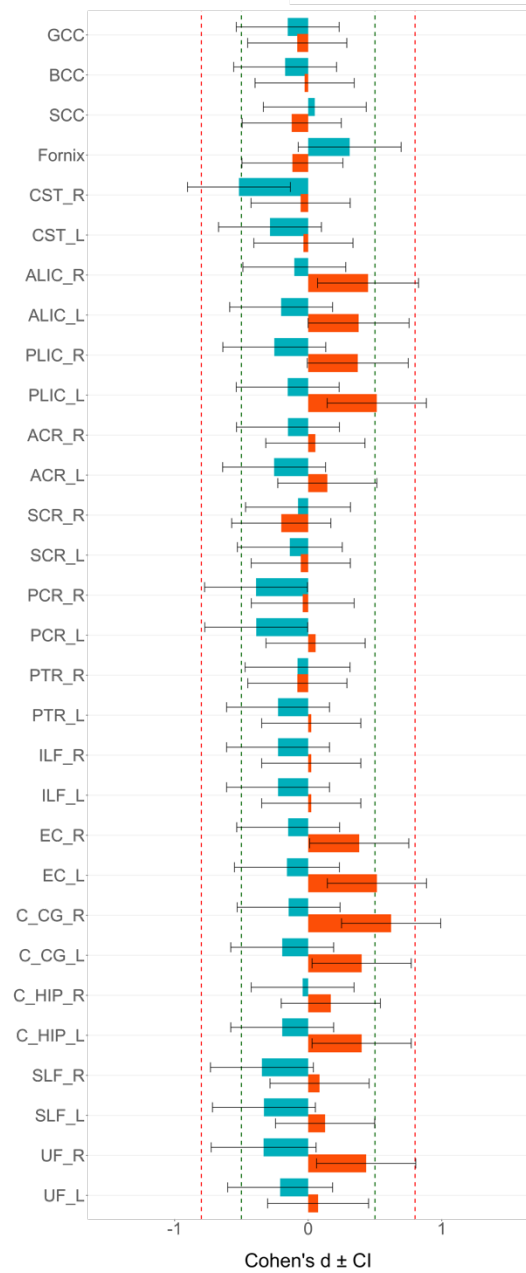
Males

A Fractional Anisotropy



Females

B Fractional Anisotropy



■ Deletion ■ Duplication

Figure 4.6 - Gender differences in Cohen d' effect sizes, when comparing deletion and duplication carriers versus controls.

Cohen d' effect sizes for group differences when comparing deletion and duplication carriers versus controls with no large CNV for fractional anisotropy in **A** males and **B** females. The thresholds where an effect size is considered to be large (0.8) or medium (0.5), according to Cohen's criteria (Cohen, 1977), are represented by a vertical red or green dashed line, respectively. White matter tracts abbreviations can be found in **Table 4.2**.

4.5. Discussion

With the aim of replicating the findings from the previous chapter, DTI-derived measures from British and Irish descendent participants from a subsample of the UK Biobank database were analysed. Here, deletion and duplication carriers of the 15q11.2 BP1-BP2 CNV were compared to thousands of controls with no large CNVs. In white matter tracts showing significant dosage effects, increases in FA in the deletion carriers and decreases in FA in duplication carriers were found, where the NoCNV group was intermediate between deletion and duplication carriers. These results largely replicate the previous findings in the deCODE Icelandic sample (Chapter 3) and therefore confirm the mirrored phenotype associated with 15q11.2 BP1-BP2 dosage on white matter microstructure. Furthermore, the largest effect for these differences was seen in the anterior and posterior limbs of the internal capsule, the same white matter tracts showing higher sensitivity to variations in the 15q11.2 BP1-BP2 region in the deCODE Icelandic sample. Significant differences were also found in the external capsule and cingulum (both cingulate gyrus and hippocampal portion), white matter tracts also shown to be affected in the previous study. Overall the effect sizes in the UK Biobank sample were smaller than the ones in the deCODE Icelandic sample. Age trajectories showed a similarity in white matter progression with age in both samples, but no relevant differences were found between males and females in the UK Biobank sample.

4.5.1. Similarities and differences between the UK Biobank sample and deCODE Icelandic sample

In Chapter 3, extensive dosage-dependent effects of 15q11.2 BP1-BP2 CNV on white matter microstructure were described in an Icelandic sample. Considering the importance of replication in science, as well as the unique nature of the Icelandic sample and the need to replicate these findings across more cosmopolitan populations, I looked at the effect of this CNV on white matter in an independent sample, selected from the UK Biobank database. This study raised important considerations. First, the reciprocal effect of the 15q11.2 BP1-BP2 CNV on white matter microstructure was replicated in the UK Biobank sample, showing a similar pattern of effects and therefore increasing the confidence of a mirrored white matter phenotype associated with this CNV. Second, the same white matter tracts revealing higher sensitivity to dosage effects of 15q11.2 BP1-BP2 in the

Icelandic sample show, again, significant differences in the UK Biobank sample, highlighting a role for the internal and external capsules. Third, the effect sizes in the UK Biobank sample were overall small, and therefore lower than the ones found in the deCODE sample. The reduced effect sizes could be a consequence of the increased heterogeneity associated with the UK Biobank sample, both in genetic and environmental factors, compared to the more homogeneous nature of the Icelandic population. Furthermore, in this study, carriers of the 15q11.2 BP1-BP2 CNV were compared to thousands of controls with different backgrounds, which also increases the heterogeneity of the sample. It is however interesting to note that, group comparisons revealed significant differences between the deletion carriers and the NoCNV controls in the UK Biobank, whereas only significant differences between deletion and duplication carriers were found in the Icelandic sample (**Figure 4.1**, in this chapter, and **Figure 3.2** in Chapter 3). This could be a result of increased statistical power achieved using large cohorts, allowing the identification of statistical differences between groups, even when their effect sizes are small (*Miller et al., 2016*). Finally, in the deCODE Icelandic sample, the deletion had a greater impact on white matter than the duplication, showing higher effect sizes when compared to the NoCNV group, which was not as clear-cut in the UK Biobank data, with the effect sizes being more similar in the deletion and duplication, when compared to NoCNV controls (**Figure 4.2** and **Table 4.3**). Moreover, some decreases in FA were found in deletion carriers from the UK Biobank data, however these effects were very small and their effect is considered negligible (Cohen d' effect < 0.2) by *Cohen, 1977* (**Figure 4.2** and **Figure 4.4**). Nevertheless, when comparing carriers to the NoCNV control group, only deletion carriers showed significant differences, whereas no changes were found between duplication carriers and NoCNV controls, and significant differences were only found in white matter tracts where deletion carriers showed increased FA.

Considering the white matter tracts showing decreased FA in deletion carriers, the fornix is of special interest since decreases in FA in this tract were also found in deletion carriers from the deCODE Icelandic sample. In the UK Biobank sample, a significant difference in MD, driven by increases in AD and RD, in deletion carriers is seen in this tract when comparing deletion to duplication carriers (**Table 4.3** and **Figure 4.1**). The functional outcomes of this 15q11.2 BP1-BP2 dosage effect on the fornix are yet unknown, however, as stated in the previous chapter, the fornix is a white matter bundle projecting from the hippocampus, a grey matter structure frequently implicated in

neurodevelopmental and neurodegenerative disorders. This structure has been shown to be implicated in cognitive disturbances and memory function (*Zhuang et al., 2012*).

In addition to the different genetic and environmental background in both samples, other important consideration is that different scanners with different field strengths, gradient directions, and b-values were used to collect the imaging data in each study, as well as different pre-processing pipelines to extract the DTI measures from the raw data. In the deCODE Icelandic sample, the MRI data were collected on a Philips Achieva 1.5T system, using 17 gradient directions and $b=800\text{s/mm}^2$, and the data were pre-processed in ExploreDTI v.4.8.3 (*Leemans et al., 2009*); whereas the UK Biobank MRI data were collected on a Siemens Skyra 3T scanner, using 50 directions and $b=1000\text{s/mm}^2$, and the pre-processing was done in FSL. Previous studies using different scanners, especially with different field strengths, have shown a striking impact on MRI data (*Kostro et al., 2014*), and specifically on DTI measures (*Dyrba et al., 2013*); and others have found different pre-processing methods to impact DTI measures as well as the statistical significance and interpretation of the results (*Maximov et al., 2015*). Nevertheless, although this could further explain some of the variability between samples, it is encouraging that similar conclusions were found in both samples despite all the variability, increasing our confidence of a consistent dosage effect of 15q11.2 BP1-BP2 on white matter microstructure.

4.5.2. Age trajectories and gender differences

The UK Biobank sample was 20 years older on average than the deCODE Icelandic sample, and the age range was narrower, making it harder to find interactions between age and CNV dosage on white matter microstructure. However, having thousands of controls with no large CNVs allowed a more reliable assessment of a typical age trajectory in the UK Biobank sample. As shown on the right side of **Figure 4.5**, the NoCNV group follows the typical pattern of gradual reduction of FA with age in the UK Biobank sample (*Krogsrud et al., 2016*), a characteristic that is not always seen in controls from the deCODE Icelandic sample (left side of **Figure 4.5** and **Figure 3.6** of Chapter 3). A striking similarity between both samples is the progression of FA with age in the deletion carriers. Again, deletion carriers seem to maintain or even slightly increase FA values with age, contrary to what happens in the NoCNV group (**Figure 4.5**). The

duplication carriers seem to follow the typical quadratic relationship of FA with age but, again, the peak of FA seems to occur later in life, where there is a more accentuated decrease in FA in late adulthood. These results are difficult to interpret, and a bigger sample including a younger group (from childhood until late adulthood) will be needed to reliably investigate the impact of 15q11.2 BP1-BP2 dosage on white matter microstructure development.

Preliminary evidence for sex differences was found in the Icelandic sample, as described in the previous chapter, where males appeared to be more sensitive to mutations in the 15q11.2 BP1-BP2 chromosomal region. However, no differences were found in the UK Biobank sample, and males and females showed a similar pattern and magnitude of effect sizes across white matter tracts (**Figure 4.6**). Therefore, sex differences were not replicated in this study. Nevertheless, the study of sex differences remains an important question when looking at the effect of these variants in the brain, and further investigations in bigger samples will be needed.

4.5.3. Limitations of the study and future directions

As stated above, several factors may have contributed to some of the variability seen between the samples. In order to approximately measure the degree of variability introduced by genetic and environmental heterogeneity, we would need a sample from the UK Biobank with similar age, cognitive, and acquisition/pre-processing characteristics, as the deCODE Icelandic sample. Processing both samples in the same way could, indeed, remove some of the variability between the samples. However, the overlap of results from the different samples showed that this effect was independent of data processing, increasing our confidence in the phenotype, as stated above. Moreover, in the previous study there were no group differences in the IQ measure, whereas this was not assessed in the present study. An important remaining question resides on how cognition in deletion carriers correlates with the increased FA, since deletion carriers were shown to have worse outcomes on cognitive function than the duplication carriers. Future work will involve looking at correlates between white matter microstructure and cognitive measures that were shown to be associated with white matter changes, such as fluid intelligence and reaction time measures (*Kievit et al., 2018; Karahan et al., 2019*), available in the UK Biobank project.

4.5.4. Conclusion

The previous results showing an effect of 15q11.2 BP1-BP2 CNV on white matter microstructure were replicated in this study using an independent sample with higher genetic and environmental heterogeneity. The converging evidence in both studies supports the hypothesis of a mirrored effect dependent on 15q11.2 BP1-BP2 CNV dosage on white matter microstructure. However, the underlying biological causes of this mirrored phenotype on white matter microstructure is still unknown. As described in the previous chapter, a role of *CYFIP1* gene on the 15q11.2 BP1-BP2 white matter phenotype is anticipated and will be explored in the next chapters using a novel *Cyfp1* haploinsufficiency rat model.

Chapter 5

White Matter Changes Associated with
haploinsufficiency of *Cyfp1* in a novel
CRISPR/Cas9 engineered rat model

5.1. Abstract

Background

In the previous chapters, global increases in FA in white matter were reported in human carriers of the 15q11.2 BP1-BP2 deletion. However, the biological basis of these changes is unknown. *CYFIP1* is a gene in this region that is known to be essential for correct dendritic spine formation in neurons via interactions in two distinct processes: inhibiting local protein synthesis and regulating actin remodelling. Although the impact of *CYFIP1* on white matter is unknown, these processes are known to play a role in axon and myelin dynamics, making *CYFIP1* a strong gene candidate for the 15q11.2 BP1-BP2 imaging phenotype. In this chapter, white matter microstructure changes will be explored in a novel *Cyfp1* haploinsufficiency rat model, recapitulating the low dosage of *CYFIP1* gene present in 15q11.2 BP1-BP2 deletion carriers.

Methods

DTI data were collected on a cohort of 24 rats (12 WT and 12 *Cyfp1*^{+/-} rats). Using similar methods to the ones applied in the human cohort in Chapter 3, brain-wide voxel differences were explored using the TBSS method, employing two different correction methods. Furthermore, regional differences were further quantified through segmentation using binary masks and tractography methods.

Results

Extensive white matter changes were found in *Cyfp1*^{+/-} rat. Here the strongest evidence points to reductions in FA in the corpus callosum, external and internal capsules and areas of fimbria/fornix. Some evidence for increased FA was seen in some areas of fimbria and stria terminalis. The most pronounced effects for decreased FA were found in the corpus callosum and external capsule. Tractography revealed that posterior areas of the corpus callosum are more affected than anterior regions.

Conclusions

These results show an impact of *Cyfipl* haploinsufficiency on white matter microstructure in a rat model, where the corpus callosum showed a higher sensitivity to dysregulations in this gene. When comparing these current data with the human findings reported in the previous chapters, it is unlikely that *CYFIP1* is solely responsible for the 15q11.2 white matter phenotype, and additional work is required to determine the contribution made by the other three genes in this CNV locus.

5.2. Introduction

The biological basis of the increased risk for psychiatric disorders due to pathogenic deletions at 15q11.2 BP1-BP2 locus is unknown. In the previous chapters, extensive white matter changes in 15q11.2 BP1-BP2 carriers were reported, specifically widespread increases in FA in deletion carriers. These data raised three main questions: (1) which of the four genes in the 15q11.2 BP1-BP2 interval are important for the disturbances in white matter microstructure, (2) what are the cellular changes underlying the white matter effects, and (3) what are the functional consequences of the white matter changes in the context of the increased risk for disorder.

In light of these questions, some evidence from previous studies was presented in Chapter 3 highlighting *NIPAI* and *CYFIP1* genes as potential responsible genes for the white matter phenotype in 15q11.2 BP1-BP2, where axonal density, guidance, organisation and myelination could be compromised by dysregulations in these genes. However, given the close molecular links between *CYFIP1* and *FMRP*, together with the fact that both FXS patients (*Green et al., 2015; Hall et al., 2016*) and 15q11.2 BP1-BP2 deletion carriers (Chapter 3) showed similar increases in FA, I first speculated that these common changes in white matter microstructure could be a consequence, at least in part, of disruptions in the *CYFIP1-FMRP* complex. Dysregulations in this complex could potentially affect the processing, localisation, or translational regulation of mRNAs encoding key proteins involved in axonal development (*Sahoo et al., 2018; B. Wang et al., 2015*).

It is important to consider that, as an actin regulator, *CYFIP1* is likely to also affect white matter via the requirement of precise regulation of the actin cytoskeleton for normal cellular development, morphology and migration (*Bauer et al., 2009; Dent and Gertler, 2003; Zuchero et al., 2015*). As examples are the studies that have linked actin regulators to oligodendrocyte-myelin dynamics. The *WAVE1* and the *ILK* regulate oligodendrocyte differentiation and axon ensheathment (*Kim et al., 2006; O'Meara et al., 2013*), while the Arp2/3 complex, a key actin nucleator, is required for initiation of myelination (*Zuchero et al., 2015*), and Rho GTPases *Cdc42* and *Rac1* regulate myelin sheath formation (*Thurnherr et al., 2006*). Rare variants in the *CYFIP1* gene and polymorphisms, within and near the gene, have also been indicated as potentially increasing susceptibility to ASD (*Toma et al., 2014; Y. Wang et al., 2015*), and

schizophrenia (*Tam et al., 2010; Yoon et al., 2014*), and could be associated with 15q11.2 BP1-BP2 clinical phenotypes.

Deletions in the *Cyfp1* gene, in mouse models, have already been shown to impact dendritic branching and maturation (*De Rubeis et al., 2013; Pathania et al., 2014; Oguro-Ando et al., 2015; Abekhouk et al., 2017*), but no studies to date have looked at the impact of variations in this gene in white matter microstructure. Therefore, prior to this study, a novel *Cyfp1*^{+/-} rat line was developed using CRISPR/Cas9 technology, modelling the reduced gene dosage of *CYFIP1* in 15q11.2 BP1-BP2 deletion carriers. In the present and in the following chapters, white matter microstructural changes associated with *Cyfp1* haploinsufficiency will be explored in this *Cyfp1*^{+/-} rat line. In this chapter, DTI methods will be used to identify regions of white matter microstructure disruption associated with reduced levels of *Cyfp1*. Here, the use of a rat line is a major advantage providing a larger brain, compared to the smaller mouse brain, resulting in enhanced imaging resolution. This increased resolution allows for the detection of more subtle changes, and also permits the use of similar processing and analyses methods to the ones used in the human cohort, increasing the translational validity of the model (*Hoyer et al., 2014*). Therefore, the analyses comprised a brain-wide voxel-based approach using the TBSS tool and a regional analyses based on segmentation of regions-of-interest from DTI maps. Additionally, tractography was performed, and tracts were manually selected from the most relevant region. The overall aim of this study was to model possible contributions by *CYFIP1* to 15q11.2 BP1-BP2 deletion phenotype on white matter microstructure.

5.3. Materials and Methods

5.3.1. Rats

The *Cyfp1* rat model was created by Cardiff University in collaboration with Horizon Discovery (St Louis, USA) using CRISPR-Cas9 targeting (<https://www.horizondiscovery.com/>) and supported by a Wellcome Trust Strategic Award (DEFINE). The creation of this model was done before the beginning of this project. Full information on the creation and validation of the rat model is in the Appendix. Information about breeding and housing is present in the General Methods in

Chapter 2. A cohort of 24 rats (WT n=12 and *Cyfp1^{+/-}* n=12) was used for imaging, where all the rats were Long Evans and 5 months old males. All the experimental procedures were performed in accordance with institutional animal welfare and ARRIVE guidelines and the UK Home Office License PPL 30/3135.

5.3.2. Diffusion tensor imaging acquisition

The rats were anaesthetised with isoflurane in oxygen at 4% and maintained at 1% during the scanning. MRI scans were acquired with a 9.4T MRI scanner (Bruker, Karlsruhe, Germany) with a 30-cm bore and a gradient strength of up to 600 mT/m. The MRI protocol included DTI acquisition with a diffusion-weighted spin-echo EPI pulse sequence having the following parameters: TR/TE=4000/22 ms, $\Delta/\delta=10.5/4.5$ ms, two EPI segments, and 60 noncollinear gradient directions with a single b-value shell at 1000 s/mm² and one image with a b-value of 0 s/mm² (referred to as b₀). Geometrical parameters were: 34 slices, each 0.32 mm thick (brain volume) and with in-plane resolution of 0.32×0.32 mm² (matrix size 80×96; FOV 25.6×30.73 mm²). The DTI protocol lasted approximately 16 minutes. In addition, high resolution, T₂-weighted images were acquired for anatomical reference with a multi-slice multi-echo pulse sequence with the following parameters: TR of 7200ms, TE of 15ms and effective TE of 45ms, rare factor was 8. Image resolution was set to 0.22 mm³ with matrix size of 128×160×50 to cover the entire brain.

5.3.3. DTI data correction and DTI maps extraction.

ExploreDTI 4.8.3 was used in the preprocessing of the rat DTI data. Prior to DTI calculation, the DWI data were first regularised. The tensor was then calculated using robust estimation algorithm and DTI images were corrected for motion and eddy-current induced distortions (*Leemans and Jones, 2009*) and mean-DWI images were generated in ExploreDTI 4.8.3. Since most of the algorithms that automatically remove non-brain tissue from imaging data are not optimised for the shape of the rat brain, skull-stripping the rat brain was done using ExploreDTI and SPM (*version 12*, UCL, London, UK) following these steps:

- (1) T₂-weighted scans were anisotropically smoothed using ExploreDTI,

- (2) both smoothed T₂-weighted and mean-DWI images were bias corrected using the segmentation tool in SPM12,
- (3) the bias corrected T₂-weighted were co-registered with a population-specific template and multiplied by a binary template mask to remove the non-brain tissue
- (4) the skull was removed from the mean DWIs using the 3D masking option in ExploreDTI.

The data was then corrected for field inhomogeneities using ExploreDTI, where the skull-stripped mean DWI images were used as a native space mask, and the skull-stripped T₂-weighted structural scans were used as transformed space mask. In this step, each DWI image was nonlinearly warped to the T₂-weighted image using non-DWIs map as a reference. Finally, ExploreDTI was used to generate FA, AD, RD and MD maps.

5.3.4. Heat maps for differences in FA between WT and *Cyfp1*^{+/-} rats

As a first exploratory assessment, differential heat maps were computed in order to explore regions in the brain where FA could be either increased or reduced in the *Cyfp1*^{+/-} rats. Each FA map was warped to a study-specific template using the old normalisation tool in SPM (*version 12*, UCL, London, UK). The average FA maps for WT and *Cyfp1*^{+/-} rats were computed as well as a differential map, subtracting the average of the *Cyfp1*^{+/-} by the average of the WT FA maps ($\Delta(\text{Cyfp1}^{+/-} - \text{WT})$).

5.3.5. Tract-Based Spatial Statistics Analysis (TBSS) of DTI

In order to perform a similar voxel-wise analysis to the one used in the human data (Chapter 3), the TBSS tool (*Smith et al., 2006*), available in FSL, was used. All FA maps were submitted to a free-search for a best registration target, where each volume was first registered to every other volume, and the one requiring minimum transformation to be registered to other volumes was selected as the best registration target. This target was used as a template into which the registration was performed. Following registration, a mean FA map was calculated, thinned to represent a mean FA skeleton, and an optimal threshold of 0.2 was applied to the mean FA skeleton to create a binary white matter skeleton mask (**Figure 5.1**). The local FA-maxima, as well as AD-, RD-, and MD-, maxima of each rat were projected onto this white matter skeleton.

For the whole-brain TBSS analysis, differences in DTI measures between the two groups (WT and *Cyfp1^{+/-}*) were assessed using voxel-wise independent t-tests, where two different contrasts were used (WT>*Cyfp1^{+/-}*, and *Cyfp1^{+/-}*>WT). The randomize function (part of FSL) was used, together with the TFCE algorithm (*Smith and Nichols, 2009*), generating cluster-size statistics based on 1000 random permutations. For multiple comparison correction, first FWE correction was used with a threshold of $p < 0.05$ – the same correction method used in the human data (Chapter 3). Since only FA changes were found within this analysis, a less conservative correction method based on FDR correction was also used, proposed by Benjamini–Hochberg (*Benjamini and Hochberg, 1995*) and described in Chapter 3.

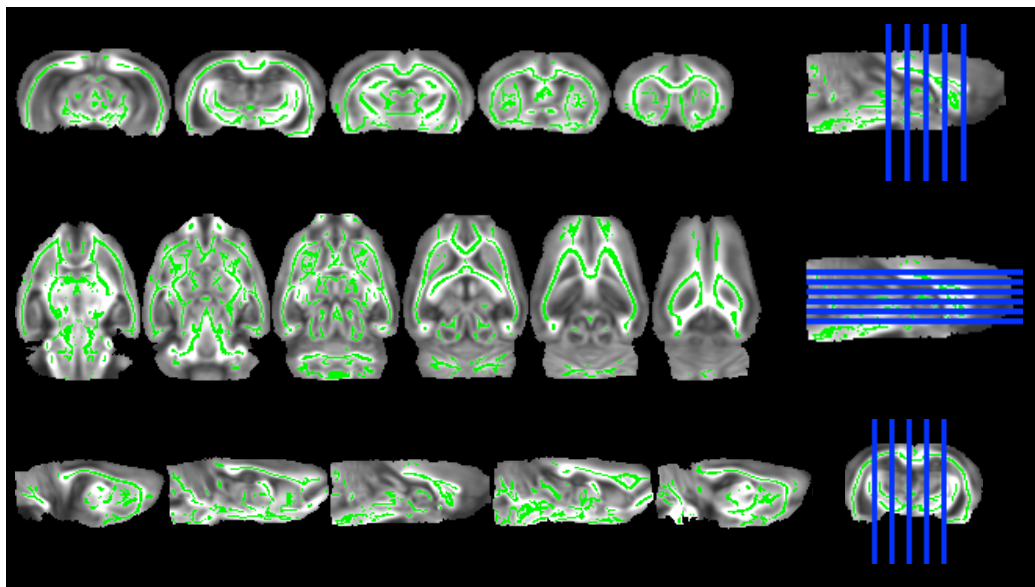


Figure 5.1 – White matter skeleton used for the Tract-Based Spatial Statistics analysis.

Mean white matter skeleton mask in green superimposed on the mean FA template image from all the 24 rats used for Tract-Based Spatial Statistics (*Smith et al., 2006*). An optimal threshold of 0.2 was applied to the mean FA skeleton to create the binary white matter skeleton mask.

5.3.6. Quantification of TBSS differences

The maps showing TBSS statistics do not provide quantifiable measures of the change in individual DTI parameters. Therefore, to further quantify the changes in areas where significant differences in FA were seen after FWE correction, ROIs were manually delineated using FSL. Several consecutive slices were outlined on the coronal plane and

the selected ROIs included the corpus callosum, internal capsule, external capsule, and fornix/fimbria regions. The CBJ13 MR-histology rat atlas at age P80 (*Calabrese et al., 2013*) was used as reference. A representation of the binary masks can be found in **Figure 5.2**. FA, AD, RD, and MD were quantified by applying these binary masks and extracting the mean values for each region across subjects.

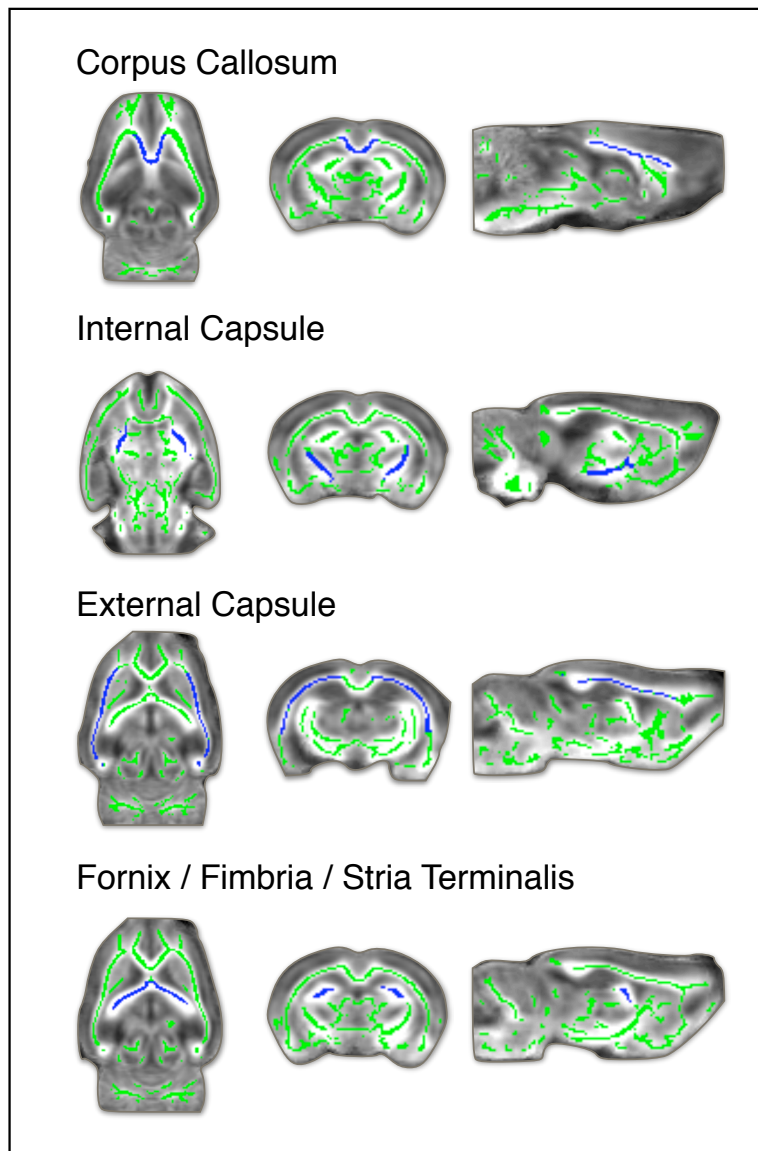


Figure 5.2 – White matter binary masks used for segmentation of specific white matter tracts.

White matter binary masks manually delineated (using FMRIB software library) for the white matter tracts that showed significant differences in the Tract-Based Spatial Statistics analysis. The binary masks are represented in blue and are superimposed on the white matter skeleton in green. The CBJ13 MR-histology rat atlas at age P80 (*Calabrese et al., 2013*) was used as reference.

5.3.7. Tractography

Tractography was performed using DTI-based algorithm, a type of deterministic tractography previously described (Basser *et al.*, 2000) and available in ExploreDTI. Here, the parameters used included a step size of 0.01 mm, curvature of 0.15 mm ($\alpha \sim 4^\circ$) and fibre length range between 1 and 100 mm. These parameters were shown to work for deterministic tractography of the mouse brain (Moldrich *et al.*, 2010). After tractography, the genu, body and splenium of the corpus callosum were manually delineated for each rat where only fibre bundles that travel through these regions were selected. All the fibre bundles were visually inspected in ExploreDTI, and fibres that did not belong to these regions were excluded (Figure 5.3). Quality of tractography was visually inspected, where 1 *Cyfp1*^{+/-} rat was removed in the analysis of the genu and splenium of the corpus callosum, and 2 *Cyfp1*^{+/-} rats were removed in the analysis of the body of the corpus callosum, since the quality of tractography was poor.

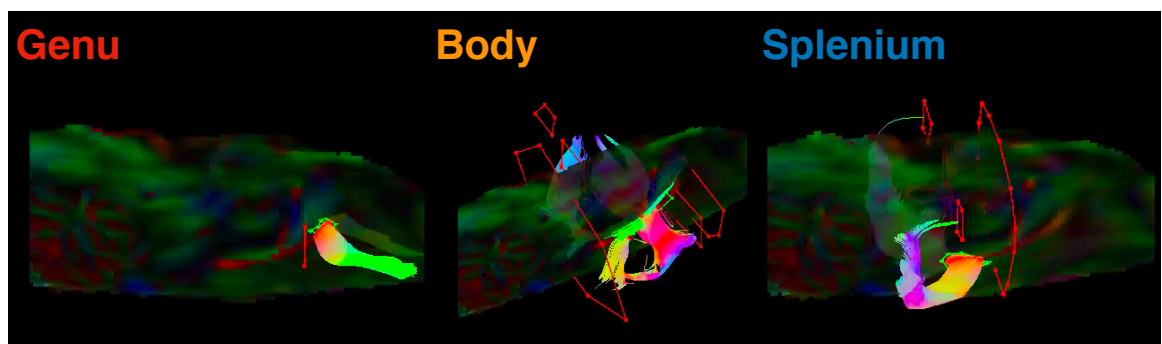


Figure 5.3 – Tractography of the corpus callosum.

Representative figure of manually delineated regions of the corpus callous (genu, body, and splenium) and respective fibres travelling through these areas. In ExploreDTI, ROIs these regions were segmented using “AND” gates (in green) and fibres of no interest were excluded using “NOT” gates (in red).

5.3.8. Statistical analysis

Both statistical analyses of the TBSS quantitative measures and tractography measures were carried out in RStudio statistical software *version 1.1.463* (R Foundation for Statistical Computing, Vienna, Austria), where two-tailed unpaired Student’s t-tests were used.

5.4. Results

5.4.1. Heat maps for differences in FA between WT and *Cyfp1*^{+/-} rats

To provide an initial characterisation of white matter microstructural changes in the whole-brain, color-coded heat maps of the FA values showing the average (of all WT and *Cyfp1*^{+/-} rats) were generated, where warm colours indicate fibre tracts with high FA (**Figure 5.4A**). The differential map ($\Delta(\text{Cyfp1}^{+/-} - \text{WT})$) showed regions of the brain where FA is decreased (in blue) and where FA is increased (in red) in *Cyfp1*^{+/-} compared to WT rats. **Figure 5.4B** show an impact of *Cyfp1* haploinsufficiency on white matter microstructure, where reductions in the corpus callosum and external capsule are seen in the *Cyfp1*^{+/-} rats. However, some increases in FA can also be noted, specifically in the stria terminalis of the *Cyfp1*^{+/-} rats, suggesting possible different effects in distinct brain regions.

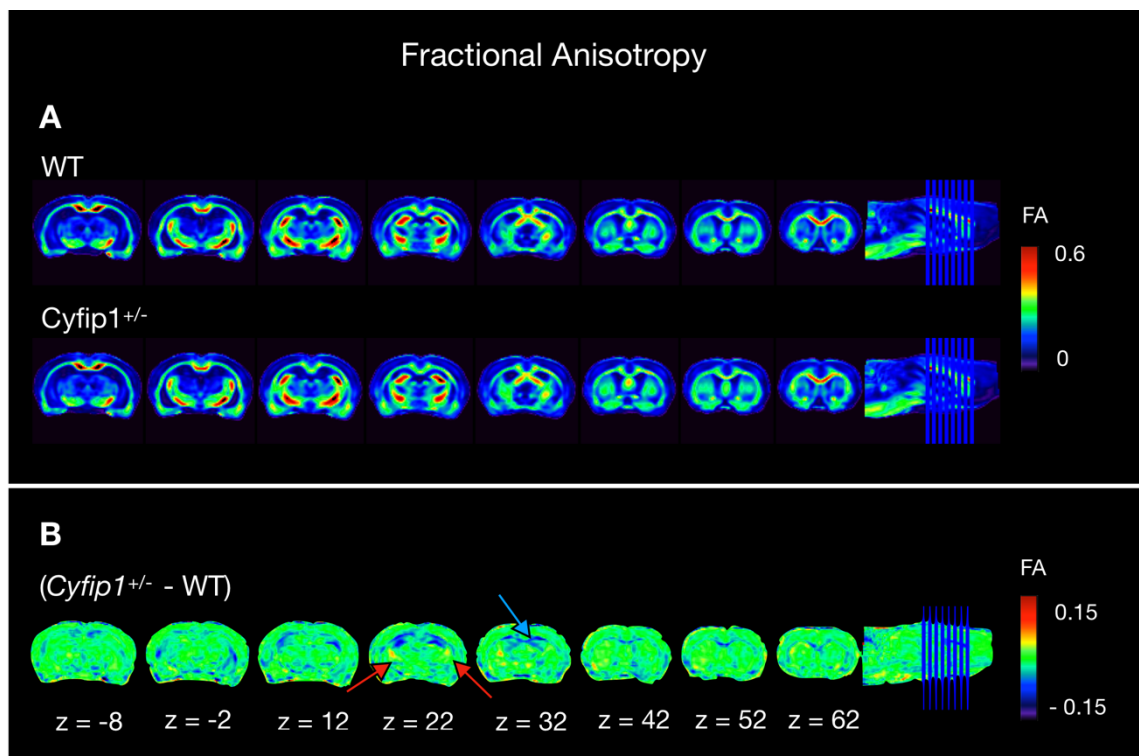


Figure 5.4 – Colour-coded heat maps for fractional anisotropy.

A Average fractional anisotropy maps (n=12 WT and n=12 *Cyfip1*^{+/-} rats) from each group. Warm colours indicate brain regions with high fractional anisotropy. **B** Differential maps between WT and *Cyfip1*^{+/-} average fractional anisotropy maps (Δ *Cyfip1*^{+/-} - WT). Warm colours indicate regions where fractional anisotropy was higher in *Cyfip1*^{+/-} rats and cold colours indicate regions where fractional anisotropy was higher in WT rats. The blue arrow points to regions of the corpus callosum, where fractional anisotropy is decreased in *Cyfip1*^{+/-} rats, and the red arrows points to regions of the fimbria/stria terminalis, where fractional anisotropy is increased in *Cyfip1*^{+/-} rats.

5.4.2. Between-group TBSS analysis – FWE correction

In order to investigate if any of these differences found in the differential heat maps were significant, group comparisons were carried out using TBSS. At first, a highly conservative FWE correction method was used, the same correction used in the human sample in Chapter 3. This approach showed significant reductions in FA in the corpus callosum, in the external and internal capsules, and in parts of the fimbria/fornix in *Cyfp1^{+/-}* rats, with no differences in AD, RD, and MD. There were no significant increases in FA using this method (**Figure 5.5**).

5.4.3. Quantification of TBSS differences

Next, I manually generated binary masks of regions of interest (corpus callosum, internal capsule, external capsule and fimbria/fornix), guided by the results from FWE correction using FSL (**Figure 5.2**), and extracted the mean FA, AD, RD and MD values in these white matter tracts. As demonstrated in **Table 5.1**, analysing the DTI data in this way (which averaged differences between WT and *Cyfp1^{+/-}* rats within a discrete fibre tract, as opposed to the voxel-by-voxel analysis which detected clusters of voxel differences in white matter tracts across the whole-brain) showed that the most significant differences were reductions in FA in the corpus callosum ($t=2.3$, $df=20.75$, $p<0.05^*$) and external capsule ($t=2.4$, $df=22$, $p<0.05^*$) in the *Cyfp1^{+/-}* rats compared to WT, as assessed with a two-tailed unpaired t-test. These data were consistent with the previous voxel-by-voxel analysis and provided the additional finding that the most extensive white matter changes in the *Cyfp1^{+/-}* rats occurred in these structures.

Table 5.1 – Group differences between *Cyfp1*^{+/-} and WT rats.

Quantification of changes in fractional anisotropy, axial diffusivity, radial diffusivity and mean diffusivity in regions where significant differences in fractional anisotropy were seen in TBSS analysis after FWE correction.

ROIs	FA		AD (10 ⁻²)		RD (10 ⁻³)		MD (10 ⁻³)	
	WT	<i>Cyfp1</i> ^{+/-}	WT	<i>Cyfp1</i> ^{+/-}	WT	<i>Cyfp1</i> ^{+/-}	WT	<i>Cyfp1</i> ^{+/-}
CC	0.49	0.46	0.14	0.13	0.69	0.71	0.92	0.91
	±0.02	±0.02*	±0.005	±0.006*	±0.05	±0.04	±0.04	±0.03
IC	0.45	0.44	0.11	0.11	0.53	0.54	0.74	0.73
	±0.02	±0.02	±0.007	±0.007	±0.03	±0.03	±0.04	±0.04
EC	0.38	0.36	0.12	0.12	0.73	0.73	0.89	0.88
	±0.02	±0.02*	±0.004	±0.003	±0.03	±0.02	±0.03	±0.02
FF	0.50	0.48	0.17	0.16	0.69	0.70	1.01	1.00
	±0.03	±0.02	±0.008	±0.004	±0.06	±0.04	±0.06	±0.03

Regions of interest (ROIs): corpus callosum (CC), internal capsule (IC), external capsule (EC) and fornix/fimbria (FF). Results obtained using TBSS-based ROI analysis, mean ± standard deviation, two-tailed unpaired t-test, *<0.05.

5.4.4. Tractography of the corpus callosum

Both whole-brain and regional analysis of the DTI data indicated a sensitivity of the corpus callosum to *Cyfp1* haploinsufficiency. In order to see if sub-regions of this structure were affected differently, tractography was performed in different segments of the corpus callosum (genu, body and splenium). This analysis allows the precise mapping of the corpus callosum tract anatomy within subjects, having the advantage of not being sensitive to the confounds of voxel-based registration (*Ciccarelli et al., 2008; McIntosh et al., 2008*). Here, corroborating the previous analysis, decreases in FA, in the *Cyfp1*^{+/-} rats, were found in all the segments of the corpus callosum, but only being significant in the splenium (t=2.8, df=21, p<0.05*) and body (t=2.3, df=18, p<0.05*) segments of the corpus callosum, compared to WT rats. Results are displayed in **Figure 5.6** and further extended to other DTI metrics (AD, RD, and MD) in **Table 5.2**.

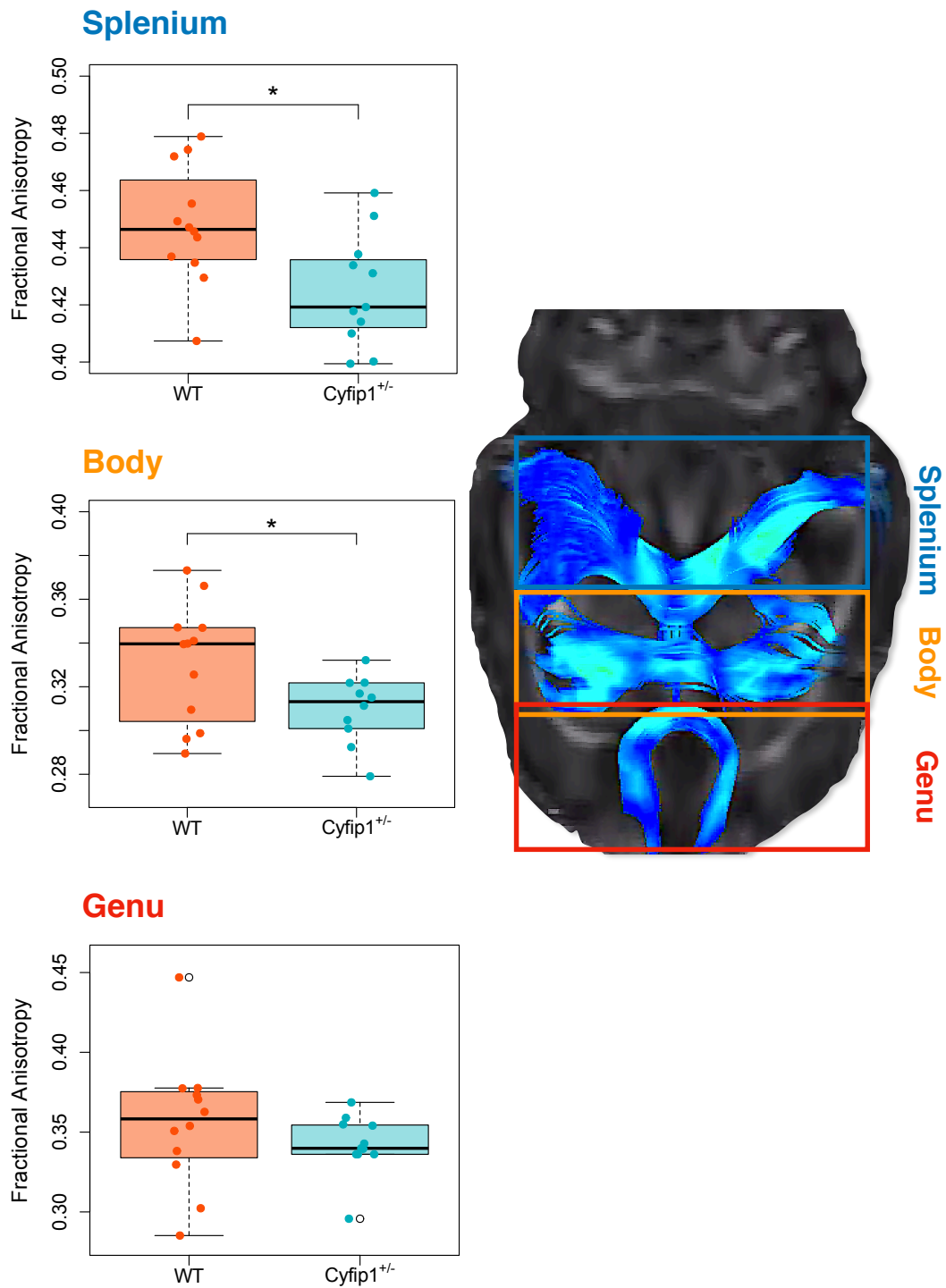


Figure 5.6 - Tractography of the splenium, body and genu of the corpus callosum.

Quantification of FA in the Splenium (n=12 WT, n=11 $Cyfip1^{+/-}$), body (n=12 WT, n=11 $Cyfip1^{+/-}$) and genu (n=12 WT, n=10 $Cyfip1^{+/-}$) of the corpus callosum. FA values show a significant reduction in the splenium ($t=2.8$, $df=21$, $p<0.05$) and body ($t=2.3$, $df=18$, $p<0.05$) segments in the $Cyfip1^{+/-}$ rats. No significant differences were found in the genu ($t=1.03$, $df=16$, $p=0.32$). Representative figure with segmented tracts was created using ExploreDTI. Results presented by mean \pm standard deviation, two-tailed unpaired t-test, $*<0.05$.

Table 5.2 – Group differences between *Cyfp1*^{+/-} and WT rats in the 3 segments of the corpus callosum. Differences are shown for FA, AD, RD and MD, where DTI measures were obtained through tractography methods. The corpus callosum was divided in 3 segments: splenium (SCC, n=12 WT, n=11 *Cyfp1*^{+/-}), body (n=12 WT, n=11 *Cyfp1*^{+/-}) and genu (GCC, n=12 WT, n=10 *Cyfp1*^{+/-}), where the regions of interest (ROI) were manually delineated. Results presented by mean ± standard deviation, two-tailed unpaired t-test, *<0.05.

ROIs	FA		AD (10 ⁻²)		RD (10 ⁻³)		MD (10 ⁻³)	
	WT	<i>Cyfp1</i> ^{+/-}	WT	<i>Cyfp1</i> ^{+/-}	WT	<i>Cyfp1</i> ^{+/-}	WT	<i>Cyfp1</i> ^{+/-}
SCC	0.45 ±0.02	0.42 ±0.02*	0.14 ±0.004	0.13 ±0.006	0.64 ±0.02	0.65 ±0.03	0.88 ±0.02	0.88 ±0.04
Body	0.33 ±0.03	0.31 ±0.02*	0.13 ±0.008	0.13 ±0.005	0.79 ±0.08	0.80 ±0.08	0.91 ±0.07	0.89 ±0.03
GCC	0.36 ±0.04	0.34 ±0.02	0.13 ±0.009	0.12 ±0.005	0.71 ±0.07	0.71 ±0.02	0.91 ±0.07	0.89 ±0.03

5.4.5. Between-group TBSS analysis – FDR correction

The FWE correction method allowed a more conservative correction and showed a consistent reduction in FA in the *Cyfp1*^{+/-} rats. However, a less conservative method might be needed to investigate more subtle changes. Therefore, the voxel-wise analysis was repeated using the FDR correction for multiple comparisons based on the Benjamini–Hochberg procedure (*Benjamini and Hochberg, 1995*), which has been previously used in rodent imaging data (*Sierra et al., 2011; Sagi et al., 2012*). This analysis, shown in **Figure 5.7**, revealed additional white matter changes including increases in FA in regions of the fornix and fimbria suggesting that *Cyfp1* haploinsufficiency may have differential effects in different brain regions. **Figure 5.7** also shows changes in other DTI metrics, after FDR correction, illustrating mostly decreases in AD and increases in RD, and MD. These effects were complementary in terms of (a) being localised in the corpus callosum and external and internal capsule, (b) being consistent with the overall predominant effects of *Cyfp1* haploinsufficiency in reducing FA and (c) being in accordance with the variations seen in the differential heat maps (**Figure 5.4**).

FDR correction

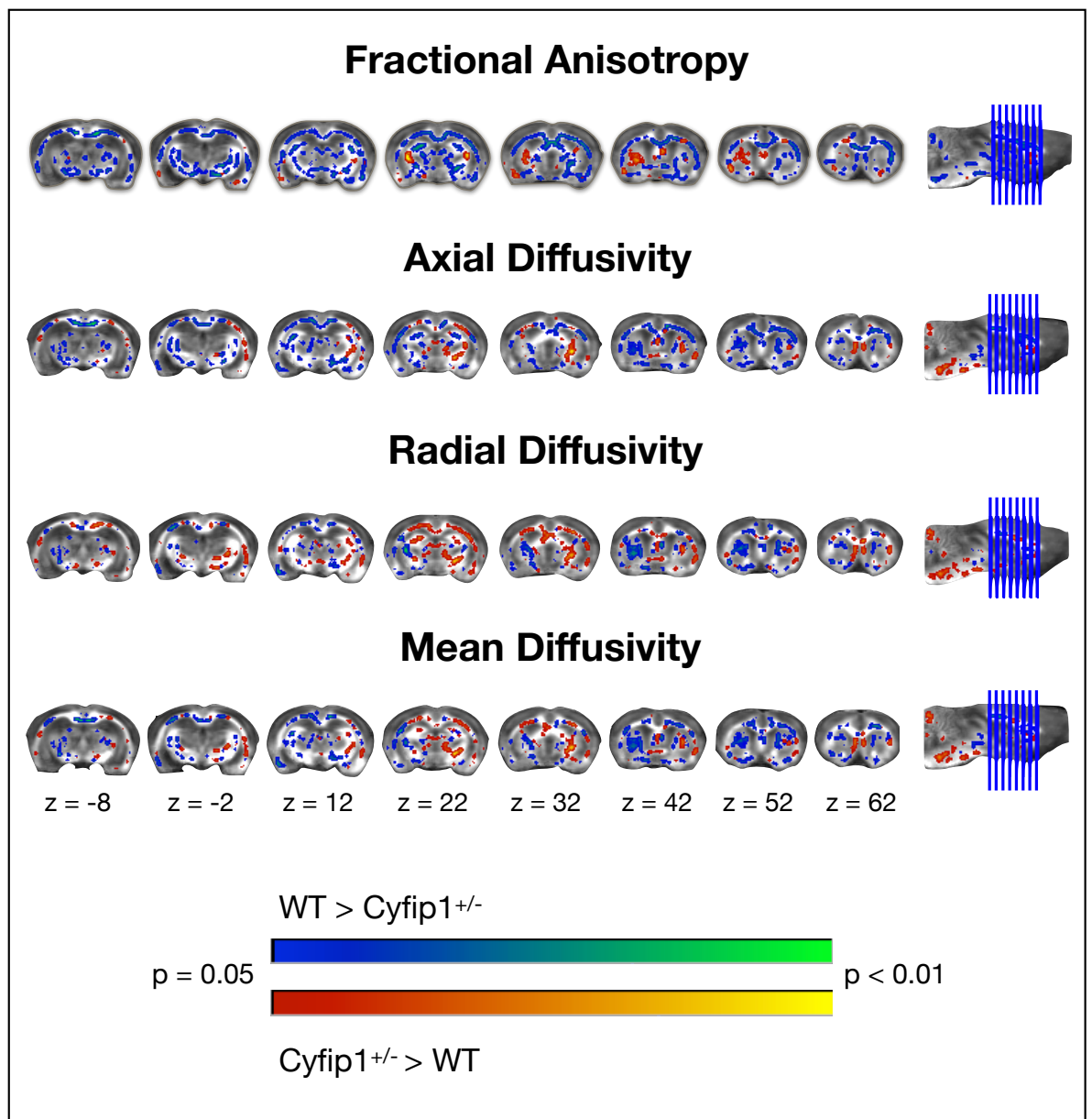


Figure 5.7 - TBSS whole-group voxel-based analysis, after FDR correction.

White matter changes comparing WT (n=12) and *Cyfip1*^{+/-} (n=12) rats, using a different method of correction. Data shows significant group differences using two-tailed unpaired t-tests based on TFCE algorithm after FDR correction based on Benjamini–Hochberg procedure (a less restricting method than FWE correction previously used) (*Benjamini and Hochberg, 1995*) for fractional anisotropy, axial diffusivity, radial diffusivity, and mean diffusivity. All the parametric maps were generated at a significance level of $p < 0.05$.

5.5. Discussion

To model possible contributions by *CYFIP1* to the 15q11.2 CNV deletion phenotype, a novel hemizygous-null *Cyfp1* rat model was created, prior to this study. The *Cyfp1*^{+/-} rat model allowed a high resolution DTI analysis using identical pre-processing to the 15q11.2 BP1-BP2 human imaging study in Chapter 3. An initial characterisation of white matter microstructural changes using differential heat maps showed an impact of *Cyfp1* haploinsufficiency in white matter microstructure, where both decreases and increases in FA were observed. To maintain a translational validity of the analysis, the same analysis method used in the human data was performed in the rat DTI data. Here, a whole-brain analysis using TBSS followed by FWE correction for multiple comparisons showed significant decreases in FA, specifically in the corpus callosum, internal and external capsule, and fimbria/fornix in the *Cyfp1*^{+/-} rats. Quantification of these changes revealed that changes in the corpus callosum and external capsule were more significant, suggesting a higher sensitivity of these regions to *Cyfp1* haploinsufficiency. Tractography analysis of different segments of the corpus callosum provided additional information suggesting that the middle (body) and posterior (splenium) segments of the corpus callosum might be more affected than the anterior (genu) segment, although all segments showed reduced FA. Finally, a whole-brain analyses was also performed using a different correction method for multiple comparisons, the FDR correction based on Benjamini–Hochberg procedure (*Benjamini and Hochberg, 1995*). This complementary analysis revealed additional white matter changes including increases in FA in regions of the fimbria and stria terminalis, similar to what was seen in the differential heat-maps, suggesting that *Cyfp1* haploinsufficiency may have differential effects in distinct brain regions.

5.5.1. Contrast between 15q11.2 BP1-BP2 deletion in human carriers and *Cyfp1* haploinsufficiency in the rat model

In the beginning of this chapter, I hypothesised that dysregulations in the *CYFIP1* gene would have an impact on white matter microstructure, given its involvement in mechanisms that potentially affect axon development and myelination, and could be associated with the white matter phenotype seen in 15q11.2 BP1-BP2. In this chapter it was shown, using DTI methods and a *Cyfp1*^{+/-} rat line, that *Cyfp1* haploinsufficiency

was associated with white matter changes in the rat model, as predicted. Changes in the *Cyfp1*^{+/-} rats consisted in significant decreases in FA that were most pronounced in the corpus callosum and external capsule, using a highly conservative correction procedure, with some evidence of increased FA in some areas of the fimbria and stria terminalis that were only apparent when using a less conservative correction method. These opposite patterns of white matter changes across different rat brain regions suggest that depletions of *Cyfp1* might have a different impact in different brain regions, as has also been shown for its homologue *Cyfp2* (Han et al., 2015). Increases in FA with little evidence of reductions were a prominent feature of the findings in the human 15q11.2 BP1-BP2 deletion carriers described in Chapters 3 and 4. Hence, while the rat and human phenotypes converged on white matter changes they mostly differed in the direction of the changes.

These results are not obviously consistent with the *CYFIP1* gene being solely responsible for the increased FA seen in the human 15q11.2 BP1-BP2 deletion carriers, but it is important to bear in mind that differences between the human and rat findings could have resulted from several factors. As described in previous chapters, 15q11.2 BP1-BP2 deletion involves three other genes in addition to *CYFIP1*. Of special interest is *NIPAI*, which is expressed in the brain and found to be involved in processes that are crucial for typical axonal growth and guidance (X. Wang et al., 2007; Tsang et al., 2009). Therefore, *a priori*, haploinsufficiency of *NIPAI*, and possibly interactions between the genes in the interval (Xiong and Oakley, 2009; Xie et al., 2014), may contribute to the 15q11.2 BP1-BP2 deletion DTI phenotype. Furthermore, it might be that changes in white matter associated with low levels of *CYFIP1/Cyfp1* gene may be similarly present in both human and rat model in addition to other molecular and cellular consequences of the copy number deletion that might have a greater contribution to DTI signal, but not necessarily to the cognitive phenotype. The possibility that there are species differences in the expression patterns of *CYFIP1/Cyfp1* and also any compensatory responses to haploinsufficiency should also be borne in mind. Furthermore, the humans and rats are likely to have been subject to differential compensatory mechanisms arising from very different environmental challenges across their lifespan (Laviola et al., 2008; Fields, 2008; Hoyer et al., 2014). An exact between-species comparison would require the assessment of *CYFIP1*-specific heterozygous humans, which are very rare in the general population. At this stage, cellular and molecular mechanisms underlying the observed white matter phenotypes cannot be understood using solely DTI, and a more

comprehensive study would require histological studies of brain tissue. The *Cyfp1^{+/-}* rat model offers an enhanced experiment tractability by allowing the direct access to brain tissue, where cellular changes will be explored in the next Chapters (6 and 7).

5.5.2. Decreased FA in the corpus callosum of the *Cyfp1^{+/-}* rats – functional outcomes

Significant decreases in FA in the *Cyfp1^{+/-}* rats were most pronounced in the corpus callosum (**Table 5.1**). The corpus callosum is the largest white matter structure containing numerous intra- and interhemispheric myelinated axonal projections, connecting the left and right cerebral hemispheres in placental mammals (*Raybaud, 2010*). Although there are no clear anatomical defined boundaries, the corpus callosum can be subdivided into functionally and morphologically distinct sub-regions, which follow the topographical organisation of cortical areas, from anterior to posterior: the genu, body, and splenium (*Witelson, 1989*), as illustrated in **Figure 5.8**. Fibre size and composition along the corpus callosum differ in each sub-region. The genu contains the highest density of thin, poorly myelinated, and slow conducting fibres, which connect the prefrontal cortex and higher order sensory areas. The density of the fibres decreases in the body and splenium, where the axons are thicker and highly myelinated. The middle portion of the body connects primary and secondary somatosensory and motor areas, whereas the posterior body connects primary and secondary auditory areas. The splenium connects visual areas in the occipital lobe (*Clarke and Zaidel, 1994; van der Knaap and van der Ham, 2011*).

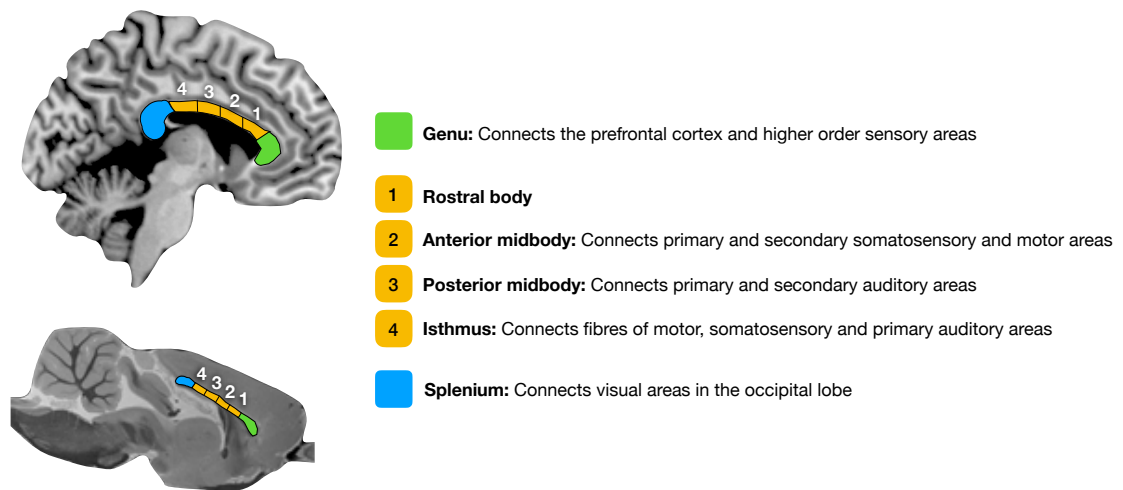


Figure 5.8 - Corpus callosum sub-regions in human (top) and rat (bottom) brain.

In this chapter, tractography was used to evaluate the effect of *Cyfp1* haploinsufficiency in these different sub-regions of the corpus callosum. While all the sub-regions showed reduced FA, significant changes were only seen in the body and splenium of the corpus callosum. Effects on corpus callosum can result in abnormal transfer between brain hemispheres and are likely to impact the function of any region that transfers information through this interhemispheric tract. Studies in mice have shown that *Cyfp1* haploinsufficiency leads to mild behavioural phenotypes (*Bozdagi et al., 2012; Chung et al., 2015*). Recently a study by *Bachmann et al., 2019* found that adult *Cyfp1^{+/-}* mice show defects in motor learning using the common rotarod behavioural test, which develops over time, appearing between young adult and adult stages. The authors also found these deficits to be reversal using behavioural training approaches at early stages. Although this study focused on spine morphology deficits, changes in the corpus callosum, especially the body sub-region, may have an impact on propagation of information from different motor areas leading to motoric deficits (*Sampaio-Baptista et al., 2013; McKenzie et al., 2014*).

Converging lines of evidence have supported the importance of the corpus callosum in neurodevelopmental disorders, where abnormalities in the corpus callosum were present in many of these conditions, including individuals at high genetic risk (*Drakesmith et al., 2019*). Volumetric studies have overall shown reductions in the total corpus callosum area in ASD (*Frazier and Hardan, 2009*), with evidence of different developmental trajectories of corpus callosum volume in children and adults with ASD

(Prigge et al., 2013). DTI studies have also shown reductions in FA in the corpus callosum in ASD patients (Alexander et al., 2007; Shukla et al., 2010; Aoki et al., 2013), with evidence of different developmental trajectories of white matter microstructure in individuals with ASD (Travers et al., 2015), suggesting an abnormal brain maturation in this region. In Williams syndrome, a study by Gagliardi et al., 2018 reported changes in white matter microstructure in patients, including decreased FA in the corpus callosum. This was later linked, by Barak et al., 2019 study to decreases in myelin thickness in the corpus callosum, which was associated with a hypersociability phenotype outcomes. In schizophrenia, behavioural abnormalities usually reflect problems in the connection between cortical areas, which ultimately points towards the corpus callosum (David, 1994). However, results are more heterogeneous when it comes to corpus callosum findings, but overall suggest reductions in volume in this area in patients with schizophrenia (van der Knaap and van der Ham, 2011; Knöchel et al., 2012).

5.5.3. Decreased FA in *Cyfp1*^{+/-} rat model – Possible cellular causes

The effect on the corpus callosum could reveal a higher sensitivity of this region to changes in *Cyfp1* levels, or could be a result of statistical power since this is the largest white matter tract in the brain, involving more imaging voxels. Of interest is the molecular work done in the *Cyfp1*^{+/-} rat line after this study, where *Cyfp1*^{+/-} rats revealed a surprising higher reduction in Cyfp1 protein level (~50%) in the corpus callosum in comparison to grey matter regions, such as the hippocampus and pre-frontal cortex (~12% and 19% respectively). These results are described in the validation of the *Cyfp1*^{+/-} rat model in Appendix 1. *CYFIP1* has been shown to be highly enriched at the synapses in dendritic spines (De Rubeis et al., 2013), where an effect of both haploinsufficiency and overexpression has been consistently reported (Pathania et al., 2014; Oguro-Ando et al., 2015). However, altogether these results suggest a sensitivity of white matter to reduced levels of *Cyfp1* gene (especially in the corpus callosum) that could potentially be a result of impaired axon development. Further investigation is needed to understand the molecular basis of this contrast between white and grey matter, and also to explore the specificity of this effect to corpus callosum, or perhaps a general effect in white matter.

As stated throughout the thesis, the focus on *Cyfp1* and white matter was guided by the assumption that dysregulations in this gene would impact local protein synthesis

and regulation of actin, which are both crucial mechanisms for generation and maintenance of neuronal networks. *Cyfp1* controls f-actin assembly by interacting with WAVE complex, and previous studies have shown that low levels of *Cyfp1* lead to abnormal increased levels of f-actin. A normally regulated, dynamic actin cytoskeleton is critical for the generation of synapses and supports normally functioning presynaptic terminals (Nelson et al., 2013). In fact, it was already shown that deletions in *Cyfp1* gene lead to spine defects, and this effects were associated with a change in equilibrium between the two distinct CYFIP1 complexes (CYFIP1 -WAVE and -FMRP complexes) (De Rubeis et al., 2013). However, actin cytoskeleton dynamics and mRNA translation mechanisms are not only important in spine formation, and a proper regulation of these mechanisms is also crucial in maintaining axonal growth cone shape, axonal guidance, as well as many important functions in glial cells (Dent and Gertler, 2003; Bauer et al., 2009; Michalski and Kothary, 2015). Furthermore, alterations of the cytoskeleton are known to be required to produce myelin, including oligodendrocyte differentiation and formation of lamellipodia and lamellipodial ‘ruffles’ that make initial contact between the oligodendrocyte and axon and are a pre-requisite for myelination to occur (Asou et al., 1995; Bauer et al., 2009). Of interest is also the study by Haberl et al., 2015 reporting white matter changes in a mouse *Fmr1* knockout, specifically reduced FA in the corpus callosum, similar to the white matter phenotype seen in the *Cyfp1*^{+/-} rat model. The mouse *Fmr1* knockout also revealed evidence of global disruptions in functional connectivity as indexed by functional magnetic resonance (fMRI). However, it is important to remember the two studies referenced in Chapter 3 showing, similarly to 15q11.2 deletion human data, increases in FA in FXS patients. These discrepancies between human and rodent data remind us that care should be taken when directly comparing disease models across different species.

5.1.1. Conclusion

In conclusion, using DTI to assess changes in white matter microstructure, disturbances to white matter were found in *Cyfp1*^{+/-} rats. Cross species comparison of the imaging phenotypes in rats and humans suggest it is unlikely that effects mediated by *CYFIP1* are solely responsible for the 15q11.2 phenotype, and additional work is required to determine the contribution made by the other three genes, *NIPA1*, *NIPA2*, and *TUBGCP5* affected in the 15q11.2 BP1-BP2 deletion. However, these findings in the *Cyfp1* rat

model give an insight into the contribution made by low dosage of *CYFIP1* to the 15q11.2 BP1-BP2 deletion phenotype. Remaining questions concern the cellular changes underlying the white matter phenotype in the rat model. This will be further explored in the following chapters by virtue of *ex-vivo* histological experiments (Chapter 6) and *in vitro* assessments (Chapter 7).

Chapter 6

Investigating the effect
of *Cyfp1* haploinsufficiency on white matter in
rat brain - an *in vivo* histological study

6.1. Abstract

Background

The diffusion tensor imaging study, described in the last chapter, has shown disturbances in white matter tracts in a novel *Cyfp1* haploinsufficiency rat line, that were most pronounced in the corpus callosum. In this chapter, possible cellular changes underlying this imaging phenotype will be explored.

Methods

Transmission electron microscopy (TEM) was used to measure the number of myelinated and unmyelinated axons, the axon diameter, myelin thickness and g-ratio (myelin thickness relative to axon diameter) of each myelinated axon. The experiment used a new cohort of rats (WT n=5, *Cyfp1*^{+/-} n=4). The number of oligodendrocyte lineage and mature cells using immunofluorescence, where sections were stained for Olig2 and CC1 proteins, was also analysed; this experiment used rats taken randomly from the same group of rats providing the DTI data from Chapter 5 (WT n=7 WT and *Cyfp1*^{+/-} n=7). Linear mixed effects (LME) models were used to analyse the effect of genotype on axon diameter, g-ratio and myelin thickness, considering variation across animals, whereas a two-tailed unpaired t-test was used to compare the number of axons and number of oligodendrocytes between groups.

Results

TEM data showed a thinning of the myelin sheath in the corpus callosum, where no differences were found in the number of unmyelinated and myelinated axons, or in axon diameter. These changes were accompanied by a reduction in the number of mature oligodendrocytes in the corpus callosum of the *Cyfp1*^{+/-} rats.

Conclusions

These results show a specific effect of *Cyfp1* haploinsufficiency on myelin, resulting in thinning of the myelin sheath. Myelin thinning was independent of changes in axon

number or diameter but was associated with a reduction in the number of mature oligodendrocytes. These results are in line with the decreased FA seen in the DTI experiment described in Chapter 5.

6.2. Introduction

The study described in Chapter 5 showed an impact of *Cyfp1* haploinsufficiency on white matter microstructure, revealing predominantly decreases in FA in *Cyfp1*^{+/-} rats that were most significant in the corpus callosum. However, the direction of this effect differed from the human data, where widespread increases in FA were seen in 15q11.2 BP1-BP2 deletion carriers. The contrast between the human and the rodent imaging data does not *a priori* completely support the initial idea that *CYFIP1* gene could be solely responsible for the 15q11.2 BP1-BP2 white matter phenotype. However, the underlying cellular causes of the imaging phenotype in the rat model are unknown, and could still be common to both rats and humans.

The decreased FA in the *Cyfp1*^{+/-} rats could result from alterations in axonal growth, guidance and/or myelination, as a result of dysregulations in the *Cyfp1*-WAVE and -FMRP complexes, which regulate cytoskeleton dynamics and mRNA translation, respectively. Taking advantage of the enhanced experimental tractability of the *Cyfp1*^{+/-} rat line, which permits direct access to brain tissue not available in human carriers of the 15q11.2 deletion, TEM methods were used in order to perform a comprehensive investigation of possible changes on axonal density, axon calibre, and myelin thickness. Furthermore, cellular changes associated with the TEM findings were investigated using immunofluorescence methods. Specifically, the number of oligodendrocyte lineage (expressing Olig2) and mature (expressing CC1) cells was quantified. The analyses focused on the corpus callosum, given that the DTI data indicated sensitivity of this structure to *Cyfp1* haploinsufficiency. The aim of this study was to further explore the cellular changes that underlie the decreased FA seen in the corpus callosum of the *Cyfp1*^{+/-} rats.

6.3. Material and Methods

6.3.1. Rats

A cohort of 9 rats (WT n=5 and *Cyfp1*^{+/-} n=4) was used for TEM. Similar to the previous chapter, all the rats were Long Evans and were 6 months old. For immunofluorescence, seven rats were randomly selected from each group in the cohort used in the DTI study,

described in the previous chapter. The animals were culled one month after the imaging experiment, and were also 6 months old. All the experimental procedures were performed in accordance with institutional animal welfare and ARRIVE guidelines and the UK Home Office License PPL 30/3135.

6.3.2. Transmission electron microscope

The rats were intracardially perfused with 0.1 M phosphate buffered saline (PBS), followed by 4% of glutaraldehyde in 0.1 M PBS. The brains were then placed on a shaker to postfix in glutaraldehyde for 4h, after which they were placed in PBS with 30% sucrose and stored at 4°C until further use. The samples were processed and data were collected by Dr. Christopher Von Ruhland at the Central Biotechnology Services in Cardiff University, and analysed by me. The brains were embedded in TAAB embedding resin. Ultra-thin sections (50 nm) were stained with aqueous 4% uranyl acetate and lead citrate. The sections were visualised on a transmission electron microscope (CM12, Philips, the Netherlands) and, for quantification, images were taken using an on-axis 2048×2048 charge-coupled device camera (Proscan, Schering, Germany). In order to obtain a representative sample, 15 regions across the extent of the anterior-posterior extent of the corpus callosum per animal were taken for quantification (see **Figure 6.1** for representative micrograph).

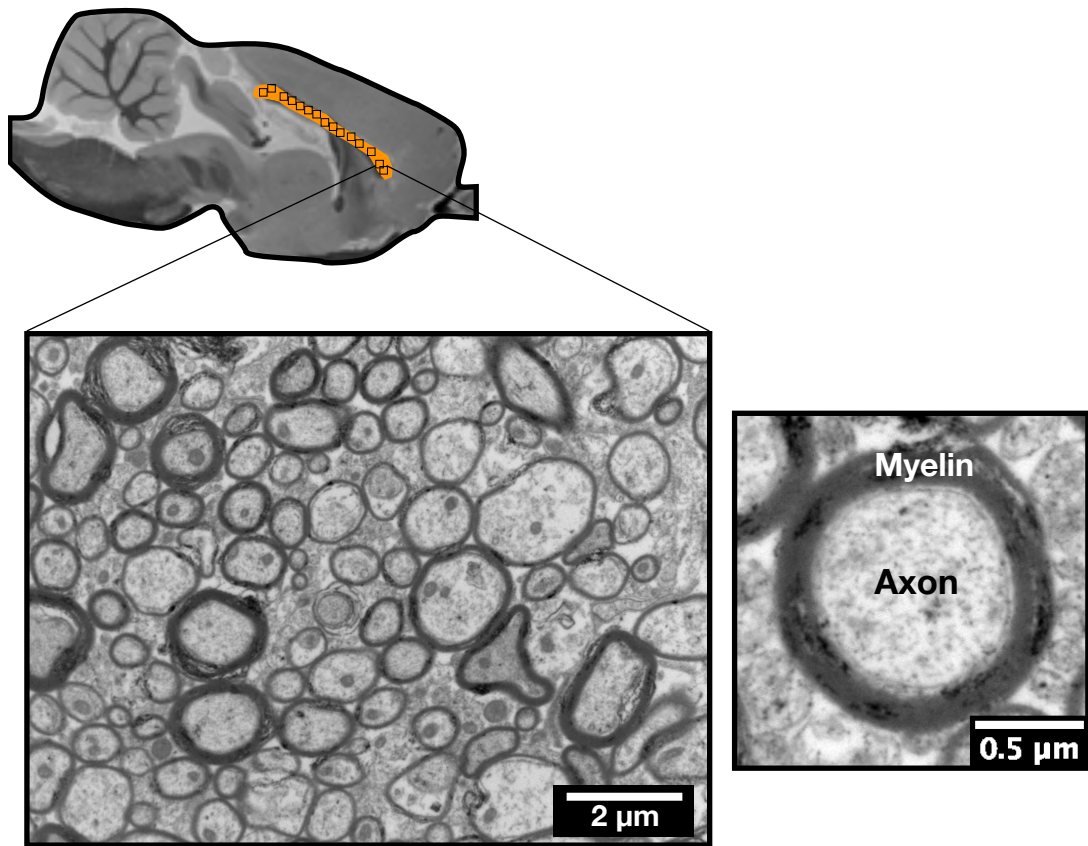


Figure 6.1 – Illustration of sampling for transmission electron microscopy, and representative figures.

For quantification, 15 regions across the extent of the anterior-posterior extent of the corpus callosum per animal were taken. In the micrographs the myelinated axons were easily identified by the surrounding myelin sheath, which is characterised by a darker thicker line around the axon. Scale bars=2 µm (left) and 0.5 µm (right).

6.3.3. Immunofluorescence

For immunofluorescence, the rats were intracardially perfused with 4% paraformaldehyde (PFA) in 0.1 M PBS. The brains were placed on a shaker to postfix in PFA for 4 h, after which they were placed in phosphate buffered 30% sucrose. Coronal cryosections of the brain, of 15 µm thickness, were made on a cryostat (CM1860 UV, Leica, UK), mounted onto a Poly-L-Lysine (PLL)-coated slides (3 sections per slide), and stored at -20 °C. For immunofluorescence, antibodies were used as follows: anti-Olig2 (ab109186, Abcam) 1:400, anti-APC [CC-1] (ab16794, Abcam) 1:400, anti-MBP (MAB386, Millipore) 1:300. For the Olig2 and CC1 double-staining, the slices were

heated in a 5% citrate buffered antigen retrieval solution (pH 6, 10x, Sigma-Aldrich Company, UK), using a water bath at 90°C for 10 min. All the slices were blocked for 1 hour with 5% donkey serum (Sigma-Aldrich Company, UK), and 0.3% Triton X-100 in PBS. The appropriate primary antibodies were applied and incubated overnight at 4 °C. On the next day, after washing, the slices were incubated for 2 hours with secondary antibodies (Alexa Fluor Life Technologies, Manchester, UK), in a concentration of 1:1000 at room temperature. Then, the slides were washed, counterstained with 1:1000 DAPI, mounted and cover-slipped. For quantification of Olig2+ and CC1+ cells, images were taken on an inverted fluorescent time lapse microscope (DMI6000B, Leica, UK), and at least 4 images from random visual fields were taken from regions including the corpus callosum and external capsule. For quantification of MBP intensity, one coronal section per rat was taken on an Axio scan (Zeiss, Germany), and the same exposure time and intensity were used for all the slides.

6.3.4. Quantification and statistical analyses

For quantification of cells the ImageJ software (version 1.51) was used. The number of myelinated and unmyelinated axons, axon diameter of myelinated fibres, myelin thickness and g-ratio (measure of myelin thickness relative to axon diameter: where lower g-ratios indicates thicker myelin sheath) of normally myelinated axons were quantified (see **Figure 6.2** for measures taken). A total of 13127 (WT n=7148, *Cyfp1*^{+/-} n=5979 axons) myelinated axons were analysed. For quantification of oligodendrocytes, the total number of Olig2+, and the overlapped Olig2+/Cc1+ cells were counted. Only cell bodies clearly identified by Olig2 and CC1 immunofluorescence and overlapping with DAPI staining were counted. MBP+ reactivity was determined by comparing immunofluorescence staining intensity. The whole region of corpus callosum and external capsule was selected in the coronal section, and quantification was done by calculating the mean intensity of the pixels above a preset intensity threshold, multiplied by the number of pixels above that threshold, and divided by the total area quantified. I performed all the cell quantifications blinded to the genotype.

Differences between WT and *Cyfp1*^{+/-} were analysed in RStudio version 1.1.463 (R Foundation for Statistical Computing, Vienna, Austria). For the TEM data, since the sample size was small (n=5 WT and n=4 *Cyfp1*^{+/-} rats) but yielded a large number of

repeated measures (WT n=7148, *Cyfp1*^{+/-} n=5979 axons), an LME model was used to take into account variation across individuals and analyse the effect of genotype on axon diameter, g-ratio and myelin thickness, where these measures were considered fixed effects, and animals were considered random effects. Since there was only one random effect, non-restricted maximum likelihood was used to estimate the model parameters. In this analysis, the axon diameter and myelin thickness values were log-transformed since the data followed a log-normal distribution, whereas the other measures followed a normal distribution. To assess differences between the number of myelinated axons, as well as the measures from the immunofluorescence experiment, a two-tailed unpaired Student's t-test was used in measures where variances between groups were similar, whereas a Welch two sample t-test was used when variances were unequal. In addition to the LME analysis, differences in myelin thickness between groups were also assessed using a Welch two sample t-test to compare the mean values of each animal between groups.

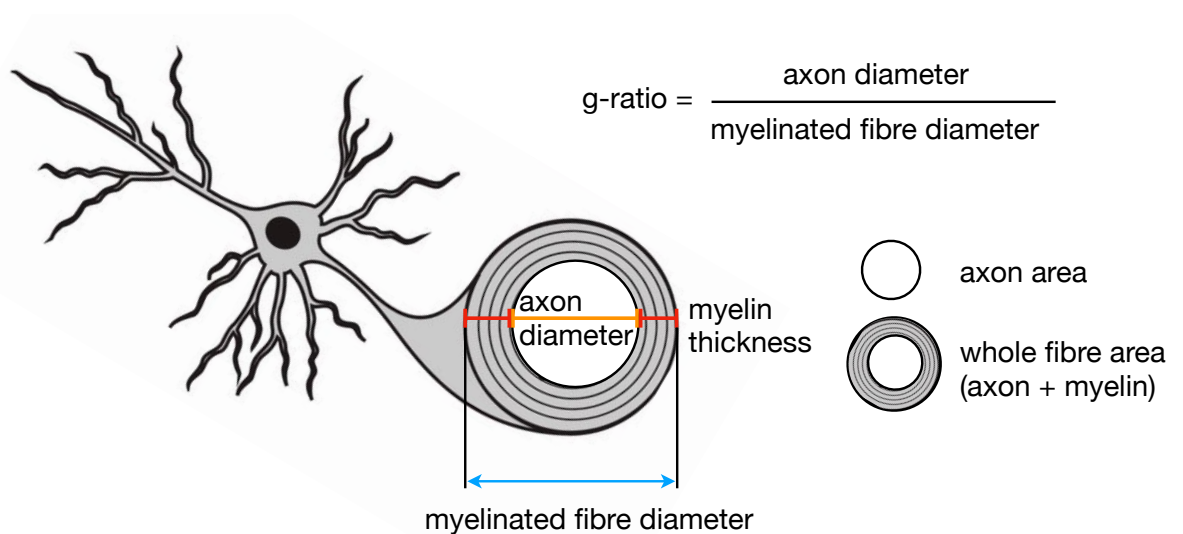


Figure 6.2 - Schematic illustration of the axon and myelin sheath and calculation of the g-ratio and myelin thickness.

The g-ratio is also known as the myelin thickness measure relative to axon diameter. A total of 13127 (WT n=7148, *Cyfp1*^{+/-} n=5979 axons) myelinated axons were analysed for the axon diameter, g-ratio and myelin thickness analyses.

6.4. Results

6.4.1. Ultra-structural analysis of axons in the corpus callosum using transmission electron microscopy

With the aim of investigating the cellular nature of the *Cyfp1*^{+/-} associated DTI changes, an ultra-structural analysis was conducted looking at the number of axons, axon diameter and myelin thickness of myelinated fibres in both *Cyfp1*^{+/-} and WT rats. The analysis focused on the corpus callosum. Quantification of the number of axons (see representative micrographs in **Figure 6.3A**) revealed no significant differences in the number of myelinated (Welch two sample t-test, df=5.15, t=0.39, p=0.7) and unmyelinated (two sample t-test, df=7, t=-0.58, p=0.58) axons (**Figure 6.3B**), between WT and *Cyfp1*^{+/-} rats. In total, 13127 myelinated fibres were quantified (7148 axons in WT and 5979 axons in *Cyfp1*^{+/-} rats) and all these axons were taken into account for axon diameter and myelin measures quantifications. Here, no genotype effects were found on axon diameter measures (**Figure 6.4C**, LME: $\chi^2(1)=0.05$, p=0.83) suggesting no differences on axon density (**Figure 6.3**) and diameter (**Figure 6.4**) in the corpus callosum of the *Cyfp1*^{+/-} rats.

To assess genotype effects on myelin two measures were taken into account: g-ratio and myelin thickness. G-ratio is a measure of myelin thickness relative to axon diameter (see measures taken in **Figure 6.2**). When plotting the frequency distribution of g-ratio values in both groups, shown in **Figure 6.5B**, an increased percentage of axons with higher g-ratio values is noticed in the *Cyfp1*^{+/-} rats. However, no significant differences were found in g-ratio when comparing all axons in each group (**Figure 6.5C**, LME: $\chi^2(1)=2.03$, p=0.15). G-ratio is dependent on axon diameter, and could be affected by a high variability on axon diameter between animals within each group. Moreover, the extent of myelination can be related to axon diameter (*Klingseisen and Lyons, 2018*) and the effects on g-ratio can be specific to certain sizes of axons. Analysing the g-ratio of axons within specific diameter ranges revealed a significant increased g-ratio in each interval in the *Cyfp1*^{+/-} rats (**Figure 6.5D**), that was more significant in larger axons. Complementary to the g-ratio analysis, frequency distribution of myelin thickness values, shown in **Figure 6.6B**, revealed a decreased percentage of axons with higher myelin thickness in the *Cyfp1*^{+/-} rats. This time a significant decrease in myelin thickness was

also seen in *Cyfp1^{+/-}* rats when compared to WT rats (**Figure 6.6C**, LME: $\chi^2(1)=14.63$, $p=0.0001^{***}$). This difference in myelin thickness was also seen when comparing the mean values of each animal (n=5 WT and n=4 *Cyfp1^{+/-}*) between groups (Welch two sample t-test, $df=3.46$, $t=3.15$, $p=0.04^*$). Furthermore, analyses of genotype effects on myelin thickness within specific diameter ranges also revealed an effect on each interval, but more significant on larger axons (**Figure 6.6D**). Additionally, there was a significant interaction effect between axon diameter and genotype on g-ratio (LME: $\chi^2(1)=26.9$, $p<0.001$). These analyses indicate decreased myelin thickness in the corpus callosum of the *Cyfp1^{+/-}* rats that was more pronounced in larger axons.

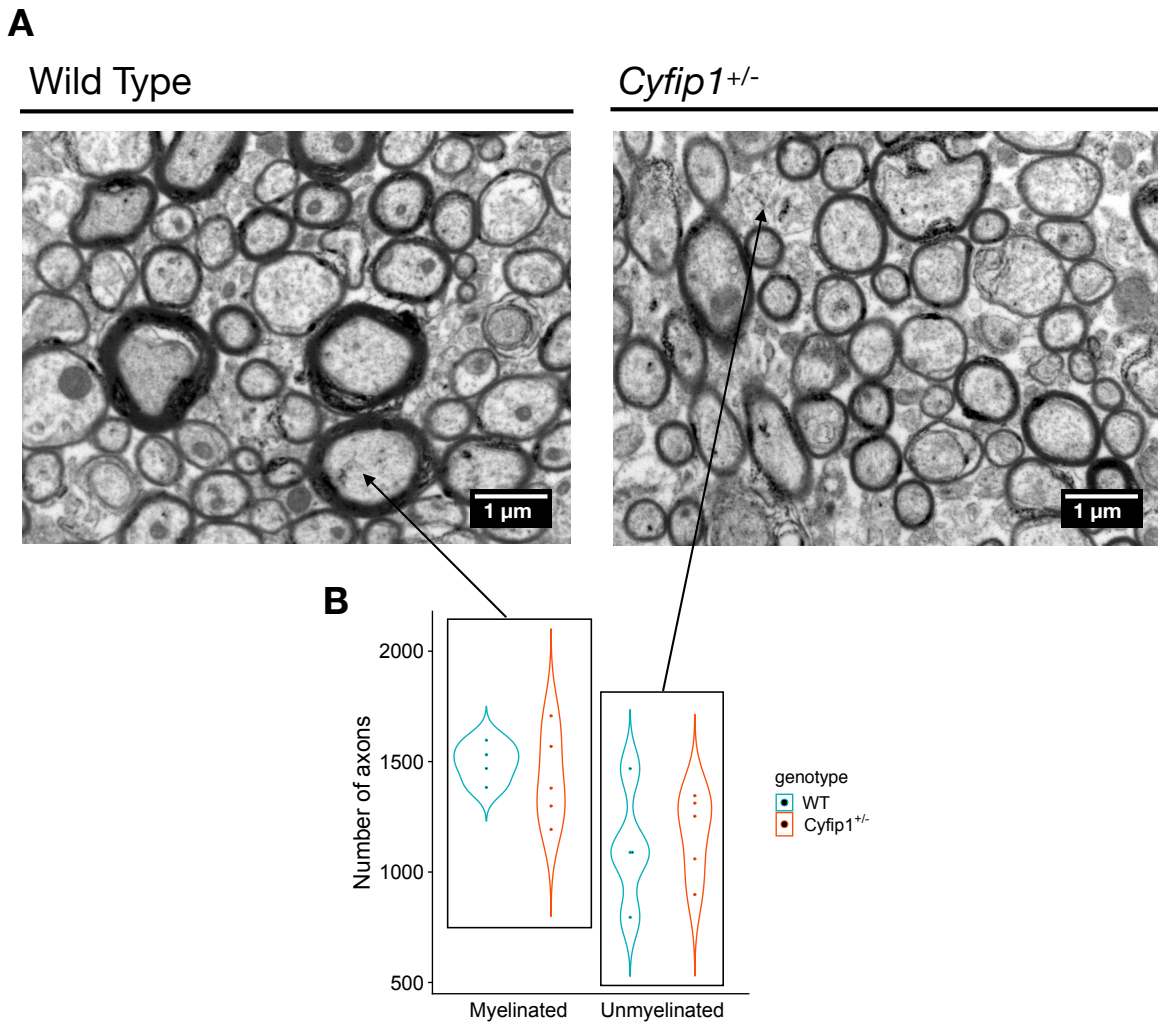


Figure 6.3 - Number of axons in WT (n=5) and *Cyfp1^{+/-}* (n=4) rats.

A Representative electron micrographs of axons in the WT and *Cyfp1^{+/-}* rats in the corpus callosum. Myelinated and unmyelinated fibres are identified by arrows. Scale bars=1 μ m. **B** Number of myelinated and unmyelinated axons per image. No differences were found between WT and *Cyfp1^{+/-}* rats in the number of myelinated (Welch two sample t-test, $df=5.15$, $t=0.39$, $p=0.7$) and unmyelinated (two sample t-test, $df=7$, $t=-0.58$, $p=0.58$) axons. Data points are represented in the figure.

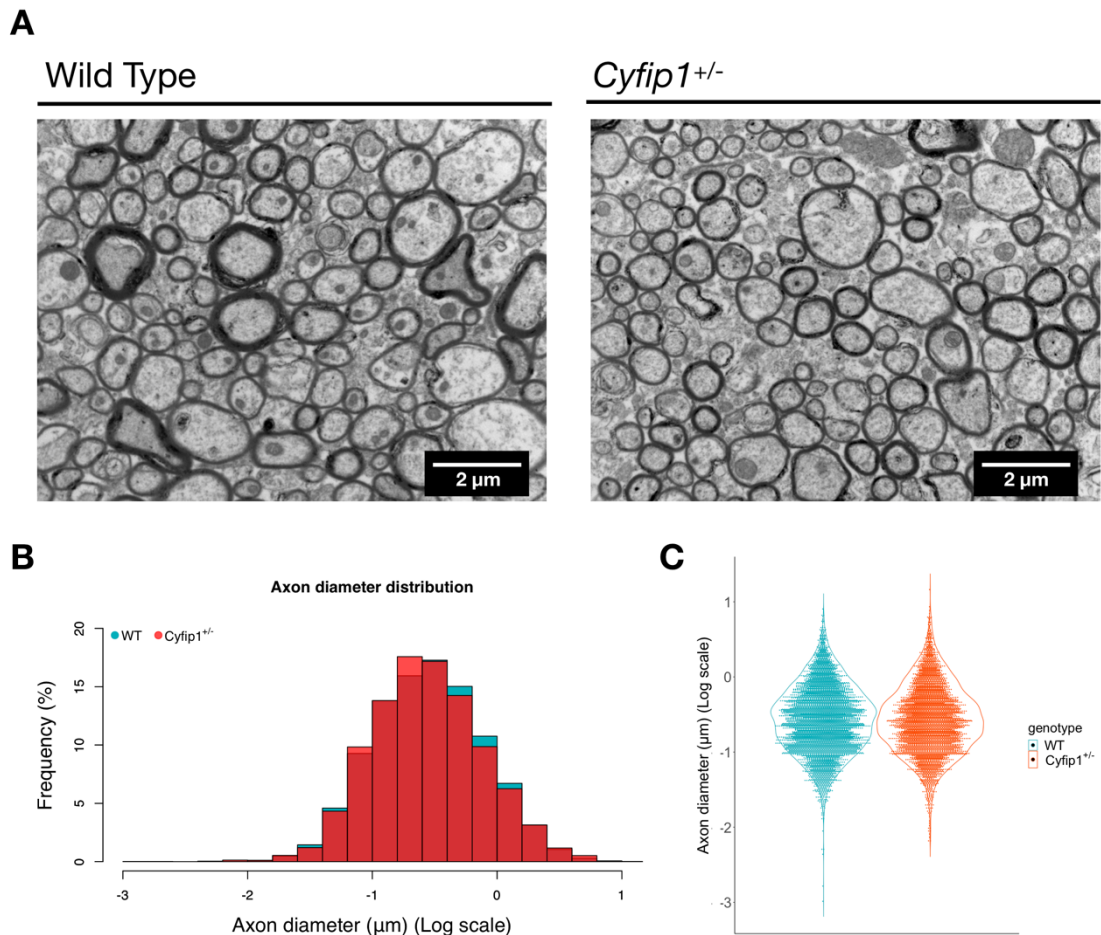


Figure 6.4 - Axon diameter in WT (n=5 animals, n=7148 axons) and *Cyfp1*^{+/-} (n=4 animals, n=5979 axons) rats.

Differences were assessed using an LME model adjusted for individual variability. **A** Representative electron micrographs of axons in the WT and *Cyfp1*^{+/-} rats in the corpus callosum. Scale bars=2 μm. **B** Histogram showing the frequency distribution of diameters of myelinated fibres. **C** Axon diameter of myelinated fibred per group. No differences were found between WT and *Cyfp1*^{+/-} rats in axon diameter (LME: $\chi^2(1)=0.05$, $p=0.83$). Data points are represented in the figure.

A

Wild Type

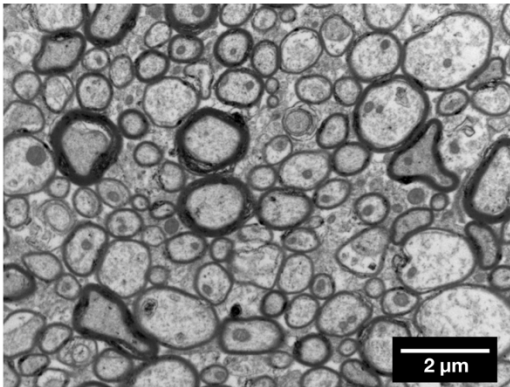
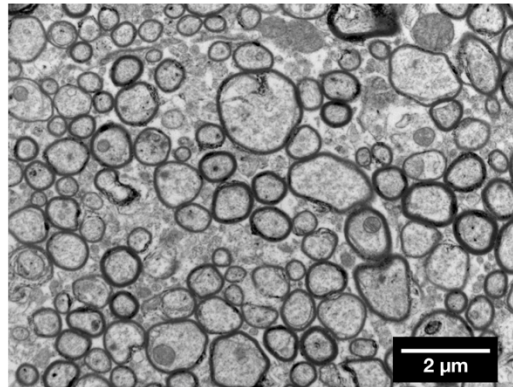
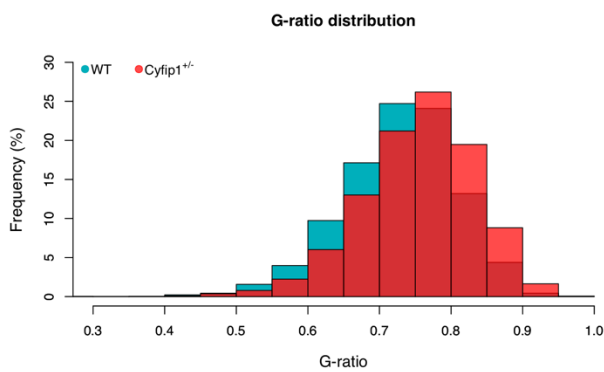
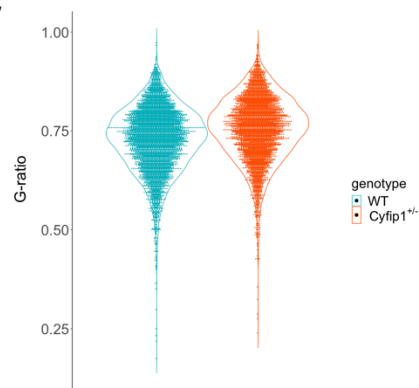
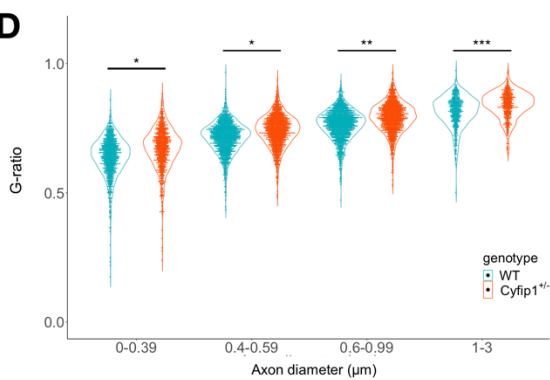
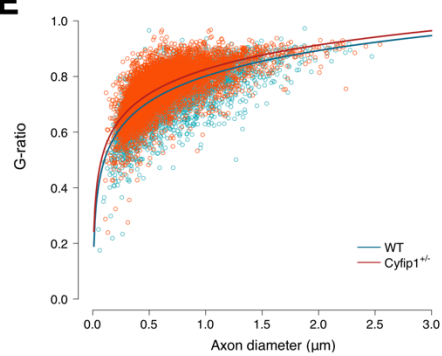
*Cyfp1*^{+/-}**B****C****D****E**

Figure 6.5 - G-ratio in WT (n=5 animals, n=7148 axons) and *Cyfp1*^{+/-} (n=4 animals, n=5979 axons) rats.

Differences were assessed using a LME model adjusted for individual variability. **A** Representative electron micrographs of axons in the WT and *Cyfp1*^{+/-} rats in the corpus callosum. Scale bars=2 μm. **B** Histogram showing the frequency distribution of g-ratio values of myelinated fibres. **C** G-ratio of myelinated fibres per group. No differences were found between WT and *Cyfp1*^{+/-} rats in g-ratio overall measure (LME: $\chi^2(1)=2.03$, $p=0.15$). **D** G-ratios calculated for small (diameter<0.4), medium-small (0.4≤diameter<0.6), medium-large (0.6≤diameter<1) and large (1≤diameter<3). Significant increases in g-ratio in *Cyfp1*^{+/-}

compared to WT rats were found in all different axon diameter ranges, and more significant in larger myelinated axons: small (n=1510 WT and 1276 *Cyfp1*^{+/-} axons; LME: $\chi^2(1)=4.23$, p=0.4*), medium-small (n=2283 WT and 2043 *Cyfp1*^{+/-} axons; LME: $\chi^2(1)=4.44$, p=0.3*), medium-large (n=2551 WT and 1993 *Cyfp1*^{+/-} axons; LME: $\chi^2(1)=7.14$, p=0.007**), and large (n=804 WT and 667 *Cyfp1*^{+/-} axons; LME: $\chi^2(1)=13.92$, p=0.0002***). **E** Scatter plot of g-ratio values across all axon diameters WT (n=7148 axons) and *Cyfp1*^{+/-} (n=5979 axons), showing a logarithmic relationship between both measures. Data points and p-values are represented in figure where, *<0.05, **<0.01, ***<0.001.

A

Wild Type

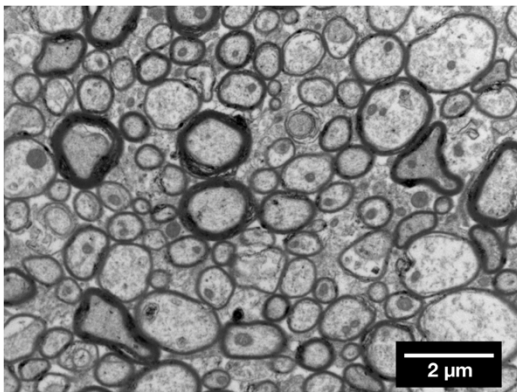
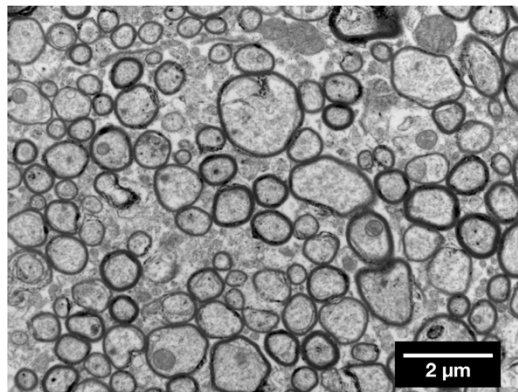
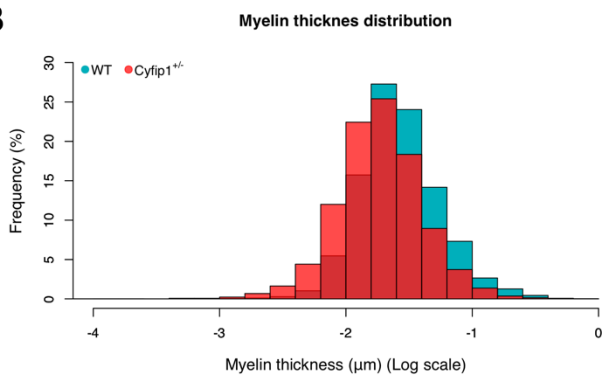
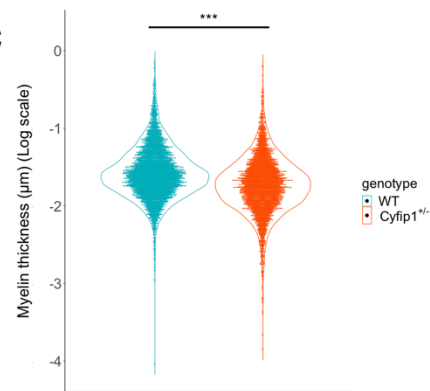
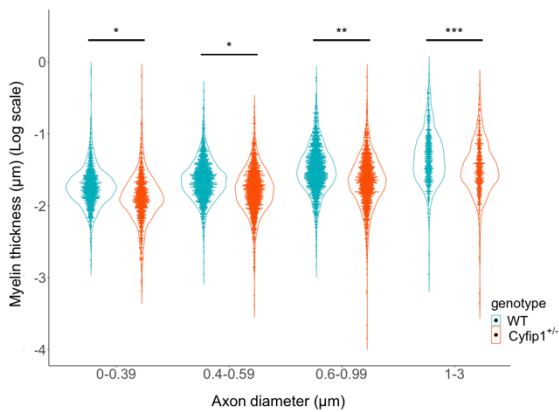
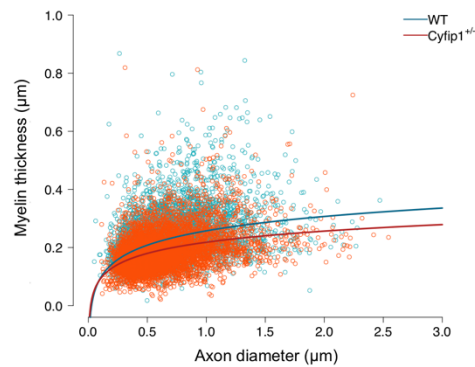
*Cyfp1*^{+/-}**B****C****D****E**

Figure 6.6 - Myelin thickness in WT (n=5 animals, n=7148 axons) and *Cyfp1*^{+/-} (n=4 animals, n=5979 axons) rats.

Differences were assessed using a LME model adjusted for individual variability. **A** Representative electron micrographs of axons in the WT and *Cyfp1*^{+/-} rats in the corpus callosum. Scale bars=2 μm. **B** Histogram showing the frequency distribution of myelin thickness values of myelinated fibres. **C** Myelin thickness of myelinated fibres per group. *Cyfp1*^{+/-} rats show significant decreased myelin thickness compared to WT rats (LME: $\chi^2(1)=14.63$, $p=0.0001$ ***). **D** Myelin thickness calculated for small (diameter<0.4), medium-small ($0.4 \leq \text{diameter} < 0.6$), medium-large ($0.6 \leq \text{diameter} < 1$) and large

($1 \leq \text{diameter} < 3$). Significant decreases in myelin thickness in *Cyfp1*^{+/-} compared to WT rats were found in all different axon diameter ranges, and more significant in larger myelinated axons: small (n=1510 WT and 1276 *Cyfp1*^{+/-} axons; LME: $\chi^2(1)=6.32$, p=0.1*), medium-small (n=2283 WT and 2043 *Cyfp1*^{+/-} axons; LME: $\chi^2(1)=5.57$, p=0.2*), medium-large (n=2551 WT and 1993 *Cyfp1*^{+/-} axons; LME: $\chi^2(1)=8.85$, p=0.003**), and large (n=804 WT and 667 *Cyfp1*^{+/-} axons; LME: $\chi^2(1)=21.92$ p=2.85e-06***). **E** Scatter plot of myelin thickness values across all axon diameters WT (n=7148 axons) and *Cyfp1*^{+/-} (n=5979 axons), showing a logarithmic relationship between both measures. Data points and p-values are represented in figure where, *<0.05, **<0.01, ***<0.001.

6.4.2. Oligodendrocyte and MBP quantification in the corpus callosum and external capsule

Myelin is produced by mature oligodendrocytes in the central nervous system, so I next investigated whether *Cyfp1* haploinsufficiency influenced the number and/or maturation of oligodendrocytes using antibodies to the specific molecular markers Olig2 and CC1. The analysis focused on the corpus callosum and external capsule. External capsule was included in this analysis since it contains fibres traveling from the corpus callosum, and significant decreased FA was also found in this region (Chapter 5). Sections were stained for Olig2 and CC1 proteins (see **Figure 6.7A** for representative images). Cells stained for Olig2 alone represented all the oligodendrocyte lineages from early progenitors to mature cells, whereas cells double-stained for Olig2 and CC1 proteins revealed specifically the mature oligodendrocyte (myelin-producing) population. In the *Cyfp1*^{+/-} rats, this analysis showed, a significant reduction in both the number of oligodendrocyte lineage cells (two sample t-test, t=2.22, df=12, p=0.04*) and mature oligodendrocytes (two sample t-test, t=2.48, df=12, p=0.03*) in comparison with WT (**Figure 6.7B**).

Complementary to the TEM analysis, the level of MBP, a specific component of the myelin sheath, was assessed by measuring the intensity of MBP+ area (see **Figure 6.8A** for representative images). Here, a reduction close to significance (two-sample t-test, t=2.16, df=12, p=0.05) was found in the corpus callosum/external capsule of the *Cyfp1*^{+/-} rats (**Figure 6.8B**).

A

WT

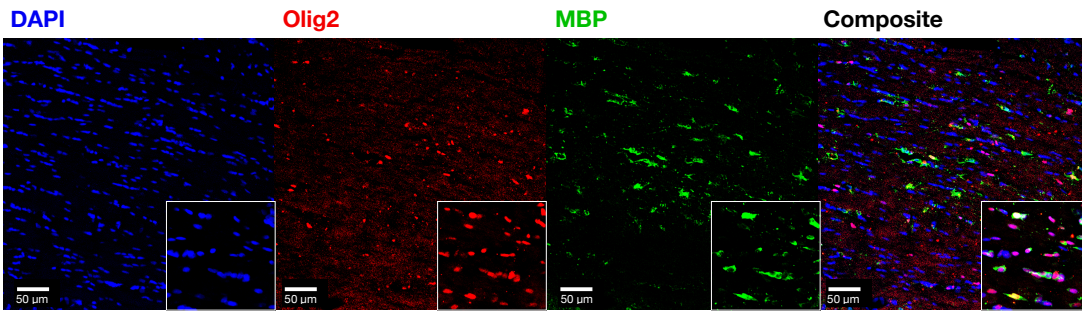
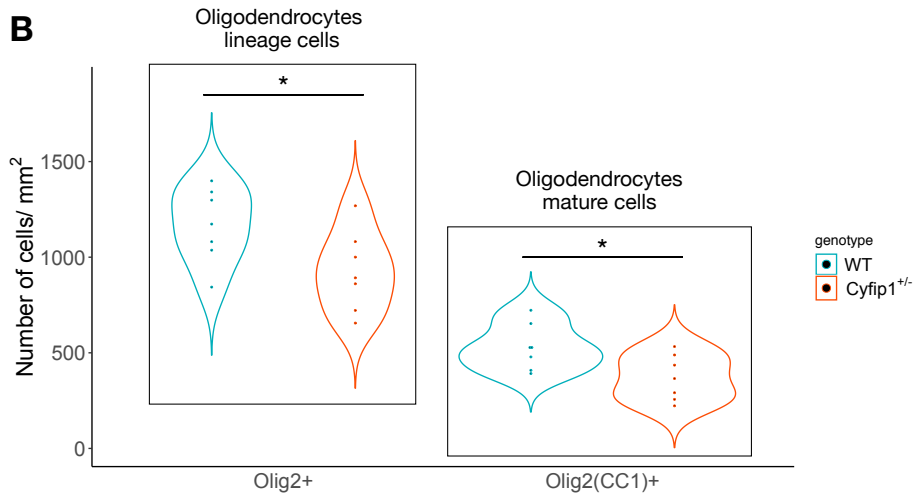
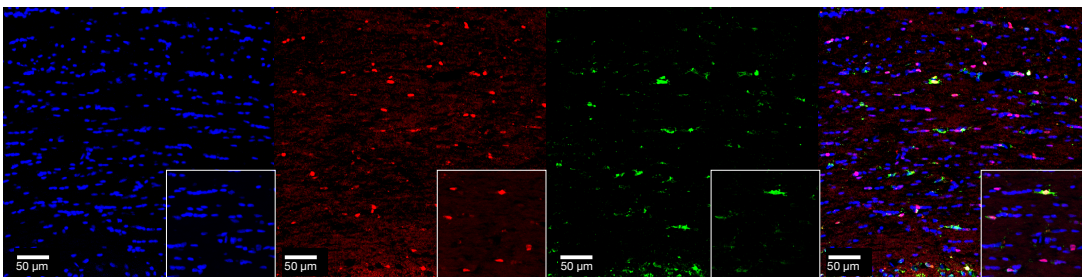
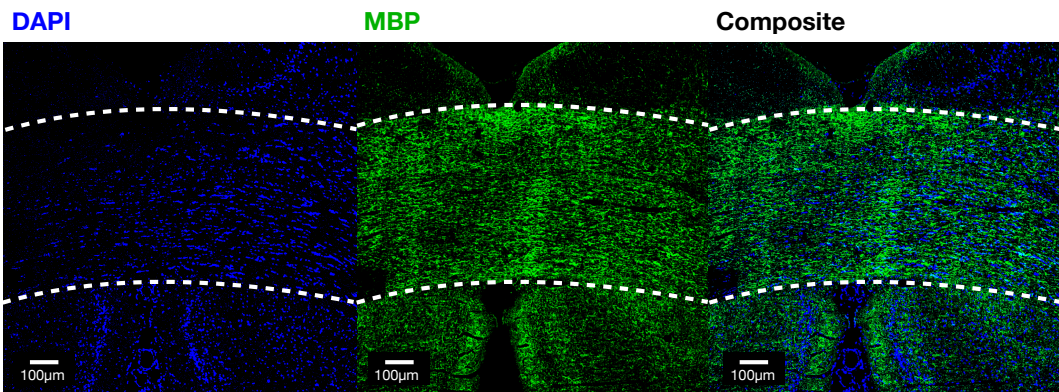
*Cyfp1*^{+/-}

Figure 6.7 – Number of oligodendrocyte lineage and mature cells in the corpus callosum of WT and *Cyfp1*^{+/-} rats (n=7 each).

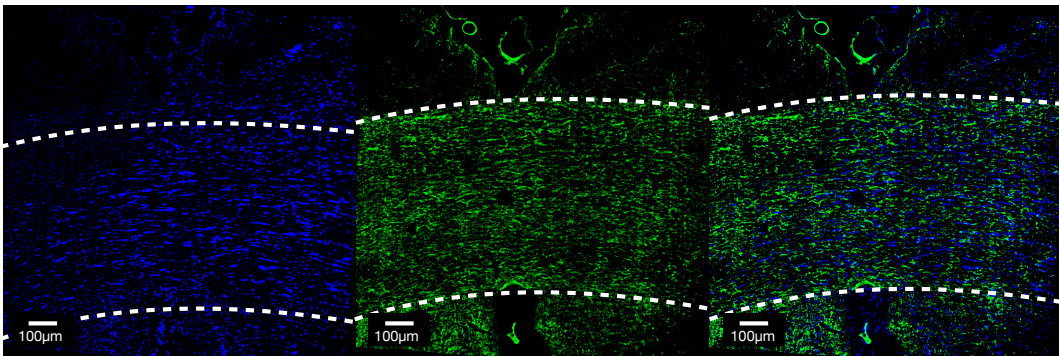
A Representative images at magnification x20 for the following immunomarkers: DAPI, Olig2, and CC1, in the corpus callosum of WT and *Cyfp1*^{+/-} rats. Scale bars=50 μm. **B** Number of oligodendrocyte lineage (represented by Olig2+ cells), and mature (represented by cells that are both Olig2+ and CC1+) cells. Significant decreases in the number of lineage (two sample t-test, $t=2.22$, $df=12$, $p\text{-value}=0.04^*$) and mature (two sample t-test, $t=2.48$, $df=12$, $p\text{-value}=0.03^*$) cells are found in the *Cyfp1*^{+/-} compared to WT rats. Data points and p-values are represented in figure where, $*<0.05$, $**<0.01$, $***<0.001$.

A

WT



Cyfp1^{+/-}



B

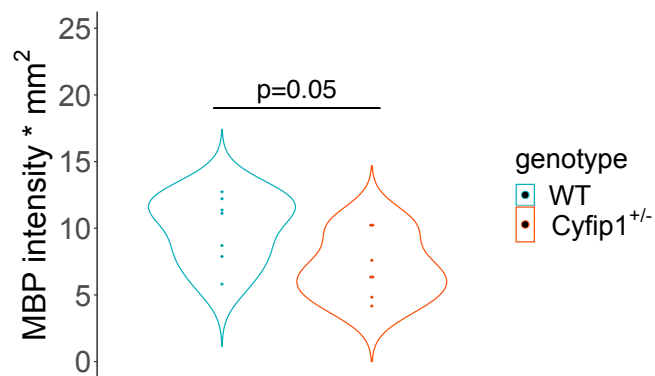


Figure 6.8 - MBP intensity levels in the corpus callosum of WT and *Cyfp1*^{+/-} rats (n=7 each).

A Representative images at magnification x10 for the following immunomarkers: DAPI and MBP, in the corpus callosum of WT and *Cyfp1*^{+/-} rats. Scale bars=100 μm. **B** MBP intensity multiplied by percentage area (mm²) of the staining. *Cyfp1*^{+/-} rats show a very close to significance decrease in MBP intensity (two-sample t-test, t=2.16, df=12, p=0.05). Data points are represented in figure.

6.5. Discussion

In order to explore the cellular causes underlying the imaging phenotype associated with the low dosage of *Cyfp1* gene, brain tissue from the *Cyfp1*^{+/-} rat line was analysed using ultra-structural and immunofluorescence methods. The ultra-structural experiment, using TEM methods, indicated a thinning of the myelin sheath in the corpus callosum of the *Cyfp1*^{+/-} rats in the absence of any changes in axonal number or diameter. Myelin is produced at the end stages of oligodendrocyte differentiation. Here, immunofluorescence methods indicated a reduction in lineage and mature oligodendrocyte cells in the corpus callosum. Furthermore, analysis of MBP levels in the corpus callosum indicated a decreased in MBP intensity in *Cyfp1*^{+/-} rats, which is in line with the myelin thinning phenotype in this region.

6.5.1. Myelin thinning in the *Cyfp1*^{+/-} rats – possible cellular mechanisms

Dysregulations in the *Cyfp1* gene, as stated previously, could result in aberrant axonal growth, guidance, and/or myelin. In this study, TEM methods showed that *Cyfp1* haploinsufficiency was indeed associated with myelin thinning in the corpus callosum in a rat model, but no evidence was found for an impact on the axonal level, in particular on axonal density and calibre. This specific effect on myelin is consistent with the decreased FA, described in the last chapter, and could be a result of disruptions in the myelination process, or demyelination as a result of abnormal neuronal dynamics. Here, the finding of a reduction on oligodendrocyte lineage and mature cells, in the corpus callosum of the *Cyfp1*^{+/-} rats, suggests an abnormal supply of myelinating oligodendrocytes, which in turn can result in myelination deficits as shown previously by others (*Boyd et al., 2013; Syed et al., 2013*).

As described in the General Introduction Chapter, an effect of *Cyfp1* on oligodendrocyte-myelin dynamics is highly relevant, since dysregulations in mechanisms involving myelin dynamics have been recently proposed in GWAS as contributors to disease pathophysiology in schizophrenia, rather than a result of environmental changes or a catalyst of downstream events (*Roussos and Haroutunian, 2014*). This could potentially underlie the brain connectivity anomalies in schizophrenia (*Lynall et al., 2010*), where other imaging and molecular profiling studies of patients with

schizophrenia have reported effects on protein signalling networks involved in the myelination process (*Aston et al., 2004; Hakak et al., 2001; Prabakaran et al., 2004; Tkachev et al., 2003*). Moreover, impaired oligodendrocyte differentiation was found in post-mortem patients with schizophrenia, where a reduction in oligodendrocyte lineage cells was reported, with no changes in the number of OPCs in the prefrontal cortex (*Mauney et al., 2015*).

A key question is how *Cyfp1* haploinsufficiency could influence oligodendrocyte-myelin dynamics. As explained in General Introduction, a main function of the CYFIP1 protein is to inhibit Arp2/3 dependent f-actin assembly, via inhibition of the WAVE1 protein and other members of the WAVE regulatory complex (*Derivery and Gautreau, 2010*). WAVE1 was found to be expressed in oligodendrocyte cells, where multiple aspects of oligodendrocyte function, including differentiation and myelination are reliant on effective cytoskeleton remodelling. Furthermore, manipulation of important actin regulators resulted in abnormal oligodendrocyte-myelin dynamics. Of particular interest is the study by *Kim et al., 2006* showing that WAVE1 localises to the leading edges where actin polymerisation is actively regulated. More importantly, this study shows a specific effect of WAVE1 knockout on oligodendrocyte-myelin dynamics, where *in vitro* oligodendrocytes, isolated from mice lacking WAVE1, had fewer processes and the mice had less myelinated fibres in the corpus callosum, but not in other regions, compared to controls. Other studies have provided evidence for a role of actin regulators on myelination, where ILK was shown to be involved in oligodendrocyte differentiation and axon ensheathment (*O'Meara et al., 2013; Michalski et al., 2016*), Arp2/3 complex was shown to be required for oligodendrocyte process outgrowth and branching but not for myelin wrapping (*Zuchero et al., 2015*), and Rho GTPases Cdc42 and Rac1 were shown to be required for correct myelin sheath formation (*Thurnherr et al., 2006*).

Oligodendrocytes extend their processes through actin-dependent mechanisms, where actin polymerisation is essential for process outgrowth (see General Introduction). Therefore, it is understandable that lower levels of f-actin, as a result of WAVE1 absence, would result in abnormal oligodendrocyte process growth. However, given the inhibitory role of *Cyfp1* on f-actin polymerisation, one would expect increased levels of f-actin as a result of *Cyfp1* haploinsufficiency. Indeed, increased levels of f-actin were found within dendritic spines in *Cyfp1*^{+/-} mice (*Pathania et al., 2014; Hsiao et al., 2016*). Several lines of evidence have established a link between *Cyfp1* and spine formation, where *Cyfp1* haploinsufficiency led to reduced spine complexity, as well as an increased

ratio of long, thin immature spines. Interestingly, as explained in General Introduction, the way oligodendrocytes extend their processes resembles spine formation in neuron cells, through a large actin-rich extension called growth cone (*Michalski and Kothary, 2015*). It is therefore possible that *Cyfp1* could have a similar influence on oligodendrocytes and affect their branching during differentiation process. Furthermore, the synthesis of major myelin proteins, such as PLP and MBP, occurs in oligodendrocytes. These proteins are only synthesised when OPCs reach maturation and are considered pre-myelinating oligodendrocytes (*Baron and Hoekstra, 2010*). Here, inhibition of their translation is crucial for oligodendrocyte development, where an early translation could be deleterious to the cell (*Boggs, 2006*). These proteins are essential for myelin compaction and formation of mature myelin, where their transport from oligodendrocytes to the myelin membrane is crucial (*Boggs, 2006; Baron and Hoekstra, 2010; Fulton et al., 2010*). FMRP was found to be expressed in oligodendrocytes, and was proposed that FMRP played a role in translation inhibition of MBP mRNA (*Wang et al., 2004*), preventing an early translation of this protein. This indicates that *Cyfp1* could also have an impact on MBP translation and/or transport of MBP to the myelin membrane. Altogether, these findings suggest that dysregulations in *Cyfp1* gene may influence oligodendrocyte differentiation and/or synthesis of myelin key proteins. Using cell culture methods to better visualise oligodendrocyte structure, I will investigate a potential effect of *Cyfp1* haploinsufficiency on oligodendrocyte differentiation in Chapter 7. Here, I will use MBP as an indicator of cell maturation and further assess the protein distribution in the cells, in order to unravel possible cellular mechanisms leading to the myelin thinning seen *in vivo*.

It is also possible that *Cyfp1* could interfere with oligodendrocytes and myelination process indirectly by affecting signalling pathways that are involved in differentiation and maturation of oligodendrocytes. Interestingly, studies have demonstrated that activation of the mammalian Target of Rapamycin (mTOR) is essential for differentiation from late OPCs to immature oligodendrocytes through two distinct signalling complexes, mTORC1 and mTORC2 (*Tyler et al., 2009, Wahl et al., 2014*). Increased *Cyfp1* dosage was found to dysregulate mTOR signalling, resulting in an enhanced expression of mTOR at the mRNA and protein level, and activation of mTOR signalling (*Oguro-Ando et al., 2015*). Reciprocally, extracts of cultured *Cyfp1* haploinsufficient primary cortical neurons from transgenic mice showed an mTOR protein reduction of 40-60% (*Abekhoukh et al., 2017*). Therefore, it is possible that

reductions in *Cyfp1* levels impact differentiation of oligodendrocytes by dysregulating mTOR signalling.

Additional complexity is apparent when considering the range of functions that may be sensitive to reduced dosage of *Cyfp1*, encompassing oligodendrocyte production, differentiation and migration; effects on neurons as opposed to oligodendrocytes, can also have an impact on axon-oligodendrocyte interactions and influence myelination in that way (*Barres and Raff, 1999*). Investigation of these possibilities, *in vivo*, would require the implementation of models that combine low dosage *Cyfp1* with gene constructs which allow the labelling oligodendrocytes at specific stages of oligodendrocyte differentiation, such as inducible Sox10 systems (*Shibata et al., 2010*).

6.5.2. Myelin thinning in the corpus callosum of *Cyfp1*^{+/-} rats – functional outcomes

Myelin is essential for high-speed conduction of electrical impulses through axons. The myelin thinning observed in the corpus callosum of the *Cyfp1*^{+/-} rats could result in network dysfunction by slowing down propagation of electrical signal between the brain and the body or within the brain itself. At the same time as this thesis project, an independent group conducted a study looking at the impact of *Cyfp1* haploinsufficiency on functional connectivity and white matter microstructure in a mouse model (*Domínguez-Iturza et al., 2019*). Of great relevance, this study found a similar thinning of the myelin sheath in the corpus callosum of the *Cyfp1*^{+/-} mice, where *Cyfp1*^{+/-} mice also showed impaired bilateral functional connectivity and motor coordination. The findings of both studies (this and *Domínguez-Iturza et al., 2019*) were published at the same time at Nature Communications. This overlap shows a quite encouraging specific effect of *Cyfp1* on myelin that is preserved across these two species (mouse and rat). Results on motor function are in line with the deficits in motor learning in *Cyfp1*^{+/-} mice, described in a previous study by *Bachmann et al., 2019*, and could be a result of this impaired bilateral connectivity, that could be caused by reductions in myelin in the corpus callosum, as explained in the previous chapter.

Of interest is also a previous study by *Inagawa et al., 1988* in mouse models with myelin deficits, specifically in *Shiverer* (deletion mutant of MBP) and *mld* (allelic mutant

to *Shiverer* with lowered MBP expression) mice, showing highly specific effects on behavioural flexibility in a reversal learning task, whereby they had difficulty changing their behaviour to reflect new reward contingencies, without deficits in original learning per se. Although no behavioural experiment is presented as part of this thesis, a parallel experiment was performed in our laboratory, by Dr. Josephine Haddon, looking at the maladaptive brain function in *Cyfp1*^{+/-} rats using behavioural tasks that assayed behavioural flexibility. These findings were published together with findings from this chapter, and Chapters 5 and 7. In our study (*Silva et al., 2019a*), we showed highly specific effects of *Cyfp1* haploinsufficiency in reversal learning, with no concomitant effects on initial learning. These effects were replicated in an independent associative mismatch task. Behavioural inflexibility, as in the *Shiverer* mice, can be related with a general thinning in myelin in the brain. However, in light of the specific findings in the corpus callosum, this structure was previously shown to correlate with behavioural flexibility in a human study using a cohort of twin pairs, where one was diagnosed with bipolar disorder and the other was clinically healthy (*Bearden et al., 2011*). In our study, the behaviour experiment was done in a separate cohort of rats, and therefore we could not correlate the behavioural deficits with changes in the corpus callosum and myelin thinning. Future work combining imaging, behaviour and histology in the same cohort of rats would permit us to explore a causal link between these two phenotypes (see General Discussion, where this issue will be further elaborated).

6.5.3. Myelin thinning in the *Cyfp1*^{+/-} rat model and relationship with human data

Myelin modulates the degree of anisotropy of water molecules inside the white matter tracts, and therefore myelin thinning is generally associated with reductions in FA (*Beaulieu, 2002; Soares et al., 2013*). Hence, the myelin thinning seen in the corpus callosum of the *Cyfp1*^{+/-} rats may be associated with the imaging phenotype described in the previous chapter. In the previous chapter, I also introduce the idea that white matter changes associated with low levels of *CYFIP1/Cyfp1* gene may be similarly present in both human and rats, despite the opposite direction of effect on FA. Here, this idea becomes more plausible since myelin is known to have a relatively modest impact on DTI signal, where changes in the axon itself lead to a stronger effect on DTI signal (*Beaulieu, 2002*). It may be that low levels of *CYFIP1/Cyfp1* gene lead to myelin deficits in both

humans and rats, but in terms of the human DTI data any effect on myelin may have been masked by other molecular and cellular changes associated with the CNV. To date, there have been no published studies of myelin (as opposed to overall white matter) changes in 15q11.2 BP1-BP2 deletion, though the current data predicts their existence and this is something that could be tested using ultrastructural MRI methods providing the necessary resolution to visualise and quantify myelinated axons directly in the living human brain (*Shi and Toga, 2017*).

6.5.4. Limitation of this study

In this study, the cohort of rats used for immunofluorescence was selected from the same cohort used for imaging in Chapter 5. Thus, I was able to explore correlations between DTI measures and number of oligodendrocytes or MBP levels in the sample, where no significant correlations were found between these measures (data not shown). A number of reasons could be behind this. First, the animals were culled one month after the imaging experiment, and during this time period variations in oligodendrocyte number and myelin could happen within each group. In the imaging data, a mean value is extracted for the whole white matter tract, whereas oligodendrocytes and MBP were quantified in specific slices of the brain. In order to compare the two measures, values of FA should be extracted from approximate regions to the ones where the staining is performed.

The results in this study are specific to the corpus callosum. However, other white matter tracts are likely to be affected, as shown in the previous chapter. Whilst an overall decrease in FA was noticed in most white matter tracts, some increases were also reported. It would be interesting to investigate if the effects of *Cyfp1* haploinsufficiency on myelin are indeed specific to the corpus callosum, or other white matter regions are similarly affected, and further explore cellular changes behind the increased FA seen in the stria terminalis in the *Cyfp1*^{+/-} rats.

6.5.5. Conclusion

TEM analysis indicated a thinning of the myelin sheath in the corpus callosum of the *Cyfp1*^{+/-} rats in the absence of any changes in axonal number or diameter. Reductions in the number of oligodendrocytes, myelin producing cells, were observed in the corpus

callosum of the *Cyfp1*^{+/-} rats suggesting that *Cyfp1* haploinsufficiency is associated with deficits in myelination. Several cellular mechanisms that become disrupted with low levels of *Cyfp1* might influence myelination by having an impact on oligodendrocyte function. In Chapter 7, the impact of *Cyfp1* on oligodendrocyte cells will be explored in a cell culture experiment.

Chapter 7

Investigating the effect
of *Cyfp1* haploinsufficiency on rat brain
oligodendrocytes - an *in vitro* cell culture study

7.1. Abstract

Background

Findings from the last chapter indicate that *Cyfp1* haploinsufficiency leads to thinning of the myelin sheath, with no apparent effect on axon density or diameter. Myelin is produced by mature oligodendrocytes, where reduction in the number of these cells suggested a disruptive myelination in the *Cyfp1*^{+/-} rats. In this chapter, cell culture methods will be used to explore specific effects of *Cyfp1* haploinsufficiency on oligodendrocyte function.

Methods

Primary OPC cultures from WT and *Cyfp1*^{+/-} neonatal rats (postnatal day 0-3) were used, where oligodendrocytes were analysed after 3 days of differentiation. Cells were stained for O4 (marking pre-oligodendrocytes to myelinating mature oligodendrocytes) and MBP (marking only mature oligodendrocytes). Here, the proportion of mature oligodendrocytes (MBP⁺ cells) was first analysed. In order to investigate a possible effect on later stages of maturation, mature oligodendrocytes were classified in 3 levels of maturation, based on the distribution of MBP⁺ staining in the cell. Finally, the area of MBP⁺ staining was quantified in oligodendrocytes on last stages of maturation.

Results

Results showed an increase in proportion of mature oligodendrocytes in *Cyfp1*^{+/-} cultures. This was due to a higher proportion of cells in initial states of maturation, where the MBP is restricted to the oligodendrocyte cell body. Oligodendrocytes on later stages of maturation presented a smaller area of MBP⁺ staining in *Cyfp1*^{+/-} cultures, compared to the WTs, where the protein failed to reach the distal parts of the highly branched oligodendrocytes.

Conclusions

Evidence in this chapter suggests that *Cyfp1* haploinsufficiency has an impact on mature oligodendrocyte function by hindering the intracellular distribution of a key myelin protein, the MBP. This suggests a possible cellular mechanism through which *Cyfp1* haploinsufficiency could interfere with the myelination process and lead to myelin thinning.

7.2. Introduction

The findings reported in the previous two chapters indicate that *Cyfp1* haploinsufficiency leads to a disruption in the myelination process dependent on oligodendrocyte-myelin dynamics, as evidenced by myelin thinning in the corpus callosum accompanied by a reduced population of mature oligodendrocytes in *Cyfp1^{+/-}* rats. Dysregulations in *Cyfp1* were already shown to have a marked impact on dendritic spine development and plasticity in mouse models (*De Rubeis et al., 2013; Pathania et al., 2014; Oguro-Ando et al., 2015*). Of potential specific relevance, during differentiation, oligodendrocytes extend long and complex projections through mechanisms that resemble dendritic growth and spine formation in neuronal cells (see Introduction for further explanation of this mechanism) (*Michalski and Kothary, 2015*). These mechanisms are highly dependent on actin dynamics, as well as a regulated transport and translation of protein and lipids, actions that could be mediated by *CYFIP1* acting as a negative regulator in the two processes.

Although data from the last chapter allowed an *in vivo* quantification of oligodendrocytes in brain tissue, this analysis does not provide enough cellular resolution to visualise the morphological characteristics of the cells. In the present work, this motivated the use of cell culture methods, providing enhanced cellular resolution for single-cell observations, where the intrinsic effects of *Cyfp1* haploinsufficiency on oligodendrocyte morphology and myelin formation could be studied. It was previously shown that oligodendrocytes can fully differentiate *in vitro*, in the absence of any axons, extending multiple processes and forming myelin membranes. Importantly, the morphological changes during oligodendrocyte differentiation resemble those observed during *in vivo* myelination (*Kachar et al., 1986; Knapp et al., 1987*).

Taking advantage of the enhanced cellular resolution, in this study I used cell culture methods to further address the question of how *Cyfp1* haploinsufficiency could impact the myelination process. Here I used two markers, O4 and MBP, in order to first investigate any differences in differentiation. O4 is expressed by oligodendrocyte cells in general, whereas MBP is a maturation marker since it is only expressed when the cells achieve maturation. MBP is a crucial protein during myelination, as explained in the General Introduction, and a reduction in MBP levels in the corpus callosum of the *Cyfp1^{+/-}* rats, was reported in the previous chapter. In brain tissue, most of the expressed

MBP comes from myelin sheaths, where this protein is widely expressed. However, the synthesis of MBP occurs in the oligodendrocytes, where its transport to the myelin membrane is needed for myelination to occur. The process through which MBP is translated and inserted in the myelin membrane is different from other myelin proteins (*Baron and Hoekstra, 2010*). Instead of the protein being synthesised in the cytoplasm adjacent to the oligodendrocyte cell body and then transported, MBP mRNA is transported in RNA granules along the microtubules within the oligodendrocyte processes (*Müller et al., 2013*). These granules contain all necessary molecules for translation and only initiate MBP translation locally at the axon-oligodendrocyte site, where freshly synthesised MBP protein is inserted within the myelin membrane (*Colman et al., 1982*).

In order to further address how *Cyfp1* haploinsufficiency could influence oligodendrocyte function, I first quantified the proportion of oligodendrocyte mature cells, and then looked at the intracellular distribution of MBP protein in oligodendrocyte at different stages of late maturation. The specific aim of the study was to start unravelling possible cellular mechanisms through which *Cyfp1* haploinsufficiency could interfere with the process of myelination and lead to myelin thinning.

7.3. Material and Methods

7.3.1. Generation of primary oligodendrocyte cultures

The protocol followed for generating oligodendrocyte cultures was previously established by *Syed et al., 2017*. This protocol is known to generate OPCs at >95%. Primary OPC cultures were isolated from neonatal Long Evans rats (postnatal day 0-3), of mixed sex. Litters remained within the breeding cage until use from P0 to P3. Here, 2 to 4 pups were used in each WT and *Cyfp1*^{+/-} cultures. Three independent biological replicates were performed. The protocol for the generation of primary oligodendrocyte cultures will be described in the next sections. Moreover, a schematic flow chart of the protocol is illustrated in **Figure 7.1**.

7.3.2. Preparation of tissue culture coating

Before isolation, all tissue culture plasticware was prepared on the same day. T75 flasks were coated with 0.01% PLL (Sigma) in PBS for 20 minutes in the incubator. Then, the flasks were washed twice with PBS and dried in the incubator for 10 to 15 minutes.

7.3.3. Dissection of neonatal rat cortex for OPC isolation

Litters of mixed sex pups were euthanised by cervical dislocation. The pups were sprayed with 70% ethanol. Using sterile curved scissors, the brains were dissected out and placed in a 10 cm Petri dish containing minimum essential medium Eagle (MEM) medium. Using a dissecting microscope and fine-tip forceps, the cerebellum was first separated from the hemispheres, and then the two hemispheres were separated in a sagittal cut from mid brain structures. Finally, the meninges were carefully removed in a caudal to rostral direction.

7.3.4. Mechanical and chemical dissociation and preparation of cells for culture

The half cortices were transferred to 7ml Bijou tubes, where 1ml of digestion medium was added in the sterile tissue culture hood for enzymatic digestion. The digestion medium contained 1 ml of MEM, 50 µl of 30 µg/ml papain (Worthington, LS003126), 15 µl of 4 mg/ml DNase I type IV (Sigma, D5025), and 10 µl of 24 mg/ml L-Cystine (Sigma, 30199). The digestion medium was filtered using a 0.2 µm syringe filter and activated in the 37 °C incubator for 15 minutes before adding the medium to the cortices. With a P1000 pipette the cortex was mechanically dissociated into flaky homogenate. The tubes containing the dissociated cortices and digestion medium were then placed in the 37 °C incubator for 30 minutes. Following incubation, the tubes were returned to the sterile hood and, using a P1000 pipette tip, the solution was pipetted up and down until a clear homogenate solution was formed. This homogenate was then transferred to a 15 ml conical tube, where Dulbecco's modified Eagle's medium (DMEM) (Sigma, D5796) was added to the solution, to make up 10 ml of solution, to stop the digestion process. The tubes were then centrifuged at 250xg for 10 minutes at 25 °C to sediment the tissue. The

supernatant was carefully aspirated in order to ensure that the majority of the digestion medium was removed. Then, 1 ml of DMEM medium containing 10% of fetal bovine serum (FBS) was added. The T75 flasks, previously coated with PPL, were filled with 9 ml of maintenance medium consisting of 500 ml of DMEM, 50 ml of 10% fetal calf serum (FCS) (Sigma, 12133C), 10 ml penicillin/streptomycin, and 10 ml of L-glutamine. The 1ml of cell suspension was then added to the flasks, where the flasks were gently rocked from side to side several times to evenly spread the culture. The flasks were then moved to the 37 °C, where the maintenance medium was changed every 3 days. Following 9 to 12 days of culturing, the OPCs are ready for isolation.

7.3.5. Removal of microglia and isolation of OPCs from astrocyte monolayer

After 9 to 12 days of culture, the cultures showed the following characteristics: a confluent layer of dark cells at the bottom, consistent mostly of astrocytes, and a cluster of small shiny cells on the top consisting of microglia and OPCs. In this cultures, it is known that microglia can be detached by mechanical shaking (*Tamashiro et al., 2012*). The medium was first aspirated from the T75 flask, and 10 ml of new maintenance medium was added. Then, to detach microglia, the flasks was placed in the orbital shaker and agitated for 1 hour (37 °C, 260 rev/min). Following this, the medium containing microglia was aspirated from the flasks and new 10 ml pre-warmed maintenance medium was added. For astrocyte removal, the flask was again placed on the shaker, and agitated overnight for 10 hours at 37 °C at 260 rev/min. The supernatant was collected and added to a 10 cm Petri dish containing 10 ml of the pre-warmed maintenance medium and incubated for 20 min at 37 °C. Then, the supernatant was pipetted to a 15 ml conical tube to centrifuge at 250xg for 10 minutes at 25 °C. The pellet was re-suspended in 1 ml of Sato's differentiation medium containing 500 ml DMEM, 5000 U/ml penicillin/streptomycin, 4 mM L-glutamine, 0.5% FCS (N4762, Sigma), 16 µg/ml Putrescine (Sigma, P6024), 400 ng/ml L-thyroxine (T4) (Sigma, T1775), 400 ng/ml tri-iodothyroxine (T3) (Sigma, IRMM469-IEA), 6.2 ng/ml progesterone (Sigma, P8783), 5 ng/ml sodium selenite (Sigma, S0133), 100 µg/ml bovine serum albumin fraction V (Sigma, 5470), 5 µg/ml insulin (Sigma, I3536). Here, T3 and T4 were first dissolved in 0.2 M NaOH and 75% MeOH before adding to DMEM. The density of cells per millilitre

was then calculated using a haemocytometer, where approximately 1×10^6 cells per flask were counted. The OPCs were then placed, at a density of 2×10^4 cells/cm² in a PLL-coated 8-well multi-chambered slide and cultured with Sato's differentiation medium. The wells containing the OPCs were cultured at 37 °C, 7.5% CO₂, and left for 3 days for differentiation.

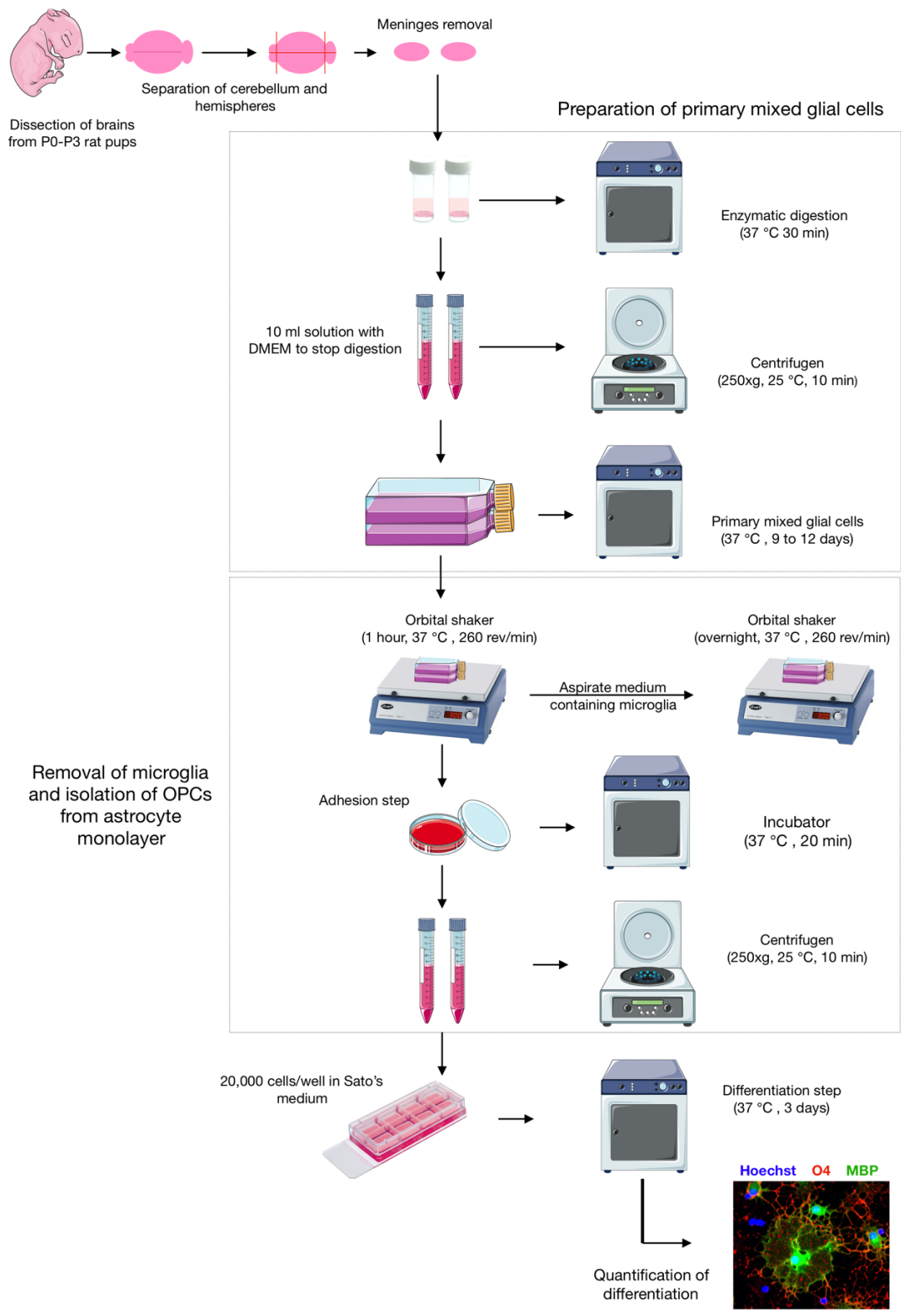


Figure 7.1 - Schematic flow chart of the experimental protocol for cultivation of OPCs.

Two diagrams are presented. The first showing the steps for preparation of primary mixed glial cells, and the second showing the steps for OPC isolation. After 3 days of differentiation in Sato's medium, the cultures are ready for immunofluorescence staining and quantification. This scheme is based on the protocol described in *Syed et al., 2017*.

7.3.6. Immunofluorescence staining of cultures

Usually after 3 days of differentiation, around 20 to 30% of the oligodendrocytes reach the maturation phase. In this study, I examined the cells at 3rd day of differentiation in order to investigate an effect on maturation rate. Therefore, after 3 days of differentiation, the cells were fixed by washing them with PBS and applying 4% of PFA solution in PBS for 10 minutes at room temperature. Following fixation, the slides were carefully washed twice with PBS. The cells were then permeabilised with blocking solution consisting of PBS, 5% donkey serum, and 0.01% Triton-X100, for 10 minutes. Cells were then stained with anti-O4 (1:200, MAB345, Millipore) and anti-MBP (1:200; MAB386, Millipore) antibodies and incubated overnight. Following primary antibody incubation, the slides were carefully washed 3 to 5 times with PBS. The corresponding secondary antibodies were then used in a 1:300 concentration (Alexa 555/488-conjugated secondary antibody, Alexa Fluor Life Technologies), and incubated for 1 hour. The slides were again washed 5 times and counterstained with Hoechst. Finally, the slides were again washed multiple times to eliminate background staining. For quantification, images were taken on an inverted fluorescent time lapse microscope (DMI6000B, Leica, UK) with x20 magnification, where 5 images from random visual fields were taken per well.

7.3.7. Quantification and statistical analyses

For quantification of cells the ImageJ software (version 1.51) was used. To assess OPC differentiation, the percentage of O4+ and the overlapped O4+/MBP+ cells, relative to Hoechst-stained nuclei were first quantified. Cells staining for O4 represent the oligodendrocyte cells from pre-oligodendrocytes to myelinating mature oligodendrocytes, whereas cells staining for O4/MBP represent the mature (non-myelinating and myelinating) cells. As explained in General Introduction, at the final stage of maturation, the oligodendrocyte processes go from process outgrowth to membrane production, where the processes resemble a ‘spider’s web-like’ appearance (**Figure 7.2**). In order to compare different levels of maturation of oligodendrocytes, O4+/MBP+ oligodendrocytes were classified into three categories considering the distribution of MBP+ staining in the cells: (i) Type 1, where the MBP staining was only present in the nucleus, (II) Type 2, ramified distribution and (iii) Type 3, membranous distribution. A representation of this characterisation is shown in **Figures 7.4B** and **7.5B**

in the Results section. Furthermore, to address the extent of MBP distribution in Type 2 and Type 3 cells, the area of MBP+ staining was quantified. During the quantification of the cells, I was not aware of the genotype. Differences between WT and *Cyfp1*^{+/-} cultured oligodendrocytes were analysed in RStudio version 1.1.463 (R Foundation for Statistical Computing, Vienna, Austria). In order to account for variability across biological repeats, an LME model was used, where biological repeats were considered random effects. Since there was only one random effect, non-restricted maximum likelihood was used to estimate the model parameters.

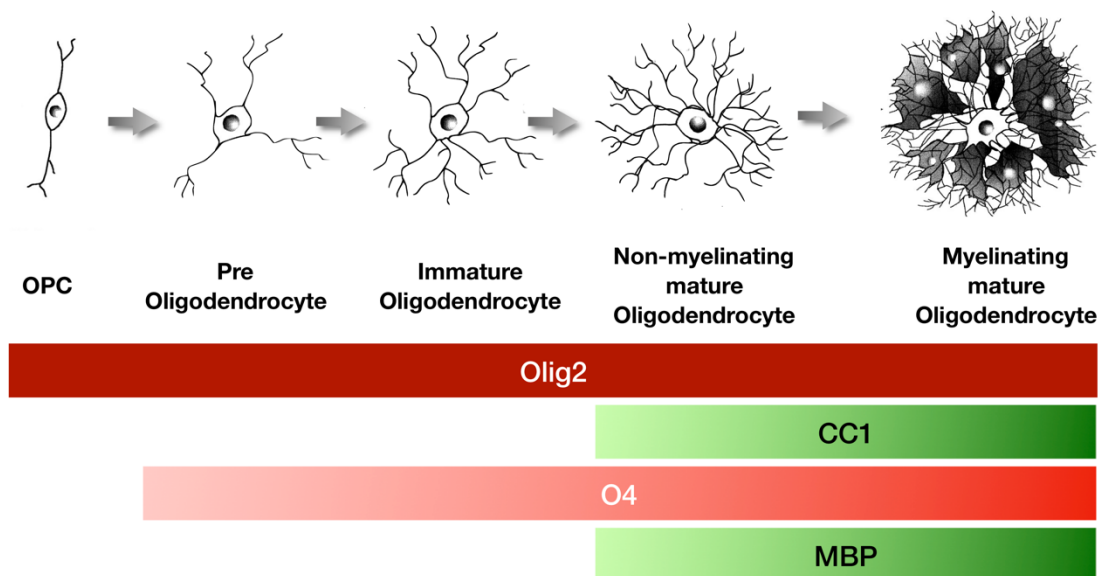


Figure 7.2 – Differentiation of oligodendrocyte lineage cells.

Morphological changes from early OPC to pre-oligodendrocyte, immature oligodendrocyte, non-myelinating mature oligodendrocyte and finally, myelinating mature oligodendrocyte. Stage-specific markers relevant for this thesis are indicated. Olig2, as explained in the previous chapter, is expressed in all oligodendrocyte lineage cells, whereas O4 is only expressed from pre-oligodendrocytes to mature oligodendrocytes. Both CC1 and MBP are maturation markers and are only expressed in non-myelinating- and myelinating mature oligodendrocytes.

7.4. Results

In this chapter, primary cell culture methods were used to further address the question of how *Cyfp1* haploinsufficiency could impact oligodendrocytes and myelination. Here, I used a standard protocol (Syed *et al.*, 2017), which generates OPCs at >95% purity from WT and *Cyfp1*^{+/-} rats. After three days of differentiation, the cells were processed for immunofluorescence staining. Similar to the last chapter, I first investigated whether *Cyfp1* haploinsufficiency influenced the number and/or maturation of oligodendrocytes. For this *in vitro* assay, I used the specific molecular markers O4 and MBP. O4 is expressed in immature and mature oligodendrocytes and MBP is only expressed in mature oligodendrocytes (**Figure 7.2**). Therefore, the number of O4+ and O4+/MBP+ cells were counted. Here, no differences were found in the percentage of cells showing a positive O4 staining (LME: $\chi^2(1)=1.57$, $p=0.21$), suggesting that there were no differences in the overall number of oligodendrocytes and therefore no effect on OPCs proliferation rate. Surprisingly, when counting the cells showing a positive staining for both O4 and MBP, *Cyfp1*^{+/-} rats showed a significant increase in this population of cells (LME: $\chi^2(1)=19.9$, $p<0.001$), suggesting an increased maturation rate in *Cyfp1*^{+/-} rats (**Figure 7.3**). In total, in WT rats 6623 cells were counted, where 4917 cells were O4+ and 1362 cells were O4+/MBP+ positive. In the *Cyfp1*^{+/-} rats, 7845 cells were counted in total, where 5789 cells were O4+ and 2012 cells were O4+/MBP+. The fact that *Cyfp1*^{+/-} cultures had more cells expressing MBP, therefore and *a priori* more mature cells, is contradictory to what we previously saw *in vivo*, in the last chapter.

A

WT

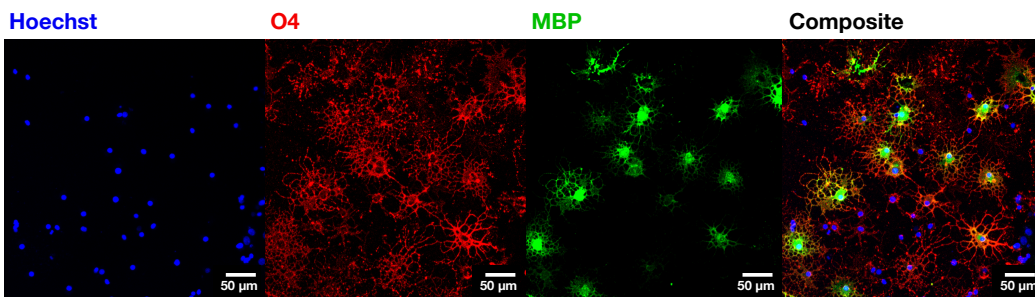
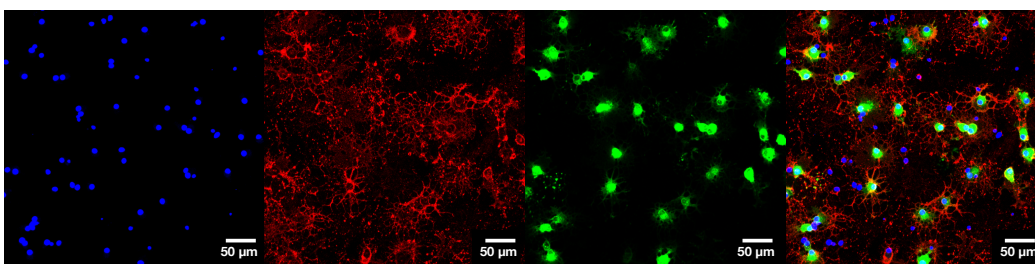
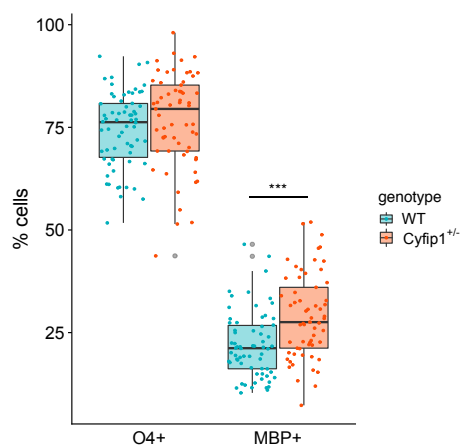
*Cyfp1*^{+/-}**B**

Figure 7.3 - *In vitro* assessment of the percentage of oligodendrocyte (O4+) and mature oligodendrocyte (MBP+) cells.

The percentage was calculated as a proportion of all cells stained with Hoechst in the culture (n=6623 WT and n=7845 cells *Cyfp1*^{+/-}). Differences were assessed using an LME model adjusted for variability between biological repeats (n=3). **A** Representative images at magnification x20 for the following immunomarkers: Hoechst, O4 and MBP in WT and *Cyfp1*^{+/-} cultures. **B** Percentage of O4+ and MBP+ cells, as a proportion of all cells. Here, no genotype effect was found in the percentage of O4+ cells (LME: $\chi^2(1)=1.57$, p=0.21), whereas a significant increase in MBP+ percentage was seen in the *Cyfp1*^{+/-} cultures (LME: $\chi^2(1)=19.9$, p<0.001***). Data points and p-values are represented in figure where, *<0.05, **<0.01, ***<0.001.

While performing the previous analysis, I further noticed that the staining pattern for MBP looked markedly different in oligodendrocyte cells from *Cyfp1^{+/-}* cultures. As can be noted in **Figure 7.4A**, *Cyfp1^{+/-}* oligodendrocytes have a more constrained distribution of MBP, where the MBP⁺ staining is more localised to the cell body. This is markedly distinct from the widely distributed pattern of MBP⁺ staining in the WT oligodendrocytes, where the MBP extends to the cell processes. I further investigated this finding by performing a quantitative analysis. To this end, I classified the MBP⁺ cells into three categories indexing the previously established maturation stages that culminate in the formation of compact myelin, taking into account the MBP distribution in the cell (*Lourenço et al., 2016*): Type 1, MBP localised only to the cell body; Type 2, any ramified MBP intracellular distribution extending into the cell processes; Type 3, final maturation stage where the MBP is distributed within the membranous processes of cells to give rise to a ‘spider’s web-like’ appearance (see **Figure 7.4B** for representative examples). This quantitative analysis confirmed the previous observation in revealing a highly significant increased percentage of Type 1 cells in the *Cyfp1^{+/-}* cultured oligodendrocytes (LME: $\chi^2(1)=68.6$, $p<0.001$ ***), with no differences in the overall percentage of cells classified as Type 2 (LME: $\chi^2(1)=0.67$, $p=0.41$) and Type 3 (LME: $\chi^2(1)=0.03$, $p=0.85$). All the percentages were calculated as a proportion of all cells in the culture (n=6623 WT and n=7845 cells *Cyfp1^{+/-}*). In total, WT cultures had 172 Type 1 cells, 735 Type 2 cells, and 456 Type 3 cells. *Cyfp1^{+/-}* cultures had 637 Type 1 cells, 905 Type 2 cells, and 454 Type 3 cells.

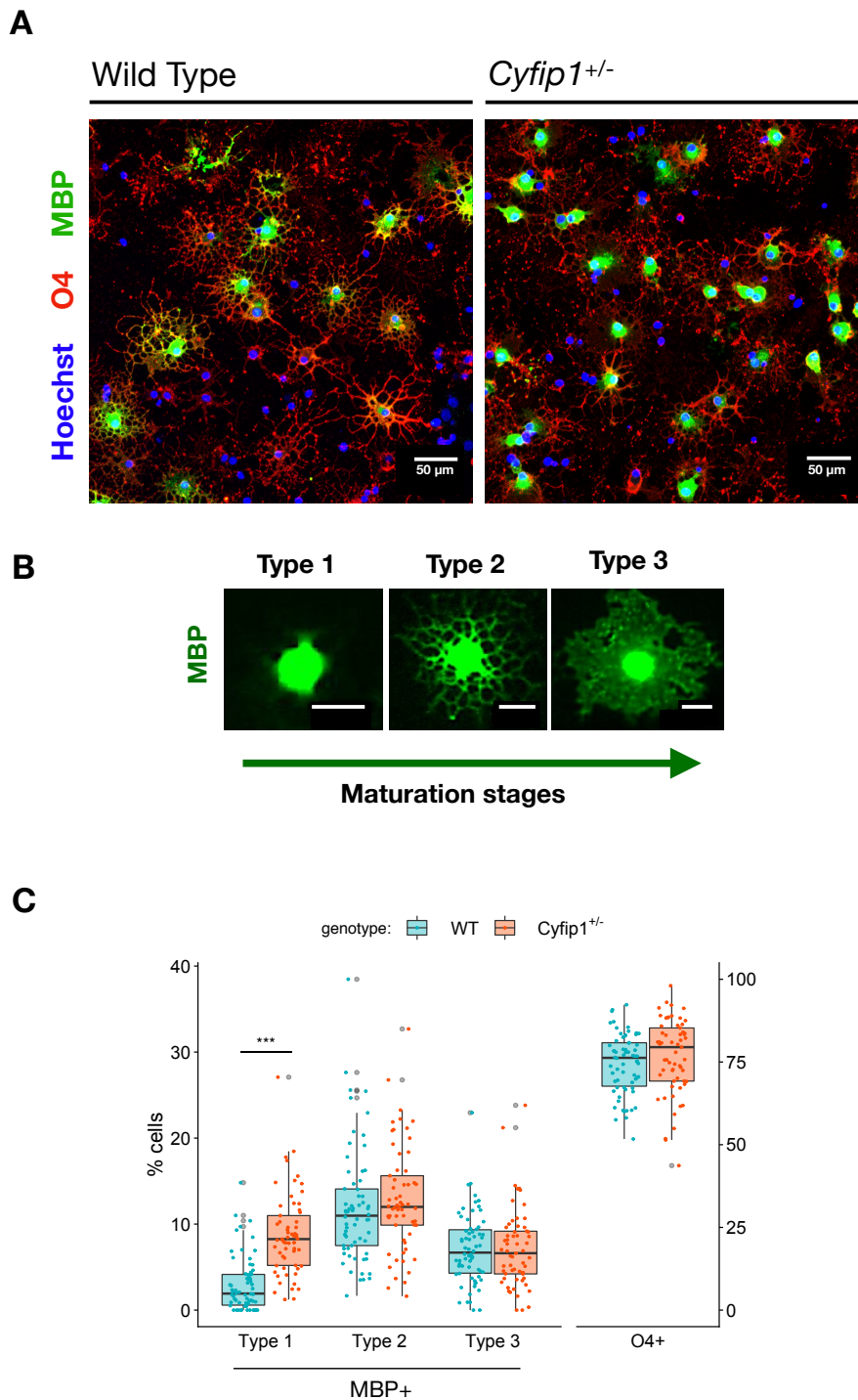


Figure 7.4 - *In vitro* assessment of the percentage of mature oligodendrocytes in different stages of maturation, as indicated by the distribution of MBP staining in the cells.

The percentage was calculated as a proportion of all cells stained with Hoechst in the culture (n=6623 WT and n=7845 cells *Cyfp1*^{+/-}). Differences were assessed using an LME model adjusted for variability between biological repeats (n=3). **A** Immunostaining of oligodendrocytes for MBP and O4 markers from WT and *Cyfp1*^{+/-} cultures, scale bar=50 μm, illustrating the punctate intracellular pattern of MBP staining in *Cyfp1*^{+/-} oligodendrocytes, relative to the more diffused, widespread pattern of staining in WT. **B** Representative images of MBP staining in oligodendrocytes exhibiting different Types of features: Type 1

(MBP localised to the cell body), Type 2 (MBP ramifying to the cell processes), Type 3 (MBP distributed within the membranous processes of cells to give rise to a 'spider's web-like' appearance), reflecting increasing maturation stages of oligodendrocytes, scale bar=20 μm . C Percentage of Type 1, Type 2 and Type 3 cells, as a proportion of all cells. Here, a significant increase in Type 1 cells was seen in the *Cyfp1*^{+/-} oligodendrocyte cultures (LME: $\chi^2(1)=68.6$, $p<0.001$ ***), whereas no difference of genotype was found in Type 2 LME: $\chi^2(1)=0.67$, $p=0.41$) and Type 3 (LME: $\chi^2(1)=0.03$, $p=0.85$) cells. The percentage of O4+ cells is again shown, where no genotype effect was found in the proportion of all oligodendrocyte cells (LME: $\chi^2(1)=1.57$, $p=0.21$). Data points and p-values are represented in figure where, * <0.05 , ** <0.01 , *** <0.001 .

The previous analysis indicated that, the increased percentage of mature cells in the *Cyfp1*^{+/-} cultures were indeed due to an increased proportion of Type 1 cells, where the MBP is expressed but only in the cell body. Here, no differences in the proportion of Type 2 and Type 3 cells was found, indicating that the *Cyfp1*^{+/-} oligodendrocytes are able to proceed to the last stages of maturation, where the processes shift from outgrowth to membrane production. However, visually the MBP staining in these cells still seemed to be somewhat constrained when compared to the WT cultures. Therefore, I next interrogated if the distribution of MBP to the distal ends of the oligodendrocyte processes could be hindered in *Cyfp1*^{+/-} cultures, even though morphologically the cells appeared to be normal. With this aim, I quantified the area of MBP+ staining in Type 2 and Type 3 cells, which showed a significant and consistent reduction in staining area for both Type 2 (LME: $\chi^2(1)=259.6$, $p<0.001$ ***) and Type 3 cells (LME: $\chi^2(1)=146.13$, $p<0.001$ ***) in *Cyfp1*^{+/-} oligodendrocytes. The area of Type 2 and Type 3 *Cyfp1*^{+/-} cells was about 50% smaller than the WT cells. Furthermore, the area of MBP staining observed in the WT cells was consistent with previous findings by others using similar culture methods ([Thurnherr et al., 2006](#)). For this analysis, the area of Type 2 cells was analysed in 491 cells from WT cultures, and in 591 cells from *Cyfp1*^{+/-} cultures. For the area quantification of Type 3 cells, 265 cells were analysed in WT cultures, whereas 341 cells were analysed in the *Cyfp1*^{+/-} cultures. Overall, these data suggest that *Cyfp1* haploinsufficiency influences the translocation of MBP to the distal parts of the highly branched mature oligodendrocyte processes, which is a critical process for myelination as explained in the General Introduction chapter of this thesis.

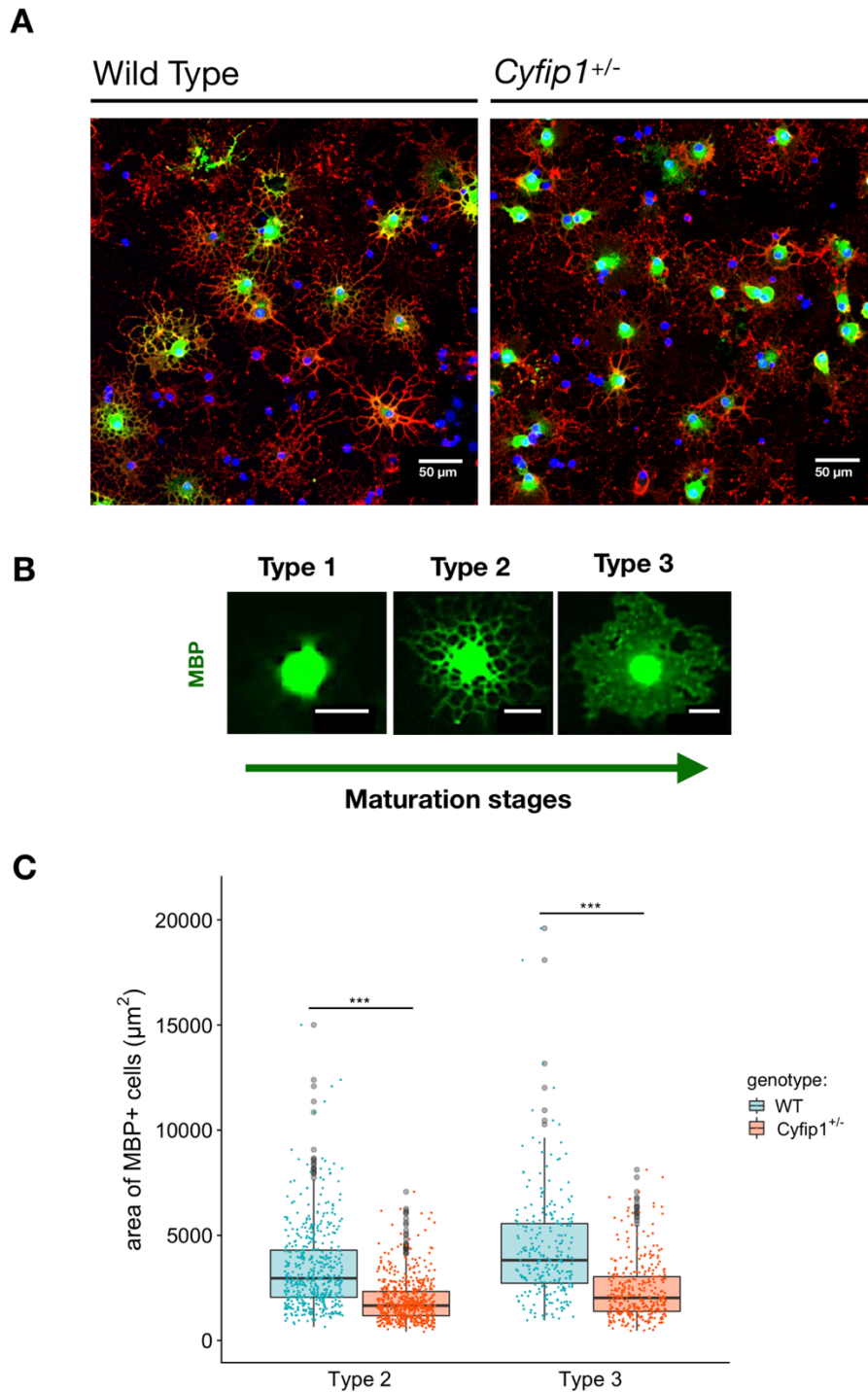


Figure 7.5 - *In vitro* assessment of the area of MBP distribution in oligodendrocytes at late stages of maturation.

Late stages of maturation were considered when MBP was distributed to the ramified processes (Type 2 cells) and when MBP was distributed to the membranous processes of the oligodendrocytes (Type 3 cells). Differences were assessed using an LME model adjusted for variability between biological repeats (n=3). **A** Immunostaining of oligodendrocytes for MBP and O4 markers from WT and *Cyfp1*^{+/-} cultures, scale bar=50 μm, illustrating the constrained distribution of MBP in *Cyfp1*^{+/-} oligodendrocytes. **B** Representative images of MBP staining in oligodendrocytes exhibiting different Types of features: Type 1 (MBP localised

to the cell body), Type 2 (MBP ramifying to the cell processes), Type 3 (MBP distributed within the membranous processes of cells to give rise to a ‘spider’s web-like’ appearance), reflecting increasing maturation stages of oligodendrocytes, scale bar=20 μ m. C Area of intracellular MBP staining in Type 2 and Type 3 cells. Here, a significant reduction in MBP staining area is seen in the *Cyfp1*^{+/-} oligodendrocyte Type 2 (LME: $\chi^2(1)=259.6$, $p<0.001$ ***) and Type 3 (LME: $\chi^2(1)=146.13$, $p<0.001$ ***) cells (about 50% of that seen in WT cells). Data points and p-values are represented in figure where, * <0.05 , ** <0.01 , *** <0.001 .

7.5. Discussion

In this study, cell culture methods were used to investigate further the effects of *Cyfp1* haploinsufficiency on oligodendrocyte function. Here, an initial assessment of oligodendrocyte differentiation showed an increased percentage of mature oligodendrocytes in the *Cyfp1*^{+/-} cultures, while no significant differences were found in oligodendrocyte general population. Then, I divided the oligodendrocyte mature cells into three morphologically different cell types, reflecting 3 different stages of late maturation. This analysis showed that the increased number of mature cells in *Cyfp1*^{+/-} cultures was a result of an abnormal increase in percentage of Type 1 cells, where the MBP staining was constrained to the cell body, and no differences were found in the number of Type 2 and Type 3 cells. Then, I looked at MBP distribution in Type 2 and Type 3 cells and found that, although these cells achieved later stages of maturation, the area of the MBP staining in *Cyfp1*^{+/-} cultures was significantly reduced in both cell type designations compared to WT cultures.

7.5.1. Constrained MBP distribution in *Cyfp1*^{+/-} cultured oligodendrocytes – possible cellular mechanisms

Several studies have shown that *Cyfp1* haploinsufficiency leads to increased levels of f-actin and newly synthesised FMRP-targeted mRNAs in neurons (*Napoli et al., 2008; Pathania et al., 2014; Hsiao et al., 2016*). Although no study to date has looked at the impact of *Cyfp1* haploinsufficiency on oligodendrocytes, it is well-established that these cells are highly dependent on actin dynamics and protein translation mechanisms to differentiate and produce myelin (see General Introduction). Increased levels of f-actin and protein translation, as a consequence of *Cyfp1* haploinsufficiency, were shown to

have a marked impact on spine morphology and physiology. In this current study, no visual evidence was found for abnormal morphology in *Cyfp1*^{+/-} oligodendrocytes. In fact, oligodendrocytes in *Cyfp1*^{+/-} cultures were able to fully mature, exhibiting the same proportion of cells with advanced morphological characteristics (Type 2 and Type 3 cells, **Figure 7.4**). However, it is important to mention that a comprehensive analysis of the oligodendrocyte cytoskeleton and number of processes was not done in this study, and therefore the current data do not discard a possible influence of *Cyfp1* on oligodendrocyte cytoskeleton morphology. Visual inspection of O4 staining, which is expressed from pre-oligodendrocyte stage onwards (**Figure 7.2**), suggests that the morphology of these cells is similar between cultures. However, quantification of this observation was difficult given the ‘spotty’ pattern of this staining. Other markers should be used to assess oligodendrocyte morphology, where some suggestions will be further discussed in the next section. Nevertheless, the findings of an abnormal distribution of MBP in *Cyfp1*^{+/-} oligodendrocytes may suggest a deficit in the transport of MBP mRNA, and/or a deficit in the translation of this protein. In order to plan future experiments addressing this hypothesis, it is important to elaborate on how *Cyfp1* could influence both the transport and/or translation inhibition of this protein.

As previously explained, MBP mRNA is transported in RNA granules, along microtubules, towards the myelin membrane. Failure in this process results in an accumulation of MBP in the oligodendrocyte cell body, culminating in myelin deficits, as demonstrated in a *taiep* mutant rat model (*Song et al., 2003*). Similarly, the *in vivo* observation of myelin thinning in *Cyfp1*^{+/-} rats, reported in the last chapter, can be a result of a failed translocation of MBP to the distal ends of the oligodendrocyte processes, as suggested *in vitro*. Interestingly, in the *taiep* mutant rat model, MBP RNA granules fail to reach the myelin membrane due to an abnormal accumulation of microtubules in the oligodendrocyte processes, that somehow hinders the transport of these granules (*Song et al., 2003*). Although the levels of f-actin were not assessed in this current study, it is possible that *Cyfp1* haploinsufficiency could lead to increased f-actin polymerisation, and therefore an accumulation of actin filaments at the oligodendrocyte processes. In the General Introduction, a study by *Zuchero et al., 2015* was mentioned, where the authors propose that MBP indirectly promotes actin disassembly (production of g-actin from f-actin), by activating depolarising proteins like cofilin and gelsolin, and this was essential for myelin wrapping. In *Zuchero et al., 2015* study it was also shown that MBP did not co-localise with actin filaments in oligodendrocytes. It is then possible that an

accumulation of actin filaments beyond the distal ends of the oligodendrocyte processes could create a physical barrier and hinder the transport of MBP RNA granules, and culminate in the observed phenotype. Furthermore, a relationship between microtubules and f-actin dynamics has been proposed, where an increment on microtubule stability or number of microtubules is associated with increased f-actin dynamics (*Wu and Bezanilla, 2018*). Whilst this hypothesis is highly speculative, it is possible that higher levels of f-actin could also affect microtubule organisation in the oligodendrocyte processes, and lead to a similar phenotype to the one observed in the *taiep* mutant rat (*Song et al., 2003*).

Inhibition of MBP protein translation before oligodendrocyte maturation, and before reaching the axon-oligodendrocyte contact site is crucial for myelin formation, where an early translation of this protein could affect the oligodendrocyte cell (*Müller et al., 2013*). A few studies have looked at FMRP as a possible mediator of MBP translation, where it was first showed that FMRP is expressed in OPCs and immature oligodendrocytes, declining as oligodendrocytes differentiated (*Wang et al., 2004*). This decline of FMRP during oligodendrocyte differentiation was accompanied by an increment in MBP protein expression at mature stages, suggesting that FMRP could regulate some aspects of myelination. Additionally, using a mouse model, *Wang et al., 2004* revealed an interaction between FMRP and the 2'untranslated region 3'UTR of MBP mRNA both *in vitro* and *in vivo*, suggesting that MBP mRNA may be one of the targets of FMRP in oligodendrocytes. It was then suggested that FMRP could repress the translation of MBP mRNA in immature oligodendrocytes, and later reduction of FMRP would allow MBP mRNA translation in mature oligodendrocytes (*Wang et al., 2004; Jeon et al., 2017*). Absence of FMRP could then lead to an early expression of MBP in immature oligodendrocytes. Given the molecular link between FMRP and CYFIP1, it is possible that FMRP inhibits MBP mRNA translation through the CYFIP1-eIF4E complex. Therefore, reduced levels of Cyfip1 protein in the rats could lead to an early translation of MBP in immature oligodendrocytes, which could explain the abnormal increment in proportion of MBP⁺ cells in *Cyfip1*^{+/-} cultures. Although a link between FMRP and MBP mRNA translation has been proposed, it is also important to mention that some contradictory findings have been reported, where no differences in expression of MBP were found in a *Fmr1* knockout mouse (*Giampetruzzi et al., 2013*). More studies are needed in order to look at a FMRP and CYFIP1 as mediators of MBP mRNA translation. Nevertheless, deficits in myelination have also been reported in *Fmr1*

knockout mouse models, specifically delayed myelination was found during the first postnatal week (*Pacey et al., 2013*).

7.5.2. Limitations of the study

The work in this study revealed initial evidence for a link between *Cyfp1* haploinsufficiency and oligodendrocyte dysfunction, by disrupting MBP protein translocation in the mature cells. However, the proposed mechanisms through which *Cyfp1* can influence this MBP distribution are speculative and further experiments need to be done. One major limitation of this study, was the fact that no comprehensive analyses were performed in order to investigate possible effects on oligodendrocyte cytoskeleton and number of processes. Furthermore, given that one of the proposed mechanisms relies on an abnormal accumulation of f-actin in the cell processes, markers for alpha-tubulin, f-actin and g-actin should be used in further experiments. Alpha-tubulin will mark for the microtubules present in the cell processes, giving us a visualisation of oligodendrocyte morphology, whereas levels of f-actin and g-actin will further elucidate on possible dysregulations in actin assembly/disassembly mechanisms. Another limitation is the fact that the presence of *Cyfp1* protein in oligodendrocytes was not measured in this study, and it will be crucial in next experiments. Here, the presence of the CYFIP1-binding WAVE1 and FMRP proteins in oligodendrocytes, where WAVE1's role in oligodendrocyte morphogenesis is well established (*Kim et al., 2006; Michalski and Kothary, 2015*), indicates that CYFIP1 protein should also be expressed in oligodendrocytes. It would also be interesting to quantify *Cyfp1* expression in different stages of differentiation, since some findings indicate that FMRP is expressed in oligodendrocytes in a differentiation stage-specific manner (*Wang et al., 2004*).

General limitations associated with *in vitro* experiments also need to be taken into account when extrapolating these results to phenotypes *in vivo*. In the last chapter, brain tissue histology revealed myelin thinning in the corpus callosum of the *Cyfp1*^{+/-} rats and a reduction in the number of mature oligodendrocyte cells in this structure. Although the evidence of an abnormal MBP distribution in cultured oligodendrocytes could lead to myelin thinning, the fact that we see more MBP⁺ cells in the *Cyfp1*^{+/-} cultures contradicts the *in vivo* observation. Understandably, both experiments rely on distinct conditions, where an obvious difference is the presence of axons *in vivo*, and absence of axons *in*

vitro. As briefly mentioned in the General Introduction, axons can influence oligodendrocyte differentiation and myelin production, where several signalling pathways are involved. Moreover, *in vitro* experiments were done on cells extracted from neonatal pups, from P0 to P3, whereas *in vivo* experiments were done in adult animals. This brings up the question whether *Cyfp1* has a different influence on oligodendrocytes during development. Finally, the *in vivo* study reported in the last chapter was focused on the corpus callosum region and different phenotypes may be apparent on distinct brain regions.

7.5.3. Conclusions

Taken together, the studies reported here and in Chapters 5 and 6 are the first addressing a role of *Cyfp1* during myelination. In this chapter, cell culture methods indicated an abnormal pattern of MBP protein distribution in *Cyfp1*^{+/-} cultured oligodendrocytes, suggesting a deficit on MBP translocation to the distal ends of the cell processes. This might be the underlying cause for the *in vivo* myelin thinning observation in *Cyfp1*^{+/-} rats, reported in Chapter 6. Therefore, this study sheds some light on possible cellular mechanisms through which *CYFIP1* could influence oligodendrocyte function and myelination. Future studies are needed in order to understand how *Cyfp1* affects MBP distribution, and distinguish between effects on mRNA transport and/or translation. Given the possible role of CYFIP1-FMRP complex in mediating MBP mRNA translation, the increased proportion of cells expressing MBP in *Cyfp1*^{+/-} oligodendrocytes could be due to an inefficient inhibition of translation. In order to assess if immature oligodendrocytes are expressing MBP in *Cyfp1*^{+/-} cultures, quantification of MBP⁺ cells can be made in cultures of OPCs after 2 days of differentiation, where MBP synthesis is initiated under control conditions. Furthermore, in order to distinguish between MBP mRNA transport and/or MBP translation, the mRNA should be targeted instead of the protein, where an interaction between *Cyfp1* and MBP mRNA could also be studied. Future experiments will be further elaborated in the General Discussion chapter.

Myelin is essential for a fast conduction of electrical impulses through axons, and myelin thinning may slow down communications between axons and lead to neural dysfunction. The overall work developed in this thesis suggests a role of *Cyfp1* in

myelination in a rat model, which may underlie the clinical and behavioural phenotypes associated with 15q11.2 BP1-BP2 deletion.

Chapter 8

General Discussion

8.1. Thesis overview

Neurodevelopmental disorders are characterised by abnormal brain development, and result in a wide spectrum of neuropsychiatric symptoms. These disorders have been conceptualised as ‘synaptopathies’, insofar as several studies have linked these disorders to altered synaptic structure and function. However, with the development of specialised methods like DTI, allowing an *in vivo* characterisation of white matter and axonal projections, new lines of evidence have emerged showing extensive white matter abnormalities in these patients, both in short and long distance connections. This has led to the question whether these white matter phenotypes are a direct cause of genetic alterations, or a secondary result of the disease process. This motivated the investigation of the impact of neurodevelopmental CNVs on white matter microstructure in clinically well individuals, where several groups have found a link between these variants and altered white matter. The work developed in this thesis investigated the impact of variations in the 15q11.2 BP1-BP2 chromosomal region on white matter microstructure. Given the importance of identifying mechanistic biomarkers, targeting the role of individual genes and how they may lead to increased risk is a significant step to improve our knowledge on these disorders. To this end, I looked at the impact of low dosage of *Cyfp1* (a gene in this region) on white matter microstructure, using a novel *Cyfp1* haploinsufficiency rat model. The following section will comprise a summary of the results presented throughout the thesis.

8.2. Summary of results

This thesis started with an investigation of white matter microstructural abnormalities in human carriers of the 15q11.2 BP1-BP2 CNV. This work is described in Chapter 3 and Chapter 4. The study described in Chapter 3 was based on a collaboration with deCODE genetics Institute in Iceland (<https://www.decode.com/>). Prior to this study, and as part of the ongoing gene discovery work in deCODE genetics, DTI data from 30 individuals with the 15q11.2 BP1-BP2 deletion, 27 individuals the reciprocal duplication, and 19 individuals with no large CNVs were collected. Using whole-brain and regional analysis, extensive global mirror effects were found in FA where deletion carriers showed widespread increases in FA, whereas duplication carriers showed decreases in FA, compared to NoCNV controls. Further preliminary and exploratory analyses suggested a possible CNV dosage-effect on age trajectories of white matter integrity, and different magnitude of effects in males and females. Overall, this was the first study, to date, showing an effect of 15q11.2 BP1-BP2 CNV on white matter microstructure.

With the aim of replicating the above findings, the study on Chapter 4 comprised an analysis on DTI-derived measures from British and Irish descendent participants from a subsample of the UK Biobank database (www.ukbiobank.ac.uk). This study was not only important to be able to establish a link between 15q11.2 BP1-BP2 and altered white matter microstructure, but also to look at these effects on a more heterogeneous sample. In this study, 54 deletion and 55 duplication carriers were compared to thousands of controls (n=15663) with no large CNVs. Again, a reciprocal effect was found with increased FA in deletion, and decreased FA in duplication, where the largest effects were found in the same white matter tracts to those described in Chapter 3. Age trajectories also showed similar white matter progressions in both samples, suggesting a possible effect of age. In the UK Biobank sample, no differences were found between males and females. Altogether, results from both studies not only establish a link between 15q11.2 BP1-BP2 CNV and altered white matter microstructure, but also show a dosage-dependent effect with a ‘mirrored phenotype’ between the deletion and duplication.

The above studies highlight the importance of investigating mechanisms through which variations in genes within the 15q11.2 BP1-BP2 interval could influence white matter microstructure. Here, the molecular link between CYFIP1 and FMRP was of high relevance, since absence of this protein is known to cause FXS, a syndrome where similar

white matter abnormalities have been reported (*Green et al., 2015; Hall et al., 2016*). This motivated the creation of a novel *Cyfp1* haploinsufficiency rat model, with the aim of modelling the low dosage of *CYFIP1* in 15q11.2 BP1-BP2 deletion carriers. In Chapters 5 to 7, a combination of DTI, histology and cell culture methods, allowed the investigation of white matter abnormalities associated with *Cyfp1* haploinsufficiency in this rat model.

In Chapter 5, DTI methods were used to look at white matter abnormalities in *Cyfp1*^{+/-} rats in the whole-brain, identifying regions with higher sensitivity to *Cyfp1* haploinsufficiency. Here, a whole-brain analysis using TBSS followed by FWE correction for multiple comparisons showed significant decreases in FA, where regional quantification showed a higher sensitivity of the corpus callosum to *Cyfp1* haploinsufficiency. Using FDR correction, a less conservative correction method for multiple comparisons, additional white matter changes were unravelled, where increases in FA in fimbria and stria terminalis were found in *Cyfp1*^{+/-} rats, suggesting a possible differential effect of *Cyfp1* haploinsufficiency in distinct brain regions. Although DTI is sensitive to white matter microstructural abnormalities in the brain this technique does not provide enough cellular resolution in order to understand the underlying cellular nature of these changes. Several factors may affect the DTI signal, such as axonal properties, like the diameter and number of axons, and myelin thickness.

In Chapter 6, ultrastructural TEM methods were first used to investigate changes on axonal density, diameter and myelin thickness, in a new cohort of rats. This analysis was focused on the corpus callosum, indicating a thinning of the myelin sheath in this structure, which was independent of any changes in axonal density or diameter. This finding was potentially highly relevant since recent evidence, combining histological and gene expression studies, have suggested deficits in myelination as a principal contributor to the atypical network connectivity seen in neurodevelopmental disorders. In the central nervous system, myelin is produced by mature oligodendrocytes, and immunofluorescence analysis indicated a decrease in the population of these cells in *Cyfp1*^{+/-} rats. This suggests an effect of *Cyfp1* haploinsufficiency on oligodendrocyte-myelin dynamics.

Using primary OPC cultures, isolated from neonatal rats (postnatal day 0-3), the study in Chapter 7 described a possible cellular mechanism through which *Cyfp1* could influence myelination. Here, although no evidence was shown for a genotypic effect on

oligodendrocyte cytoskeleton morphology, *Cyfp1*^{+/-} oligodendrocytes exhibited an abnormal intracellular distribution of MBP, a key myelin protein. *Cyfp1*^{+/-} oligodendrocytes showed a relatively constrained distribution of MBP protein in the cell body, compared to the widespread distribution encompassing the cell processes in WT cells. These data indicate a failure in MBP translocation to the oligodendrocyte cell processes in *Cyfp1*^{+/-} cultures. The transport of MBP mRNA to the distal ends of the cell processes, and consequent translation at the axon-oligodendrocyte contact site, is crucial for a variety of mechanisms leading to myelin formation, and can therefore underlie the *in vivo* myelin thinning observation in *Cyfp1*^{+/-} rats.

8.3. Link between human and rat model findings

Evidence from the DTI studies in Chapters 3 and 4 show that variations at 15q11.2 BP1-BP2 lead to white matter abnormalities. In the beginning of this thesis, it was hypothesised that *CYFIP1* could be a potential contributor to these white matter abnormalities, given its known involvement in mechanisms that potentially affect axon development and myelination. In Chapter 5, using DTI methods and a *Cyfp1*^{+/-} rat line, it was indeed shown that *Cyfp1* haploinsufficiency was associated with white matter changes, as predicted. However, as noted previously, although the rat and human phenotypes converged on white matter changes, they differed in the direction of effects, with predominant increased FA in human deletion carriers and decreased FA in *Cyfp1*^{+/-} rats. Understandably, a direct comparison between the human and the rat data is not possible, where apparent species differences could underlie these opposite effects.

In Chapter 5, it is also noted that the 15q11.2 BP1-BP2 involves three other genes in addition to *CYFIP1* that may also have an impact on white matter microstructure. Therefore, one possible way to address specie differences would be to create a new a rat model, encompassing a full deletion of the four genes in this region: *NIPAI1*, *NIPAI2*, *TUBGCP5* and *CYFIP1*. Here, assuming this were technically feasible and the resulting animals viable, if similar changes were seen between the rats and humans, one could hypothesise with greater confidence that other genes in this region could also contribute to the 15q11.2 BP1-BP2 deletion phenotype, though it would remain difficult to predict phenotypic consequences arising from possible interactions between the four genes, including the case of effects on white matter. The creation of animal models with

mutations in each individual gene in this region could help further answer this question. A gene candidate for white matter abnormalities is the *NIPAI*, known to mediate BMP signalling that is involved in axonal growth and guidance. It has been proposed that deletions in *NIPAI* could result in axonal overgrowth, leading to increased axonal density, which could underlie the increased FA seen in human carriers. The DTI studies on human carriers also showed a reciprocal effect of the 15q11.2 BP1-BP2 CNV on white matter microstructure, where bidirectional dosage led to opposite changes in FA. Therefore, given that a dosage-dependent effect of *Cyfp1* on spine morphology was previously found, it would be interesting to also investigate the effects of *Cyfp1* overexpression on white matter microstructure.

Data from Chapter 6 revealed additional detail to cellular changes possibly underlying the imaging phenotype, revealing a specific impact of *Cyfp1* haploinsufficiency on myelin thickness. Here, *Cyfp1*^{+/-} rats showed myelin thinning in the corpus callosum, which is consistent with the decreased FA reported in Chapter 5. An obvious question is whether myelin deficits could also be present in human 15q11.2 BP1-BP2 deletion carriers. It is known that myelin modulates the degree of anisotropy of water molecules inside the white matter tracts, and therefore affects the DTI signal, where less myelin is associated with reduced FA. However, the influence of myelin is relatively modest when compared to changes in the axon itself, that lead to stronger effects on DTI signal. Therefore, it is hypothesised in Chapter 6 that these myelin changes can also be present in humans, but could be masked by other alterations on white matter structure that lead to the observed increased FA. As mentioned in Chapter 6, one way to investigate this matter would be to distinguish between myelin and axonal changes. Some MRI methods are proven to be more specific to myelin changes than DTI, such as magnetization transfer ratio, myelin water imaging and susceptibility mapping (*Heath et al., 2018*). Furthermore, the development of ultrastructural MRI methods, such as Connectome scanners, could theoretically provide enough resolution to disentangle changes in myelin from other axonal properties (*Shi and Toga, 2017*). Cardiff University Brain Research Imaging Centre (CUBRIC) houses a Siemens 3 Tesla Connectome system, the first facility with a connectome scanner outside of the United States. Future projects could involve the use of this scanner in a cohort of 15q11.2 BP1-BP2 CNV carriers. However, there is still a great need to validate these imaging methods (*Shi and Toga, 2017*). Nevertheless, the human findings suggest that deviations from normal gene dosage in each direction can culminate in abnormalities in brain development. This

illustrates the importance of studying how chromosomal imbalances can have different impacts on neural processes, which might have important implications for designing targeted therapeutic interventions in the future.

8.4. *Cyfp1* haploinsufficiency and oligodendrocyte function – a proposed mechanism

The work described in Chapter 7 indicates an impact of *Cyfp1* haploinsufficiency on MBP protein distribution in *Cyfp1*^{+/-} oligodendrocytes, where MBP protein is constrained to the cell body not reaching the end processes of the cells. An abnormal transport of MBP mRNA, and/or a deficit in translation inhibition of the protein could result in the observed phenotype. In Chapter 7, I propose two different mechanisms through which *Cyfp1* haploinsufficiency could impact these two processes. Knowing that oligodendrocyte-myelin dynamics rely on constant actin remodelling leads to the question as to whether alterations in actin content could influence MBP transport. Here, it is known that CYFIP1 acts as a negative regulator of actin polymerisation (production of f-actin), and reduced dosage of *Cyfp1* leads to increased levels of f-actin in dendritic spines in mice. Therefore, I suggested that *Cyfp1* haploinsufficiency in rats could lead to an abnormal accumulation of f-actin in the processes of *Cyfp1*^{+/-} oligodendrocytes, creating a physical barrier to MBP transport to the myelin membrane. MBP transport occurs via microtubules, and changes in these structures have been shown to highly impact MBP distribution in oligodendrocytes (*Song et al., 2003; Lyons et al., 2009*). Given that f-actin dynamics are coordinated with microtubule formation and maturation (*Wu and Bezanilla, 2018*), it is also possible that increased levels of f-actin could have an impact on microtubule organisation. **Figure 8.1A** illustrates this proposed mechanism, where *Cyfp1* haploinsufficiency leads to an accumulation of actin filaments that affects microtubule organisation, hindering the transport of the MBP mRNA stress granules to the distal end of the oligodendrocytes' processes.

One way to test this hypothesis would be by using *in situ* hybridization methods to track the location and movement of MBP mRNA. A study by *Laursen et al., 2011* was able to target MBP mRNA in oligodendrocytes, employing an MBP-specific digoxigenin labelled probe. Single-molecule fluorescent *in situ* hybridization (smFISH) method could also be used, allowing the detection of single RNA molecules at the single-cell level and

single-molecule resolution (*Haimovich et al., 2017*). Furthermore, RNAscope® Technology is a novel in situ hybridization assay for detection of single molecules of targeted RNA in cells. This technique provides a higher specificity, compared to smFISH, by amplifying target-specific signals but not background noise from non-specific hybridization (<https://acdbio.com/science/how-it-works>).

As explained previously, MBP is only expressed in mature oligodendrocytes, and inhibition of its translation during oligodendrocyte differentiation is crucial for cell development. Some studies have suggested a role of FMRP as a repressor of MBP mRNA translation. Hence, considering that FMRP acts as a repressor of translation of some mRNAs in combination with CYFIP1, it is possible that decreased levels of CYFIP1 could lead to an early translation of MBP in immature oligodendrocytes, as proposed in **Figure 8.1B**. To test this hypothesis, OPCs cultures could be analysed after 2 days of differentiation, where MBP synthesis is just initiated under control conditions. Furthermore, an RNA immunoprecipitation assay can be used to analyse proteins that interact and modify the function of mRNAs. This assay could be used to investigate the interaction between MBP mRNA and Cyfip1 protein. Additionally, in order to test different *Cyfip1* dosage effects on MBP distribution, overexpression and conditional full-knockout of *Cyfip1* in oligodendrocytes can be studied. An investigation of *CYFIP1* influence on MBP distribution in human 15q11.2 BP1-BP2 carriers could potentially be done by using human blood cells from these carriers, to be reprogrammed into human neural stem cells (hNSCs) (*Thier et al., 2019*) in order to generate oligodendrocytes *in vitro* (*Rodrigues et al., 2017*).

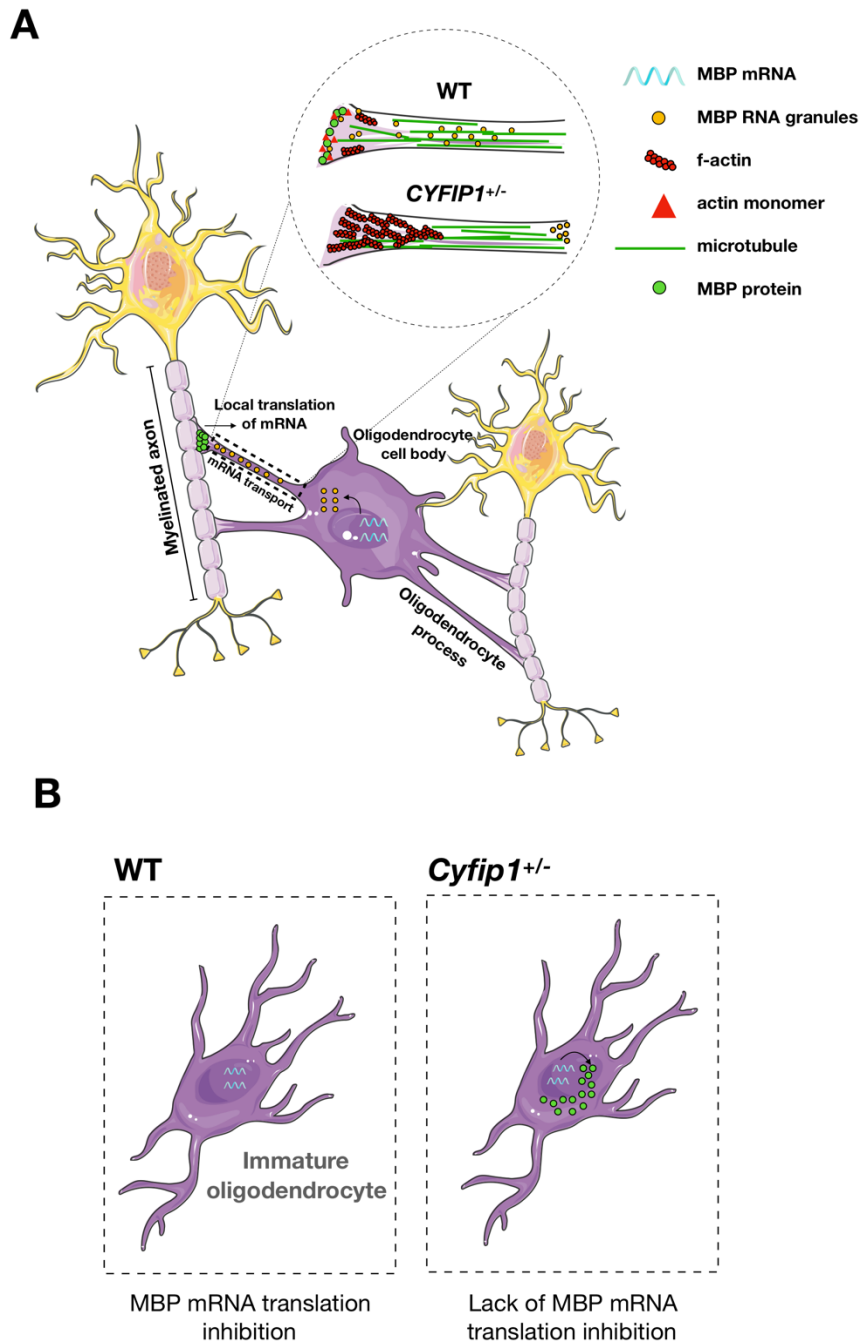


Figure 8.1 - Proposed mechanisms through which *Cyfip1* haploinsufficiency could impact MBP mRNA transport and/or MBP translation inhibition in oligodendrocyte cells.

A Schematic representation of axon ensheathment by an oligodendrocyte, where MBP mRNA is transported in stress granules from the cell body towards the axon-oligodendrocyte contact site. Here, it is proposed that *Cyfip1* haploinsufficiency hinders this process by leading to increased production of f-actin. Increased f-actin would result in accumulation of actin filaments in the oligodendrocyte processes and disorganisation of microtubules, which could present a physical barrier to the transport of MBP mRNA. **B** Schematic representation of an immature oligodendrocyte under normal conditions (WT), where MBP mRNA translation is inhibited; and under abnormal conditions (as hypothesised for *Cyfip1*^{+/-} oligodendrocytes), where MBP mRNA translation occurs before maturation.

8.5. Functional outcomes of impaired myelination in *Cyfp1*^{+/-} rats

TEM analysis, in Chapter 6, revealed a thinning of the myelin sheath in the corpus callosum of *Cyfp1*^{+/-} rats. This myelin thinning seems to be preserved across species, where an independent group (*Domínguez-Iturza et al., 2019*) found myelin thinning in *Cyfp1*^{+/-} mice, also in the corpus callosum. *Domínguez-Iturza et al., 2019* also found impaired bilateral functional connectivity and motor coordination in *Cyfp1*^{+/-} mice. Motor learning has also been shown to be impaired in *Cyfp1*^{+/-} mice in *Bachmann et al., 2019*. The corpus callosum connects and mediates information between the two brain hemispheres, and some white matter tracts connecting motor areas travel through the body of the corpus callosum. Therefore, myelin thinning in this region can be the underlying reason of abnormal bilateral connectivity and motor problems.

Results in Chapter 7 suggest that this myelin thinning might be a result of oligodendrocyte dysfunction, where apparent deficits in MBP protein distribution were observed in *Cyfp1*^{+/-} oligodendrocytes *in vitro*. As stated in Chapter 6, an earlier study on *Shiverer* mice showed that reduced levels of MBP are associated with specific effects on behavioural flexibility using a reversal learning task, with no deficits on initial learning (*Inagawa et al., 1988*). In our laboratory, parallel experiments (not reported in this thesis) looking at the effect *Cyfp1* haploinsufficiency on behavioural flexibility were performed, and published together with the findings from Chapter 5, 6 and 7 (*Silva et al., 2019a*). Here, two different tasks were used: reversal learning and associative mismatch task. In the reversal learning task, the *Cyfp1*^{+/-} rats showed greater early preservation in choosing the previously rewarded stimulus, where effects were highly specific to the reversal element of the task, with no related effects on initial learning. This pattern of normal initial learning but impaired behavioural flexibility was also apparent in the associative mismatch task.

Inability to alter behaviour in response to environment changes has been highly associated with orbitofrontal cortex and ventral prefrontal cortex in humans and rats (*Schoenbaum et al., 2002; Chudasama and Robbins, 2003; Hornak et al., 2004*). Although the TEM analysis in Chapter 6 was restricted to the corpus callosum, the DTI whole-brain analysis in Chapter 5 suggests that other white matter tracts might also be affected in *Cyfp1*^{+/-} rats. *In vitro* findings, in Chapter 7, also suggest a general effect of *Cyfp1* on myelination. Hence, myelin thinning in white matter structures relevant to

behaviour flexibility could lead to this abnormal behaviour. Although the role of the corpus callosum in behaviour flexibility is not established, this structure was previously shown to correlate with behaviour flexibility (*Bearden et al., 2011*), as explained in Chapter 6. The corpus callosum (along with the internal capsule) is also known to carry white matter bundles containing axons projecting from the frontal cortex and striatal regions, and development of the corpus callosum coincides with the maturation of the frontal cortex, mutually influencing each other's development (*Putnam et al., 2008; Ozalay et al., 2013*). Therefore, changes in the corpus callosum structure could influence structures relevant for behavioural flexibility. The behavioural assays performed in the *Cyfp1^{+/-}* rats were done in a separate cohort of animals, not allowing correlation analyses between behaviour and white matter properties. Future experiments combining *in vivo* DTI, behaviour assays, and histology in the same cohort of animals could reveal white matter structures associated with behavioural changes in the *Cyfp1^{+/-}* rats, where the role of the corpus callosum on behaviour flexibility could be investigated.

An increasing body of evidence suggests that myelin also plays a role in circuit plasticity, where alterations in oligodendrocyte-myelin dynamics can occur during cognitive processing and learning. Several studies, in rodents and humans, have shown an association between learning a new task and white matter alterations in relevant brain regions (*McKenzie et al., 2014; Hofstetter and Assaf, 2017; Metzler-Baddeley et al., 2017*). *McKenzie et al., 2014* showed that the production of newly formed oligodendrocytes is accelerated in mice learning a new motor skill, where mice had to learn how to run on a complex modified wheel, with irregularly spaced rungs. The authors further showed that myelination was essential for learning this new skill by blocking the oligodendrocyte production before and after learning this task. Here, mice only had difficulties performing this task when oligodendrocyte manipulation was done prior to learning. This suggests that myelination was crucial for learning a new complex task, but not required to recall a pre-learned skill. This effect is not specific to motor learning, where other studies have found white matter plasticity associated with other behavioural assays. *Hofstetter and Assaf, 2017* looked at the influence of short learning tasks on white matter plasticity in both humans and rats, where humans performed a 2 hours spatial learning task, and rats underwent training for 1 day in a Morris water maze task. DTI data were acquired in both cohorts, before and after learning. In both species, changes in water diffusion were found in the fornix and were correlated with improvement in behavioural measures, showing a correlation between white matter and learning. *Metzler-Baddeley et*

al., 2017 used MRI methods with higher specificity to myelin changes to investigate myelin plasticity in adaptive working-memory training in humans. After 2 months of training, participants who underwent adaptive working memory training reported increases in myelin-associated metrics in relevant brain regions, compared to participants who practiced a non-challenging task. Interestingly, the group who performed a repetitive non-challenging task showed opposite changes, revealing negative outcomes in myelin-associated metrics. This pattern of opposing results indicate that myelin remodelling might only occur during ‘higher-level’ cognitive functions.

Considering the hypothesis that *Cyfp1* haploinsufficiency leads to impaired myelination, one can postulate that *Cyfp1*^{+/-} rats have less myelin plasticity as a response to learning new complex tasks. Flexible thinking is considered a component of ‘higher-level’ cognition, involving the ability to adapt to new environmental cues. It is therefore possible that myelin remodelling is necessary to establish a new behaviour that contradicts the previously learned one. In order to test if reduced myelin plasticity in *Cyfp1*^{+/-} rats contributes to their behavioural inflexibility, we have designed a new experiment in our laboratory to look at changes in white matter properties after biconditional training. *In vivo* imaging data were acquired from *Cyfp1*^{+/-} and WT rats before and after training, where magnetisation transfer ratio (MTR) maps, as a proxy of myelin content, together with DTI and structural MRI data were collected. After the second scan, the brains were extracted to perform histological analysis (using TEM and immunofluorescence methods) in order to look at cellular alterations after training (see **Figure 8.2** for experiment design). For histology, a behavioural-naïve control cohort was used, to explore cellular differences due to training. This will be the first study investigating a role of myelin plasticity during flexible thinking, and will further allow the identification of white matter connections important for this task; where the role of the corpus callosum in behavioural flexibility will also be studied.

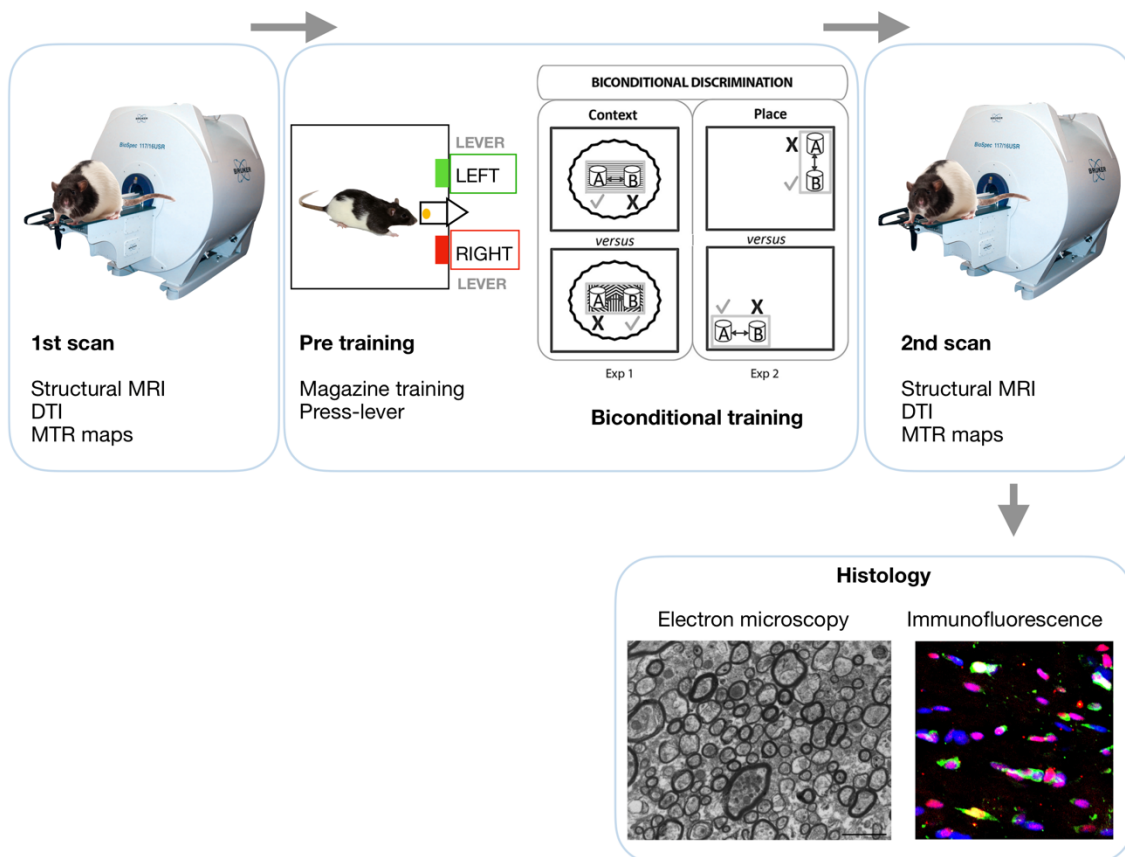


Figure 8.2 - Experiment design to test alterations in white matter microstructure after biconditional discrimination learning.

In this ongoing experiment, the mediation effect through which *Cyfp1* haploinsufficiency affects biconditional learning due to alterations in myelin plasticity will be investigated. In order to focus on myelin content, magnetisation transfer ratio (MTR) maps were acquired, a technique that is more specific to myelin changes than DTI. Structural MRI, DTI, and MTR maps were collected before and after learning. At the end of the second scan, the brain tissue was taken for histology procedures, where electron microscopy and immunofluorescence techniques will be used to investigate cellular changes after training. Schematic representation of biconditional discrimination paradigm was taken from *Dumont et al., 2015*.

8.6. Conclusions and future directions

The work developed in this thesis has made novel contributions to understanding how genetic variations at 15q11.2 BP1-BP2 chromosomal region may contribute to white matter microstructural abnormalities that can result in network dysfunction. Conclusions of this thesis can be summarised as follows:

- Chromosomal imbalances in the 15q11.2 BP1-BP2 chromosomal region leads to abnormal white matter microstructural, where bidirectional dosage results in opposite changes in DTI metrics.
- *Cyfp1* haploinsufficiency also leads to white matter abnormalities in *Cyfp1*^{+/-} rats. However, the direction of changes are opposite to those found in 15q11.2 BP1-BP2 deletion carriers.
- In *Cyfp1*^{+/-} rats, *Cyfp1* haploinsufficiency is associated with myelin thinning in the corpus callosum, and with a reduction of mature oligodendrocytes.
- Cultured oligodendrocytes from neonatal pups (P0 to P3) suggest an abnormal distribution of MBP protein in *Cyfp1*^{+/-} oligodendrocytes, an important protein for myelination.

Altogether, these results suggest that *Cyfp1* influences myelination in the central nervous system, which may underlie the 15q11.2 BP1-BP2 cognitive phenotypes. Here, it was clear that a link between the rat and human data is still uncertain, and more experiments using different types of imaging acquisition in the humans may help answering this question. *In vitro* assays, using cells from this novel *Cyfp1*^{+/-} rat line, will provide further information about *Cyfp1*'s role on oligodendrocyte function, and therefore understanding the mechanisms through which *Cyfp1* influences myelination. Finally, ongoing work in our laboratory is trying to establish a link between altered myelin plasticity in *Cyfp1*^{+/-} rats and maladaptive brain function in the context of adaptive myelination, whereby changes in learning impacts acutely on myelination. These proposed experiments will be important to establish biomarkers for the altered neurodevelopmental processes leading to the increased psychiatric risk and behavioural problems associated with the 15q11.2 BP1-BP2 CNV.

References

- Abe, O., Takao, H., Gono, W., Sasaki, H., Murakami, M., Kabasawa, H., Kawaguchi, H., Goto, M., Yamada, H., Yamasue, H., Kasai, K., Aoki, S., Ohtomo, K., 2010. Voxel-based analysis of the diffusion tensor. *Neuroradiology* 52, 699–710. <https://doi.org/10.1007/s00234-010-0716-3>
- Abekhouk, S., Bardoni, B., 2014. CYFIP family proteins between autism and intellectual disability: links with Fragile X syndrome. *Front. Cell. Neurosci.* 8. <https://doi.org/10.3389/fncel.2014.00081>
- Abekhouk, S., Sahin, H.B., Grossi, M., Zongaro, S., Maurin, T., Madrigal, I., Kazue-Sugioka, D., Raas-Rothschild, A., Doulazmi, M., Carrera, P., Stachon, A., Scherer, S., Drula Do Nascimento, M.R., Trembleau, A., Arroyo, I., Szatmari, P., Smith, I.M., Milà, M., Smith, A.C., Giangrande, A., Caillé, I., Bardoni, B., 2017. New insights into the regulatory function of CYFIP1 in the context of WAVE- and FMRP-containing complexes. *Dis. Model. Mech.* 10, 463–474. <https://doi.org/10.1242/dmm.025809>
- Abel, K.M., Drake, R., Goldstein, J.M., 2010. Sex differences in schizophrenia. *Int. Rev. Psychiatry* 22, 417–428. <https://doi.org/10.3109/09540261.2010.515205>
- Abrahams, B.S., Geschwind, D.H., 2008. Advances in autism genetics: on the threshold of a new neurobiology. *Nat. Rev. Genet.* 9, 341–355. <https://doi.org/10.1038/nrg2346>
- Aggarwal, S., Yurlova, L., Snaidero, N., Reetz, C., Frey, S., Zimmermann, J., Pähler, G., Janshoff, A., Friedrichs, J., Müller, D.J., Goebel, C., Simons, M., 2011. A size barrier limits protein diffusion at the cell surface to generate lipid-rich myelin-membrane sheets. *Dev. Cell* 21, 445–456. <https://doi.org/10.1016/j.devcel.2011.08.001>
- Ainger, K., Avossa, D., Morgan, F., Hill, S.J., Barry, C., Barbarese, E., Carson, J.H., 1993. Transport and localization of exogenous myelin basic protein mRNA microinjected into oligodendrocytes. *J. Cell Biol.* 123, 431–441. <https://doi.org/10.1083/jcb.123.2.431>
- Alba-Ferrara, L.M., de Erausquin, G.A., 2013. What does anisotropy measure? Insights from increased and decreased anisotropy in selective fiber tracts in schizophrenia. *Front. Integr. Neurosci.* 7. <https://doi.org/10.3389/fnint.2013.00009>
- Alexander, A.L., Lee, J.E., Lazar, M., Boudos, R., DuBray, M.B., Oakes, T.R., Miller, J.N., Lu, J., Jeong, E.-K., McMahan, W.M., Bigler, E.D., Lainhart, J.E., 2007. Diffusion tensor imaging of the corpus callosum in Autism. *NeuroImage* 34, 61–73. <https://doi.org/10.1016/j.neuroimage.2006.08.032>
- Alfaro-Almagro, F., Jenkinson, M., Bangerter, N.K., Andersson, J.L.R., Griffanti, L., Douaud, G., Sotiropoulos, S.N., Jbabdi, S., Hernandez-Fernandez, M., Vallee, E., Vidaurre, D., Webster, M., McCarthy, P., Rorden, C., Daducci, A., Alexander, D.C., Zhang, H., Dragonu, I., Matthews, P.M., Miller, K.L., Smith, S.M., 2018.

Image processing and Quality Control for the first 10,000 brain imaging datasets from UK Biobank. *NeuroImage* 166, 400–424. <https://doi.org/10.1016/j.neuroimage.2017.10.034>

Alkan, C., Coe, B.P., Eichler, E.E., 2011. Genome structural variation discovery and genotyping. *Nat. Rev. Genet.* 12, 363–376. <https://doi.org/10.1038/nrg2958>

Almeida, R.G., Czopka, T., Ffrench-Constant, C., Lyons, D.A., 2011. Individual axons regulate the myelinating potential of single oligodendrocytes in vivo. *Dev. Camb. Engl.* 138, 4443–4450. <https://doi.org/10.1242/dev.071001>

Amorim, I.S., Lach, G., Gkogkas, C.G., 2018. The Role of the Eukaryotic Translation Initiation Factor 4E (eIF4E) in Neuropsychiatric Disorders. *Front. Genet.* 9. <https://doi.org/10.3389/fgene.2018.00561>

Anagnostou, E., Taylor, M.J., 2011. Review of neuroimaging in autism spectrum disorders: what have we learned and where we go from here. *Mol. Autism* 2, 4. <https://doi.org/10.1186/2040-2392-2-4>

Aoki, Y., Abe, O., Nippashi, Y., Yamasue, H., 2013. Comparison of white matter integrity between autism spectrum disorder subjects and typically developing individuals: a meta-analysis of diffusion tensor imaging tractography studies. *Mol. Autism* 4, 25. <https://doi.org/10.1186/2040-2392-4-25>

Ashburner, J., Friston, K.J., 2000. Voxel-Based Morphometry—The Methods. *NeuroImage* 11, 805–821. <https://doi.org/10.1006/nimg.2000.0582>

Asou, H., Hamada, K., Sakota, T., 1995. Visualization of a single myelination process of an oligodendrocyte in culture by video microscopy. *Cell Struct. Funct.* 20, 59–70.

Association, A.P., 2013. Diagnostic and Statistical Manual of Mental Disorders (DSM-5®). American Psychiatric Pub.

Aston, C., Jiang, L., Sokolov, B.P., 2004. Microarray analysis of postmortem temporal cortex from patients with schizophrenia. *J. Neurosci. Res.* 77, 858–866. <https://doi.org/10.1002/jnr.20208>

Aung, W.Y., Mar, S., Benzinger, T.L., 2013. Diffusion tensor MRI as a biomarker in axonal and myelin damage. *Imaging Med.* 5, 427–440. <https://doi.org/10.2217/iim.13.49>

Austin, M.A., Harding, S., McElroy, C., 2003. Genebanks: A Comparison of Eight Proposed International Genetic Databases. *Public Health Genomics* 6, 37–45. <https://doi.org/10.1159/000069544>

Baaré, W.F.C., Hulshoff Pol, H.E., Boomsma, D.I., Posthuma, D., de Geus, E.J.C., Schnack, H.G., van Haren, N.E.M., van Oel, C.J., Kahn, R.S., 2001. Quantitative Genetic Modeling of Variation in Human Brain Morphology. *Cereb. Cortex* 11, 816–824. <https://doi.org/10.1093/cercor/11.9.816>

Bachmann, S.O., Sledziowska, M., Cross, E., Kalbassi, S., Waldron, S., Chen, F., Ranson, A., Baudouin, S.J., 2019. Behavioral training rescues motor deficits in *Cyfp1*

- haploinsufficiency mouse model of autism spectrum disorders. *Transl. Psychiatry* 9, 29. <https://doi.org/10.1038/s41398-018-0338-9>
- Bacon, C., Lakics, V., Machesky, L., Rumsby, M., 2007. N-WASP regulates extension of filopodia and processes by oligodendrocyte progenitors, oligodendrocytes, and Schwann cells-implications for axon ensheathment at myelination. *Glia* 55, 844–858. <https://doi.org/10.1002/glia.20505>
- Baiano, M., David, A., Versace, A., Churchill, R., Balestrieri, M., Brambilla, P., 2007. Anterior cingulate volumes in schizophrenia: A systematic review and a meta-analysis of MRI studies. *Schizophr. Res.* 93, 1–12. <https://doi.org/10.1016/j.schres.2007.02.012>
- Baker, M., 2016. 1,500 scientists lift the lid on reproducibility. *Nat. News* 533, 452. <https://doi.org/10.1038/533452a>
- Banerjee, A., Ifrim, M.F., Valdez, A.N., Raj, N., Bassell, G.J., 2018. Aberrant RNA translation in fragile X syndrome: From FMRP mechanisms to emerging therapeutic strategies. *Brain Res., RNA Metabolism in Neurological Disease 2018* 1693, 24–36. <https://doi.org/10.1016/j.brainres.2018.04.008>
- Bar, E., Barak, B., 2019. Microglia roles in synaptic plasticity and myelination in homeostatic conditions and neurodevelopmental disorders. *Glia* 0. <https://doi.org/10.1002/glia.23637>
- Bardoni, B., Abekhoukh, S., 2014. CYFIP family proteins between autism and intellectual disability: links with Fragile X syndrome. *Front. Cell. Neurosci.* 8. <https://doi.org/10.3389/fncel.2014.00081>
- Barnea-Goraly, N., Eliez, S., Hedeus, M., Menon, V., White, C.D., Moseley, M., Reiss, A.L., 2003. White matter tract alterations in fragile X syndrome: preliminary evidence from diffusion tensor imaging. *Am. J. Med. Genet. B Neuropsychiatr. Genet.* 118, 81–88.
- Baron, W., Hoekstra, D., 2010. On the biogenesis of myelin membranes: Sorting, trafficking and cell polarity. *FEBS Lett., Frontiers in Membrane Biochemistry* 584, 1760–1770. <https://doi.org/10.1016/j.febslet.2009.10.085>
- Baron, W., Ozgen, H., Klunder, B., de Jonge, J.C., Nomden, A., Plat, A., Trifilieff, E., de Vries, H., Hoekstra, D., 2015. The Major Myelin-Resident Protein PLP Is Transported to Myelin Membranes via a Transcytotic Mechanism: Involvement of Sulfatide. *Mol. Cell. Biol.* 35, 288–302. <https://doi.org/10.1128/MCB.00848-14>
- Barres, B.A., Raff, M.C., 1999. Axonal Control of Oligodendrocyte Development. *J. Cell Biol.* 147, 1123–1128.
- Basser, P.J., Mattiello, J., LeBihan, D., 1994a. MR diffusion tensor spectroscopy and imaging. *Biophys. J.* 66, 259–267. [https://doi.org/10.1016/S0006-3495\(94\)80775-1](https://doi.org/10.1016/S0006-3495(94)80775-1)

- Basser, P. J., Mattiello, J., Lebihan, D., 1994b. Estimation of the Effective Self-Diffusion Tensor from the NMR Spin Echo. *J. Magn. Reson. B* 103, 247–254. <https://doi.org/10.1006/jmrb.1994.1037>
- Basser, P.J., Pajevic, S., Pierpaoli, C., Duda, J., Aldroubi, A., 2000. In vivo fiber tractography using DT-MRI data. *Magn. Reson. Med.* 44, 625–632. [https://doi.org/10.1002/1522-2594\(200010\)44:4<625::AID-MRM17>3.0.CO;2-O](https://doi.org/10.1002/1522-2594(200010)44:4<625::AID-MRM17>3.0.CO;2-O)
- Bassett, A.S., Chow, E.W.C., AbdelMalik, P., Gheorghiu, M., Husted, J., Weksberg, R., 2003. The Schizophrenia Phenotype in 22q11 Deletion Syndrome. *Am. J. Psychiatry* 160, 1580–1586. <https://doi.org/10.1176/appi.ajp.160.9.1580>
- Basu, S., Lamprecht, R., 2018. The Role of Actin Cytoskeleton in Dendritic Spines in the Maintenance of Long-Term Memory. *Front. Mol. Neurosci.* 11. <https://doi.org/10.3389/fnmol.2018.00143>
- Bauer, N.G., Richter-Landsberg, C., Ffrench-Constant, C., 2009. Role of the oligodendroglial cytoskeleton in differentiation and myelination. *Glia* 57, 1691–1705. <https://doi.org/10.1002/glia.20885>
- Baumann, P.S., Griffa, A., Fournier, M., Golay, P., Ferrari, C., Alameda, L., Cuenod, M., Thiran, J.-P., Hagmann, P., Do, K.Q., Conus, P., 2016. Impaired fornix–hippocampus integrity is linked to peripheral glutathione peroxidase in early psychosis. *Transl. Psychiatry* 6, e859. <https://doi.org/10.1038/tp.2016.117>
- Bearden, C.E., Erp, V., M, T.G., Dutton, R.A., Boyle, C., Madsen, S., Luders, E., Kieseppa, T., Tuulio-Henriksson, A., Huttunen, M., Partonen, T., Kaprio, J., Lönqvist, J., Thompson, P.M., Cannon, T.D., 2011. Mapping Corpus Callosum Morphology in Twin Pairs Discordant for Bipolar Disorder. *Cereb. Cortex* 21, 2415–2424. <https://doi.org/10.1093/cercor/bhr030>
- Bearden, C.E., van Erp, T.G.M., Dutton, R.A., Tran, H., Zimmermann, L., Sun, D., Geaga, J.A., Simon, T.J., Glahn, D.C., Cannon, T.D., Emanuel, B.S., Toga, A.W., Thompson, P.M., 2007. Mapping Cortical Thickness in Children with 22q11.2 Deletions. *Cereb. Cortex* 17, 1889–1898. <https://doi.org/10.1093/cercor/bhl097>
- Beaulieu, C., 2002. The basis of anisotropic water diffusion in the nervous system - a technical review. *NMR Biomed.* 15, 435–455. <https://doi.org/10.1002/nbm.782>
- Belmonte, M.K., Gomot, M., Baron-Cohen, S., 2010. Visual attention in autism families: ‘unaffected’ sibs share atypical frontal activation. *J. Child Psychol. Psychiatry* 51, 259–276. <https://doi.org/10.1111/j.1469-7610.2009.02153.x>
- Benjamini, Y., Hochberg, Y., 1995. Controlling the False Discovery Rate: A Practical and Powerful Approach to Multiple Testing. *J. R. Stat. Soc. Ser. B Methodol.* 57, 289–300.
- Bercury, K.K., Macklin, W.B., 2015. Dynamics and Mechanisms of CNS Myelination. *Dev. Cell* 32, 447–458. <https://doi.org/10.1016/j.devcel.2015.01.016>

- Bernstein, H.-G., Steiner, J., Guest, P.C., Dobrowolny, H., Bogerts, B., 2015. Glial cells as key players in schizophrenia pathology: recent insights and concepts of therapy. *Schizophr. Res., White Matter Pathology* 161, 4–18. <https://doi.org/10.1016/j.schres.2014.03.035>
- Biomarkers Definitions Working Group, 2001. Biomarkers and surrogate endpoints: Preferred definitions and conceptual framework. *Clin. Pharmacol. Ther.* 69, 89–95. <https://doi.org/10.1067/mcp.2001.113989>
- Bishop, D., Rutter, M., 2009. Neurodevelopmental Disorders: Conceptual Issues, in: *Rutter's Child and Adolescent Psychiatry*. John Wiley & Sons, Ltd, pp. 32–41. <https://doi.org/10.1002/9781444300895.ch3>
- Bittel, D.C., Kibiryeve, N., Butler, M.G., 2006. Expression of 4 Genes Between Chromosome 15 Breakpoints 1 and 2 and Behavioral Outcomes in Prader-Willi Syndrome. *Pediatrics* 118, e1276–e1283. <https://doi.org/10.1542/peds.2006-0424>
- Boggs, J.M., 2006. Myelin basic protein: a multifunctional protein. *Cell. Mol. Life Sci. CMLS* 63, 1945–1961. <https://doi.org/10.1007/s00018-006-6094-7>
- Bora, E., Fornito, A., Radua, J., Walterfang, M., Seal, M., Wood, S.J., Yücel, M., Velakoulis, D., Pantelis, C., 2011. Neuroanatomical abnormalities in schizophrenia: A multimodal voxelwise meta-analysis and meta-regression analysis. *Schizophr. Res.* 127, 46–57. <https://doi.org/10.1016/j.schres.2010.12.020>
- Boyd, A., Zhang, H., Williams, A., 2013. Insufficient OPC migration into demyelinated lesions is a cause of poor remyelination in MS and mouse models. *Acta Neuropathol. (Berl.)* 125, 841–859. <https://doi.org/10.1007/s00401-013-1112-y>
- Bozdagi, O., Sakurai, T., Dorr, N., Pilorge, M., Takahashi, N., Buxbaum, J.D., 2012. Haploinsufficiency of *Cyfip1* Produces Fragile X-Like Phenotypes in Mice. *PLoS ONE* 7, e42422. <https://doi.org/10.1371/journal.pone.0042422>
- Braat, S., D'Hulst, C., Heulens, I., De Rubeis, S., Mientjes, E., Nelson, D.L., Willemsen, R., Bagni, C., Van Dam, D., De Deyn, P.P., Kooy, R.F., 2015. The GABAA receptor is an FMRP target with therapeutic potential in fragile X syndrome. *Cell Cycle Georget. Tex* 14, 2985–2995. <https://doi.org/10.4161/15384101.2014.989114>
- Bruining, H., de Sonneville, L., Swaab, H., de Jonge, M., Kas, M., van Engeland, H., Vorstman, J., 2010. Dissecting the Clinical Heterogeneity of Autism Spectrum Disorders through Defined Genotypes. *PLoS ONE* 5. <https://doi.org/10.1371/journal.pone.0010887>
- Burnside, R.D., Pasion, R., Mikhail, F.M., Carroll, A.J., Robin, N.H., Youngs, E.L., Gadi, I.K., Keitges, E., Jaswaney, V.L., Papenhausen, P.R., Potluri, V.R., Risheg, H., Rush, B., Smith, J.L., Schwartz, S., Tepperberg, J.H., Butler, M.G., 2011. Microdeletion/microduplication of proximal 15q11.2 between BP1 and BP2: a susceptibility region for neurological dysfunction including developmental and language delay. *Hum. Genet.* 130, 517–528. <https://doi.org/10.1007/s00439-011-0970-4>

- Butler, M.G., 2017. Clinical and genetic aspects of the 15q11.2 BP1–BP2 microdeletion disorder. *J. Intellect. Disabil. Res.* 61, 568–579. <https://doi.org/10.1111/jir.12382>
- Butler, M.G., Bittel, D.C., Kibiryeve, N., Talebizadeh, Z., Thompson, T., 2004. Behavioral Differences Among Subjects With Prader-Willi Syndrome and Type I or Type II Deletion and Maternal Disomy. *Pediatrics* 113, 565–573. <https://doi.org/10.1542/peds.113.3.565>
- Button, K.S., Ioannidis, J.P.A., Mokrysz, C., Nosek, B.A., Flint, J., Robinson, E.S.J., Munafò, M.R., 2013. Power failure: why small sample size undermines the reliability of neuroscience. *Nat. Rev. Neurosci.* 14, 365–376. <https://doi.org/10.1038/nrn3475>
- Cafferkey, M., Ahn, J.W., Flinter, F., Ogilvie, C., 2014. Phenotypic features in patients with 15q11.2(BP1-BP2) deletion: Further delineation of an emerging syndrome. *Am. J. Med. Genet. A.* 164, 1916–1922. <https://doi.org/10.1002/ajmg.a.36554>
- Calabrese, E., Badea, A., Watson, C., Johnson, G.A., 2013. A quantitative magnetic resonance histology atlas of postnatal rat brain development with regional estimates of growth and variability. *NeuroImage* 71, 196–206. <https://doi.org/10.1016/j.neuroimage.2013.01.017>
- Carson, J.H., Worboys, K., Ainger, K., Barbarese, E., 1997. Translocation of myelin basic protein mRNA in oligodendrocytes requires microtubules and kinesin. *Cell Motil. Cytoskeleton* 38, 318–328. [https://doi.org/10.1002/\(SICI\)1097-0169\(1997\)38:4<318::AID-CM2>3.0.CO;2-#](https://doi.org/10.1002/(SICI)1097-0169(1997)38:4<318::AID-CM2>3.0.CO;2-#)
- Catani, M., Howard, R.J., Pajevic, S., Jones, D.K., 2002. Virtual in Vivo Interactive Dissection of White Matter Fasciculi in the Human Brain. *NeuroImage* 17, 77–94. <https://doi.org/10.1006/nimg.2002.1136>
- Chai, J.-H., Locke, D.P., Grealley, J.M., Knoll, J.H.M., Ohta, T., Dunai, J., Yavor, A., Eichler, E.E., Nicholls, R.D., 2003. Identification of Four Highly Conserved Genes between Breakpoint Hotspots BP1 and BP2 of the Prader-Willi/Angelman Syndromes Deletion Region That Have Undergone Evolutionary Transposition Mediated by Flanking Duplicons. *Am. J. Hum. Genet.* 73, 898–925.
- Chang, Y.S., Owen, J.P., Pojman, N.J., Thieu, T., Bukshpun, P., Wakahiro, M.L.J., Marco, E.J., Berman, J.I., Spiro, J.E., Chung, W.K., Buckner, R.L., Roberts, T.P.L., Nagarajan, S.S., Sherr, E.H., Mukherjee, P., 2016. Reciprocal white matter alterations due to 16p11.2 chromosomal deletions versus duplications: White Matter Microstructure in 16p11.2 CNVs. *Hum. Brain Mapp.* 37, 2833–2848. <https://doi.org/10.1002/hbm.23211>
- Chaste, P., Sanders, S.J., Mohan, K.N., Klei, L., Song, Y., Murtha, M.T., Hus, V., Lowe, J.K., Willsey, A.J., Moreno-De-Luca, D., Yu, T.W., Fombonne, E., Geschwind, D., Grice, D.E., Ledbetter, D.H., Lord, C., Mane, S.M., Martin, D.M., Morrow, E.M., Walsh, C.A., Sutcliffe, J.S., State, M.W., Martin, C.L., Devlin, B., Beaudet, A.L., Cook, E.H., Kim, S.-J., 2014. Modest Impact on Risk for Autism Spectrum Disorder of Rare Copy Number Variants at 15q11.2, Specifically Breakpoints 1 to 2: Effects 15q11.2 CNV on autism risk. *Autism Res.* 7, 355–362. <https://doi.org/10.1002/aur.1378>

- Chen, E., Sharma, M.R., Shi, X., Agrawal, R.K., Joseph, S., 2014. Fragile X mental retardation protein regulates translation by binding directly to the ribosome. *Mol. Cell* 54, 407–417. <https://doi.org/10.1016/j.molcel.2014.03.023>
- Chen, Z., Borek, D., Padrick, S.B., Gomez, T.S., Metlagel, Z., Ismail, A., Umetani, J., Billadeau, D.D., Otwinowski, Z., Rosen, M.K., 2010. Structure and Control of the Actin Regulatory WAVE Complex. *Nature* 468, 533–538. <https://doi.org/10.1038/nature09623>
- Cheng, C.-M., Chang, W.-H., Chen, M.-H., Tsai, C.-F., Su, T.-P., Li, C.-T., Tsai, S.-J., Hsu, J.-W., Huang, K.-L., Lin, W.-C., Chen, T.-J., Bai, Y.-M., 2018. Co-aggregation of major psychiatric disorders in individuals with first-degree relatives with schizophrenia: a nationwide population-based study. *Mol. Psychiatry* 23, 1756–1763. <https://doi.org/10.1038/mp.2017.217>
- Cheng, Y., Chou, K.-H., Chen, I.-Y., Fan, Y.-T., Decety, J., Lin, C.-P., 2010. Atypical development of white matter microstructure in adolescents with autism spectrum disorders. *NeuroImage* 50, 873–882. <https://doi.org/10.1016/j.neuroimage.2010.01.011>
- Chudasama, Y., Robbins, T.W., 2003. Dissociable contributions of the orbitofrontal and infralimbic cortex to pavlovian autoshaping and discrimination reversal learning: further evidence for the functional heterogeneity of the rodent frontal cortex. *J. Neurosci. Off. J. Soc. Neurosci.* 23, 8771–8780.
- Chung, L., Wang, X., Zhu, L., Towers, A.J., Cao, X., Kim, I.H., Jiang, Y., 2015. Parental origin impairment of synaptic functions and behaviors in cytoplasmic FMRP interacting protein 1 (Cyfip1) deficient mice. *Brain Res.* 1629, 340–350. <https://doi.org/10.1016/j.brainres.2015.10.015>
- Ciccarelli, O., Catani, M., Johansen-Berg, H., Clark, C., Thompson, A., 2008. Diffusion-based tractography in neurological disorders: concepts, applications, and future developments. *Lancet Neurol.* 7, 715–727. [https://doi.org/10.1016/S1474-4422\(08\)70163-7](https://doi.org/10.1016/S1474-4422(08)70163-7)
- Cingolani, L.A., Goda, Y., 2008. Actin in action: the interplay between the actin cytoskeleton and synaptic efficacy. *Nat. Rev. Neurosci.* 9, 344–356. <https://doi.org/10.1038/nrn2373>
- Cioni, J.-M., Wong, H.W., Bressan, D., Kodama, L., Harris, W.A., Holt, C.E., 2018. Axon-Axon Interactions Regulate Topographic Optic Tract Sorting via CYFIP2-Dependent WAVE Complex Function. <https://doi.org/10.17863/CAM.17682>
- Clarke, J.M., Zaidel, E., 1994. Anatomical-behavioral relationships: Corpus callosum morphometry and hemispheric specialization. *Behav. Brain Res.* 64, 185–202. [https://doi.org/10.1016/0166-4328\(94\)90131-7](https://doi.org/10.1016/0166-4328(94)90131-7)
- Coe, B.P., Witherspoon, K., Rosenfeld, J.A., van Bon, B.W.M., Vulto-van Silfhout, A.T., Bosco, P., Friend, K.L., Baker, C., Buono, S., Vissers, L.E.L.M., Schuurs-Hoeijmakers, J.H., Hoischen, A., Pfundt, R., Krumm, N., Carvill, G.L., Li, D., Amaral, D., Brown, N., Lockhart, P.J., Scheffer, I.E., Alberti, A., Shaw, M., Pettinato, R., Tervo, R., de Leeuw, N., Reijnders, M.R.F., Torchia, B.S., Peeters,

- H., O’Roak, B.J., Fichera, M., Hehir-Kwa, J.Y., Shendure, J., Mefford, H.C., Haan, E., Gécz, J., de Vries, B.B.A., Romano, C., Eichler, E.E., 2014. Refining analyses of copy number variation identifies specific genes associated with developmental delay. *Nat. Genet.* 46, 1063–1071. <https://doi.org/10.1038/ng.3092>
- Cohen, J., 1977. CHAPTER 1 - The Concepts of Power Analysis, in: *Statistical Power Analysis for the Behavioral Sciences (Revised Edition)*. Academic Press, pp. 1–17. <https://doi.org/10.1016/B978-0-12-179060-8.50006-2>
- Colman, D.R., Kreibich, G., Frey, A.B., Sabatini, D.D., 1982. Synthesis and incorporation of myelin polypeptides into CNS myelin. *J. Cell Biol.* 95, 598–608. <https://doi.org/10.1083/jcb.95.2.598>
- Comery, T.A., Harris, J.B., Willems, P.J., Oostra, B.A., Irwin, S.A., Weiler, I.J., Greenough, W.T., 1997. Abnormal dendritic spines in fragile X knockout mice: Maturation and pruning deficits. *Proc. Natl. Acad. Sci.* 94, 5401–5404. <https://doi.org/10.1073/pnas.94.10.5401>
- Contractor, A., Klyachko, V.A., Portera-Cailliau, C., 2015. Altered neuronal and circuit excitability in Fragile X Syndrome. *Neuron* 87, 699–715. <https://doi.org/10.1016/j.neuron.2015.06.017>
- Cory, G.O.C., Ridley, A.J., 2002. Braking WAVES. *Nature* 418, 732–733. <https://doi.org/10.1038/418732a>
- Cox, D.M., Butler, M.G., 2015. The 15q11.2 BP1–BP2 Microdeletion Syndrome: A Review. *Int. J. Mol. Sci.* 16, 4068–4082. <https://doi.org/10.3390/ijms16024068>
- Cropley, V.L., Klauser, P., Lenroot, R.K., Bruggemann, J., Sundram, S., Bousman, C., Pereira, A., Di Biase, M.A., Weickert, T.W., Weickert, C.S., Pantelis, C., Zalesky, A., 2016. Accelerated Gray and White Matter Deterioration With Age in Schizophrenia. *Am. J. Psychiatry* 174, 286–295. <https://doi.org/10.1176/appi.ajp.2016.16050610>
- Dai, Z., Pendergast, A.M., 1995. Abi-2, a novel SH3-containing protein interacts with the c-Abl tyrosine kinase and modulates c-Abl transforming activity. *Genes Dev.* 9, 2569–2582. <https://doi.org/10.1101/gad.9.21.2569>
- Davenport, E.C., Szulc, B.R., Drew, J., Taylor, J., Morgan, T., Higgs, N.F., López-Doménech, G., Kittler, J.T., 2019. Autism and Schizophrenia-Associated CYFIP1 Regulates the Balance of Synaptic Excitation and Inhibition. *Cell Rep.* 26, 2037–2051.e6. <https://doi.org/10.1016/j.celrep.2019.01.092>
- David, A.S., 1994. Schizophrenia and the corpus callosum: Developmental, structural and functional relationships. *Behav. Brain Res.* 64, 203–211. [https://doi.org/10.1016/0166-4328\(94\)90132-5](https://doi.org/10.1016/0166-4328(94)90132-5)
- de Groot, M., Vernooij, M.W., Klein, S., Ikram, M.A., Vos, F.M., Smith, S.M., Niessen, W.J., Andersson, J.L.R., 2013. Improving alignment in Tract-based spatial statistics: evaluation and optimization of image registration. *NeuroImage* 76, 400–411. <https://doi.org/10.1016/j.neuroimage.2013.03.015>

- de Kovel, C.G.F., Trucks, H., Helbig, I., Mefford, H.C., Baker, C., Leu, C., Kluck, C., Muhle, H., von Spiczak, S., Ostertag, P., Obermeier, T., Kleefuss-Lie, A.A., Hallmann, K., Steffens, M., Gaus, V., Klein, K.M., Hamer, H.M., Rosenow, F., Brilstra, E.H., Trenité, D.K.-N., Swinkels, M.E.M., Weber, Y.G., Unterberger, I., Zimprich, F., Urak, L., Feucht, M., Fuchs, K., Møller, R.S., Hjalgrim, H., De Jonghe, P., Suls, A., Rückert, I.-M., Wichmann, H.-E., Franke, A., Schreiber, S., Nürnberg, P., Elger, C.E., Lerche, H., Stephani, U., Koeleman, B.P.C., Lindhout, D., Eichler, E.E., Sander, T., 2010. Recurrent microdeletions at 15q11.2 and 16p13.11 predispose to idiopathic generalized epilepsies. *Brain J. Neurol.* 133, 23–32. <https://doi.org/10.1093/brain/awp262>
- Dent, E.W., Gertler, F.B., 2003. Cytoskeletal Dynamics and Transport in Growth Cone Motility and Axon Guidance. *Neuron* 40, 209–227. [https://doi.org/10.1016/S0896-6273\(03\)00633-0](https://doi.org/10.1016/S0896-6273(03)00633-0)
- Derivery, E., Gautreau, A., 2010. Generation of branched actin networks: assembly and regulation of the N-WASP and WAVE molecular machines. *BioEssays* 32, 119–131. <https://doi.org/10.1002/bies.200900123>
- Derivery, E., Lombard, B., Loew, D., Gautreau, A., 2009. The Wave complex is intrinsically inactive. *Cell Motil.* 66, 777–790. <https://doi.org/10.1002/cm.20342>
- De Rubeis, S., Pasciuto, E., Li, K.W., Fernández, E., Di Marino, D., Buzzi, A., Ostroff, L.E., Klann, E., Zwartkruis, F.J.T., Komiyama, N.H., Grant, S.G.N., Pujol, C., Choquet, D., Achsel, T., Posthuma, D., Smit, A.B., Bagni, C., 2013. CYFIP1 Coordinates mRNA Translation and Cytoskeleton Remodeling to Ensure Proper Dendritic Spine Formation. *Neuron* 79, 1169–1182. <https://doi.org/10.1016/j.neuron.2013.06.039>
- Di Marino, D., D’Annessa, I., Tancredi, H., Bagni, C., Gallicchio, E., 2015. A unique binding mode of the eukaryotic translation initiation factor 4E for guiding the design of novel peptide inhibitors. *Protein Sci. Publ. Protein Soc.* 24, 1370–1382. <https://doi.org/10.1002/pro.2708>
- Doherty, J.L., Owen, M.J., 2014. Genomic insights into the overlap between psychiatric disorders: implications for research and clinical practice. *Genome Med.* 6, 29. <https://doi.org/10.1186/gm546>
- Domingues, H.S., Cruz, A., Chan, J.R., Relvas, J.B., Rubinstein, B., Pinto, I.M., 2018. Mechanical plasticity during oligodendrocyte differentiation and myelination. *Glia* 66, 5–14. <https://doi.org/10.1002/glia.23206>
- Domínguez-Iturza, N., Lo, A.C., Shah, D., Armendáriz, M., Vannelli, A., Mercaldo, V., Trusel, M., Li, K.W., Gastaldo, D., Santos, A.R., Callaerts-Vegh, Z., D’Hooge, R., Mameli, M., Linden, A.V. der, Smit, A.B., Achsel, T., Bagni, C., 2019. The autism- and schizophrenia-associated protein CYFIP1 regulates bilateral brain connectivity and behaviour. *Nat. Commun.* 10, 1–13. <https://doi.org/10.1038/s41467-019-11203-y>
- Doornbos, M., Sikkema-Raddatz, B., Ruijvenkamp, C.A.L., Dijkhuizen, T., Bijlsma, E.K., Gijbers, A.C.J., Hilhorst-Hofstee, Y., Hordijk, R., Verbruggen, K.T., Kerstjens-Frederikse, W.S. (Mieke), van Essen, T., Kok, K., van Silfhout, A.T.,

- Breuning, M., van Ravenswaaij-Arts, C.M.A., 2009. Nine patients with a microdeletion 15q11.2 between breakpoints 1 and 2 of the Prader–Willi critical region, possibly associated with behavioural disturbances. *Eur. J. Med. Genet., Emerging microdeletion and microduplication syndromes* 52, 108–115. <https://doi.org/10.1016/j.ejmg.2009.03.010>
- Drakesmith, M., Parker, G.D., Smith, J., Linden, S.C., Rees, E., Williams, N., Owen, M.J., Bree, M. van den, Hall, J., Jones, D.K., Linden, D.E.J., 2019. Genetic risk for schizophrenia and developmental delay is associated with shape and microstructure of midline white-matter structures. *Transl. Psychiatry* 9, 102. <https://doi.org/10.1038/s41398-019-0440-7>
- Dumont, J.R., Amin, E., Wright, N.F., Dillingham, C.M., Aggleton, J.P., 2015. The impact of fornix lesions in rats on spatial learning tasks sensitive to anterior thalamic and hippocampal damage. *Behav. Brain Res.* 278, 360–374. <https://doi.org/10.1016/j.bbr.2014.10.016>
- Dyrba, M., Ewers, M., Wegrzyn, M., Kilimann, I., Plant, C., Oswald, A., Meindl, T., Pievani, M., Bokde, A.L.W., Fellgiebel, A., Filippi, M., Hampel, H., Klöppel, S., Hauenstein, K., Kirste, T., Teipel, S.J., Group, the E. study, 2013. Robust Automated Detection of Microstructural White Matter Degeneration in Alzheimer’s Disease Using Machine Learning Classification of Multicenter DTI Data. *PLOS ONE* 8, e64925. <https://doi.org/10.1371/journal.pone.0064925>
- Ecker, C., Bookheimer, S.Y., Murphy, D.G.M., 2015. Neuroimaging in autism spectrum disorder: brain structure and function across the lifespan. *Lancet Neurol.* 14, 1121–1134. [https://doi.org/10.1016/S1474-4422\(15\)00050-2](https://doi.org/10.1016/S1474-4422(15)00050-2)
- Ecker, C., Murphy, D., 2014. Neuroimaging in autism—from basic science to translational research. *Nat. Rev. Neurol.* 10, 82–91. <https://doi.org/10.1038/nrneurol.2013.276>
- Eden, S., Rohatgi, R., Podtelejnikov, A.V., Mann, M., Kirschner, M.W., 2002. Mechanism of regulation of WAVE1-induced actin nucleation by Rac1 and Nck. *Nature* 418, 790–793. <https://doi.org/10.1038/nature00859>
- Eliez, S., Schmitt, J.E., White, C.D., Reiss, A.L., 2000. Children and Adolescents With Velocardiofacial Syndrome: A Volumetric MRI Study. *Am. J. Psychiatry* 157, 409–415. <https://doi.org/10.1176/appi.ajp.157.3.409>
- Emery, B., 2010. Regulation of Oligodendrocyte Differentiation and Myelination. *Science* 330, 779–782. <https://doi.org/10.1126/science.1190927>
- Fejgin, K., Nielsen, J., Birknow, M.R., Bastlund, J.F., Nielsen, V., Lauridsen, J.B., Stefansson, H., Steinberg, S., Sorensen, H.B.D., Mortensen, T.E., Larsen, P.H., Klewe, I.V., Rasmussen, S.V., Stefansson, K., Werge, T.M., Kallunki, P., Christensen, K.V., Didriksen, M., 2014. A Mouse Model that Recapitulates Cardinal Features of the 15q13.3 Microdeletion Syndrome Including Schizophrenia- and Epilepsy-Related Alterations. *Biol. Psychiatry, Schizophrenia and Bipolar Disorder: New Insights into Novel Mechanisms* 76, 128–137. <https://doi.org/10.1016/j.biopsych.2013.08.014>

- Feuk, L., Carson, A.R., Scherer, S.W., 2006. Structural variation in the human genome. *Nat. Rev. Genet.* 7, 85. <https://doi.org/10.1038/nrg1767>
- Fields, R.D., 2015. A new mechanism of nervous system plasticity: activity-dependent myelination. *Nat. Rev. Neurosci.* 16, 756–767. <https://doi.org/10.1038/nrn4023>
- Fields, R.D., 2008. White matter in learning, cognition and psychiatric disorders. *Trends Neurosci.* 31, 361–370. <https://doi.org/10.1016/j.tins.2008.04.001>
- Fitzsimmons, J., Kubicki, M., Shenton, M., 2013. Review of functional and anatomical brain connectivity findings in schizophrenia. *Curr. Opin. Psychiatry* 26, 172–187. <https://doi.org/10.1097/YCO.0b013e32835d9e6a>
- Fitzsimmons, J., Kubicki, M., Smith, K., Bushnell, G., Estepar, R.S.J., Westin, C.-F., Nestor, P.G., Niznikiewicz, M.A., Kikinis, R., McCarley, R.W., Shenton, M.E., 2009. Diffusion tractography of the fornix in schizophrenia. *Schizophr. Res.* 107, 39–46. <https://doi.org/10.1016/j.schres.2008.10.022>
- Flynn, S.W., Lang, D.J., Mackay, A.L., Goghari, V., Vavasour, I.M., Whittall, K.P., Smith, G.N., Arango, V., Mann, J.J., Dwork, A.J., Falkai, P., Honer, W.G., 2003. Abnormalities of myelination in schizophrenia detected in vivo with MRI, and post-mortem with analysis of oligodendrocyte proteins. *Mol. Psychiatry* 8, 811–820. <https://doi.org/10.1038/sj.mp.4001337>
- Fombonne, E., 2009. Epidemiology of Pervasive Developmental Disorders. *Pediatr. Res.* 65, 591–598. <https://doi.org/10.1203/PDR.0b013e31819e7203>
- Forsingdal, A., Fejgin, K., Nielsen, V., Werge, T., Nielsen, J., 2016. 15q13.3 homozygous knockout mouse model display epilepsy-, autism- and schizophrenia-related phenotypes. *Transl. Psychiatry* 6, e860. <https://doi.org/10.1038/tp.2016.125>
- Fox, M.A., Afshari, F.S., Alexander, J.K., Colello, R.J., Fuss, B., 2006. Growth cone-like sensorimotor structures are characteristic features of postmigratory, premyelinating oligodendrocytes. *Glia* 53, 563–566. <https://doi.org/10.1002/glia.20293>
- Francis, A.N., Bhojraj, T.S., Prasad, K.M., Montrose, D., Eack, S.M., Rajarethinam, R., van Elst, L.T., Keshavan, M.S., 2013. Alterations in the cerebral white matter of genetic high risk offspring of patients with schizophrenia spectrum disorder. *Prog. Neuropsychopharmacol. Biol. Psychiatry* 40, 187–192. <https://doi.org/10.1016/j.pnpbp.2012.08.003>
- Frank, M., 2000. MAL, a proteolipid in glycosphingolipid enriched domains: functional implications in myelin and beyond. *Prog. Neurobiol.* 60, 531–544. [https://doi.org/10.1016/S0301-0082\(99\)00039-8](https://doi.org/10.1016/S0301-0082(99)00039-8)
- Frazier, T.W., Hardan, A.Y., 2009. A meta-analysis of the corpus callosum in autism. *Biol. Psychiatry* 66, 935–941. <https://doi.org/10.1016/j.biopsych.2009.07.022>
- Fulton, D., Paez, P.M., Campagnoni, A.T., 2010. The multiple roles of myelin protein genes during the development of the oligodendrocyte. *ASN NEURO* 2. <https://doi.org/10.1042/AN20090051>

- Gagliardi, C., Arrigoni, F., Nordio, A., De Luca, A., Peruzzo, D., Decio, A., Leemans, A., Borgatti, R., 2018. A Different Brain: Anomalies of Functional and Structural Connections in Williams Syndrome. *Front. Neurol.* 9. <https://doi.org/10.3389/fneur.2018.00721>
- Garey, L., 2010. When cortical development goes wrong: schizophrenia as a neurodevelopmental disease of microcircuits. *J. Anat.* 217, 324–333. <https://doi.org/10.1111/j.1469-7580.2010.01231.x>
- Giampetruzzi, A., Carson, J.H., Barbarese, E., 2013. FMRP and myelin protein expression in oligodendrocytes. *Mol. Cell. Neurosci., RNA and splicing regulation in neurodegeneration* 56, 333–341. <https://doi.org/10.1016/j.mcn.2013.07.009>
- Gilmore, J.H., Kang, C., Evans, D.D., Wolfe, H.M., Smith, J.K., Lieberman, J.A., Lin, W., Hamer, R.M., Styner, M., Gerig, G., 2010. Prenatal and Neonatal Brain Structure and White Matter Maturation in Children at High Risk for Schizophrenia. *Am. J. Psychiatry* 167, 1083–1091. <https://doi.org/10.1176/appi.ajp.2010.09101492>
- Good, C.D., Scahill, R.I., Fox, N.C., Ashburner, J., Friston, K.J., Chan, D., Crum, W.R., Rossor, M.N., Frackowiak, R.S.J., 2002. Automatic Differentiation of Anatomical Patterns in the Human Brain: Validation with Studies of Degenerative Dementias. *NeuroImage* 17, 29–46. <https://doi.org/10.1006/nimg.2002.1202>
- Gottesman, I.I., 1991. Schizophrenia genesis: The origins of madness. Schizophrenia genesis: The origins of madness. W H Freeman/Times Books/ Henry Holt & Co, New York, NY, US.
- Goytain, A., Hines, R.M., El-Husseini, A., Quamme, G.A., 2007. NIPA1 (SPG6), the Basis for Autosomal Dominant Form of Hereditary Spastic Paraplegia, Encodes a Functional Mg²⁺ Transporter. *J. Biol. Chem.* 282, 8060–8068. <https://doi.org/10.1074/jbc.M610314200>
- Grabli, D., McCairn, K., Hirsch, E.C., Agid, Y., Féger, J., François, C., Tremblay, L., 2004. Behavioural disorders induced by external globus pallidus dysfunction in primates: I. Behavioural study. *Brain J. Neurol.* 127, 2039–2054. <https://doi.org/10.1093/brain/awh220>
- Graciarena, M., Seiffe, A., Nait-Oumesmar, B., Depino, A.M., 2019. Hypomyelination and Oligodendroglial Alterations in a Mouse Model of Autism Spectrum Disorder. *Front. Cell. Neurosci.* 12. <https://doi.org/10.3389/fncel.2018.00517>
- Green, T., Barnea-Goraly, N., Raman, M., Hall, S.S., Lightbody, A.A., Bruno, J.L., Quintin, E.-M., Reiss, A.L., 2015. Specific effect of the fragile-X mental retardation-1 gene (FMR1) on white matter microstructure. *Br. J. Psychiatry* 207, 143–148. <https://doi.org/10.1192/bjp.bp.114.151654>
- Griffiths, I., Klugmann, M., Anderson, T., Yool, D., Thomson, C., Schwab, M.H., Schneider, A., Zimmermann, F., McCulloch, M., Nadon, N., Nave, K.A., 1998. Axonal swellings and degeneration in mice lacking the major proteolipid of myelin. *Science* 280, 1610–1613. <https://doi.org/10.1126/science.280.5369.1610>

- Grossman, A.W., Elisseou, N.M., McKinney, B.C., Greenough, W.T., 2006. Hippocampal pyramidal cells in adult *Fmr1* knockout mice exhibit an immature-appearing profile of dendritic spines. *Brain Res.* 1084, 158–164. <https://doi.org/10.1016/j.brainres.2006.02.044>
- Guðmundsson, E., 2016. Staðlað greindarpróf fyrir fullorðna á Íslandi: WASIIS. Standardized intelligence test for adults in Iceland: WASIIS.
- Guilmatre, A., Dubourg, C., Mosca, A.-L., Legallic, S., Goldenberg, A., Drouin-Garraud, V., Layet, V., Rosier, A., Briault, S., Bonnet-Brilhault, F., Laumonnier, F., Odent, S., Le Vacon, G., Joly-Helas, G., David, V., Bendavid, C., Pinoit, J.-M., Henry, C., Impallomeni, C., Germano, E., Tortorella, G., Di Rosa, G., Barthelemy, C., Andres, C., Faivre, L., Frébourg, T., Saugier Veber, P., Champion, D., 2009. Recurrent rearrangements in synaptic and neurodevelopmental genes and shared biologic pathways in schizophrenia, autism, and mental retardation. *Arch. Gen. Psychiatry* 66, 947–956. <https://doi.org/10.1001/archgenpsychiatry.2009.80>
- Gupta, S., Ellis, S.E., Ashar, F.N., Moes, A., Bader, J.S., Zhan, J., West, A.B., Arking, D.E., 2014. Transcriptome analysis reveals dysregulation of innate immune response genes and neuronal activity-dependent genes in autism. *Nat. Commun.* 5, 5748. <https://doi.org/10.1038/ncomms6748>
- Haan, N., Carter, J., Westacott, L.J., Owen, M.J., Gray, W.P., Hall, J., Wilkinson, L.S., 2018. Haploinsufficiency of the schizophrenia risk gene *Cyfp1* causes abnormal postnatal hippocampal neurogenesis through a novel microglia dependent mechanism. *bioRxiv* 417832. <https://doi.org/10.1101/417832>
- Haas, B.W., Barnea-Goraly, N., Lightbody, A.A., Patnaik, S.S., Hoefl, F., Hazlett, H., Piven, J., Reiss, A.L., 2009. Early white-matter abnormalities of the ventral frontostriatal pathway in fragile X syndrome. *Dev. Med. Child Neurol.* 51, 593–599. <https://doi.org/10.1111/j.1469-8749.2009.03295.x>
- Haberl, M.G., Zerbi, V., Veltien, A., Ginger, M., Heerschap, A., Frick, A., 2015. Structural-functional connectivity deficits of neocortical circuits in the *Fmr1*-/- mouse model of autism. *Sci. Adv.* 1, e1500775. <https://doi.org/10.1126/sciadv.1500775>
- Haimovich, G., Ecker, C.M., Dunagin, M.C., Eggan, E., Raj, A., Gerst, J.E., Singer, R.H., 2017. Intercellular mRNA trafficking via membrane nanotube-like extensions in mammalian cells. *Proc. Natl. Acad. Sci.* 114, E9873–E9882. <https://doi.org/10.1073/pnas.1706365114>
- Hakak, Y., Walker, J.R., Li, C., Wong, W.H., Davis, K.L., Buxbaum, J.D., Haroutunian, V., Fienberg, A.A., 2001. Genome-wide expression analysis reveals dysregulation of myelination-related genes in chronic schizophrenia. *Proc. Natl. Acad. Sci. U. S. A.* 98, 4746–4751. <https://doi.org/10.1073/pnas.081071198>
- Hall, A., 1998. Rho GTPases and the Actin Cytoskeleton. *Science* 279, 509–514. <https://doi.org/10.1126/science.279.5350.509>

- Hall, S.S., Dougherty, R.F., Reiss, A.L., 2016. Profiles of aberrant white matter microstructure in fragile X syndrome. *NeuroImage Clin.* 11, 133–138. <https://doi.org/10.1016/j.nicl.2016.01.013>
- Han, K., Chen, H., Gennarino, V.A., Richman, R., Lu, H.-C., Zoghbi, H.Y., 2015. Fragile X-like behaviors and abnormal cortical dendritic spines in Cytoplasmic FMR1-interacting protein 2-mutant mice. *Hum. Mol. Genet.* 24, 1813–1823. <https://doi.org/10.1093/hmg/ddu595>
- Hanley, J.G., 2014. Actin-dependent mechanisms in AMPA receptor trafficking. *Front. Cell. Neurosci.* 8. <https://doi.org/10.3389/fncel.2014.00381>
- Hanson, E., Bernier, R., Porche, K., Jackson, F.I., Goin-Kochel, R.P., Snyder, L.G., Snow, A.V., Wallace, A.S., Campe, K.L., Zhang, Y., Chen, Q., D'Angelo, D., Moreno-De-Luca, A., Orr, P.T., Boomer, K.B., Evans, D.W., Kanne, S., Berry, L., Miller, F.K., Olson, J., Sherr, E., Martin, C.L., Ledbetter, D.H., Spiro, J.E., Chung, W.K., 2015. The Cognitive and Behavioral Phenotype of the 16p11.2 Deletion in a Clinically Ascertained Population. *Biol. Psychiatry, Autism Genotypes and Phenotypes* 77, 785–793. <https://doi.org/10.1016/j.biopsych.2014.04.021>
- Hartley, S.L., MacLean, W.E., Butler, M.G., Zarcone, J., Thompson, T., 2005. Maladaptive behaviors and risk factors among the genetic subtypes of Prader–Willi syndrome. *Am. J. Med. Genet. A.* 136A, 140–145. <https://doi.org/10.1002/ajmg.a.30771>
- He, C.X., Portera-Cailliau, C., 2013. The trouble with spines in fragile X syndrome: density, maturity and plasticity. *Neuroscience* 251, 120–128. <https://doi.org/10.1016/j.neuroscience.2012.03.049>
- Heath, F., Hurley, S.A., Johansen-Berg, H., Sampaio-Baptista, C., 2018. Advances in noninvasive myelin imaging. *Dev. Neurobiol.* 78, 136–151. <https://doi.org/10.1002/dneu.22552>
- Helgason, A., Nicholson, G., Stefánsson, K., Donnelly, P., 2003. A Reassessment of Genetic Diversity in Icelanders: Strong Evidence from Multiple Loci for Relative Homogeneity Caused by Genetic Drift. *Ann. Hum. Genet.* 67, 281–297. <https://doi.org/10.1046/j.1469-1809.2003.00046.x>
- Heutink, P., Oostra, B.A., 2002. Gene finding in genetically isolated populations. *Hum. Mol. Genet.* 11, 2507–2515. <https://doi.org/10.1093/hmg/11.20.2507>
- Ho, K.S., Wassman, E.R., Baxter, A.L., Hensel, C.H., Martin, M.M., Prasad, A., Twede, H., Vanzo, R.J., Butler, M.G., 2016. Chromosomal Microarray Analysis of Consecutive Individuals with Autism Spectrum Disorders Using an Ultra-High Resolution Chromosomal Microarray Optimized for Neurodevelopmental Disorders. *Int. J. Mol. Sci.* 17. <https://doi.org/10.3390/ijms17122070>
- Hoefl, F., Barnea-Goraly, N., Haas, B.W., Golarai, G., Ng, D., Mills, D., Korenberg, J., Bellugi, U., Galaburda, A., Reiss, A.L., 2007. More Is Not Always Better: Increased Fractional Anisotropy of Superior Longitudinal Fasciculus Associated

with Poor Visuospatial Abilities in Williams Syndrome. *J. Neurosci.* 27, 11960–11965. <https://doi.org/10.1523/JNEUROSCI.3591-07.2007>

- Hofstetter, S., Assaf, Y., 2017. The rapid development of structural plasticity through short water maze training: A DTI study. *NeuroImage* 155, 202–208. <https://doi.org/10.1016/j.neuroimage.2017.04.056>
- Homberg, J.R., Kyzar, E.J., Scattoni, M.L., Norton, W.H., Pittman, J., Gaikwad, S., Nguyen, M., Poudel, M.K., Ullmann, J.F.P., Diamond, D.M., Kaluyeva, A.A., Parker, M.O., Brown, R.E., Song, C., Gainetdinov, R.R., Gottesman, I.I., Kalueff, A.V., 2016. Genetic and environmental modulation of neurodevelopmental disorders: Translational insights from labs to beds. *Brain Res. Bull.* 125, 79–91. <https://doi.org/10.1016/j.brainresbull.2016.04.015>
- Horev, G., Ellegood, J., Lerch, J.P., Son, Y.-E.E., Muthuswamy, L., Vogel, H., Krieger, A.M., Buja, A., Henkelman, R.M., Wigler, M., Mills, A.A., 2011. Dosage-dependent phenotypes in models of 16p11.2 lesions found in autism. *Proc. Natl. Acad. Sci.* 108, 17076–17081. <https://doi.org/10.1073/pnas.1114042108>
- Hornak, J., O’Doherty, J., Bramham, J., Rolls, E.T., Morris, R.G., Bullock, P.R., Polkey, C.E., 2004. Reward-related reversal learning after surgical excisions in orbito-frontal or dorsolateral prefrontal cortex in humans. *J. Cogn. Neurosci.* 16, 463–478. <https://doi.org/10.1162/089892904322926791>
- Hoyer, C., Gass, N., Weber-Fahr, W., Sartorius, A., 2014. Advantages and Challenges of Small Animal Magnetic Resonance Imaging as a Translational Tool. *Neuropsychobiology* 69, 187–201. <https://doi.org/10.1159/000360859>
- Hsiao, K., Harony-Nicolas, H., Buxbaum, J.D., Bozdagi-Gunal, O., Benson, D.L., 2016. Cyfip1 Regulates Presynaptic Activity during Development. *J. Neurosci.* 36, 1564–1576. <https://doi.org/10.1523/JNEUROSCI.0511-15.2016>
- Hu, W.F., Chahrour, M.H., Walsh, C.A., 2014. The Diverse Genetic Landscape of Neurodevelopmental Disorders. *Annu. Rev. Genomics Hum. Genet.* 15, 195–213. <https://doi.org/10.1146/annurev-genom-090413-025600>
- Hubl, D., Koenig, T., Strik, W., Federspiel, A., Kreis, R., Boesch, C., Maier, S.E., Schroth, G., Lovblad, K., Dierks, T., 2004. Pathways that make voices: white matter changes in auditory hallucinations. *Arch. Gen. Psychiatry* 61, 658–668. <https://doi.org/10.1001/archpsyc.61.7.658>
- Huganir, R.L., Nicoll, R.A., 2013. AMPARs and Synaptic Plasticity: The Last 25 Years. *Neuron* 80, 704–717. <https://doi.org/10.1016/j.neuron.2013.10.025>
- Hughes, E.G., Kang, S.H., Fukaya, M., Bergles, D.E., 2013. Oligodendrocyte progenitors balance growth with self-repulsion to achieve homeostasis in the adult brain. *Nat. Neurosci.* 16, 668–676. <https://doi.org/10.1038/nn.3390>
- Iafate, A.J., Feuk, L., Rivera, M.N., Listewnik, M.L., Donahoe, P.K., Qi, Y., Scherer, S.W., Lee, C., 2004. Detection of large-scale variation in the human genome. *Nat. Genet.* 36, 949. <https://doi.org/10.1038/ng1416>

- Inagawa, K., Watanabe, S., Tsukada, Y., Mikoshiba, K., 1988. The role of myelination in learning performance observed in two strains of myelin-deficient mutant mice (shiverer and mld). *Behav. Neural Biol.* 50, 184–192. [https://doi.org/10.1016/S0163-1047\(88\)90871-0](https://doi.org/10.1016/S0163-1047(88)90871-0)
- Ioannidis, J.P.A., 2005. Why Most Published Research Findings Are False. *PLOS Med.* 2, e124. <https://doi.org/10.1371/journal.pmed.0020124>
- Irwin, S.A., Galvez, R., Greenough, W.T., 2000. Dendritic Spine Structural Anomalies in Fragile-X Mental Retardation Syndrome. *Cereb. Cortex* 10, 1038–1044. <https://doi.org/10.1093/cercor/10.10.1038>
- Ismail, A.M., Padrick, S.B., Chen, B., Umetani, J., Rosen, M.K., 2009. The WAVE regulatory complex is inhibited. *Nat. Struct. Mol. Biol.* 16, 561–563. <https://doi.org/10.1038/nsmb.1587>
- Ismail, S., Essawi, M., 2012. Genetic polymorphism studies in humans. *Middle East J. Med. Genet.* 1, 57–63. <https://doi.org/10.1097/01.MXE.0000415225.85003.47>
- Itsara, A., Cooper, G.M., Baker, C., Girirajan, S., Li, J., Absher, D., Krauss, R.M., Myers, R.M., Ridker, P.M., Chasman, D.I., Mefford, H., Ying, P., Nickerson, D.A., Eichler, E.E., 2009. Population analysis of large copy number variants and hotspots of human genetic disease. *Am. J. Hum. Genet.* 84, 148–161. <https://doi.org/10.1016/j.ajhg.2008.12.014>
- Jacquemont, S., Coe, B.P., Hersch, M., Duyzend, M.H., Krumm, N., Bergmann, S., Beckmann, J.S., Rosenfeld, J.A., Eichler, E.E., 2014. A Higher Mutational Burden in Females Supports a “Female Protective Model” in Neurodevelopmental Disorders. *Am. J. Hum. Genet.* 94, 415–425. <https://doi.org/10.1016/j.ajhg.2014.02.001>
- Jäkel, S., Dimou, L., 2017. Glial Cells and Their Function in the Adult Brain: A Journey through the History of Their Ablation. *Front. Cell. Neurosci.* 11. <https://doi.org/10.3389/fncel.2017.00024>
- Jakobsson, M., Scholz, S.W., Scheet, P., Gibbs, J.R., VanLiere, J.M., Fung, H.-C., Szpiech, Z.A., Degan, J.H., Wang, K., Guerreiro, R., Bras, J.M., Schymick, J.C., Hernandez, D.G., Traynor, B.J., Simon-Sanchez, J., Matarin, M., Britton, A., van de Leemput, J., Rafferty, I., Bucan, M., Cann, H.M., Hardy, J.A., Rosenberg, N.A., Singleton, A.B., 2008. Genotype, haplotype and copy-number variation in worldwide human populations. *Nature* 451, 998–1003. <https://doi.org/10.1038/nature06742>
- Jeon, S.J., Ryu, J.H., Bahn, G.H., 2017. Altered Translational Control of Fragile X Mental Retardation Protein on Myelin Proteins in Neuropsychiatric Disorders. *Biomol. Ther.* 25, 231–238. <https://doi.org/10.4062/biomolther.2016.042>
- Jeurissen, B., Leemans, A., Tournier, J.-D., Jones, D.K., Sijbers, J., 2013. Investigating the prevalence of complex fiber configurations in white matter tissue with diffusion magnetic resonance imaging. *Hum. Brain Mapp.* 34, 2747–2766. <https://doi.org/10.1002/hbm.22099>

- Jin, X., Riew, T.-R., Kim, H.L., Choi, J.-H., Lee, M.-Y., 2018. Morphological characterization of NG2 glia and their association with neuroglial cells in the 3-nitropropionic acid-lesioned striatum of rat. *Sci. Rep.* 8, 1–17. <https://doi.org/10.1038/s41598-018-24385-0>
- Jones, D.K., Horsfield, M.A., Simmons, A., 1999. Optimal strategies for measuring diffusion in anisotropic systems by magnetic resonance imaging. *Magn. Reson. Med.* 42, 515–525. [https://doi.org/10.1002/\(SICI\)1522-2594\(199909\)42:3<515::AID-MRM14>3.0.CO;2-Q](https://doi.org/10.1002/(SICI)1522-2594(199909)42:3<515::AID-MRM14>3.0.CO;2-Q)
- Jones, D.K., Knösche, T.R., Turner, R., 2013. White matter integrity, fiber count, and other fallacies: The do's and don'ts of diffusion MRI. *NeuroImage* 73, 239–254. <https://doi.org/10.1016/j.neuroimage.2012.06.081>
- Jones, D.K., Leemans, A., 2011. Diffusion tensor imaging. *Magn. Reson. Neuroimaging Methods Protoc.* 127–144.
- Jones, D.K., Symms, M.R., Cercignani, M., Howard, R.J., 2005. The effect of filter size on VBM analyses of DT-MRI data. *NeuroImage* 26, 546–554. <https://doi.org/10.1016/j.neuroimage.2005.02.013>
- Kachar, B., Behar, T., Dubois-Dalcq, M., 1986. Cell shape and motility of oligodendrocytes cultured without neurons. *Cell Tissue Res.* 244, 27–38. <https://doi.org/10.1007/BF00218378>
- Kagawa, T., Yoshida, S., Shiraishi, T., Hashimoto, M., Inadomi, D., Sato, M., Tsuzuki, T., Miwa, K., Yuasa, K., 2017. Basic principles of magnetic resonance imaging for beginner oral and maxillofacial radiologists. *Oral Radiol.* 33, 92–100. <https://doi.org/10.1007/s11282-017-0274-z>
- Kambeitz, J., Kambeitz-Ilankovic, L., Leucht, S., Wood, S., Davatzikos, C., Malchow, B., Falkai, P., Koutsouleris, N., 2015. Detecting Neuroimaging Biomarkers for Schizophrenia: A Meta-Analysis of Multivariate Pattern Recognition Studies. *Neuropsychopharmacology* 40, 1742–1751. <https://doi.org/10.1038/npp.2015.22>
- Kappenman, E.S., Keil, A., 2017. Introduction to the special issue on recentring science: Replication, robustness, and reproducibility in psychophysiology. *Psychophysiology* 54, 3–5. <https://doi.org/10.1111/psyp.12787>
- Karahan, E., Costigan, A.G., Graham, K.S., Lawrence, A.D., Zhang, J., 2019. Cognitive and white-matter compartment models reveal selective relations between corticospinal tract microstructure and simple reaction time. *J. Neurosci.* 2954–18. <https://doi.org/10.1523/JNEUROSCI.2954-18.2019>
- Kassmann, C.M., Lappe-Siefke, C., Baes, M., Brügger, B., Mildner, A., Werner, H.B., Natt, O., Michaelis, T., Prinz, M., Frahm, J., Nave, K.-A., 2007. Axonal loss and neuroinflammation caused by peroxisome-deficient oligodendrocytes. *Nat. Genet.* 39, 969–976. <https://doi.org/10.1038/ng2070>
- Kates, W.R., Burnette, C.P., Jabs, E.W., Rutberg, J., Murphy, A.M., Grados, M., Geraghty, M., Kaufmann, W.E., Pearlson, G.D., 2001. Regional cortical white

matter reductions in velocardiofacial syndrome: a volumetric MRI analysis. *Biol. Psychiatry* 49, 677–684.

- Kendall, K.M., Rees, E., Escott-Price, V., Einon, M., Thomas, R., Hewitt, J., O'Donovan, M.C., Owen, M.J., Walters, J.T.R., Kirov, G., 2016. Cognitive Performance Among Carriers of Pathogenic Copy Number Variants: Analysis of 152,000 UK Biobank Subjects. *Biol. Psychiatry*.
<https://doi.org/10.1016/j.biopsych.2016.08.014>
- Kendler, K.S., 2010. Advances in Our Understanding of Genetic Risk Factors for Autism Spectrum Disorders. *Am. J. Psychiatry* 167, 1291–1293.
<https://doi.org/10.1176/appi.ajp.2010.10081160>
- Kettenmann, H., Verkhratsky, A., 2008. Neuroglia: the 150 years after. *Trends Neurosci.* 31, 653–659. <https://doi.org/10.1016/j.tins.2008.09.003>
- Kevenaar, J.T., Hoogenraad, C.C., 2015. The axonal cytoskeleton: from organization to function. *Front. Mol. Neurosci.* 8. <https://doi.org/10.3389/fnmol.2015.00044>
- Kievit, R.A., Fuhrmann, D., Borgeest, G.S., Simpson-Kent, I.L., Henson, R.N.A., 2018. The neural determinants of age-related changes in fluid intelligence: a pre-registered, longitudinal analysis in UK Biobank. *Wellcome Open Res.* 3. <https://doi.org/10.12688/wellcomeopenres.14241.2>
- Kim, H.-J., DiBernardo, A.B., Sloane, J.A., Rasband, M.N., Solomon, D., Kosaras, B., Kwak, S.P., Vartanian, T.K., 2006. WAVE1 Is Required for Oligodendrocyte Morphogenesis and Normal CNS Myelination. *J. Neurosci.* 26, 5849–5859. <https://doi.org/10.1523/JNEUROSCI.4921-05.2006>
- Kirov, G., 2015. CNVs in neuropsychiatric disorders. *Hum. Mol. Genet.* 24, R45–R49. <https://doi.org/Kirov,> George
<<http://orca.cf.ac.uk/view/cardiffauthors/A0312379.html>> 2015. CNVs in neuropsychiatric disorders. *Human Molecular Genetics* 24 (R1) , R45-R49. [10.1093/hmg/ddv253](https://doi.org/10.1093/hmg/ddv253) <<http://dx.doi.org/10.1093/hmg/ddv253>>
- Kirov, G., Grozeva, D., Norton, N., Ivanov, D., Mantripragada, K.K., Holmans, P., Craddock, N., Owen, M.J., O'Donovan, M.C., 2009. Support for the involvement of large copy number variants in the pathogenesis of schizophrenia. *Hum. Mol. Genet.* 18, 1497–1503. <https://doi.org/10.1093/hmg/ddp043>
- Kirov, G., Rees, E., Walters, J.T.R., Escott-Price, V., Georgieva, L., Richards, A.L., Chambert, K.D., Davies, G., Legge, S.E., Moran, J.L., McCarroll, S.A., O'Donovan, M.C., Owen, M.J., 2014. The penetrance of copy number variations for schizophrenia and developmental delay. *Biol. Psychiatry* 75, 378–385. <https://doi.org/10.1016/j.biopsych.2013.07.022>
- Klein, S., Staring, M., Murphy, K., Viergever, M.A., Pluim, J.P.W., 2010. elastix: a toolbox for intensity-based medical image registration. *IEEE Trans. Med. Imaging* 29, 196–205. <https://doi.org/10.1109/TMI.2009.2035616>

- Klingseisen, A., Lyons, D.A., 2018. Axonal Regulation of Central Nervous System Myelination: Structure and Function. *The Neuroscientist* 24, 7–21. <https://doi.org/10.1177/1073858417703030>
- Knapp, P.E., Bartlett, W.P., Skoff, R.P., 1987. Cultured oligodendrocytes mimic in vivo phenotypic characteristics: Cell shape, expression of myelin-specific antigens, and membrane production. *Dev. Biol.* 120, 356–365. [https://doi.org/10.1016/0012-1606\(87\)90238-7](https://doi.org/10.1016/0012-1606(87)90238-7)
- Knöchel, C., Oertel-Knöchel, V., Schönmeier, R., Rotarska-Jagiela, A., van de Ven, V., Prvulovic, D., Haenschel, C., Uhlhaas, P., Pantel, J., Hampel, H., Linden, D.E.J., 2012. Interhemispheric hypoconnectivity in schizophrenia: Fiber integrity and volume differences of the corpus callosum in patients and unaffected relatives. *NeuroImage* 59, 926–934. <https://doi.org/10.1016/j.neuroimage.2011.07.088>
- Kobayashi, K., Kuroda, S., Fukata, M., Nakamura, T., Nagase, T., Nomura, N., Matsuura, Y., Yoshida-Kubomura, N., Iwamatsu, A., Kaibuchi, K., 1998. p140Sra-1 (Specifically Rac1-associated Protein) Is a Novel Specific Target for Rac1 Small GTPase. *J. Biol. Chem.* 273, 291–295. <https://doi.org/10.1074/jbc.273.1.291>
- Kostro, D., Abdulkadir, A., Durr, A., Roos, R., Leavitt, B.R., Johnson, H., Cash, D., Tabrizi, S.J., Scahill, R.I., Ronneberger, O., Klöppel, S., Track-HD Investigators, 2014. Correction of inter-scanner and within-subject variance in structural MRI based automated diagnosing. *NeuroImage* 98, 405–415. <https://doi.org/10.1016/j.neuroimage.2014.04.057>
- Kozma, R., Ahmed, S., Best, A., Lim, L., 1995. The Ras-related protein Cdc42Hs and bradykinin promote formation of peripheral actin microspikes and filopodia in Swiss 3T3 fibroblasts. *Mol. Cell. Biol.* 15, 1942–1952. <https://doi.org/10.1128/MCB.15.4.1942>
- Kretschmann, H.J., 1988. Localisation of the corticospinal fibres in the internal capsule in man. *J. Anat.* 160, 219–225.
- Krogsrud, S.K., Fjell, A.M., Tamnes, C.K., Grydeland, H., Mork, L., Due-Tønnessen, P., Bjørnerud, A., Sampaio-Baptista, C., Andersson, J., Johansen-Berg, H., Walhovd, K.B., 2016. Changes in white matter microstructure in the developing brain—A longitudinal diffusion tensor imaging study of children from 4 to 11 years of age. *NeuroImage* 124, 473–486. <https://doi.org/10.1016/j.neuroimage.2015.09.017>
- Kunda, P., Craig, G., Dominguez, V., Baum, B., 2003. Abi, Sra1, and Kette Control the Stability and Localization of SCAR/WAVE to Regulate the Formation of Actin-Based Protrusions. *Curr. Biol.* 13, 1867–1875. <https://doi.org/10.1016/j.cub.2003.10.005>
- Kurusu, S., Takenawa, T., 2009. The WASP and WAVE family proteins. *Genome Biol.* 10, 226. <https://doi.org/10.1186/gb-2009-10-6-226>
- Laursen, L.S., Chan, C.W., French-Constant, C., 2011. Translation of myelin basic protein mRNA in oligodendrocytes is regulated by integrin activation and hnRNP-K. *J. Cell Biol.* 192, 797–811. <https://doi.org/10.1083/jcb.201007014>

- Laviola, G., Hannan, A.J., Macrì, S., Solinas, M., Jaber, M., 2008. Effects of enriched environment on animal models of neurodegenerative diseases and psychiatric disorders. *Neurobiol. Dis.* 31, 159–168. <https://doi.org/10.1016/j.nbd.2008.05.001>
- Lee, S.H., Dominguez, R., 2010. Regulation of Actin Cytoskeleton Dynamics in Cells. *Mol. Cells* 29, 311–325.
- Leemans, A., Jeurissen, B., Sijbers, J., Jones, D.K., 2009. ExploreDTI: a graphical toolbox for processing, analyzing, and visualizing diffusion MR data, in: 17th Annual Meeting of Intl Soc Mag Reson Med. p. 3537.
- Leemans, A., Jones, D.K., 2009. The B-matrix must be rotated when correcting for subject motion in DTI data. *Magn. Reson. Med.* 61, 1336–1349. <https://doi.org/10.1002/mrm.21890>
- Legge, S.E., Jones, H.J., Kendall, K.M., Pardiñas, A.F., Menzies, G., Bracher-Smith, M., Escott-Price, V., Rees, E., Davis, K.A.S., Hotopf, M., Savage, J.E., Posthuma, D., Holmans, P., Kirov, G., Owen, M.J., O'Donovan, M.C., Zammit, S., Walters, J.T.R., 2019. Genetic association study of psychotic experiences in UK Biobank. *bioRxiv* 583468. <https://doi.org/10.1101/583468>
- Lenz, K.M., Nelson, L.H., 2018. Microglia and Beyond: Innate Immune Cells As Regulators of Brain Development and Behavioral Function. *Front. Immunol.* 9. <https://doi.org/10.3389/fimmu.2018.00698>
- Li, H.H., Roy, M., Kuscuoglu, U., Spencer, C.M., Halm, B., Harrison, K.C., Bayle, J.H., Splendore, A., Ding, F., Meltzer, L.A., Wright, E., Paylor, R., Deisseroth, K., Francke, U., 2009. Induced chromosome deletions cause hypersociability and other features of Williams-Beuren syndrome in mice. *EMBO Mol. Med.* 1, 50–65. <https://doi.org/10.1002/emmm.200900003>
- Lin, A.C., Holt, C.E., 2008. Function and regulation of local axonal translation. *Curr. Opin. Neurobiol., Development* 18, 60–68. <https://doi.org/10.1016/j.conb.2008.05.004>
- Linden, D.E.J., 2012. The Challenges and Promise of Neuroimaging in Psychiatry. *Neuron* 73, 8–22. <https://doi.org/10.1016/j.neuron.2011.12.014>
- Linden, D.E.J., Fallgatter, A.J., 2009. Neuroimaging in Psychiatry: From Bench to Bedside. *Front. Hum. Neurosci.* 3. <https://doi.org/10.3389/neuro.09.049.2009>
- Locke, D.P., Se graves, R., Nicholls, R.D., Schwartz, S., Pintel, D., Albertson, D.G., Eichler, E.E., 2004. BAC microarray analysis of 15q11–q13 rearrangements and the impact of segmental duplications. *J. Med. Genet.* 41, 175–182. <https://doi.org/10.1136/jmg.2003.013813>
- Lourenço, T., Paes de Faria, J., Bippes, C.A., Maia, J., Lopes-da-Silva, J.A., Relvas, J.B., Grãos, M., 2016. Modulation of oligodendrocyte differentiation and maturation by combined biochemical and mechanical cues. *Sci. Rep.* 6. <https://doi.org/10.1038/srep21563>

- Lozano, R., Rosero, C.A., Hagerman, R.J., 2014. Fragile X spectrum disorders. *Intractable Rare Dis. Res.* 3, 134–146. <https://doi.org/10.5582/irdr.2014.01022>
- Lunn, K.F., Baas, P.W., Duncan, I.D., 1997. Microtubule organization and stability in the oligodendrocyte. *J. Neurosci. Off. J. Soc. Neurosci.* 17, 4921–4932.
- Luo, L., 2002. Actin Cytoskeleton Regulation in Neuronal Morphogenesis and Structural Plasticity. *Annu. Rev. Cell Dev. Biol.* 18, 601–635. <https://doi.org/10.1146/annurev.cellbio.18.031802.150501>
- Lüscher, C., Malenka, R.C., 2012. NMDA Receptor-Dependent Long-Term Potentiation and Long-Term Depression (LTP/LTD). *Cold Spring Harb. Perspect. Biol.* 4. <https://doi.org/10.1101/cshperspect.a005710>
- Luse, S.A., 1959. The fine structure of the morphogenesis of myelin. *Prog. Neurobiol.* 4, 59–95.
- Lynall, M.-E., Bassett, D.S., Kerwin, R., McKenna, P.J., Kitzbichler, M., Müller, U., Bullmore, E., 2010. Functional connectivity and brain networks in schizophrenia. *J. Neurosci. Off. J. Soc. Neurosci.* 30, 9477–9487. <https://doi.org/10.1523/JNEUROSCI.0333-10.2010>
- Lyons, D.A., Naylor, S.G., Scholze, A., Talbot, W.S., 2009. Kif1b is essential for mRNA localization in oligodendrocytes and development of myelinated axons. *Nat. Genet.* 41, 854–858. <https://doi.org/10.1038/ng.376>
- Ma, L., Rohatgi, R., Kirschner, M.W., 1998. The Arp2/3 complex mediates actin polymerization induced by the small GTP-binding protein Cdc42. *Proc. Natl. Acad. Sci.* 95, 15362–15367. <https://doi.org/10.1073/pnas.95.26.15362>
- Malhotra, D., Sebat, J., 2012. CNVs: Harbingers of a Rare Variant Revolution in Psychiatric Genetics. *Cell* 148, 1223–1241. <https://doi.org/10.1016/j.cell.2012.02.039>
- Marcotrigiano, J., Gingras, A.C., Sonenberg, N., Burley, S.K., 1999. Cap-dependent translation initiation in eukaryotes is regulated by a molecular mimic of eIF4G. *Mol. Cell* 3, 707–716.
- Martin, K.C., Barad, M., Kandel, E.R., 2000. Local protein synthesis and its role in synapse-specific plasticity. *Curr. Opin. Neurobiol.* 10, 587–592. [https://doi.org/10.1016/S0959-4388\(00\)00128-8](https://doi.org/10.1016/S0959-4388(00)00128-8)
- Mauney, S.A., Pietersen, C.Y., Sonntag, K.-C., Woo, T.-U.W., 2015. Differentiation of Oligodendrocyte Precursors is Impaired in the Prefrontal Cortex in Schizophrenia. *Schizophr. Res.* 169, 374–380. <https://doi.org/10.1016/j.schres.2015.10.042>
- Maximov, I.I., Thönneßen, H., Konrad, K., Amort, L., Neuner, I., Shah, N.J., 2015. Statistical Instability of TBSS Analysis Based on DTI Fitting Algorithm. *J. Neuroimaging* 25, 883–891. <https://doi.org/10.1111/jon.12215>
- McCarthy, S.E., McCombie, W.R., Corvin, A., 2014. Unlocking the treasure trove: from genes to schizophrenia biology. *Schizophr. Bull.* 40, 492–496. <https://doi.org/10.1093/schbul/sbu042>

- McIntosh, A.M., Job, D.E., Moorhead, T.W.J., Harrison, L.K., Lawrie, S.M., Johnstone, E.C., 2005. White Matter Density in Patients with Schizophrenia, Bipolar Disorder and Their Unaffected Relatives. *Biol. Psychiatry* 58, 254–257. <https://doi.org/10.1016/j.biopsych.2005.03.044>
- McIntosh, A.M., Muñoz Maniega, S., Lymer, G.K.S., McKirdy, J., Hall, J., Sussmann, J.E.D., Bastin, M.E., Clayden, J.D., Johnstone, E.C., Lawrie, S.M., 2008. White matter tractography in bipolar disorder and schizophrenia. *Biol. Psychiatry* 64, 1088–1092. <https://doi.org/10.1016/j.biopsych.2008.07.026>
- McKenzie, I.A., Ohayon, D., Li, H., Faria, J.P. de, Emery, B., Tohyama, K., Richardson, W.D., 2014. Motor skill learning requires active central myelination. *Science* 346, 318–322. <https://doi.org/10.1126/science.1254960>
- McLaughlin, K., Travers, B.G., Dadalko, O.I., Dean, D.C., Tromp, D., Adluru, N., Destiche, D., Freeman, A., Prigge, M.D., Froehlich, A., Duffield, T.C., Zielinski, B.A., Bigler, E.D., Lange, N., Anderson, J.S., Alexander, A.L., Lainhart, J.E., 2018. Longitudinal development of thalamic and internal capsule microstructure in autism spectrum disorder. *Autism Res. Off. J. Int. Soc. Autism Res.* 11, 450–462. <https://doi.org/10.1002/aur.1909>
- Menjot de Champfleury, N., Lima Maldonado, I., Moritz-Gasser, S., Machi, P., Le Bars, E., Bonafé, A., Duffau, H., 2013. Middle longitudinal fasciculus delineation within language pathways: A diffusion tensor imaging study in human. *Eur. J. Radiol., Special Section: Imaging of the Peripheral Nervous System* 82, 151–157. <https://doi.org/10.1016/j.ejrad.2012.05.034>
- Metzler-Baddeley, C., Foley, S., Santis, S. de, Charron, C., Hampshire, A., Caeyenberghs, K., Jones, D.K., 2017. Dynamics of White Matter Plasticity Underlying Working Memory Training: Multimodal Evidence from Diffusion MRI and Relaxometry. *J. Cogn. Neurosci.* 29, 1509. https://doi.org/10.1162/jocn_a_01127
- Michalski, J.-P., Cummings, S.E., O’Meara, R.W., Kothary, R., 2016. Integrin-linked kinase regulates oligodendrocyte cytoskeleton, growth cone, and adhesion dynamics. *J. Neurochem.* 136, 536–549. <https://doi.org/10.1111/jnc.13446>
- Michalski, J.-P., Kothary, R., 2015. Oligodendrocytes in a Nutshell. *Front. Cell. Neurosci.* 9, 340. <https://doi.org/10.3389/fncel.2015.00340>
- Miki, H., Sasaki, T., Takai, Y., Takenawa, T., 1998. Induction of filopodium formation by a WASP-related actin-depolymerizing protein N-WASP. *Nature* 391, 93. <https://doi.org/10.1038/34208>
- Miller, K.L., Alfaro-Almagro, F., Bangerter, N.K., Thomas, D.L., Yacoub, E., Xu, J., Bartsch, A.J., Jbabdi, S., Sotiropoulos, S.N., Andersson, J.L.R., Griffanti, L., Douaud, G., Okell, T.W., Weale, P., Dragonu, I., Garratt, S., Hudson, S., Collins, R., Jenkinson, M., Matthews, P.M., Smith, S.M., 2016. Multimodal population brain imaging in the UK Biobank prospective epidemiological study. *Nat. Neurosci.* 19, 1523–1536. <https://doi.org/10.1038/nn.4393>

- Mizuno, A., Villalobos, M.E., Davies, M.M., Dahl, B.C., Müller, R.-A., 2006. Partially enhanced thalamocortical functional connectivity in autism. *Brain Res.* 1104, 160–174. <https://doi.org/10.1016/j.brainres.2006.05.064>
- Moldrich, R.X., Pannek, K., Hoch, R., Rubenstein, J.L., Kurniawan, N.D., Richards, L.J., 2010. Comparative mouse brain tractography of diffusion magnetic resonance imaging. *NeuroImage* 51, 1027–1036. <https://doi.org/10.1016/j.neuroimage.2010.03.035>
- Monoranu, C.M., Apfelbacher, M., Grünblatt, E., Puppe, B., Alafuzoff, I., Ferrer, I., Al-Saraj, S., Keyvani, K., Schmitt, A., Falkai, P., Schittenhelm, J., Halliday, G., Kril, J., Harper, C., McLean, C., Riederer, P., Roggendorf, W., 2009. pH measurement as quality control on human post mortem brain tissue: a study of the BrainNet Europe consortium. *Neuropathol. Appl. Neurobiol.* 35, 329–337. <https://doi.org/10.1111/j.1365-2990.2008.01003a.x>
- Mori, S., Crain, B.J., Chacko, V.P., Zijl, P.C.M.V., 1999. Three-dimensional tracking of axonal projections in the brain by magnetic resonance imaging. *Ann. Neurol.* 45, 265–269. [https://doi.org/10.1002/1531-8249\(199902\)45:2<265::AID-ANA21>3.0.CO;2-3](https://doi.org/10.1002/1531-8249(199902)45:2<265::AID-ANA21>3.0.CO;2-3)
- Mori, S., Wakana, S., Zijl, P.C.M. van, Nage-Poetscher, L.M., 2005. *MRI Atlas of Human White Matter*. Elsevier.
- Morris, C.A., Demsey, S.A., Leonard, C.O., Dilts, C., Blackburn, B.L., 1988. Natural history of Williams syndrome: Physical characteristics. *J. Pediatr.* 113, 318–326. [https://doi.org/10.1016/S0022-3476\(88\)80272-5](https://doi.org/10.1016/S0022-3476(88)80272-5)
- Morrow, E.M., 2010. Genomic Copy Number Variation in Disorders of Cognitive Development. *J. Am. Acad. Child Adolesc. Psychiatry* 49, 1091–1104. <https://doi.org/10.1016/j.jaac.2010.08.009>
- Mukai, J., Dhillia, A., Drew, L.J., Stark, K.L., Cao, L., MacDermott, A.B., Karayiorgou, M., Gogos, J.A., 2008. Palmitoylation-dependent neurodevelopmental deficits in a mouse model of 22q11 microdeletion. *Nat. Neurosci.* 11, 1302–1310. <https://doi.org/10.1038/nn.2204>
- Müller, C., Bauer, N.M., Schäfer, I., White, R., 2013. Making myelin basic protein -from mRNA transport to localized translation. *Front. Cell. Neurosci.* 7. <https://doi.org/10.3389/fncel.2013.00169>
- Murphy, S.M., Preble, A.M., Patel, U.K., O'Connell, K.L., Dias, D.P., Moritz, M., Agard, D., Stults, J.T., Stearns, T., 2001. GCP5 and GCP6: Two New Members of the Human γ -Tubulin Complex. *Mol. Biol. Cell* 12, 3340–3352.
- Murthy, S.K., Nygren, A.O.H., Shakankiry, H.M.E., Schouten, J.P., Khayat, A.I.A., Ridha, A., Ali, M.T.A., 2007. Detection of a novel familial deletion of four genes between BP1 and BP2 of the Prader-Willi/Angelman syndrome critical region by oligo-array CGH in a child with neurological disorder and speech impairment. *Cytogenet. Genome Res.* 116, 135–140. <https://doi.org/10.1159/000097433>

- Nakahata, Y., Yasuda, R., 2018. Plasticity of Spine Structure: Local Signaling, Translation and Cytoskeletal Reorganization. *Front. Synaptic Neurosci.* 10. <https://doi.org/10.3389/fnsyn.2018.00029>
- Nakai, N., Takumi, T., Nakai, J., Sato, M., 2018. Common Defects of Spine Dynamics and Circuit Function in Neurodevelopmental Disorders: A Systematic Review of Findings From in Vivo Optical Imaging of Mouse Models. *Front. Neurosci.* 12. <https://doi.org/10.3389/fnins.2018.00412>
- Nakatani, J., Tamada, K., Hatanaka, F., Ise, S., Ohta, H., Inoue, K., Tomonaga, S., Watanabe, Y., Chung, Y.J., Banerjee, R., Iwamoto, K., Kato, T., Okazawa, M., Yamauchi, K., Tanda, K., Takao, K., Miyakawa, T., Bradley, A., Takumi, T., 2009. Abnormal Behavior in a Chromosome- Engineered Mouse Model for Human 15q11-13 Duplication Seen in Autism. *Cell* 137, 1235–1246. <https://doi.org/10.1016/j.cell.2009.04.024>
- Napoli, I., Mercaldo, V., Boyl, P.P., Eleuteri, B., Zalfa, F., Di Marino, D., Mohr, E., Massimi, M., Falconi, M., Witke, W., Costa-Mattioli, M., Sonenberg, N., Achsel, T., Bagni, C., 2008. The fragile X syndrome protein represses activity-dependent translation through CYFIP1, a new 4E-BP. *Cell* 134, 1042–1054. <https://doi.org/10.1016/j.cell.2008.07.031>
- Narayan, S., Kass, K.E., Thomas, E.A., 2007. Chronic haloperidol treatment results in a decrease in the expression of myelin/oligodendrocyte-related genes in the mouse brain. *J. Neurosci. Res.* 85, 757–765. <https://doi.org/10.1002/jnr.21161>
- Nave, K.-A., 2010. Myelination and support of axonal integrity by glia. *Nature* 468, 244–252. <https://doi.org/10.1038/nature09614>
- Nawaz, S., Sánchez, P., Schmitt, S., Snaidero, N., Mitkovski, M., Velte, C., Brückner, B.R., Alexopoulos, I., Czopka, T., Jung, S.Y., Rhee, J.S., Janshoff, A., Witke, W., Schaap, I.A.T., Lyons, D.A., Simons, M., 2015. Actin filament turnover drives leading edge growth during myelin sheath formation in the central nervous system. *Dev. Cell* 34, 139–151. <https://doi.org/10.1016/j.devcel.2015.05.013>
- Nebel, R.A., Zhao, D., Pedrosa, E., Kirschen, J., Lachman, H.M., Zheng, D., Abrahams, B.S., 2016. Reduced CYFIP1 in Human Neural Progenitors Results in Dysregulation of Schizophrenia and Epilepsy Gene Networks. *PLOS ONE* 11, e0148039. <https://doi.org/10.1371/journal.pone.0148039>
- Need, A.C., Ge, D., Weale, M.E., Maia, J., Feng, S., Heinzen, E.L., Shianna, K.V., Yoon, W., Kasperavičiūtė, D., Gennarelli, M., Strittmatter, W.J., Bonvicini, C., Rossi, G., Jayathilake, K., Cola, P.A., McEvoy, J.P., Keefe, R.S.E., Fisher, E.M.C., Jean, P.L.S., Giegling, I., Hartmann, A.M., Möller, H.-J., Ruppert, A., Fraser, G., Crombie, C., Middleton, L.T., Clair, D.S., Roses, A.D., Muglia, P., Francks, C., Rujescu, D., Meltzer, H.Y., Goldstein, D.B., 2009. A Genome-Wide Investigation of SNPs and CNVs in Schizophrenia. *PLOS Genet.* 5, e1000373. <https://doi.org/10.1371/journal.pgen.1000373>
- Nelson, J.C., Stavoe, A.K.H., Colón-Ramos, D.A., 2013. The actin cytoskeleton in presynaptic assembly. *Cell Adhes. Migr.* 7, 379–387. <https://doi.org/10.4161/cam.24803>

- Nielsen, J., Fejgin, K., Sotty, F., Nielsen, V., Mørk, A., Christoffersen, C.T., Yavich, L., Lauridsen, J.B., Clausen, D., Larsen, P.H., Egebjerg, J., Werge, T.M., Kallunki, P., Christensen, K.V., Didriksen, M., 2017. A mouse model of the schizophrenia-associated 1q21.1 microdeletion syndrome exhibits altered mesolimbic dopamine transmission. *Transl. Psychiatry* 7, 1–12. <https://doi.org/10.1038/s41398-017-0011-8>
- Niemi, M.E.K., Martin, H.C., Rice, D.L., Gallone, G., Gordon, S., Kelemen, M., McAloney, K., McRae, J., Radford, E.J., Yu, S., Gecz, J., Martin, N.G., Wright, C.F., Fitzpatrick, D.R., Firth, H.V., Hurles, M.E., Barrett, J.C., 2018. Common genetic variants contribute to risk of rare severe neurodevelopmental disorders. *Nature* 562, 268. <https://doi.org/10.1038/s41586-018-0566-4>
- Nilsson, S.R., Fejgin, K., Gastambide, F., Vogt, M.A., Kent, B.A., Nielsen, V., Nielsen, J., Gass, P., Robbins, T.W., Saksida, L.M., Stensbøl, T.B., Tricklebank, M.D., Didriksen, M., Bussey, T.J., 2016. Assessing the Cognitive Translational Potential of a Mouse Model of the 22q11.2 Microdeletion Syndrome. *Cereb. Cortex N. Y. N* 1991 26, 3991–4003. <https://doi.org/10.1093/cercor/bhw229>
- Nilsson, S.R.O., Celada, P., Fejgin, K., Thelin, J., Nielsen, J., Santana, N., Heath, C.J., Larsen, P.H., Nielsen, V., Kent, B.A., Saksida, L.M., Stensbøl, T.B., Robbins, T.W., Bastlund, J.F., Bussey, T.J., Artigas, F., Didriksen, M., 2016. A mouse model of the 15q13.3 microdeletion syndrome shows prefrontal neurophysiological dysfunctions and attentional impairment. *Psychopharmacology (Berl.)* 233, 2151–2163. <https://doi.org/10.1007/s00213-016-4265-2>
- Nimchinsky, E.A., Oberlander, A.M., Svoboda, K., 2001. Abnormal development of dendritic spines in FMR1 knock-out mice. *J. Neurosci. Off. J. Soc. Neurosci.* 21, 5139–5146.
- Nishiyama, T., Sasaki, T., Takaishi, K., Kato, M., Yaku, H., Araki, K., Matsuura, Y., Takai, Y., 1994. rac p21 is involved in insulin-induced membrane ruffling and rho p21 is involved in hepatocyte growth factor- and 12-O-tetradecanoylphorbol-13-acetate (TPA)-induced membrane ruffling in KB cells. *Mol. Cell. Biol.* 14, 2447–2456.
- Nuninga, J.O., Bohlken, M.M., Koops, S., Fiksinski, A.M., Mandl, R.C.W., Breetvelt, E.J., Duijff, S.N., Kahn, R.S., Sommer, I.E.C., Vorstman, J.A.S., 2018. White matter abnormalities in 22q11.2 deletion syndrome patients showing cognitive decline. *Psychol. Med.* 48, 1655–1663. <https://doi.org/10.1017/S0033291717003142>
- Oguro-Ando, A., Rosensweig, C., Herman, E., Nishimura, Y., Werling, D., Bill, B.R., Berg, J.M., Gao, F., Coppola, G., Abrahams, B.S., Geschwind, D.H., 2015. Increased CYFIP1 dosage alters cellular and dendritic morphology and dysregulates mTOR. *Mol. Psychiatry* 20, 1069–1078. <https://doi.org/10.1038/mp.2014.124>
- Olszewski, A.K., Kikinis, Z., Gonzalez, C.S., Coman, I.L., Makris, N., Gong, X., Rathi, Y., Zhu, A., Antshel, K.M., Fremont, W., Kubicki, M.R., Bouix, S., Shenton, M.E., Kates, W.R., 2017. The social brain network in 22q11.2 deletion syndrome:

- a diffusion tensor imaging study. *Behav. Brain Funct. BBF* 13. <https://doi.org/10.1186/s12993-017-0122-7>
- O'Meara, R.W., Michalski, J.-P., Anderson, C., Bhanot, K., Rippstein, P., Kothary, R., 2013. Integrin-Linked Kinase Regulates Process Extension in Oligodendrocytes via Control of Actin Cytoskeletal Dynamics. *J. Neurosci.* 33, 9781–9793. <https://doi.org/10.1523/JNEUROSCI.5582-12.2013>
- Omotade, O.F., Pollitt, S.L., Zheng, J.Q., 2017. Actin-based growth cone motility and guidance. *Mol. Cell. Neurosci., Cytoskeleton-dependent regulation of neuronal network formation* 84, 4–10. <https://doi.org/10.1016/j.mcn.2017.03.001>
- Osterweil, E.K., 2019. Upsetting the excitatory-inhibitory balance hypothesis of autism. *Sci. Transl. Med.* 11, eaax2730. <https://doi.org/10.1126/scitranslmed.aax2730>
- Owen, M.J., Craddock, N., O'Donovan, M.C., 2010. Suggestion of Roles for Both Common and Rare Risk Variants in Genome-wide Studies of Schizophrenia. *Arch. Gen. Psychiatry* 67, 667–673. <https://doi.org/10.1001/archgenpsychiatry.2010.69>
- Owen, M.J., O'Donovan, M.C., 2017. Schizophrenia and the neurodevelopmental continuum:evidence from genomics. *World Psychiatry Off. J. World Psychiatr. Assoc. WPA* 16, 227–235. <https://doi.org/10.1002/wps.20440>
- Ozalay, O., Calli, C., Kitis, O., Cagdas Eker, M., Donat Eker, O., Ozan, E., Coburn, K., Saffet Gonul, A., 2013. The relationship between the anterior corpus callosum size and prefrontal cortex volume in drug-free depressed patients. *J. Affect. Disord.* 146, 281–285. <https://doi.org/10.1016/j.jad.2012.06.040>
- Pacey, L.K.K., Xuan, I.C.Y., Guan, S., Sussman, D., Henkelman, R.M., Chen, Y., Thomsen, C., Hampson, D.R., 2013. Delayed myelination in a mouse model of fragile X syndrome. *Hum. Mol. Genet.* 22, 3920–3930. <https://doi.org/10.1093/hmg/ddt246>
- Palframan, D., 1997. Multi-axial Classification of Child and Adolescent Psychiatric Disorders. *J. Psychiatry Neurosci.* 22, 341–342.
- Pathania, M., Davenport, E.C., Muir, J., Sheehan, D.F., López-Doménech, G., Kittler, J.T., 2014. The autism and schizophrenia associated gene CYFIP1 is critical for the maintenance of dendritic complexity and the stabilization of mature spines. *Transl. Psychiatry* 4, e374. <https://doi.org/10.1038/tp.2014.16>
- Pedraza, L., Huang, J.K., Colman, D., 2009. Disposition of axonal caspr with respect to glial cell membranes: Implications for the process of myelination. *J. Neurosci. Res.* 87, 3480–3491. <https://doi.org/10.1002/jnr.22004>
- Peltonen, L., Palotie, A., Lange, K., 2000. Use of population isolates for mapping complex traits. *Nat. Rev. Genet.* 1, 182. <https://doi.org/10.1038/35042049>
- Pergola, G., Selvaggi, P., Trizio, S., Bertolino, A., Blasi, G., 2015. The role of the thalamus in schizophrenia from a neuroimaging perspective. *Neurosci. Biobehav.*

- Peters, L., Bulthé, J., Daniels, N., Op de Beeck, H., De Smedt, B., 2018. Dyscalculia and dyslexia: Different behavioral, yet similar brain activity profiles during arithmetic. *NeuroImage Clin.* 18, 663–674.
<https://doi.org/10.1016/j.nicl.2018.03.003>
- Pierpaoli, C., Basser, P.J., 1996. Toward a quantitative assessment of diffusion anisotropy. *Magn. Reson. Med.* 36, 893–906.
- Pierpaoli, C., Jezzard, P., Basser, P.J., Barnett, A., Di Chiro, G., 1996. Diffusion tensor MR imaging of the human brain. *Radiology* 201, 637–648.
<https://doi.org/10.1148/radiology.201.3.8939209>
- Pinto, D., Marshall, C., Feuk, L., Scherer, S.W., 2007. Copy-number variation in control population cohorts. *Hum. Mol. Genet.* 16, R168–R173.
<https://doi.org/10.1093/hmg/ddm241>
- Pollard, T.D., Borisy, G.G., 2003. Cellular Motility Driven by Assembly and Disassembly of Actin Filaments. *Cell* 112, 453–465.
[https://doi.org/10.1016/S0092-8674\(03\)00120-X](https://doi.org/10.1016/S0092-8674(03)00120-X)
- Powell, S.K., Gregory, J., Akbarian, S., Brennand, K.J., 2017. Application of CRISPR/Cas9 to the Study of Brain Development and Neuropsychiatric Disease. *Mol. Cell. Neurosci.* 82, 157–166. <https://doi.org/10.1016/j.mcn.2017.05.007>
- Prabakaran, S., Swatton, J.E., Ryan, M.M., Huffaker, S.J., Huang, J.T.-J., Griffin, J.L., Wayland, M., Freeman, T., Dudbridge, F., Lilley, K.S., Karp, N.A., Hester, S., Tkachev, D., Mimmack, M.L., Yolken, R.H., Webster, M.J., Torrey, E.F., Bahn, S., 2004. Mitochondrial dysfunction in schizophrenia: evidence for compromised brain metabolism and oxidative stress. *Mol. Psychiatry* 9, 684–697, 643.
<https://doi.org/10.1038/sj.mp.4001511>
- Prigge, M.B.D., Lange, N., Bigler, E.D., Merkle, T.L., Neeley, E.S., Abildskov, T.J., Froehlich, A.L., Nielsen, J.A., Cooperrider, J.R., Cariello, A.N., Ravichandran, C., Alexander, A.L., Lainhart, J.E., 2013. Corpus Callosum Area in Children and Adults with Autism. *Res. Autism Spectr. Disord.* 7, 221–234.
<https://doi.org/10.1016/j.rasd.2012.09.007>
- Puig, J., Pedraza, S., Blasco, G., Daunis-i-Estadella, J., Prados, F., Remollo, S., Prats-Galino, A., Soria, G., Boada, I., Castellanos, M., Serena, J., 2011. Acute Damage to the Posterior Limb of the Internal Capsule on Diffusion Tensor Tractography as an Early Imaging Predictor of Motor Outcome after Stroke. *Am. J. Neuroradiol.* 32, 857–863. <https://doi.org/10.3174/ajnr.A2400>
- Pujana, M.A., Nadal, M., Guitart, M., Armengol, L., Gratacòs, M., Estivill, X., 2002. Human chromosome 15q11-q14 regions of rearrangements contain clusters of LCR15 duplicons. *Eur. J. Hum. Genet.* 10, 26.
<https://doi.org/10.1038/sj.ejhg.5200760>

- Purcell, S.M., Moran, J.L., Fromer, M., Ruderfer, D., Solovieff, N., Roussos, P., O'Dushlaine, C., Chambert, K., Bergen, S.E., Kähler, A., Duncan, L., Stahl, E., Genovese, G., Fernández, E., Collins, M.O., Komiyama, N.H., Choudhary, J.S., Magnusson, P.K.E., Banks, E., Shakir, K., Garimella, K., Fennell, T., DePristo, M., Grant, S.G.N., Haggarty, S.J., Gabriel, S., Scolnick, E.M., Lander, E.S., Hultman, C.M., Sullivan, P.F., McCarroll, S.A., Sklar, P., 2014. A polygenic burden of rare disruptive mutations in schizophrenia. *Nature* 506, 185–190. <https://doi.org/10.1038/nature12975>
- Putnam, M.C., Wig, G.S., Grafton, S.T., Kelley, W.M., Gazzaniga, M.S., 2008. Structural Organization of the Corpus Callosum Predicts the Extent and Impact of Cortical Activity in the Nondominant Hemisphere. *J. Neurosci.* 28, 2912–2918. <https://doi.org/10.1523/JNEUROSCI.2295-07.2008>
- Rainier, S., Chai, J.-H., Tokarz, D., Nicholls, R.D., Fink, J.K., 2003. NIPA1 gene mutations cause autosomal dominant hereditary spastic paraplegia (SPG6). *Am. J. Hum. Genet.* 73, 967–971. <https://doi.org/10.1086/378817>
- Raybaud, C., 2010. The corpus callosum, the other great forebrain commissures, and the septum pellucidum: anatomy, development, and malformation. *Neuroradiology* 52, 447–477. <https://doi.org/10.1007/s00234-010-0696-3>
- Raynaud-Messina, B., Merdes, A., 2007. Gamma-tubulin complexes and microtubule organization. *Curr. Opin. Cell Biol.* 19, 24–30. <https://doi.org/10.1016/j.ceb.2006.12.008>
- Readhead, C., Hood, L., 1990. The dysmyelinating mouse mutations shiverer (shi) and myelin deficient (shimld). *Behav. Genet.* 20, 213–234.
- Readhead, C., Popko, B., Takahashi, N., Shine, H.D., Saavedra, R.A., Sidman, R.L., Hood, L., 1987. Expression of a myelin basic protein gene in transgenic shiverer mice: correction of the dysmyelinating phenotype. *Cell* 48, 703–712. [https://doi.org/10.1016/0092-8674\(87\)90248-0](https://doi.org/10.1016/0092-8674(87)90248-0)
- Redon, R., Ishikawa, S., Fitch, K.R., Feuk, L., Perry, G.H., Andrews, T.D., Fiegler, H., Shapero, M.H., Carson, A.R., Chen, W., Cho, E.K., Dallaire, S., Freeman, J.L., González, J.R., Gratacòs, M., Huang, J., Kalaitzopoulos, D., Komura, D., MacDonald, J.R., Marshall, C.R., Mei, R., Montgomery, L., Nishimura, K., Okamura, K., Shen, F., Somerville, M.J., Tchinda, J., Valsesia, A., Woodwark, C., Yang, F., Zhang, Junjun, Zerjal, T., Zhang, Jane, Armengol, L., Conrad, D.F., Estivill, X., Tyler-Smith, C., Carter, N.P., Aburatani, H., Lee, C., Jones, K.W., Scherer, S.W., Hurles, M.E., 2006. Global variation in copy number in the human genome. *Nature* 444, 444. <https://doi.org/10.1038/nature05329>
- Rees, E., Kendall, K., Pardiñas, A.F., Legge, S.E., Pocklington, A., Escott-Price, V., MacCabe, J.H., Collier, D.A., Holmans, P., O'Donovan, M.C., Owen, M.J., Walters, J.T.R., Kirov, G., 2016. Analysis of Intellectual Disability Copy Number Variants for Association With Schizophrenia. *JAMA Psychiatry* 73, 963–969. <https://doi.org/10.1001/jamapsychiatry.2016.1831>

- Rees, E., O'Donovan, M.C., Owen, M.J., 2015. Genetics of schizophrenia. *Curr. Opin. Behav. Sci., Behavioral genetics* 2, 8–14. <https://doi.org/10.1016/j.cobeha.2014.07.001>
- Rees, E., Walters, J.T.R., Georgieva, L., Isles, A.R., Chambert, K.D., Richards, A.L., Mahoney-Davies, G., Legge, S.E., Moran, J.L., McCarroll, S.A., O'Donovan, M.C., Owen, M.J., Kirov, G., 2014. Analysis of copy number variations at 15 schizophrenia-associated loci. *Br. J. Psychiatry* 204, 108–114. <https://doi.org/10.1192/bjp.bp.113.131052>
- Richter, J.D., Bassell, G.J., Klann, E., 2015. Dysregulation and restoration of translational homeostasis in fragile X syndrome. *Nat. Rev. Neurosci.* 16, 595–605. <https://doi.org/10.1038/nrn4001>
- Richter, J.D., Sonenberg, N., 2005. Regulation of cap-dependent translation by eIF4E inhibitory proteins. *Nature* 433, 477–480. <https://doi.org/10.1038/nature03205>
- Ridley, A.J., Hall, A., 1992. The small GTP-binding protein rho regulates the assembly of focal adhesions and actin stress fibers in response to growth factors. *Cell* 70, 389–399. [https://doi.org/10.1016/0092-8674\(92\)90163-7](https://doi.org/10.1016/0092-8674(92)90163-7)
- Ridley, A.J., Paterson, H.F., Johnston, C.L., Diekmann, D., Hall, A., 1992. The small GTP-binding protein rac regulates growth factor-induced membrane ruffling. *Cell* 70, 401–410. [https://doi.org/10.1016/0092-8674\(92\)90164-8](https://doi.org/10.1016/0092-8674(92)90164-8)
- Ripke, S., O'Dushlaine, C., Chambert, K., Moran, J.L., Kähler, A.K., Akterin, S., Bergen, S.E., Collins, A.L., Crowley, J.J., Fromer, M., Kim, Y., Lee, S.H., Magnusson, P.K.E., Sanchez, N., Stahl, E.A., Williams, S., Wray, N.R., Xia, K., Bettella, F., Borglum, A.D., Bulik-Sullivan, B.K., Cormican, P., Craddock, N., de Leeuw, C., Durmishi, N., Gill, M., Golimbet, V., Hamshere, M.L., Holmans, P., Hougaard, D.M., Kendler, K.S., Lin, K., Morris, D.W., Mors, O., Mortensen, P.B., Neale, B.M., O'Neill, F.A., Owen, M.J., Milovancevic, M.P., Posthuma, D., Powell, J., Richards, A.L., Riley, B.P., Ruderfer, D., Rujescu, D., Sigurdsson, E., Silagadze, T., Smit, A.B., Stefansson, H., Steinberg, S., Suvisaari, J., Tosato, S., Verhage, M., Walters, J.T., Multicenter Genetic Studies of Schizophrenia Consortium, Levinson, D.F., Gejman, P.V., Kendler, K.S., Laurent, C., Mowry, B.J., O'Donovan, M.C., Owen, M.J., Pulver, A.E., Riley, B.P., Schwab, S.G., Wildenauer, D.B., Dudbridge, F., Holmans, P., Shi, J., Albus, M., Alexander, M., Campion, D., Cohen, D., Dikeos, D., Duan, J., Eichhammer, P., Godard, S., Hansen, M., Lerer, F.B., Liang, K.-Y., Maier, W., Mallet, J., Nertney, D.A., Nestadt, G., Norton, N., O'Neill, F.A., Papadimitriou, G.N., Ribble, R., Sanders, A.R., Silverman, J.M., Walsh, D., Williams, N.M., Wormley, B., Psychosis Endophenotypes International Consortium, Arranz, M.J., Bakker, S., Bender, S., Bramon, E., Collier, D., Crespo-Facorro, B., Hall, J., Iyegbe, C., Jablensky, A., Kahn, R.S., Kalaydjieva, L., Lawrie, S., Lewis, C.M., Lin, K., Linszen, D.H., Mata, I., McIntosh, A., Murray, R.M., Ophoff, R.A., Powell, J., Rujescu, D., Van Os, J., Walshe, M., Weisbrod, M., Wiersma, D., Wellcome Trust Case Control Consortium 2, Bramon, E., Corvin, A.P., O'Donovan, M.C., Stefansson, K., Scolnick, E., Purcell, S., McCarroll, S.A., Sklar, P., Hultman, C.M., Sullivan, P.F., 2013. Genome-wide association analysis identifies 13 new risk loci for schizophrenia. *Nat. Genet.* 45, 1150–1159. <https://doi.org/10.1038/ng.2742>

- Rodrigues, G.M.C., Gaj, T., Adil, M.M., Wahba, J., Rao, A.T., Lorbeer, F.K., Kulkarni, R.U., Diogo, M.M., Cabral, J.M.S., Miller, E.W., Hockemeyer, D., Schaffer, D.V., 2017. Defined and Scalable Differentiation of Human Oligodendrocyte Precursors from Pluripotent Stem Cells in a 3D Culture System. *Stem Cell Rep.* 8, 1770–1783. <https://doi.org/10.1016/j.stemcr.2017.04.027>
- Ross, R.G., Stevens, K.E., Proctor, W.R., Leonard, S., Kisley, M.A., Hunter, S.K., Freedman, R., Adams, C.E., 2010. Research Review: Cholinergic mechanisms, early brain development, and risk for schizophrenia. *J. Child Psychol. Psychiatry* 51, 535–549. <https://doi.org/10.1111/j.1469-7610.2009.02187.x>
- Rotarska-Jagiela, A., Oertel-Knoechel, V., DeMartino, F., van de Ven, V., Formisano, E., Roebroek, A., Rami, A., Schoenmeyer, R., Haenschel, C., Hendler, T., Maurer, K., Vogeley, K., Linden, D.E.J., 2009. Anatomical brain connectivity and positive symptoms of schizophrenia: A diffusion tensor imaging study. *Psychiatry Res. Neuroimaging* 174, 9–16. <https://doi.org/10.1016/j.psychresns.2009.03.002>
- Roussos, P., Haroutunian, V., 2014. Schizophrenia: susceptibility genes and oligodendroglial and myelin related abnormalities. *Front. Cell. Neurosci.* 8. <https://doi.org/10.3389/fncel.2014.00005>
- Sagi, Y., Tavor, I., Hofstetter, S., Tzur-Moryosef, S., Blumenfeld-Katzir, T., Assaf, Y., 2012. Learning in the Fast Lane: New Insights into Neuroplasticity. *Neuron* 73, 1195–1203. <https://doi.org/10.1016/j.neuron.2012.01.025>
- Sahoo, P.K., Smith, D.S., Perrone-Bizzozero, N., Twiss, J.L., 2018. Axonal mRNA transport and translation at a glance. *J. Cell Sci.* 131, jcs196808. <https://doi.org/10.1242/jcs.196808>
- Sahoo, T., Bacino, C.A., German, J.R., Shaw, C.A., Bird, L.M., Kimonis, V., Anselm, I., Waisbren, S., Beaudet, A.L., Peters, S.U., 2007. Identification of novel deletions of 15q11q13 in Angelman syndrome by array-CGH: molecular characterization and genotype-phenotype correlations. *Eur. J. Hum. Genet. EJHG* 15, 943–949. <https://doi.org/10.1038/sj.ejhg.5201859>
- Sale, A., Berardi, N., Maffei, L., 2014. Environment and Brain Plasticity: Towards an Endogenous Pharmacotherapy. *Physiol. Rev.* 94, 189–234. <https://doi.org/10.1152/physrev.00036.2012>
- Sampaio-Baptista, C., Khrapitchev, A.A., Foxley, S., Schlagheck, T., Scholz, J., Jbabdi, S., DeLuca, G.C., Miller, K.L., Taylor, A., Thomas, N., Kleim, J., Sibson, N.R., Bannerman, D., Johansen-Berg, H., 2013. Motor Skill Learning Induces Changes in White Matter Microstructure and Myelination. *J. Neurosci.* 33, 19499–19503. <https://doi.org/10.1523/JNEUROSCI.3048-13.2013>
- Satterthwaite, T.D., Wolf, D.H., Calkins, M.E., Vandekar, S.N., Erus, G., Ruparel, K., Roalf, D.R., Linn, K.A., Elliott, M.A., Moore, T.M., Hakonarson, H., Shinohara, R.T., Davatzikos, C., Gur, R.C., Gur, R.E., 2016. Structural Brain Abnormalities in Youth With Psychosis Spectrum Symptoms. *JAMA Psychiatry* 73, 515–524. <https://doi.org/10.1001/jamapsychiatry.2015.3463>

- Scamvougeras, A., Kigar, D.L., Jones, D., Weinberger, D.R., Witelson, S.F., 2003. Size of the human corpus callosum is genetically determined: an MRI study in mono and dizygotic twins. *Neurosci. Lett.* 338, 91–94. [https://doi.org/10.1016/S0304-3940\(02\)01333-2](https://doi.org/10.1016/S0304-3940(02)01333-2)
- Schenck, A., Bardoni, B., Langmann, C., Harden, N., Mandel, J.-L., Giangrande, A., 2003. CYFIP/Sra-1 Controls Neuronal Connectivity in *Drosophila* and Links the Rac1 GTPase Pathway to the Fragile X Protein. *Neuron* 38, 887–898. [https://doi.org/10.1016/S0896-6273\(03\)00354-4](https://doi.org/10.1016/S0896-6273(03)00354-4)
- Schenck, A., Bardoni, B., Moro, A., Bagni, C., Mandel, J.-L., 2001. A highly conserved protein family interacting with the fragile X mental retardation protein (FMRP) and displaying selective interactions with FMRP-related proteins FXR1P and FXR2P. *Proc. Natl. Acad. Sci.* 98, 8844–8849. <https://doi.org/10.1073/pnas.151231598>
- Schoenbaum, G., Nugent, S.L., Saddoris, M.P., Setlow, B., 2002. Orbitofrontal lesions in rats impair reversal but not acquisition of go, no-go odor discriminations. *Neuroreport* 13, 885–890.
- Schuetze, M., Park, M.T.M., Cho, I.Y., MacMaster, F.P., Chakravarty, M.M., Bray, S.L., 2016. Morphological Alterations in the Thalamus, Striatum, and Pallidum in Autism Spectrum Disorder. *Neuropsychopharmacology* 41, 2627–2637. <https://doi.org/10.1038/npp.2016.64>
- Sebat, J., Lakshmi, B., Troge, J., Alexander, J., Young, J., Lundin, P., Månér, S., Massa, H., Walker, M., Chi, M., Navin, N., Lucito, R., Healy, J., Hicks, J., Ye, K., Reiner, A., Gilliam, T.C., Trask, B., Patterson, N., Zetterberg, A., Wigler, M., 2004. Large-Scale Copy Number Polymorphism in the Human Genome. *Science* 305, 525–528. <https://doi.org/10.1126/science.1098918>
- Sellgren, C.M., Gracias, J., Watmuff, B., Biag, J.D., Thanos, J.M., Whittredge, P.B., Fu, T., Worringer, K., Brown, H.E., Wang, J., Kaykas, A., Karmacharya, R., Goold, C.P., Sheridan, S.D., Perlis, R.H., 2019. Increased synapse elimination by microglia in schizophrenia patient-derived models of synaptic pruning. *Nat. Neurosci.* 22, 374–385. <https://doi.org/10.1038/s41593-018-0334-7>
- Seok, J.-H., Park, H.-J., Chun, J.-W., Lee, S.-K., Cho, H.S., Kwon, J.S., Kim, J.-J., 2007. White matter abnormalities associated with auditory hallucinations in schizophrenia: A combined study of voxel-based analyses of diffusion tensor imaging and structural magnetic resonance imaging. *Psychiatry Res. Neuroimaging* 156, 93–104. <https://doi.org/10.1016/j.psychres.2007.02.002>
- Sheehan, D.V., Lecrubier, Y., Sheehan, K.H., Amorim, P., Janavs, J., Weiller, E., Hergueta, T., Baker, R., Dunbar, G.C., 1998. The Mini-International Neuropsychiatric Interview (M.I.N.I.): the development and validation of a structured diagnostic psychiatric interview for DSM-IV and ICD-10. *J. Clin. Psychiatry* 59 Suppl 20, 22-33;quiz 34-57.
- Shergill, S.S., Kanaan, R.A., Chitnis, X.A., O'Daly, O., Jones, D.K., Frangou, S., Williams, S.C.R., Howard, R.J., Barker, G.J., Murray, R.M., McGuire, P., 2007.

- A Diffusion Tensor Imaging Study of Fasciculi in Schizophrenia. *Am. J. Psychiatry* 164, 467–473. <https://doi.org/10.1176/ajp.2007.164.3.467>
- Sherman, D.L., Brophy, P.J., 2005. Mechanisms of axon ensheathment and myelin growth. *Nat. Rev. Neurosci.* 6, 683. <https://doi.org/10.1038/nrn1743>
- Shi, Y., Alin, K., Goff, S.P., 1995. Abl-interactor-1, a novel SH3 protein binding to the carboxy-terminal portion of the Abl protein, suppresses v-abl transforming activity. *Genes Dev.* 9, 2583–2597. <https://doi.org/10.1101/gad.9.21.2583>
- Shi, Y., Toga, A.W., 2017. Connectome imaging for mapping human brain pathways. *Mol. Psychiatry* 22, 1230–1240. <https://doi.org/10.1038/mp.2017.92>
- Shibata, S., Yasuda, A., Renault-Mihara, F., Suyama, S., Katoh, H., Inoue, T., Inoue, Y.U., Nagoshi, N., Sato, M., Nakamura, M., Akazawa, C., Okano, H., 2010. Sox10- Venus mice: a new tool for real-time labeling of neural crest lineage cells and oligodendrocytes. *Mol. Brain* 3, 31. <https://doi.org/10.1186/1756-6606-3-31>
- Shinawi, M., Liu, P., Kang, S.-H.L., Shen, J., Belmont, J.W., Scott, D.A., Probst, F.J., Craigen, W.J., Graham, B.H., Pursley, A., Clark, G., Lee, J., Proud, M., Stocco, A., Rodriguez, D.L., Kozel, B.A., Sparagana, S., Roeder, E.R., McGrew, S.G., Kurczynski, T.W., Allison, L.J., Amato, S., Savage, S., Patel, A., Stankiewicz, P., Beaudet, A.L., Cheung, S.W., Lupski, J.R., 2010. Recurrent reciprocal 16p11.2 rearrangements associated with global developmental delay, behavioural problems, dysmorphism, epilepsy, and abnormal head size. *J. Med. Genet.* 47, 332–341. <https://doi.org/10.1136/jmg.2009.073015>
- Shukla, D.K., Keehn, B., Lincoln, A.J., Müller, R.-A., 2010. White matter compromise of callosal and subcortical fiber tracts in children with autism spectrum disorder: a diffusion tensor imaging study. *J. Am. Acad. Child Adolesc. Psychiatry* 49, 1269–1278, 1278.e1–2. <https://doi.org/10.1016/j.jaac.2010.08.018>
- Sierra, A., Laitinen, T., Lehtimäki, K., Rieppo, L., Pitkänen, A., Gröhn, O., 2011. Diffusion tensor MRI with tract-based spatial statistics and histology reveals undiscovered lesioned areas in kainate model of epilepsy in rat. *Brain Struct. Funct.* 216, 123–135. <https://doi.org/10.1007/s00429-010-0299-0>
- Sigurdsson, T., Stark, K.L., Karayiorgou, M., Gogos, J.A., Gordon, J.A., 2010. Impaired hippocampal–prefrontal synchrony in a genetic mouse model of schizophrenia. *Nature* 464, 763–767. <https://doi.org/10.1038/nature08855>
- Silbersweig, D.A., Rauch, S.L., 2017. Neuroimaging in Psychiatry: A Quarter Century of Progress. *Harv. Rev. Psychiatry* 25, 195. <https://doi.org/10.1097/HRP.000000000000177>
- Silva, A.I., Haddon, J.E., Syed, Y.A., Trent, S., Lin, T.-C.E., Patel, Y., Carter, J., Haan, N., Honey, R.C., Humby, T., Assaf, Y., Owen, M.J., Linden, D.E.J., Hall, J., Wilkinson, L.S., 2019a. Cyfip1 haploinsufficient rats show white matter changes, myelin thinning, abnormal oligodendrocytes and behavioural inflexibility. *Nat. Commun.* 10, 1–13. <https://doi.org/10.1038/s41467-019-11119-7>

- Silva, A.I., Ulfarsson, M.O., Stefansson, H., Gustafsson, O., Walters, G.B., Linden, D.E.J., Wilkinson, L.S., Drakesmith, M., Owen, M.J., Hall, J., Stefansson, K., 2019b. Reciprocal White Matter Changes Associated With Copy Number Variation at 15q11.2 BP1-BP2: A Diffusion Tensor Imaging Study. *Biol. Psychiatry* 85, 563–572. <https://doi.org/10.1016/j.biopsych.2018.11.004>
- Simons, M., Nave, K.-A., 2016. Oligodendrocytes: Myelination and Axonal Support. *Cold Spring Harb. Perspect. Biol.* 8, a020479. <https://doi.org/10.1101/cshperspect.a020479>
- Sinnaeve, D., 2012. The Stejskal–Tanner equation generalized for any gradient shape—an overview of most pulse sequences measuring free diffusion. *Concepts Magn. Reson. Part A* 40A, 39–65. <https://doi.org/10.1002/cmr.a.21223>
- Sloan, S.A., Barres, B.A., 2014. Mechanisms of astrocyte development and their contributions to neurodevelopmental disorders. *Curr. Opin. Neurobiol., SI: Development and regeneration* 27, 75–81. <https://doi.org/10.1016/j.conb.2014.03.005>
- Small, J.V., Stradal, T., Vignal, E., Rottner, K., 2002. The lamellipodium: where motility begins. *Trends Cell Biol.* 12, 112–120. [https://doi.org/10.1016/S0962-8924\(01\)02237-1](https://doi.org/10.1016/S0962-8924(01)02237-1)
- Smith, S.M., Jenkinson, M., Johansen-Berg, H., Rueckert, D., Nichols, T.E., Mackay, C.E., Watkins, K.E., Ciccarelli, O., Cader, M.Z., Matthews, P.M., Behrens, T.E.J., 2006. Tract-based spatial statistics: Voxelwise analysis of multi-subject diffusion data. *NeuroImage* 31, 1487–1505. <https://doi.org/10.1016/j.neuroimage.2006.02.024>
- Smith, S.M., Nichols, T.E., 2009. Threshold-free cluster enhancement: Addressing problems of smoothing, threshold dependence and localisation in cluster inference. *NeuroImage* 44, 83–98. <https://doi.org/10.1016/j.neuroimage.2008.03.061>
- Snaidero, N., Möbius, W., Czopka, T., Hekking, L.H.P., Mathisen, C., Verkleij, D., Goebbels, S., Edgar, J., Merkler, D., Lyons, D.A., Nave, K.-A., Simons, M., 2014. Myelin membrane wrapping of CNS axons by PI(3,4,5)P3-dependent polarized growth at the inner tongue. *Cell* 156, 277–290. <https://doi.org/10.1016/j.cell.2013.11.044>
- Snaidero, N., Velte, C., Myllykoski, M., Raasakka, A., Ignatev, A., Werner, H.B., Erwig, M.S., Möbius, W., Kursula, P., Nave, K.-A., Simons, M., 2017. Antagonistic Functions of MBP and CNP Establish Cytosolic Channels in CNS Myelin. *Cell Rep.* 18, 314–323. <https://doi.org/10.1016/j.celrep.2016.12.053>
- Soares, J.M., Marques, P., Alves, V., Sousa, N., 2013. A hitchhiker’s guide to diffusion tensor imaging. *Front. Neurosci.* 7. <https://doi.org/10.3389/fnins.2013.00031>
- Sobottka, B., Ziegler, U., Kaech, A., Becher, B., Goebels, N., 2011. CNS live imaging reveals a new mechanism of myelination: the liquid croissant model. *Glia* 59, 1841–1849. <https://doi.org/10.1002/glia.21228>

- Song, J., Carson, J.H., Barbarese, E., Li, F.-Y., Duncan, I.D., 2003. RNA transport in oligodendrocytes from the taiep mutant rat. *Mol. Cell. Neurosci.* 24, 926–938. [https://doi.org/10.1016/S1044-7431\(03\)00254-9](https://doi.org/10.1016/S1044-7431(03)00254-9)
- Song, J., Goetz, B.D., Baas, P.W., Duncan, I.D., 2001. Cytoskeletal Reorganization during the Formation of Oligodendrocyte Processes and Branches. *Mol. Cell. Neurosci.* 17, 624–636. <https://doi.org/10.1006/mcne.2001.0974>
- Stefansson, H., Meyer-Lindenberg, A., Steinberg, S., Magnusdottir, B., Morgen, K., Arnarsdottir, S., Bjornsdottir, G., Walters, G.B., Jonsdottir, G.A., Doyle, O.M., Tost, H., Grimm, O., Kristjansdottir, S., Snorrason, H., Davidsdottir, S.R., Gudmundsson, L.J., Jonsson, G.F., Stefansdottir, B., Helgadottir, I., Haraldsson, M., Jonsdottir, B., Thygesen, J.H., Schwarz, A.J., Didriksen, M., Stensbøl, T.B., Brammer, M., Kapur, S., Halldorsson, J.G., Hreidarsson, S., Saemundsen, E., Sigurdsson, E., Stefansson, K., 2013. CNVs conferring risk of autism or schizophrenia affect cognition in controls. *Nature* 505, 361–366. <https://doi.org/10.1038/nature12818>
- Stefansson, H., Rujescu, D., Cichon, S., Pietiläinen, O.P.H., Ingason, A., Steinberg, S., Fossdal, R., Sigurdsson, E., Sigmundsson, T., Buizer-Voskamp, J.E., Hansen, T., Jakobsen, K.D., Muglia, P., Francks, C., Matthews, P.M., Gylfason, A., Halldorsson, B.V., Gudbjartsson, D., Thorgeirsson, T.E., Sigurdsson, A., Jonasdottir, Adalbjorg, Jonasdottir, Aslaug, Bjornsson, A., Mattiasdottir, S., Blondal, T., Haraldsson, M., Magnusdottir, B.B., Giegling, I., Möller, H.-J., Hartmann, A., Shianna, K.V., Ge, D., Need, A.C., Crombie, C., Fraser, G., Walker, N., Lonnqvist, J., Suvisaari, J., Tuulio-Henriksson, A., Paunio, T., Toulopoulou, T., Bramon, E., Di Forti, M., Murray, R., Ruggeri, M., Vassos, E., Tosato, S., Walshe, M., Li, T., Vasilescu, C., Mühleisen, T.W., Wang, A.G., Ullum, H., Djurovic, S., Melle, I., Olesen, J., Kiemeny, L.A., Franke, B., Kahn, R.S., Linszen, D.H., Os, J. van, Wiersma, D., Bruggeman, R., Cahn, W., Haan, L. de, Krabbendam, L., Myin-Germeys, I., Sabatti, C., Freimer, N.B., Gulcher, J.R., Thorsteinsdottir, U., Kong, A., Andreassen, O.A., Ophoff, R.A., Georgi, A., Rietschel, M., Werge, T., Petursson, H., Goldstein, D.B., Nöthen, M.M., Peltonen, L., Collier, D.A., Clair, D.S., Stefansson, K., 2008. Large recurrent microdeletions associated with schizophrenia. *Nature* 455, 232–236. <https://doi.org/10.1038/nature07229>
- Steffen, A., Rottner, K., Ehinger, J., Innocenti, M., Scita, G., Wehland, J., Stradal, T.E.B., 2004. Sra-1 and Nap1 link Rac to actin assembly driving lamellipodia formation. *EMBO J.* 23, 749–759. <https://doi.org/10.1038/sj.emboj.7600084>
- Stejskal, E.O., Tanner, J.E., 1965. Spin Diffusion Measurements: Spin Echoes in the Presence of a Time-Dependent Field Gradient. *J. Chem. Phys.* 42, 288–292. <https://doi.org/10.1063/1.1695690>
- Steward, O., Schuman, E.M., 2003. Compartmentalized Synthesis and Degradation of Proteins in Neurons. *Neuron* 40, 347–359. [https://doi.org/10.1016/S0896-6273\(03\)00635-4](https://doi.org/10.1016/S0896-6273(03)00635-4)
- Sullivan, P.F., Daly, M.J., O'Donovan, M., 2012. Genetic architectures of psychiatric disorders: the emerging picture and its implications. *Nat. Rev. Genet.* 13, 537–551. <https://doi.org/10.1038/nrg3240>

- Syed, Y.A., Abdulla, S.A., Kotter, M.R.N., 2017. Studying the Effects of Semaphorins on Oligodendrocyte Lineage Cells, in: Terman, J.R. (Ed.), *Semaphorin Signaling: Methods and Protocols*, Methods in Molecular Biology. Springer New York, New York, NY, pp. 363–378. https://doi.org/10.1007/978-1-4939-6448-2_26
- Syed, Y.A., Baer, A., Hofer, M.P., González, G.A., Rundle, J., Myrta, S., Huang, J.K., Zhao, C., Rossner, M.J., Trotter, M.W.B., Lubec, G., Franklin, R.J.M., Kotter, M.R., 2013. Inhibition of phosphodiesterase-4 promotes oligodendrocyte precursor cell differentiation and enhances CNS remyelination. *EMBO Mol. Med.* 5, 1918–1934. <https://doi.org/10.1002/emmm.201303123>
- Tam, G.W.C., van de Lagemaat, L.N., Redon, R., Strathdee, K.E., Croning, M.D.R., Malloy, M.P., Muir, W.J., Pickard, B.S., Deary, I.J., Blackwood, D.H.R., Carter, N.P., Grant, S.G.N., 2010. Confirmed rare copy number variants implicate novel genes in schizophrenia. *Biochem. Soc. Trans.* 38, 445–451. <https://doi.org/10.1042/BST0380445>
- Tamashiro, T.T., Dalgard, C.L., Byrnes, K.R., 2012. Primary Microglia Isolation from Mixed Glial Cell Cultures of Neonatal Rat Brain Tissue. *J. Vis. Exp. JoVE*. <https://doi.org/10.3791/3814>
- Tamura, M., Mukai, J., Gordon, J.A., Gogos, J.A., 2016. Developmental Inhibition of Gsk3 Rescues Behavioral and Neurophysiological Deficits in a Mouse Model of Schizophrenia Predisposition. *Neuron* 89, 1100–1109. <https://doi.org/10.1016/j.neuron.2016.01.025>
- Taylor, W.D., Hsu, E., Krishnan, K.R.R., MacFall, J.R., 2004. Diffusion tensor imaging: background, potential, and utility in psychiatric research. *Biol. Psychiatry* 55, 201–207. <https://doi.org/10.1016/j.biopsych.2003.07.001>
- Thelin, J., Halje, P., Nielsen, J., Didriksen, M., Petersson, P., Bastlund, J.F., 2017. The translationally relevant mouse model of the 15q13.3 microdeletion syndrome reveals deficits in neuronal spike firing matching clinical neurophysiological biomarkers seen in schizophrenia. *Acta Physiol.* 220, 124–136. <https://doi.org/10.1111/apha.12746>
- Thermenos, H.W., Keshavan, M.S., Juelich, R.J., Molokotos, E., Whitfield-Gabrieli, S., Brent, B.K., Makris, N., Seidman, L.J., 2013. A review of neuroimaging studies of young relatives of individuals with schizophrenia: a developmental perspective from schizotaxia to schizophrenia. *Am. J. Med. Genet. Part B Neuropsychiatr. Genet. Off. Publ. Int. Soc. Psychiatr. Genet.* 162B, 604–635. <https://doi.org/10.1002/ajmg.b.32170>
- Thier, M.C., Hommerding, O., Panten, J., Pinna, R., García-González, D., Berger, T., Wörsdörfer, P., Assenov, Y., Scognamiglio, R., Przybylla, A., Kaschutnig, P., Becker, L., Milsom, M.D., Jauch, A., Utikal, J., Herrmann, C., Monyer, H., Edenhofer, F., Trumpp, A., 2019. Identification of Embryonic Neural Plate Border Stem Cells and Their Generation by Direct Reprogramming from Adult Human Blood Cells. *Cell Stem Cell* 24, 166–182.e13. <https://doi.org/10.1016/j.stem.2018.11.015>

- Thurnherr, T., Benninger, Y., Wu, X., Chrostek, A., Krause, S.M., Nave, K.-A., Franklin, R.J.M., Brakebusch, C., Suter, U., Relvas, J.B., 2006. Cdc42 and Rac1 Signaling Are Both Required for and Act Synergistically in the Correct Formation of Myelin Sheaths in the CNS. *J. Neurosci.* 26, 10110–10119. <https://doi.org/10.1523/JNEUROSCI.2158-06.2006>
- Tkachev, D., Mimmack, M.L., Ryan, M.M., Wayland, M., Freeman, T., Jones, P.B., Starkey, M., Webster, M.J., Yolken, R.H., Bahn, S., 2003. Oligodendrocyte dysfunction in schizophrenia and bipolar disorder. *Lancet Lond. Engl.* 362, 798–805. [https://doi.org/10.1016/S0140-6736\(03\)14289-4](https://doi.org/10.1016/S0140-6736(03)14289-4)
- Toma, C., Torricco, B., Hervás, A., Valdés-Mas, R., Tristán-Noguero, A., Padillo, V., Maristany, M., Salgado, M., Arenas, C., Puente, X.S., Bayés, M., Cormand, B., 2014. Exome sequencing in multiplex autism families suggests a major role for heterozygous truncating mutations. *Mol. Psychiatry* 19, 784–790. <https://doi.org/10.1038/mp.2013.106>
- Tournier, J.-D., Yeh, C.-H., Calamante, F., Cho, K.-H., Connelly, A., Lin, C.-P., 2008. Resolving crossing fibres using constrained spherical deconvolution: Validation using diffusion-weighted imaging phantom data. *NeuroImage* 42, 617–625. <https://doi.org/10.1016/j.neuroimage.2008.05.002>
- Travers, B., Adluru, N., Ennis, C., Tromp, D., Destiche, D., Doran, S., Bigler, E., Lange, N., Lainhart, J., Alexander, A., 2012. Diffusion Tensor Imaging in Autism Spectrum Disorder: A Review. *Autism Res. Off. J. Int. Soc. Autism Res.* 5, 289–313. <https://doi.org/10.1002/aur.1243>
- Travers, B.G., Tromp, D.P.M., Adluru, N., Lange, N., Destiche, D., Ennis, C., Nielsen, J.A., Froehlich, A.L., Prigge, M.B.D., Fletcher, P.T., Anderson, J.S., Zielinski, B.A., Bigler, E.D., Lainhart, J.E., Alexander, A.L., 2015. Atypical development of white matter microstructure of the corpus callosum in males with autism: a longitudinal investigation. *Mol. Autism* 6. <https://doi.org/10.1186/s13229-015-0001-8>
- Trent, S., Hall, J., Connelly, W.M., Errington, A.C., 2019. Cyfip1 Haploinsufficiency Does Not Alter GABAA Receptor δ -Subunit Expression and Tonic Inhibition in Dentate Gyrus PV+ Interneurons and Granule Cells. *eNeuro* 6, ENEURO.0364-18.2019. <https://doi.org/10.1523/ENEURO.0364-18.2019>
- Tsang, H.T.H., Edwards, T.L., Wang, X., Connell, J.W., Davies, R.J., Durrington, H.J., O’Kane, C.J., Luzio, J.P., Reid, E., 2009. The hereditary spastic paraplegia proteins NIPA1, spastin and spartin are inhibitors of mammalian BMP signalling. *Hum. Mol. Genet.* 18, 3805–3821. <https://doi.org/10.1093/hmg/ddp324>
- Tyler, W.A., Gangoli, N., Gokina, P., Kim, H.A., Covey, M., Levison, S.W., Wood, T.L., 2009. Activation of the Mammalian Target of Rapamycin (mTOR) is Essential for Oligodendrocyte Differentiation. *J. Neurosci. Off. J. Soc. Neurosci.* 29, 6367–6378. <https://doi.org/10.1523/JNEUROSCI.0234-09.2009>
- Ulfarsson, M.O., Walters, G.B., Gustafsson, O., Steinberg, S., Silva, A., Doyle, O.M., Brammer, M., Gudbjartsson, D.F., Arnarsdottir, S., Jonsdottir, G.A., Gisladdottir, R.S., Bjornsdottir, G., Helgason, H., Ellingsen, L.M., Halldorsson, J.G.,

- Saemundsen, E., Stefansdottir, B., Jonsson, L., Eiriksdottir, V.K., Eiriksdottir, G.R., Johannesdottir, G.H., Unnsteinsdottir, U., Jonsdottir, B., Magnusdottir, B.B., Sulem, P., Thorsteinsdottir, U., Sigurdsson, E., Brandeis, D., Meyer-Lindenberg, A., Stefansson, H., Stefansson, K., 2017. 15q11.2 CNV affects cognitive, structural and functional correlates of dyslexia and dyscalculia. *Transl. Psychiatry* 7, e1109. <https://doi.org/10.1038/tp.2017.77>
- Uranova, N., Orlovskaya, D., Vikhрева, O., Zimina, I., Kolomeets, N., Vostrikov, V., Rachmanova, V., 2001. Electron microscopy of oligodendroglia in severe mental illness. *Brain Res. Bull.* 55, 597–610. [https://doi.org/10.1016/s0361-9230\(01\)00528-7](https://doi.org/10.1016/s0361-9230(01)00528-7)
- Uranova, N.A., Vostrikov, V.M., Vikhрева, O.V., Zimina, I.S., Kolomeets, N.S., Orlovskaya, D.D., 2007. The role of oligodendrocyte pathology in schizophrenia. *Int. J. Neuropsychopharmacol.* 10, 537–545. <https://doi.org/10.1017/S1461145707007626>
- Valente, K.D., Varela, M.C., Koiffmann, C.P., Andrade, J.Q., Grossmann, R., Kok, F., Marques-Dias, M.J., 2013. Angelman syndrome caused by deletion: A genotype–phenotype correlation determined by breakpoint. *Epilepsy Res.* 105, 234–239. <https://doi.org/10.1016/j.eplepsyres.2012.12.005>
- van Berckel, B.N., Bossong, M.G., Boellaard, R., Kloet, R., Schuitemaker, A., Caspers, E., Luurtsema, G., Windhorst, A.D., Cahn, W., Lammertsma, A.A., Kahn, R.S., 2008. Microglia activation in recent-onset schizophrenia: a quantitative (R)-[11C]PK11195 positron emission tomography study. *Biol. Psychiatry* 64, 820–822. <https://doi.org/10.1016/j.biopsych.2008.04.025>
- van der Knaap, L.J., van der Ham, I.J.M., 2011. How does the corpus callosum mediate interhemispheric transfer? A review. *Behav. Brain Res.* 223, 211–221. <https://doi.org/10.1016/j.bbr.2011.04.018>
- Van, L., Boot, E., Bassett, A., 2017. Update on the 22q11.2 deletion syndrome and its relevance to schizophrenia. *Curr. Opin. Psychiatry* 30, 191–196. <https://doi.org/10.1097/YCO.0000000000000324>
- Vandermosten, M., Boets, B., Poelmans, H., Sunaert, S., Wouters, J., Ghesquiere, P., 2012. A tractography study in dyslexia: neuroanatomic correlates of orthographic, phonological and speech processing. *Brain* 135, 935–948. <https://doi.org/10.1093/brain/awr363>
- Varela, M.C., Kok, F., Setian, N., Kim, C.A., Koiffmann, C.P., 2005. Impact of molecular mechanisms, including deletion size, on Prader–Willi syndrome phenotype: study of 75 patients. *Clin. Genet.* 67, 47–52. <https://doi.org/10.1111/j.1399-0004.2005.00377.x>
- Vargas, D.L., Nascimbene, C., Krishnan, C., Zimmerman, A.W., Pardo, C.A., 2005. Neuroglial activation and neuroinflammation in the brain of patients with autism. *Ann. Neurol.* 57, 67–81. <https://doi.org/10.1002/ana.20315>

- Vassos, E., Collier, D.A., Holden, S., Patch, C., Rujescu, D., St Clair, D., Lewis, C.M., 2010. Penetrance for copy number variants associated with schizophrenia. *Hum. Mol. Genet.* 19, 3477–3481. <https://doi.org/10.1093/hmg/ddq259>
- Verkerk, A.J.M.H., Pieretti, M., Sutcliffe, J.S., Fu, Y.-H., Kuhl, D.P.A., Pizzuti, A., Reiner, O., Richards, S., Victoria, M.F., Zhang, F., Eussen, B.E., van Ommen, G.-J.B., Blonden, L.A.J., Riggins, G.J., Chastain, J.L., Kunst, C.B., Galjaard, H., Thomas Caskey, C., Nelson, D.L., Oostra, B.A., Warren, S.T., 1991. Identification of a gene (FMR-1) containing a CGG repeat coincident with a breakpoint cluster region exhibiting length variation in fragile X syndrome. *Cell* 65, 905–914. [https://doi.org/10.1016/0092-8674\(91\)90397-H](https://doi.org/10.1016/0092-8674(91)90397-H)
- Vostrikov, V.M., Uranova, N.A., Orlovskaya, D.D., 2007. Deficit of perineuronal oligodendrocytes in the prefrontal cortex in schizophrenia and mood disorders. *Schizophr. Res.* 94, 273–280. <https://doi.org/10.1016/j.schres.2007.04.014>
- Wager, T.D., Lindquist, M.A., Nichols, T.E., Kober, H., Van Snellenberg, J.X., 2009. Evaluating the consistency and specificity of neuroimaging data using meta-analysis. *NeuroImage* 45, S210-221. <https://doi.org/10.1016/j.neuroimage.2008.10.061>
- Wahl, S.E., McLane, L.E., Bercury, K.K., Macklin, W.B., Wood, T.L., 2014. Mammalian Target of Rapamycin Promotes Oligodendrocyte Differentiation, Initiation and Extent of CNS Myelination. *J. Neurosci.* 34, 4453–4465. <https://doi.org/10.1523/JNEUROSCI.4311-13.2014>
- Wake, H., Lee, P.R., Fields, R.D., 2011. Control of local protein synthesis and initial events in myelination by action potentials. *Science* 333, 1647–1651. <https://doi.org/10.1126/science.1206998>
- Walther, S., Federspiel, A., Horn, H., Razavi, N., Wiest, R., Dierks, T., Strik, W., Müller, T.J., 2011. Alterations of white matter integrity related to motor activity in schizophrenia. *Neurobiol. Dis.* 42, 276–283. <https://doi.org/10.1016/j.nbd.2011.01.017>
- Wang, B., Pan, L., Wei, M., Wang, Q., Liu, W.-W., Wang, N., Jiang, X.-Y., Zhang, X., Bao, L., 2015. FMRP-Mediated Axonal Delivery of miR-181d Regulates Axon Elongation by Locally Targeting Map1b and Calm1. *Cell Rep.* 13, 2794–2807. <https://doi.org/10.1016/j.celrep.2015.11.057>
- Wang, C., Aleksic, B., Ozaki, N., 2015. Glia-related genes and their contribution to schizophrenia. *Psychiatry Clin. Neurosci.* 69, 448–461. <https://doi.org/10.1111/pcn.12290>
- Wang, H., Ku, L., Osterhout, D.J., Li, W., Ahmadian, A., Liang, Z., Feng, Y., 2004. Developmentally-programmed FMRP expression in oligodendrocytes: a potential role of FMRP in regulating translation in oligodendroglia progenitors. *Hum. Mol. Genet.* 13, 79–89. <https://doi.org/10.1093/hmg/ddh009>
- Wang, K., Li, M., Hadley, D., Liu, R., Glessner, J., Grant, S.F.A., Hakonarson, H., Bucan, M., 2007. PennCNV: An integrated hidden Markov model designed for high-

resolution copy number variation detection in whole-genome SNP genotyping data. *Genome Res.* 17, 1665–1674. <https://doi.org/10.1101/gr.6861907>

- Wang, X., Shaw, W.R., Tsang, H.T.H., Reid, E., O’Kane, C.J., 2007. *Drosophila* spichthyn inhibits BMP signaling and regulates synaptic growth and axonal microtubules. *Nat. Neurosci.* 10, 177–185. <https://doi.org/10.1038/nn1841>
- Wang, Y., Zeng, Z., Cai, Y., 2015. Identification of Schizophrenia-Associated Gene Polymorphisms Using Hybrid Filtering Feature Selection with Structural Information, in: Yin, X., Ho, K., Zeng, D., Aickelin, U., Zhou, R., Wang, H. (Eds.), *Health Information Science*. Springer International Publishing, Cham, pp. 174–184.
- Warland, A., Kendall, K.M., Rees, E., Kirov, G., Caseras, X., 2019. Schizophrenia-associated genomic copy number variants and subcortical brain volumes in the UK Biobank. *Mol. Psychiatry* 1. <https://doi.org/10.1038/s41380-019-0355-y>
- Watson, C.G., Stopp, C., Wypij, D., Bellinger, D.C., Newburger, J.W., Rivkin, M.J., 2018. Altered White Matter Microstructure Correlates with IQ and Processing Speed in Children and Adolescents Post-Fontan. *J. Pediatr.* 200, 140-149.e4. <https://doi.org/10.1016/j.jpeds.2018.04.022>
- Whalley, H.C., Nickson, T., Pope, M., Nicol, K., Romaniuk, L., Bastin, M.E., Semple, S.I., McIntosh, A.M., Hall, J., 2015. White matter integrity and its association with affective and interpersonal symptoms in borderline personality disorder. *NeuroImage Clin.* 7, 476–481. <https://doi.org/10.1016/j.nicl.2015.01.016>
- Wheeler, A.L., Voineskos, A.N., 2014. A review of structural neuroimaging in schizophrenia: from connectivity to connectomics. *Front. Hum. Neurosci.* 8. <https://doi.org/10.3389/fnhum.2014.00653>
- Wheeler-Kingshott, C.A.M., Cercignani, M., 2009. About “axial” and “radial” diffusivities. *Magn. Reson. Med.* 61, 1255–1260. <https://doi.org/10.1002/mrm.21965>
- White, R., Gonsior, C., Bauer, N.M., Krämer-Albers, E.-M., Luhmann, H.J., Trotter, J., 2012. Heterogeneous Nuclear Ribonucleoprotein (hnRNP) F Is a Novel Component of Oligodendroglial RNA Transport Granules Contributing to Regulation of Myelin Basic Protein (MBP) Synthesis. *J. Biol. Chem.* 287, 1742–1754. <https://doi.org/10.1074/jbc.M111.235010>
- White, R., Gonsior, C., Krämer-Albers, E.-M., Stöhr, N., Hüttelmaier, S., Trotter, J., 2008. Activation of oligodendroglial Fyn kinase enhances translation of mRNAs transported in hnRNP A2-dependent RNA granules. *J. Cell Biol.* 181, 579–586. <https://doi.org/10.1083/jcb.200706164>
- White, T., Andreasen, N.C., Nopoulos, P., 2002. Brain volumes and surface morphology in monozygotic twins. *Cereb. Cortex N. Y. N* 1991 12, 486–493.
- Winston, G.P., 2012. The physical and biological basis of quantitative parameters derived from diffusion MRI. *Quant. Imaging Med. Surg.* 2, 254. <https://doi.org/10.3978/j.issn.2223-4292.2012.12.05>

- Witelson, S.F., 1989. Hand and sex differences in the isthmus and genu of the human corpus callosum. A postmortem morphological study. *Brain J. Neurol.* 112 (Pt 3), 799–835. <https://doi.org/10.1093/brain/112.3.799>
- Woerner, C., Overstreet, K., 1999. Wechsler abbreviated scale of intelligence (WASI). San Antonio TX Psychol. Corp.
- Woo, Y.J., Wang, T., Guadalupe, T., Nebel, R.A., VINO, A., Del Bene, V.A., Molholm, S., Ross, L.A., Zwiers, M.P., Fisher, S.E., Foxe, J.J., Abrahams, B.S., 2016. A Common CYFIP1 Variant at the 15q11.2 Disease Locus Is Associated with Structural Variation at the Language-Related Left Supramarginal Gyrus. *PLOS ONE* 11, e0158036. <https://doi.org/10.1371/journal.pone.0158036>
- Wu, M., Chang, L.C., Walker, L., Lemaitre, H., Barnett, A.S., Marengo, S., Pierpaoli, C., 2008. Comparison of EPI distortion correction methods in diffusion tensor MRI using a novel framework. *Med. Image Comput. Comput.-Assist. Interv. MICCAI Int. Conf. Med. Image Comput. Comput.-Assist. Interv.* 11, 321–329.
- Wu, S.-Z., Bezanilla, M., 2018. Actin and microtubule cross talk mediates persistent polarized growth. *J. Cell Biol.* 217, 3531–3544. <https://doi.org/10.1083/jcb.201802039>
- Xie, H., Zhang, Y., Zhang, P., Wang, J., Wu, Y., Wu, X., Netoff, T., Jiang, Y., 2014. Functional Study of NIPA2 Mutations Identified from the Patients with Childhood Absence Epilepsy. *PLOS ONE* 9, e109749. <https://doi.org/10.1371/journal.pone.0109749>
- Xiong, Y., Oakley, B.R., 2009. In vivo analysis of the functions of γ -tubulin-complex proteins. *J. Cell Sci.* 122, 4218–4227. <https://doi.org/10.1242/jcs.059196>
- Yan, Z., Kim, E., Datta, D., Lewis, D.A., Soderling, S.H., 2016. Synaptic Actin Dysregulation, a Convergent Mechanism of Mental Disorders? *J. Neurosci.* 36, 11411–11417. <https://doi.org/10.1523/JNEUROSCI.2360-16.2016>
- Yeatman, J.D., Dougherty, R.F., Rykhlevskaia, E., Sherbondy, A.J., Deutsch, G.K., Wandell, B.A., Ben-Shachar, M., 2011. Anatomical properties of the arcuate fasciculus predict phonological and reading skills in children. *J. Cogn. Neurosci.* 23, 3304–3317. https://doi.org/10.1162/jocn_a_00061
- Yoon, K.-J., Nguyen, H.N., Ursini, G., Zhang, F., Kim, N.-S., Wen, Z., Makri, G., Nauen, D., Shin, J.H., Park, Y., Chung, R., Pekle, E., Zhang, C., Towe, M., Hussaini, S.M.Q., Lee, Y., Rujescu, D., St Clair, D., Kleinman, J.E., Hyde, T.M., Krauss, G., Christian, K.M., Rapoport, J.L., Weinberger, D.R., Song, H., Ming, G.-L., 2014. Modeling a genetic risk for schizophrenia in iPSCs and mice reveals neural stem cell deficits associated with adherens junctions and polarity. *Cell Stem Cell* 15, 79–91. <https://doi.org/10.1016/j.stem.2014.05.003>
- Young, K.M., Psachoulia, K., Tripathi, R.B., Dunn, S.-J., Cossell, L., Attwell, D., Tohyama, K., Richardson, W.D., 2013. Oligodendrocyte Dynamics in the Healthy Adult CNS: Evidence for Myelin Remodeling. *Neuron* 77, 873–885. <https://doi.org/10.1016/j.neuron.2013.01.006>

- Zhang, F., Gu, W., Hurles, M.E., Lupski, J.R., 2009. Copy Number Variation in Human Health, Disease, and Evolution. *Annu. Rev. Genomics Hum. Genet.* 10, 451–481. <https://doi.org/10.1146/annurev.genom.9.081307.164217>
- Zhang, Y., Chen, K., Sloan, S.A., Bennett, M.L., Scholze, A.R., O’Keeffe, S., Phatnani, H.P., Guarnieri, P., Caneda, C., Ruderisch, N., Deng, S., Liddelw, S.A., Zhang, C., Daneman, R., Maniatis, T., Barres, B.A., Wu, J.Q., 2014. An RNA-Sequencing Transcriptome and Splicing Database of Glia, Neurons, and Vascular Cells of the Cerebral Cortex. *J. Neurosci.* 34, 11929–11947. <https://doi.org/10.1523/JNEUROSCI.1860-14.2014>
- Zhao, Q., Li, T., Zhao, X., Huang, K., Wang, T., Li, Z., Ji, J., Zeng, Z., Zhang, Z., Li, K., Feng, G., St Clair, D., He, L., Shi, Y., 2013. Rare CNVs and Tag SNPs at 15q11.2 Are Associated With Schizophrenia in the Han Chinese Population. *Schizophr. Bull.* 39, 712–719. <https://doi.org/10.1093/schbul/sbr197>
- Zhuang, L., Wen, W., Trollor, J.N., Kochan, N.A., Reppermund, S., Brodaty, H., Sachdev, P., 2012. Abnormalities of the fornix in mild cognitive impairment are related to episodic memory loss. *J. Alzheimers Dis. JAD* 29, 629–639. <https://doi.org/10.3233/JAD-2012-111766>
- Zuchero, J.B., Fu, M., Sloan, S.A., Ibrahim, A., Olson, A., Zaremba, A., Dugas, J.C., Wienbar, S., Caprariello, A.V., Kantor, C., Leonoudakis, D., Lariosa-Willingham, K., Kronenberg, G., Gertz, K., Soderling, S.H., Miller, R.H., Barres, B.A., 2015. CNS myelin wrapping is driven by actin disassembly. *Dev. Cell* 34, 152–167. <https://doi.org/10.1016/j.devcel.2015.06.011>
- Zufferey, F., Sherr, E.H., Beckmann, N.D., Hanson, E., Maillard, A.M., Hippolyte, L., Macé, A., Ferrari, C., Kutalik, Z., Andrieux, J., Aylward, E., Barker, M., Bernier, R., Bouquillon, S., Conus, P., Delobel, B., Faucett, W.A., Goin-Kochel, R.P., Grant, E., Harewood, L., Hunter, J.V., Lebon, S., Ledbetter, D.H., Martin, C.L., Männik, K., Martinet, D., Mukherjee, P., Ramocki, M.B., Spence, S.J., Steinman, K.J., Tjernagel, J., Spiro, J.E., Reymond, A., Beckmann, J.S., Chung, W.K., Jacquemont, S., 2012. A 600 kb deletion syndrome at 16p11.2 leads to energy imbalance and neuropsychiatric disorders. *J. Med. Genet.* 49, 660–668. <https://doi.org/10.1136/jmedgenet-2012-101203>

Appendix 1

A.1 Creation of the *Cyfp1*^{+/-} rat

A.1.1 CRISPR-Cas9 targeting

Proprietary bioinformatics software (Horizon Discovery, St. Louis, USA) was used to design a short guide RNA (sgRNA) targeting a Protospacer Adjacent Motif (PAM) sequence within exon 7 of the rat *Cyfp1* gene (GGCAGATCCACAATCCATCCagg) on chromosome 1 (**Figure A.1**).

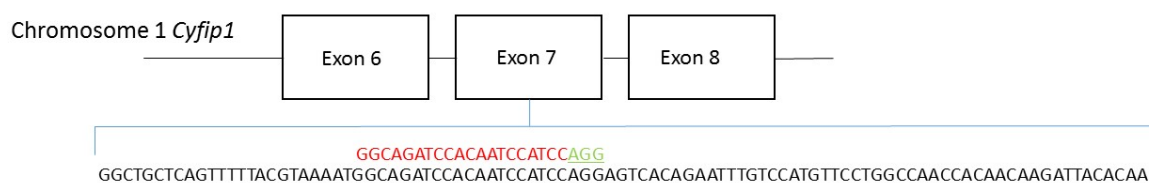


Figure A.1 - Targeting of the *Cyfp1* gene with sgRNA in exon 7. Targeting of the sgRNA was restricted to the first two thirds of the Open Reading Frame of the *Cyfp1* rat gene (first 21 of 32 exons, Refseq: NC_005100.4, NM_001107517.1). Upstream targeting at the 5' end was also avoided due to the possible presence of cryptic promoters. The guide was designed and selected with the use of a commercially available online CRISPR design tool (commercial algorithm) to locate the appropriate PAM sequences and ideal locations for the sgRNA. An oligo was generated containing the specific guide sequence along with the appropriate scaffold and the oligo then acted as a template in an *in vitro* transfection (IVT) reaction to generate the sgRNA.

An initial *in vitro* assessment of efficiency of the sgRNA-Cas9 was performed by nucleofecting the sgRNA-Cas9 into rat C6 glial cells. Genomic DNA (gDNA) PCR products were subsequently generated from nucleofected C6 cells using primers flanking the sgRNA site (FOR: GCCAAAGCTTCCCCTAAAGT; REV: TGGGCGTCAAGTACATTCTG; 497bp amplicon). gDNA PCR products were screened for NHEJ activity and deletion mutations using the SURVEYOR Cel-1 Mutation

Detection Assay (Integrated DNA Technologies, following manufacturer's instructions, **Figure A.2**).

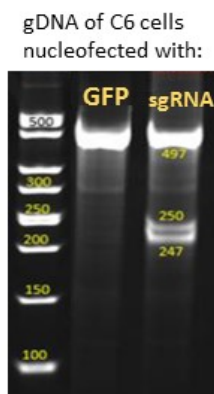


Figure A.2 – *In vitro* assessment of targeting efficiency. gDNA was obtained from C6 glial cells nucleofected with sgRNA-Cas9 and Green Fluorescent Protein (GFP). C6 cells nucleofected with GFP only acted as a visual positive of successful nucleofection (cells fluoresce green) and a genetic negative control of NHEJ activity. Meanwhile, NHEJ activity is observed in C6 cells nucleofected with sgRNA-Cas9 via the observation of smaller cel-1 bands and the relative intensity of these bands compared to the intensity of the larger wild-type band (497 bp) can be used to estimate NHEJ activity.

A.1.2 Embryonic microinjection of sgRNA-Cas9

Embryo donor female Long Evans rats were super-ovulated with pregnant mare serum (PMS) and given human chorionic gonadotrophin (HCG) 48 hrs post PMS administration. Females were immediately mated to stud males after HCG administration. Embryo donor females were euthanized 18-24 hrs after mating and their one-cell fertilized embryos were isolated by harvesting the reproductive tract and rupturing the ampulae. A total of 270 embryos were then put in culture media in a CO₂ incubator until ready for microinjection. All 270 one-cell stage embryos were microinjected with the validated sgRNA-Cas9 over four sessions and then implanted into synchronized pseudopregnant Long Evans recipient females, resulting in 18 live births.

A.1.3 Positive founders and confirmation of 4bp deletion

Of the 18 live births, 7 pups demonstrated NHEJ activity (39% efficiency) as measured by the SURVEYOR assay (with gDNA derived from P14 tissue biopsies). To further identify positive founders, sequencing experiments of the gDNA PCR products were performed and revealed one positive female showing a 4bp out of frame heterozygous

deletion in exon 7 of the *Cyfp1* gene at location Chromosome 1: 36974-36977 and a resulting bioinformatics prediction of an early stop codon in exon 8 (**Figure A.3**) Therefore, the efficiency ratio of generating rats carrying the required deletion was 5.5% (1 from 18 live births).

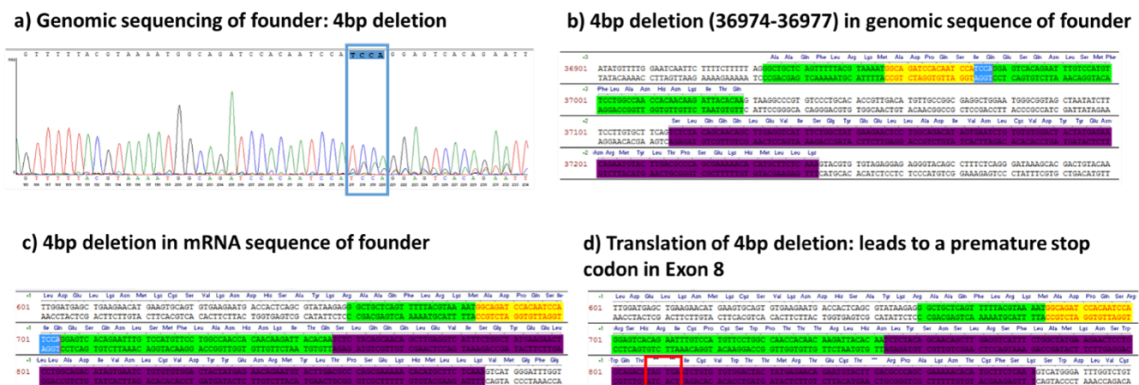


Figure A.3 - Genomic sequencing of the *Cyfp1* 4bp heterozygous deletion founder. a) Manual reading of each double peak in the sequencing chromatograph (ABI Sequence Scanner) show that upstream of the deletion i) the sequence read becomes mixed and ii) the sequence of the secondary peaks from the modified allele align with wild-type sequence, except they occur 4bp further upstream. This reveals the size and position of the modified allele. b) The 4bp deletion in the founder genomic sequence is highlighted in blue (Exon 7 highlighted in green; sgRNA site highlighted in yellow; exon 8 highlighted in purple) c) 4bp deletion in the mRNA sequence of the founder. d) The translation of mRNA from the 4bp-deleted sequence is bioinformatically predicted to create an early stop codon in Exon 8 (codons TAG and TGA, region outlined by red box).

A.1.4 Assessment of potential off-target effects

Recent analysis has shown that Cas9-mediated off-target effects are relatively common (*Anderson et al., 2018*), which found that 23% of 81-genome-editing projects exhibited OTEs across mouse and rat models. *Anderson et al., 2018* highlights the importance of validating the specificity of CRISPR-Cas9 gene editing and recommends an assessment of sgRNA design, in-silico prediction of potential OT sites and importantly biological assays, that together allow confidence that any OT engineered gene changes fall well below the background mutation frequency that can occur spontaneously.

To address this issue, we present an expanded analysis of potential OT sites in **Table A.1**. Here it is shown that the sgRNA guide designed against rat *Cyfp1* has a MIT specificity score (Hsu et al., 2013) of 100% against the *Cyfp1* gene and an overall score of 73.3% when factored against 49 OT sites. Previously in authoritative reviews it has been considered that a cut-off score of 66%, and above is sufficient to effectively eliminate the likelihood of OTE (Hsu et al., 2013) and this proposition has recently been confirmed by others (Anderson et al., 2018). Further, it has previously been shown that 2 mismatches (MM) – in concatenated or interspaced form - reduce Cas9 cleavage activity to low levels and can be further reduced to negligible levels if they occur within close proximity (12bp) to the PAM region (Hsu et al., 2013). Moreover, 3 concatenated mismatches were sufficient to eliminate detectable cleavage in the majority of loci tested, and more so, if these were interspaced and/or proximal to PAM. We also generated a list of top 10 potential off-target (OT) sites, based on the sgRNA sequence used (GGCAGATCCACAATCCATCCagg), and ranked using the MIT website <http://crispr.mit.edu/>. Closer inspection of our list of Top 10 OT sites in **Table A.2**, shows that all have a minimum of 3 MMs and sites 1 and 3 both possess a MM in close proximity to the PAM.

Table A.1 - MIT predicted off target sites for the Cyfip1 sgRNA in-silico.

Numbered Ots	MIT specificity scores - using Benchling (previously MIT website)			Gene	Overall specificity score 73.3 % Locus
	Sequence	PAM	Score		
	GGCAGATCCACAATCCATCC	AGG	100	Cyfip1 (ENSRNOG00000011945)	chr1:+114295724
OT1	GGAAAATCCACCATCCATCC	TGG	1.4		chr2:-95793954
OT2	GCCAAATCCACAATCCATGC	CAG	1.3		chr14:+5813530
OT3	GTATCATCCACAATCCATCC	AAG	1.3		chr4:+109037870
OT4	CTCAGAAACACAATCCATCC	CAG	1		chr3:+90820151
OT5	GGTAGCCCCACAATCCATCC	CAG	1		chr8:+90295695
OT6	TGTACAGCCACAATCCATCC	AAG	1		chr8:+45237516
OT7	GTCCGAACCCCAATCCATCC	TAG	1		chr2:-85528916
OT8	TGGAAATCCACAATCCATCT	CAG	0.9		chr2:+223864733
OT9	AGCAGATCCAGATCCATCC	AGG	0.7		chr4:+72665650
OT10	AGCATATACACAATCCATTC	CAG	0.7		chr7:-113365387
OT11	TGCATACCCAGAATCCATCC	TAG	0.6		chr6:-128916162
OT12	AGCATAACCAGAATCCATCC	GGG	0.6		chr11:+79708047
OT13	GCTAGATCCTCAGTCCATCC	TGG	0.6		chr2:-172781048
OT14	AGCAGATGCCCAATCCATTC	GAG	0.6		chr18:-63836841
OT15	GACAAAGCCAAAATCCATCC	AGG	0.6		chr3:+28891768
OT16	GTCAGAGACAGAATCCATCC	AAG	0.6		chr4:-170865117
OT17	TGCACAGCCACAATCCTTCC	AGG	0.5		chr14:+13356994
OT18	AGCACTTCCACCATCCATCC	AGG	0.5		chr4:-180525716
OT19	AACTGATCCACAATTCATCC	CAG	0.5		chr8:-8347020
OT20	CACAGATCTACAATCCCTCC	CAG	0.5		chr3:-176292068
OT21	GGCAGATCCAGAACCATCC	CGG	0.5		chr6:-43384274
OT22	TGTAGATCCTCAATACATCC	AGG	0.5		chr7:+67511010
OT23	TCCAGATCCAGAATCCCTCC	TAG	0.4		chr11:-36121578
OT24	GGCAGGTTCTGAATCCATCC	CAG	0.4		chr8:+24534839
OT25	GACACACCCCACTCCATCC	AGG	0.4		chr19:-55314147
OT26	AGCAGAGTCACAATCCATGC	AAG	0.4		chr2:-261967831
OT27	GGCAGCTGCGCAATCCATCA	TGG	0.4		chr3:-173954380
OT28	GGCAAATTCATGATCCATCC	AAG	0.4		chr10:+8354081
OT29	GGCACATTGACAATCCTTCC	CAG	0.4		chr2:-126822158
OT30	GGCGGACCCCCAGTCCATCC	AGG	0.4	Cyfip2 (ENSRNOG00000006557)	chr10:-31364956
OT31	TGCACATCCGCAATCCACCC	CAG	0.4		chr10:-92422723
OT32	TGCAGATACATATCCATCC	CAG	0.4		chr15:+1789082
OT33	GGAAATGTCCACAGTCCATCC	AGG	0.4		chr18:-31761206
OT34	GGAAATTTCCACATCCATCC	TGG	0.4		chr15:-61472675
OT35	AGCACATCCACTCTCCATCC	CAG	0.3		chr19:-30859164
OT36	GATAGATCCACTGTCCATCC	TGG	0.3		chr5:+63159170
OT37	AGCAGACTCACAATTCATCC	TAG	0.3		chr2:-85469475
OT38	ACCAGATCCCACTCCTTCC	CAG	0.3		chr5:+135998305
OT39	GGCACATCCACAATCCAGCA	AAG	0.3		chr1:+146539887
OT40	TTGAGATCCACAATCTATCC	TAG	0.3		chr2:+103959476
OT41	TGCAGAACCACTATCCATCT	CGG	0.3		chrX:-63694162
OT42	AGCAGCTCCAGAATCCATCA	TGG	0.3		chr1:-146566385
OT43	TGCAGATCTAAAATCCATCT	GGG	0.3		chrX:-143494363
OT44	GCCAGCTCCAAAATCCATCT	AAG	0.3		chr3:+127954078
OT45	TGCAGTTCCAGGATCCATCC	AAG	0.3	ENSRNOG00000020103	chr18:+30285706
OT46	GTCAGAACCAGAATCCCTCC	TGG	0.3		chr5:+75274315
OT47	GAAAGATCCATAATTCATCC	TGG	0.3		chr2:+253045233
OT48	TGCAAATCCACAGTCCATTC	AGG	0.3		chr5:-85205106
OT49	GCCAGGGCCACAATCCATAC	AGG	0.3	Grm3 (ENSRNOG00000005519)	chr4:-21535579

Table A.2 – Top 10 predicted off target sites for the Cyfip1 sgRNA with a breakdown of mismatches and individual MIT scores.

	Sequence	Genomic Coordinates	Mismatches	MM proximal to PAM (12bp core)	Interspaced MM	MIT score
Injected US sgRNA sequence	GGCAGATCCACAATCCATCCAGG	Chr1:+114295729	0	0	0	100
OT Site 1	GGAAATCCACCATCCATCCTGG	chr2:-115534496	3	1	3	1.4
OT Site 2	GTATCATCCACAATCCATCCAAG	chr4:+173741171	4	0	0	1.3
OT Site 3	GCCAAATCCACAATCCATGCCAG	chr14:+5796700	3	1	3	1.3
OT Site 4	CTCAGAAACAATCCATCCAG	chr3:+97482256	4	0	2	1
OT Site 5	TGTACAGCCACAATCCATCCAAG	chr8:+43715985	4	0	4	1
OT Site 6	GTCCGAACCCAATCCATCCTAG	chr2:-105200718	4	1	4	1
OT Site 7	TGGAATCCACAATCCATCTCAG	chr2:+241911684	4	1	4	0.9
OT Site 8	AGCAGATCCAGATTCATCCAGG	chr4:+137367617	3	2	3	0.7
OT Site 9	TGCATACCCGAATCCATCCTAG	chr6:-138113252	4	1	4	0.6
OT Site10	AGCATAACCGAATCCATCCGGG	chr11:-81022173	4	1	4	0.6

It is also important to notice recent discussions in the gene editing field as to the extent to which in-silico predicted OT sites (MIT website, Benchling) reflect true biological OT sites of Cas9-mediated activity. To some extent, this has been addressed experimentally by *Anderson et al., 2018*, whereby 30 robust OT sites were identified by two sequencing methodologies (whole-genome sequencing and TEG-sequencing) and found that 25 of these, i.e. 83%, were predicted using in silico methodologies. Therefore, in light of these results we can be reasonably confident that the Top 10 OTE table generated for the Cyfip1 sgRNA is reflective of bone-fide biological OT sites.

Furthermore, using a Surveyor assay, all the Top 10 predicted OT sites were negative, i.e. no OTE were detected when we explicitly tested for them using wet methods. Corresponding gDNA PCR primer pairs were designed to flank each potential OT site (**Figure A.4a**). Extracted gDNA from the founder animal and wild-type controls were used as template for PCR, before each gDNA PCR product underwent the SURVEYOR assay (**Figure A.4b**). The lack of NHEJ activity, as indicated by a lack of smaller secondary products, revealed no evidence for genomic disruptions at the selected sites and was further confirmed by sequencing the 10 OT site gDNA products (data not shown).

a) Top 10 potential off-target sites (MIT) for sgRNA

	Off Target Sequence	genomic coordinates	F primer	R primer
Injected gRNA sequence	GGCAGATCCACAATCCATCCAGG	chr1: 115302084-115302106		
OT Site 1	GGA ^{AA} ATCCACCATCCATCCAGG	chr2: 95670408-95670430	tgaaggcaggaactctdgg	tgacagatgcaccaagtggt
OT Site 2	GTATCATCCACAATCCATCCAAAG	chr4: 111917803-111917825	agtcactgctgcctcaatctct	tacacccctccccacaata
OT Site 3	GCCAAATCCACAATCCATCCAGG	chr14: 5746379-5746401	ttctttatgccctctgctg	gctttcacatgggggttaa
OT Site 4	CTCAGAA ^{AC} CACAATCCATCCAGG	chr3: 86410011-86410033	tcccatcttgcatagtgact	ctttcaccctggaggctgtt
OT Site 5	TGTACAGCCACAATCCATCCAAAG	chr8: 44004281-44004303	gatgggtagaacacccaactg	ccaccatagdcaccgaaat
OT Site 6	GTC ^{CG} AA ^{CCC} CAATCCATCCAGG	chr2: 84878323-84878345	ctgggaagcataaagggaag	ttgcagctatctgtccagct
OT Site 7	TGGAAATCCACAATCCATCCAGG	chr2: 216880248-216880270	caccaggatccccaagtcta	ctgcctcaaaatcccagctgt
OT Site 8	AGCAGATCCAGATCCATCCAGG	chr4: 70983405-70983427	gocattctgggataccatgt	acctctgtgggaagcaaga
OT Site 9	AGCATAACCCAGATCCATCCAGG	chr11: 78421166-78421188	tcctctctgctccagta	cgcaggacaagtggtgatt
OT Site 10	TGCATACCCAGAATCCATCCAGG	chr6: 129397603-129397625	cagagcaggtgtggaaga	cgtttaatcagcagtgcaag

b) SURVEYOR assay of Top 10 potential off-target sites

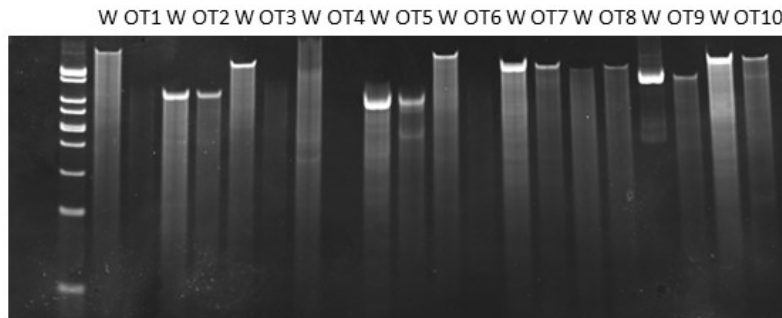


Figure A.4 - In-silico identification of the Top 10 sgRNA off-target sites and NHEJ activity assessed by the SURVEYOR assay. a) The top 10 OT sites were computed by taking into account the following i) total number of mismatches (either 3-4 mismatches, highlighted in red), ii) mismatch absolute position (to accommodate for the relatively high disturbance of mismatches falling close to the PAM site) and iii) mean pairwise distance between mismatches to account for the steric effect of closely neighbouring mismatches in disrupting sgRNA -DNA interaction. A total of 156 off-target sites were found, although only 14 of which were intragenic. Corresponding PCR primer pairs were designed to flank the top 10 potential off target sites. b) Using extracted gDNA from the founder animal and wild-type controls, gDNA products were made to flank each potential OT site (~300-500bp amplicon) and run on the SURVEYOR assay. None of the 10 OT sites tested revealed NHEJ activity and was later corroborated with sequencing data.

A.1.5 Breeding, re-derivation and maintenance at Charles River, UK

The F1 founder female was mated with male wild types at Horizon Discovery and generated F2 progeny containing the mutation confirming germ-line transmission. A total of five male positives were exported to Charles River, Lyon, France for re-derivation by embryo transfer. The resulting specific pathogen free (SPF) progeny were sent to Charles River, Margate, UK for routine breeding and generation of experimental groups for phenotypic testing. The standard breeding protocol was a heterozygous x wild-type cross giving rise to 1:1 average *Cyfp1*^{+/-} /wild-type progeny allowing full use of the litter and the generation of litter-mate controls. In most cases and unless otherwise stated, the genetic modification was transmitted through the male, resulting in the litters being raised

by wild-type dams. On occasion, transmission was through the female, this was to check for parent-of-origin effects; no POE have been found. The *Cyfp1^{+/-}* rat model is viable and Charles River has reported no adverse effects on breeding performance, development, general health; and in addition, no deviation from the expected Mendelian 1:1 ratio of *Cyfp1^{+/-}* to wild-types and no skewing of the sex ratios.

A.1.6 Housing of experimental groups at Cardiff

All experiments were carried out using adult male littermate Long Evans rats (4.5 - 9 months old) that had been produced at Charles River, UK and delivered to Cardiff at 8-10 weeks of age. Rats were housed in groups of mixed wild-type/*Cyfp1^{+/-}* in conventional, environmentally enriched cages, maximum 4 to a cage, with unrestricted food and water access and a standard 12h light-dark cycle (08:00 to 20:00). Room temperature was maintained at $21 \pm 2^\circ\text{C}$ and humidity at $55 \pm 10\%$. Animal husbandry was carried out by technical staff at Cardiff University. All procedures were performed in accordance with ARRIVE guidelines, the local regulations set by Cardiff University and the Animal (Scientific Procedures) Act 1986.

A.1.7 PCR Genotyping

Genotyping was carried out twice, an initial assay from tissue sent from Charles River prior to transport of the rats to Cardiff and then a further confirmatory assay post-mortem, in both cases the genotyping was carried out by the investigators in Cardiff. DNA was extracted using Qiagen DNEasy Blood & Tissue Kit, Cat No./ID: 69506 and PCR carried out using a 2-primer design with primer sequences: **Forward** - TAGGGCTGCTCAGTTTTTACG, **Reverse** - TTGTTGTGGTTGG CCAGGAA. For the cycling conditions 2 ul of sample was added to 23 ul of PCR Mastermix solution (12.5 ul Promega GoTaq® G2 Green Mastermix M7822, M7823, 1 ul of each primer and 8.5 ul nuclease-free water) and placed in a thermal cycler under the following conditions: 1.) 95 °C for 10:00, 2.) 95 °C for 00:40, 3.) 60C for 00:40, 4.) 72 °C for 01:00, 5.) 40 cycles of steps 2-4, 6.) 72 °C for 05:00 and 7.) 8 °C for ever. The resulting PCR products for the mutant and wild-type sequences differed by 8bp, which produces a single band (wild-type) or a double band (*Cyfp1^{+/-}*), **Figure A.5**. To achieve this level of resolution, 10 ul PCR product and 3ul Promega 6X Blue/Orange Loading Dye (G1881) were pipetted into a well in a 4% agarose gel and run for 1.5-2 hours at 150v.



Figure A.5 - Gel image showing PCR products from *Cyfip1*^{+/-} and wild-type rats using ear tissue; wild-type products show as a single band, *Cyfip1*^{+/-} products as a double band, using this 2-primer design there was 100% concordance between the initial and post mortem genotype determinations.

A.1.8 Molecular verification and characterisation of the *Cyfip1*^{+/-} rat model

A.1.8.1 qRT-PCR

The effect of the heterozygous genomic heterozygous premature stop codon on transcription was tested by measuring *Cyfip1* mRNA gene expression in the brain tissue of *Cyfip1*^{+/-} rats via quantitative real-time PCR. Rats were sacrificed by carbon dioxide inhalation and whole brains from mutant adult males were extracted, alongside wild-type littermate controls (5.5 - 8months old, n=11 per genotype) and hemi-brain dissected and stored on dry ice before storage at -80 °C. In a separate group of animals (4.5 - 5 months old, n=10 per genotype) prefrontal cortex (PFC) and hippocampal regions from both brain hemispheres were dissected free-hand and frozen on dry ice before storage at -80 °C. RNA was extracted from the hippocampus and PFC (one hemisphere only), and hemi-brains, using RNeasy Kits (Qiagen), followed by DNase treatment of RNA (TURBO DNA-free Kit, Ambion, Life Technologies) and cDNA synthesis (RNA to cDNA EcoDry Premix, Random Hexamers, Clontech). cDNA samples were prepared in triplicate in 96-well reaction plates for SYBR-green-based quantitative real-time PCR (SensiFAST, HI-ROX, Biorline), according to manufacturer's instructions using a StepOnePlus System (Applied Biosystems, Thermo Fisher Scientific). *Cyfip1*-specific primers, along with

Gapdh and *Hprt* primers (housekeeping genes), were bioinformatically designed and assessed to span at least one exon-exon boundary and to match only for its target mRNA sequence in rat (primer-BLAST and nBLAST, NCBI), before being commercially synthesised (Sigma-Aldrich). Primer efficiencies were experimentally determined through a dilution series of brain region-specific wildtype cDNA (efficiency of 90-110% was required, annealing temperature set at 60 °C). All samples were run in triplicate and individual $-\Delta\text{Ct}$ values (relative to *Gapdh* and *Hprt*) were used to quantify mRNA gene expression. Primers used for qRT-PCR were as follows: *Cyfp1* (FOR: GAGGAGAATAAGTCCCGGTGG, REV: GTAGCGTGCCAGCTCAGAAA; targeting exon 11-12); *Gapdh* (FOR: TCTCTGCTCCTCCCTGTTCT, REV: TACGGCCAAATCCGTTTACA); *Hprt* (FOR: TCCTCCTCAGACCGCTTTTC, REV: ATCACTAATCACGACGCTGGG). As illustrated in **Figure A.6** quantification by qRT-PCR confirmed that the genomic disruption of *Cyfp1* leads to reduced *Cyfp1* mRNA expression in *Cyfp1*^{+/-} rats, with a reduction seen in the hemi-brain, hippocampus and PFC compared to wild-types (HEMI-BRAIN GENE ($F_{(1,16)}=63.094$, $p=0.0001$), HIPP GENE ($F_{(1,18)}=27.192$, $p=0.0001$), PFC GENE ($F_{(1,18)}=39.831$, $p=0.0001$); 1-way ANOVA on $-\Delta\text{Ct}$ data). We also confirmed that *Cyfp1* haploinsufficiency did not change *Cyfp2* expression (data not shown).

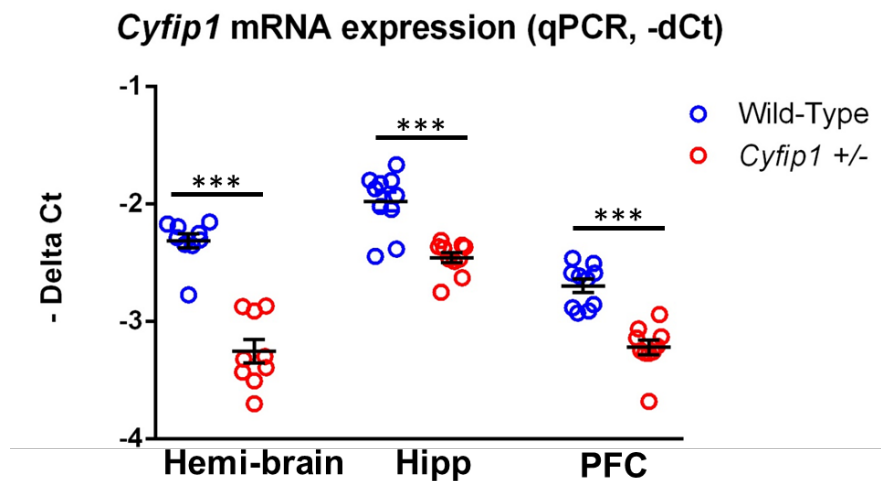


Figure A.6- *Cyfp1* mRNA expression in the hemi-brain, hippocampus and PFC and of wild-type and *Cyfp1*^{+/-} rats. Measurement of $-\Delta\text{Ct}$ by qRT-PCR revealed reductions of *Cyfp1* mRNA in the hemi-brain of *Cyfp1*^{+/-} rats compared with wild-types (wild-type: -2.312 ± 0.187 , *Cyfp1*^{+/-}: -3.253 ± 0.302 ; equivalent to a 47.9% decrease using $2^{-\Delta\Delta\text{Ct}}$). Similarly, *Cyfp1* mRNA expression in *Cyfp1*^{+/-} rats was reduced compared with wild-types in the hippocampus (wild-type: -1.976 ± 0.256 , *Cyfp1*^{+/-}: -2.455 ± 0.139 ; equivalent

to a 28.3% decrease) and PFC (wild-type: -2.695 ± 0.178 , *Cyfp1*^{+/-}: -3.219 ± 0.193 ; 30.5% reduction). Four hemi-brains were of insufficient RNA quality to perform qRT-PCR (n=2 per genotype). Individual $-\Delta\text{Ct}$ data is graphed with error bars representing SEM. 1-way ANOVA performed on individual data points, with normality assessed by Shapiro-Wilk tests. * = P<0.05, ** = P<0.01, *** = P<0.001.

A.1.8.2 Immunofluorescent western blotting

Semi-quantitative immunofluorescent western blotting assays were employed to measure Cyfp1 protein in the brain of *Cyfp1*^{+/-} rats and thereby determine whether the disruption already observed at the genomic (see section 3 and 7) and mRNA expression level (see previous section) was maintained at the level of Cyfp1 protein. The remaining, contralaterally dissected hippocampus and PFC (see section 8.1, n=10 per genotype), hemi-brains from a separate cohort of rats (n=11 per genotype, 5.5m - 8m old), were homogenized manually with a glass Dounce homogeniser in 1 ml of ice-cold lysis RIPA buffer (RIPA Lysis and Extraction Buffer, ThermoFisher Scientific) containing protease inhibitors (cOmplete Mini EDTA-free Protease Inhibitor, Roche, 1 tablet/ 10 ml RIPA). Additionally, Cyfp1 protein level was quantified in the corpus callosum, given that the work developed in this thesis focused on this region. A new cohort of rats (n=9 WT and 10 *Cyfp1*^{+/-} rats). was used for this analysis. The corpus callosum were manually dissected from the brains and visually inspected under the microscope. The homogenates were centrifuged at 12,000 rpm for 20 minutes at 4°C and aliquots of supernatant containing proteins stored at -80°C. A total of 40 µg of protein (quantified using Pierce BCA Protein Kit Assay, as per manufacturer's instructions, ThermoFisher Scientific) in Laemmli sample buffer containing 1/20 β-mercaptoethanol (Bio-rad) were denatured at 95°C for 5 min prior to separation on a 4-12% gradient Bis-Tris Midi gel (NuPAGE, ThermoFisher Scientific) in 1x Bolt MES SDS Running Buffer (ThermoFisher Scientific) at a constant voltage of 115 V for 1 hr. Transfer was performed in 1 x Bolt Transfer Buffer (ThermoFisher Scientific) to Amersham Protran nitrocellulose membranes (GE Healthcare Life Sciences) at a constant voltage of 85 V for 2 hr 15 min at 4 °C. Blots were blocked in 5% non-fat milk (Blocking Agent, Amersham, GE Healthcare Life Sciences) in 0.01 M Tris buffered saline solution containing 0.2% Tween 20 (TBST), and this TBST solution was used for all subsequent washes. Primary and fluorescent secondary antibodies were similarly diluted in TBST containing 0.2% Tween 20 and 5% milk and they were used at the following concentrations: Cyfp1 (AB6046, Millipore),

1:1,000; Gapdh (ab8245, Abcam), 1:5,000; IRDye® 680RD Goat anti-Rabbit IgG (Li-Cor, 926-68071), 1:15,000 and IRDye® 680RD Donkey anti-Mouse IgG (Li-Cor, 926-68072), 1:15,000. Incubation of blots in primary antibody solutions were at 4°C overnight, whilst fluorescent secondary antibodies were for 1 hr at RT. Blots were visualised using the 700 nm channel of the Odyssey CLx Imaging System (Li-Cor) and densitometric quantification was performed on scanned blot films using ImageStudio Lite software (Li-Cor). Densitometry data was normalised to the protein Calnexin (Cal) and between-blot variance was minimised by normalising each *Cyfp1*^{+/-} sample signal to the average signal of all the wildtype samples on the same blot.

Figure A.7 shows an overall 27% reduction in Cyfp1 protein levels in the hemi-brain samples of *Cyfp1*^{+/-} compared with wild-types (Hemi-brain Cyfp1 prot (F(1,20)=2.087, p=0.164); 1-way ANOVA). Similar levels of mean reductions were found in the hippocampal and prefrontal cortex samples (Hipp Cyfp1 prot, (F(1,18)=0.985, p=0.334), 1-way ANOVA; PFC Cyfp1 prot (F(1,20)=1.738, p=0.204), 1-way ANOVA). Due to a great degree of variability, these reductions were not significant. Surprisingly, when looking at the protein level in the corpus callosum, a 51.6% decrease of Cyfp1 protein is seen revealing a significant reduction despite the presence of some variability (Corpus callosum Cyfp1 prot, (F(1,17)=7.778, p=0.013), 1-way ANOVA). The increased variability in the hemi brain, hippocampal and prefrontal cortex samples was common to both the wild-type and *Cyfp1*^{+/-} rats, so it is unlikely to be due to the genetic manipulation *per se*. Whether these data reflect a degree of variability in the extent to which the reductions in mRNA translate into systematic reductions in protein levels, at least in the hippocampus and PFC, remains to be determined.

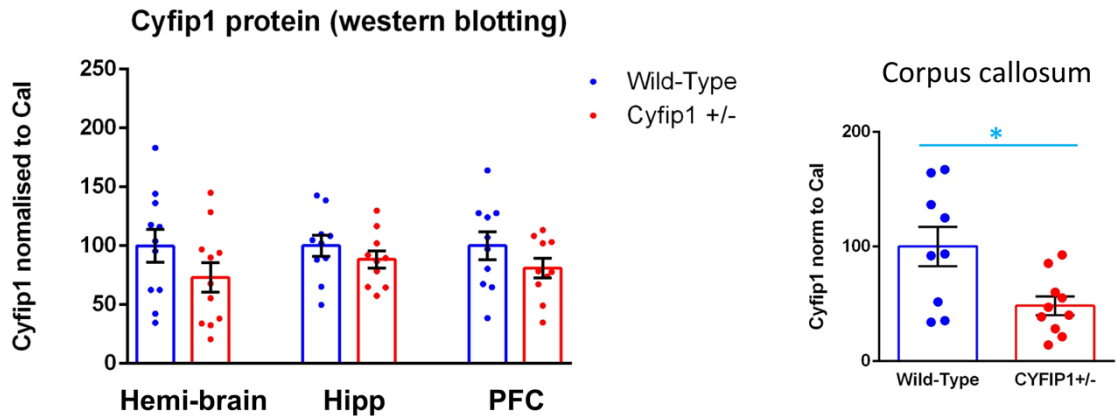


Figure A.7 - Cyfip1 protein levels in the hemi-brain, hippocampus and PFC of wild-type and *Cyfip1*^{+/-} rats. Measurement of protein levels by immunofluorescent western blotting revealed reductions of Cyfip1 protein in the hemi-brain (27% reduction), hippocampus (11.6% reduction), pre-frontal cortex (19,1% reduction), and corpus callosum (51.6% reduction) of *Cyfip1*^{+/-} rats compared with wild-types. Due to the high variability within each group, only differences in the corpus callosum were significant. Densitometric data given relative to the average of all wild-type samples (100%) and normalised to protein control, Calnexin (Cal). Bars represent SEM, and 1-way ANOVA performed on individual data points. * = P<0.05, ** = P<0.01, *** = P<0.001.

Supplementary References

- Anderson, K.R., Haeussler, M., Watanabe, C., Janakiraman, V., Lund, J., Modrusan, Z., Stinson, J., Bei, Q., Buechler, A., Yu, C., Thamminana, S.R., Tam, L., Sowick, M.-A., Alcantar, T., O’Neil, N., Li, J., Ta, L., Lima, L., Roose-Girma, M., Rairdan, X., Durinck, S., Warming, S., 2018. CRISPR off-target analysis in genetically engineered rats and mice. *Nat. Methods* 15, 512–514. <https://doi.org/10.1038/s41592-018-0011-5>
- Hsu, P.D., Scott, D.A., Weinstein, J.A., Ran, F.A., Konermann, S., Agarwala, V., Li, Y., Fine, E.J., Wu, X., Shalem, O., Cradick, T.J., Marraffini, L.A., Bao, G., Zhang, F., 2013. DNA targeting specificity of RNA-guided Cas9 nucleases. *Nat. Biotechnol.* 31, 827–832. <https://doi.org/10.1038/nbt.2647>

A.2 Supplementary material for Chapter 3

A.2.1 TBSS analysis excluding individuals who are related

Table A3. Individual information on dosage, age, gender, total intracranial volume, and family relationships. Individuals who are related are highlighted with a certain colour, and the colour code is specified in the KEY column. The individuals who were removed from the analyses to produce **Figures A.8** are specified on column 6. Dosage: 1= deletion, 2=NoCNV, 3=duplication.

Subject	dosage	age	gender	TIV	
Subj 1	2	59	1	1612.33	
Subj 2	2	41	1	1767.58	removed
Subj 3	2	37	1	1642.45	
Subj 4	2	49	2	1500.51	
Subj 5	2	56	1	1916.71	
Subj 6	2	36	2	1329.03	
Subj 7	2	22	1	1640.82	
Subj 8	2	42	1	1860.66	
Subj 9	2	39	2	1629.37	
Subj 10	2	26	2	1638.81	
Subj 11	2	31	2	1420.73	
Subj 12	2	37	1	1569.75	
Subj 13	2	28	2	1486.33	
Subj 14	3	62	1	1769.55	
Subj 15	3	45	1	1616.38	
Subj 16	1	44	2	1575.26	
Subj 17	1	32	2	1376.6	
Subj 18	1	27	1	1558.38	
Subj 19	1	56	2	1385.12	
Subj 20	1	38	1	1544.59	
Subj 21	1	27	1	1860.96	
Subj 22	1	41	2	1479.42	

KEY

- nephew-aunt
- half-siblings
- mother-daughter
- siblings
- siblings
- daughter-father
- son-mother
- siblings
- uncle-niece
- first cousins
- first cousins

Subject	dosage	age	gender	TIV	
Subj 23	3	52	2	1546.55	removed
Subj 24	1	65	1	1547.32	
Subj 25	1	45	2	1458.81	
Subj 26	3	26	2	1333.78	removed
Subj 27	3	53	1	1715.04	
Subj 28	3	51	2	1484.94	removed
Subj 29	2	35	1	1701.68	
Subj 30	1	24	1	1662.12	
Subj 31	3	58	2	1382.59	
Subj 32	1	27	1	1593.04	removed
Subj 33	1	37	2	1543.53	
Subj 34	1	23	2	1414.08	removed
Subj 35	3	40	2	1509.29	
Subj 36	1	57	2	1416.03	
Subj 37	3	26	2	1464.85	
Subj 38	3	49	1	1499.49	
Subj 39	3	28	1	1676.73	
Subj 40	2	25	1	1791.84	
Subj 41	2	50	1	1676.31	
Subj 42	3	22	2	1607.84	
Subj 43	3	51	1	1552.31	
Subj 44	1	46	2	1589.06	
Subj 45	3	54	1	1706.39	removed
Subj 46	1	50	1	1692.26	
Subj 47	3	23	1	1770.81	
Subj 48	1	56	1	1426.4	
Subj 49	1	60	2	1505.46	
Subj 50	3	22	1	1607.08	
Subj 51	1	61	1	1643.26	
Subj 52	3	59	2	1530.1	removed
Subj 53	1	50	1	1526.48	
Subj 54	3	51	2	1458.54	
Subj 55	3	41	1	1725.68	
Subj 56	3	35	2	1467.06	

Subject	dosage	age	gender	TIV	
Subj 57	3	27	2	1547.91	
Subj 58	1	55	1	1749.57	
Subj 59	3	48	2	1412.99	
Subj 60	1	54	2	1328.75	removed
Subj 61	2	35	2	1295.43	
Subj 62	3	57	1	1551.93	
Subj 63	3	37	2	1379.58	
Subj 64	3	36	2	1506.7	
Subj 65	1	34	1	1630.99	
Subj 66	1	42	2	1465.2	
Subj 67	1	47	2	1272.6	removed
Subj 68	3	65	2	1418.19	
Subj 69	1	40	2	1475.89	
Subj 70	1	21	1	1675.78	
Subj 71	1	53	1	1449.1	
Subj 72	1	32	2	1447.54	
Subj 73	1	41	2	1370.07	removed
Subj 74	3	56	1	1638.58	
Subj 75	2	53	1	1821.95	
Subj 76	2	39	1	1700.44	

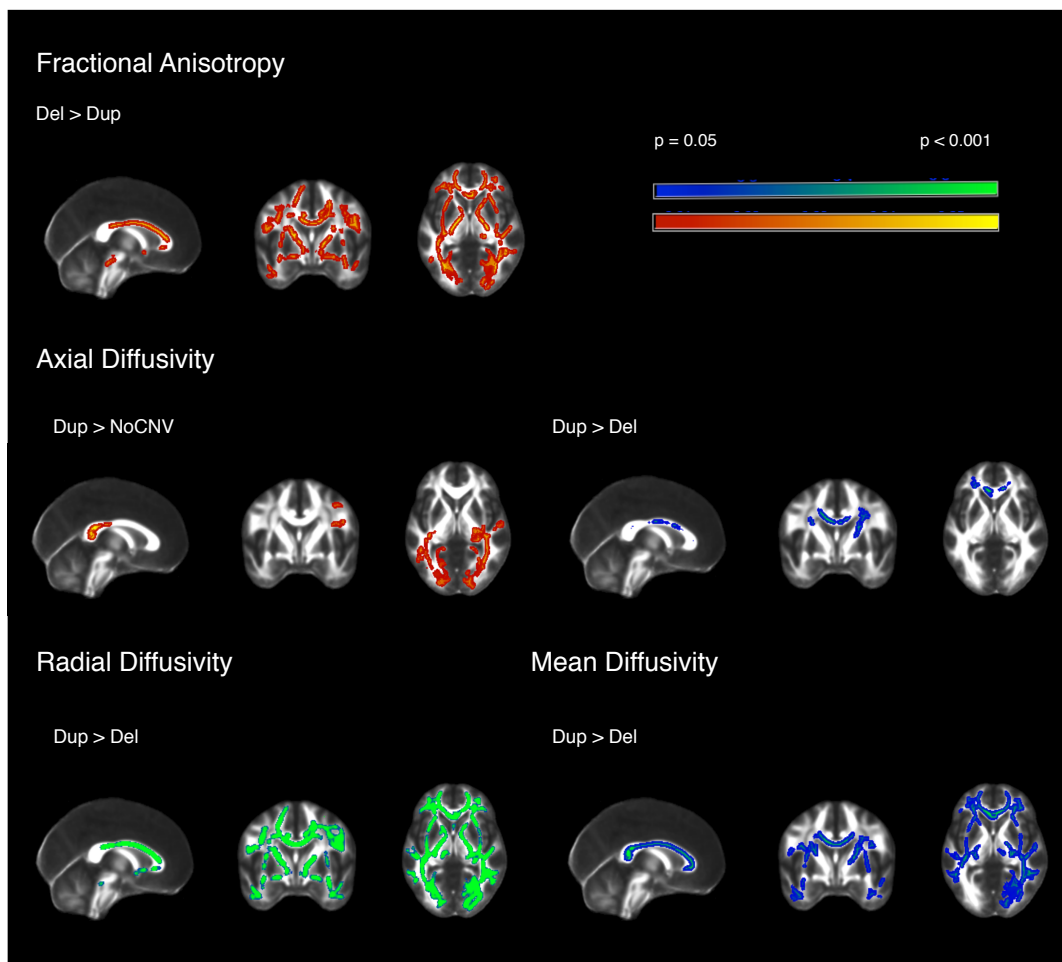


Figure A.8 - TBSS whole-group voxel-based analysis excluding individuals who are related. Significant results for the two-sample t-test showing group differences between deletion (Del, $n = 25$), duplication (Dup, $n = 22$), and no large copy number variants (NoCNV, $n = 18$) groups for fractional anisotropy (FA), axial diffusivity (AD), radial diffusivity (RD), and mean diffusivity (MD) maps. Here, only contrasts that gave rise to significant results after correction are displayed ($p < 0.05$, corrected). Within the significant results, red and blue code for less significant results and yellow and green for more significant results. The deletion showed widespread increased FA, and decreased AD, RD, and MD compared with duplication group. The duplication showed increased AD compared with NoCNV group.

Reciprocal White Matter Changes Associated With Copy Number Variation at 15q11.2 BP1-BP2: A Diffusion Tensor Imaging Study

Ana I. Silva, Magnus O. Ulfarsson, Hreinn Stefansson, Omar Gustafsson, G. Bragi Walters, David E.J. Linden, Lawrence S. Wilkinson, Mark Drakesmith, Michael J. Owen, Jeremy Hall, and Kari Stefansson

ABSTRACT

BACKGROUND: The 15q11.2 BP1-BP2 cytogenetic region has been associated with learning and motor delays, autism, and schizophrenia. This region includes a gene that codes for the cytoplasmic FMR1 interacting protein 1 (CYFIP1). The CYFIP1 protein is involved in actin cytoskeletal dynamics and interacts with the fragile X mental retardation protein. Absence of fragile X mental retardation protein causes fragile X syndrome. Because abnormal white matter microstructure has been reported in both fragile X syndrome and psychiatric disorders, we looked at the impact of 15q11.2 BP1-BP2 dosage on white matter microstructure.

METHODS: Combining a brain-wide voxel-based approach and a regional-based analysis, we analyzed diffusion tensor imaging data from healthy individuals with the deletion ($n = 30$), healthy individuals with the reciprocal duplication ($n = 27$), and IQ-matched control subjects with no large copy number variants ($n = 19$), recruited from a large genotyped population sample.

RESULTS: We found global mirror effects (deletion > control > duplication) on fractional anisotropy. The deletion group showed widespread increased fractional anisotropy when compared with duplication. Regional analyses revealed a greater effect size in the posterior limb of the internal capsule and a tendency for decreased fractional anisotropy in duplication.

CONCLUSIONS: These results show a reciprocal effect of 15q11.2 BP1-BP2 on white matter microstructure, suggesting that reciprocal chromosomal imbalances may lead to opposite changes in brain structure. Findings in the deletion overlap with previous white matter differences reported in fragile X syndrome patients, suggesting common pathogenic mechanisms derived from disruptions of cytoplasmic CYFIP1-fragile X mental retardation protein complexes. Our data begin to identify specific components of the 15q11.2 BP1-BP2 phenotype and neurobiological mechanisms of potential relevance to the increased risk for disorder.

Keywords: 15q11.2 BP1-BP2, Copy number variant, CYFIP1, Diffusion tensor imaging, Fragile X syndrome, Genetics

<https://doi.org/10.1016/j.biopsych.2018.11.004>

Copy number variants (CNVs) are rare structural variations of the genome arising from unbalanced meiotic rearrangements that can result in carriers possessing a deletion or duplication of parts of one of the chromosome pairs. An increased burden of CNVs has been observed in several neurodevelopmental and psychiatric diseases, including autism spectrum disorder (ASD), attention-deficit/hyperactivity disorder (ADHD), intellectual disability, and schizophrenia (1,2). How these damaging variants modify risk for psychopathology is still not well understood at the mechanistic level, but given their relatively high penetrance and cross-disorder pleiotropic effects, significant impact on brain structure and function is anticipated.

Altered white matter (WM) structure has been consistently reported in psychiatric disorders. For instance, in the case of schizophrenia, neuroimaging studies have shown

abnormal structural and functional connectivity at both microscopic and macroscopic levels, and such data have been central in supporting various “dysconnectivity” hypotheses of mental disease (3,4). It follows that a key question for neurobiological research is whether CNVs that are associated with neurodevelopmental disorders, including schizophrenia, are also associated with changes in WM and brain connectivity.

The 15q11.2 BP1-BP2 cytogenetic microdeletion is emerging as a recognized syndrome and has been associated with developmental, speech, language, and motor delays (5,6), and also with increased susceptibility for epilepsy (7), ADHD (5), ASD (8), and schizophrenia (9). Moreover, recent ultra high-resolution chromosomal microarray analyses report the 15q11.2 BP1-BP2 deletion as the most frequent finding in

those with only ASD or with ASD combined with intellectual disability and congenital anomalies (10). The reciprocal duplication has also been associated with increased risk for ASD (11), although its significance is still unclear (8).

Not all the individuals with the BP1-BP2 microdeletion/microduplication are clinically affected, and the genes in this region have variable expressivity. Yet, healthy individuals with the deletion and without a current clinical diagnosis frequently report mild-to-moderate impairments in motor function and deficits across several cognitive domains, including an increased incidence of difficulties in mathematics and reading skills (11,12), while healthy individuals with the duplication perform to a similar level as population control subjects (12). In a recent study by Ulfarsson *et al.* (13), these cognitive deficits were shown to be accompanied by structural changes in the brain, as assessed by structural magnetic resonance imaging (MRI), in individuals with a deletion or duplication showing reciprocal structural effects, as well as by different patterns of brain activation in tests of reading and mathematics. However, the effect on WM microstructure cannot be assessed with standard MRI, and diffusion tensor imaging (DTI) studies are needed.

The 15q11.2 BP1-BP2 region is adjacent to the areas affected in the Prader-Willi and Angelman syndromes, conditions resulting from deletions of the BP1-BP3 (type I) or the BP2-BP3 (type II) regions at 15q11.2, with the BP1-BP2 deletion partly overlapping the type I but not type II Prader-Willi/Angelman region. Individuals with type I deletion report more severe neurodevelopmental disturbances compared with individuals with the smaller type II deletion (14,15). The isolated BP1-BP2 region spans ~500 kb and encompasses four different genes: nonimprinted in Prader-Willi/Angelman syndrome 1 gene (*NIPA1*), nonimprinted in Prader-Willi/Angelman syndrome 2 gene (*NIPA2*), cytoplasmic FMR1 interacting protein 1 (*CYFIP1*), and tubulin gamma complex associated protein 5 gene (*TUBGCP5*) (16). The four genes probably play a role in brain development and function, and some work has been done to understand the extent and mechanism through which they contribute to increased risk for psychiatric disorder in the 15q11.2 BP1-BP2 region (5). For instance, the *NIPA1* gene is known to mediate Mg^{2+} transport and was associated with autosomal dominant hereditary spastic paraplegia (17), which might be caused by abnormal bone morphogenic protein (BMP) signaling as a result of dysregulations in *NIPA1* (18). The *NIPA2* gene encodes for proteins used in renal Mg^{2+} transport and metabolism and, when mutated, can cause childhood absence epilepsy (19). *TUBGCP5* is highly expressed in the subthalamic nuclei, a region linked to obsessive-compulsive disorder and ADHD (20). More is known about the *CYFIP1* gene, which is considered a prominent candidate gene contributing to 15q11.2 BP1-BP2 brain and psychological phenotypes (21). Haploinsufficiency of *Cyfp1* in mouse models, recapitulating the predicted low dosage of *CYFIP1* in 15q11.2 BP1-BP2 microdeletion, has been shown to impact two main processes: 1) the regulation of cytoskeleton remodeling by the binding of CYFIP1 protein to RAC1, and subsequent activation of the WAVE regulatory complex neurons (22,23); and 2) via direct interaction of the CYFIP1 protein with fragile X mental retardation protein

(FMRP), the repression of eIF4E-mediated translation of FMRP target messenger RNAs (24). These actions of CYFIP1 protein in the brain have the potential to influence WM, the former through effects on neuronal structure and integrity and the latter via interactions with FMRP, mutations that are known to be associated with changes in WM structure (25). Loss of FMRP function, due to an expansion repeat in the *FMR1* gene on the long arm of the X chromosome, is a cause of fragile X syndrome (FXS), the most common monogenic form of inherited intellectual disability (26).

Recently, two studies (27,28) used DTI to investigate differences in WM microstructure, comparing subjects with FXS with subjects without FXS but with similar IQ and levels of autistic symptoms (minimizing confounding effects owing to intellectual ability), and found increased fractional anisotropy (FA) as well as decreased radial diffusivity (RD) and mean diffusivity (MD) in several WM tracts in FXS subjects. Therefore, it might be anticipated, given the close molecular links between CYFIP1 and FMRP, that some degree of phenotypic overlap may be present in FXS and 15q11.2 BP1-BP2 deletion.

In the present work, we employed a DTI approach to assess WM microstructural changes associated with the 15q11.2 BP1-BP2 region in an adult cohort, selected from the Icelandic population, without a known diagnosis of schizophrenia or autism, thereby potentially avoiding the confounding effects of the disorders clinical signs. Combining brain-wide voxel-based approach (FSL Tract-Based Spatial Statistics [TBSS]) with an atlas-based analysis, allowing quantification of the magnitude of regional changes, we hypothesized that we would see a similar pattern of effects as reported for FXS: increased FA in 15q11.2 BP1-BP2 deletion. We also assessed healthy adults with the reciprocal duplication to evaluate the extent of any reciprocal effects on the neural phenotype. Our data begin to identify specific components of the 15q11.2 BP1-BP2 phenotype and mechanisms of potential relevance to the increased risk for disorder.

METHODS AND MATERIALS

Participants

In total, 30 individuals with the 15q11.2 BP1-BP2 deletion, 27 with the reciprocal duplication, and 19 control subjects with no large CNVs (NoCNV) were recruited from a large genotyped sample of approximately 160,000 subjects representing half of the Icelandic population, in which none of the subjects had any other large CNVs. Subjects between 21 and 66 years of age were included in this study, and the number of female and male subjects was the same (38 men and 38 women) and balanced in each condition group. All the subjects were clinically healthy, such that subjects were excluded if they had ICD-10 or DSM-IV diagnoses for schizophrenia or schizoaffective or bipolar disorder; were diagnosed with autism, intellectual disability, or developmental delay at the State Diagnostic and Counselling Centre of Iceland (serves children and adolescents with a disability); met psychoses criteria on the Mini-International Neuropsychiatric Interview (29); were diagnosed with schizophrenia, schizoaffective or bipolar disorder, autism, intellectual disability, or developmental delay according to self-reports (or

Table 1. Subject Characteristics

Group	Age, Years	Male/Female	IQ Score ^a	Subjects (N = 76)
Deletion	42.83 ± 12.5 (21–65)	14/16	101.2 ± 13.8	30
NoCNV	38.95 ± 10.56 (22–59)	12/7	108.3 ± 16.9	19
Duplication	43.48 ± 13.51 (22–66)	12/15	100.8 ± 11.8	27

Values are mean ± SD (range) or *n*. The IQ score included four subtests (vocabulary, similarities, block design, and matrix reasoning).

NoCNV, no large copy number variants.

^aIcelandic version of the Wechsler Abbreviated Scale of Intelligence (12). The test was performed in all individuals with the deletion, in 11 of 19 individuals in the NoCNV group, and in 26 of 27 individuals with the duplication.

reports from parents); or were using antipsychotic medication. Approval for this study was obtained from the National Bioethics Committee of Iceland and the Icelandic Data Protection Authority.

The IQ scores were assessed using an Icelandic version of the Wechsler Adult Intelligence Scale (30,31) including four subtests (vocabulary, similarities, block design, and matrix reasoning). Further details on how these individuals were genotyped and on how the cognitive assessment was performed can be found in Stefansson *et al.*'s (12) study. There were no significant differences in the IQs between groups. Although all the individuals with the deletion were tested, only 11 of 19 from the NoCNV group and 26 of 27 from the duplication group were tested. Demographic information is described in Table 1, and family relationships between subjects are described in Supplemental Table S2.

Diffusion Tensor Imaging

Water diffusion is anisotropic in healthy nerve fibers, diffusing freely along the fiber tracts but restricted in the perpendicular direction (32). DTI is sensitive to these anisotropic changes, which makes this technique particularly useful for evaluating WM microstructure (33). DTI findings are commonly reported in terms of scalars such as FA, axial diffusivity (AD), RD, and MD.

Diffusion MRI Acquisition and Preprocessing

MRI data were acquired on a Philips Achieva 1.5T system (Phillips Healthcare, Eindhoven, the Netherlands). A diffusion-weighted echo-planar imaging sequence with sensitivity encoding acceleration was used. Seventeen noncolinear gradient diffusion-weighted images (DWIs) at $b = 800$ s/mm² and one nonweighted ($b = 0$ s/mm²) image were acquired with the following parameters: echo time = 72 ms, repetition time = 9024 ms, 60 slices, slice thickness = 2 mm, field of view = 240 × 240 mm, acquisition matrix = 144 × 144, resulting in data acquired with a 1.67 × 1.67 × 2 mm voxel resolution.

Diffusion-weighted data were preprocessed using ExploreDTI v.4.8.3 (34) in MATLAB R2015a (The MathWorks, Inc., Natick, MA). First, the Brain Extraction Tool (35) (<http://www.fmrib.ox.ac.uk/fsl/>) was used to remove nonbrain tissue. Within the ExploreDTI pipeline, eddy currents and head motion correction was performed using an affine registration to the non-diffusion-weighted B₀ images, with appropriate rotation of the encoding vectors (36). Field inhomogeneities were corrected using the approach of Wu *et al.* (37). Each DWI was nonlinearly warped to the T₁-weighted image using the FA maps from the DWIs as a reference. Warps were computed

using Elastix (38), by using normalized mutual information as the cost function and constraining deformations to the phase-encoding direction. The corrected DWIs were therefore transformed to the same (undistorted) space as the T₁-weighted structural images. ExploreDTI was used to generate whole-brain maps of FA, AD, RD, and MD.

TBSS Analysis of DTI

The corrected FA, AD, RD, and MD maps were analyzed using the FSL's TBSS tool. TBSS is a whole-brain analysis (39) that starts with a nonlinear registration of the FA maps to a standard FA template (FMRIB58_FA, FMRIB Software Library FA adult template). Then, FA maps are thinned and averaged to create a study-specific WM skeleton template, and the registered FA maps are aligned to this template. An optimal FA threshold of 0.2 was chosen for the binary skeleton mask. Afterward, all the AD, RD, and MD maps were also registered to the FMRIB58_FA template.

General linear models were created to investigate copy number effects at 15q11.2 BP1-BP2. Statistically significant differences were first assessed with a multiple regression model (duplication > NoCNV > deletion and deletion > NoCNV > duplication). Total intracranial volume, age, and sex were included as covariates of no interest. Differences in DTI measures between groups were assessed using voxelwise independent *t* tests (deletion vs. NoCNV, duplication vs. NoCNV, and deletion vs. duplication), in which six different contrasts were used to assess group differences (Table 2). The randomize function from FSL was used with the

Table 2. Summary of Between-Group FSL Tract-Based Spatial Statistics Analyses Results

Contrast	Whole-Group Analysis			
	FA	AD	RD	MD
Del > NoCNV	+	–	–	–
NoCNV > Del	–	–	–	–
NoCNV > Dup	–	–	–	–
Dup > NoCNV	–	+	–	–
Del > Dup	++	–	–	–
Dup > Del	–	+	++	+

Significant voxelwise comparisons ($p < .05$) are indicated by a plus sign (+) (less significant) or two plus signs (++) (more significant), and nonsignificant results ($p > .05$) are indicated by a minus sign (–). All the *p* values were corrected using the threshold-free cluster enhancement algorithm in FSL Tract-Based Spatial Statistics.

AD, axial diffusivity; Del, deletion; Dup, duplication; FA, fractional anisotropy; MD, mean diffusivity; NoCNV, no large copy number variants; RD, radial diffusivity.

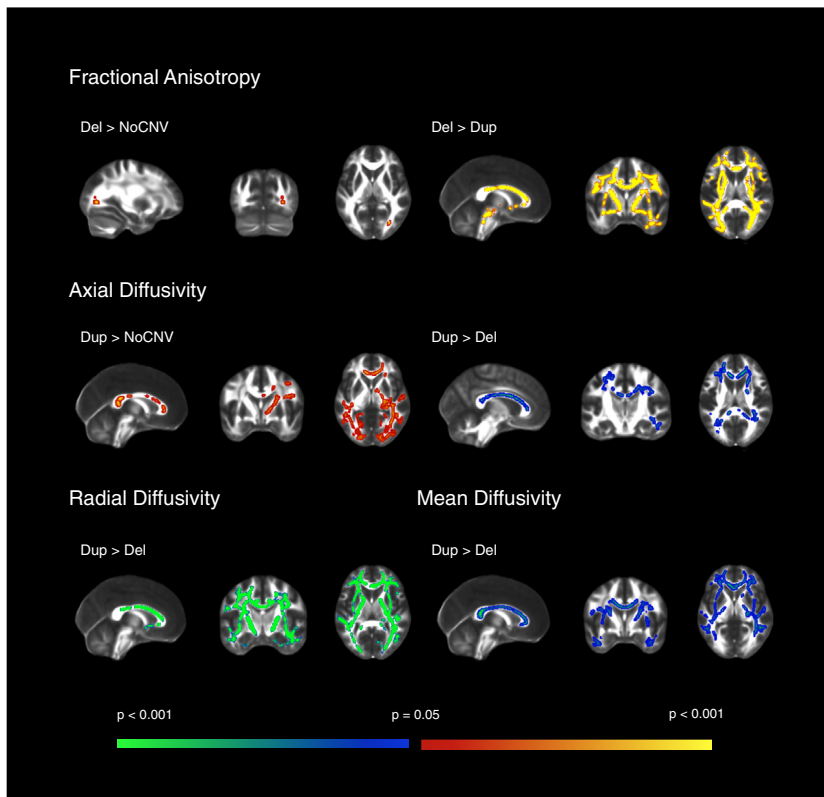


Figure 1. FSL Tract-Based Spatial Statistics whole-group voxel-based analysis. Significant results for the two-sample *t* test showing group differences between subjects with the deletion (Del) ($n = 30$), duplication (Dup) ($n = 27$), and no large copy number variants (NoCNV) ($n = 19$) for fractional anisotropy, axial diffusivity, radial diffusivity, and mean diffusivity maps. Here, only contrasts that gave rise to significant results after correction are displayed ($p < .05$, corrected). Within the significant results, red and blue code for less significant results and yellow and green for more significant results. The deletion showed widespread increased fractional anisotropy compared with the duplication and NoCNV groups, and decreased axial diffusivity, radial diffusivity, and mean diffusivity compared with the duplication group. The duplication group showed increased axial diffusivity compared with NoCNV group.

threshold-free cluster enhancement approach (40), generating cluster-size statistics based on 5000 random permutations to calculate probabilities corrected for multiple comparisons. Significant results were considered with a corrected p value $< .05$ ($p < .025$ for each tail of the two-tailed test). Anatomical WM regions showing significant group differences were identified with the John Hopkins University WM atlas (ICBM-DTI-81) (41).

Regional DTI Metrics Statistical Analyses

Region values of FA, AD, RD, and MD were obtained by averaging over the intersecting voxels between the WM DTI maps with the John Hopkins University WM atlas (ICBM-DTI-81), which comprises 48 tracts (41). To investigate between-group regional differences in FA, AD, RD, and MD, linear regression analysis was performed for each DTI measure and for each WM tract, regressing out age, sex, and total intracranial volume as covariates of no interest. For these, RStudio version 1.1.463 (R Foundation for Statistical Computing, Vienna, Austria) was used to test differences between groups.

To account for multiple testing in the pairwise comparisons, we used the standard false discovery rate method based on the Benjamini-Hochberg approach (42), taking into account the relation between different WM tracts and between DTI metrics. Only significant false discovery rate-adjusted p values are reported. Cohen's *d* effect sizes were calculated for differences between the deletion and duplication groups (43). An

interaction between sex and 15q11.2 BP1-BP2 dosage was also evaluated.

RESULTS

Between-Group TBSS Analysis

TBSS was used to assess groupwise microstructural differences in major WM pathways throughout the brain. *F* statistics showed extensive significant differences in the direction deletion $>$ NoCNV $>$ duplication in FA, and duplication $>$ NoCNV $>$ deletion in AD, RD, and MD. Further pairwise comparisons showed extensive and global increase in FA, and decreased AD, RD, and MD in the deletion group compared with the duplication group. These differences were seen in major WM tracts, such as the corpus callosum, superior longitudinal fasciculus, inferior longitudinal fasciculus (ILF), and internal capsule (IC). Moreover, the deletion group also showed increased FA when compared with the NoCNV group in the posterior thalamic radiation. The duplication group showed significantly increased AD when compared with the NoCNV group. The contrasts that gave rise to significant voxelwise results ($p < .05$, corrected) are summarized in Table 2 and TBSS results are displayed in Figure 1.

Between-Group Regional Analyses

Results from the atlas-based segmentation were consistent with the TBSS. Plots of the data confirmed the overall pattern of increased FA in the deletion group compared with the

Impact of 15q11.2 BP1-BP2 CNV on White Matter

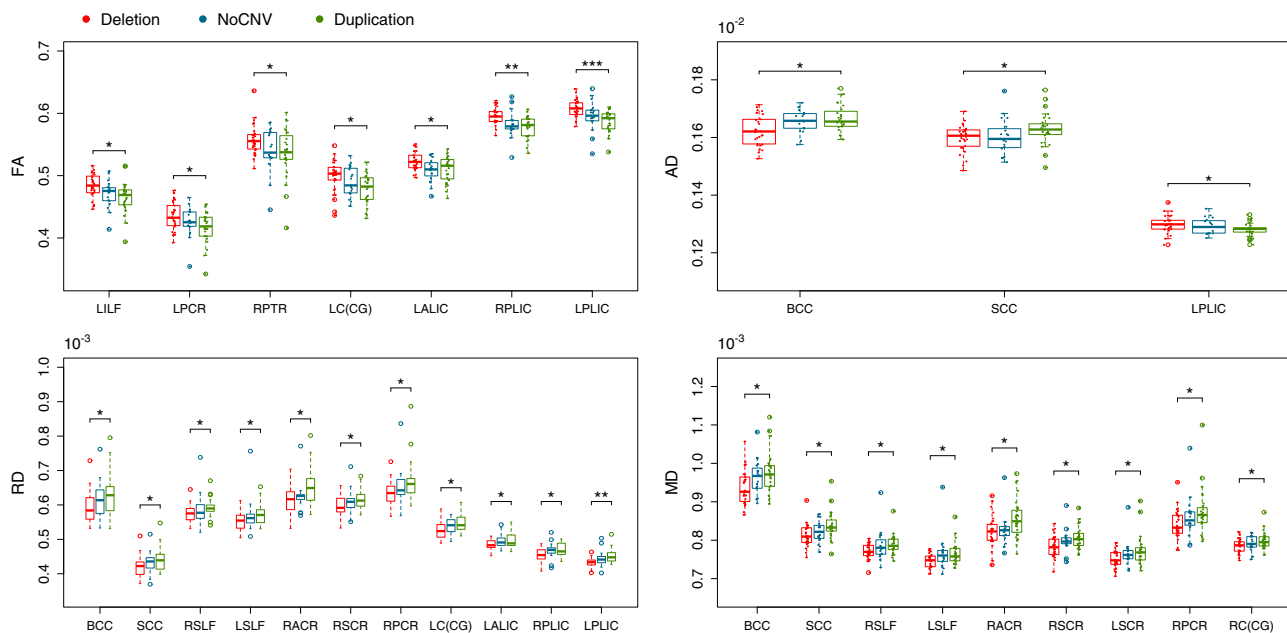


Figure 2. Boxplots showing group differences for atlas-based analyses. Significant group differences in fractional anisotropy (FA), axial diffusivity (AD), radial diffusivity (RD), and mean diffusivity (MD) are shown after multiple comparisons correction ($p < .05$). * $p < .05$, ** $p < .01$, *** $p < .001$. BCC, body of corpus callosum; LALIC, left anterior limb of the internal capsule; LC(CG), left cingulum (cingulate gyrus portion); LILF, left inferior longitudinal fasciculus; LPCR, left posterior corona radiata; LPLIC, left posterior limb of the internal capsule; LSCR, left superior corona radiata; LSLF, left superior longitudinal fasciculus; NoCNV, no large copy number variants; RACR, right anterior corona radiata; RC(CG), right cingulum (cingulate gyrus portion); RPCR, right posterior corona radiata; RPLIC, right posterior limb of the internal capsule; RPTR, right posterior thalamic radiation; RSCR, right superior corona radiata; RSLF, right superior longitudinal fasciculus; SCC, splenium of the corpus callosum.

duplication group, with the NoCNV group lying intermediate between these groups (Figure 2). However, the deletion group showed greater effect sizes than the duplication group when compared with the NoCNV group (Supplemental Table S1). Because the pairwise comparisons were only significant between the deletion and duplication groups, we only show Cohen's effect size plots for comparisons of the deletion group versus the duplication group. Cohen's effect sizes for FA and AD are displayed in Figure 3, and for all the DTI measures in Supplemental Figure S1. The largest effect size was observed for higher FA and lower RD in the posterior limb of the IC (PLIC). Across the whole brain, the effect size was medium in FA (Cohen's $d = 0.69$), RD (Cohen's $d = -0.68$), and MD (Cohen's $d = -0.63$), and small for AD (Cohen's $d = -0.38$), according to Cohen's criteria (43). Findings are summarized in Table 3 and extended in Supplemental Table S1. As some of the subjects are related, we reanalyzed the data using only one member from each family and found the results to be consistent with initial findings/primary analyses. However, a few WM tracts became nonsignificant, possibly owing to the loss of power from reducing the cohort to 65 subjects (Supplemental Figures S3 and S4).

Sex Differences

A sex-by-dosage interaction model was used to investigate sex differences in relation to 15q11.2 BP1-BP2 dosage. Although we found no significant interaction effect in the whole-group analysis, we found significant differences in effect size when analyzing men and women separately, as

assessed by using a two-tailed unpaired t test. Men showed larger effect size for increased FA ($t = 2.56$, $p = .013$) compared with women, and an overall large effect size in the whole brain (Cohen's $d = 0.99$), whereas women showed a small effect size (Cohen's $d = 0.47$). Moreover, men showed large effect sizes in more regions, namely in the genu and body of the corpus callosum, left ILF, anterior and posterior corona radiata, posterior thalamic radiation, cerebral peduncle, anterior limb of the IC, and PLIC. Women, however, showed a large effect size for increased FA in the left cingulum (cingulate gyrus portion) that is not seen in men (Supplemental Figure S2).

DISCUSSION

In a whole-brain exploratory analysis, we found consistently increased FA and decreased RD and MD in individuals with the 15q11.2 BP1-BP2 deletion compared with individuals in the reciprocal duplication group. The duplication group showed significantly increased AD relative to the NoCNV and deletion groups (Figure 1). Additional regional analyses (Figure 2) indicated that, in most WM tracts, the NoCNV group was intermediate between the deletion and duplication groups, suggesting a "mirror phenotype" (12). However, the deletion showed a greater impact on WM microstructure by showing larger effect sizes than in the duplication group (Supplemental Table S1).

We found the greatest effects in FA and RD bilaterally in the PLIC (Figure 2 and Supplemental Figure S1). The PLIC carries sensory information from the thalamus to the cortex, a key

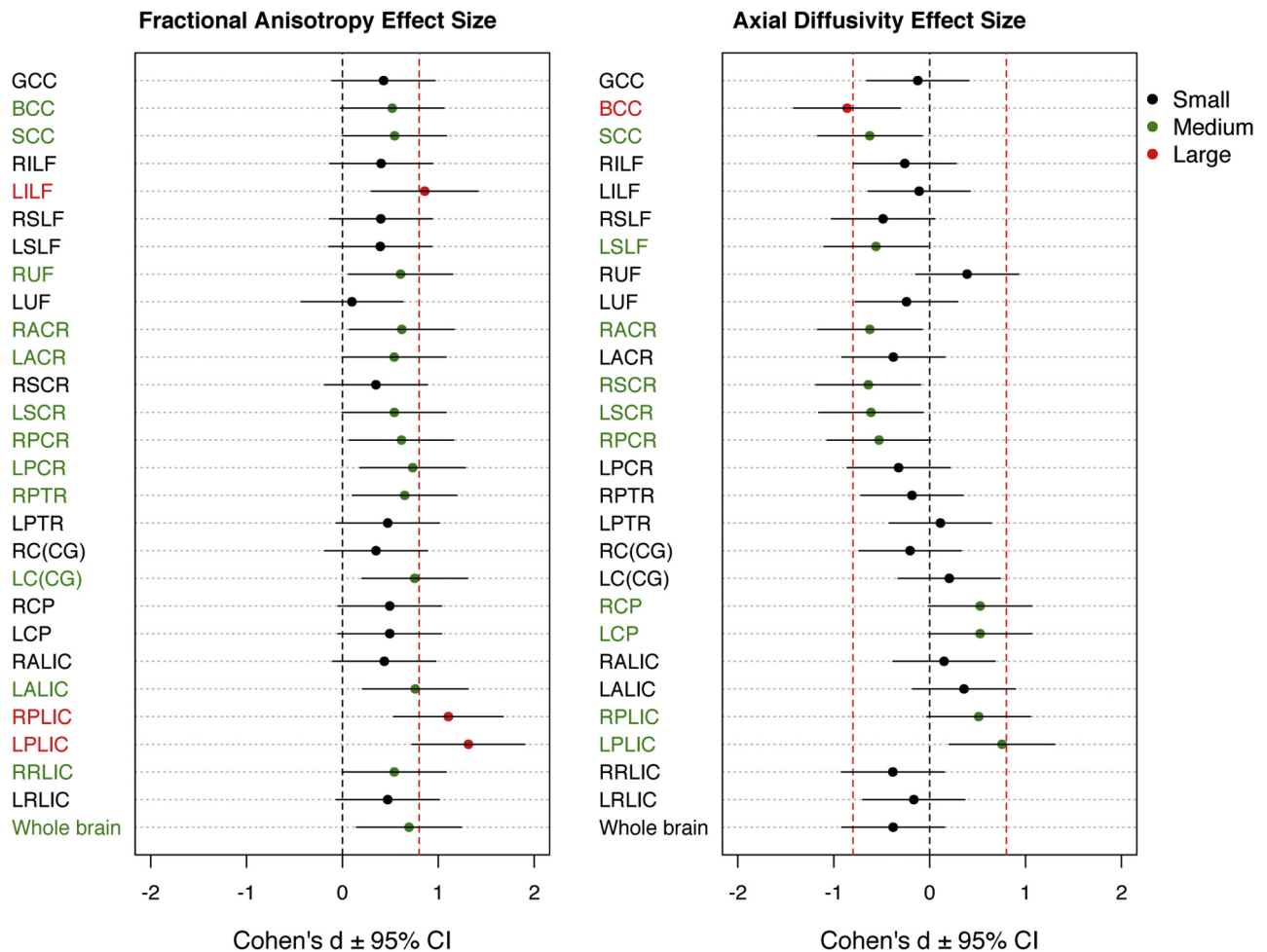


Figure 3. Effect sizes on deletion versus duplication for fractional anisotropy (left) and axial diffusivity (right). The threshold where an effect size is considered to be large [0.8, according to Cohen's criteria (43)] is represented by the vertical red dashed line. Black, green, and red dots represent small, medium, and large effect sizes, respectively. BCC, body of corpus callosum; CI, confidence interval; GCC, genu of the corpus callosum; LACR, left anterior corona radiata; LALIC, left anterior limb of the internal capsule; LC(CG), left cingulum (cingulate gyrus); LCP, left cerebral peduncle; LILF, left inferior longitudinal fasciculus; LPCR, left posterior corona radiata; LPLIC, left posterior limb of the internal capsule; LPTR, left posterior thalamic radiation; LRLIC, left retrolenticular part of internal capsule; LSCR, left superior corona radiata; LSLF, left superior longitudinal fasciculus; LUF, left uncinate fasciculus; RACR, right anterior corona radiata; RALIC, right anterior limb of the internal capsule; RC(CG), right cingulum (cingulate gyrus); RCP, right cerebral peduncle; RILF, right inferior longitudinal fasciculus; RPCR, right posterior corona radiata; RPLIC, right posterior limb of the internal capsule; RPTR, right posterior thalamic radiation; RRLIC, right retrolenticular part of internal capsule; RSCR, right superior corona radiata; RSLF, right superior longitudinal fasciculus; RUF, right uncinate fasciculus; SCC, splenium of the corpus callosum.

sensorimotor relay area implicated in schizophrenia (44) and ASD (45). In schizophrenia, reductions in FA have been reported in the IC (4). However, in ASD patients, functional connectivity between motor regions of the thalamus and cortex was found to be hyperconnected (46), and a longitudinal study showed that the thalamus and IC undergo an atypical development trajectory in ASD, in which increasing connectivity from childhood through adolescence and adulthood was seen (47). The increased FA in the PLIC seen in the deletion group could be a result of an abnormal thalamus and IC development, which could relate to motor delays frequently reported in the BP1-BP2 deletion. Thus, a younger group is needed to look at the age trajectory of FA and its correlates with motor function outcome. We also found a large effect size

in FA in the left ILF, a major WM tract thought to be critical to semantic processing and involved in dyslexia. Dyslexia and dyscalculia are common features in 15q11.2 BP1-BP2 deletion, and individuals with the deletion were previously shown to have a smaller fusiform gyrus (13), a structure that was shown to play a role in reading and mathematics and that connects to the ILF (48).

Although all DTI changes seem to be consistent throughout the brain, regional analysis shows increases and decreases in AD in different WM tracts in the deletion (Figure 2 and 3). Previously, AD has been related to axonal damage and RD with axonal density and myelin (49). FA reflects the relative contribution of AD and RD. Because we find global increased FA, including areas where AD is decreased, the RD

Table 3. Comparisons Between the Deletion and Duplication of the 15q11.2 BP1-BP2 Region on FA, AD, RD, and MD

Dependent Variable	ROI	t	p Value (FDR Corrected)	Effect Size	
FA Del vs. Dup	LILF	-3.15	.02 ^a	0.86	
	LPCR	-2.85	.03 ^a	0.73	
	RPTR	-2.68	.04 ^a	0.65	
	LC(CG)	-2.93	.03 ^a	0.75	
	LALIC	-2.97	.03 ^a	0.76	
	RPLIC	-4.31	.003 ^b	1.11	
	LPLIC	-5.06	.0006 ^c	1.31	
AD Del vs. Dup	BCC	3.55	.02 ^a	-0.86	
	SCC	-2.62	.04 ^a	-0.62	
	LPLIC	-2.88	.03 ^a	0.75	
RD Del vs. Dup	BCC	2.89	.03 ^a	-0.65	
	SCC	2.88	.03 ^a	-0.68	
	RSLF	2.69	.04 ^a	-0.70	
	LSLF	2.69	.04 ^a	-0.69	
	RACR	3.01	.03 ^a	-0.73	
	RSCR	2.78	.03 ^a	-0.71	
	RPCR	2.78	.03 ^a	-0.69	
	LC(CG)	3.22	.03 ^a	-0.83	
	LALIC	2.80	.03 ^a	-0.72	
	RPLIC	3.32	.02 ^a	-0.84	
	LPLIC	4.48	.002 ^b	-1.16	
	MD Del vs. Dup	BCC	3.38	.02 ^a	-0.77
		SCC	3.31	.02 ^a	-0.78
RSLF		2.99	.03 ^a	-0.78	
LSLF		2.95	.03 ^a	-0.77	
RACR		3.03	.03 ^a	-0.76	
RSCR		2.89	.03 ^a	-0.75	
LSCR		2.60	.04 ^a	-0.65	
RPCR		2.63	.03 ^a	-0.66	
RC(CG)		2.97	.03 ^a	-0.67	

AD, axial diffusivity; BCC, body of corpus callosum; Del, deletion; Dup, duplication; FA, fractional anisotropy; FDR, false discovery rate; LALIC, left anterior limb of the internal capsule; LC(CG), left cingulum (cingulate gyrus portion); LILF, left inferior longitudinal fasciculus; LPCR, left posterior corona radiata; LPLIC, left posterior limb of the internal capsule; LSCR, left superior corona radiata; LSLF, left superior longitudinal fasciculus; MD, mean diffusivity; RACR, right anterior corona radiata; RC(CG), right cingulum (cingulate gyrus portion); RD, radial diffusivity; ROI, region of interest; RPCR, right posterior corona radiata; RPLIC, right posterior limb of the internal capsule; RPTR, right posterior thalamic radiation; RSCR, right superior corona radiata; RSLF, right superior longitudinal fasciculus; SCC, splenium of the corpus callosum.

^ap < .05.

^bp < .01.

^cp < .001.

contribution seems to be stronger. The global decreased RD in the corpus callosum (and other areas) found here could be a result of increased axonal density that may also explain the increased WM volume found previously in the corpus callosum in healthy individuals with the deletion (12,13). Furthermore, areas with reduced AD could be a result of reduced axonal integrity.

Increased FA arising from abnormal WM organization has been reported before in patients with Williams syndrome, a chromosomal disorder associated with visuospatial deficits, in which higher FA in the superior longitudinal fasciculus tract was correlated with deficits in visuospatial construction (50). The globally increased FA in the deletion group could point to either a compensatory mechanism in response to primary deficits, as a protection against disease onset, or a diffuse dysregulation of neuronal dynamics, increasing the risk for psychiatric disorder. Hence, a central question is how each gene within this CNV region could contribute to this phenotype. All four genes in this region are highly conserved and expressed in human central nervous system, and may play a role in 15q11.2 BP1-BP2-associated phenotypes. Moreover, mutations in each gene were associated with different disorders: *NIPA1* with autosomal-dominant hereditary spastic paraplegia (17), *NIPA2* with childhood absence epilepsy (19), *TUBGCP5* with ADHD and obsessive-compulsive disorder (20), and *CYFIP1* with increasing susceptibility to ASD (51) and with schizophrenia (52). Furthermore, dysregulations in mechanisms related to *NIPA1* and *CYFIP1* genes might have an impact on WM microstructure. *NIPA1* was found to inhibit the BMP signaling via interaction with BMP receptor type II (18), which is crucial for typical axonal growth, guidance, and differentiation. In a *Drosophila* model, enhanced BMP signaling resulted in abnormal distal axonal overgrowth at the presynaptic neuromuscular junction (53), which could result in increased axonal density. *CYFIP1*, on the other hand, has a crucial role in actin remodeling during neural wiring, in which dysregulations could result in changes in axonal density, organization, and myelination (54,55).

Recently, two articles by the same group [Green *et al.* (27) and Hall *et al.* (28)] reported increased FA and decreased RD and MD in FXS patients compared with IQ-matched control subjects. There is, therefore, a marked degree of overlap between our current findings in 15q11.2 BP1-BP2 deletion and WM changes in FXS, consistent a priori with the suggested molecular link between *CYFIP1* and FMRP. The question arises, what common neural mechanism(s) may contribute to this overlap in WM phenotype? Here, evidence that both FMRP and *CYFIP1* influence diverse aspects of synaptic function, as well as effects on dendritic architecture, may be of relevance (56–58). Both *Fmr1* knockout and *Cyfp1* hemizygous-null adult mice have in common an increased ratio of immature-to-mature spines (59–63). While the relationship between neuronal density and number of synapses per neuron is still not well understood, the observed increased FA in FXS (26,27) and 15q11.2 BP1-BP2 deletion (this study) could be caused by an increased neuronal density as an adaptive response to an increased number of immature spines and reduced functional synapses.

Further speculations as to cellular/molecular mechanisms underlying the observed WM changes should, at this stage, be made with caution. DTI data are difficult to relate in a definitive way to underlying cellular changes, and their investigation would require postmortem or biopsy. To overcome this, translational models of human disease in animals are an attractive alternative to explore individual genotype-phenotype relationships (64). Therefore, owing to the

potential role of *CYFIP1* in WM microstructure phenotypes associated with the 15q11.2 BP1-BP2 region, it would be informative to assess DTI data using low-dosage *Cyfp1* animal models. Furthermore, direct access to brain tissue would allow an analysis of underlying cellular changes relevant to the DTI findings.

Clinical phenotypes of reciprocal CNVs have been broadly classified into four general categories: mirrored, identical, overlapping, and unique (65). The 16p11.2 (66), 1q21.1 (67), 3q29 (68), and 17p11.2 (69) CNVs have been associated with mirrored phenotypes. Comparable to what we have reported here, increased FA was found in individuals with the 16p11.2 deletion, and opposite changes were found in individuals with the reciprocal duplication (70). The extensive reciprocal effects on WM reported here, and in previous studies (12,13), show that the 15q11.2 BP1-BP2 also affects WM microstructure in a dosage-dependent way. When it comes to neuropsychiatric and behavioral findings at this locus, the picture is less clear (6). The microdeletion has been associated with developmental delay, schizophrenia, and autism, whereas duplication is generally not considered as a risk locus for schizophrenia (71) and has not come out as a significant risk variant for developmental delay in recent large-scale genetic studies (72). Moreover, the microdeletion has been shown to have a greater impact on cognitive function in healthy individuals, particularly in the acquisition of mathematical skills and reading, whereas individuals in the duplication group performed similarly to the NoCNV group (12,13). In this study, the microdeletion also shows a greater impact on WM microstructure, with larger effect sizes than the microduplication (Supplemental Table S1), but the lack of cognitive data in this sample did not allow us to find correlations between increased FA and cognition.

A limitation of this study was the impossibility to correct regions with crossing fibers, and reductions in the number of fibers in these regions might give rise to increased FA. The fact that we see an overall increased FA, and not only in crossing fiber regions, makes this less likely to be the main cause of the group differences. In the current analysis, we could not find a sex-by-dosage interaction, but men showed larger effect sizes than women (Supplemental Figure S2), suggesting sex-dependent changes in WM. Although the molecular causality behind this sex difference is still unclear, sex bias has been observed in neurodevelopmental disorders (73). Moreover, 15q11.2 BP1-BP2 was shown to have a greater impact on ASD-related phenotype in men than women (8). Further larger studies will, however, be required to determine the exact interaction of sex and 15q11.2 BP1-BP2 dosage.

Using complementary methods of analysis, this study shows a consistent pattern of WM microstructure alterations, which are consistent with recent FXS DTI studies, beginning to reveal brain mechanisms underlying the complex routes to psychopathology mediated by mutations at the 15q11.2 BP1-BP2 cytogenetic region. The reciprocal effects on WM microstructure, described here, suggest that deviations from normal gene dosage in each direction can lead to abnormalities in brain development, underlining the importance of studying how reciprocal chromosomal imbalances impact neural processes, which might have important implications for therapeutic intervention.

ACKNOWLEDGMENTS AND DISCLOSURES

This work was supported by Innovative Medicines Initiative Joint Undertaking Grant Nos. 115008 (NEWMEDS [to KS]) and 115300 (EUAIMS [to KS]), of which resources were composed of European Federation of Pharmaceutical Industries and Associations in-kind contribution and financial contribution from European Union Seventh Framework Programme (EU-FP7/2007-2013) Grant No. 602450 (IMAGEMEND) and FP7-People-2011-IAPP Grant No. 286213 (PsychDPC); Wellcome Trust Strategic Award "DEFINE" Grant No. 100202/Z/12/Z (to JH); and core support from the Neuroscience and Mental Health Research Institute, Cardiff University (PhD grant to AS). Approval for this study was obtained from the National Bioethics Committee of Iceland and the Icelandic Data Protection Authority.

We are grateful to the participants and we thank the nurses and staff at the Research Recruitment Centre and technicians and staff at Röntgen Domus.

MOU, HS, OG, GBW, and KS are employees of deCODE genetics/Amgen. The remaining authors report no biomedical financial interests or potential conflicts of interest.

ARTICLE INFORMATION

From the Cardiff University Brain Research Imaging Centre (AIS, DEJL, MD), School of Psychology; Neuroscience and Mental Health Research Institute (AIS, DEJL, LSW, MJO, JH); and Division of Psychological Medicine and Clinical Neurosciences (AIS, DEJL, LSW, MJO, JH) and MRC Centre for Neuropsychiatric Genetics and Genomics (LSW, MJO, JH), School of Medicine, Cardiff University, Cardiff, United Kingdom; and deCODE genetics/Amgen (MOU, HS, OG, GBW, KS); and the Faculty of Electrical Engineering (MOU) Faculty of Medicine (GBW), University of Iceland, Reykjavik, Iceland.

JH and KS contributed equally to this work.

Address correspondence to Jeremy Hall, M.D., Ph.D., Neuroscience and Mental Health Research Institute, Hadyn Ellis Building, Cathays, Cardiff, CF24 4HQ; E-mail: hallj10@cardiff.ac.uk; or Kari Stefansson, M.D., Ph.D., deCODE genetics/Amgen, Sturlugata 8, IS-101 Reykjavik, Iceland; E-mail: kstefans@decode.is.

Received May 30, 2018; revised Nov 7, 2018; accepted Nov 12, 2018.

Supplementary material cited in this article is available online at <https://doi.org/10.1016/j.biopsych.2018.11.004>.

REFERENCES

1. Kirov G (2015): CNVs in neuropsychiatric disorders. *Hum Mol Genet* 24:R45–R49.
2. Grayton HM, Fernandes C, Rujescu D, Collier DA (2012): Copy number variations in neurodevelopmental disorders. *Prog Neurobiol* 99:81–91.
3. van den Heuvel MP, Fornito A (2014): Brain networks in schizophrenia. *Neuropsychol Rev* 24:32–48.
4. McIntosh AM, Job DE, Moorhead TWJ, Harrison LK, Lawrie SM, Johnstone EC (2005): White matter density in patients with schizophrenia, bipolar disorder and their unaffected relatives. *Biol Psychiatry* 58:254–257.
5. Cox DM, Butler MG (2015): The 15q11.2 BP1–BP2 microdeletion syndrome: A review. *Int J Mol Sci* 16:4068–4082.
6. Butler MG (2017): Clinical and genetic aspects of the 15q11.2 BP1–BP2 microdeletion disorder. *J Intellect Disabil Res* 61:568–579.
7. de Kovel CGF, Trucks H, Helbig I, Mefford HC, Baker C, Leu C, et al. (2010): Recurrent microdeletions at 15q11.2 and 16p13.11 predispose to idiopathic generalized epilepsies. *Brain J Neurol* 133:23–32.
8. Chaste P, Sanders SJ, Mohan KN, Klei L, Song Y, Murtha MT, et al. (2014): Modest impact on risk for autism spectrum disorder of rare copy number variants at 15q11.2, specifically breakpoints 1 to 2: Effects 15q11.2 CNV on autism risk. *Autism Res* 7:355–362.
9. Stefansson H, Rujescu D, Cichon S, Pietiläinen OPH, Ingason A, Steinberg S, et al. (2008): Large recurrent microdeletions associated with schizophrenia. *Nature* 455:232–236.
10. Ho KS, Wassman ER, Baxter AL, Hensel CH, Martin MM, Prasad A, et al. (2016): Chromosomal microarray analysis of consecutive individuals with autism spectrum disorders using an ultra-high resolution

Impact of 15q11.2 BP1-BP2 CNV on White Matter

- chromosomal microarray optimized for neurodevelopmental disorders. *Int J Mol Sci* 17:2070.
11. Burnside RD, Pasion R, Mikhail FM, Carroll AJ, Robin NH, Youngs EL, *et al.* (2011): Microdeletion/microduplication of proximal 15q11.2 between BP1 and BP2: A susceptibility region for neurological dysfunction including developmental and language delay. *Hum Genet* 130:517–528.
 12. Stefansson H, Meyer-Lindenberg A, Steinberg S, Magnusdottir B, Morgen K, Arnarsdottir S, *et al.* (2013): CNVs conferring risk of autism or schizophrenia affect cognition in controls. *Nature* 505:361–366.
 13. Ulfarsson MO, Walters GB, Gustafsson O, Steinberg S, Silva A, Doyle OM, *et al.* (2017): 15q11.2 CNV affects cognitive, structural and functional correlates of dyslexia and dyscalculia. *Transl Psychiatry* 7:e1109.
 14. Butler MG, Bittel DC, Kibiryeva N, Talebizadeh Z, Thompson T (2004): Behavioral differences among subjects with Prader-Willi syndrome and type I or type II deletion and maternal disomy. *Pediatrics* 113:565–573.
 15. Bittel DC, Kibiryeva N, Butler MG (2006): Expression of 4 genes between chromosome 15 breakpoints 1 and 2 and behavioral outcomes in Prader-Willi syndrome. *Pediatrics* 118:e1276–e1283.
 16. Chai J-H, Locke DP, Grealis JM, Knoll JHM, Ohta T, Dunai J, *et al.* (2003): Identification of four highly conserved genes between breakpoint hotspots BP1 and BP2 of the Prader-Willi/Angelman syndromes deletion region that have undergone evolutionary transposition mediated by flanking duplicons. *Am J Hum Genet* 73:898–925.
 17. Rainier S, Chai J-H, Tokarz D, Nicholls RD, Fink JK (2003): NIPA1 gene mutations cause autosomal dominant hereditary spastic paraplegia (SPG6). *Am J Hum Genet* 73:967–971.
 18. Tsang HTH, Edwards TL, Wang X, Connell JW, Davies RJ, Durrington HJ, *et al.* (2009): The hereditary spastic paraplegia proteins NIPA1, spastin and spartin are inhibitors of mammalian BMP signaling. *Hum Mol Genet* 18:3805–3821.
 19. Xie H, Zhang Y, Zhang P, Wang J, Wu Y, Wu X, *et al.* (2014): Functional study of NIPA2 mutations identified from the patients with childhood absence epilepsy. *PLoS One* 9:e109749.
 20. Grabli D, McCairn K, Hirsch EC, Agid Y, Féger J, François C, *et al.* (2004): Behavioural disorders induced by external globus pallidus dysfunction in primates: I. Behavioural study. *Brain J Neurol* 127:2039–2054.
 21. Yoon K-J, Nguyen HN, Ursini G, Zhang F, Kim N-S, Wen Z, *et al.* (2014): Modeling a genetic risk for schizophrenia in iPSCs and mice reveals neural stem cell deficits associated with adherens junctions and polarity. *Cell Stem Cell* 15:79–91.
 22. Chen Z, Borek D, Padrick SB, Gomez TS, Metlagel Z, Ismail A, *et al.* (2010): Structure and control of the actin regulatory WAVE complex. *Nature* 468:533–538.
 23. De Rubeis S, Pasciuto E, Li KW, Fernández E, Di Marino D, Buzzi A, *et al.* (2013): CYFIP1 coordinates mRNA translation and cytoskeleton remodeling to ensure proper dendritic spine formation. *Neuron* 79:1169–1182.
 24. Napoli I, Mercaldo V, Boyl PP, Eleuteri B, Zalfa F, De Rubeis S, *et al.* (2008): The fragile X syndrome protein represses activity-dependent translation through CYFIP1, a New 4E-BP. *Cell* 134:1042–1054.
 25. Barnea-Goraly N, Eliez S, Hedeus M, Menon V, White CD, Moseley M, *et al.* (2003): White matter tract alterations in fragile X syndrome: Preliminary evidence from diffusion tensor imaging. *Am J Med Genet B Neuropsychiatr Genet* 118:81–88.
 26. Lozano R, Rosero CA, Hagerman RJ (2014): Fragile X spectrum disorders. *Intractable Rare Dis Res* 3:134–146.
 27. Green T, Barnea-Goraly N, Raman M, Hall SS, Lightbody AA, Bruno JL, *et al.* (2015): Specific effect of the fragile-X mental retardation-1 gene (FMR1) on white matter microstructure. *Br J Psychiatry* 207:143–148.
 28. Hall SS, Dougherty RF, Reiss AL (2016): Profiles of aberrant white matter microstructure in fragile X syndrome. *Neuroimage Clin* 11:133–138.
 29. Sheehan DV, Lecrubier Y, Sheehan KH, Amorim P, Janavs J, Weiller E, *et al.* (1998): The Mini-International Neuropsychiatric Interview (M.I.N.I.): The development and validation of a structured diagnostic psychiatric interview for DSM-IV and ICD-10. *J Clin Psychiatry* 59(suppl 20):22–33, quiz 34–57.
 30. Woerner C, Overstreet K (1999): Wechsler Abbreviated Scale of Intelligence (WASI). San Antonio, TX: Psychological Corporation.
 31. Guðmundsson E (2016): Staðlað greindarpróf fyrir fullorðna á Íslandi: WASIIS. (Standardized intelligence test for adults in Iceland: WASIIS.). Available at: <https://www.hirsla.lsh.is/handle/2336/620069>. Accessed September 20, 2018.
 32. Jones DK, Leemans A (2011): Diffusion tensor imaging. In: Modo M, Bulte JWM, editors. *Magnetic Resonance Neuroimaging: Methods and Protocols*. Totowa, NJ: Humana Press, 127–144.
 33. Soares JM, Marques P, Alves V, Sousa N (2013): A hitchhiker's guide to diffusion tensor imaging. *Front Neurosci* 7:31.
 34. Leemans A, Jeurissen B, Sijbers J, Jones DK (2009): ExploreDTI: A graphical toolbox for processing, analyzing, and visualizing diffusion MR data. *Proc Intl Soc Mag Reson Med* 17:3537.
 35. Smith SM (2002): Fast robust automated brain extraction. *Hum Brain Mapp* 17:143–155.
 36. Leemans A, Jones DK (2009): The B-matrix must be rotated when correcting for subject motion in DTI data. *Magn Reson Med* 61:1336–1349.
 37. Wu M, Chang LC, Walker L, Lemaitre H, Barnett AS, Marengo S, *et al.* (2008): Comparison of EPI distortion correction methods in diffusion tensor MRI using a novel framework. *Med Image Comput Comput Assist Interv* 11:321–329.
 38. Klein S, Staring M, Murphy K, Viergever MA, Pluim JPW (2010): elastix: A toolbox for intensity-based medical image registration. *IEEE Trans Med Imaging* 29:196–205.
 39. Smith SM, Jenkinson M, Johansen-Berg H, Rueckert D, Nichols TE, Mackay CE, *et al.* (2006): Tract-based spatial statistics: Voxelwise analysis of multi-subject diffusion data. *Neuroimage* 31:1487–1505.
 40. Smith SM, Nichols TE (2009): Threshold-free cluster enhancement: Addressing problems of smoothing, threshold dependence and localisation in cluster inference. *Neuroimage* 44:83–98.
 41. Mori S, Wakana S, van Zijl PCM, Nagae-Poetscher LM (2005): *MRI Atlas of Human White Matter*, 1st ed. New York: Elsevier.
 42. Benjamini Y, Hochberg Y (1995): Controlling the false discovery rate: A practical and powerful approach to multiple testing. *J R Stat Soc Ser B Methodol* 57:289–300.
 43. Cohen J (1977): Chapter 1. The concepts of power analysis. In: *Statistical Power Analysis for the Behavioral Sciences* (Revised Edition). San Diego, CA: Academic Press, 1–17.
 44. Pergola G, Selvaggi P, Trizio S, Bertolino A, Blasi G (2015): The role of the thalamus in schizophrenia from a neuroimaging perspective. *Neurosci Biobehav Rev* 54:57–75.
 45. Doll CA, Broadie K (2014): Impaired activity-dependent neural circuit assembly and refinement in autism spectrum disorder genetic models. *Front Cell Neurosci* 8:30.
 46. Mizuno A, Villalobos ME, Davies MM, Dahl BC, Müller R-A (2006): Partially enhanced thalamocortical functional connectivity in autism. *Brain Res* 1104:160–174.
 47. McLaughlin K, Travers BG, Dadalco OI, Dean DC, Tromp D, Adluru N, *et al.* (2018): Longitudinal development of thalamic and internal capsule microstructure in autism spectrum disorder. *Autism Res* 11:450–462.
 48. Kiernan JA (2012): Anatomy of the temporal lobe. *Epilepsy Res Treat* 2012:176157.
 49. Hecke WV, Emsell L, Sunaert S (2015): *Diffusion Tensor Imaging: A Practical Handbook*. New York: Springer.
 50. Hoeft F, Barnea-Goraly N, Haas BW, Golarai G, Ng D, Mills D, *et al.* (2007): More is not always better: Increased fractional anisotropy of superior longitudinal fasciculus associated with poor visuospatial abilities in Williams syndrome. *J Neurosci* 27:11960–11965.
 51. Toma C, Torrico B, Hervás A, Valdés-Mas R, Tristán-Noguero A, Padillo V, *et al.* (2014): Exome sequencing in multiplex autism families suggests a major role for heterozygous truncating mutations. *Mol Psychiatry* 19:784–790.

52. Tam GWC, van de Lagemaat LN, Redon R, Strathdee KE, Croning MDR, Malloy MP, *et al.* (2010): Confirmed rare copy number variants implicate novel genes in schizophrenia. *Biochem Soc Trans* 38:445–451.
53. Wang X, Shaw WR, Tsang HTH, Reid E, O'Kane CJ (2007): *Drosophila* spichthyn inhibits BMP signaling and regulates synaptic growth and axonal microtubules. *Nat Neurosci* 10:177–185.
54. Dent EW, Gertler FB (2003): Cytoskeletal dynamics and transport in growth cone motility and axon guidance. *Neuron* 40:209–227.
55. Bauer NG, Richter-Landsberg C, Ffrench-Constant C (2009): Role of the oligodendroglial cytoskeleton in differentiation and myelination. *Glia* 57:1691–1705.
56. Sidorov MS, Auerbach BD, Bear MF (2013): Fragile X mental retardation protein and synaptic plasticity. *Mol Brain* 6:15.
57. Antar LN, Li C, Zhang H, Carroll RC, Bassell GJ (2006): Local functions for FMRP in axon growth cone motility and activity-dependent regulation of filopodia and spine synapses. *Mol Cell Neurosci* 32:37–48.
58. Li C, Bassell GJ, Sasaki Y (2009): Fragile X mental retardation protein is involved in protein synthesis-dependent collapse of growth cones induced by semaphorin-3A. *Front Neural Circuits* 3:11.
59. Tessier CR, Broadie K (2008): *Drosophila* fragile X mental retardation protein developmentally regulates activity-dependent axon pruning. *Development* 135:1547–1557.
60. Nimchinsky EA, Oberlander AM, Svoboda K (2001): Abnormal development of dendritic spines in FMR1 knock-out mice. *J Neurosci* 21:5139–5146.
61. Pathania M, Davenport EC, Muir J, Sheehan DF, López-Doménech G, Kittler JT (2014): The autism and schizophrenia associated gene CYFIP1 is critical for the maintenance of dendritic complexity and the stabilization of mature spines. *Transl Psychiatry* 4:e374.
62. Oguro-Ando A, Rosensweig C, Herman E, Nishimura Y, Werling D, Bill BR, *et al.* (2015): Increased CYFIP1 dosage alters cellular and dendritic morphology and dysregulates mTOR. *Mol Psychiatry* 20:1069–1078.
63. Abekhouk S, Sahin HB, Grossi M, Zongaro S, Maurin T, Madrigal I, *et al.* (2017): New insights into the regulatory function of CYFIP1 in the context of WAVE- and FMRP-containing complexes. *Dis Model Mech* 10:463–474.
64. Schofield PN, Hoehndorf R, Gkoutos GV (2012): Mouse genetic and phenotypic resources for human genetics. *Hum Mutat* 33:826–836.
65. Golzio C, Katsanis N (2013): Genetic architecture of reciprocal CNVs. *Curr Opin Genet Dev* 23:240–248.
66. Weiss LA, Shen Y, Korn JM, Arking DE, Miller DT, Fossdal R, *et al.* (2008): Association between microdeletion and microduplication at 16p11.2 and autism. *N Engl J Med* 358:667–675.
67. Brunetti-Piéri N, Berg JS, Scaglia F, Belmont J, Bacino CA, Sahoo T, *et al.* (2008): Recurrent reciprocal 1q21.1 deletions and duplications associated with microcephaly or macrocephaly and developmental and behavioral abnormalities. *Nat Genet* 40:1466–1471.
68. Ballif BC, Theisen A, Coppinger J, Gowans GC, Hersh JH, Madan-Khetarpal S, *et al.* (2008): Expanding the clinical phenotype of the 3q29 microdeletion syndrome and characterization of the reciprocal microduplication. *Mol Cytogenet* 1:8.
69. Lacaria M, Saha P, Potocki L, Bi W, Yan J, Girirajan S, *et al.* (2012): A duplication CNV that conveys traits reciprocal to metabolic syndrome and protects against diet-induced obesity in mice and men. *PLoS Genet* 8:e1002713.
70. Chang YS, Owen JP, Pojman NJ, Thieu T, Bukshpun P, Wakahiro MLJ, *et al.* (2016): Reciprocal white matter alterations due to 16p11.2 chromosomal deletions versus duplications: White matter microstructure in 16p11.2 CNVs. *Hum Brain Mapp* 37:2833–2848.
71. Kirov G, Rees E, Walters JTR, Escott-Price V, Georgieva L, Richards AL, *et al.* (2014): The penetrance of copy number variations for schizophrenia and developmental delay. *Biol Psychiatry* 75:378–385.
72. Coe BP, Witherspoon K, Rosenfeld JA, van Bon BWM, Vulto-van Silfhout AT, Bosco P, *et al.* (2014): Refining analyses of copy number variation identifies specific genes associated with developmental delay. *Nat Genet* 46:1063–1071.
73. Rinehart NJ, Cornish KM, Tonge BJ (2011): Gender differences in neurodevelopmental disorders: Autism and fragile x syndrome. *Curr Top Behav Neurosci* 8:209–229.

ARTICLE

<https://doi.org/10.1038/s41467-019-11119-7>

OPEN

Cyfp1 haploinsufficient rats show white matter changes, myelin thinning, abnormal oligodendrocytes and behavioural inflexibility

Ana I. Silva ^{1,2,3}, Josephine E. Haddon^{1,2,4}, Yasir Ahmed Syed^{1,5}, Simon Trent^{1,2}, Tzu-Ching E. Lin^{1,2}, Yateen Patel^{1,2}, Jenny Carter^{1,2}, Niels Haan ^{1,2}, Robert C. Honey⁴, Trevor Humby^{1,4}, Yaniv Assaf⁶, Michael J. Owen ^{1,2}, David E.J. Linden^{1,2,3,7}, Jeremy Hall^{1,2} & Lawrence S. Wilkinson^{1,2,4}

The biological basis of the increased risk for psychiatric disorders seen in 15q11.2 copy number deletion is unknown. Previous work has shown disturbances in white matter tracts in human carriers of the deletion. Here, in a novel rat model, we recapitulated low dosage of the candidate risk gene *CYFIP1* present within the 15q11.2 interval. Using diffusion tensor imaging, we first showed extensive white matter changes in *Cyfp1* mutant rats, which were most pronounced in the corpus callosum and external capsule. Transmission electron microscopy showed that these changes were associated with thinning of the myelin sheath in the corpus callosum. Myelin thinning was independent of changes in axon number or diameter but was associated with effects on mature oligodendrocytes, including aberrant intracellular distribution of myelin basic protein. Finally, we demonstrated effects on cognitive phenotypes sensitive to both disruptions in myelin and callosal circuitry.

¹Neuroscience and Mental Health Research Institute, MRC Centre for Neuropsychiatric Genetics and Genomics, Hadyr Ellis Building, Cathays, Cardiff CF24 4HQ, UK. ²Division of Psychological Medicine and Clinical Neurosciences, School of Medicine, Cardiff University, Cardiff, CF24 4HQ, UK. ³Cardiff University Brain Research Imaging Centre, School of Psychology, Cardiff University, Maindy Road, Cardiff CF24 4HQ, UK. ⁴School of Psychology, Cardiff University, Cardiff, Park Place CF10 3AT, UK. ⁵School of Bioscience, The Sir Martin Evans Building, Museum Ave, Cardiff CF10 3AX, UK. ⁶Department of Neurobiology, Tel-Aviv University, Ramat Aviv, 6997801 Tel-Aviv, Israel. ⁷School of Mental Health and Neuroscience, Maastricht University, Maastricht, 6229 ER, The Netherlands. Correspondence and requests for materials should be addressed to J.H. (email: Hallj10@cardiff.ac.uk) or to L.S.W. (email: wilkinsonl@cardiff.ac.uk)

Low gene dosage of the cytoplasmic FMRP interacting protein 1 (*CYFIP1*) gene is a candidate risk factor for psychopathology by virtue of its involvement in the pathogenic 15q11.2 BP1-BP2 copy number variant (CNV). Heterozygous deletion of this genomic interval leads to a two- to four fold increase in risk for intellectual disability and psychiatric problems, including schizophrenia, autism, as well as a significant increase in the risk for epilepsy^{1,2}. The deletion contains four genes: non-imprinted in Prader-Willi/Angelman syndrome 1 gene (*NIPAI1*), non-imprinted in Prader-Willi/Angelman syndrome 2 gene (*NIPA2*), *CYFIP1* and tubulin gamma complex associated protein 5 gene (*TUBGCP5*)³. Whilst all these genes are expressed in the brain and may be of potential relevance to psychopathology, *CYFIP1* haploinsufficiency is considered to be a likely significant contributor to the 15q11.2 BP1-BP2 psychiatric phenotype due to its known involvement in a number of key brain plasticity-related functions. These include alterations in dendritic spine morphology and branching, mediated by interactions in two distinct complexes: the WAVE regulatory complex to modulate ARP2/3 dependent actin cytoskeleton dynamics, and *CYFIP1*-eIF4E complex to suppress protein translation at the synapse through interactions with fragile X mental retardation 1 protein (FMRP), the gene product of *FMR1*⁴. Mutations in *FMR1* are causative for fragile X syndrome, a condition associated with intellectual disability and a range of psychiatric symptoms⁵.

Changes in white matter microstructure have been reported consistently in major psychiatric disorders including schizophrenia, autism and intellectual disability⁶. Moreover, using diffusion tensor imaging (DTI) methods, in recently published findings we found extensive white matter changes in 15q11.2 BP1-BP2 CNV carriers, specifically widespread increases in fractional anisotropy (FA) in deletion carriers⁷. Some of the biggest changes we observed were in the posterior limb of the internal capsule and corpus callosum. Prominent effects in the corpus callosum are consistent with previous findings by others of increased corpus callosum volume in 15q11.2 BP1-BP2 deletion subjects⁸. The human data raise three main questions; which of the four genes in the 15q11.2 BP1-BP2 interval are important for the disturbances in white matter microstructure, what are the cellular changes underlying the white matter effects, and what are the functional consequences of the white matter changes in the context of the increased risk for disorder. Given the potential major impact of *CYFIP1* in 15q11.2 BP1-BP2 associated phenotypes, in the present work we addressed these questions by taking advantage of the enhanced experimental tractability of a *Cyfp1* haploinsufficiency rat line (hereafter designated *Cyfp1*^{+/-}) created using CRISPR/Cas9 technology modelling the reduced gene dosage of *CYFIP1* in 15q11.2 BP1-BP2 deletion carriers.

Our focus on white matter microstructure was also guided by evidence that *CYFIP1* is an actin regulator, and thus likely to affect white matter via the requirement of precise regulation of the actin cytoskeleton for normal cellular development, morphology and migration. Hence, *CYFIP1* haploinsufficiency has the potential to disrupt axonal organisation via both effects on axonal guidance⁹ and the myelin component of white matter tracts^{10,11}. Myelin is produced by mature oligodendrocytes and several studies have linked actin regulators to oligodendrocyte-myelin dynamics. The Wiskott-Aldrich Syndrome protein family member 1 (WAVE1) and the integrin-linked kinase (ILK) regulate oligodendrocyte differentiation and axon ensheathment^{12,13}, while the Arp2/3 complex, a key actin nucleator, is required for initiation of myelination¹¹, and Rho GTPases Cdc42 and Rac1 regulate myelin sheath formation¹⁴.

We therefore hypothesised there would be white matter abnormalities in the *Cyfp1*^{+/-} rat line possibly linked to underlying changes in axonal architecture including myelin. We

also anticipated functional effects on brain and behaviour on the basis that axon-myelin perturbations can have marked effects on brain network activity caused by disruptions in the temporal coherence of action potential integration across different brain regions^{15,16}. Synchronisation of synaptic signals is crucial in learning, and a previous study in *shiverer* (deletion mutant of myelin basic protein (MBP)) and *mld* (allelic mutant to *shiverer* with lowered MBP expression) mice¹⁵ showed that deficits in myelination had a specific effect on behavioural flexibility in a reversal learning task. In the present work therefore, we looked for evidence of maladaptive brain function in the *Cyfp1*^{+/-} rats using behavioural tasks that assayed behavioural flexibility.

Results

***Cyfp1* haploinsufficiency disrupts white matter microstructure.** Full details of the creation of the *Cyfp1*^{+/-} rat model are in the Supplementary Methods. CRISPR/Cas9 targeting led to a 4 bp out of frame heterozygous deletion in exon 7 of the *Cyfp1* gene at location Chromosome 1: 36974–36977 and a resulting bioinformatics prediction of an early stop codon in exon 8, which was verified functionally using qPCR and Western Blot to measure reductions in mRNA and protein respectively.

To investigate white matter microstructure in the *Cyfp1*^{+/-} rat brain a cohort of 24 behaviourally naïve male rats (wild-type (WT) $n=12$, *Cyfp1*^{+/-} $n=12$) were anaesthetised with isoflurane in oxygen at 4% and maintained at 1%, and DTI data were collected using a 9.4 T MRI scanner, utilising 60 noncollinear gradient directions with a single b-value shell at 1000 sm^{-2} . Group comparisons were carried out using Tract-Based Spatial Statistics (TBSS)¹⁷ available in FMRIB Software Library (FSL), with a randomise function allowing voxel-wise nonparametric permutation analysis of the DTI maps projected onto a whole brain white matter skeleton (Supplementary Fig. 1). The randomise function was used with the threshold-free cluster enhancement (TFCE)¹⁸, generating cluster-size statistics based on 1000 random permutations. Behaviourally naïve animals were used in the light of evidence showing behaviour itself can influence white matter^{19,20}. Figure 1 shows the regions where significant differences in white matter microstructure were found after correction for multiple comparisons. Figure 1a shows the pattern of changes using a highly conservative family-wise error (FWE) correction. This approach showed consistent reductions in FA in the corpus callosum, in the external and internal capsule, and in parts of the fimbria/fornix in *Cyfp1*^{+/-} rats, with no differences in axial diffusivity (AD), radial diffusivity (RD) and mean diffusivity (MD). We complemented the highly conservative FWE correction method used in human imaging studies with the False Discovery Rate (FDR) correction for multiple comparisons based on the Benjamini–Hochberg procedure²¹, used previously in rodent imaging data^{19,22}. This analysis, shown in Fig. 1b, revealed additional white matter changes including increases in FA in regions of the fornix and fimbria suggesting that *Cyfp1* haploinsufficiency may have differential effects in different brain regions. Figure 1b also shows changes in other DTI metrics, after FDR correction, illustrating mostly decreases in AD and increases in RD, and MD. These effects were complementary in terms of (a) being localised in the corpus callosum and external and internal capsule and (b) being consistent with the overall predominant effects of *Cyfp1* haploinsufficiency in reducing FA.

We next manually generated binary masks of regions of interest (corpus callosum, internal capsule, external capsule and fimbria/fornix), guided by the results from FWE correction using FSL (Supplementary Fig. 2), and assessed mean FA, AD, RD and MD in these white matter tracts. As can be seen in Table 1,

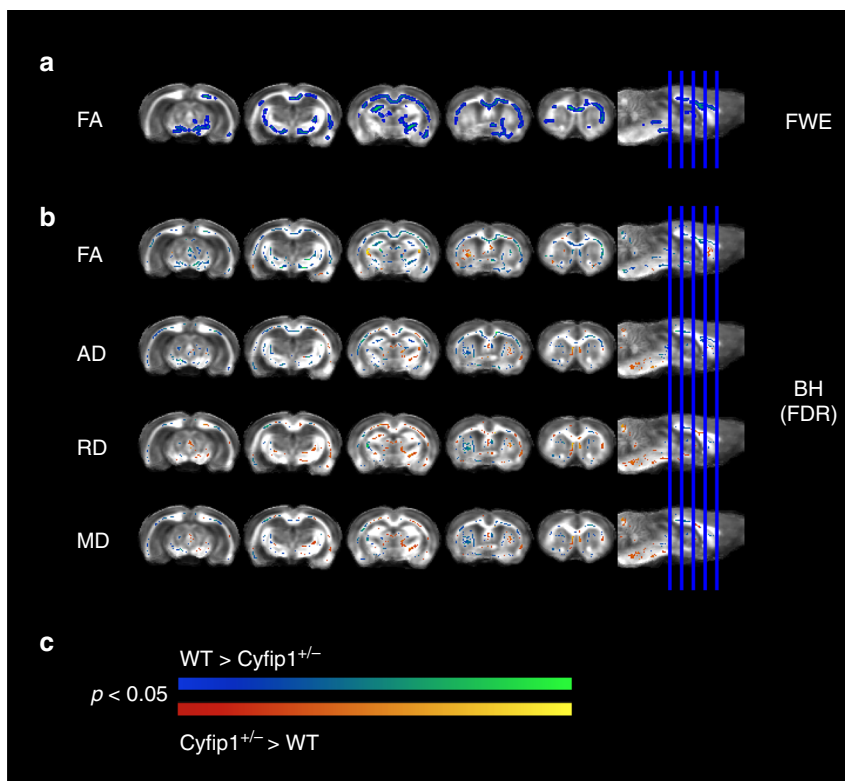


Fig. 1 *Cyfip1* haploinsufficiency disrupts white matter microstructure. White matter changes comparing WT ($n = 12$) and *Cyfip1*^{+/-} ($n = 12$) rats. Data shows significant group differences using two-tailed unpaired *t*-tests based on Threshold-Free Cluster Enhancement (TFCE) algorithm after **a** family-wise error (FWE) rate correction for fractional anisotropy (FA), and **b** false discovery rate (FDR) correction based on the Benjamini–Hochberg procedure for FA, axial diffusivity (AD), radial diffusivity (RD) and mean diffusivity (MD). All the parametric maps were generated at a significance level of $p < 0.05$. **c** Scale bars indicating the direction of the changes in both **a**, **b**, where relative decreases in *Cyfip1*^{+/-} rats are represented by a gradient of blue (less significant) to green (more significant), and relative increases in *Cyfip1*^{+/-} are represented by a gradient of red (less significant) to yellow (more significant)

Table 1 Quantification of DTI changes in regions where significant differences in FA were seen in TBSS analysis after FWE correction

ROIs	FA		AD (10^{-2})		RD (10^{-3})		MD (10^{-3})	
	WT	<i>Cyfip1</i> ^{+/-}	WT	<i>Cyfip1</i> ^{+/-}	WT	<i>Cyfip1</i> ^{+/-}	WT	<i>Cyfip1</i> ^{+/-}
CC	0.49 ± 0.02	0.46 ± 0.02 ^a	0.14 ± 0.005	0.13 ± 0.006 ^a	0.69 ± 0.05	0.71 ± 0.04	0.92 ± 0.04	0.91 ± 0.03
IC	0.45 ± 0.02	0.44 ± 0.02	0.11 ± 0.007	0.11 ± 0.007	0.53 ± 0.03	0.54 ± 0.03	0.74 ± 0.04	0.73 ± 0.04
EC	0.38 ± 0.02	0.36 ± 0.02 ^a	0.12 ± 0.004	0.12 ± 0.003	0.73 ± 0.03	0.73 ± 0.02	0.89 ± 0.03	0.88 ± 0.02
FF	0.50 ± 0.03	0.48 ± 0.02	0.17 ± 0.008	0.16 ± 0.004	0.69 ± 0.06	0.70 ± 0.04	1.01 ± 0.06	1.00 ± 0.03

Source data are provided as a Source Data file

FA fractional anisotropy, AD axial diffusivity, RD radial diffusivity, MD mean diffusivity values from WT and *Cyfip1*^{+/-} rats, ROIs regions of interest, CC corpus callosum, IC internal capsule, EC external capsule, FF fornix/fimbria

Results obtained using TBSS-based ROI analysis, mean ± standard deviation, two-tailed unpaired *t*-test, ^a $p < 0.05$

analysing the DTI data in this way (which averaged differences between WT and *Cyfip1*^{+/-} rats within a discrete fibre tract, as opposed to the voxel-by-voxel analysis which detected clusters of voxel differences in white matter tracts across the whole brain) showed that the most significant differences were reductions in FA in the corpus callosum ($t = 2.3$, $df = 20.75$, $p < 0.05$) and external capsule ($t = 2.4$, $df = 22$, $p < 0.05$) in the *Cyfip1*^{+/-} rats compared to WT, as assessed with a two-tailed unpaired *t*-test. These data were consistent with the previous voxel-by-voxel analysis and provided the additional finding that the most extensive white matter changes in the *Cyfip1*^{+/-} rats occurred in these structures.

***Cyfip1* haploinsufficiency affects myelin in corpus callosum.** We next investigated the cellular nature of the *Cyfip1* associated

DTI changes. DTI measures can be affected by several factors and previous studies have linked decreases in FA in white matter tracts with less myelin, lower axonal density, axonal damage, or changes in axonal organisation^{23,24}. To assess cellular changes, we carried out an ultra-structural analysis, blind to genotype, using transmission electron microscopy in behaviourally naïve animals focusing on the corpus callosum, given the DTI data indicating the sensitivity of this structure to *Cyfip1* haploinsufficiency. The experiment used a new cohort of rats (WT $n = 5$, *Cyfip1*^{+/-} $n = 4$). In order to obtain a representative sample, we sampled 15 regions across the anterior-posterior extent of the corpus callosum encompassing the genu, body and splenium, from sagittal brain sections (representative micrographs in Fig. 2a). We measured the number of myelinated and unmyelinated axons, the inner diameter and the outer diameter (including the myelin

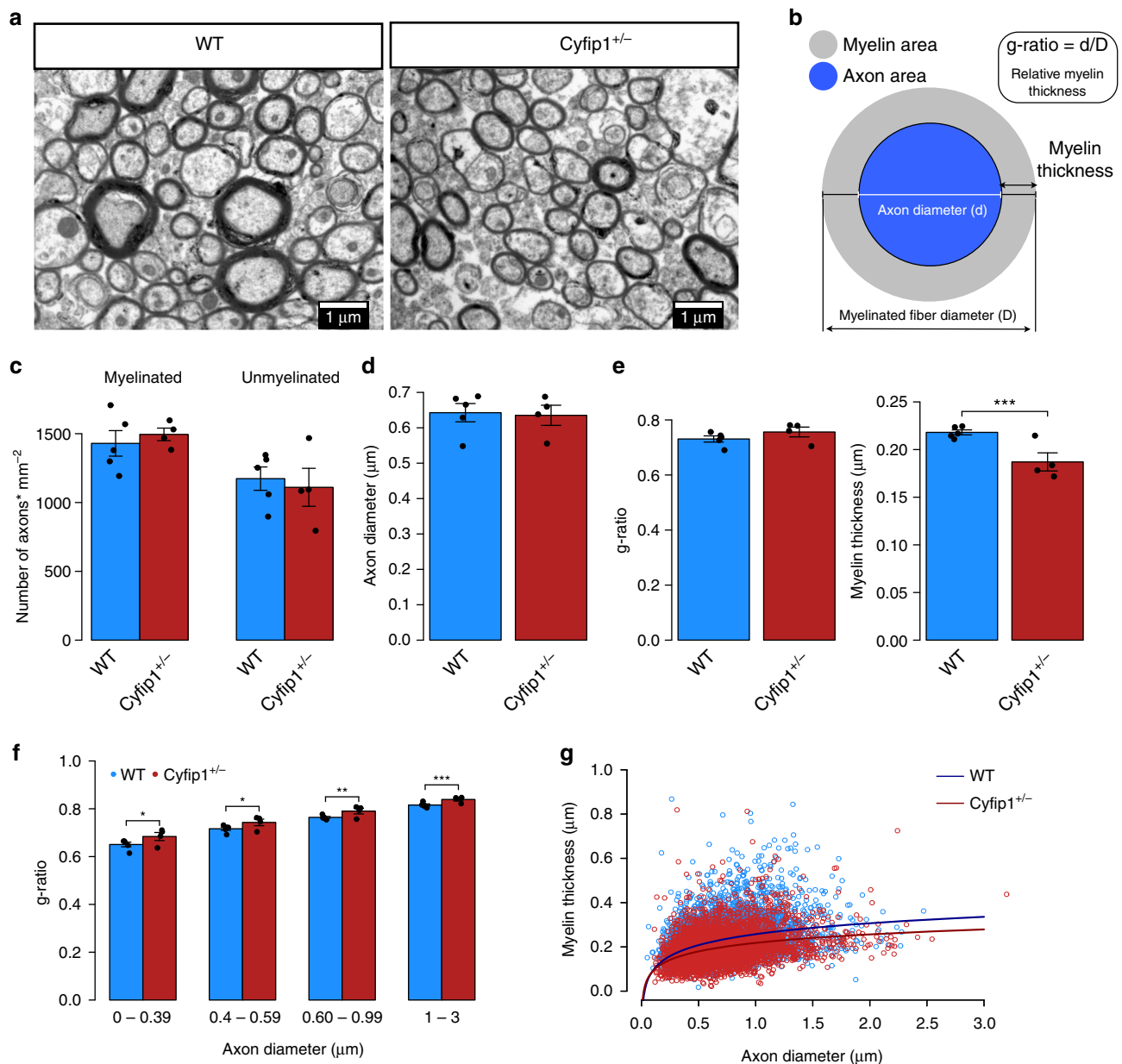


Fig. 2 Decreased myelin thickness in the corpus callosum in the *Cyfip1*^{+/-} rats. **a** Representative electron micrographs of axons in the WT ($n = 5$ animals and $n = 7148$ axons) and *Cyfip1*^{+/-} ($n = 4$ animals and $n = 5979$ axons) rats. **b** Schematic illustration of the axon and myelin sheath and calculation of the g-ratio and myelin thickness. **c** Mean number of myelinated ($t = -0.63$, $df = 5.72$, $p = 0.55$, ns) and unmyelinated axons per group ($t = 0.39$, $df = 5.15$, $p = 0.71$, ns), assessed with a two-tailed unpaired *t*-test. **d** Mean axon diameter of myelinated fibres per group (LME: $\chi^2(1) = 0.05$, $p = 0.83$). **e** Mean g-ratio per group (LME: $\chi^2(1) = 2.03$, $p = 0.15$) and mean myelin thickness per group (LME: $\chi^2(1) = 14.63$,***), showing significant decreased myelin thickness in *Cyfip1*^{+/-} rats. **f** mean g-ratios calculated for small ($n = 1510$ WT and 1276 *Cyfip1*^{+/-} axons; LME: $\chi^2(1) = 4.23$,*), medium-small ($n = 2283$ WT and 2043 *Cyfip1*^{+/-} axons; LME: $\chi^2(1) = 4.44$,*), medium-large ($n = 2551$ WT and 1993 *Cyfip1*^{+/-} axons; LME: $\chi^2(1) = 7.14$,**), and large ($n = 804$ WT and 667 *Cyfip1*^{+/-} axons; LME: $\chi^2(1) = 13.92$,***) myelinated axons, showing significant increases in g-ratio in all different axon diameter ranges, and more significant in larger axons. **g** Scatter plot of myelin thickness values across all axon diameters WT ($n = 7148$ axons) and *Cyfip1*^{+/-} ($n = 5979$ axons). Differences between axon diameter, g-ratio and myelin thickness measures were assessed using linear mixed effects (LME) models adjusted for individual variability. Data are mean \pm SEM; * <0.05 , ** <0.01 , *** <0.001 . Source data are provided as a Source Data file

sheath) of each axon, and then calculated the myelin thickness and the g-ratio (myelin thickness relative to axon diameter, where smaller g-ratios indicate greater myelin thickness) of each myelinated axon (see measures taken in Fig. 2b).

We used linear mixed effects (LME) models to analyse the effect of genotype on axon diameter, g-ratio and myelin thickness, considering variation across animals, whereas a two-tailed unpaired *t*-test was used to compare the number of axons

between groups. In this analysis, the myelin thickness was log-transformed since the data followed a log-normal distribution, whereas the other measures followed a normal distribution. No genotype differences were found in the number of unmyelinated ($t = 0.39$, $df = 5.15$, $p = 0.71$) and myelinated ($t = -0.63$, $df = 5.72$, $p = 0.55$) axons (Fig. 2c), or in the diameter of the axons (Fig. 2d, LME: $\chi^2(1) = 0.05$, $p = 0.83$), suggesting no differences in axonal density and calibre in the corpus callosum of

the *Cyfp1*^{+/-} rats. The analyses did not show a significant increase in g-ratio when comparing all axons in each group (LME: $\chi^2(1) = 2.03$, $p = 0.15$), however it revealed a significant reduction in myelin thickness in the *Cyfp1*^{+/-} rats (LME: $\chi^2(1) = 14.63$, $p < 0.001$), both shown in Fig. 2e. The fact that we did not see a significant difference in g-ratio could have resulted from variability in the average of axon diameters within animals in the same group, which is related to g-ratio (Supplementary Fig. 3). Furthermore, we needed to consider that the extent of myelination can be related to axon diameter²⁵, and whether the effects on the g-ratio were specific to certain sizes of axons. Analysing the g-ratio of axons within specific diameter ranges revealed a significant increased g-ratio in each interval in the *Cyfp1*^{+/-} rats (Fig. 2f), that was more significant in larger axons. These analyses indicate decreased myelin thickness in the corpus callosum of the *Cyfp1*^{+/-} rats that is more pronounced in larger axons.

Cyfp1^{+/-} rats have less oligodendrocytes in corpus callosum.

Myelin is produced by mature oligodendrocytes, so we next tested whether *Cyfp1* haploinsufficiency influenced the number and/or the maturation of oligodendrocytes using antibodies to the specific molecular markers Olig2 and Cc1. This experiment used rats taken randomly from the same group of rats providing the DTI data shown in Fig. 1 (WT $n = 7$ WT and *Cyfp1*^{+/-} $n = 7$). The analysis focused on the corpus callosum and external capsule and at least four random sections were taken for quantification in each rat from coronal sections. Sections were stained for Olig2 and Cc1 proteins. Cells stained for Olig2 alone represented all the oligodendrocyte lineages from early progenitors to mature cells, whereas cells double-stained for Olig2 and Cc1 proteins revealed specifically the mature oligodendrocyte (myelin-producing) population. In the *Cyfp1*^{+/-} rats, this analysis showed a

significant reduction in both the number of oligodendrocyte lineage cells (Fig. 3a; $t = 2.18$, $df = 11.94$, $p < 0.05$) and mature oligodendrocytes ($t = 2.48$, $df = 11.99$, $p < 0.05$) in comparison with WT. We also found a significant reduction in the level of MBP (Fig. 3b, $t = 2.16$, $df = 11.96$, $p = 0.052$) in the corpus callosum/external capsule of the *Cyfp1*^{+/-} rats. The significance was assessed using a two-tailed unpaired *t*-test.

***Cyfp1*^{+/-} rats have aberrant MBP distribution in oligodendrocytes.** We used primary cell culture methods to address further the question of how *Cyfp1* haploinsufficiency might impact on oligodendrocytes and myelination. We used standard protocols²⁶, which generate oligodendrocyte precursor cells (OPC) at $\geq 95\%$ purity from WT and *Cyfp1*^{+/-} rats. Three independent biological replicates were performed. After 3 days of differentiation the cells were processed for immunohistochemistry with antibodies to O4 and MBP. Cells stained for O4 alone mark the early, immature stages of oligodendrocyte differentiation and combined O4/MBP staining mark later mature stages of oligodendrocyte differentiation. For the imaging analysis five images from random visual fields were taken per well and a minimum of 1000 cells quantified per experimental group/ replicate, as previously, we used a LME models for statistical analysis to account for variation across biological repeats (where these were considered random effects).

We focused on MBP, which is both a marker for mature oligodendrocyte differentiation and essential for the production of myelin²⁷. With the enhanced cellular resolution possible with cultured oligodendrocytes, we immediately noticed that the staining pattern for MBP looked markedly different in cells originating from *Cyfp1*^{+/-} brain tissue compared to WT. Specifically, as illustrated in Fig. 4a, there appeared to be a more punctate organisation in *Cyfp1*^{+/-} cells where MBP staining was

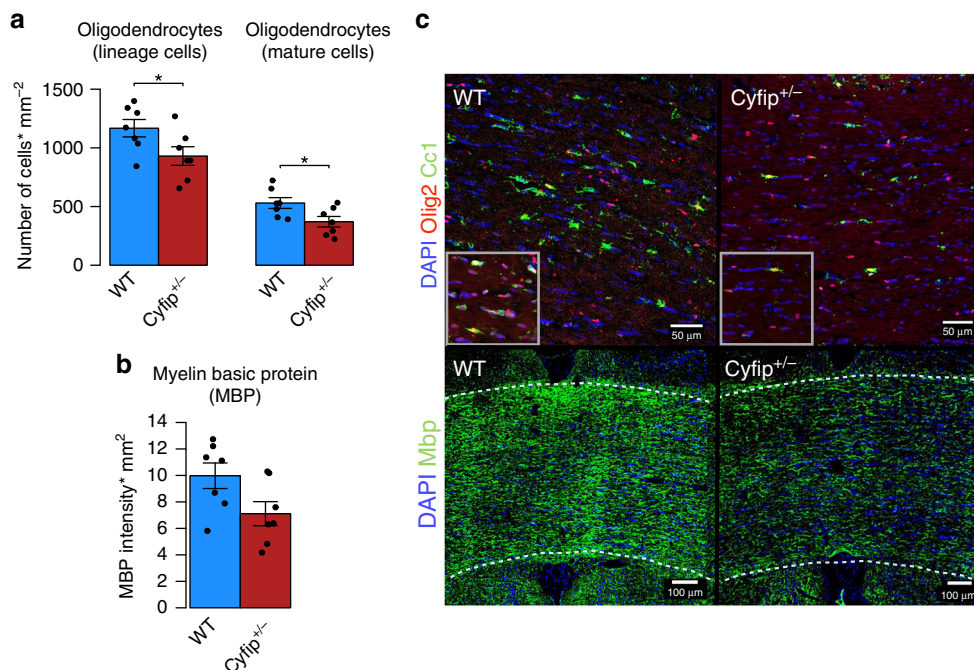


Fig. 3 Altered number of oligodendrocyte lineage and mature cells, and levels of myelin basic protein (MBP), in the corpus callosum of the *Cyfp1*^{+/-} rats. **a** Mean number of oligodendrocyte lineage ($n = 7$ each; $t = 2.18$, $df = 11.94$, *), stained with Olig2, and mature ($n = 7$ each; $t = 2.48$, $df = 11.99$, *), stained with Olig2 and Cc1, cells per mm². **b** Mean MBP intensity multiplied by the percentage area (mm²) of the staining ($n = 7$ each; $t = 2.16$, $df = 11.96$, $p = 0.052$). **c** Representative images (at magnification $\times 20$ (top) and $\times 10$ (bottom)) for the following immunomarkers: DAPI, Olig2, Cc1 and Mbp in the corpus callosum of the WT and *Cyfp1*^{+/-} rats. Scale bars = 50 μm (top) and 100 μm (bottom). Differences between groups were assessed using a two-tailed unpaired *t*-test. Data are mean \pm SEM; * < 0.05 , ** < 0.01 , *** < 0.001 . Source data are provided as a Source Data file

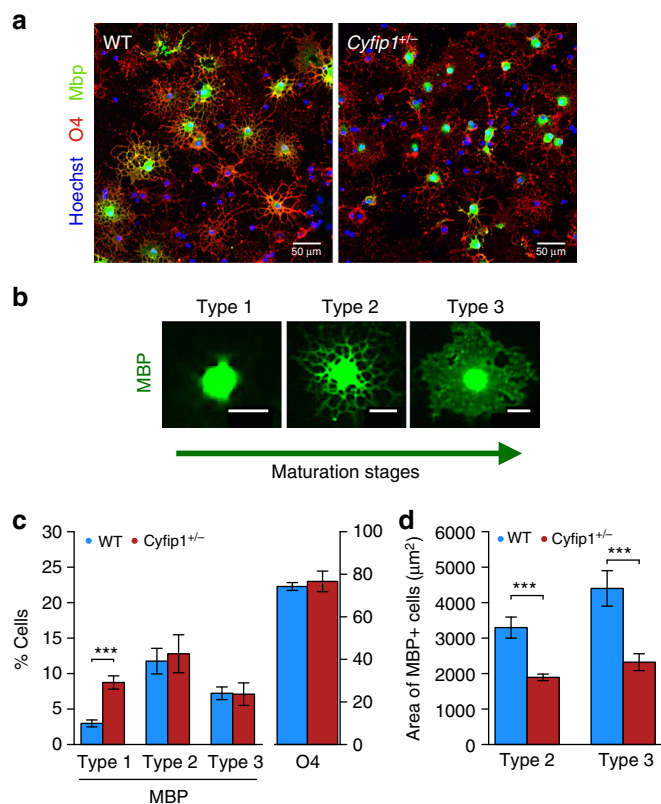


Fig. 4 *Cyfip1* haploinsufficiency influences the intracellular distribution of myelin basic protein (MBP) in cultured oligodendrocytes. **a** Immunostaining of oligodendrocytes for MBP and O4 from wild type (WT) and *Cyfip1*^{+/-}, scale bar = 50 μm, illustrating the punctate intracellular pattern of staining of MBP in *Cyfip1*^{+/-} relative to the more diffused, widespread pattern of staining in WT. **b** Representative images of oligodendrocytes staining for MBP exhibiting features of Type 1 (MBP localised to the cell body), Type 2 (MBP ramifying into the cell processes), Type 3 (MBP distributed throughout the cell and within the membranes of cell processes) reflecting increasing maturation stages of oligodendrocytes, scale bar = 20 μm. **c** the effects of genotype on the percentage of Type 1 ($n = 172$ WT and 637 *Cyfip1*^{+/-} cells; LME: $\chi^2(1) = 68.49$, ***), Type 2 ($n = 735$ WT and 905 *Cyfip1*^{+/-} cells; LME: $\chi^2(1) = 0.59$, $p = 0.44$), Type 3 ($n = 456$ WT and 454 *Cyfip1*^{+/-} cells; LME: $\chi^2(1) = 0.02$, $p = 0.88$), and O4 + cells ($n = 4917$ WT and 5789 *Cyfip1*^{+/-} cells; LME: $\chi^2(1) = 1.44$, $p = 0.23$), as a proportion of all cells ($n = 6623$ WT and 7845 *Cyfip1*^{+/-} cells) in the culture (stained with Hoechst); this panel also illustrates the effects of genotype on the overall proportion of differentiating oligodendrocytes as indexed by all cells staining for O4. **d** effects of genotype on the area of intracellular MBP staining in Type 2 ($n = 491$ WT and 591 *Cyfip1*^{+/-} cells; LME: $\chi^2(1) = 258.03$, ***) and Type 3 ($n = 265$ WT and 341 *Cyfip1*^{+/-} cells; LME: $\chi^2(1) = 145.52$, ***) oligodendrocytes, as depicted in the representative images in b. Values were obtained from 3 independent experiments. Differences between number of cells and area were quantified using linear mixed effects (LME) models adjusted for variability in each biological repeat. Data are mean \pm SEM; * <0.05 , ** <0.01 , *** <0.001 . Source data are provided as a Source Data file

localised mainly to the cell body region, compared to a more widely distributed pattern of cellular staining in WT that extended into the cell processes. We interrogated this finding in more detail using a quantitative analysis that classified MBP + cells into three previously established categories indexing the maturation stages of oligodendrocytes that culminates in the formation of compact myelin²⁸: Type 1, MBP localised only to the cell body; Type 2, any ramified MBP intracellular distribution

extending into the cell processes; Type 3, final maturation stage where MBP is throughout the cell and distributed within the membranous processes of cells to give rise to a ‘spider’s web-like’ appearance (see Fig. 4b for representative examples). The quantitative data confirmed the previous qualitative observation in revealing a highly significant increased incidence of Type 1 cells in *Cyfip1*^{+/-} (LME: $\chi^2(1) = 68.49$, $p < 0.001$, Fig. 4c). Furthermore, whilst there were no significant genotype differences in the overall proportion of cells classified, broadly, as Type 2 (LME: $\chi^2(1) = 0.59$, $p = 0.44$) or Type 3 (LME: $\chi^2(1) = 0.02$, $p = 0.88$, Fig. 4c), within each of these classifications *Cyfip1*^{+/-} oligodendrocytes showed a more constrained cellular distribution of MBP as indicated by a highly significant and consistent reduction in the area of MBP staining in the *Cyfip1*^{+/-} population, which amounted to about 50% of that seen in WT cells (LME: $\chi^2(1) = 258.03$, $p < 0.001$, Fig. 4d). The area of MBP staining observed in the WT cells was consistent with previous findings by others using similar culture methods¹⁴. Furthermore, the effects of *Cyfip1* haploinsufficiency occurred in the absence of any observable genotype effects on MBP + oligodendrocyte cell size/gross morphology or the overall number of differentiating oligodendrocytes present in the cultures as evidenced by the total numbers of O4 + cells. (Fig. 4c, LME: $\chi^2(1) = 1.44$, $p = 0.23$). Together, these data were consistent with *Cyfip1* haploinsufficiency hindering the translocation of MBP to the distal parts of the highly branched mature oligodendrocyte, a process that is critical for successful differentiation and the production of myelin²⁹, and likely therefore to be of relevance to the previous finding of myelin thinning in the *Cyfip1*^{+/-} rats.

***Cyfip1* haploinsufficiency affects behavioural flexibility.** We next assessed whether the *Cyfip1* related imaging and cellular phenotypes were associated with effects on behaviour. Behavioural changes have been observed in rodent models of reduced myelination including *shiverer* and *mld* mice with modifications in myelin basic protein¹⁵. Both mutants showed highly specific effects on behavioural flexibility in a reversal learning task, whereby they had difficulty changing their behaviour to reflect the new reward contingencies, without concomitant deficits in learning deficits *per se*¹⁵. Furthermore, both human^{30–35} and animal studies^{36,37} have also shown that disruptions to connectivity involving callosal circuitry and circuits involving the internal and external capsules impact on a number of psychological functions, in particular those mediating attention and response control, especially response inhibition.

To assay behavioural flexibility, we utilised a touch screen-based appetitive reversal learning task in a separate cohort of experimental rats (WT $n = 7$, *Cyfip1*^{+/-} $n = 10$). The reversal learning task first allowed an assessment of basic appetitive learning where rats had to learn that one visual stimulus was associated with reward (the S+) and another stimulus was not (S–), with the two stimuli counterbalanced across animals. This was followed by reversal of the contingencies (see Supplementary Fig. 4 for flowchart of task design). Successful reversal learning can be aligned to tasks used in clinical studies (i.e. the Stroop task, SART, stop signal) to examine cognitive processes supporting flexible control of behaviour^{38–44}. All rats successfully completed the early stages of pre-training in the reversal learning task where they had to learn to collect food from the magazine and to touch stimuli presented on the touchscreen to earn rewards, achieving these to criterion in a similar number of sessions (Magazine Training (mean \pm s.e.m): WT = 2.7 \pm 0.5, *Cyfip1*^{+/-} = 3.7 \pm 0.3, ANOVA: GENOTYPE ($F(1,15) = 2.79$, $p = 0.12$); Touch Training: WT = 15.6 \pm 2.2, *Cyfip1*^{+/-} = 13.3 \pm 2.1, GENOTYPE

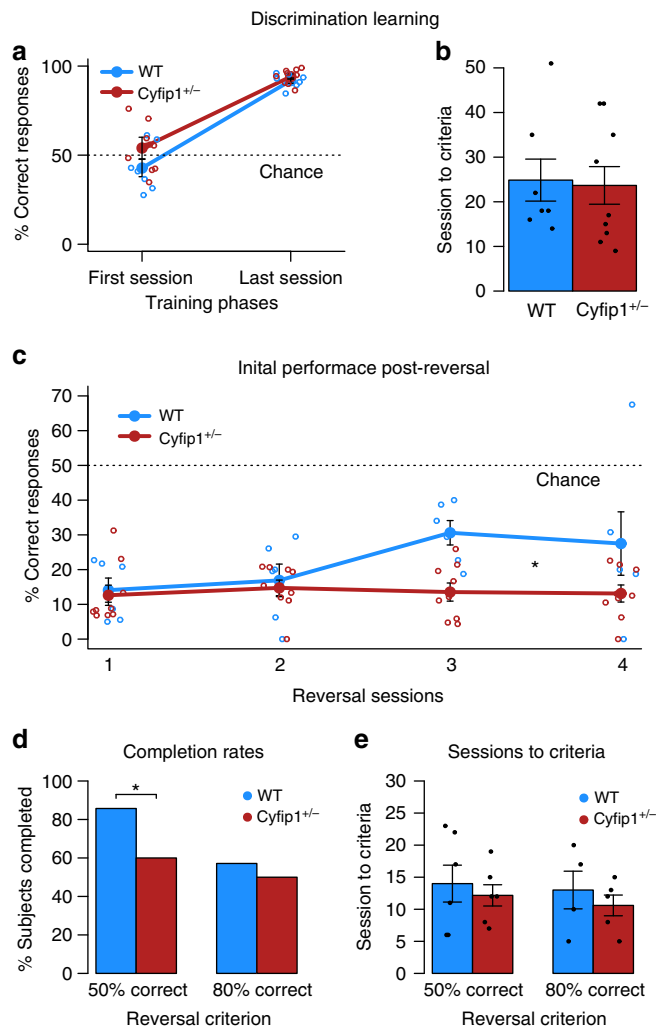


Fig. 5 *Cyfip1* haploinsufficient rats show deficits in behavioural flexibility in a reversal learning paradigm. WT ($n = 7$) and *Cyfip1*^{+/-} ($n = 9$) rats successfully acquire the visual discrimination in the touchscreen boxes, reaching the same level of performance (% correct) **a** during the last session of training, and **b** reaching criteria in a similar number of sessions (ANOVA: $F(1,14) = 0.03, p = 0.86$). One *Cyfip1*^{+/-} rat did not complete initial learning. **c** *Cyfip1*^{+/-} rats show more persistent responses to the original stimulus response contingencies during the first few sessions of reversal, (WT ($n = 6$) and *Cyfip1*^{+/-} ($n = 9$), ANOVA: GENOTYPE X SESSION interaction, $F(3,39) = 3.76, *$), where one of the WT rats did not start reversal learning task. **d** A larger proportion of *Cyfip1*^{+/-} rats failed to reach the 50% correct criterion during reversal than WT rats, (Chi-squared: $\chi^2 = 9.61, *$). **e** However, those that do reach criteria do so in a similar number of sessions as WT rats (effect of GENOTYPE, ANOVA: 50% criteria ($F(1,10) = 0.31, p = 0.59$), and 80% criteria ($F(1,7) = 0.44, p = 0.57$). Data are mean \pm SEM. * <0.05 , ** <0.01 , *** <0.001 . The raw number of animals completing each task can be seen in Supplementary Table 1a. Source data are also provided as a Source Data file

($F(1,15) = 0.53, p = 0.48$). Then the rats moved on to the visual discrimination training where the two stimuli were present. As illustrated in Fig. 5a, both groups achieved high levels of performance to a criterion of 80% correct trials across two successive days and there was no difference in the number of sessions required to reach criterion between the groups (Fig. 5b, ANOVA: GENOTYPE ($F(1,14) = 0.03, p = 0.86$)). One *Cyfip1*^{+/-} was not included in these and subsequent analyses as they failed to

reach criterion on the visual discrimination task (see also Supplementary Table 1a).

Following acquisition of the initial visual discrimination the contingencies were reversed. This manipulation had the expected effect where perseverating with the previously correct choice led to scores were that were below chance levels (i.e., 50%). However, in contrast to the basic learning of the visual discrimination, there was an effect of genotype when the reward contingencies were reversed in the immediate post-reversal sessions (see Fig. 5c). In this part of the task,^{45,46} the *Cyfip1*^{+/-} rats continued to respond to the original S + over successive sessions, while the WT began to switch their choices to the new S + (a 2 x 2 ANOVA revealed a main effect of SESSION ($F(3,39) = 3.67, p < 0.05$) and a GENOTYPE x SESSION interaction ($F(3,39) = 3.76, p < 0.05$), where a main effect of GENOTYPE was marginally significant ($F(1,13) = 4.32, p = 0.06$)). Further analysis of simple main effects revealed an effect of SESSION in the WT ($F(3,39) = 7.34, p < 0.01$) but not in the *Cyfip1*^{+/-} group ($F(3,39) = 0.09, p = 0.96$), and an effect of GENOTYPE on sessions 3 and 4 following reversal (Minimum $F(1,52) = 9.42, p < 0.01$).

In subsequent sessions with the reversed contingencies the rats gradually reached a criterion of 50% correct. However, fewer *Cyfip1*^{+/-} than WT rats reached this criterion (Fig. 5d, Chi-squared: $\chi^2 = 9.61, p < 0.05$). However, again, group differences were apparent in those fewer *Cyfip1*^{+/-} rats that successfully reached this criterion (Fig. 5d, Chi-squared: $\chi^2 = 9.61, p < 0.05$). Here, three *Cyfip1*^{+/-} rats failed to complete early reversal compared to only one WT. Effectively this sub-group of rats were never able to successfully inhibit the previously learned response despite being given ample opportunity to do so that extended to the end of the experiment (rats that completed this phase of reversal did so in an average of 13 sessions, whereas those that failed to learn the reversed contingencies had an average of 22 sessions before the end of the experiment). Figure 5d also illustrates the high degree of behavioural specificity shown by the *Cyfip1*^{+/-} rats in the task; insofar as genotype differences were not evident in the relative proportion of those rats that were able to successfully inhibit the previous response strategy, and went on to learn the new contingency to 80% criterion (two WT rats, and one *Cyfip1*^{+/-} rat failed to reach 80% criterion and so were not included in subsequent analyses of sessions to criterion). Moreover, *Cyfip1*^{+/-} rats that completed these stages of reversal (reaching 50 and 80% correct) did so in a similar number of sessions to WTs, where separate ANOVAs revealed no effect of GENOTYPE on sessions to either 50% criteria ($F(1,10) = 0.31, p = 0.59$), or 80% criteria ($F(1,7) = 0.44, p = 0.57$) (Fig. 5e; see also Supplementary Table 1a for the number of rats completing each stage of the reversal task; the total sessions and trials across the whole task are also shown in Table 1b).

We further assessed the effects of *Cyfip1* haploinsufficiency on the ability to change behaviour in the face of changed contingencies (WT $n = 21$, *Cyfip1*^{+/-} $n = 15$) using an established associative mismatch task⁴⁷⁻⁵⁰ when the contingencies involving sensory events were changed. Here, rats first received two audio-visual sequences (i.e. Tone → Steady Light, Click → Flashing Light; the combinations were counterbalanced across animals). As reported previously⁴⁷⁻⁵⁰, presentations of the initially novel visual stimuli resulted in an orienting response towards the light cue that habituated over the course of the four training sessions, as animals came to expect the presentation of the light following the auditory cue. There were no effects of genotype on behaviour in this part of the task or on habituation to the test apparatus, Fig. 6a, where a 2 x 2 ANOVA on activity during habituation to the chambers revealed a main effects of BLOCK ($F(5,170) = 119.5, p < 0.05$) but no other effect of genotype or interaction (Maximum $F(5,170) = 0.4, p = 0.85$). A

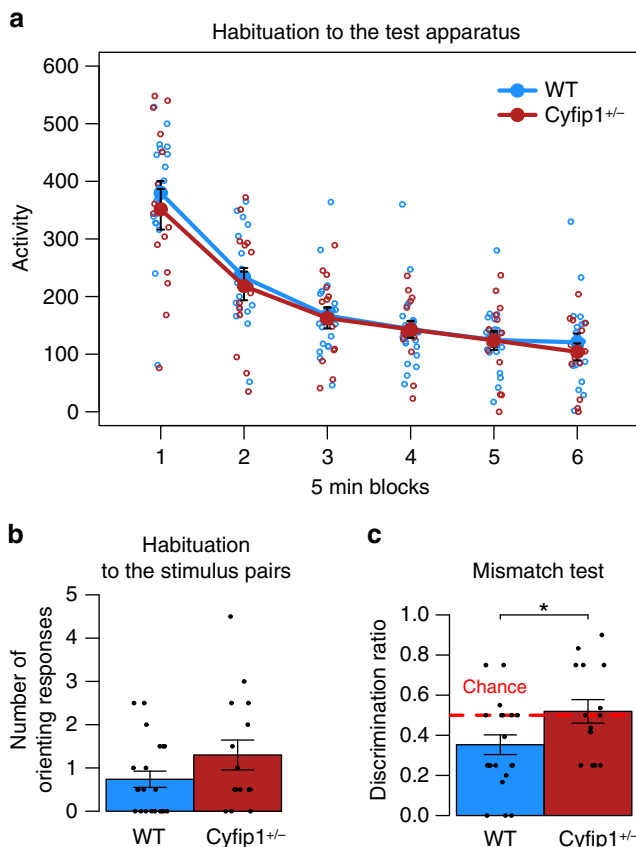


Fig. 6 *Cyfip1* haploinsufficient rats show deficits in flexible responses in orienting behaviour on a mismatch task. **a** There are no genotype effects on habituation to the experimental apparatus. Both WT ($n = 21$) and *Cyfip1*^{+/-} ($n = 15$) show reduced activity to the experimental chambers over the course of each 30-min long session (5 min blocks). **b** Both WT and *Cyfip1*^{+/-} rats showed reduced orienting to the auditory-visual sequences presented during training (ANOVA: $F(1,34) = 2.4$, $p = 0.62$), and **c** WT rats preferentially responded to the novel mismatched visual stimuli over the familiar matched stimuli (discrimination ratio < 0.50). In contrast, *Cyfip1*^{+/-} rats showed no preference, responding equally to both matched and mismatched visual cues (ANOVA: $F(1,34) = 5.92$, *). * < 0.05 , ** < 0.01 , *** < 0.001 . Source data are provided as a Source Data file

one-way ANOVA revealed no differences in orienting to the cued visual stimuli at the end of the training phase (Fig. 6b, GENOTYPE ($F(1,34) = 2.4$, $p = 0.62$)).

During testing rats were presented with both the original training trials (match; i.e. Tone→Steady Light, Click→Flashing Light) and novel mismatch combinations of the same cues (e.g. Tone→Flashing Light, Click→Steady Light), WT rats showed the normal preference^{47–50} to orient to the visual cues on mismatch trails (relative to match trails) demonstrating their ability to respond to the changed contingencies. In contrast, the *Cyfip1*^{+/-} rats failed to show this preference, instead showing no preference for responding to either the habituated (match) or the novel (mismatch) cues (Fig. 6c, ANOVA: GENOTYPE ($F(1,34) = 5.92$, $p < 0.05$) as indicated by the discrimination ratios (total orienting to matched/total orienting to both matched + mismatched). This pattern of behaviour represents further evidence of a deficit in behavioural flexibility associated with *Cyfip1* haploinsufficiency. In this case, the deficit was revealed by a failure to respond when the contingencies involving sensory events were changed.

Discussion

We used a CRISPR/Cas9 engineered rat line to model the contribution of *Cyfip1* haploinsufficiency to white matter changes observed in carriers of the pathogenic 15q11.2 BP1-BP2 deletion. The *Cyfip1*^{+/-} rat model allowed us to carry out a DTI analysis with high resolution using identical preprocessing to our 15q11.2 BP1-BP2 human imaging study, and employ rigorous statistics including exploratory voxel-wise assessments permitting comparisons of genotype effects across brain regions. The *Cyfip1*^{+/-} rat line provided enhanced experimental tractability in terms of direct access to brain tissue, with interpretation of DTI changes at the cellular and molecular level, and also allowed relevant behavioural analyses under controlled conditions.

A main finding of the DTI experiments were significant decreases in FA that were most pronounced in the corpus callosum and external capsule. More widespread changes in white matter were apparent when using a less conservative correction method including increased FA in some areas of the fornix/fimbria. The precise relationship between DTI measures and cellular changes is subject to ongoing debate²⁴ and whilst DTI can identify white matter changes it cannot definitively distinguish between disruptions to axons and/or myelin. Consequently, at the outset the DTI effects we obtained in the rat model could have been related to changes in axon microstructure or myelin, or both.

Transmission electron microscopy indicated a thinning of the myelin sheath in the corpus callosum of the *Cyfip1*^{+/-} rats in the absence of any changes in axonal number or diameter. Myelin is produced at the end stages of oligodendrocyte differentiation and we found reductions in later stage mature oligodendrocytes in corpus callosum in-vivo. However, whilst previous evidence in other contexts has shown that changes in oligodendrocyte number can be associated with myelin thickness^{51,52} this still leaves the question of the cellular mechanism(s) by which *Cyfip1* haploinsufficiency could interfere with the process of myelination and lead to myelin thinning.

We addressed the issue of cellular mechanism taking advantage of the enhanced cellular resolution offered by cultured primary oligodendrocyte. We showed evidence that *Cyfip1* haploinsufficiency impacts on mature oligodendrocyte function by hindering the intracellular distribution of a key protein, MBP, where in the *Cyfip1* mutants the protein localised to the cell body and failed to achieve the normal highly distributed pattern of expression encompassing the distal cell processes and membranes. The myelination process is initiated by events occurring at the distal parts of the highly branched mature oligodendrocyte and hence, our finding of a deficit in translocation of MBP to those regions is consistent with and provides a mechanism for our in vivo observations of myelin thinning in the *Cyfip1*^{+/-} animals. Several previous studies have established a critical role for MBP in initiating and supporting the production of myelin in mature oligodendrocytes triggered by contact with axons, where a principle function of MBP is to organise the compaction of oligodendrocyte plasma membranes to form myelin⁵³. However and of key relevance, previous studies such as those reporting the effects of mutations *Kif1b*²⁹ have also demonstrated myelin deficits, including myelin thinning, that are associated with abnormal intracellular distributions of MBP highly reminiscent of the pattern seen in the *Cyfip1*^{+/-} animals.

The effects of *Cyfip1* haploinsufficiency on oligodendrocytes and myelination may be related to deficits in actin physiology via interactions with the WAVE complex. Multiple aspects of oligodendrocyte function, including cell proliferation, differentiation, migration and myelination are reliant on effective cytoskeleton remodelling¹⁰. In mouse models manipulating

WAVE1 protein directly impacts on the ability to form myelin in the corpus callosum¹². MBP stimulates the production of soluble G-actin from F-actin as part of the mechanism controlling the necessary disassembly of actin filaments in the distal processes of oligodendrocytes¹¹ which is a crucial step for myelination⁵⁴. Consequently, our findings showing a failure of MBP to be located appropriately precisely where these interactions take place would impact adversely on myelin formation. Whether any effects mediated by MBP abnormalities seen here also involve the previously reported aberrant F-actin dynamics⁵⁵ in *Cyfp1*^{+/-} mouse models, remains to be established.

Effects related to the close interaction between CYFIP1 and FMRP affecting protein translation cannot be discounted, especially in view of a degree of overlap between white matter changes in the *Cyfp1*^{+/-} rat model and a mouse *Fmr1* knockout, specifically reduced FA in the corpus callosum⁵⁶. The mouse *Fmr1* knockout also revealed evidence of global disruptions in functional connectivity as indexed by fMRI⁵⁶. Prior to myelination, mRNAs encoding MBP are transported into the oligodendrocyte processes, where local translation of MBP mRNAs occurs, so perturbations in CYFIP1-FMRP interactions could presumably affect MBP mRNA translation. However, whilst there is some in vitro evidence linking FMRP with regulation of mRNA translation in developing oligodendrocytes⁵⁷, current data does not allow further speculation regarding FMRP mediated effects on the phenotypes seen in the *Cyfp1*^{+/-} rat model. Additional complexity is apparent when considering the range of functions that may be sensitive to reduced dosage of *Cyfp1*, encompassing oligodendrocyte production, differentiation and migration; effects on neurons as opposed to oligodendrocytes, can also have an impact on axon-oligodendrocyte interactions and influence myelination in that way⁵⁸.

We assessed the extent to which the imaging and cellular data were associated with behavioural effects. Behavioural flexibility has been shown to be sensitive to abnormalities in myelination in mouse models of myelin deficits¹⁵. Furthermore, in humans, corpus callosum morphology correlates with behavioural flexibility in a study using a cohort of twin pairs, where one was diagnosed with bipolar disorder and the other was clinically healthy³⁰. We therefore focused the behavioural analyses on psychological processes supporting such flexibility. We first showed that during reversal learning, *Cyfp1*^{+/-} rats showed greater early perseveration in choosing the previously rewarded stimulus. The effects in the *Cyfp1*^{+/-} rats were highly specific to the reversal element of the task, with no concomitant effects on initial learning.

The pattern of normal initial learning but impaired behavioural flexibility was also evident when assessed independently in an associative mismatch task. In this case, the changed contingencies involved the relationships between the components of audio-visual sequences. This task has been described previously⁴⁷⁻⁵⁰, and characterised with respect to its psychological origin^{47,49}, the conditions under which it is observed^{48,50} and its underlying brain substrates, where there is evidence that hippocampal circuitry is involved, and mediation of related psychological processes by callosal circuitry⁵⁹⁻⁶¹. We again observed a highly specific effect of *Cyfp1* haploinsufficiency on the orienting behaviour generated when there was a mismatch between the trained and tested audio-visual sequences, with the *Cyfp1*^{+/-} rats not showing the expected increase in orienting to a familiar visual stimulus that was unpredicted by the auditory cue that preceded it. An inability to alter behaviour in response to changes in the environment has been strongly associated with orbitofrontal cortex (particularly during reversal learning⁶²) and ventral prefrontal cortex damage in humans⁶³ and rats^{62,64}. Whilst the role of the corpus callosum in behavioural flexibility has not been

as extensively investigated, it is known to be important in the functional integrity of brain regions that are classically linked with behavioural flexibility^{32,64,65}. The corpus callosum (along with the internal capsule) carries white matter bundles containing axons projecting from the frontal cortex and striatal regions³², and pruning and myelination of the corpus callosum coincides with cortical maturation in the frontal cortex, mutually influencing each other's development^{65,66}.

Increases in FA with little evidence of reductions were a prominent feature of our findings in human 15q11.2 BP1-BP2 deletion carriers⁷. Hence, while the rat model and human phenotype converged on white matter changes they differed in the direction of the change. Differences between the human and rat findings could have resulted from several factors. First, the 15q11.2 BP1-BP2 deletion involves three other genes in addition to *CYFIP1*, especially *NIPA1* which is expressed in the brain and was found to inhibit the bone morphogenic protein (BMP), crucial for typical axonal growth and guidance^{67,68}. Therefore, a priori, haploinsufficiency of *NIPA1*, and possibly the other genes in the interval^{69,70}, may impact on the 15q11.2 BP1-BP2 deletion DTI phenotype. The possibility that there are species differences in the expression patterns of *CYFIP1/Cyfp1* and also any compensatory responses to haploinsufficiency should also be borne in mind. Furthermore, the humans and rats are likely to have been subject to differential compensatory mechanisms arising from very different environmental challenges across their lifespan^{6,71,72}. Moreover, as changes in myelin thickness impact relatively modestly on DTI measures²⁴ it may be that whilst myelin changes may be present in both human and the rat model, in terms of the human DTI data any effect on myelin may have been masked by other molecular and cellular consequences of the copy number deletion. To date, there have been no published studies of myelin (as opposed to overall white matter) changes in 15q11.2 BP1-BP2 deletion, though the current data predicts their existence and this is something that could be tested using ultrastructural magnetic resonance imaging (MRI) methods providing the necessary resolution to visualise and quantify myelinated axons directly in the living human brain⁷³. Nonetheless, whilst an exact between-species comparison would require an assessment of *CYFIP1*-specific heterozygous humans, we have demonstrated a clear link between *Cyfp1* haploinsufficiency and white matter microstructure.

In conclusion, we have employed a novel rat model of *Cyfp1* haploinsufficiency to probe the neurobiological and behavioural mechanisms underlying the significantly enhanced risk for psychopathology linked to the 15q11.2 BP1-BP2 deletion. We found disturbances to white matter as seen in human carriers, and showed effects on myelin thickness associated with an abnormal intracellular distribution of MBP, together with evidence of highly specific effects on behavioural flexibility. Cross species comparison of the imaging phenotypes in rats and humans suggest it is unlikely that effects mediated by *CYFIP1* are solely responsible for the 15q11.2 phenotype, and additional work is required to determine the contribution made by the other three genes, *NIPA1*, *NIPA2*, and *TUBGCP5* affected in the 15q11.2 BP1-BP2 deletion. However, these findings in the *Cyfp1* rat model give an insight into the contribution made by low dosage of *CYFIP1* to the 15q11.2 BP1-BP2 deletion phenotype.

Methods

Rats. The *Cyfp1* rat model was created by Cardiff University in collaboration with Horizon Discovery (St Louis, USA) using CRISPR-Cas9 targeting (<https://www.horizondiscovery.com/>) and supported by a Wellcome Trust Strategic Award (DEFINE). Full information on the creation and validation of the rat model is in the Supplementary Methods section. All the rats used in this study were Long Evans males. The rats were produced from breeding stocks held at Charles River (UK) using a WT x HET design resulting in an average 1:1 WT to *Cyfp1*^{+/-}, the

mutation was transmitted in Mendelian fashion with no sex bias and the rats were healthy and viable showing no general ill effects of the mutation. The rats were transported to Cardiff at 8–10 weeks of age. At Cardiff the rats were housed in mixed-genotype groups of 2–3 rats. The rats had free access to food and water (except for those used in the reversal learning task, see below) and lived under the condition of a 12 hr light/day cycle (lights on at 7:00 am), room temperature $21 \pm 2^\circ\text{C}$. Rats used in DTI were 5-months-old. The rats were euthanised 1 month after the scanning and used for immunofluorescence. The rats used for electron microscopy were 6-months-old. The rats used for behavioural experiments were 6–9-months-old. The reversal learning task was motivated by liquid reward (10% sucrose solution w/v) and to enhance working in the task, the rats were subject to water restriction immediately prior to and during task training, in which case the rats were given 2 h access to water per day. The water restriction schedule has no adverse effects on the health or welfare of the rats, being designed to give rise to a temporary increase in motivation for the liquid reinforcement, and across the whole day the rats on the schedule drink as much fluid as under free access conditions. All the experimental procedures were performed in accordance with institutional animal welfare, ethical and ARRIVE guidelines and under the UK Home Office License PPL 30/3135 (Animals (Scientific Procedures) Act 1986).

Diffusion tensor imaging acquisition. A cohort of 24 rats (WT $n = 12$ and *Cyfp1*^{+/-} $n = 12$) were anaesthetised with isoflurane in oxygen at 4% and maintained at 1% during the scanning. MRI scans were acquired with a 9.4 T MRI scanner (Bruker, Karlsruhe, Germany) with a 30-cm bore and a gradient strength of up to 600 mTm^{-1} . The MRI protocol included DTI acquisition with a diffusion-weighted (DW) spin-echo echo-planar-imaging (EPI) pulse sequence having the following parameters: TR/TE = 4000/22 ms, $\Delta/\delta = 10.5/4.5$ ms, two EPI segments, and 60 noncollinear gradient directions with a single *b*-value shell at 1000 smm^{-2} and one image with a *b*-value of 0 smm^{-2} (referred to as *b*0). Geometrical parameters were: 34 slices, each 0.32 mm thick (brain volume) and with in-plane resolution of $0.32 \times 0.32\text{ mm}^2$ (matrix size 80×96 ; FOV $25.6 \times 30.73\text{ mm}^2$). The DTI protocol lasted ~16 min. In addition, high resolution, T2 weighted images were acquired for anatomical reference with a multi-slice multi-echo pulse sequence with the following parameters: TR of 7200 ms, TE of 15 ms and effective TE of 45 ms, rare factor was 8. Image resolution was set to 0.22 mm^3 with matrix size of $128 \times 160 \times 50$ to cover the entire brain.

DTI data correction and DTI maps extraction. ExploreDTI 4.8.3⁷⁴ and SPM (version 12, UCL, London, UK) were used in the preprocessing of the rat DTI data. First, eddy-current induced distortion and motion correction were performed and mean-DWI images were extracted using ExploreDTI. Non-brain tissue was removed from the mean-DWI and the T₂-weighted images following these steps: (1) T₂-weighted scans were anisotropic smoothed using ExploreDTI, (2) both smoothed T₂-weighted and mean DWI images were bias corrected using the segmentation tool in SPM12, (3) the bias corrected T₂-weighted were coregistered with a population-specific template and multiplied by a mask to remove the non-brain tissue, (4) the skull was removed from the mean DWIs using the 3D masking option in ExploreDTI. Then, data was corrected for field inhomogeneities, using ExploreDTI, where the skull-stripped mean DWIs images were used as a native space mask, and the skull-stripped T₂-weighted structural scans were used as transformed space mask. Each DWI image was nonlinearly warped to the T₂-weighted image using non-DWIs map as a reference. ExploreDTI was used to generate FA, AD, RD and MD maps.

Preprocessing for Tract-Based Spatial Statistics. For the voxel-wise analyses of DTI data, Tract-Based Spatial Statistics (TBSS) method was implemented, which is part of the FSL. All FA maps were submitted to a free-search for a best registration target, where each volume was first registered to every other volume, and the one requiring minimum transformation to be registered to other volumes was selected as the best registration target. This target was used as a template into which the registration was performed. Following registration, a mean FA map was calculated, thinned to represent a mean FA skeleton, and an optimal threshold of 0.2 was applied to the mean FA skeleton to create a binary white matter skeleton mask (Supplementary Fig. 1). The local FA-maxima, as well as the AD, RD and MD, of each rat were projected onto this white matter skeleton.

ex vivo transmission electron microscopy and immunofluorescence. For transmission electron microscopy, a new cohort of nine rats (WT $n = 5$ and *Cyfp1*^{+/-} $n = 4$) was used. For immunofluorescence seven brains were randomly selected (WT $n = 7$ and *Cyfp1*^{+/-} $n = 7$) from the cohort used for DTI. In both cohorts, the rats were intracardially perfused with 0.1 M phosphate buffered saline (PBS), followed by 4% of glutaraldehyde in 0.1 M PBS in the cohort used for electron microscopy, and 4% paraformaldehyde in 0.1 M PBS (PFA) in the cohort used for immunofluorescence. For transmission electron microscopy, the brains were placed on a shaker to postfix in glutaraldehyde for 4 h, after which they were placed in phosphate buffered saline and stored at 4°C until further use. Then the brains were embedded in TAAB embedding resin. Ultra-thin sections (50 nm) were stained with aqueous 4% uranyl acetate and lead citrate. The sections were visualised on a transmission electron microscope (CM12, Philips, the Netherlands)

and, for quantification, images were taken using an on-axis 2048×2048 charge-coupled device camera (Proscan, Schering, Germany). In order to obtain a representative sample, 15 regions across the extent of the anterior-posterior extent of the corpus callosum per animal were taken for quantification. For immunofluorescence, the brains were placed on a shaker to postfix in PFA for 4 h, after which they were placed in phosphate buffered 30% sucrose. Coronal cryosections of the brain, of $15\ \mu\text{m}$ thickness, were made on a cryostat (CM1860 UV, Leica, UK), mounted onto a Poly-L-Lysine (PLL)-coated slides (three sections per slide), and stored at -20°C . For immunofluorescence, antibodies were used as follows: anti-Olig2 (ab109186, Abcam) 1:400, anti-APC [CC-1] (ab16794, Abcam) 1:400, anti-MBP (MAB386, Millipore) 1:300. For the Olig2 and Cc1 doublestaining, the slices were heated in a 5% citrate buffered antigen retrieval solution (pH 6, 10x, Sigma-Aldrich Company, UK), using a water bath at 90% for 10 min. All the slices were blocked for 1 h with 5% donkey serum (Sigma-Aldrich Company, UK), and 0.3% Triton X-100 in PBS. The appropriate primary antibodies were applied and incubated overnight at 4°C . On the next day, after washing, the slices were incubated for 2 h with secondary antibodies (Alexa Fluor Life Technologies, Manchester, UK), in a concentration of 1:1000 at room temperature. Then, the slides were washed, counterstained with 1:1000 DAPI, mounted and cover-slipped. For quantification of Olig2 + and Cc1 + cells, images were taken on an inverted fluorescent time lapse microscope (DMI6000B, Leica, UK), and at least 4 images from random visual fields were taken from regions including the corpus callosum and external capsule. For quantification of MBP intensity, one coronal section per rat was taken on an Axio scan (Zeiss, Germany), and the same exposure time and intensity were used for all the slides.

in vitro immunofluorescence. Primary OPC cultures were isolated from neonatal Long Evans (postnatal day 0–3) rat from cortices following a standard protocol²⁶. This protocol is known to generate OPC at $\geq 95\%$. Briefly, cerebral cortices were dissected, and the meninges were removed. Following the enzymatic digestion for an hour, the cell suspension was placed into cell culture flasks. The mixed glial cultures were grown for ~10 days in Dulbecco modified Eagle medium supplemented with 10% foetal calf serum at 37°C in 7.5% CO₂. On day 10, the flasks were shaken for 1 h at 260 rpm on an orbital shaker to remove the loosely attached microglia and were then shaken at 260 rpm overnight to dislodge the loosely attached oligodendrocyte precursors. OPCs were seeded onto PLL-coated eight well chamber slides (2×10^4 cells/well), in Sato's medium supplemented with 0.5% foetal calf serum (FCS) in order to induce differentiation. After 3 days of differentiation, the cells were fixed using 4% PFA in PBS for 10 min following two washes with PBS. Cells were stained with anti-O4 (1:200; MAB345, Millipore) and anti-MBP (1:200; MAB386, Millipore) antibodies (Alexa 555/488-conjugated secondary antibody, 1:300; Alexa Fluor Life Technologies). For quantification, images were taken on an inverted fluorescent time lapse microscope (DMI6000B, Leica, UK) with $\times 20$ magnification, where 5 images from random visual fields were taken per well. Three independent biological replicates were performed.

Reversal learning. A separate group of 17 rats were used in the reversal learning task (WT $n = 7$, *Cyfp1*^{+/-} $n = 10$). Testing was conducted in a touchscreen-based automated operant system that consisted of an operant chamber with a flat-screen monitor equipped with an infrared touchscreen with accompanying Animal Behaviour Environment Test (ABET) II software (Campden Instruments, Leics). Session duration was 30 min, or until 100 trials were completed under all training conditions. Pre-training consisted of two stages (Magazine Training and Touch Training) these gradually shaped the screen-touching behaviour required for the reversal learning touchscreen task proper. Following successful completion of pre-training Visual Discrimination Training began (Supplementary Fig. 4); two stimuli were presented at a time (S+ and S-, counterbalanced across animals), on either side of the screen. The rat had to touch the correct stimulus (S+) to elicit reward. Reward delivery was accompanied by illumination of the tray light and a tone. Entry to collect the reward turned off the tray light and started the inter-trial interval (ITI -5s) following which the rat initiated the next trial by a second magazine entry. Touching the incorrect stimulus (S-) terminated the trial and the house-light was turned on for a time-out period of 5 s and no reward given, following the time-out the ITI period began after which the rat had to initiate the next trial by executing a magazine entry. Once the rats reached performance criteria (Completing 50 + trials with 80–85% correct, for 2 consecutive sessions), the contingencies were reversed (previous S+ now S-; previous S- now S+) and behaviour monitored (see Supplementary Figure 4 for schematic of task design).

Mismatch task. A different group of 36 rats performed the mismatch task (WT $n = 21$, *Cyfp1*^{+/-} $n = 15$). On the first 4 days, the rats were placed in the experimental apparatus (a modified skinner box allowing presentations of auditory and visual stimuli) for 30 min. Following this general habituation to the apparatus they received 4 days of training with two audiovisual sequences. One auditory stimulus (a 2 kHz tone) preceded the constant presentation of a light, whereas a second auditory stimulus (a 10 Hz series of clicks) preceded the flashing presentation of the same light stimuli (i.e. Tone → Steady Light, Click → Flashing Light; the combinations were randomly counterbalanced across animals). All stimuli were presented for 10 sec. There were 10 presentations of both audiovisual sequences on each of the first

3 days of training and six presentations of both sequences on day 4 that served as warm-up trials for the eight test trials that immediately followed. The inter-trial-interval was 2 min. Rats received two types of test trials, match and mismatch. The order in which the two types of test trials were presented was counterbalanced. Match test trials were presentations of the same audiovisual sequences that had been presented during training (e.g. Tone→Steady Light, Click→Flashing Light), whereas on mismatch trials the auditory stimuli preceding the visual stimuli were exchanged (e.g. Tone→Flashing Light, Click→Steady Light). All experimental sessions were recorded using a video recorder and orienting responses subsequently scored by observers who were blind to the genotype of the rats and the nature of the test trials (match or mismatch). An Orienting Response (OR) was defined as the tip of a rat's snout being located in the side of the apparatus that contained the light and pointing in the direction of the light.

Statistical analyses. Differences in DTI measures between the two groups (WT and *Cyfp1^{+/-}*) were assessed using voxel-wise independent *t*-tests, where two different contrasts were used (WT > *Cyfp1^{+/-}*, and *Cyfp1^{+/-}* > WT). Using the randomise function (part of FSL), the null distribution was built over 1000 random permutations, using the TFCE¹⁸ algorithm where cluster-like structures are enhanced, and the results are shown for $p < 0.05$. For multiple comparison correction, first FWE correction was used. Since only FA changes were found within this analysis, we also used a less conservative correction method based on FDR correction, purposed by Benjamini–Hochberg²¹. To quantify the changes in areas where significant differences in FA were seen after FWE correction, regions of interest (ROIs) were manually delineated using FSL. Several consecutive slices were outlined on the coronal plane and the selected ROIs included the corpus callosum, internal capsule, external capsule, and fornix/fimbria regions. The CBJ13 MR-histology rat atlas at age P80⁷⁵ was used as reference. A representation of the binary masks can be found in Supplementary Fig. 2. FA, AD, RD and MD were quantified by applying these binary masks and extracting the mean values for each region across subjects.

For quantification of cells the ImageJ software (version 1.51) was used. The number of myelinated and unmyelinated axons, axon diameter, myelin thickness and g-ratio (measure of myelin thickness relative to axon diameter: where lower g-ratios indicates thicker myelin sheath) of normally myelinated axons were quantified. A total of 13127 (WT $n = 7148$, *Cyfp1^{+/-}* $n = 5979$ axons) myelinated axons were analysed. For quantification of oligodendrocytes *ex vivo*, the total number of Olig2⁺, and the overlapped Olig2⁺/Cc1⁺ cells were counted. Only cell bodies clearly identified by Olig2 and Cc1 immunofluorescence and overlapping with DAPI staining were counted. MBP⁺ reactivity was determined by comparing immunofluorescence staining intensity. The whole region of corpus callosum and external capsule was selected in the coronal section, and quantification was done by calculating the mean intensity of the pixels above a preset intensity threshold, multiplied by the number of pixels above that threshold, and divided by the total area quantified. For *in vitro* quantification, to assess OPC differentiation, the percentage of O4⁺ and MBP⁺ cells relative to Hoechst-stained nuclei were quantified. In order to compare different levels of maturation of oligodendrocytes, MBP-positive oligodendrocytes were classified into three categories considering the distribution of MBP in the cells: (i) type 1, where the MBP staining was only present in the nucleus, (ii) type 2, ramified distribution and (iii) type 3, membranous distribution. Furthermore, to quantify MBP distribution in type 2 and type 3 cells, the area of MBP⁺ staining was quantified.

All the cell quantifications were conducted with the investigator blinded to the phenotype. Differences between WT and *Cyfp1^{+/-}* were analysed in RStudio version 1.1.463 (R Foundation for Statistical Computing, Vienna, Austria). In order to compare all the axons in each group while taking into account variation across individuals, we used linear mixed effects models to analyse the effect of genotype on axon diameter, g-ratio and myelin thickness, where these measures were considered fixed effects, and animals were considered random effects. Since we only had one random effect, we used non-restricted maximum likelihood to estimate the model parameters. In this analysis, the myelin thickness was log-transformed since the data followed a log-normal distribution, whereas the other measures followed a normal distribution. For *in-vitro* analyses, linear mixed effects models were also used to consider variation across biological repeats (where these were considered random effects). All the other measures were analysed using two-tailed unpaired Student's *t*-test. Data are given as mean ± s.e.m.

Visual discrimination and reversal learning performance was assessed using ANOVA with factors of GENOTYPE and SESSION. Any significant interaction was subsequently examined by analysing the Simple Effects. Completion rates for the rats during the different phases of reversal were assessed non-parametrically using Chi-squared test. Performance in the mismatch task was assessed using ANOVA with factor of GENOTYPE and BLOCK during the habituation to the test apparatus phase of training and factor GENOTYPE in the habituation to the stimulus pairs and mismatch test phases. Orienting responses in the mismatch test phase were analysed as a discrimination ratio (total orienting to matched/total orienting to both matched + mismatched).

Reporting summary. Further information on research design is available in the Nature Research Reporting Summary linked to this article.

Data availability

All data from this study are available from the corresponding author upon reasonable request. The source data underlying Table 1, Fig. 2c–g, Fig. 3a–b, Fig. 4c–d, Fig. 5a–e, Fig. 6a–c, and Supplementary Figs. VI and VII are provided as a Source Data file.

Received: 23 November 2018 Accepted: 20 June 2019

Published online: 01 August 2019

References

- Cox, D. M. & Butler, M. G. The 15q11.2 BP1–BP2 Microdeletion syndrome: a review. *Int. J. Mol. Sci.* **16**, 4068–4082 (2015).
- Butler, M. G. Clinical and genetic aspects of the 15q11.2 BP1–BP2 microdeletion disorder. *J. Intellect. Disabil. Res.* **61**, 568–579 (2017).
- Chai, J.-H. et al. Identification of four highly conserved genes between breakpoint hotspots BP1 and BP2 of the prader-willi/angelman syndromes deletion region that have undergone evolutionary transposition mediated by flanking duplicons. *Am. J. Hum. Genet.* **73**, 898–925 (2003).
- De Rubeis, S. et al. CYFIP1 coordinates mRNA translation and cytoskeleton remodeling to ensure proper dendritic spine formation. *Neuron* **79**, 1169–1182 (2013).
- Lozano, R., Rosero, C. A. & Hagerman, R. J. Fragile X spectrum disorders. *Intractable Rare Dis. Res.* **3**, 134–146 (2014).
- Fields, R. D. White matter in learning, cognition and psychiatric disorders. *Trends Neurosci.* **31**, 361–370 (2008).
- Silva, A. I. et al. Reciprocal white matter changes associated with copy number variation at 15q11.2 BP1–BP2: A Diffusion Tensor Imaging Study. *Biol. Psychiatry* **85**, 563–572 (2019).
- Ulfarsson, M. O. et al. 15q11.2 CNV affects cognitive, structural and functional correlates of dyslexia and dyscalculia. *Transl. Psychiatry* **7**, e1109 (2017).
- Dent, E. W. & Gertler, F. B. Cytoskeletal dynamics and transport in growth cone motility and axon guidance. *Neuron* **40**, 209–227 (2003).
- Bauer, N. G., Richter-Landsberg, C. & Ffrench-Constant, C. Role of the oligodendroglial cytoskeleton in differentiation and myelination. *Glia* **57**, 1691–1705 (2009).
- Zuchero, J. B. et al. CNS myelin wrapping is driven by actin disassembly. *Dev. Cell* **34**, 152–167 (2015).
- Kim, H.-J. et al. WAVE1 is required for oligodendrocyte morphogenesis and normal CNS myelination. *J. Neurosci.* **26**, 5849–5859 (2006).
- O'Meara, R. W. et al. Integrin-linked kinase regulates process extension in oligodendrocytes via control of actin cytoskeletal dynamics. *J. Neurosci.* **33**, 9781–9793 (2013).
- Thurnherr, T. et al. Cdc42 and Rac1 signaling are both required for and act synergistically in the correct formation of myelin sheaths in the CNS. *J. Neurosci.* **26**, 10110–10119 (2006).
- Inagawa, K., Watanabe, S., Tsukada, Y. & Mikoshiba, K. The role of myelination in learning performance observed in two strains of myelin-deficient mutant mice (shiverer and mld). *Behav. Neural Biol.* **50**, 184–192 (1988).
- Fields, R. D. A new mechanism of nervous system plasticity: activity-dependent myelination. *Nat. Rev. Neurosci.* **16**, 756–767 (2015).
- Smith, S. M. et al. Tract-based spatial statistics: Voxelwise analysis of multi-subject diffusion data. *NeuroImage* **31**, 1487–1505 (2006).
- Smith, S. M. & Nichols, T. E. Threshold-free cluster enhancement: addressing problems of smoothing, threshold dependence and localisation in cluster inference. *NeuroImage* **44**, 83–98 (2009).
- Hofstetter, S. & Assaf, Y. The rapid development of structural plasticity through short water maze training: A DTI study. *NeuroImage* **155**, 202–208 (2017).
- McKenzie, I. A. et al. Motor skill learning requires active central myelination. *Science* **346**, 318–322 (2014).
- Benjamini, Y. & Hochberg, Y. Controlling the false discovery rate: a practical and powerful approach to multiple testing. *J. R. Stat. Soc. Ser. B Methodol.* **57**, 289–300 (1995).
- Sierra, A. et al. Diffusion tensor MRI with tract-based spatial statistics and histology reveals undiscovered lesioned areas in kainate model of epilepsy in rat. *Brain Struct. Funct.* **216**, 123–135 (2011).
- Le Bihan, D. Molecular diffusion, tissue microdynamics and microstructure. *NMR Biomed.* **8**, 375–386 (1995).
- Beaulieu, C. The basis of anisotropic water diffusion in the nervous system - a technical review. *NMR Biomed.* **15**, 435–455 (2002).
- Klingseisen, A. & Lyons, D. A. Axonal regulation of central nervous system myelination: structure and function. *Neuroscientist* **24**, 7–21 (2018).
- Syed, Y. A., Abdulla, S. A. & Kotter, M. R. N. Studying the Effects of Semaphorins on Oligodendrocyte Lineage Cells. in *Semaphorin Signaling*:

- Methods and Protocols* (ed. Terman, J. R.) 363–378 (Springer, New York, 2017). https://doi.org/10.1007/978-1-4939-6448-2_26
27. Boggs, J. M. Myelin basic protein: a multifunctional protein. *Cell. Mol. Life Sci. CMLS* **63**, 1945–1961 (2006).
 28. Lourenço, T. et al. Modulation of oligodendrocyte differentiation and maturation by combined biochemical and mechanical cues. *Sci. Rep.* **6**, 21563 (2016).
 29. Lyons, D. A., Naylor, S. G., Scholze, A. & Talbot, W. S. Kif1b is essential for mRNA localization in oligodendrocytes and development of myelinated axons. *Nat. Genet.* **41**, 854–858 (2009).
 30. Bearden, C. E. et al. Mapping corpus callosum morphology in twin pairs discordant for bipolar disorder. *Cereb. Cortex* **21**, 2415–2424 (2011).
 31. Lochner, C. et al. Evidence for fractional anisotropy and mean diffusivity white matter abnormalities in the internal capsule and cingulum in patients with obsessive-compulsive disorder. *J. Psychiatry Neurosci. JPN* **37**, 193–199 (2012).
 32. Haber, S. N. & Behrens, T. E. J. The neural network underlying incentive-based learning: implications for interpreting circuit disruptions in psychiatric disorders. *Neuron* **83**, 1019–1039 (2014).
 33. Alm, K. H., Rolheiser, T., Mohamed, F. B. & Olson, I. R. Fronto-temporal white matter connectivity predicts reversal learning errors. *Front. Hum. Neurosci.* **9**, 343 (2015).
 34. Balevich, E. C. et al. Corpus callosum size and diffusion tensor anisotropy in adolescents and adults with schizophrenia. *Psychiatry Res. Neuroimaging* **231**, 244–251 (2015).
 35. Onnink, A. M. H. et al. Deviant white matter structure in adults with attention-deficit/hyperactivity disorder points to aberrant myelination and affects neuropsychological performance. *Prog. Neuropsychopharmacol. Biol. Psychiatry* **63**, 14–22 (2015).
 36. Magnuson, M. E., Thompson, G. J., Pan, W.-J. & Keilholz, S. D. Effects of severing the corpus callosum on electrical and BOLD functional connectivity and spontaneous dynamic activity in the rat brain. *Brain Connect* **4**, 15–29 (2013).
 37. Coizet, V. et al. Organization of the anterior limb of the internal capsule in the rat. *J. Neurosci.* **37**, 2539–2554 (2017).
 38. Waltz, J. A. & Gold, J. M. Probabilistic reversal learning impairments in schizophrenia: further evidence of orbitofrontal dysfunction. *Schizophr. Res.* **93**, 296–303 (2007).
 39. Kaland, N., Smith, L. & Mortensen, E. L. Brief report: cognitive flexibility and focused attention in children and adolescents with asperger syndrome or high-functioning autism as measured on the computerized version of the wisconsin card sorting test. *J. Autism Dev. Disord.* **38**, 1161–1165 (2008).
 40. Dickson, P. E. et al. Effects of stimulus salience on touchscreen serial reversal learning in a mouse model of fragile X syndrome. *Behav. Brain Res.* **252**, 126–135 (2013).
 41. Hamilton, D. A. & Brigman, J. L. Behavioral flexibility in rats and mice: contributions of distinct frontocortical regions. *Genes Brain Behav.* **14**, 4–21 (2015).
 42. Uddin, L. Q. et al. Brain state differentiation and behavioral inflexibility in Autism. *Cereb. Cortex* **25**, 4740–4747 (2015).
 43. Lancaster, T. M. et al. Associations between polygenic risk for schizophrenia and brain function during probabilistic learning in healthy individuals. *Hum. Brain Mapp.* **37**, 491–500 (2016).
 44. Reddy, L. F., Waltz, J. A., Green, M. F., Wynn, J. K. & Horan, W. P. Probabilistic reversal learning in schizophrenia: stability of deficits and potential causal mechanisms. *Schizophr. Bull.* **42**, 942–951 (2016).
 45. Gabriel, M. & Orona, E. Parallel and serial processes of the prefrontal and cingulate cortical systems during behavioral learning. *Brain Res. Bull.* **8**, 781–785 (1982).
 46. Bussey, T. J., Muir, J. L., Everitt, B. J. & Robbins, T. W. Dissociable effects of anterior and posterior cingulate cortex lesions on the acquisition of a conditional visual discrimination: facilitation of early learning vs. impairment of late learning. *Behav. Brain Res.* **82**, 45–56 (1996).
 47. Honey, R. C. & Good, M. Associative components of recognition memory. *Curr. Opin. Neurobiol.* **10**, 200–204 (2000).
 48. Honey, R. C. & Good, M. Associative modulation of the orienting response: distinct effects revealed by hippocampal lesions. *J. Exp. Psychol. Anim. Behav. Process.* **26**, 3–14 (2000).
 49. Honey, R. C., Jordanova, M. D. & Good, M. Latent inhibition and habituation: Evaluation of an associative analysis. in *Latent inhibition: Cognition, neuroscience and applications to schizophrenia* 163–182 (Cambridge University Press, 2010). <https://doi.org/10.1017/CBO9780511730184.009>
 50. Honey, R. C., Watt, A. & Good, M. Hippocampal lesions disrupt an associative mismatch process. *J. Neurosci.* **18**, 2226–2230 (1998).
 51. Boyd, A., Zhang, H. & Williams, A. Insufficient OPC migration into demyelinated lesions is a cause of poor remyelination in MS and mouse models. *Acta Neuropathol. (Berl.)* **125**, 841–859 (2013).
 52. Syed, Y. A. et al. Inhibition of phosphodiesterase-4 promotes oligodendrocyte precursor cell differentiation and enhances CNS remyelination. *EMBO Mol. Med.* **5**, 1918–1934 (2013).
 53. Raasakka, A. et al. Membrane association landscape of myelin basic protein portrays formation of the myelin major dense line. *Sci. Rep.* **7**, 4974 (2017).
 54. Nawaz, S. et al. Actin filament turnover drives leading edge growth during myelin sheath formation in the central nervous system. *Dev. Cell* **34**, 139–151 (2015).
 55. Pathania, M. et al. The autism and schizophrenia associated gene CYFIP1 is critical for the maintenance of dendritic complexity and the stabilization of mature spines. *Transl. Psychiatry* **4**, e374 (2014).
 56. Haberl, M. G. et al. Structural-functional connectivity deficits of neocortical circuits in the Fmr1-/- mouse model of autism. *Sci. Adv.* **1**, e1500775 (2015).
 57. Jeon, S. J., Ryu, J. H. & Bahn, G. H. Altered translational control of fragile x mental retardation protein on myelin proteins in neuropsychiatric disorders. *Biomol. Ther.* **25**, 231–238 (2017).
 58. Barres, B. A. & Raff, M. C. Axonal control of oligodendrocyte development. *J. Cell Biol.* **147**, 1123–1128 (1999).
 59. Banich, M. T. The missing link: the role of interhemispheric interaction in attentional processing. *Brain Cogn.* **36**, 128–157 (1998).
 60. Niogi, S., Mukherjee, P., Ghajar, J. & McCandliss, B. D. Individual differences in distinct components of attention are linked to anatomical variations in distinct white matter tracts. *Front. Neuroanat.* **4**, 2 (2010).
 61. Chechlacz, M., Humphreys, G. W., Sotiropoulos, S. N., Kennard, C. & Cazzoli, D. Structural organization of the corpus callosum predicts attentional shifts after continuous theta burst stimulation. *J. Neurosci.* **35**, 15353–15368 (2015).
 62. Chudasama, Y. & Robbins, T. W. Dissociable contributions of the orbitofrontal and infralimbic cortex to pavlovian autoshaping and discrimination reversal learning: further evidence for the functional heterogeneity of the rodent frontal cortex. *J. Neurosci.* **23**, 8771–8780 (2003).
 63. Hornak, J. et al. Reward-related reversal learning after surgical excisions in orbito-frontal or dorsolateral prefrontal cortex in humans. *J. Cogn. Neurosci.* **16**, 463–478 (2004).
 64. Schoenbaum, G., Nugent, S. L., Saddoris, M. P. & Setlow, B. Orbitofrontal lesions in rats impair reversal but not acquisition of go, no-go odor discriminations. *Neuroreport* **13**, 885–890 (2002).
 65. Ozalay, O. et al. The relationship between the anterior corpus callosum size and prefrontal cortex volume in drug-free depressed patients. *J. Affect. Disord.* **146**, 281–285 (2013).
 66. Putnam, M. C., Wig, G. S., Grafton, S. T., Kelley, W. M. & Gazzaniga, M. S. Structural organization of the corpus callosum predicts the extent and impact of cortical activity in the nondominant hemisphere. *J. Neurosci.* **28**, 2912–2918 (2008).
 67. Tsang, H. T. H. et al. The hereditary spastic paraplegia proteins NIPA1, spastin and spartin are inhibitors of mammalian BMP signalling. *Hum. Mol. Genet.* **18**, 3805–3821 (2009).
 68. Wang, X., Shaw, W. R., Tsang, H. T. H., Reid, E. & O’Kane, C. J. Drosophila spichthyn inhibits BMP signaling and regulates synaptic growth and axonal microtubules. *Nat. Neurosci.* **10**, 177–185 (2007).
 69. Xie, H. et al. Functional study of NIPA2 mutations identified from the patients with childhood absence epilepsy. *PLoS ONE* **9**, e109749 (2014).
 70. Xiong, Y. & Oakley, B. R. In vivo analysis of the functions of γ -tubulin-complex proteins. *J. Cell Sci.* **122**, 4218–4227 (2009).
 71. Laviola, G., Hannan, A. J., Macri, S., Solinas, M. & Jaber, M. Effects of enriched environment on animal models of neurodegenerative diseases and psychiatric disorders. *Neurobiol. Dis.* **31**, 159–168 (2008).
 72. Hoyer, C., Gass, N., Weber-Fahr, W. & Sartorius, A. Advantages and challenges of small animal magnetic resonance imaging as a translational tool. *Neuropsychobiology* **69**, 187–201 (2014).
 73. Shi, Y. & Toga, A. W. Connectome imaging for mapping human brain pathways. *Mol. Psychiatry* **22**, 1230–1240 (2017).
 74. Leemans, A., Jeurissen, B., Sijbers, J. & Jones, D. K. ExploreDTI: a graphical toolbox for processing, analyzing, and visualizing diffusion MR data. in *Proc. 17th Annual Meeting of International Society for Magnetic Resonance in Medicine (ISMRM)*, Berkeley, CA (2009).
 75. Calabrese, E., Badea, A., Watson, C. & Johnson, G. A. A quantitative magnetic resonance histology atlas of postnatal rat brain development with regional estimates of growth and variability. *NeuroImage* **71**, 196–206 (2013).

Acknowledgements

This work was also supported by a Wellcome Trust Strategic Award ‘DEFINE’ grant no. 100202/Z/12/Z and core support from the Neuroscience and Mental Health Research Institute, Cardiff University, UK. We acknowledge technical support for the DTI studies from Andrew Stewart, School of Biosciences, Cardiff University and excellent animal husbandry and care by the Joint Biological Services Unit personal at Cathays Animal

Facility, Cardiff University. We also acknowledge technical support for the transmission electron microscopy acquisition from Dr. Christopher Von Ruhland, Central Biotechnology Services, Cardiff University.

Author contributions

A.I.S., J.E.H., Y.A.S., D.E.J.L., J.H. and L.S.W. planned, designed and instigated the study. S.T. conducted the molecular specification of the novel heterozygous *Cyfp1* rat line. Y.P., Y.A. and J.C. conducted the DTI imaging acquisition, and A.I.S., Y.A., D.E.J.L., J.H. and L.S.W. analysed the DTI data. A.I.S., Y.A.S. and N.H. obtained and analysed the transmission electron microscopy data, immunofluorescence, and cell culture data. J.E.H., A.I.S., J.H., T.E.L., R.C.H., T.H. and L.S.W. carried out and analysed the behavioural studies. A.I.S., J.E.H., J.H., M.J.O., D.E.J.L., R.C.H. and L.S.W. wrote and reviewed the paper.

Additional information

Supplementary Information accompanies this paper at <https://doi.org/10.1038/s41467-019-11119-7>.

Competing interests: The authors declare no competing interests.

Reprints and permission information is available online at <http://npg.nature.com/reprintsandpermissions/>

Peer review information: *Nature Communications* thanks Jacob Ellegood and other anonymous reviewer(s) for their contribution to the peer review of this work. Peer reviewer reports are available.

Publisher's note: Springer Nature remains neutral with regard to jurisdictional claims in published maps and institutional affiliations.



Open Access This article is licensed under a Creative Commons Attribution 4.0 International License, which permits use, sharing, adaptation, distribution and reproduction in any medium or format, as long as you give appropriate credit to the original author(s) and the source, provide a link to the Creative Commons license, and indicate if changes were made. The images or other third party material in this article are included in the article's Creative Commons license, unless indicated otherwise in a credit line to the material. If material is not included in the article's Creative Commons license and your intended use is not permitted by statutory regulation or exceeds the permitted use, you will need to obtain permission directly from the copyright holder. To view a copy of this license, visit <http://creativecommons.org/licenses/by/4.0/>.

© The Author(s) 2019